THE MECHANICS AND DESIGN OF A NON-TEARING FLOOR CONNECTION USING SLOTTED REINFORCED CONCRETE BEAMS

A THESIS
SUBMITTED IN PARTIAL FULFILMENT
OF THE REQUIREMENTS FOR THE DEGREE OF
MASTER OF ENGINEERING
AT THE
UNIVERSITY OF CANTERBURY

By
Eu Ving Au
March 2010

Supervisors:
Professor Des Bull
Associate Professor Stefano Pampanin

Department of Civil and Natural Resources Engineering
University of Canterbury
Christchurch, New Zealand

Abstract

Ductile plastic hinge zones in beams of reinforced concrete frames are known to incur extensive damage and elongate. This 'beam elongation' can inflict serious damage to adjacent floor diaphragms, raising concerns of life safety. In light of this, the slotted reinforced concrete beam was investigated as a promising non-tearing floor substitute for conventional design. It consists of a conventional reinforced concrete beam, modified with a narrow vertical slot adjacent to the column face, running approximately three-quarters of the beam depth. Seismic rotations occur about the remaining concrete "top-hinge", such that deformations are concentrated in the bottom bars of the beam, away from the floor slab, and beam elongation is minimised.

The inclusion of the slot raised several design issues which needed to be addressed. These were the shear transfer across the top-hinge, buckling of bottom longitudinal reinforcement, low cycle fatigue, bond anchorage of reinforcement in interior joints, interior joint design, detailing with floor units and beam torsion resulting from eccentric floor gravity loads. These issues were conceptually investigated in this project. It was found that most issues could be resolved by providing additional reinforcement and/or specifying alternative detailing.

As part of the experimental investigation, quasi-static cyclic tests were performed on in-plane beam-column joint subassemblies. Specimens tested included exterior and interior joint subassemblies with slotted-beams and a conventional exterior joint as a benchmark. This was followed by a test on a slotted-beam interior joint subassembly with precast floor units and imposed gravity load. Experimental tests revealed significant reductions in damage to both the beam and floor when compared to conventional beams. Issues of bar buckling, bond-slip and altered joint behaviour were also highlighted, but were resolved in the final test.

A simple analytical procedure to predict the moment-rotation response of slotted-beams was developed and verified with experimental results. This was used to perform sensitivity studies to determine appropriate limits for the concrete top-hinge depth, top-to-bottom reinforcement ratio and depth of diagonal shear reinforcement.

For the numerical investigation, a multi-spring model was developed to represent the flexural response of slotted-beams. This was verified with experimental tests and implemented into a five-storey, three-bay frame for earthquake time history analyses. To provide a benchmark, a conventional frame was also setup using the plastic hinge element developed by Peng (2009). Time history analyses showed that the slotted-beam frame response was very similar to the response of a conventional frame. Due to greater hysteretic damping, there was a slight reduction in the average interstorey drift and lateral displacement envelopes. The slotted-beam frame also exhibited 40% smaller residual drifts than the conventional frame.

The research carried out in this thesis showed slotted reinforced concrete beams to be an effective non-tearing floor solution, which could provide a simple and practical substitute for conventional reinforced concrete design.

Acknowledgements

The research presented in this thesis was undertaken at the University of Canterbury under the supervision of Professor Des Bull and Associate Professor Stefano Pampanin. First and foremost, I would sincerely like to thank them both for all their time, effort and guidance.

The financial support provided by the New Zealand Foundation for Research, Science and Technology (FRST) through the "Future Building Systems" research program is greatly acknowledged. Without this support, this project would not have been possible.

I would like to thank the technical staff of the Civil and Natural Resource Engineering Department. In particular, I give a big thanks to Mosese Fifita for all his help in the Structures Laboratory. Thanks also to Russell McConchie, Tim Perigo, Stuart Toase and Peter Coursey for their assistance.

I would like to say thank you to my fellow post-graduate students for all their help, advice and friendship. Particular thanks would have to go to Kam Weng Yuen for his help introducing me into the laboratory, and Brian Peng for all his help with numerical analyses.

I would also like to give a special thanks to all my friends and family for their support and encouragement. To my parents, David and Christine, thank you so much for bringing me up the way you have and for all your love and support. To my fiancé, Rebekah, thank you for all your love and encouragement. Without contest, meeting you was the highlight of my post-graduate studies.

Finally, I would like to thank Jesus Christ for the opportunity to complete a Master's degree. I thank Him for the love and grace He gave dying on the cross that I, and anyone who comes to Him, may have life and have it to the full (John 10:10).

Table of Contents

List of Figures

List of Tables

List of Equations

No. 5 Bar (15.9 mm): $\varepsilon_{ap} = 0.08(2N_f)^{-0.5}$

No. 6 Bar (19.1 mm): $\varepsilon_{ap} = 0.16(2N_f)^{-0.57}$

No. 7 Bar (22.2 mm): $\varepsilon_{ap} = 0.13(2N_f)^{-0.51}$ ...(3-14) 3-14

No. 8 Bar (25.4 mm): $\varepsilon_{ap} = 0.09(2N_f)^{-0.42}$

No. 9 Bar (28.7 mm): $\varepsilon_{ap} = 0.07(2N_f)^{-0.37}$

$$D_{Total} = \sum_{i=1}^{n} D_i = \sum_{i=1}^{n} \frac{1}{N_{f,i}} = \sum_{i=1}^{n} 2\left(\frac{\varepsilon_f'}{\varepsilon_{ap}}\right)^{1/c}$$ ...(3-15) 3-14

Where $D_{Total} \geq 1.0$ denotes low cycle fatigue failure

$$\frac{d_b}{h_c'} \leq \frac{4u_a}{\xi_m \lambda_o f_y}$$ ...(3-16)..... 3-22

$$\frac{d_b}{h_c'} \leq 2.66\frac{\sqrt{f'_c}}{\lambda_o f_y}$$ ...(3-17)..... 3-24

$$\therefore V_{jh} = T + T' - V_{col} = (A_{s1} + A_{s2})\lambda_o f_y - V_{col}$$ ...(3-18) 3-26

$V_{jh} = (C_c' + C_s') + (T_s - C_c) - V_{col}$ or $T_s' + C_s - V_{col}'$ $\therefore V_{jh} = 2\lambda_o A_s f_y - V_{col}$ ...(3-19). 3-26

$$V_{jv} = \frac{h_b}{h_c} V_{jh}$$ ...(3-20)..... 3-27

$V_{jh} = V_{ch}' + V_{sh}'$

Where: $V_{ch}' = C_c' + B_s' - V_{col}$

$V_{sh}' = T_s' + C_s' - B_s'$

$B_s' = 1.25u_o \times 0.8c = (C_s' + T_s')c / h_c$

...(3-21)..... 3-28

$V_{jh} = V_{ch} + V_{sh}$

Where: $V_{ch} = B_s - V_{col}$

$V_{sh} = V_{sh}' + \Delta V_{sh}$

$B_s = \xi_b u_o \times 0.8c = 0.8\xi_b (C_s + T_s)c / h_c$

...(3-22)..... 3-29

$$V_{sh} = f_{yh} A_{jh} = \frac{6V_{jh}^{*}}{f'_c b_j h_c}\left(\alpha_i f_y A_s^{*}\right)$$

Where: $\alpha_i = \left(1.4 - 1.6\frac{C_j N_o^{*}}{f'_c A_g}\right)\alpha_n$ ...(3-23)..... 3-31

$$\frac{6V_{jh}^{*}}{f'_c b_j h_c} \geq 0.85$$

$$M_{n,slab} = A_s f_y (t_{topping} - d_{starter} - a/2) + \mu V_{slab}^{*}(t_{unit} + a/2)$$

Where: $a = \frac{A_s f_y - \mu V_{slab}^{*}}{\alpha f'_c b}$ ...(3-24)..... 3-41

$$F_{h1}^{*} = \frac{V_{Eo-G}^{*}(x_2 - b/2) + V_{slab}^{*}(b - x_2) + M_{n,slab}}{(x_2 - x_1)}$$

$$F_{h2}^{*} = \frac{V_{G+Eo}^{*}(b/2 - x_1) + V_{slab}^{*}(b - x_1) + M_{n,slab}}{(x_2 - x_1)}$$

...(3-25) 3-42

$\delta_l = \theta_b h_b < 0.04 h_b$ ...(3-26) 3-46

$\delta_g = \theta_b\left(\frac{h_b}{2} - t_{slab}\right)$ ...(3-27)..... 3-46

$\delta_{geo} = \theta_b(t_{slab} - c)$ ...(3-28)..... 3-47

$t_{backer} = \theta_b(t_{slab} - d')$ ...(3-29)..... 3-47

$\frac{d_b}{h_c'} \leq \frac{4u_a}{\xi_m \lambda_o f_y}$ ...(4-1)..... 4-41

Horizontal equilibrium: $F_s + F_s' + F_h - C_c = 0$ ...(6-1) 6-2

Gap opening : $M_n = F_s(d - c) + F_s'(d' - c) + F_h(d_h - c) + C_c(a/2 - c)$

Gap closing : $M_n = F_s(d - c) + F_s'(d' - c) + F_h(d_h - c) + C_c(d_c - a/2 - c)$

...(6-2) 6-2

$\Delta_s = \theta_b(d - c)$ and $\Delta_s' = \theta_b(d' - c)$ ...(6-3)..... 6-3

$\varepsilon_s = \frac{\Delta_s + 2/3 L_{sp} \alpha \varepsilon_y}{L_{ub} + 2L_{sp}}$ ...(6-4) 6-3

$$\varepsilon_s' = \frac{\Delta_s'}{4/3L_{sp}'} \quad ...(6\text{-}5) \quad 6\text{-}3$$

$$L_{sp} = 0.022 f_y d_b \quad ...(6\text{-}6) \quad 6\text{-}4$$

$$\varepsilon_s \le \varepsilon_y : \quad f_s = E_s \varepsilon_s$$
$$\varepsilon_y < \varepsilon_s \le \varepsilon_{sh} : \quad f_s = f_y$$
$$\varepsilon_{sh} < \varepsilon_s \le \varepsilon_u : \quad f_s = f_u + (f_y - f_u)\left(\frac{\varepsilon_u - \varepsilon_s}{\varepsilon_u - \varepsilon_{sh}}\right)^p \quad ...(6\text{-}7) \quad 6\text{-}4$$

$$\text{where :} \quad p = \frac{\log\left(\frac{f_u - f_{sh1}}{f_u - f_y}\right)}{\log\left(\frac{\varepsilon_u - \varepsilon_{sh1}}{\varepsilon_u - \varepsilon_{sh}}\right)}$$

$$\varepsilon_{shift} = \varepsilon_s - \varepsilon_{sp}$$
$$\text{Where :} \quad \varepsilon_{sp} = \varepsilon_{s,old} - \varepsilon_y > 0 \quad ...(6\text{-}8) \quad 6\text{-}5$$

$$\text{Gap opening : } \Delta_c = \theta_b \times c$$
$$\text{Gap closing : } \Delta_c = \theta_b (d_c - c) \quad ...(6\text{-}9) \quad 6\text{-}6$$

$$\varepsilon_c = \frac{\Delta_c}{L_{pc}'} \quad ...(6\text{-}10) \quad 6\text{-}6$$

Where L_{pc}' is between $2/3L_{sp}'$ and $4/3L_{sp}'$

$$\varepsilon_c = \left[\frac{\theta_b L_{cant}}{\left(L_{cant} - \frac{L_p}{2}\right)L_p} + \phi_y\right] \times c \quad ...(6\text{-}11) \quad 6\text{-}6$$

$$f_c = \frac{f'_{cc}\, xr}{r - 1 + x^r}$$

$$x = \frac{\varepsilon_c}{\varepsilon_{cc}}$$

$$\varepsilon_{cc} = \varepsilon_{co}\left[1 + 5\left(\frac{f'_{cc}}{f'_{co}} - 1\right)\right] \quad ...(6\text{-}12) \dots 6\text{-}7$$

$$r = \frac{E_c}{E_c - E_{\sec}}$$

$$E_c = 5000\sqrt{f'_{co}}$$

$$E_{\sec} = \frac{f'_{cc}}{\varepsilon_{cc}}$$

$$\varepsilon_{cu} = \varepsilon_{sp} + 0.04\left(\frac{f'_{cc}}{f'_{co}} - 1\right) \quad ...(6\text{-}13) \dots 6\text{-}8$$

$$\varepsilon_c > 2\varepsilon_{co}: \quad f_c = \left(\frac{f'_{co}(2\varepsilon_{co}/\varepsilon_{cc})r}{r - 1 + (2\varepsilon_{co}/\varepsilon_{cc})^r}\right)\left(1 - \frac{\varepsilon_c - 2\varepsilon_{co}}{\varepsilon_{sp} - 2\varepsilon_{co}}\right) \quad ...(6\text{-}14) \dots 6\text{-}8$$

$$\Delta_h = \theta_b(d_h - c) \quad ...(6\text{-}15) \dots 6\text{-}10$$

$$\varepsilon_h = \frac{\Delta_h}{L_{p,h}} \quad ...(6\text{-}16) \dots 6\text{-}10$$

Where : $L_{p,h}$ is between $4/3L_{sp}$ and $2L_{sp}$

$$F_h = A_h f_{s,h} \cos\theta_h \quad ...(6\text{-}17) \dots 6\text{-}10$$

$$L_p = \frac{V_{yc}\, s}{A_v f_{vy}} \quad ...(7\text{-}1) \dots 7\text{-}2$$

$$L_{yield} = \frac{M_{\max} - M_y}{M_{\max}} L_{cant} + \frac{d - d'}{2} + L_{sp} \quad ...(7\text{-}2) \dots 7\text{-}2$$

$$D = L_p \sin\theta_{strut} \quad ...(7\text{-}3) \dots 7\text{-}2$$

$$k_p = \frac{F_{+ve} - F_{-ve}}{\Delta_{+ve} - \Delta_{-ve}} \quad ...(A\text{-}1) \dots A\text{-}1$$

$$E_D = \sum_{cycle} (\Delta_{i+1} - \Delta_i) \frac{(F_i + F_{i+1})}{2} \quad \text{...(A- 2)} \quad \text{A-1}$$

$$\xi_{eq} = \frac{1}{4\pi} \frac{E_D}{E_{So}} \quad \text{...(A- 3)} \quad \text{A-2}$$

where : $E_{So} = k\Delta_o{}^2 / 2$

$$\delta_{el} = \frac{\delta_{bottom} - \delta_{top}}{2} \quad \text{...(A- 4)} \quad \text{A-2}$$

$$\Delta_{bv} = \delta_{pot,v} - x_{pot}\theta_b \quad \text{...(A- 5)} \quad \text{A-3}$$

$$\Delta_{total} = \Delta_c + \Delta_{b,fl} + \Delta_{b,fe} + \Delta_j \quad \text{...(A- 6)} \quad \text{A-4}$$

$$\Delta_c = \frac{F(L_c - h_b)^3}{12E_cI_c} \quad \text{...(A- 7)} \quad \text{A-4}$$

$$\text{Exterior joint} : \Delta_{b,fl} = F\left(\frac{L_c}{L_b}\right)^2 \frac{(L_b - h_c)^3}{6E_cI_b}$$

$$\text{Interior joint} : \Delta_{b,fl} = F\left(\frac{L_c}{L_b}\right)^2 \frac{(L_b - h_c)^3}{12E_cI_b} \quad \text{...(A- 8)} \quad \text{A-4}$$

$$\theta_b = \frac{\delta_{bottom} - \delta_{top}}{h_p} \quad \text{...(A- 9)} \quad \text{A-4}$$

$$\Delta_{b,fe} = \frac{L_c}{L_b}\theta_b(L_b - h_c) \quad \text{...(A- 10)} \quad \text{A-5}$$

Joint shear distortion : $\gamma_j = \frac{\Delta_s}{Dv}$

$$\text{where} : \Delta_s = \frac{|\delta_{ds}|}{\cos R}$$
$$\delta_{ds} = \delta_{jd} - \delta_{dh} - \delta_{dv} \quad \text{...(A- 11)} \quad \text{A-6}$$
$$\delta_{dh} = \frac{\delta_{jt} + \delta_{jb}}{2}\cos R$$
$$\delta_{dv} = \frac{\delta_{jl} + \delta_{jr}}{2}\sin R$$

$$\Delta_j = \gamma_1(L_b - h_c)\frac{L_c}{L_b} + \gamma_2(L_c - h_b) - \gamma_2 h_c \frac{L_c}{L_b} - \gamma_1 h_b$$
$$= \gamma_j\left(L_c - h_c\frac{L_c}{L_b}\right) - \gamma_j h_b \quad \text{...(A- 12)} \quad \text{A-6}$$

Exterior joint : $V_{jh} = \frac{M_b}{jd}\left(1 - \frac{L_b}{L_c}\frac{jd}{(L_b - h_c)}\right)$

Interior joint : $V_{jh} = \frac{M_b}{jd}\left(1 - \frac{L_b}{L_c}\frac{jd}{(L_b - h_c)}\right)$ ...(A- 13) A-7

$$K_j = \frac{\rho_v n \cot^2\alpha}{1 + 4\rho_v n\left(\frac{b_w}{b_{ws}}\right)(1 + 0.39\cot^2\alpha)^2} E_c A_j \quad \text{...(A- 14)} \quad \text{A-7}$$

$$\gamma_j = \frac{V_{jh}}{K_j} \quad \text{...(A- 15)} \quad \text{A-7}$$

$$c = \frac{\delta_1 d_2 - \delta_2 d_1}{\delta_1 - \delta_2} \quad \text{...(A- 16)} \quad \text{A-8}$$

$$\Delta_{component} = \delta_1 + \frac{(\delta_2 - \delta_1)}{(d_2 - d_1)}(d_{component} - d_1) \quad \text{...(A- 17)} \quad \text{A-8}$$

Nomenclature

A_b	=	Area of longitudinal bar
A_{cv}	=	Area of concrete resisting shear
A_g	=	Gross section area
A_{jh}	=	Area horizontal joint steel
A_{jv}	=	Area vertical joint steel
A_s	=	Area of bottom longitudinal reinforcement in beam
A_s'	=	Area of top longitudinal reinforcement in beam
A_{sh}	=	Area of shear reinforcement at spacing s
A_{te}	=	Area of one leg of stirrup tie
A_v	=	Area of shear reinforcement perpendicular to the span within spacing s
a	=	Depth of Whitney equivalent concrete compression block
B_s	=	Longitudinal reinforcement force transferred to the joint concrete strut mechanism via bond
b	=	Section width
b_j	=	Effective joint width
b_w	=	Width of web
C_c	=	Concrete compressive force
c	=	Neutral axis depth
c_c	=	Cover concrete depth
d	=	Effective beam depth (Distance from extreme top fibre to centroid of bottom longitudinal reinforcement)

d' = Distance from extreme top fibre to centroid of top longitudinal reinforcement

d_b = Longitudinal bar diameter

d_{bh} = Diagonal shear hanger bar diameter

d_c = Depth of concrete top-hinge in slotted beam

d_h = Depth to diagonal shear hanger at the beam-column interface

$d_{starter}$ = Depth to starter bar centreline from floor surface

E_c = Elastic modulus of concrete

E_D = Hysteretic energy dissipated per cycle

E_s = Elastic modulus of steel

F = Interstorey shear force

F_h = Horizontal force component in diagonal shear hanger

F_s = Force in bottom longitudinal reinforcement

F_s' = Force in top longitudinal reinforcement

f'_c = Specified 28 day concrete compressive strength

f_s = Stress in bottom longitudinal reinforcement

f_s' = Stress in top longitudinal reinforcement

f_y = Yield strength of longitudinal reinforcement

f_{yt} = Yield strength of transverse reinforcement

f_u = Ultimate strength of steel reinforcement

H_e = Effective height

h_b = Beam depth

h_c = Column depth

h_c' = Effective column depth providing bond to longitudinal reinforcement

I_b = Beam moment of inertia

I_c = Column moment of inertia

I_g = Gross section moment of inertia

jd = Moment lever arm

K_e = Effective secant stiffness

k_p = Peak-to-peak stiffness

L = Centreline span

L_b = Beam span length between column centrelines

L_c = Column interstorey height

L_{cant} = Beam cantilever length to point of contraflexure

L_{db} = Development length of bar

L_n = Clear span

L_p = Plastic hinge length

L_p' = Strain length of top longitudinal reinforcement

L_{pc}' = Strain length of compression concrete in top-hinge

L_{slot} = Slot width

L_{sp} = Strain penetration length

L_{ub} = Unbonded length of steel reinforcement including width of slot

L_{yield} = Effective length of steel spring in plastic hinge element (Peng, 2009)

M^* = Section design moment at ultimate limit state

M_E = Moment demand from elastic analysis

M_{max} = Maximum expected moment in beam plastic hinge

M_n = Nominal flexural strength

M_o = Overstrength moment

M_{slab}^* = End-moment applied to beam from floor slab

M_y = Beam yield moment

m_e = Effective mass

N^* = Design axial load at ultimate limit state

N_o^* = Design axial load derived from overstrength earthquake actions

N_n = Nominal axial strength of section

$N(T,D)$ = Near-fault factor from NZS1170.5:2004

R_u = Return period factor for ultimate limit state from NZS1170.5:2004

s, s_h = Transverse steel spacing

T_e = Effective period

$t_{topping}$ = Cast-in-place floor topping thickness

t_{unit} = Precast floor unit thickness

u_a = Average bond stress/strength of deformed bars passing through an interior joint

V^* = Design shear force at ultimate limit state

V_{base} = Base shear

V_c = Nominal shear strength provided by concrete

V_{ch} = Horizontal joint shear resisted by concrete strut mechanism

V_{col} = Column shear force

V_E = Shear force demand from elastic analysis

V_E^* = Design earthquake shear force at ultimate limit state

V_{Eo} = Overstrength earthquake shear force

V_G^* = Design gravity shear force at ultimate limit state

V_{jh} = Horizontal joint shear force

V_n = Total nominal shear strength of section

V_s = Nominal shear strength provided by shear reinforcement

V_{sh} = Horizontal joint shear resisted by truss mechanism

V_{slab}^* = Shear force introduced to beam from floor slab

V_{yc} = Beam shear force at cyclic flexural yield

v_n = Nominal shear stress in section

Z = Hazard factor from NZS1170.5:2004

α = Factor accounting for greater strain penetration at higher strains (Pampanin et al., 2000; Palermo, 2004)

α_1 = Concrete stress block factor defined in NZS3101:2006 clause 7.4.2.7

β_1 = Concrete stress block factor defined in NZS3101:2006 clause 7.4.2.7

Δ = Interstorey displacement

$\Delta_{b,fe}$ = Beam fixed-end rotation contribution to interstorey displacement

$\Delta_{b,fl}$ = Elastic beam flexural contribution to interstorey displacement

Δ_c = Elastic column flexural contribution to interstorey displacement

Δ_d = Design displacement

Δ_j = Joint shear deformation contribution to interstorey displacement

ΔV_{sh} = Excess strut force resisted by bottom joint stirrups

$\Delta\varepsilon_p$ = Change in peak plastic strain for a given load-cycle ($=\Delta\varepsilon_s-2\varepsilon_y$)

δ = Measured deformation in linear potentiometer (elongation = positive)

ε_a = Strain amplitude

ε_{ap} = Plastic strain amplitude

ε_c = Concrete strain at extreme compression fibre

ε_s = Strain in bottom longitudinal reinforcement in beam

ε_s' = Strain in top longitudinal reinforcement in beam

ε_{sh} = Steel strain at the onset of strain hardening

ε_{sp} = Plastic steel strain

ε_y = Steel yield strain

ε_u = Steel strain at the peak ultimate stress

φ = Strength reduction factor

φ_o = Flexural overstrength factor or steel overstrength factor

γ_j = Joint shear deformation

λ_o = Material overstrength factor

μ = Friction coefficient

θ = Drift/rotation

θ_b = Beam rotation

θ_h = Inclination of diagonal hanger from horizontal

ρ = Bottom longitudinal reinforcement ratio

ρ' = Top longitudinal reinforcement ratio

ρ_t = Column longitudinal reinforcement ratio

ρ_v = beam-column joint steel ratio

ω = Dynamic magnification factor

ξ_b = Bond factor defined in Figure 3-20

ξ_{eq} = Equivalent viscous damping

CHAPTER 1 INTRODUCTION

1.1 Context of Research

Since the 1970's, reinforced concrete frame design in New Zealand has been based upon Capacity Design Philosophy, which seeks to prevent building collapse by ensuring the formation a ductile beam-sway mechanism (Park and Paulay, 1975). This is done by detailing ductile plastic hinge zones in beams and at the base of ground floor columns, and allocating reserve capacity to other elements such that they remain elastic. Whilst past earthquakes have shown capacity design to be successful in preventing total building collapse, they have also highlighted the extensive damage which occurs in yielding plastic hinges (Hall, 1995; Aragumi Corporation, 1995). In some cases, the post-earthquake damaged structure was beyond economic repair and had to be torn down.

In addition to incurring extensive damage, plastic hinge zones are also known to elongate. This 'beam elongation' has been shown to be on the order of 2-5% of the beam depth per plastic hinge (Zerke and Durrani, 1989, 1990; Megget and Fenwick, 1989; Restrepo, Park and Buchanan, 1990), and hence is capable of impairing a structure's ability to withstand collapse. Firstly, beam elongation can indirectly increase the overstrength of yielding plastic hinges, which can result in hinging of columns and the formation of an undesirable soft-storey mechanism. The increase in overstrength is the result of axial beam compression induced as floor units attempt to restrain the elongation, and the activation of slab reinforcement as the elongation extends into the floor diaphragm (Lau, Fenwick and Davidson, 2007; Peng, 2009). Secondly, recent research conducted at the University of Canterbury has highlighted the extensive damage to floor diaphragms from beam elongation (Matthews, 2004). Issues identified were the potential loss of floor gravity support and loss of diaphragm action which ties the structure together. These issues present a clear risk to life safety.

Therefore there exists a need for a structural system that minimises the damage incurred in yielding regions during a seismic event, which also addresses the inadvertent damage to floor diaphragms from beam elongation. To allow fast and easy implementation into New Zealand practice, the solution should also be simple and as similar as possible to what is currently done in industry. While low-damaging post-tensioned rocking systems have been developed

(See Section 2.2), these are fairly new to the construction industry and still exhibit beam elongation and the associated tearing of floor diaphragms.

1.2 The Slotted Reinforced Concrete Beam

The slotted reinforced concrete beam is a solution capable of addressing the aforementioned need. A slotted reinforced concrete beam is similar to a conventional reinforced concrete (RC) beam, but with a narrow vertical gap at the column face, running approximately three-quarters of the beam depth as shown in Figure 1-1. The bottom longitudinal reinforcement is continuous through the gap, with an unbonded length in the beam to reduce local strains. This unbonded length is accomplished by encasing the deformed bars in steel or plastic tubes. Diagonal steel hangers through the concrete top-hinge allow the transfer of beam shear forces across the slot and into the joint.

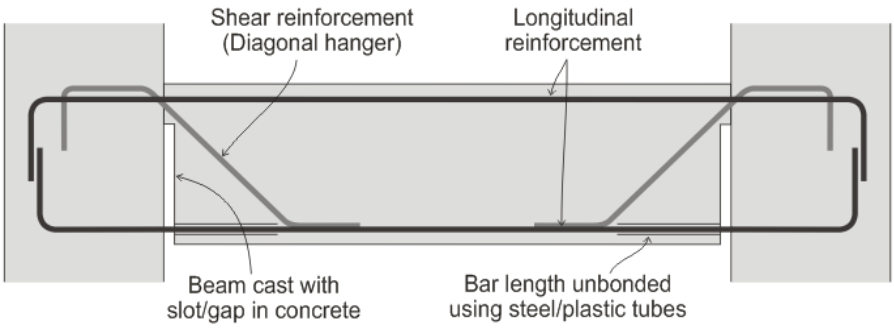

Figure 1-1: Illustration of a slotted reinforced concrete beam

The inclusion of a slot adjacent to the column face allows seismic rotations to be accommodated via opening and closing of the slot. Rotations occur about the remaining concrete depth such that the neutral axis remains within this "concrete top-hinge" as shown in Figure 1-2. Herein, the term "neutral axis" when used for a slotted-beam, infers the zero strain fibre location in the slotted-beam section immediately adjacent the column face. The flexural strength of the slotted-connection is governed by yielding of the bottom reinforcement, which provides hysteretic energy dissipation. During positive (gap-opening) moments, bottom reinforcement yields in tension; and during negative (gap-closing) moments, yielding occurs in compression. To limit elongation of top longitudinal reinforcement and ensure the neutral axis remains within the top-hinge during negative moments, top reinforcement should be sized larger than the bottom reinforcement.

This gap opening and closing behaviour provides numerous benefits. Firstly, the slot effectively acts as an artificial crack preventing plastic cracking from extending into the rest

of the beam. This greatly reduces the amount of damage in the beam connection. Secondly, rotation about the top-hinge minimises deformations at the top of the beam and the floor slab level, which minimises the damage to adjacent floors. Thirdly, because deformations are accommodated by gap-closing on one side and gap-opening at the other, slotted-beams exhibit negligible beam elongation. This minimises all the issues associated with beam elongation, namely the tearing of adjacent floor diaphragms, and beam overstrength enhancements from floor slab contributions and axial load effects.

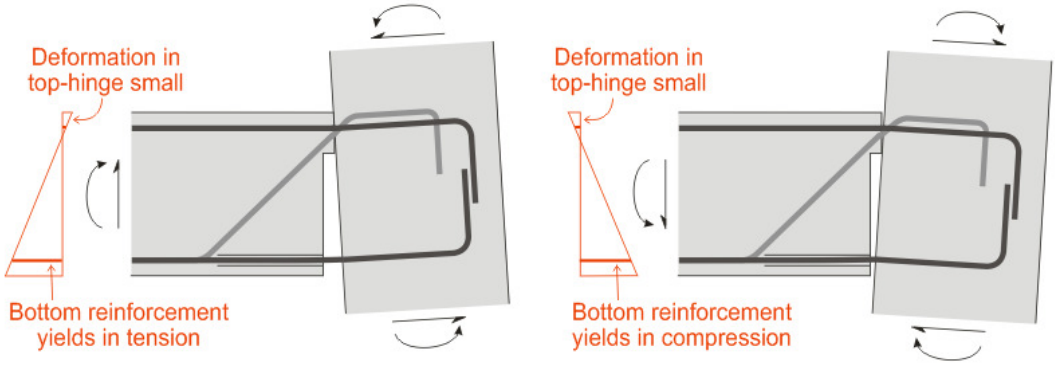

(a) Positive (gap opening) moment **(b) Negative (gap closing) moment**

Figure 1-2: Accommodation of rotation via opening and closing of slot

Because the slotted reinforced concrete beam is so similar to a conventional reinforced concrete beam (herein referred to as a 'monolithic beam'), it can be constructed via precast-emulation methods commonly used in New Zealand. That is, slotted-beams can be brought on-site precast, lifted into place and connected to precast columns with cast-in-situ joints. No specially designed corbels or connectors are required, just ordinary deformed reinforcing bars. Slotted reinforced concrete beams present a practical non-tearing floor substitute for existing reinforced concrete construction, which can be easily implemented into the construction industry.

Experimental tests on slotted reinforced concrete beams were first carried out in Japan by Ohkubo, Matsuoka, Yoshioka and Anderson in 1999. Then in 2004, Ohkubo and Hamamoto carried out tests which included floor units. These investigations showed significant reductions in damage to the connection and floor slab. While a satisfactory moment-rotation response was achieved, these specimens were not subject to a rigorous loading protocol as required by American Concrete Institute (ACI) acceptance criteria (2005). In addition, much of this literature is in Japanese and information on the mechanics or design of slotted-beams is not readily available. This research project seeks to test slotted-beam specimens in accordance with ACI acceptance criteria (2005) and extend on available English literature.

An emphasis has been placed on producing design recommendations and a solution that can be easily implemented into New Zealand practice.

1.3 Research Objectives

The purpose of this research project was to develop and test an appropriate detail for a slotted reinforced concrete beam that can be used as a non-tearing floor substitute for conventional reinforced concrete design in New Zealand. The chosen detail should be cheap and constructible using similar methods to what is currently done in practice. To bring the concept closer to industry use, design recommendations are sought.

Specific research objectives are summarised below:

- Theoretically investigate design issues associated with slotted reinforced concrete beams; namely shear transfer, longitudinal bar buckling, low cycle fatigue, anchorage of bottom longitudinal reinforcement in interior joints, joint design and detailing with floor slabs. This involves describing the mechanism causing the issue and attempting to provide a solution via design or detailing recommendations.

- Carry out experimental investigations on beam-column subassemblies to compare the response of slotted-beams with a conventional monolithic beam and verify the reduction in damage to the connection. These experimental tests will also be used to investigate alternative reinforcement details and verify design recommendations.

- Carry out an experimental investigation on a beam-column subassembly with precast floor units to verify the reduction in damage to the floor and investigate effects of beam torsion resulting from eccentric floor gravity loads. This experimental test will be used in conjunction with previous tests to verify design and detailing recommendations.

- Develop analytical and numerical models to predict the response of slotted-beam connections. These models will be calibrated and verified with experimental tests.

- Using non-linear earthquake time history analysis, numerically investigate the response of a frame using slotted-beam connections and compare it to the response of a frame using conventional monolithic connections. The numerical model developed for slotted-beams and existing models for conventional RC beams will be used.

1.4 Outline of Thesis

This thesis is comprised of nine chapters. This chapter previously described the need for a simple non-tearing floor connection and introduced the slotted reinforced concrete beam as a promising solution. An outline of the research objectives for this project was also given.

CHAPTER 2 gives a review of relevant research leading up to the first development of the slotted reinforced concrete beam. The basis for existing reinforced concrete design is explained, followed by the subsequent development of dry-jointed ductile precast connections to address damage issues in conventional connections. Because of damage still inflicted to floor diaphragms in all of these systems, research towards developing a non-tearing floor connection, and subsequently the slotted reinforced concrete beam, is briefly summarised.

CHAPTER 3 provides a conceptual investigation of design issues related to slotted reinforced concrete beams; namely shear transfer, longitudinal bar buckling, low cycle fatigue, anchorage of reinforcement in interior joints, interior joint design and floor slab effects. An explanation of the mechanics behind each issue is given, and where possible, a solution is suggested via detailing or design recommendations. The last section of this chapter gives a design example for a slotted-beam and compares it to the design of a conventional monolithic beam.

CHAPTER 4 and CHAPTER 5 report on the experimental investigations carried out as part of this project. CHAPTER 4 reports on the testing of in-plane exterior and interior beam-column joint subassemblies using the slotted connection, and a conventional exterior joint specimen which acted as a benchmark. CHAPTER 5 reports on the testing of an in-plane interior joint slotted-beam specimen with precast floor units. Each chapter describes specimen details, the construction process, experimental setup, and presents the results from testing.

CHAPTER 6 presents an analytical procedure developed to predict the moment-rotation response of slotted reinforced concrete beams. An outline of the procedure is given, followed by sensitivity studies to assess the effect of changing various beam parameters. Lastly, the procedure is verified against results from experimental tests.

CHAPTER 7 reports on the numerical investigation portion of this project. The chapter describes an existing multi-spring model for conventional RC beams and the development of a similar multi-spring model for slotted-beams. Both models are verified with experimental tests before being implemented into a two-dimensional five-storey frame for earthquake time history analyses. Results from time history analyses are presented and the difference in frame response between the two systems is discussed.

CHAPTER 8 provides a summary of the research conducted and highlights major conclusions that were drawn. The final sub-section discusses areas requiring further research.

CHAPTER 9 compiles a list of references from relevant literature sources that were used.

Finally, included at the end of this thesis are appendices to supplement the information given in the main chapters. APPENDIX A gives details of methods used to process test result data and decompose specimen displacements assuming elastic beam, column and joint deformations. APPENDIX B provides additional photographic logs from experimental tests carried out. APPENDIX C provides a copy of datafiles for subassembly and frame models that were setup in Ruaumoko2D. Lastly, APPENDIX D presents additional time history results plots for each earthquake record used.

CHAPTER 2 RESEARCH BACKGROUND

2.1 New Zealand Reinforced Concrete Design

2.1.1 Introduction of Precast-emulation Construction

Since the early 1960's, there has been a steady increase in the use of precast concrete for structural components in New Zealand. This has largely been due to the benefits of higher quality control, reductions in site formwork, site labour and increases in speed of construction. By the end of the 1980's, precast concrete had become prominent in moment resisting frames and structural walls.

Outside of New Zealand, precast concrete elements used as seismic structural components have been shown to perform poorly during earthquakes (Hall, 1994; Wyllie and Filson, 1989). The poor seismic performance of these precast structural elements has been attributed to non-ductile behaviour of connections as a result of inadequate detailing.

While the then current New Zealand design standard, NZS3101:1982, provided well for the seismic design of cast-in-place concrete, it did not address all seismic design aspects of precast construction. Despite the lack of codified precast design, significant developments in the use of precast concrete were made as the result of innovation from industry. In 1988, a Study Group of the New Zealand Concrete Society, the New Zealand National Society for Earthquake Engineering and the Centre for Advanced Engineering was formed to collate and summarise existing data, and recommend practices for the design and construction of structural precast concrete in buildings (CAE, 1991). The outcomes from this Study Group are published in a manual titled "Guidelines for the Use of Structural Precast Concrete in Buildings" (first printed in August 1991).

Past earthquakes and extensive laboratory testing have shown well designed and detailed cast-in-place reinforced concrete frames to prevent collapse during severe earthquakes (CAE, 1991). As a result, current precast construction simply involves economically connecting precast elements such that the seismic performance will be as that for a monolithic structure (Park, 1986; Park, 2002). Figure 2-1 below illustrates some common arrangements of precast emulation of cast-in-place construction. All three systems shown are characterised by precast members connected by "wet" (cast-in-place) joints.

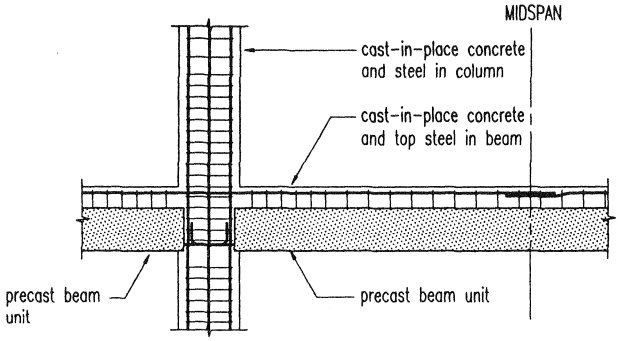

(a) System 1 - Precast Beam Units Between Columns

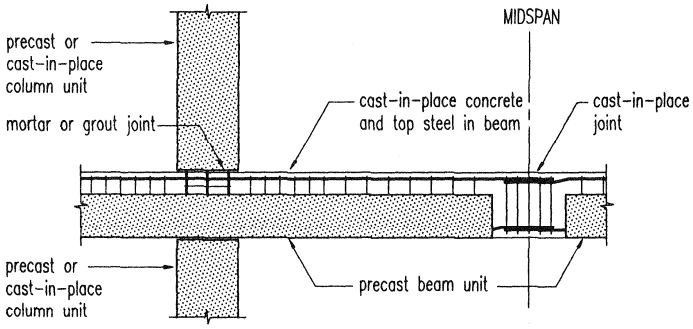

(b) System 2 - Precast Beam Units Through Columns

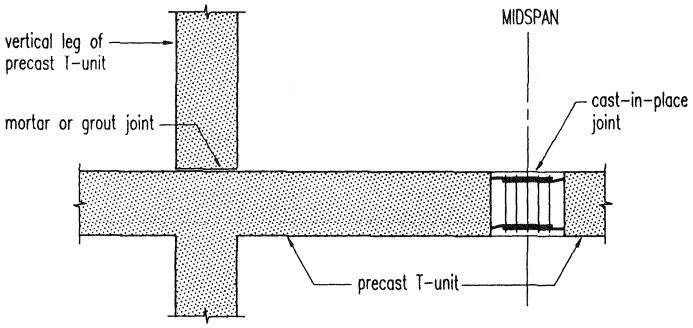

(c) System 3 - Precast T-Units

Figure 2-1: Precast emulation of cast-in-place concrete construction (CAE, 1991)

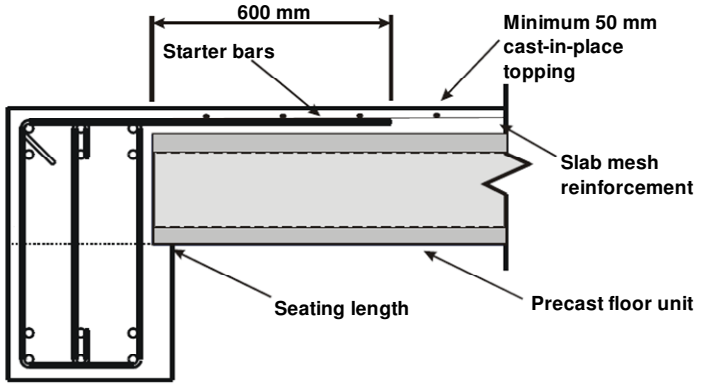

Figure 2-2: Conventional precast floor-to-beam connection

Similarly, Figure 2-2 shows the conventional method for connecting precast floor units to semi-precast beams. Beam units arrive onsite with the bottom half precast. The precast floor units are then lowered onto the beam, and the remaining portion of the beam is cast-in-place along with the slab topping. Deformed starter bars are provided to transfer diaphragm forces to the beam. The majority of New Zealand precast construction today emulates monolithic cast-in-place construction.

2.1.2 Capacity Design Philosophy

In addition to emulating monolithic structures, to prevent collapse and ensure adequate ductility can be achieved, current New Zealand design is based upon the capacity design philosophy. Capacity design was developed during the 1970's by discussion groups of the National Society for Earthquake Engineering and by Park and Paulay (1975). Prior to the 1970's, structural members were designed to be just strong enough to resist design actions determined from linear elastic analyses. As a result, the post-elastic mechanism that formed in buildings during a severe earthquake was a matter of chance.

Capacity design seeks to predefine the post-elastic mechanism by designing the structure with a weak beam-strong column hierarchy of strength to prevent soft-storey and global collapse. In reinforced concrete frames, beam ends and base columns are identified to yield and are suitably detailed for design strength and ductility (Paulay and Priestley, 1992; Park, 2002). All other regions of the structure are then designed with reserve capacity above the overstrength actions coming from these yielding regions, such that they remain elastic. Figure 2-3 illustrates desirable mechanisms of post-elastic deformation as according to the New Zealand Concrete Structures Standard NZS3101:2006. Recent earthquakes, such as Loma Prieta (1989), Northridge (1994) and Kobe (1995), have confirmed the adequacy of capacity design in preventing building collapse (Hall, 1995; Aragumi Corporation, 1995).

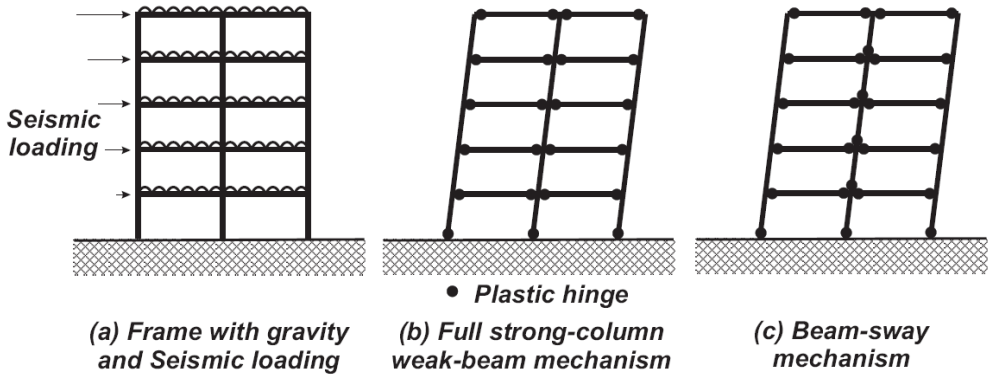

Figure 2-3: Desirable post-elastic mechanisms in monolithic moment resisting frames

2.1.3 Drawbacks and Deficiencies of Current Practice

Despite the adequacy of capacity design in preventing overall building collapse, post-earthquake reports have also highlighted the extensive economic losses incurred due to repair of damage and downtime (Hall, 1995; Aragumi Corporation, 1995). The 1995 Kobe earthquake revealed modern buildings that behaved as intended, but were still demolished due to the excessive cost of repair. The system which prevents collapse via energy dissipation in suitably detailed plastic hinges, consequently damages the structure extensively at these locations.

In addition to undergoing extensive damage, plastic hinge zones at beam ends are known to elongate during cyclic deformations. This phenomenon is well described in Fenwick and Megget (1993), and is commonly referred to as 'beam elongation'. Two contributions are commonly recognised: firstly, the 'material contribution' due to residual tensile steel strains, and secondly, the 'geometrical contribution' due to rotation of a finite-depth beam about the neutral axis depth. Experimental tests by numerous researchers (Zerke and Durrani, 1989, 1990; Megget and Fenwick, 1989; Restrepo, Park and Buchanan, 1990) have shown this elongation can be of the order of 2-5% percent of the member depth per plastic hinge and thus can have a major influence on the response of the structure and its ability to withstand collapse (Fenwick and Davidson, 1995).

Firstly, beam growth induces axial forces in beams and mobilizes slab reinforcement in adjacent floor units. This can significantly increase beam overstrength moments and hence column moment demands, altering the hierarchy of strength such that undesirable column hinging may occur (Lau, Fenwick and Davidson, 2007; Peng, 2009). Secondly, beam elongation will result in extensive cracking and tearing of floor slabs adjacent to the beam as shown in Figure 2-4c. This can result in the loss of diaphragm action, where inertial forces from the floor diaphragm are no longer able to cross into vertical lateral-load resisting elements as shown in Figure 2-4b (Bull, 2003). Diaphragm action plays a critical role in the lateral resistance of a structure by tying the whole structural system together. Lastly, beam elongation can result in the loss of gravity support and unseating failure of floor slabs as shown in Figure 2-4d (Matthews, 2004). Despite the clear risk to life safety, the former two effects are not adequately dealt with in current design practice. The latest New Zealand Standard NZS3101:2006 has increased seating widths for the latter effect; however a recent

publication from the Department of Housing and Building (2009) suggests that these may still not be enough.

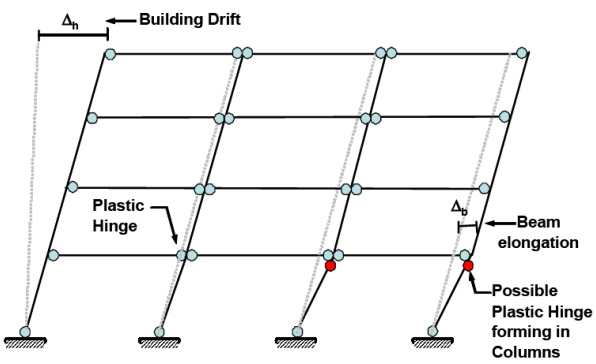

(a) Column hinging due to beam elongation

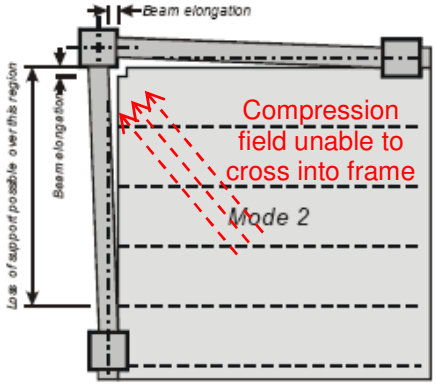

(b) Loss of diaphragm action (Bull, 2003)

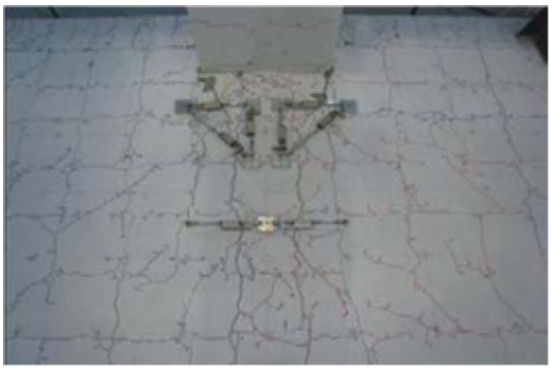

(c) Tearing of floor slab (Peng et al., 2008)

(d) Unseating failure of floor slab (Matthews, 2004)

Figure 2-4: Effects of beam elongation

Recent earthquake events and research highlighting these deficiencies have thus extended performance objectives beyond solely preventing collapse to limiting damage, leading to the introduction of a Performance Based Seismic Engineering framework. The SEAOC Vision 2000 Committee (1995) defined Performance Based Seismic Engineering as "a set of engineering procedures for design and construction of structures to achieve predictable levels of performance in response to specified levels of earthquake, within definable levels of reliability". The Performance Design Objective Matrix shown in Figure 2-5 illustrates how the desired performance level is coupled to the level of seismic hazard for structures with different performance objectives.

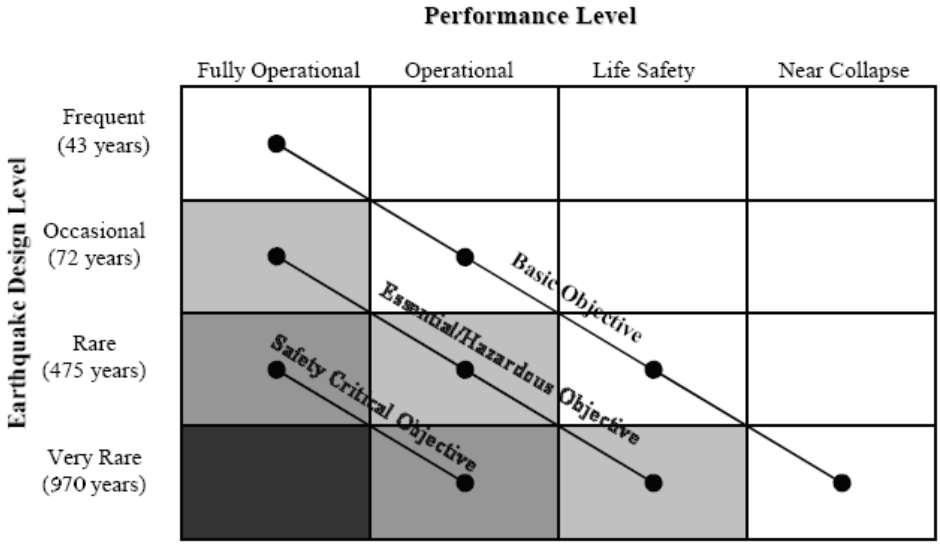

Figure 2-5: Seismic Performance Design Objective Matrix

(SEAOC Vision 2000 Committee, 1995)

To meet these higher performance objectives, systems which prevent collapse and also avoid excessive damage during earthquakes need to be developed. Dry jointed ductile precast systems, such as those developed during the PRESSS (Precast Structural Seismic Systems) program and by NIST (National Institute of Standards and Technology), attempted to address this need and are discussed in the following section.

2.2 Development of Dry-jointed Ductile Precast Connections

The majority of dry-jointed ductile precast systems developed over the last two decades rely on a rocking motion mechanism at the interface of beam and column elements. Energy dissipated via rocking motion was first studied by Housner in 1963, but the concept was not applied to connections in moment resisting frames until some years later. In 1987, a multiphase research program was initiated by the National Institute of Standards and Technology (NIST). Then in 1991, a separate research program, called Precast Seismic Structural Systems (PRESSS), was initiated as a joint United States-Japanese undertaking. Despite significant progress made in reducing damage to beam and column elements and providing re-centering capability, few solutions adequately addressed the problem of geometric beam elongation or sought to reduce damage to floor slabs.

2.2.1 NIST Research Program

The NIST program was initiated in response to the lack of available data on the seismic performance of precast concrete connections in moment resisting frames. The objective of this program was to investigate and develop guidelines for the design of precast beam-column connections in regions of high seismic activity (Cheok and Lew, 1991).

In Phase I of the programme, Cheok and Lew (1990) tested four monolithic and two grouted post-tensioned precast concrete beam-column subassemblies. Test results showed the post-tensioned precast specimens to be stronger than and as ductile as the monolithic specimens. However, the post-tensioned connections only dissipated 30% of the energy dissipated in the monolithic sections per cycle. Subject to further testing, it was concluded that post-tensioned precast beam-column connections were a viable solution for precast connections in high seismic regions.

Phase II and III of the programme sought to improve the energy absorption characteristics of the precast concrete connection (Cheok and Stone, 1991, 1993). This was done by changing post-tensioning bars to prestressing strands and locating post-tensioning steel closer to the beam centroid. While the energy dissipated per cycle still remained less than that of the monolithic specimens, due to the higher displacement ductilities achieved in the precast specimens, total energy dissipated was comparable to that of a conventional section (Cheok and Lew, 1993).

In Phase IV, tests on ten configurations of a 'hybrid' precast beam-column connection were carried out (Cheok, Stone, Stanton, Seagren, 1994; Stone, Cheok and Stanton, 1995). The hybrid system consisted of post-tensioning steel to clamp the beam and column precast units together and mild steel for energy dissipation. The post-tensioning steel was ungrouted to provide self-centering behaviour – a concept proposed by Priestley and Tao (1993). The hybrid system was shown to be superior to conventional monolithic connections, exhibiting comparable moment capacity, energy dissipation and greater drift capacity.

Despite the 'hybrid' rocking system showing negligible damage to beam and column elements, opening of the beam-column interface would still induce considerable geometric beam elongation and cause extensive damage to adjacent floors. Tests with floor slabs were not carried out to confirm this hypothesis.

2.2.2 PRESSS Research Program

The PRESSS program was initiated in 1991, as a joint coordinated United States-Japan research effort. The research objective was to develop effective seismic structural systems for precast buildings and prepare design recommendations for incorporation into building codes (Priestley, 1991). Phase I involved the development and evaluation of structural concepts for application in precast concrete buildings in seismic regions. Phase II took the most promising concepts from Phase I and proceeded with experimental tests on beam-column connection subassemblages.

Priestley and Tao (1993) proposed the concept of using partially debonded post-tensioning tendons through a rocking beam-column connection, to explicitly provide a re-centering force. This was verified in experimental tests of two ungrouted post-tensioned, jointed precast beam-column joint subassemblies (Priestley and MacRae, 1996). Both specimens suffered only minor damage up to 3% drifts, and had negligible residual displacements.

Palmieri, Saqan, French and Kreger (1996) tested eight beam-column connections that investigated behavioural concepts of tension-compression yielding, substantial energy dissipation and nonlinear-elastic response. The four specimens tested to observe tension-compression yielding consisted of precast beam and column units joined with mild steel or high strength threaded bar. Only one specimen was tested to observe the effects of substantial energy dissipation. Two post-tensioned and one pre-tensioned precast beam-column specimens were tested to observe nonlinear-elastic response. Further details of these tests are given in Palmieri et al. (1996). Palmieri and French (1996) also gives further information on other concepts proposed but not tested, such as armouring of the rocking interface.

The beam-column connection tests of particular interest to this thesis are specimens UT-GAP and UMn-GAP. These were tension-compression yielding specimens which included a one inch gap between the beam and column face, over three-quarters of the beam depth. Schematics of the two test specimens are shown in Figure 2-6. This was the original development of the ‘slotted beam’ concept. Whilst the other rocking connections were still subject to geometric beam elongation, for these slotted-connections, lateral movement was accommodated by rotation about the bottom-hinge via opening and closing of the slot, such that there was minimal beam elongation. Locating the gap at the top of the connection allowed for easy fabrication by simply lowering the beam on to corbels, while locating the

gap at the bottom would prevent large cracking in adjacent floor panels. Specimen UT-GAP performed satisfactorily through drift levels of 2.5%, however pinching of the hysteresis loops was observed due to flexural and shear deformations in the corbel connection. Specimen UMn-GAP performed satisfactorily up to 2% drift, upon which brittle fracture occurred in the top reinforcement adjacent to the couplers.

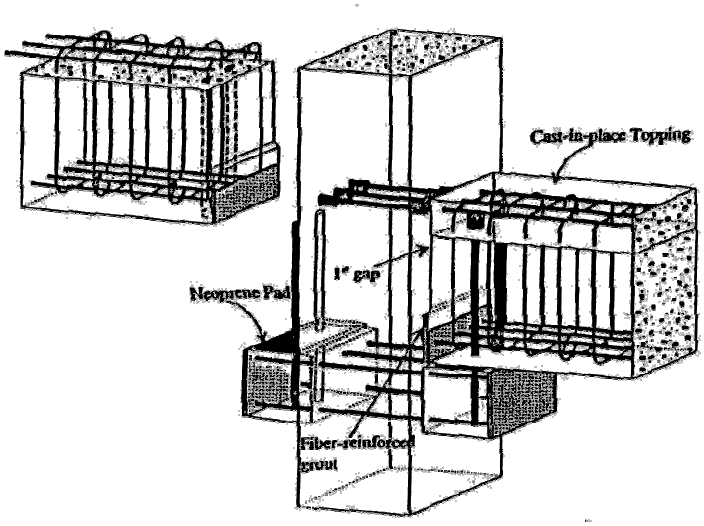

(a) Specimen UT-GAP

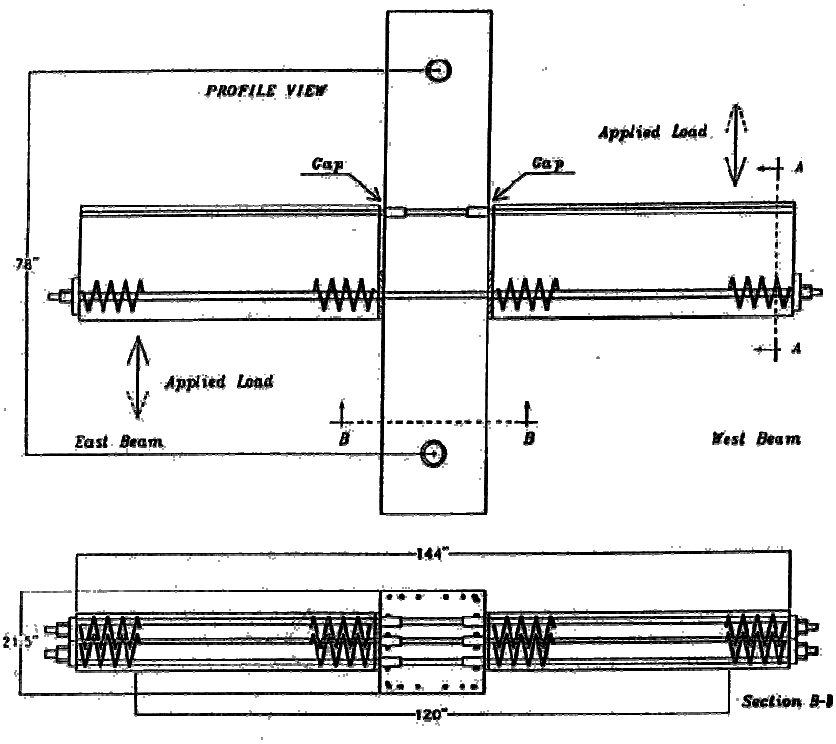

(b) Specimen UMn-GAP

Figure 2-6: Tension-compression yield specimens utilising the 'slotted-beam' concept (Palmieri et al., 1996)

Phase III of the PRESSS program finished with a test of a 60 percent scale five-storey precast/prestressed concrete building under simulated seismic loading (Nakaki, Stanton and Sritharan, 1999). The test building consisted of two seismic frames in one direction and a shear wall in the orthogonal direction. Four ductile frame connection systems were tested. These were tension-compression yielding (TCY) gap connections, TCY connections, hybrid connections and pretensioned connections. The prestressed frame behaved particularly well, suffering only minor spalling of cover concrete and some crushing of the fiber grout pads at the beam-column interface (Priestley, Sritharan, Conley and Pampanin, 1999). Residual drifts in this frame were negligible as a result of the unbonded prestressing steel. The TCY frame dissipated more energy, but suffered greater damage and had greater residual drifts. The TCY gap connection, shown in Figure 2-7, utilised the slotted beam concept and was similar to the specimen tested by Palmieri et al. (1996). The bottom bars were post-tensioned to clamp the frame together. During testing, vertical slip at the beam-column interface was observed due to insufficient clamping force. This resulted in damage occurring earlier and significant spalling of the beam soffit. Thus a viable working solution of the gap system was not yet achieved.

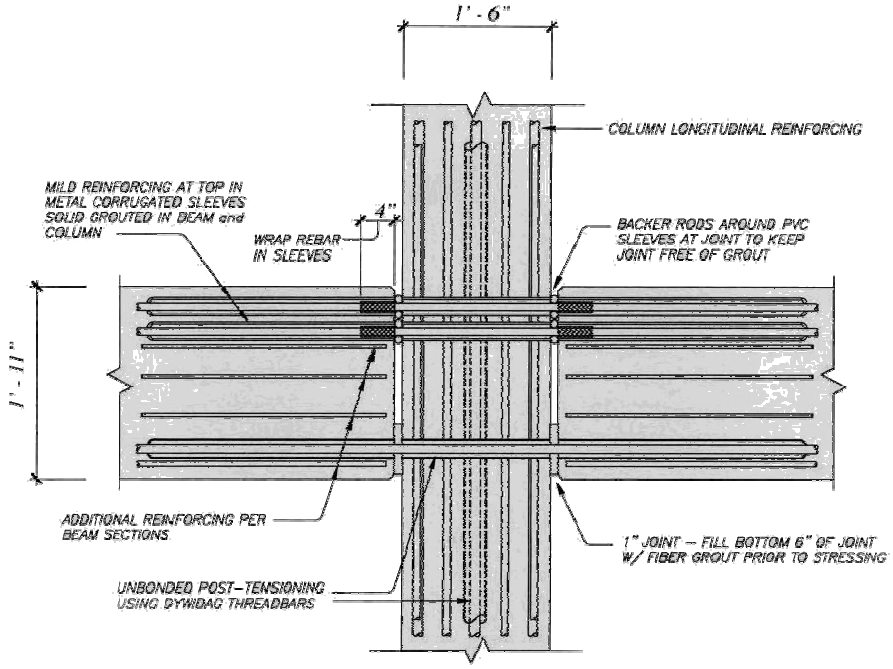

Figure 2-7: TCY gap connection in PRESSS five-storey frame (Nakaki et al., 1999)

2.2.3 Other Recent Developments

More recently, Pampanin, Pagani and Zambelli (2004) extended dry-jointed ductile connections developed during the PRESSS program to gravity load dominated frames. Two systems were presented: the Brooklyn Cable-stayed solution which used inclined bars, and the Brooklyn Suspended solution which used a draped unbonded post-tensioned tendon to balance gravity loads. A permanent steel corbel/bracket (shown in Figure 2-8) was also introduced to transfer vertical shear forces, as oppose to relying solely on friction at the interface as developed in the PRESSS-program.

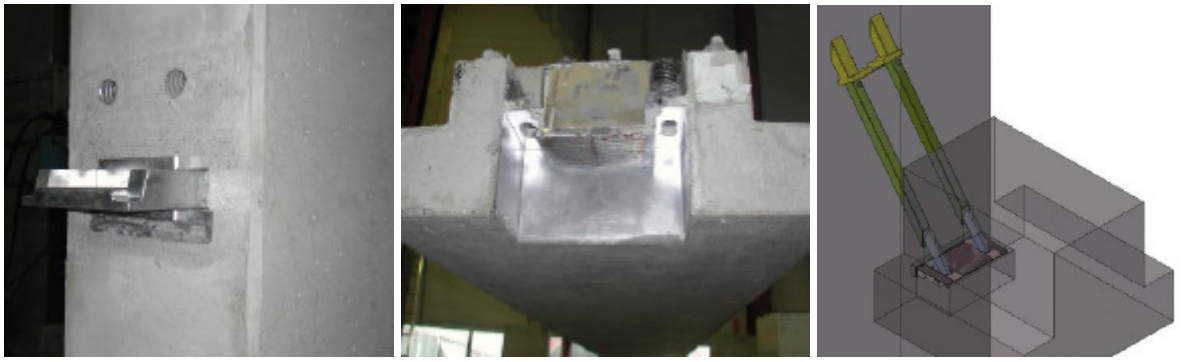

Figure 2-8: Alternative solutions of steel shear corbel/bracket (Hercules systems, proprietary of B.S. Italia srl)

At the University of Canterbury, Davies (2004) and Arnold (2004) tested a more heavily armoured joint with a bullet-shaped shear key. Li (2006) later simplified the connection to reduce welding and improve construction tolerances; and extended testing to consider 3D effects and biaxial seismic loading. Concurrently, Pampanin (2005) and Pampanin, Amaris, Akguzel, and Palermo (2006) tested various rocking systems with replaceable external mild steel energy dissipaters. These could be external, or set within the beam cross-section for architectural purposes as shown in Figure 2-9.

Figure 2-9: Replaceable external mild steel energy dissipaters

2.3 Development of Non-tearing Floor Solutions

While previous dry-jointed ductile frame solutions were successful in reducing damage to beam and column elements and eliminating residual drifts, they did not address problems of geometric beam elongation and tearing of connected floor slabs. Furthermore, although the concept of a slotted beam to reduce beam elongation was introduced, no viable solution was adequately developed. This section outlines later studies which sought to address these remaining issues.

2.3.1 Articulated Floor System

In dry-jointed ductile 'hybrid' precast connections, deformations are accommodated via rocking at the beam-column interface, resulting in considerable gap opening at the interface. This deformation has the ability to heavily damage connected floor slabs. To address this, Pampanin, Amaris, Akguzel and Palermo (2006) conceptualised an articulated floor system capable of accommodating displacement incompatibilities between the floor and frame. This system, shown in Figure 2-10, connects the floor unit to lateral beams using mechanical shear keys. These shear keys allow the slab to slide in orthogonal directions relative to the adjacent beams. Also, due the low flexural stiffness of the shear keys, torsional deformations of the beam relative to the slab can also be accommodated.

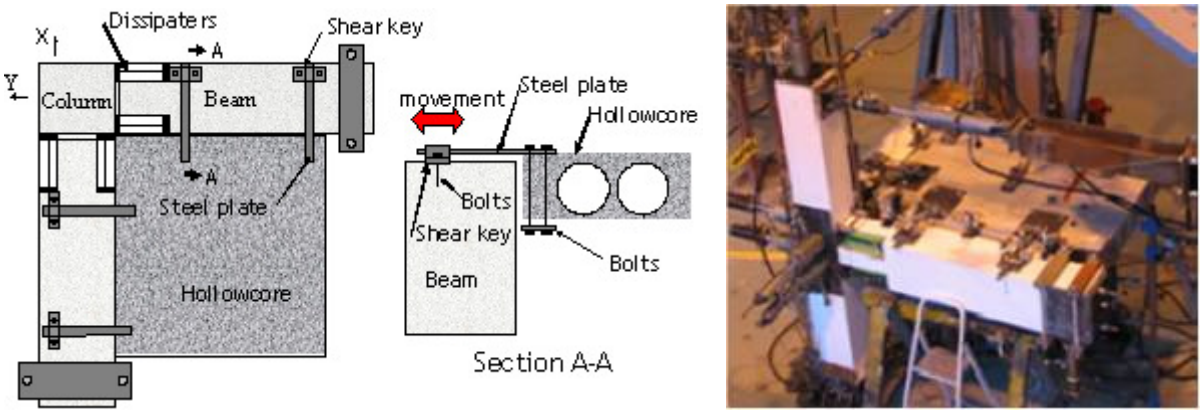

Figure 2-10: Articulated floor system

2.3.2 Hybrid Frame System with Non-tearing Floor Connections

Amaris, Pampanin, Bull and Carr (2007, 2008) investigated a non-tearing floor solution for dry-jointed ductile precast connections that could be used with traditional floor-to-frame connections – that is, precast floor units with cast-in-situ topping and continuity starter bars.

This system adopted the slotted-beam concept, allowing rotations at the beam-column interface to be accommodated via opening and closing of the gap. This behaviour has the benefit of negligible beam elongation from both material and geometric contributions. A metallic corbel was used as a top-hinge, which carried shear forces and concentrated deformations away from the floor level such that tearing of floors would be minimised. Two anti-symmetric draped post-tensioned tendons provided moment capacity and a re-centering force, while external mild steel provided energy dissipation. External beam-column subassemblies and a two-storey one-bay frame were tested, and showed low damage, high connection flexibility and negligible beam elongation. Despite the satisfactory response, construction difficulties were highlighted.

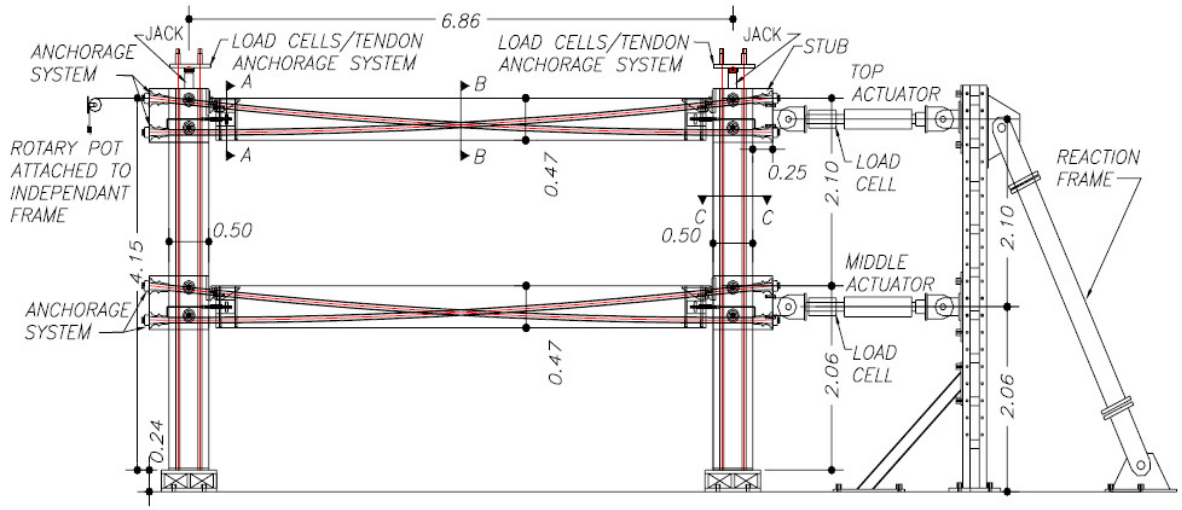

(a) Two-storey, one-bay frame tested

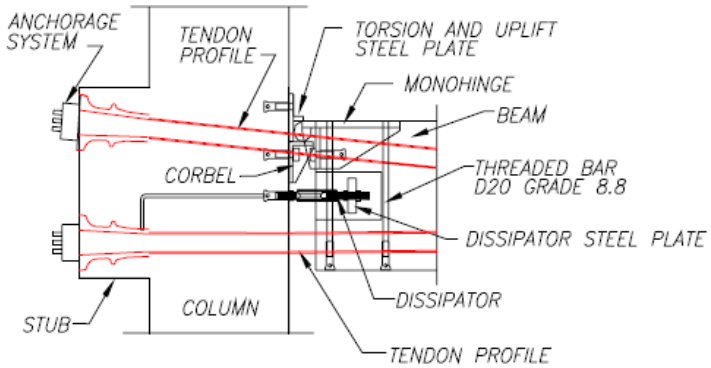

(b) Non-tearing floor connection details

Figure 2-11: Hybrid frame system with non-tearing floor connection (Amaris et al., 2008)

2.3.3 Slotted Reinforced Concrete Beam

Ohkubo, Matsuoka, Yoshioka and Anderson (1999) tested a conventional reinforced concrete beam-column connection with a bottom slot. Unlike previous studies, these specimens had no prestressing tendons, but were monolithic, with no dry-jointed beam-column interface. This was the first development of the slotted reinforced concrete beam – that is, a monolithic reinforced concrete beam utilising the slotted-connection.

Bottom reinforcement was continuous through the slot, with an unbonded length achieved by encasing the bars in ungrouted steel tubes. Unbonding bottom reinforcement reduced strains in the longitudinal bars, allowing greater deformations before fracture. Initial testing showed a poor performance, with a heavily pinched hysteretic response as shown in Figure 2-12. This was due to an inadequate shear transfer mechanism, resulting in the formation of a large diagonal crack beginning at the end of the bottom reinforcement unbonded length. This crack, termed the 'S-crack', is shown on the right of Figure 2-12. Further testing was carried out with the addition of diagonal shear hangers to transfer shear forces into the beam-column joint. These tests showed the diagonal reinforcement to be effective in transferring shear into the joint. A stable flexural response was achieved up to a drift of 4.0%, upon which strength degradation occurred due to buckling of the bottom reinforcement.

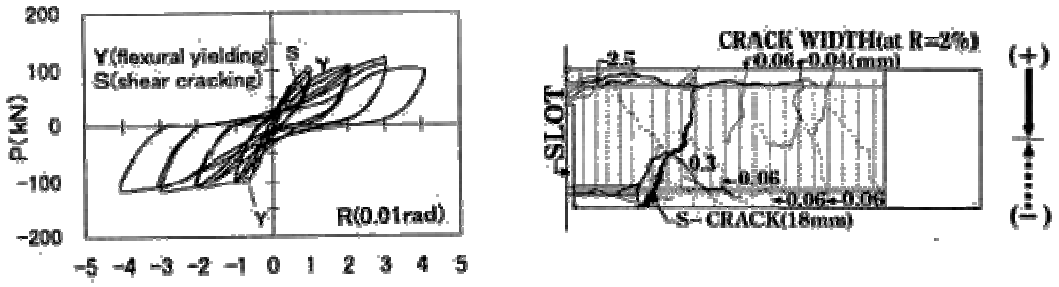

Figure 2-12: Pinched hysteresis response and S-crack from initial tests by Ohkubo et al. (1999)

Ohkubo and Hamamoto (2004) later tested interior beam-column subassemblies with floor slabs to observe damage and tearing to the adjacent floor panels. Two slotted-beam specimens were tested. A conventional monolithic specimen was also tested to provide a benchmark for comparison. Significant reductions in cracking and damage were observed in the slotted beam specimens compared to the monolithic case as shown in Figure 2-13 below. In addition, the slotted beam specimens were found to provide greater energy dissipation above drifts of 1%. While the hysteretic response showed no pinching, tests were only

carried out to drift levels of 3% and specimens were not subject to a rigorous loading protocol as required by ACI acceptance criteria (2005).

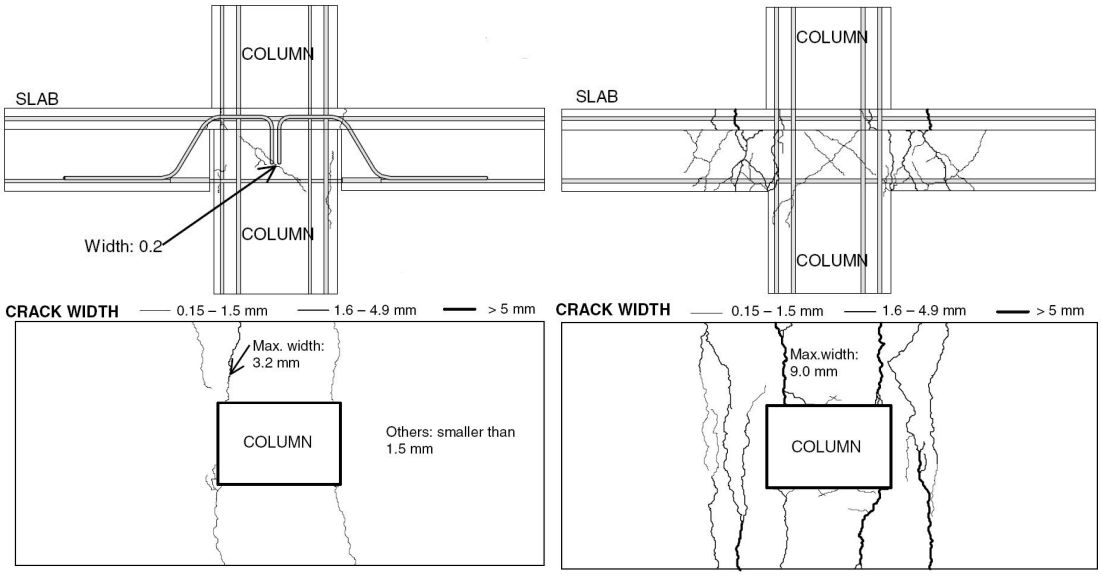

(a) Slotted beam connection **(b) Monolithic beam connection**

Figure 2-13: Joint and floor crack patterns from tests carried out by Ohkubo and Hamamoto (2004)

Although the slotted reinforced concrete beam studied by Ohkubo et al. (1999, 2004) does not provide any re-centering capability like the post-tensioned systems described in Section 2.2, it exhibits negligible beam elongation and does not use specially designed corbels or energy dissipation devices. It can also be constructed easily using precast-emulation methods commonly used in New Zealand. As a result, there are fewer barriers to implementation into New Zealand practice. This research project sought to investigate the slotted reinforced concrete beam further, to understand their behaviour, make design recommendations and address unresolved issues of bar buckling, low cycle fatigue, bar anchorage, joint design and detailing with floor slabs.

CHAPTER 3 MECHANICS AND DESIGN OF SLOTTED REINFORCED CONCRETE BEAMS

This chapter conceptually investigates design issues related to slotted reinforced concrete beams; and covers aspects such as flexural design, shear design, beam elongation, longitudinal bar buckling, low cycle fatigue, anchorage of reinforcement in interior joints, interior joint behaviour and detailing with floor slabs. In light of the described mechanical behaviour and results from experimental tests carried out, tentative design recommendations are made to address each issue. At the end of the chapter, a design example for an interior joint with slotted-beams is given alongside a conventional reinforced concrete beam design for comparison.

3.1 Design of Longitudinal Reinforcement

3.1.1 Bottom Reinforcement for Flexural Strength

Because the flexural response of a slotted-beam is governed by yielding of bottom reinforcement, only this reinforcement needs to be sized for the flexural demand. Figure 3-1 illustrates the forces in a slotted-beam section at positive (gap opening) and negative (gap closing) nominal strength moments. Because flexural forces induced in diagonal shear reinforcement are close to the neutral axis and moment strength is govern by yielding of bottom reinforcement, forces in diagonal reinforcement will have little influence on the moment strength and thus have been omitted for simplicity.

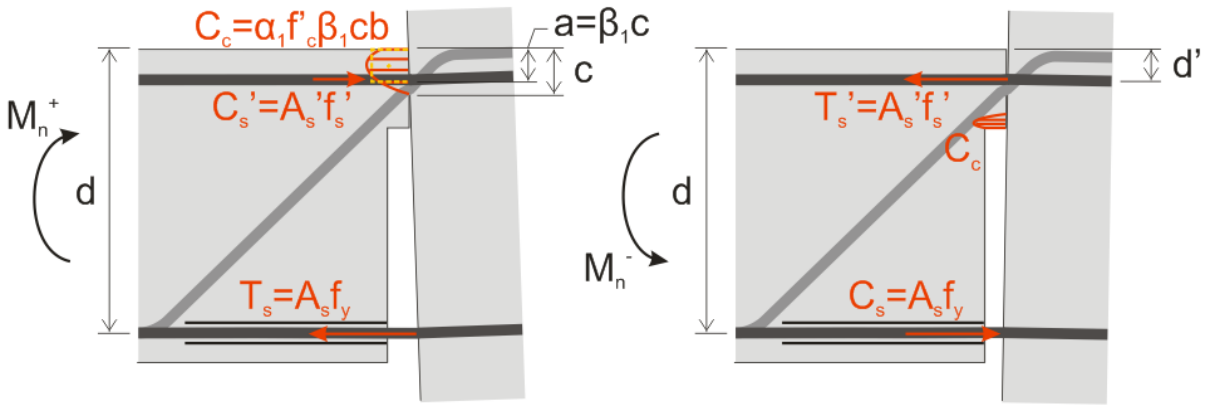

(a) Positive (gap opening) moment **(b) Negative (gap closing) moment**

Figure 3-1: Evaluation of nominal flexural strength for slotted-beams

The positive nominal flexural strength, M_n^+, can be calculated as it is done for a conventional reinforced concrete (RC) beam – that is, by multiplying the bottom reinforcement yield force about a lever arm as in Equation 3-1. This is an approximation that conservatively ignores the force in the top reinforcement and any additional confinement to the concrete hinge from the column face. A_s and f_y are the area and yield strength of the bottom reinforcement respectively, and d and a are the beam effective depth and Whitney equivalent rectangular concrete stress block depth respectively.

$$M_n^+ = A_s f_y (d - a/2) \qquad ...(3\text{-}1)$$

Unlike conventional RC beams, the flexural mechanism is not the same for negative moments in a slotted-beam. Compression yielding of bottom reinforcement governs the strength, and there is no concrete compression at the beam soffit, due to the slot, as is normally seen in a conventional RC beam. Provided there has not been excessive elongation through the top-hinge, there will be concrete compression at the bottom of the concrete top-hinge as shown in Figure 3-1b. Ignoring this compressive force because it is near the neutral axis, the negative nominal flexural strength can be accurately approximated as in Equation 3-2, where *d'* is the depth to the top reinforcement.

$$M_n^- = A_s f_y (d - d') \qquad ...(3\text{-}2)$$

The current New Zealand code, NZS3101:2006, specifies maximum and minimum reinforcement ratios as given in Equations 3-3 and 3-4, where the reinforcement ratio, ρ, is defined as A_s/bd. b is the width of the concrete compression block.

$$\rho_{\max} = \frac{f_c' + 10}{6 f_y} \le 0.025 \qquad ...(3\text{-}3)$$

$$\rho_{\min} = \frac{\sqrt{f_c'}}{4 f_y} \qquad ...(3\text{-}4)$$

The maximum reinforcement ratio ensures that the limiting flexural capacity occurs via ductile yielding of reinforcement, as oppose to brittle failure of compression concrete. Because the positive flexural behaviour of a slotted-beam is characterised by tensile yielding of bottom reinforcement and compression of the top concrete fibre like a conventional monolithic beam, this check should also be applied to slotted-beams.

Similarly, the minimum reinforcement ratio ensures there is sufficient tensile reinforcement to prevent brittle failure of the section at first cracking. If there is very little reinforcement, the first cracking moment may be higher than the yield moment, such that first crack becomes a brittle mechanism. Because the gap in a slotted-beam acts as an artificial crack, brittle failure at first cracking will not occur. Thus this check is not required for slotted-beams. However, a minimum reinforcement ratio guards against excessively deep sections with little reinforcement. This limits the plastic straining of bottom reinforcement, which needs to be controlled in slotted-beams due to low cycle fatigue. For this reason, some minimum reinforcement limit should be specified for slotted-beams. This is discussed later in Section 3.5.

Because flexural behaviour is governed by yielding of bottom reinforcement, these reinforcement limits do not apply to the top longitudinal reinforcement.

3.1.2 Top Reinforcement for Crack and Elongation Control

As mentioned in the previous section, top reinforcement does not have to be sized for the flexural demand. Instead it needs to be sized to limit cracking and elongation through the concrete top-hinge. The benefits of negligible beam elongation and reduced damage to floors are the result of the neutral axis remaining within the top-hinge, such that flexural deformations within the top-hinge and in adjacent floor slabs are small. This behaviour will only occur if axial tensile deformations in top longitudinal reinforcement during gap closing moments are restrained. If excessive yielding occurs, elongation through the top-hinge will occur and the neutral axis will drop during gap-closing rotations. Top reinforcement must therefore be designed to limit these deformations, and ideally to remain elastic.

Applying horizontal equilibrium to Figure 3-1b, it can be seen that the force in the top reinforcement will be greater than the force in the bottom reinforcement. For top reinforcement to remain elastic it must be capable of resisting yielding of bottom reinforcement and any overstrength from strain hardening, plus an additional concrete compressive force at the bottom of the top-hinge. In Section 6.2.7, a parametric study was carried out on the top-to-bottom reinforcement ratio, $A_s'f_y'/A_sf_y$. It was found that for top reinforcement to remain elastic, $A_s'f_y'/A_sf_y$ had to be greater than 2.5. A ratio this high can become very impractical to design and construct.

During the test of specimen SB2 which had $A_s'f_y'/A_sf_y$=1.8, slight yielding of top reinforcement was shown to have a marginal increase on beam elongation and cracking. From the parametric study in Section 6.2.7, when $A_s'f_y'/A_sf_y$ was greater than 2.0, top reinforcement strains remained small within six times the yield strain. Thus $A_s'f_y'/A_sf_y$=2.0 is a reasonable top reinforcement content that should be targeted in design, which can also be practically achieved. If Grade 300 steel is used for bottom reinforcement and Grade 500 used for top reinforcement, only a 10% increase in the bar diameter is required in the top compared to the bottom.

As an additional note, experimental tests have shown that diagonal hanger reinforcement also helps to restrain longitudinal elongation through the top-hinge. To avoid congestion through the top-hinge, often Grade 500 hanger reinforcement may be required to allow smaller bar sizes.

3.2 Shear Transfer Mechanism

In conventional reinforced concrete beams, shear is carried by both concrete and steel contributions. A truss analogy can be drawn as illustrated in Figure 3-2, where concrete transfers shear via diagonal struts and vertical stirrups tie the truss together (Collins and Mitchell, 1980; Park and Paulay, 1975). Because of these diagonal shear struts, NZS3101:2006 allows the shear force demand at the column face to be taken as the shear force one effective beam depth away from the column face. In slotted-beams, the inclusion of a gap adjacent to the column face prevents these diagonal struts from crossing into the beam-column joint, such that shear must be transferred via other means (See Figure 3-4b).

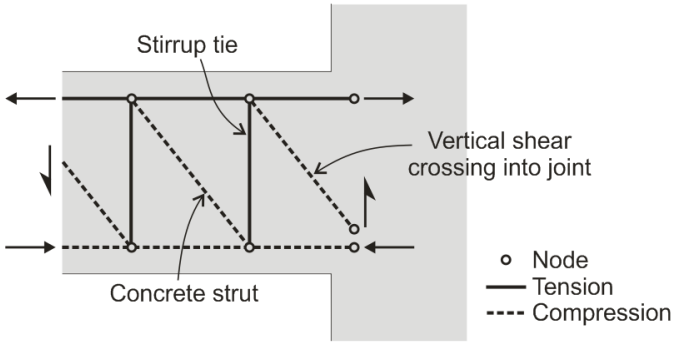

Figure 3-2: Shear truss analogy for monolithic beams

Ohkubo et al. (1999) first studied the shear transfer mechanism in slotted-beams and successfully used diagonal reinforcement, similar to that shown in Figure 3-3, to carry shear into the joint. This method is simple, efficient, can be easily designed and hence was adopted

in this research. An additional detail to that tested by Ohkubo et al. is recommended, and is that the upper bend in the diagonal hanger should be located well within the column to capture the induced strut as shown in Figure 3-3. This ensures shear forces are transferred via axial deformations in the hanger rather than dowel action. Dowel action requires excessive deformation to be mobilised and will result in undesirable shear sliding. The shear carried by diagonal reinforcement can be designed according to current NZS3101:2006 provisions in clause 9.3.9.4.4 using:

$$V_s = A_v f_{yt} \sin \theta_h \qquad ...(3\text{-}5)$$

V_s is the nominal shear strength provided by the diagonal reinforcement, A_v is the area of diagonal reinforcement, f_{yt} is the lower characteristic yield strength, and θ_h the inclination of the reinforcement from horizontal.

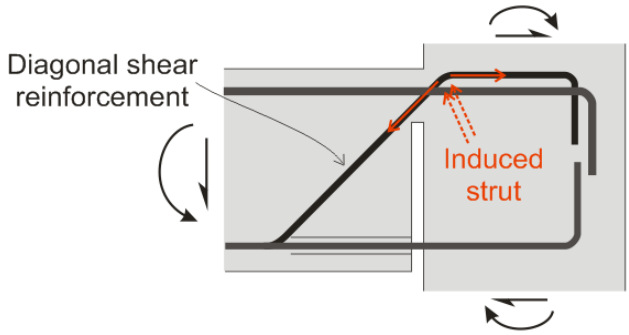

Figure 3-3: Diagonal shear reinforcement

Figure 3-4 illustrates conceptual shear load paths for slotted-beams using strut and tie. Despite the small concrete section, testing has indicated some shear transfer through the concrete (See Section 4.3.11). Possible load paths for the concrete shear contribution have been shown in red.

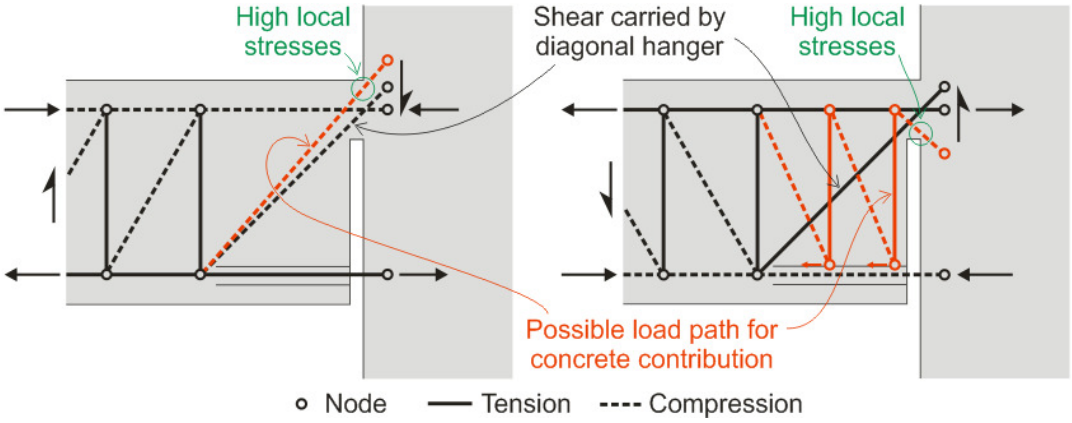

(a) Gap opening rotations **(b) Gap closing rotations**

Figure 3-4: Conceptual load paths for shear transfer in slotted-beams

For gap opening rotations (Figure 3-4a), the response is similar to a conventional beam. When conventional beams form plastic hinges, shear must be transferred primarily via a diagonal strut, most of which coincides with the compression field at the extreme fibre which forms due to flexural actions. It is suggested that the same occurs with slotted-beams with the aid of compression in diagonal reinforcement.

For gap closing rotations (Figure 3-4b), this diagonal strut cannot cross into the bottom of the joint, so shear is carried primarily by the diagonal hanger. The majority of the beam shear arrives at the bottom bend of the hanger and is carried into the joint via tension. However during experimental tests, increasing strains in the hanger and diagonal cracking in the region after the bottom bend are observed, suggesting additional shear transfer to the hanger after the bottom bend. It is hypothesized that as the diagonal hanger elongates under tension, stirrups along the unbonded length of the bottom longitudinal reinforcement are also activated in tension. This provides a mechanism for additional shear to enter into the hanger and eventually a concrete load path through the top-hinge. This load path coincides with the small compression field that forms at the bottom of the top-hinge due to flexural rotation.

ACI 318-05 and NZS3101:2006 code provisions for concrete shear contribution originate from the 1960's (ACI-ASCE Committee 326, 1962), and are based on concrete tensile strength, aggregate size, crack widths and the shear truss model in Figure 3-2. For simplicity they assume that shear stresses are uniform, such that the given concrete shear strength, v_c, actually has no physical meaning. Other more recent methods, based on modified compression field theory (Bentz, Vecchio and Collins, 2006), are capable of producing the actual shear stress distribution, but still rely on the same Bernoulli stress distribution. Because the presence of a slot creates a highly disturbed zone of stresses, such theories cannot be applied to slotted-beams.

Flexural cracking of the concrete top-hinge means it is unlikely that there will be any contribution resulting from concrete tensile strength. Thus the concrete shear contribution in slotted-beams is more likely the result of high localised stresses from aggregate interlock and friction in the flexural compression field. Such behaviour is difficult to accurately quantify and how reliable this mechanism is after some yielding of top reinforcement and cracking is uncertain. Thus for safety and simplicity, it is recommended that the concrete shear contribution is ignored and that the diagonal shear reinforcement be designed to carry the total shear demand. Because of the absence of diagonal shear struts, the shear force demand

at the column face should be taken as that at the column face and not one effective depth out as done for conventional RC beams.

The strut and tie model in Figure 3-4b highlights an important detailing aspect that the unbonded length should be terminated before the bottom bend of the diagonal hanger. If the unbonded length extends beyond the bottom bend as shown in Figure 3-5a, then the horizontal force introduced to the node at the bottom bend can only be restrained by the tensile strength of the concrete. This will result in the formation of an unrestrained shear-crack as observed in experimental tests carried out by Ohkubo et al. (1999). Note that although the beam soffit is in compression from flexure, the crack is opened by a downwards shear deformation.

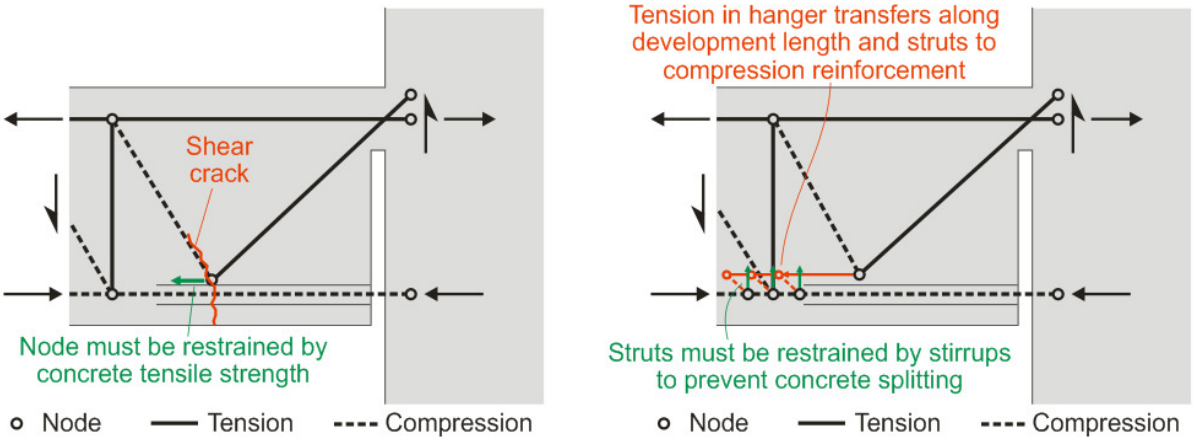

(a) Shear-crack formation **(b) Alternative load-path**

Figure 3-5: Strut and tie when unbonded length extends beyond bottom bend of hanger

An alternative load-path is possible, and is shown in Figure 3-5b. If the diagonal hanger has a development length beyond the obtuse bend, the tension can be resisted along this length and strut back to longitudinal reinforcement in compression. To ensure concrete splitting parallel to the bars does not occur, additional stirrups are required to provide the green tie force shown. Because concrete splitting is a major issue, especially with large diameter (25 mm) bars, this detail is not preferred and was not investigated in this project. Note that in Figure 3-5b, the green and orange forces are actually in the same horizontal plane as the bottom longitudinal reinforcement.

3.3 Beam Elongation

One of the major benefits of slotted-beams over conventional monolithic beams is that they exhibit negligible beam elongation. This markedly reduces damage to adjacent floor slabs,

which ensures diaphragm action is maintained during seismic events. Beam elongation is minimised because end-rotations can be accommodated via opening and closing of the slot as shown in Figure 3-6. Although the left-hand-side connection elongates δ_{el}^{+}, the right-hand-side connection contracts δ_{el}^{-}, such that the overall beam elongation observed at the beam centreline is minimal.

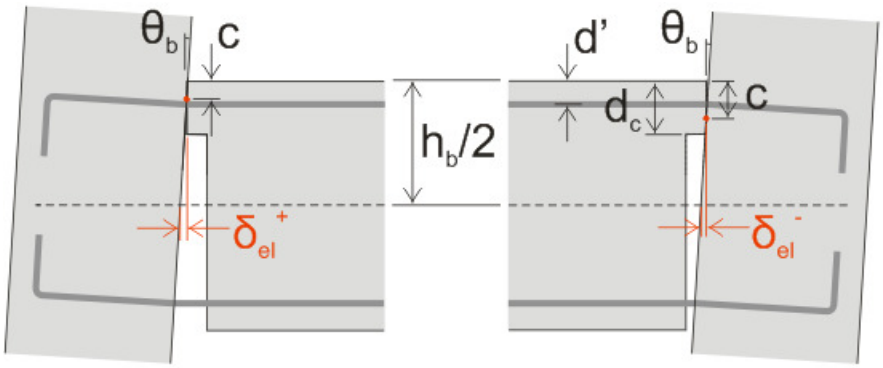

Figure 3-6: Beam elongation and contraction in slotted-beams

Two contributions to beam elongation are commonly recognised in conventional reinforced concrete beams: firstly, the 'material contribution' due to residual tensile steel strains, and secondly, the 'geometrical contribution' due to the rotation of a finite-depth beam about the neutral axis depth. Because the behaviour of a slotted-beam is governed by tension-compression yielding of the bottom reinforcement only, the 'material contribution' is limited to very minor yielding of top reinforcement. In addition, because the rotation occurs about a shallow concrete top-hinge, the 'geometric contribution' is also minimised.

From Figure 3-6, the elongation or contraction observed at the beam centreline at either connection can be expressed as:

$$\delta_{el} = \theta_b \left(\frac{h_b}{2} - c \right) \qquad \text{...(3-6)}$$

Ignoring the neutral axis depth, this expression can be altered to give a theoretical upper bound for the beam elongation on the left-hand-side (LHS):

$$\delta_{el}^{+} < \theta_b \frac{h_b}{2} \qquad \text{...(3-7)}$$

Similarly for the right-hand-side (RHS) connection, because horizontal force equilibrium requires that the neutral axis must remain below the top reinforcement, a theoretical upper-bound for the contraction at the beam centreline can be given by:

$$\delta_{el}^{-} < \theta_b \left(\frac{h_b}{2} - d' \right) \qquad \text{...(3-8)}$$

Provided that permanent elongation of the top reinforcement is limited, the neutral axis should remain within the concrete top-hinge, such that a theoretical lower-bound for the beam contraction can be expressed as:

$$\delta_{el}^{-} \geq \theta_b \left(\frac{h_b}{2} - d_c \right) \qquad \text{...(3-9)}$$

Figure 3-7 plots these theoretical upper and lower bounds against experimentally observed beam elongations and contractions for slotted-beam specimens SB1, SB2 and SB3. It can be seen that Equation 3-7 provides an accurate upper-bound to the observed beam elongation during gap opening rotations. Equation 3-8 also provides a reliable upper bound to beam contractions but is less accurate. Equation 3-9 however does not provide an absolute lower bound to the observed contractions. The RHS beam of specimen SB2 exhibited greater yielding of top reinforcement, allowing the neutral axis to drop below the concrete top-hinge which violates the assumption made for Equation 3-9.

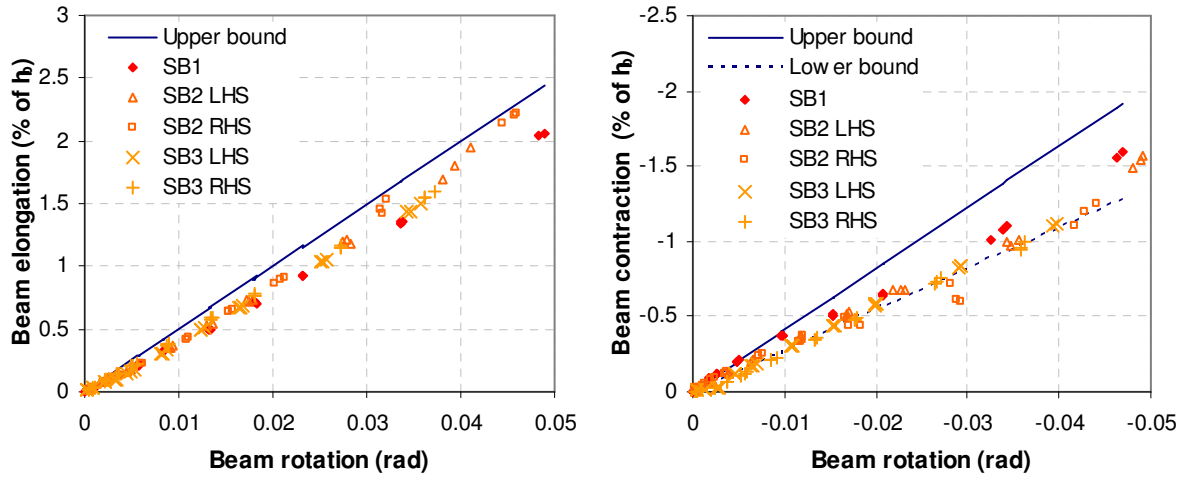

(a) Gap opening **(b) Gap closing**

Figure 3-7: Comparison of theoretical upper and lower bounds with experimental slotted-beam elongations and contractions

Assuming excessive yielding of top reinforcement is retrained, an upper bound to the overall elongation in a slotted-beam can be found by taking the difference of Equations 3-7 and 3-9. This gives:

$$\delta_{el,total} \leq \theta_b d_c \qquad ...(3\text{-}10)$$

Literature recognises beam elongation in conventional monolithic beams to range between 2-5% of the beam depth (Zerke et al., 1989, 1990; Megget et al., 1989; Restrepo et al., 1990). In a recent draft publication, the Department of Building and Housing (2009) in conjunction with the Structural Engineering Society of New Zealand (SESOC) suggested the following empirical formula for the beam elongation per plastic hinge:

$$\delta_{el,monolithic} = \theta_b h_b \leq 0.04 h_b \qquad ...(3\text{-}11)$$

This equates to an overall elongation at the beam centreline of $2\theta_b h_b$ for a monolithic beam forming two plastic hinges at each end. Considering the depth of the top-hinge in a slotted-beam will be on the order of 0.2 to 0.25 times the beam depth, a comparison of Equation 3-10 with Equation 3-11 suggests a slotted-beam will only exhibit 1/8th to 1/10th of the beam elongation observed in monolithic beams.

3.4 Longitudinal Bar Buckling

Because bottom longitudinal bars in slotted-beams are subject to extensive deformations in compression, they are more susceptible to buckling than reinforcement in conventional reinforced concrete beams. Because the strength of a slotted-connection is derived from yielding of this reinforcement, any buckling will result in severe strength degradation. High bending strains induced at the edges of the bar from buckling may then result in bar fracture on subsequent tensile excursions. It is therefore imperative that buckling is prevented to ensure the survival of the connection during an earthquake.

In tests carried out during this project (See CHAPTERS 4 and 5), buckling was observed to occur predominantly along the unbonded length immediately adjacent to the slot. Figure 3-8 illustrates the possible buckling mechanism causing this. Under a downwards vertical shear, the beam will move downwards relative to the column. This will induce a slight curved eccentricity along the unbonded length as the bar is forced to bend downwards as it enters the debonding tube as shown in Figure 3-8a. As the slot closes more, this eccentricity will

initiate buckling along the unbonded length resulting in spalling of the beam soffit as shown in Figure 3-8b.

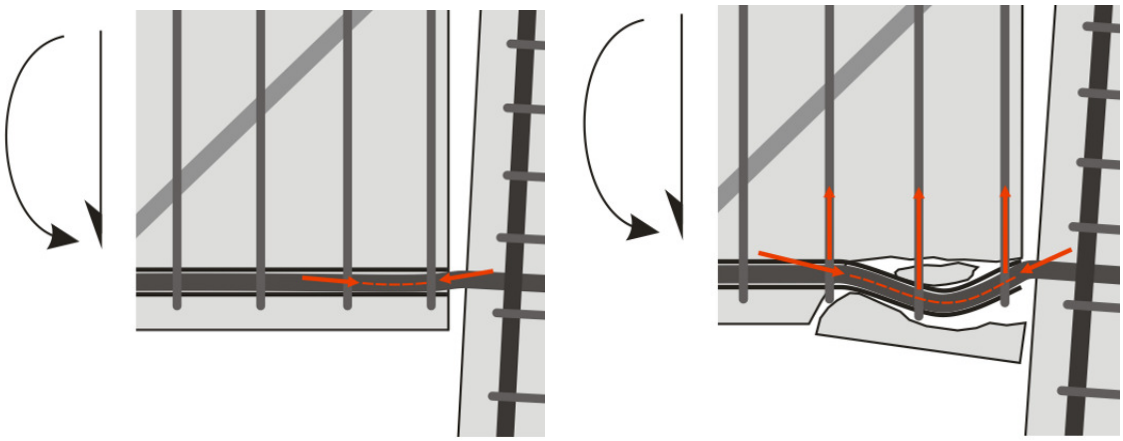

(a) Slight eccentricity from vertical movement **(b) Buckling resulting in spalling**

Figure 3-8: Illustration of buckling mechanism in bottom reinforcement

If the stirrup spacing is large, buckling will occur in the first stirrup spacing next to the slot as observed in the test of specimen SB1. If the stirrup spacing is small, a higher buckling mode may occur which extends across multiple stirrups along the unbonded length. This was observed in the LHS beams of specimens SB2 and SB3. Alternatively, if the tie immediately adjacent to the slot is not strong enough, buckling may extend out into the slot as observed in tests carried out by Leslie (2010). Testing revealed that existing stirrup spacing provisions of $6d_b$ in NZS3101:2006 are insufficient to prevent buckling of bottom longitudinal reinforcement in slotted-beams. So to prevent buckling of these bars, extra restraint must be provided in the region along the unbonded length of these bars.

From finite element microanalysis, Dhakal et al. (2000, 2002) proposed that buckling was unlikely to occur if the ratio given by Equation 3-12 was satisfied. In this expression, L is the buckling length, d_b is the bar diameter and f_y is the bar yield stress. Assuming first mode buckling, that is L is equal to one stirrup spacing, this equates to a stirrup spacing of $4.6d_b$ for Grade 300 reinforcement. In light of this, during experimental testing, two methods to restrain buckling were investigated. The first was to reduce the stirrup spacing to $3d_b$, and the second was to reduce the spacing to $4d_b$ and provide additional support to longitudinal bars along the unbonded length by debonding using steel tubes. The latter method was found to be more effective and successfully prevented buckling and soffit spalling. Solely decreasing the stirrup spacing was insufficient, because the bar simply buckled at a higher mode – that is,

across multiple stirrup spacings. The added flexural stiffness of the steel tube helped to restrain this higher mode buckling.

$$\frac{L}{d_b}\sqrt{\frac{f_y}{100}} < 8 \qquad \text{...(3-12)}$$

Therefore, to prevent buckling of bottom longitudinal reinforcement, the stirrup spacing for slotted-beams should be reduced beyond existing NZS3101:2006 provisions. Currently, NZS3101:2006 requires a maximum spacing, s_{max}, of the smaller of $d/4$ or $6d_b$ within $2h_b$ of the column face, which is considered the potential plastic hinge zone (PPHZ). Outside this, the maximum spacing is specified as the smaller of $d/2$ and 600 mm. It is recommended that these provisions are kept for a slotted-beam with the addition of a $4d_b$ maximum spacing limit along the unbounded length L_{ub}. This is illustrated below in Figure 3-9. The reason for the reduced spacing of $4d_b$ along L_{ub} is to account for the greater likelihood of buckling along this length due to extensive compression yielding. The existing code provision of the smaller of $d/4$ and $6d_b$ within a length of $2h_b$ should be kept because of yield penetration of bottom reinforcement into the beam beyond the debonding steel tubes just like in a typical plastic hinge zone. Outside $2h_b$ the slotted-beam is simply a conventional RC beam and so existing NZS3101:2006 provisions apply.

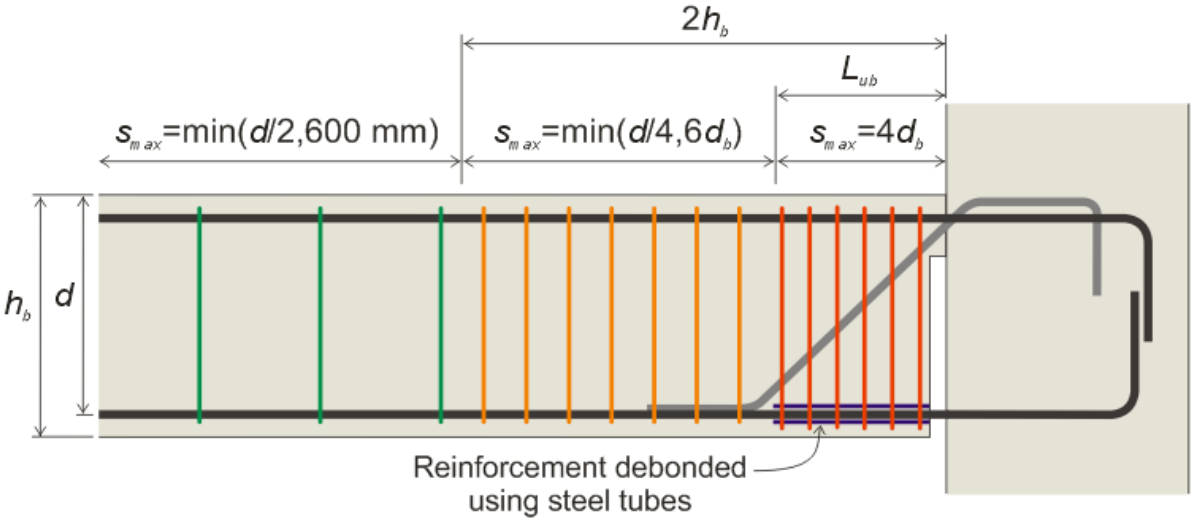

Figure 3-9: Recommended maximum stirrup spacings for anti-buckling in slotted-beams

In addition to reducing the maximum stirrup spacing, steel tubes should be used to provide the unbonded length of the bottom longitudinal reinforcement. The steel tube should be thick enough to withstand buckling itself, and the internal diameter should minimise the clearance

between the tube and bar. Too much clearance will allow the bar to buckle within the tube, causing an eccentricity which may result in buckling of the tube as well. Further research is required to determine appropriate tube wall thicknesses for a variety of cases.

Another area requiring further research is whether current provisions for the lateral tie size need to be increased. NZS3101:2006 requires lateral ties to be able to resist 1/16th of the yield force in the bar or group of bars that it restrains when spaced at $6d_b$ centres. Because the maximum spacing along the unbonded length of slotted-beams has been reduced to $4d_b$, in the meantime and until further research is conducted, it is recommended that lateral ties be conservatively designed to resist 1/16th of the yield force in the bar or group of bars that it restrains when spaced at $4d_b$ centres.

3.5 Low Cycle Fatigue

Longitudinal bars in conventional reinforced concrete beams yield extensively in tension but undergo limited yielding in compression. However, in slotted-beams, bottom reinforcement yields extensively in both tension and compression. As a result, the connection is more at risk to low cycle fatigue failure via fracture of this reinforcement. To help delay this failure mode, a length of the bottom reinforcement is unbonded to reduce the total accumulated plastic strain. This section investigates the low cycle fatigue response of slotted-beams. A method to predict the low cycle fatigue failure of longitudinal reinforcement using existing theory is presented, and then used to compare the low cycle fatigue response of slotted-beams with conventional monolithic beams.

The Coffin-Manson equation (Coffin, 1954; Manson, 1953) relates the plastic-strain amplitude for constant amplitude cyclic loading, ε_{ap}, with the number of cycles until failure, N_f, as follows:

$$\varepsilon_{ap} = \frac{\Delta\varepsilon_p}{2} = \varepsilon_f'(2N_f)^c \qquad \text{...(3-13)}$$

Where ε_f' and c are empirical constants

Mander, Panthaki, and Kasalanati (1994) and Brown and Kunnath (2004) calibrated the above equation to experimental fatigue life data for different sized deformed bars to give the formulae in Equation 3-14 below. Data came from bars that were tested in uni-axial tension and compression, under equi-amplitude loading, at strain amplitudes between ±0.01 and

±0.03. This happens to accurately simulate the strain history that can be expected in the bottom reinforcement of slotted-beams. Bars had a support spacing of $6d_b$ to ensure compression yield before buckling occurred, which is consistent with maximum stirrup spacing provisions in NZS3101:2006. Failure was taken as the initiation of a fatigue crack in the bar. Brown and Kunnath (2004) showed fatigue life resistance improved with increasing bar diameter at low total strain amplitudes, ε_a, less than 0.02, but worsened at higher total strain amplitudes greater than 0.025.

$$\begin{aligned}
&\text{No. 5 Bar (15.9 mm)}: \quad \varepsilon_{ap} = 0.08(2N_f)^{-0.5} \\
&\text{No. 6 Bar (19.1 mm)}: \quad \varepsilon_{ap} = 0.16(2N_f)^{-0.57} \\
&\text{No. 7 Bar (22.2 mm)}: \quad \varepsilon_{ap} = 0.13(2N_f)^{-0.51} \\
&\text{No. 8 Bar (25.4 mm)}: \quad \varepsilon_{ap} = 0.09(2N_f)^{-0.42} \\
&\text{No. 9 Bar (28.7 mm)}: \quad \varepsilon_{ap} = 0.07(2N_f)^{-0.37}
\end{aligned} \qquad \text{...(3-14)}$$

These expressions can be used in conjunction with Miner's rule (1945), given in Equation 3-15, to evaluate the damage accumulation, D_{Total}, in longitudinal reinforcement. D_i is the damage index for a given cycle, for which an accumulated index of 1.0 denotes low cycle fatigue failure. So provided that the load history is known, the plastic strain amplitude can be evaluated, and thus the onset of low cycle fatigue failure can be predicted. In this project, numerical multi-spring models of beam-column connections were used to obtain the plastic strain amplitude in reinforcement for a given drift loading. For details of these multi-spring models refer to CHAPTER 7.

$$D_{Total} = \sum_{i=1}^{n} D_i = \sum_{i=1}^{n} \frac{1}{N_{f,i}} = \sum_{i=1}^{n} 2\left(\frac{\varepsilon_f'}{\varepsilon_{ap}}\right)^{1/c} \qquad \text{...(3-15)}$$

Where $D_{Total} \geq 1.0$ denotes low cycle fatigue failure

Figure 3-10 plots the predicted accumulated damage index for monolithic beam specimen RCB1 and slotted-beam specimens SB1 and SB3 which were tested as part of the experimental investigation carried out for this project (See CHAPTERS 4 and 5). The interstorey drift sequence applied is given in Section 4.2.2 for specimens RCB1 and SB1 and in Section 5.2.2 for specimen SB3. These drift protocols were adopted in accordance with ACI acceptance criteria for new moment frame connections (ACI Committee 374, 2005).

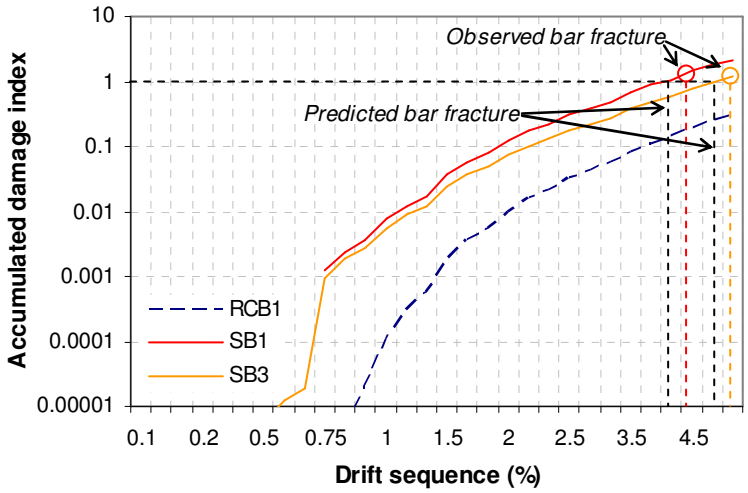

Figure 3-10: Low cycle fatigue prediction for tested specimens RCB1, SB1 and SB3

As expected, it is shown that the damage accumulation in both slotted-beam specimens is significantly higher than that in the conventional monolithic specimen. Longitudinal reinforcement in specimen RCB1 was very unlikely to fracture from low cycle fatigue. However, specimen SB1 was predicted to fail on the third cycle at 3.5% drift, and specimen SB3 on the second cycle at 4.5% drift. During the actual tests, bottom bars fractured on the first cycle at 4.5% drift for specimen SB1 and on the third cycle at 4.5% drift for specimen SB3. In both cases, this was one cycle later than expected from theory. Given the inherent scatter in low cycle fatigue life data from which the expressions in Equation 3-14 were calibrated to, the low cycle fatigue method presented appears to provide a reasonable prediction of the onset of bar fracture. Note that this method ignores any influence from surrounding concrete on the reinforcement and any bending or eccentricity resulting from flexure and shear sliding in the actual beam-column connection.

Whilst Miner's rule is simple to use, it does have limitations such as the omission of mean stress effects (Krawinkler, 1983). Mean stress effects result when positive and negative strain amplitudes are not the same – that is, when there is a non-zero mean stress. A tensile mean stress is detrimental to the fatigue life, whereas a compressive mean stress is beneficial (Koh and Stephens, 1991). The effect is more significant for longer fatigue lives where the strain amplitude is small (ε_a<0.005) and predominantly elastic. Fortunately, the bottom reinforcement in slotted-beams tends to be subject to equi-amplitude straining at higher strain amplitudes, such that mean stress effects are negligible. This is not so for conventional monolithic beams which are strained more in tension than in compression, at strain amplitudes less than half that observed in slotted-beam reinforcement. Thus the prediction shown above for monolithic specimen RCB1 may be slightly unconservative.

To further investigate the low cycle fatigue response of slotted-beams compared to conventional monolithic beams, a parametric study was performed on the two numerical full-scale beam-column joint subassembly models shown in Figure 3-11 – one used a slotted-beam connection and the other a conventional monolithic connection. In the multi-spring connection, the reinforcement ratio and beam depth was altered such that each beam still had the same moment capacity. Table 3-1 summarises the five beam configurations investigated. For all beams, 30 MPa concrete and Grade 300 reinforcement was used. For the slotted-beams, the top-hinge depth was taken as 0.25d, the unbonded length as 0.9(d-d'), and top reinforcement sized such that $A_s'f_y'/A_sf_y$=2.

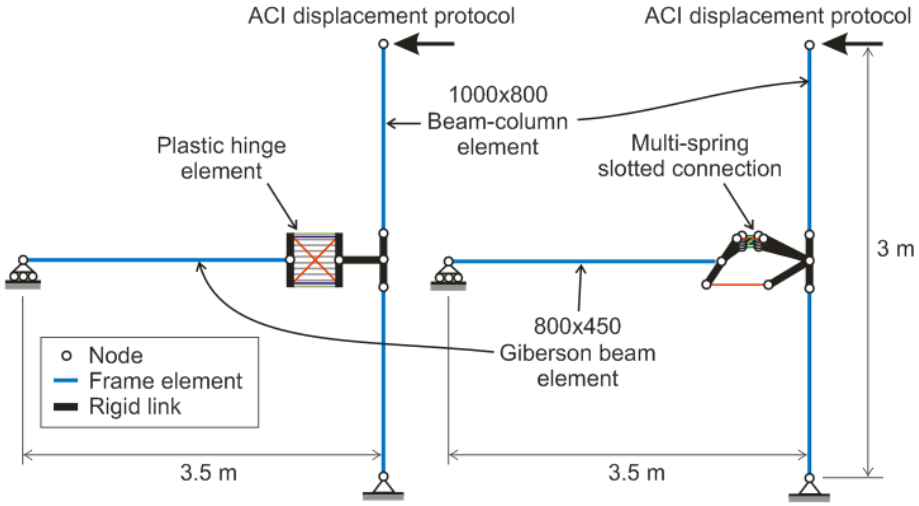

(a) Monolithic connection **(b) Slotted-beam connection**

Figure 3-11: Numerical full-scale joint subassembly models investigated

Table 3-1: Beam connection configurations investigated

ρ_s	h_b (mm)	d (mm)	b (mm)	A_s (mm^2)	M_n (kNm)
0.005	1060	1000	450	2250	655
0.008	860	800	450	2864	655
0.011	760	700	450	3326	655
0.014	680	620	450	3832	655
0.017	620	560	450	4339	655

Figure 3-12 plots the accumulation of plastic strain and damage in each connection when the subassembly models were subject to the same ACI drift sequence described in Section 4.2.2. Figure 3-12a shows that the plastic strain accumulation in slotted-beams is 2-3 times greater than that in an equivalent monolithic connection. This explains why the damage accumulation is significantly worst for slotted-beams. Figure 3-12b shows that the damage accumulation reduces as the reinforcement ratio is increased. This is because as the reinforcement area is increased, the beam depth can be decreased for a given moment

capacity. For shallower beams, yielding reinforcement is closer to the neutral axis such that strains are smaller. Thus a minimum reinforcement ratio limit should be specified for slotted-beams to ensure sufficient low cycle fatigue resistance.

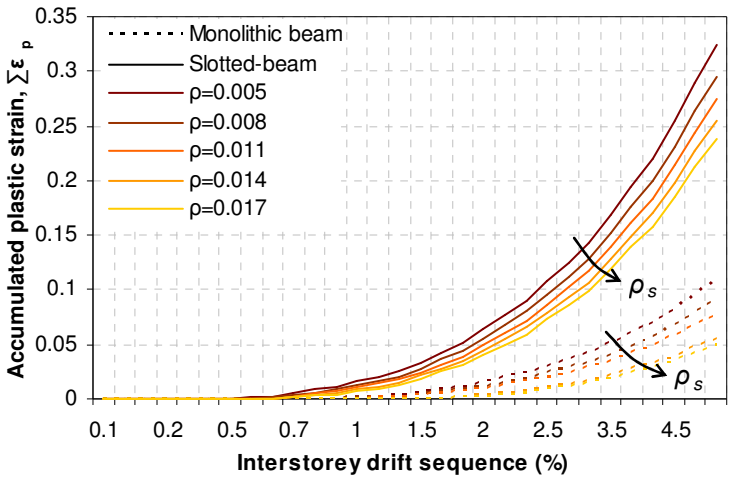

(a) Accumulated plastic strain during drift sequence

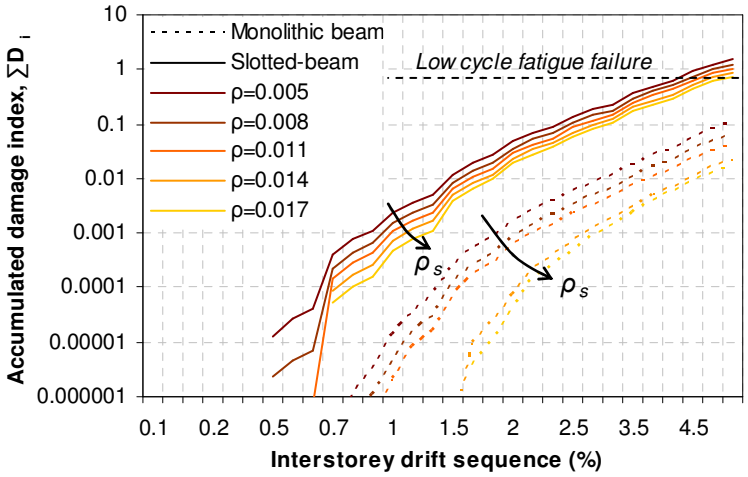

(b) Accumulated damage index during drift sequence

Figure 3-12: Effect of reinforcement ratio of low cycle fatigue performance

ACI acceptance criteria requires that the connection is capable of completing the third cycle to 3.5% drift without any strength degradation greater than 25% (ACI Committee 374, 2005). Assuming reinforcement fracture occurs when the accumulated damage index reaches unity, Figure 3-12b shows that slotted-connections with reinforcement ratios of 0.008 and greater satisfy ACI requirements. Given that specimens experimentally tested in this project had reinforcement ratios of 0.006 and fell only one 3.5% cycle short of ACI criteria, a minimum reinforcement ratio for slotted-beams between 0.006 and 0.008 appears reasonable.

To investigate the effect of the unbonded length on the low cycle fatigue response, Figure 3-13 plots the damage accumulation for the beam configuration with ρ=0.011 for different unbonded lengths ranging between 0.7(*d-d'*) and 1.1(*d-d'*). It shows that increasing the unbonded length from 0.7(*d-d'*) to 1.1(*d-d'*) allows the connection to undergo another two cycles at 4.5% drift before predicted bar fracture. Thus it is important to maximise the unbonded length to maximise low cycle fatigue performance. The only restriction on the unbonded length is that it must be terminated before the bottom bend in the diagonal hanger reinforcement. Thus for 45° diagonal reinforcement, the maximum unbonded length is likely to range between 0.9(*d-d'*) and *d-d'*.

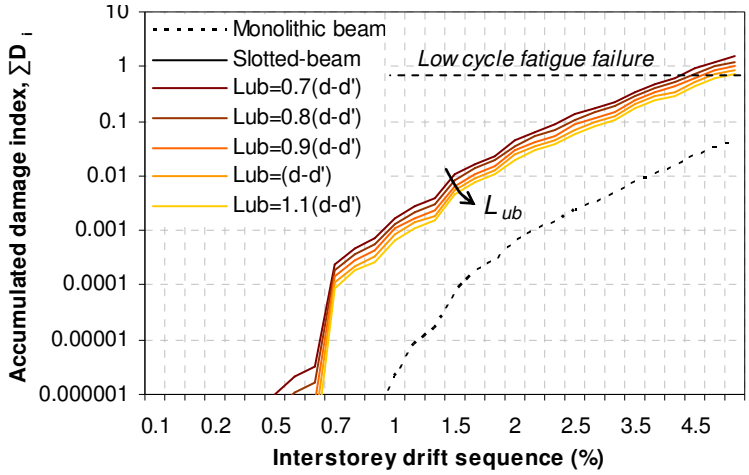

Figure 3-13: Effect of unbonded length on low cycle fatigue performance

As a final comment on low cycle fatigue, it should be noted that the above method does not consider strain rate effects on low cycle fatigue resistance. Research has shown the fracture toughness of mild steel to increase for increasing strain rates up to 10^{-3} strain/s, and then decrease with increasing strain rates beyond this (Srinivas and Kamat, 2001). From numerical time history analyses with actual earthquake records (See Section 7.3), peak strain rates on the order of 5×10^{-2} – 8×10^{-2} strain/s can be expected in the bottom longitudinal reinforcement of slotted-beams. This falls in the strain rate range where fracture toughness decreases. But for the particular mild steel tested by Srinivas et al., the fracture toughness at these strain rates was still slightly higher than the fracture toughness at quasi-static testing strain rates. This means that dynamic strain rates during a seismic event may not have a detrimental effect on the low cycle fatigue performance of a slotted-beam beyond what is observed in quasi-static tests. Further testing at realistic seismic strain rates should be carried out using New Zealand mild steel reinforcing bar to confirm this.

3.6 Anchorage of Bottom Reinforcement in Interior Joints

Because the flexural strength of a slotted-beam is governed by yielding of bottom longitudinal reinforcement, anchorage of this reinforcement through interior beam-column joints is essential to ensure strength is maintained. If bond-slip of this reinforcement was to occur, these bars would not reach full yield, and thus the flexural strength of the connection would be reduced. This was observed in the experimental test of specimen SB2 (See Section 4.3.12) where bond-slip led to significant strength degradation.

In conventional monolithic beams, bottom longitudinal bars passing through interior columns are normally subject to elastic push on one side and overstrength-yield pull on the other. Because of the presence of concrete acting in compression, often a degree of bond-slip is allowed to occur without much degradation in flexural strength. For slotted-beams, because there is no concrete acting in compression at the beam soffit, the bottom reinforcement is subject to overstrength yield push and pull, with no additional restraint from concrete acting in compression. Thus the bond stress condition is more severe for slotted-beams and current design provisions for monolithic beams should be modified for slotted-beams.

To illustrate the difference in bond behaviour, Figure 3-15 shows a conceptual comparison of the bond stress development between a monolithic beam and a slotted-beam. For this illustration, a monolithic beam section equivalent to tested specimen RCB1 and a slotted-beam section equivalent to tested specimen SB1 are adopted (For section details, see Section 4.1). Steel forces were calculated from the monotonic moment-rotation analysis shown in Figure 3-14, and average bond stress values were calculated assuming a column depth of 400 mm. Snapshots of the bond conditions are illustrated for beam rotations of 0.00025 rad, 0.015 rad and 0.025 rad; which respectively correspond to limit states of first yield in the slotted-beam, strain hardening and cover concrete crushing. The author would like to emphasise that the stress distributions drawn are only conceptual and based on engineering judgement. Because bond stress is a complex problem dependent on many factors such as concrete strength, confinement, bar diameter, bar spacing, anchorage length, load rate and cyclic load history (Eligehaussen, Popov and Bertero, 1983; ACI Committee 408, 1992), the bond stress distribution is seldom uniquely defined. The stress distributions given below were modified from representative distributions suggested by Cheung et al. (1991) and Paulay and Priestley (1992).

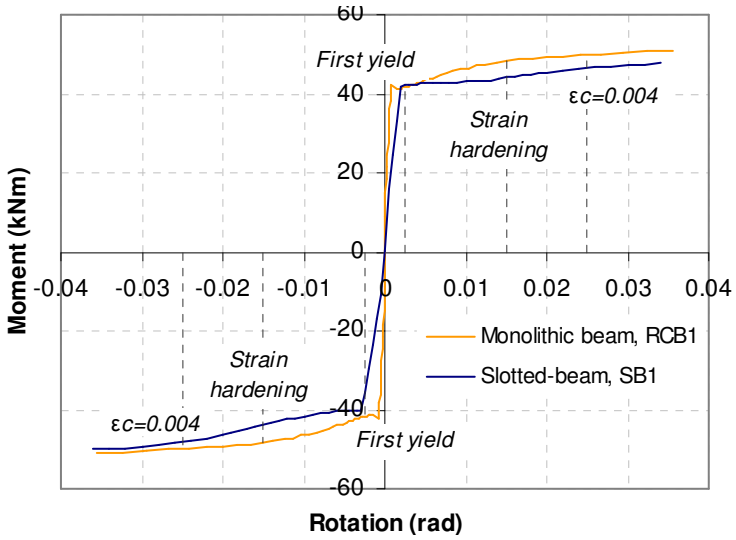

Figure 3-14: Monotonic moment-rotation analysis for sections RCB1 and SB1

At first yield (θ_b=0.00025), there is likely to be little bond deterioration in the joint so the bond stress distribution is likely to be close to uniform. Less uniformity can be expected in the slotted-beam because the total force, which must be transferred via bond, is greater due to larger bar compression on the right-hand-side. Due to yield penetration, the effective column depth providing bond decreases. For simplicity $0.8h_c$ has been assumed. At this limit state, the average bond stress for the slotted-beam is 5.8 MPa, which is already reasonably higher than 3.7 MPa for the monolithic beam.

As reinforcement begins to strain harden, the force which must be resisted increases, and thus the average bond stress for both joints also increases. Cyclic yield penetration into the joint and gradual bond deterioration results in limited bond-slip such that the bond stress is no longer uniform as shown. The stress distribution shown for the monolithic beam is that suggested by Paulay and Priestley (1992). While behaviour on the tension side of the joint is similar for the slotted-beam, significantly more stress must be transferred on the compression side. This alters the bond stress distribution, such that stresses are concentrated more on the compression side when compared to the distribution in the monolithic joint.

After many large drift cycles, concrete cone pullout at the column face may occur in the slotted-beam which reduces the effective column depth providing bond even further – here $0.7h_c$ has been assumed. This in turn increases the average bond stress even more. Cone pullout may also occur in the monolithic joint; however this is less pronounced because complete spalling is unlikely due to additional confinement provided by beam concrete. At the ultimate limit state shown, the average bond stress in the slotted-beam joint is almost

twice that in the monolithic joint; and the maximum local bond stress in the slotted-beam, as illustrated in this case, is double the average bond stress.

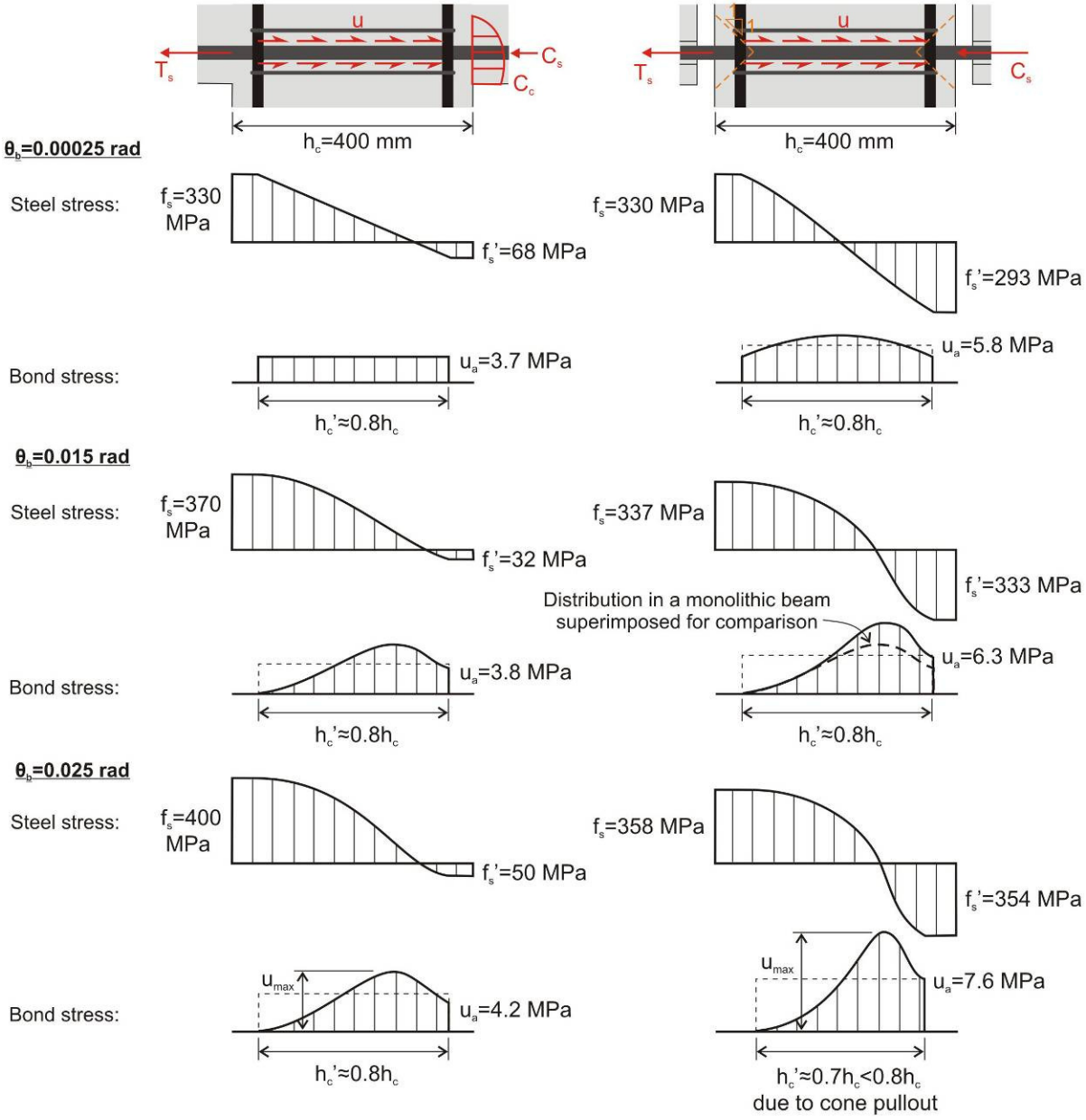

(a) Monolithic beam **(b) Slotted-beam**

Figure 3-15: Conceptual comparison of bond stress development in interior joints with monolithic beams and slotted-beams

Figure 3-15 highlights three major differences in the bond behaviour of interior joints with slotted-beams compared to monolithic beams. Firstly, yielding of both tension and compression reinforcement means a much larger force must be anchored by bond. Secondly, because the stress in compression reinforcement is significantly higher, the shape of the bond stress distribution changes and becomes more skewed to the compression side of the joint.

Thirdly, concrete cone pullout, which is likely to occur after repeated cycles, will further reduce the effective depth providing bond. As an aside, although yielding of both tension and compression reinforcement can occur in conventional monolithic beams when cyclic displacements are large enough, this compression yielding occurs at much smaller strains than those that occur in a slotted-beam; therefore the degradation to the bond is not as significant.

A fourth difference which was not considered above is additional steel forces due to cyclic strain hardening. Tests on slotted-beams revealed additional post-yield hardening as a result of cyclic plastic straining of bottom reinforcement. The extent of this additional hardening is dependent on the load history applied, but will increase the forces which must be anchored by bond. Existing provisions for anchoring reinforcement in interior joints for conventional beams need to be modified for these four factors before being applied to slotted-beams.

Current NZS3101:2006 provisions for bond through an interior joint are based on theory described in Paulay and Priestley (1992) with an added 5% safety reduction. Ignoring this safety reduction, modification factors for axial load, bar location during casting and joint type, the basic equation given in Paulay and Priestley can be expressed as:

$$\frac{d_b}{h_c'} \leq \frac{4u_a}{\xi_m \lambda_o f_y} \qquad ...(3\text{-}16)$$

Where d_b is the longitudinal bar diameter, h_c' is the effective column depth providing bond, u_a is the average bond stress/strength, λ_o is the overstrength factor for the reinforcement and ξ_m is a factor which accounts for the relative magnitude of force in compression reinforcement compared to tension reinforcement. NZS3101:2006 simply assumes $0.8h_c$ for h_c' and takes λ_o as 1.25. u_a is approximated as $0.67u_{max}$ for monolithic beams, which comes from the assumed bond stress distribution in Figure 3-15. Given that maximum local bond stresses of $u_{max}=2.5\sqrt{f'_c}$ have been observed (Eligehausen et al., 1983), this gives $u_a=1.675\sqrt{f'_c}$. ξ_m is defined as $(T_s+C_s')/T_s$, and is normally taken as 1.55. Each of these terms must be modified to allow the same equation to be applied to interior joints with slotted-beams.

Firstly, to account for yielding of both tension and compression reinforcement on either side of the joint, ξ_m should be taken as 2.0. The bar force on the compression side of the joint is

approximately equal to the force on the tension side, and so the force that must be resisted by bond is $T_s+C_s' \approx 2T_s$.

To account for the change in bond stress distribution, the average bond stress/strength, u_a, should be altered accordingly. Because little experimental investigation has been carried out into the bond stress distribution in slotted-beams, the distribution illustrated in Figure 3-15 should be considered very tentatively. This mechanism, however, does suggest a reduction in the ratio of u_a/u_{max} from 0.67. Observed bond stress distributions from the test of specimen SB3 (See Section 5.3.8) are consistent with this hypothesis, with a maximum u_a/u_{max} ratio of 0.51 reached at 2.5% drift.

Past tests on slotted-beam interior joints have obtained average bond stresses of between $1.0\sqrt{f'_c}$ and $1.3\sqrt{f'_c}$ without bond-slip failure occurring (Ohkubo et al., 2004; Leslie, 2010). Just prior to bond failure occurring in specimen SB2 (See Section 4.3.12), an average bond stress of $1.48\sqrt{f'_c}$ was reached. These values are all less than $1.675\sqrt{f'_c}$ adopted for the safe design of conventional beams, which also suggests a reduction in the u_a/u_{max} ratio. Therefore it is probable that the maximum average bond stress for slotted-beams lies in the range of $1.3\sqrt{f'_c}$ to $1.5\sqrt{f'_c}$. However there is insufficient experimental data available to allow a safe value to be specified with the level of confidence required for design. It is well-known that bond strength is inherently an unreliable figure. Specified bond strengths adopted today originate from 95 percentile lines of best fit through extensive test data. Furthermore, just to be consistent with the theory adopted in NZS3101:2006, here the maximum bond stress, u_{max}, has been assumed to be a function of $\sqrt{f'_c}$. However this is not always the case, and other researchers have proposed empirical expressions for the maximum bond stress as a function of f'_c (Vandewalle, 1992; Huang et al., 1996) and $f'^{2/3}_c$ (Fédération internationale du béton, 2000). Further testing of slotted-beams is recommended, along similar lines of tests carried out by Zhu and Jirsa (1983) for conventional beams, to ensure influences from joint shear and column flexure are included.

To account for the reduction in the effective column depth providing bond from concrete cone pullout at the column face, Figure 3-16 proposes a new estimation of h_c' assuming a reduction from 45° cone pullouts at each face. The test of specimen SB2 showed these cones intersected with horizontal stirrups adjacent to the bar at approximately 45°. The depth of pullout can therefore be minimised by locating adjacent column and joint stirrups as close as

possible to the longitudinal beam reinforcement. In such cases, h_c' should be taken no greater than $0.8h_c$ as adopted for conventional beams in NZS3101:2006.

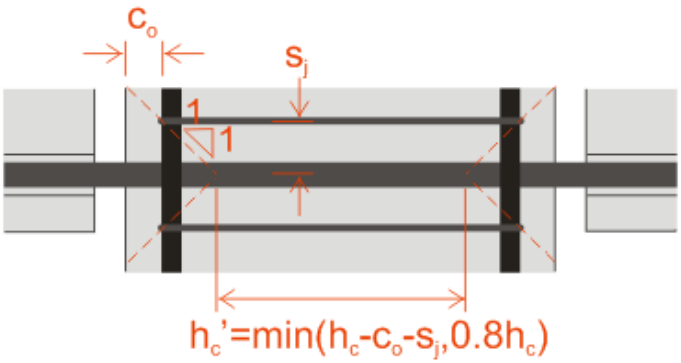

Figure 3-16: Estimation of effective column depth providing bond

The final modification that must be made is to account for the greater strain hardening in the bottom reinforcement due to cyclic tension-compression yielding. Instead of adopting λ_o=1.25, values on the order of 1.3-1.4 may be more appropriate for Grade 300 reinforcement in slotted-beams. The test of specimen SB1 revealed flexural overstrength factors on the order of 1.3 for positive moments and 1.4 for negative moments (See Table 4-6); and bottom longitudinal reinforcement in specimen SB3 exhibited material overstrength factors in the range of 1.3 to 1.4 (See Figure 5-37b). It should be noted that this cyclic strain hardening is dependent on the load history applied, and the drift protocol used for this project can be considered as rather severe. Recent numerical time history analyses by Muir (2009) revealed that this overstrength may not be as significant as experimental testing may suggest.

To give an idea of how these modifications may affect column widths required to provide sufficient bar anchorage, say u_a=1.4√f'$_c$. After applying a 95% safety reduction, Equation 3-16 then becomes:

$$\frac{d_b}{h_c'} \le 2.66\frac{\sqrt{f'_c}}{\lambda_o f_y} \qquad \text{...(3-17)}$$

Assuming h_c'=0.8h_c, λ_o=1.3, 30 MPa concrete and Grade 300 reinforcement, this gives d_b/h_c=1/33 for a slotted-beam. For a conventional RC beam, the bond equation from NZS3101:2006 gives d_b/h_c=1/21. Thus column widths greater than 1.5 times the size required for conventional beams can be expected when using slotted-beams. This is undesirable but is a limitation of slotted-beams.

In cases where such a large column depth cannot be provided, Figure 3-17 shows alternative conceptual anchorage details. However each has their own drawbacks. Using separate bars with 90° hooks may result in an over-congested joint unless the beam is relatively wide. Because of buckling problems, bottom bars should not be cranked into the joint. Welded or mechanical anchorages could be used, but concrete stresses should be checked for local crushing. Effects of welding on steel properties should also be considered. Lastly, it may be possible to use ducts filled with high strength grout to improve the u_a term in Equation 3-16. These details are only conceptual ideas, and no investigation was carried out to determine the effectiveness of these methods.

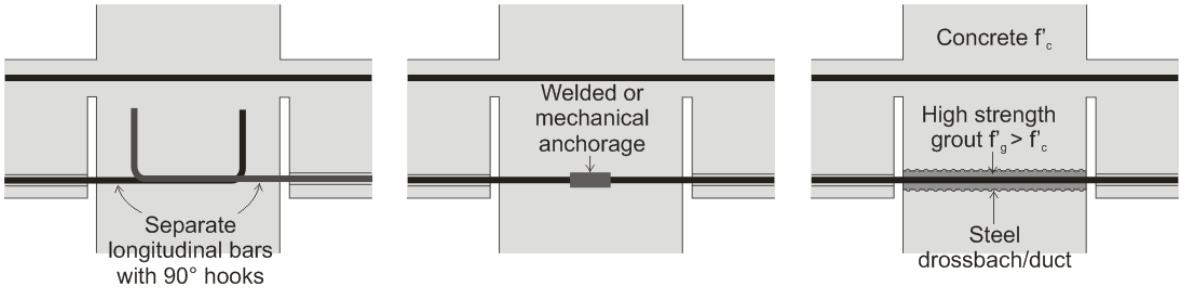

Figure 3-17: Alternative anchorage details for bottom reinforcement in interior joints

Although it will generally not govern, d_b/h_c ratios for top reinforcement in slotted-beams should also be checked. For top reinforcement, current code provisions do apply as concrete compression does exist. It should be noted that λ_o could probably be reduced to 1.1 instead of 1.25 for Grade 300 reinforcement (1.4 for Grade 500), as strain hardening of top reinforcement should not occur. 1.1 should be adopted as oppose to 1.0 to account for the fact that actual strengths are higher than specified lower characteristic strengths (Paulay and Priestley, 1992).

3.7 Interior Joint Design

3.7.1 Joint Shear Force Demand

Figure 3-18a illustrates the external actions acting on an interior beam-column joint with traditional monolithic beam connections. The joint shear force demand is usually determined from horizontal equilibrium rather than vertical equilibrium because horizontal forces are more easily defined. Applying horizontal equilibrium to the monolithic joint, the horizontal joint shear force demand is commonly written as (Paulay and Priestley, 1992):

$$V_{jh} = C_c' + C_s' + T - V_{col} = T' + C_c + C_s - V_{col}'$$

$$\therefore V_{jh} = T + T' - V_{col} = (A_{s1} + A_{s2})\lambda_o f_y - V_{col} \qquad ...(3\text{-}18)$$

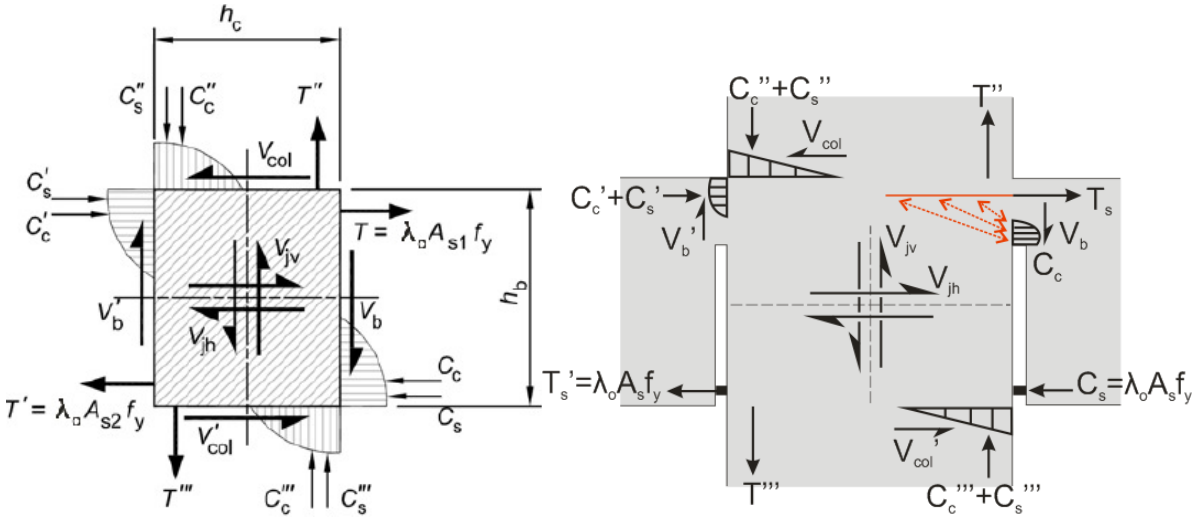

(a) Monolithic beam **(b) Slotted-beam**

Figure 3-18: External actions on interior beam-column joints with conventional monolithic beams and slotted-beams

Similarly, Figure 3-18b shows the external forces acting on an interior joint with slotted-beams. These forces differ slightly from that of a conventional joint. Firstly, there is no concrete compression at the bottom of the right-hand-side beam due to the slot. Secondly, because of a prying effect in the right-hand-side beam, the tensile force in the top reinforcement, T_s, is greater than the compression in the bottom reinforcement, C_s. From equilibrium, T_s is equal to C_c+C_s. Like conventional joints, the horizontal joint shear demand can be computed by applying horizontal equilibrium:

$$V_{jh} = (C_c' + C_s') + (T_s - C_c) - V_{col} \quad \text{or} \quad T_s' + C_s - V_{col}'$$

$$\therefore V_{jh} = 2\lambda_o A_s f_y - V_{col} \qquad ...(3\text{-}19)$$

Thus the horizontal joint shear in a slotted-beam is, in general, no different to that for an equivalently reinforced monolithic beam despite the difference in external forces. The derivation of the vertical joint shear force is more cumbersome due to the addition of axial load and multiple layers of reinforcement. For conventional joints it is common and sufficiently accurate to estimate its value from joint equilibrium as (Paulay and Priestley, 1992):

$$V_{jv} = \frac{h_b}{h_c} V_{jh} \qquad ...(3\text{-}20)$$

Because the joint panel zone for a slotted-beam does not differ much from a traditional joint, it is reasonable to assume this expression also applies to slotted-beams.

3.7.2 Joint Shear Strength

Conventional reinforced concrete beam-column joints resist joint shear via the two mechanisms illustrated in Figure 3-19 (Paulay and Priestley, 1992). Shown on the left is the 'concrete strut mechanism', where shear is resisted by a diagonal compression field running from opposite corners of the joint. The strut is induced by concrete compression forces resulting from flexure, and an additional force from longitudinal steel in compression which is transferred via bond. The remaining joint shear is resisted by stirrup reinforcement, which is termed the 'truss mechanism' and is shown on the right of the figure.

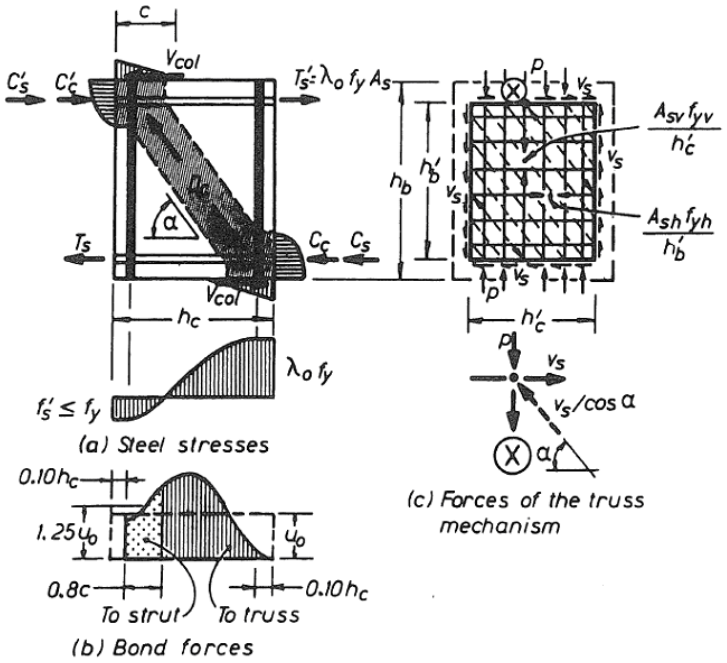

Figure 3-19: Concrete strut and truss joint shear mechanisms in conventional reinforced concrete beams (Paulay & Priestley, 1992)

The total horizontal joint shear strength derived from the two mechanisms can thus be expressed as:

$$
\begin{aligned}
&V_{jh} = V_{ch}' + V_{sh}' \\
&\text{Where : } V_{ch}' = C_c' + B_s' - V_{col} \\
&\qquad V_{sh}' = T_s' + C_s' - B_s' \\
&\qquad B_s' = 1.25u_o \times 0.8c = (C_s' + T_s')c / h_c
\end{aligned}
\qquad \text{...(3-21)}
$$

V_{jh} is the total horizontal joint shear, V_{ch}' is the horizontal contribution from the concrete strut mechanism, V_{sh}' is the horizontal contribution from the truss mechanism and B_s' is reinforcement force transferred to the strut mechanism via bond. As shown in Figure 3-19, u_o is the average bond force per unit length along the reinforcement, and c is the neutral axis depth of the column across which bond forces can contribute to the strut mechanism.

These two mechanisms can be applied to interior joints with slotted-beams but with some minor changes. Because of the slot, no concrete compression force can form at the bottom of the joint as highlighted in Figure 3-20. Thus the contribution to the concrete strut mechanism must be derived solely from the transfer of bottom reinforcement compression via bond stresses, B_s. More often than not, the horizontal force V_{ch} introduced to the concrete strut by the bottom reinforcement will be less than the force V_{ch}' introduced at the top of the joint. The top of the joint is essentially the same as a monolithic beam and can derive its strut contribution from both concrete compression, C_c', and bond, B_s'. As a result, a portion of the strut force introduced at the top of the joint will have to be resisted by horizontal shear reinforcement at the bottom of the joint, herein denoted as $\Delta V_{sh} = V_{ch}' - V_{ch} = V_{sh} - V_{sh}'$. V_{sh} and V_{sh}' are the horizontal joint shear forces resisted by the truss mechanism at the bottom and top of the joint respectively.

Evidence of this mechanism is reflected in the horizontal joint stirrup strain profile obtained from the test of specimen SB2 (See Section 4.3.13). The strain profile was observed to increase towards to the bottom of the joint, rather than being symmetric as is commonly observed in monolithic interior joints (Park and Raitong, 1988; Cheung et al., 1991). This is illustrated conceptually on the right of Figure 3-20. V_{sh}' is the contribution to the truss mechanism from the top of the joint, which will produce a symmetric joint stirrup strain profile as shown. But due to the excess strut force ΔV_{sh} that must be restrained, joint strains increase toward the bottom of the joint as shown in red.

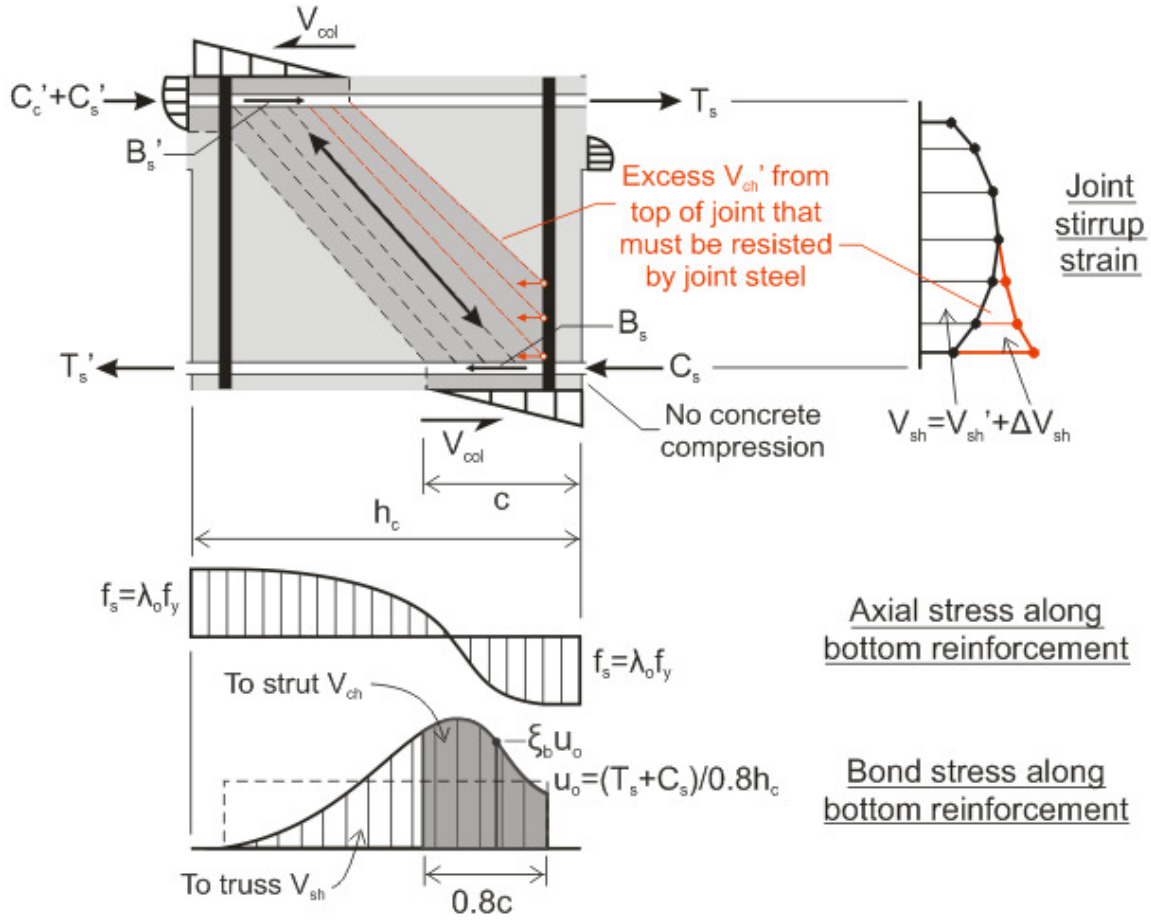

Figure 3-20: Concrete strut mechanism for interior joints with slotted-beams

Applying similar concepts from Equation 3-21 to the bottom of the slotted-beam joint in Figure 3-20, the contribution from the two mechanisms can be expressed as:

$$
\begin{aligned}
&V_{jh} = V_{ch} + V_{sh} \\
&\text{Where}: \; V_{ch} = B_s - V_{col} \\
&\qquad\quad V_{sh} = V_{sh}' + \Delta V_{sh} \\
&\qquad\quad B_s = \xi_b u_o \times 0.8c = 0.8\xi_b (C_s + T_s) c / h_c
\end{aligned}
\qquad \text{...(3-22)}
$$

Here V_{sh} is the total shear carried by joint stirrups, including the contribution from the truss mechanism V_{sh}' and that from the excess strut force ΔV_{sh}. B_s is the bottom reinforcement force transferred to the strut mechanism via bond. To keep the expression as general as possible, ξ_b is a factor which when multiplied by u_o gives the average bond force along the column width $0.8c$ as shown in Figure 3-20. It will be dependent on the bond stress distribution and the ratio c/h_c. For monolithic beams, Paulay and Priestley (1992) adopt 1.25 as in Equation 3-21. But because of the changes to the bond stress mechanism as discussed in Section 3.6, this factor will be higher for slotted-beams.

From the test of specimen SB2, the maximum excess strut force resisted by joint stirrups was found to be 30-40% of the shear resisted by the truss mechanism in an equivalent monolithic joint. This was for an axial load ratio of N^*/f'_cA_g=0.038. Back calculated values for ξ_b ranged between 1.73 and 2.05.

To assess the effect of the joint aspect ratio, axial load and ξ_b on the excess strut force, Figure 3-21 shows the results of a parametric analysis that was carried out. The same beam section as specimen SB2 was used, but the column depth and axial load was altered and the corresponding joint forces computed using Equation 3-22. In this figure, the excess strut force has been expressed as a fraction of the truss mechanism shear in an equivalent monolithic joint, $V_{sh,monolithic}$, which was calculated using Equation 3-21.

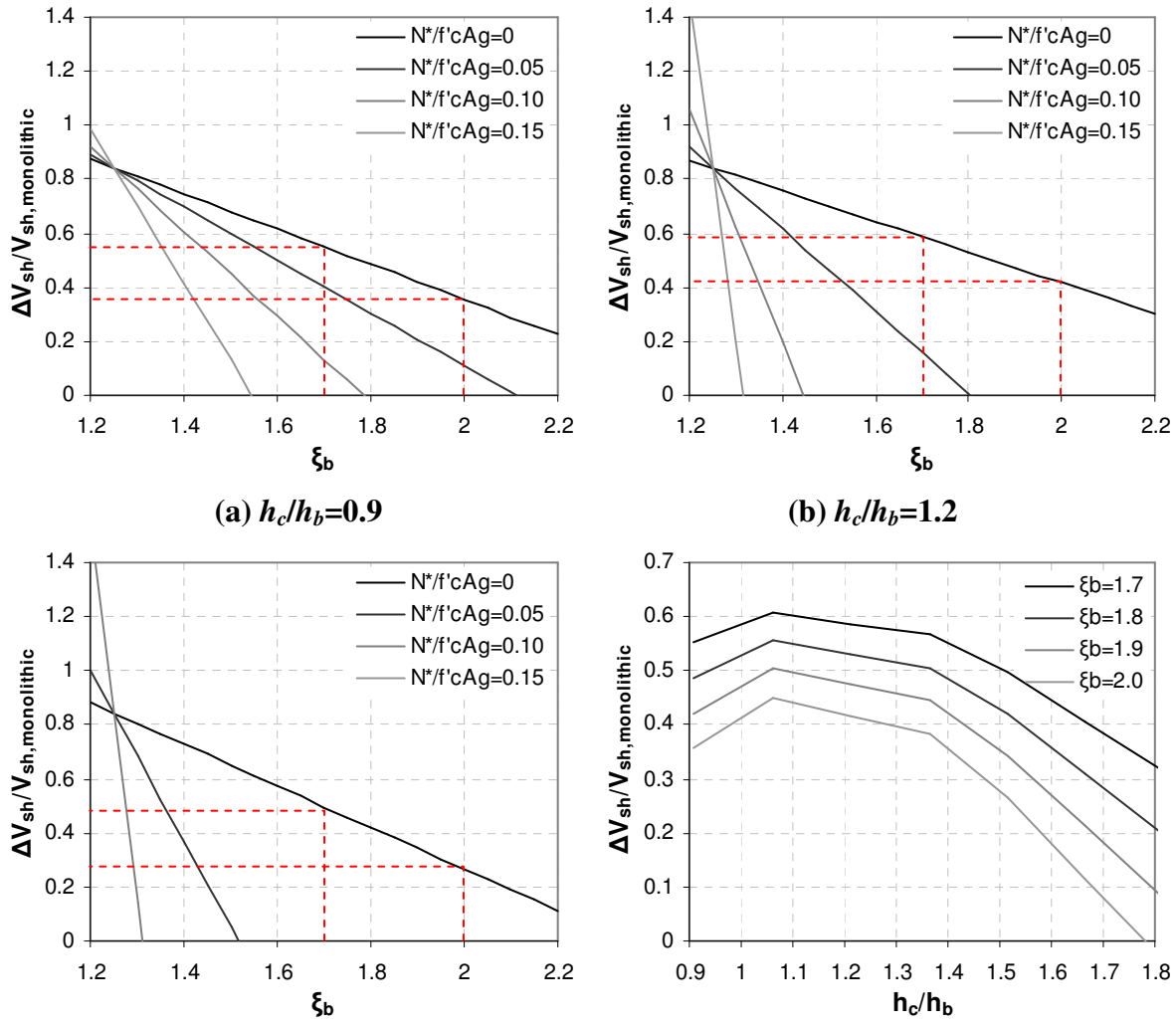

Figure 3-21: Effect of joint aspect ratio (h_c/h_b), axial load (N^*/f'_cA_g) and bond factor ξ_b on the excess strut force (ΔV_{sh})

It is shown that the excess strut force is relatively insensitive to the joint aspect ratio when there is zero axial load. For realistic ξ_b values between 1.7 and 2.0, the excess strut force remains around 30-60% of the truss mechanism shear force. Note that lower values of ξ_b are more conservative. Slight increases in axial load are shown to significantly reduce the excess strut force, and this effect is accentuated as the column width is increased. This is because any level of axial load increases the column neutral axis depth, which increases the length over which longitudinal beam reinforcement can contribute to the strut mechanism via bond.

Ignoring beneficial effects of axial load, it can be concluded that the joint stirrups in a slotted-beam interior joint should be increased by 30-60% from that required in an equivalent monolithic joint. In addition, these extra stirrups should be located in the bottom half of the joint. Although the test of specimen SB2 revealed some of the excess strut force to be resisted by stirrups in the upper half of the joint, the majority of the force is concentrated in the bottom half of the joint.

To allow a practical implementation of the assertion made in the previous paragraph, this additional joint reinforcement should be specified as a percentage of the required joint reinforcement for an equivalent monolithic joint as computed from code equations, and not Equation 3-21. This is because the common practicing engineer will only use code equations, which contain conservative assumptions such that the specified increase of 30-60% may become too difficult to construct. The design equation for horizontal joint reinforcement in interior beam-column joints given in NZS3101:2006 is:

$$V_{sh} = f_{yh} A_{jh} = \frac{6V_{jh}^{*}}{f'_c b_j h_c}\left(\alpha_i f_y A_s^{*}\right)$$

$$\text{Where:} \quad \alpha_i = \left(1.4 - 1.6\frac{C_j N_o^{*}}{f'_c A_g}\right)\alpha_n \qquad \text{...(3-23)}$$

$$\frac{6V_{jh}^{*}}{f'_c b_j h_c} \geq 0.85$$

Although this equation is based on theory from Paulay and Priestley (1992), it differs from Equation 3-21 which was used to calculate $V_{sh,monolithic}$ values in Figure 3-21. Firstly, the code equation relies on a column neutral axis depth approximation of $(0.25+0.85N_o^{*}/f'_cA_g)h_c$, which can be overly conservative, especially for higher levels of axial load. Secondly, $6V_{jh}^{*}/f'_cb_jh_c$ is an extra term that is not present in Equation 3-21, which is used to provide a

lower limit to support the truss mechanism by specifying that it must be greater than 0.85. This limit was imposed because there was no test data for cases with $6V_{jh}^{*}/f'_c b_j h_c$<0.85 when the equation was first introduced into the New Zealand code. Because lower reinforcement ratios are usually used in practice, for most cases this limit governs.

Figure 3-22a shows the results of the same parametric analysis given in Figure 3-21d, but this time the excess strut force has been expressed as a fraction of the truss mechanism shear in an equivalent monolithic joint as calculated from the code, $V_{sh,NZS3101}$. Due to conservative code assumptions, the percentage increase in the required joint reinforcement to resist the excess strut force is now only 20-35%.

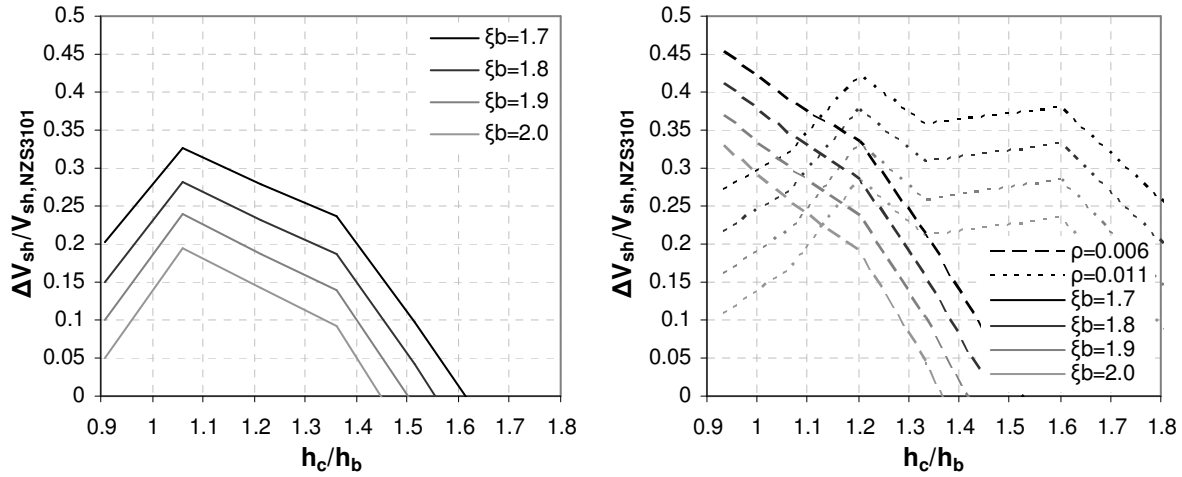

(a) Slotted-beam section SB2 **(b) 750 mm deep slotted-beam**

Figure 3-22: Effect of joint aspect ratio (h_c/h_b), axial load ($N^*/f'_c A_g$) and bond factor ξ_b on the excess strut force (ΔV_{sh})

So far, only one slotted-beam section has been considered. Figure 3-22b plots the same results for 750 mm deep slotted-beams with longitudinal reinforcement ratios of 0.006 and 0.011. In this case, the percentage increase in joint reinforcement to resist the excess strut force is between 25-40%. For all three beam sections in Figure 3-22, the code limit of $6V_{jh}^{*}/f'_c b_j h_c \geq 0.85$ governed.

Therefore, as a tentative recommendation, the joint reinforcement for an interior beam-column with slotted-beams should be increased by 25-40% from that given by NZS3101:2006 equations. These extra stirrups should be located in the bottom half of the joint, which can be achieved by either increasing the stirrup size or decreasing the stirrup spacing in this region. Stirrup sets immediately adjacent to bottom beam reinforcement which cannot be considered to contribute to A_{jh} according to NZS3101:2006, can be

considered to contribute to ΔA_{jh}. Therefore, often ΔA_{jh} can be achieved with only the addition of one or two extra stirrup sets. Figure 3-38 in Section 3.9 gives an example of the difference in detailing for a monolithic and slotted interior beam-column joint.

The recommendation above conservatively ignores any beneficial effects of axial load. It has been shown that a small level of axial load greatly reduces the excess strut force, however accurate consideration of the axial load ratio requires a much more detailed analysis. As a final note, this recommendation has only been validated for cases where the code limit of $6V_{jh}^{*}/f'_c b_j h_c \geq 0.85$ governs. Cases where this limit is not likely to govern are when adjoining beams have a high reinforcement ratio and the column depth is small. However because slotted-beams often require a large column depth to provide anchorage to bottom reinforcement, this limit is likely to always govern for slotted-beams.

It is considered that the vertical joint shear behaviour of a slotted interior beam-column joint will be the same as that for a conventional joint. The presence of the slot only alters the mechanism in which horizontal forces enter the joint, and where beam shear enters the joint during gap-closing rotations. During gap-closing rotations, vertical beam shear will enter the joint at the top via diagonal shear reinforcement passing through the top-hinge. This differs from conventional beams where beam shear will enter the joint at the bottom via a diagonal strut. This change in behaviour should not affect the vertical joint mechanism because overall the same forces are still entering the joint. Thus no modification to existing NZS3101:2006 provisions for vertical joint reinforcement are needed for slotted-beams.

3.7.3 Anchorage of Diagonal Hangers in Interior Joints

Diagonal hanger reinforcement should be anchored into interior beam-column joints using 90° hooks. Although it is possible to have a continuous hanger through an interior joint, it would be difficult to ensure the bar was bent correctly and fitted properly across the joint. This leaves 90° end hooks as the simplest means of anchorage.

In line with conventional thinking, designers may be tempted locate the hooks on opposite ends of the column, as shown in Figure 3-23a, in attempt to capture the concrete strut mechanism in the joint. However as discussed in Section 3.7.2, the forces introduced to the concrete strut at the top of the joint will exceed that introduced at the bottom. As a result, this excess strut force must be resisted by horizontal stirrups at the bottom of the joint as shown in orange in Figure 3-23a. So clearly, locating hanger hooks on the far sides of the column

may overstress the stirrups at the bottom of the joint. Obviously this detail cannot be avoided if the hook development length, L_{dh}, requires the full depth of the column. The joint shear reinforcement recommendations from Section 3.7.2 were calibrated from the test of specimen SB2 which adopted this anchorage detail and hence accounts for this effect. A drawback of this anchorage detail is that there must be sufficient joint width to allow hangers from either side of the joint to be cranked past each other.

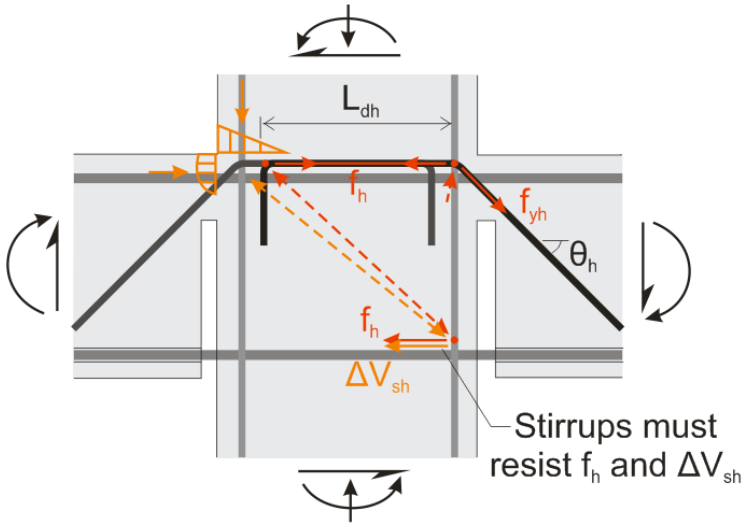

(a) Two 90° hooks cranked past each other

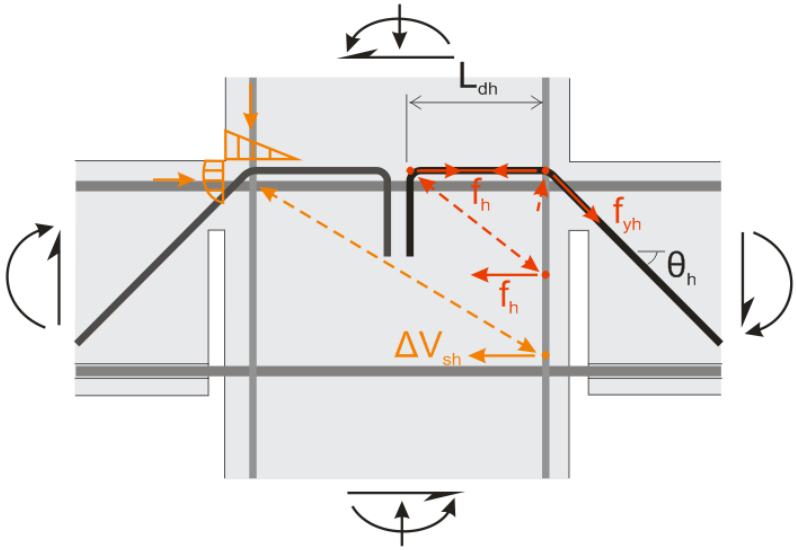

(b) Two 90° hooks at the centre of the joint

Figure 3-23: Possible anchorage details of diagonal hangers in interior joints

A more efficient detail for anchoring diagonal hangers in interior joints is shown in Figure 3-23b. This does require a wide column; however this is likely to be already available due to anchorage requirements for bottom longitudinal beam reinforcement. This detail will not overstress stirrups at the bottom of the joint, and is easier to construct as hangers do not need

to be cranked past each other. Additional consideration must be taken to ensure the forces from the hanger development length and hook do not overstress horizontal joint stirrups in the upper half of the joint. This anchorage detail was not investigated in-depth and further research should be carried out to ascertain whether additional joint reinforcement should be provided.

3.8 Floor Slab Effects

The purpose of using a slotted-beam is to create a non-tearing floor connection by reducing deformations induced at the floor slab level. This section discusses various floor slab effects such as prying, effective flange contributions to flexural strength, beam torsion and floor seating widths, which should be considered when detailing slotted-beams with precast floors.

3.8.1 Slab Prying Effects

To simplify construction and ease implementation into current practice, the slotted-beam can be constructed using precast-emulation methods commonly used in New Zealand. Slotted-beams can be brought onsite with only the bottom half precast, and once floor units have been seated on the beam, the rest of the beam can be cast simultaneously with the floor topping. As a result, the floor topping will be cast integrally with the concrete top-hinge. This will allow floor slab concrete to act in compression as an effective flange, resulting in prying at the slab surface during gap-closing rotations. Because of the additional concrete compression from this effective flange, the neutral axis must drop to maintain horizontal equilibrium. This will induce greater deformations at the slab surface, resulting in greater cracking and prying of the slab as shown in Figure 3-24.

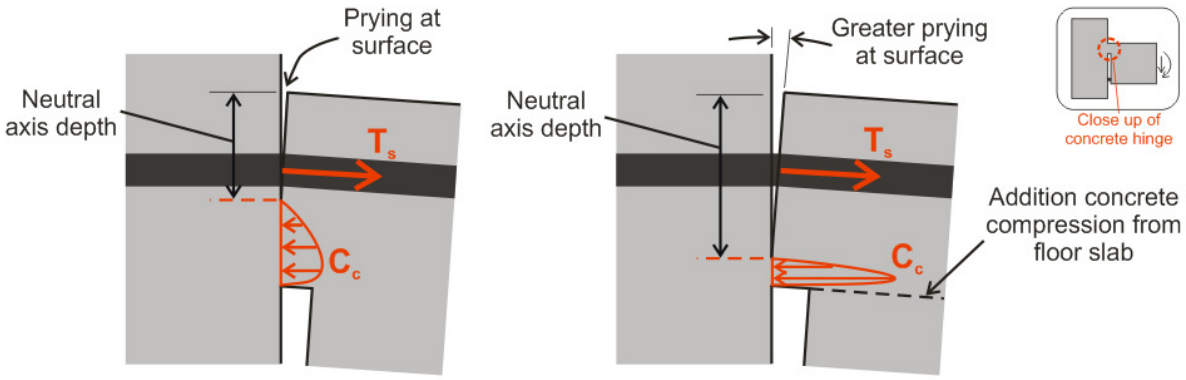

(a) Concrete top-hinge without floor slab (b) Concrete top-hinge with floor slab

Figure 3-24: Prying effect of floor slab

Therefore, to reduce slab concrete compression contributions and minimise this prying effect, the slab depth adjacent to the slotted section should be less than the concrete top-hinge depth. Figure 3-25 and Figure 3-26 illustrate connection details to achieve this when precast floor units span parallel to the slotted-beam and when they span onto the slotted-beam itself.

When precast floor units span parallel to the slotted-beam, the timber infill detail proposed by Matthews, Bull and Mander (2003) is recommended. This detail was originally proposed to accommodate the displacement incompatibility between the frame and precast floor units shown in Figure 3-25b. But, as shown in Figure 3-25a, it also allows the floor slab adjacent to the slotted section to be cast with a smaller depth than the concrete top-hinge.

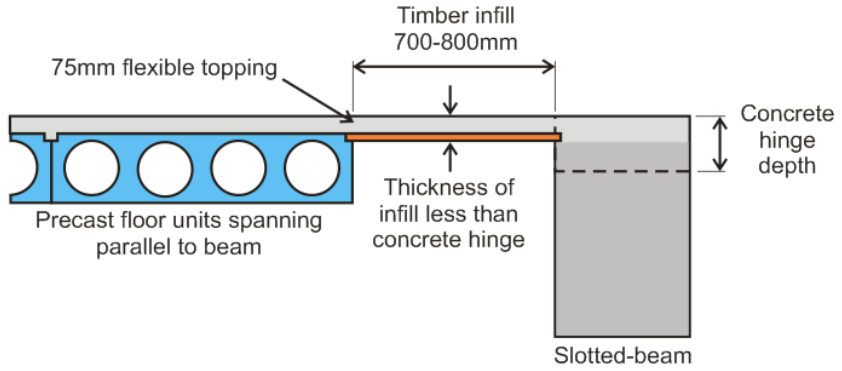

(a) Timber infill detail

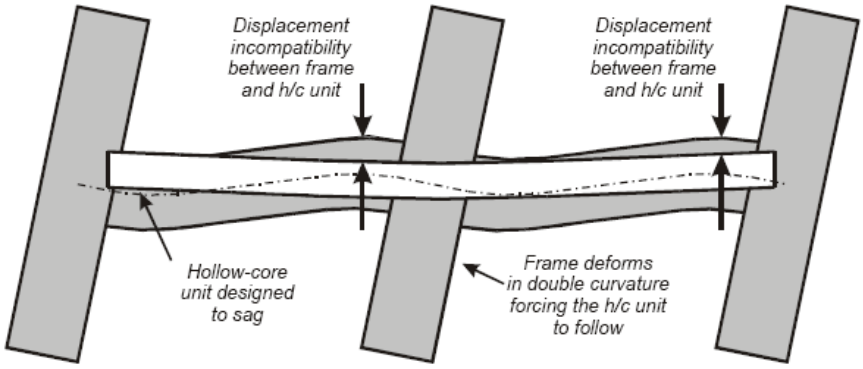

(b) Displacement incompatibility between frame and precast floor units

Figure 3-25: Floor slab-to-beam connection detail for precast floor units spanning parallel to slotted-beam as proposed by Matthews et al. (2003)

When precast floor units span directly onto the slotted-beam, the slab can be cast thinner than the concrete top-hinge using timber infills as shown in Figure 3-26. If the column is narrow, the timber infill can span across the width of the column. However if the column is wide, a precast floor unit or transverse beam spanning onto the column may be required.

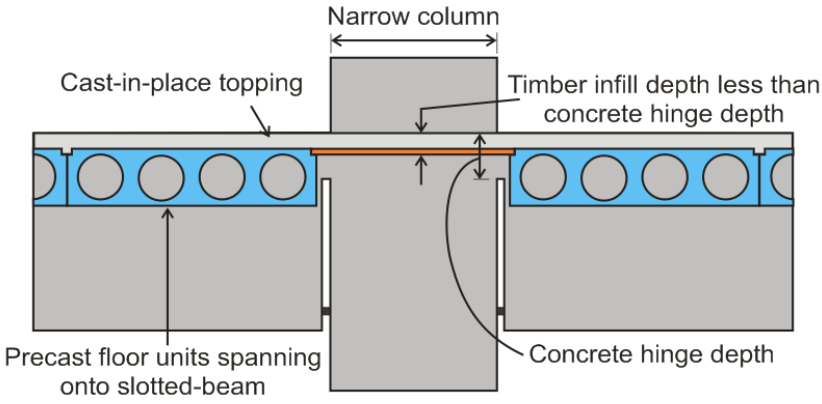

(a) Detail for narrow columns

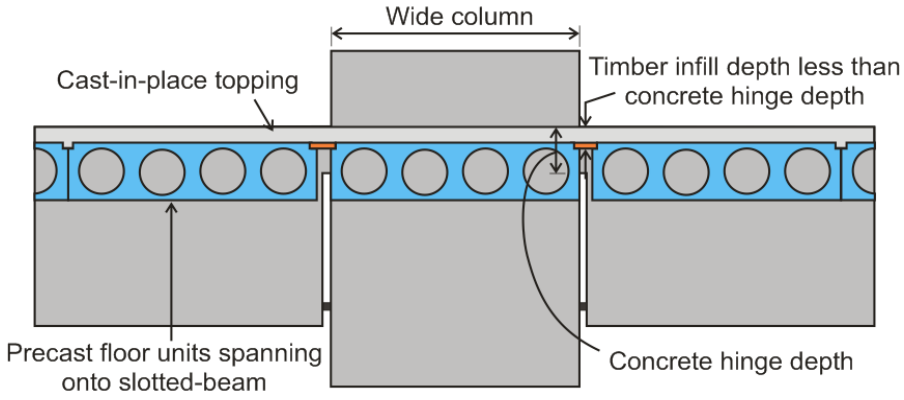

(b) Detail for wide columns

Figure 3-26: Proposed floor slab-to-beam connection details for precast floor units spanning onto slotted-beams

3.8.2 Effective Flange Contributions to Connection Strength

For conventional reinforced concrete beams, floor slab concrete and reinforcement can increase the moment capacity of plastic hinges. This strength enhancement is usually computed by assuming an effective flange width which contributes to the section strength. NZS3101:2006 has conservative provisions for this width for calculating the nominal moment capacity, which were derived from experimental tests carried out by Cheung, Park and Paulay (1991).

This flange effect can also significantly increase overstrength beam moments. This is undesirable when it comes to designing adjacent columns which must have reserve capacity above these overstrength actions. The strength increase can be particularly large for negative moments where slab reinforcement contributes in tension, which can be further exacerbated by the elongation of plastic hinges. Tests by Lau, Fenwick and Davidson (2007) revealed a strength increase of up to 80% with the addition of floor units. Current NZS3101:2006

provisions for overstrength effective widths are only tentative, but recent work by Peng (2009) has shown these to be greatly unconservative for interior joints. The test carried out by Peng attained overstrength column shear demands 1.76 to 2 times the column shear resulting from nominal beam strengths without flange effects. NZS3101:2006 however only gave overstrength shear demands 1.55 to 1.73 times the shear resulting from nominal beam strengths. Thus monolithic beam overstrength moments can become particularly demanding when effective flange contributions from floor units are considered.

This is not so for slotted-beams, which have limited effective flange contributions due deformations being concentrated at the bottom of the beam and away from the floor slab. Because yielding of bottom reinforcement governs the strength of a slotted-beam, forces at the floor slab level have little influence on the strength of the connection. In Section 6.2.11, a parametric analysis was carried out investigating the effect of including slab flexural contributions by assuming increasing effective flange widths. It was shown that contributions from slab reinforcement and concrete in compression had negligible effect on nominal yield moments but increased post-yield overstrength moments. The extent of this effect however was very much dependent on the activated slab width assumed. From the test of specimen SB3, the overstrength column shear demand was 1.6 times the shear resulting from nominal beam strengths at 3.5% drift. This is significantly less than that attained by Peng (2009) for conventional monolithic beams.

The effective flange width that should be adopted for slotted-beams was not investigated in-depth in this project. The experimental test on specimen SB3 and tests on conventional beams by Peng revealed that the effective width is further dependent on the torsional stiffness of any transverse beam or floor unit framing into the column. Further research is required to determine appropriate flange widths for different configurations – that is, interior and exterior joints, with and without transverse beams, etc.

3.8.3 Induced Beam Torsion from Floor Gravity Loads

Figure 3-27 is a cross-section through a generic frame, showing one-way floor slabs seated on slotted-beams framing into the page. The floor slabs will induce a downwards shear, V_{slab}^{*}, and a continuity moment, M_{slab}^{*}, where they are seated on the beam. For the beam supporting floor units only on one side, these actions will translate into a torsional demand. Because slotted beams have a reduced concrete cross-sectional area, this torsion must be resisted primarily by a force couple in the diagonal steel hangers.

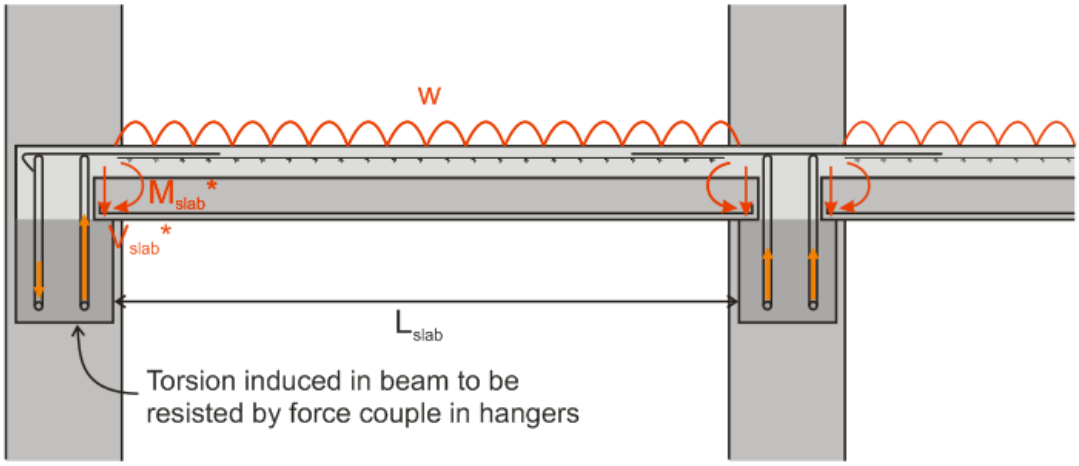

Figure 3-27: Induced beam torsion from floor gravity loads

The critical load case is clearly not the static gravity load case shown in Figure 3-27, but will rather be that caused by a combination of gravity and earthquake loads. In tests carried out on monolithic beams designed according to NZS3101, combined earthquake and gravity torsional actions have been observed to result in significant beam twist as plastic hinge zones deteriorate and torsional stiffness is lost (Matthews, 2004; Lindsay, 2004). This consequently results in flexural strength degradation due to buckling of beam longitudinal reinforcement. For slotted-beams, it can be expected that this strength degradation will be significantly more severe. Any lateral eccentricity caused by beam twist may initiate early buckling of bottom reinforcement and subsequent bar fractures. It is therefore imperative that this beam twist is properly restrained in slotted-beams.

Figure 3-28 shows the four load cases that can occur under biaxial earthquake actions. V_{Eo}^{*} is the earthquake beam shear force demand, which induces tension in the hangers for drifts into the page, and compression for drifts out of the page. V_{slab}^{*} is the slab gravity shear which acts downwards independent of the earthquake direction; and $M_{n,slab}$ is the fixed-end moment demand applied to the beam from the slab, which is dependent on the transverse earthquake direction. Because it is highly likely that starter bars will yield, the nominal moment capacity has been adopted as the applied moment value. Note that vertical earthquake accelerations have not been considered here, but can further exacerbate torsional demands.

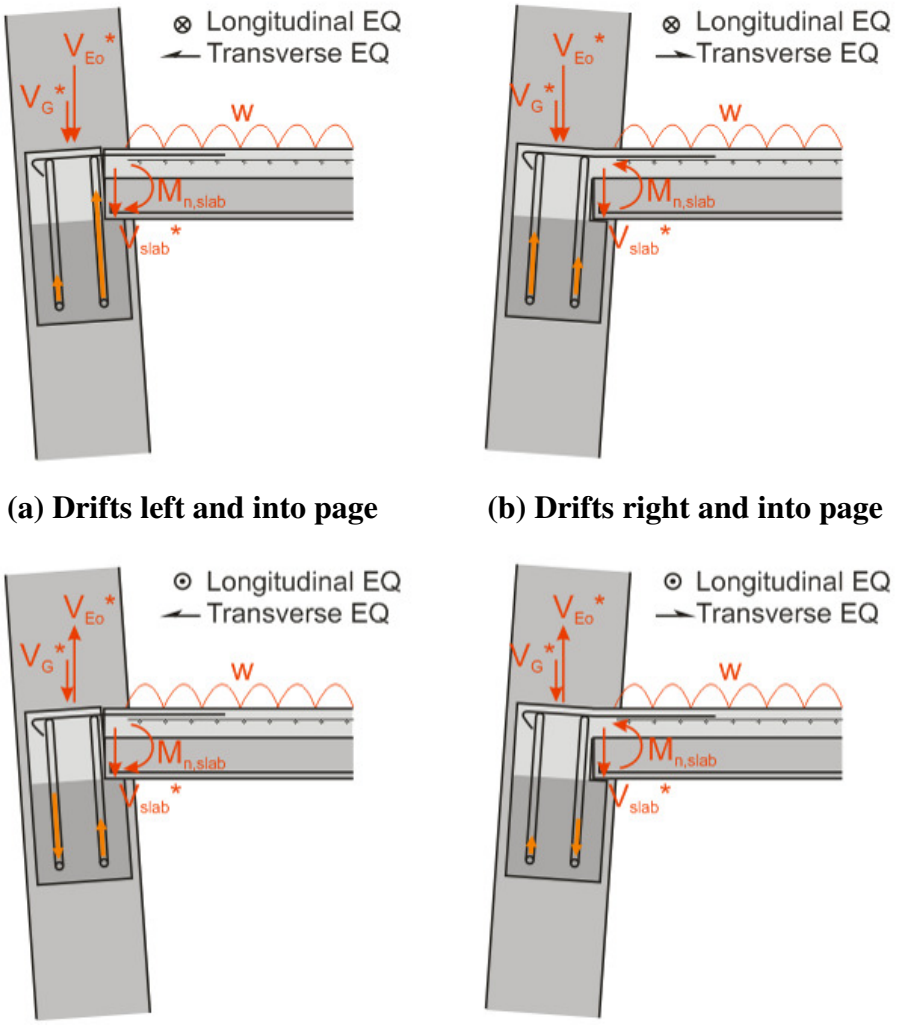

(a) Drifts left and into page **(b) Drifts right and into page**

(c) Drifts left and out of page **(d) Drifts right and out of page**

Figure 3-28: Induced beam torsion from floor gravity and biaxial earthquake actions

From vector summation, Figure 3-28a gives the worst case tension in the inner diagonal hanger, while Figure 3-28c gives the worst case compression on the outer diagonal hanger. These are the critical cases that shall be considered herein.

Because the end moment from the slab is the nominal capacity, the torsional demand on the beam can be reduced by minimising $M_{n,slab}$. Continuity moments are not relied upon for the gravity capacity of floor slabs, so minimising $M_{n,slab}$ presents no adverse effects. Figure 3-29 illustrates a seating detail, first proposed by Matthews et al. (2003) to accommodate relative displacements between precast floors and beams, which can be used to reduce the moment provided by the seated slab.

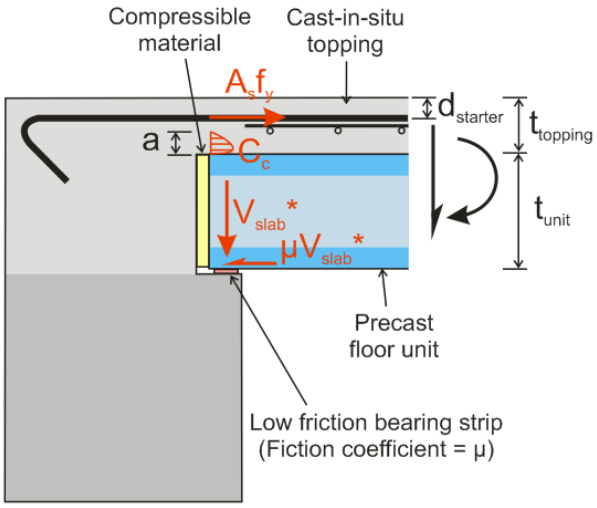

Figure 3-29: Seating detail to reduce $M_{n,slab}$ (Matthews et al., 2003)

The compressible backing material and low friction bearing strip (McDowell bearing strip for example) allows the bottom of the floor unit to slide in and out as the beam rotates relative to the slab, such that deformations are accommodated via closing and opening of the compressible gap. The compressible backing material therefore effectively reduces the section depth, such that $M_{n,slab}$ is reduced. For downward rotations of the slab relative to the beam, it can be calculated as:

$$M_{n,slab} = A_s f_y (t_{topping} - d_{starter} - a/2) + \mu V_{slab}^{*} (t_{unit} + a/2)$$

$$\text{Where:} \quad a = \frac{A_s f_y - \mu V_{slab}^{*}}{\alpha f'_c b} \qquad \text{...(3-24)}$$

The nominal moment is dependent on the slab span length (which effects V_{slab}^{*}) and the bearing strip friction coefficient, μ. Friction coefficients between 0.5 and 0.7 are normally specified by suppliers, however because friction is usually considered for resistance, it is likely these are lower characteristic values. This is un-conservative in this case as the co-efficient is being used to estimate the torsional moment demand on the beam. Further research into actual friction coefficients is therefore required.

Given the critical torsional actions in Figure 3-30 and adopting two diagonal hangers, the design forces for each hanger can be calculated from moment equilibrium to be:

$$F_{h1}^{*} = \frac{V_{Eo-G}^{*}(x_2 - b/2) + V_{slab}^{*}(b - x_2) + M_{n,slab}}{(x_2 - x_1)}$$

$$F_{h2}^{*} = \frac{V_{G+Eo}^{*}(b/2 - x_1) + V_{slab}^{*}(b - x_1) + M_{n,slab}}{(x_2 - x_1)} \quad \text{...(3-25)}$$

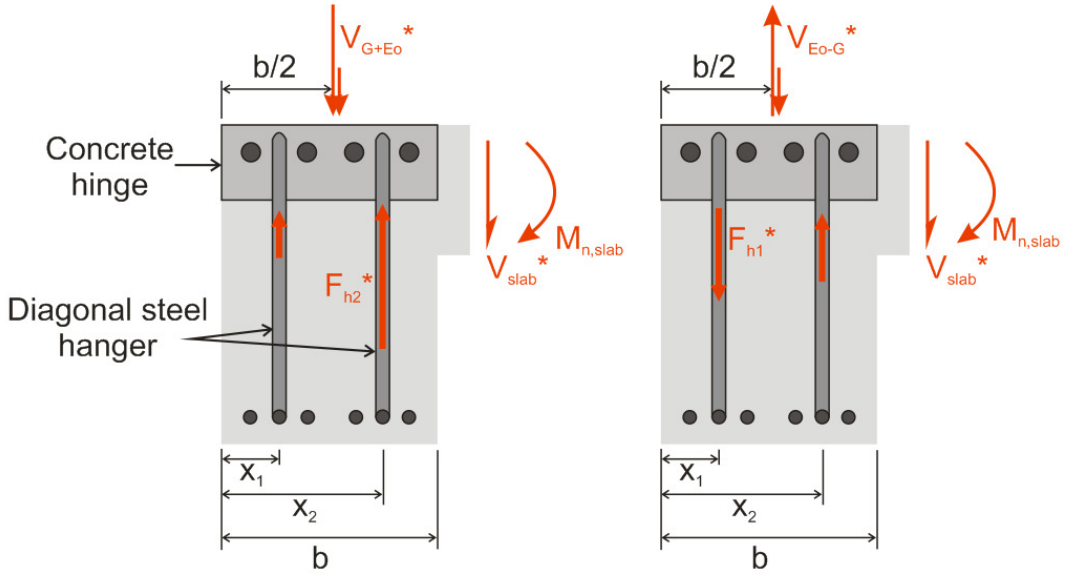

(a) Maximum hanger tension **(b) Maximum hanger compression**

Figure 3-30: Torsional design actions for two diagonal hangers

To help quantify the magnitude of these forces, Table 3-2 summarises the critical hanger design actions for first floor beams in the five-storey prototype frame building given in Section 5.1.1. Beam dimensions of 750 mm × 500 mm, V_{Eo}^{*} of 235 kN, hanger spacing (x_2-x_1) of 260 mm, μ of 1.0 and a reduced combined gravity floor load ($G+\psi_c Q$) of 9.08 kPa have been assumed. To show the effect of the floor span length, actions for a variable length of support slab, L_{slab}, are given.

Table 3-2: Critical torsional design actions for first floor beams in five-storey prototype frame building, using two diagonal hangers

L_{slab} (m)	V_{slab}^{*} (kN)	$M_{n,slab}$ (kNm)	Max compression F_{h1}^{*} (kN)	Max tension F_{h2}^{*} (kN)
5.5	62.4	20.6	214	299
6.5	73.8	22.8	228	324
7.5	85.1	25.0	242	349
8.5	96.5	27.2	255	374
9.5	107.8	29.4	269	399
10.5	119.2	31.5	283	424

The maximum practical bar size currently available in New Zealand is 32 mm diameter deformed bar with a lower characteristic yield strength of 500 MPa (HD32 Grade 500). A

single HD32 hanger inclined at 45° has a design shear strength (vertical component) of 284 kN. Therefore the maximum practical bar size available in New Zealand is sufficient to resist the maximum compression force expected in the outer hanger, but not the maximum tension force expected in the inner hanger. So unless an HD40 hanger is used, which has a design shear strength of 444 kN, a third hanger must be included.

Figure 3-31 illustrates a reinforcement detail utilising a third hanger in such a way as to maximise the lever arm resisting torsional actions. The third hanger is located in the ledge supporting the slab and carries on up into the joint over a length of floor which is constructed using a timber infill. For further information on this detail, refer to tested specimen SB3 in CHAPTER 5, which tested this detail.

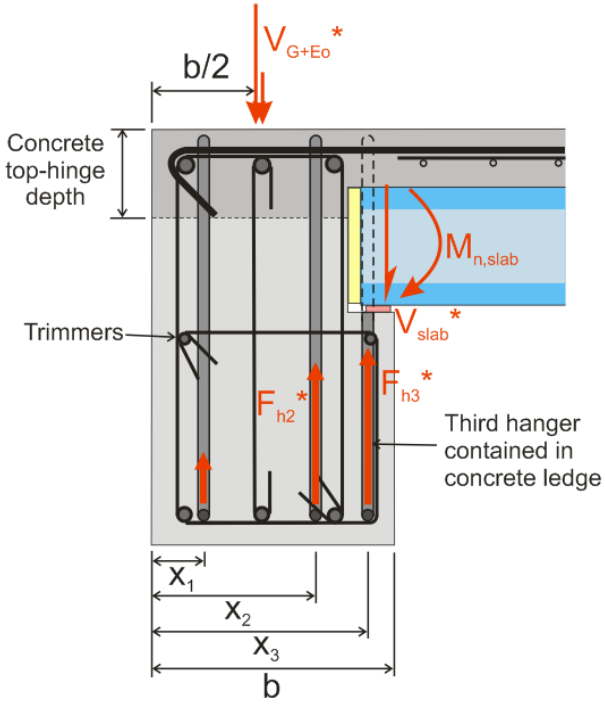

Figure 3-31: Reinforcement detail adopting three diagonal hangers to resist torsion

The system with three hangers is statically in-determinant and therefore provides an extra degree of redundancy. Hanger forces can be computed by implementing the model in Figure 3-32 into a spreadsheet or static analysis software. It conservatively assumes the torsional stiffness of the slotted-beam is provided solely from diagonal reinforcement. In reality, concrete friction across the top-hinge section will provide some rigid stiffness, but once the friction capacity is exceeded, this stiffness will be minimal. The stiffness provided from the hangers can be computed from the vertical component of their axial stiffness, AE/L. From strain gauge test data, $2L_{sp}$ appears to be a reasonable assumption for the stiffness length parameter L. L_{sp} is the yield penetration length of the diagonal hanger, which is commonly

adopted as 0.022 times the bar's yield strength (in MPa) times the bar's diameter (in mm). Alternatively, hanger actions can be estimated using Equation 3-25 by lumping the two inner hangers together and assuming equal force in both hangers. This assumption implies yielding of the outermost hanger is allowed.

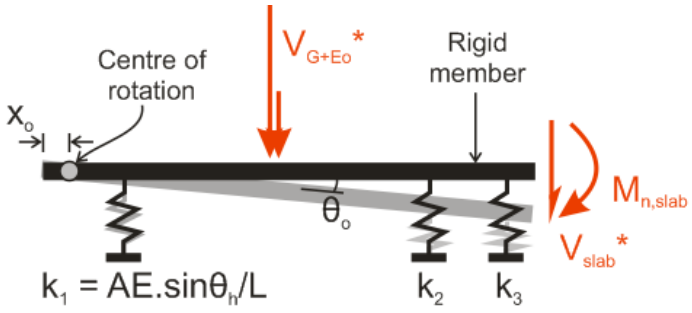

Figure 3-32: Schematic representation of slotted-beam with three hangers

Table 3-3 summarises tensile hanger design actions for the first floor beams of the same prototype frame used for Table 3-2, but for beams using three hangers. 28 mm diameter, Grade 500 deformed bars (HD28) were assumed for the internal hangers, whilst an HD32 bar was assumed for the outer hanger. x_1, x_2 and x_3, as defined in Figure 3-31, were taken as 120 mm, 350 mm and 450 mm respectively. V_{Eo}^*, V_{slab}^* and $M_{n,slab}$ are the same as for Table 3-2.

Table 3-3: Critical torsional design actions for first floor beams in five-storey prototype frame building, using three diagonal hangers

L_{slab} (m)	θ_o (rad)	x_o (mm)	Max tension F_{h2}^* (kN)	Max tension F_{h3}^* (kN)
5.5	0.0024	-4.2	119	153
6.5	0.0029	40.2	127	167
7.5	0.0034	71.3	134	182
8.5	0.0039	94.3	141	196
9.5	0.0044	112.0	149	211
10.5	0.0049	126.0	156	226

Table 3-3 shows that the inclusion of a third hanger allows all reasonable floor spans to be supported using more practical bar sizes. HD28 bars inclined at 45°, which have a design shear strength of 218 kN, can be used for the innermost hanger; and for spans less than 6.5m, HD25 bars (design shear strength of 174 kN) can be used.

It has been shown that it is possible to resist torsional forces acting on a slotted-beam using three diagonal shear hangers. The next concern is whether the elastic twist of the beam will induce enough eccentricity within the bottom reinforcement to initiate early buckling. The

left-hand-side beam of tested specimen SB3 exhibited beam twists between 0.005 and 0.008 radians without buckling. However, this test was uni-directional and in the plane of the frame. It is recommended that full biaxial testing is carried out to properly check the worst case torsional demands on a slotted-beam.

3.8.4 Seating Widths for Floor Units

To reduce torsional demands on slotted-beams and accommodate rotation of floor units relative to supporting beams, the seating detail proposed by Matthews et al. (2003) in Figure 3-33 is recommended for slotted-beams. This detail effectively behaves as a slotted connection, where a low friction bearing strip allows rotations to be accommodated via opening and closing of a gap created by a compressible backer. A minimum seating width must be provided to allow the unit to slide in without contacting the beam and to slide out without moving off the support. Other factors such as shrinkage, construction tolerances and elongation of seismic beams spanning parallel to the floor units must also be considered in the seating width provided.

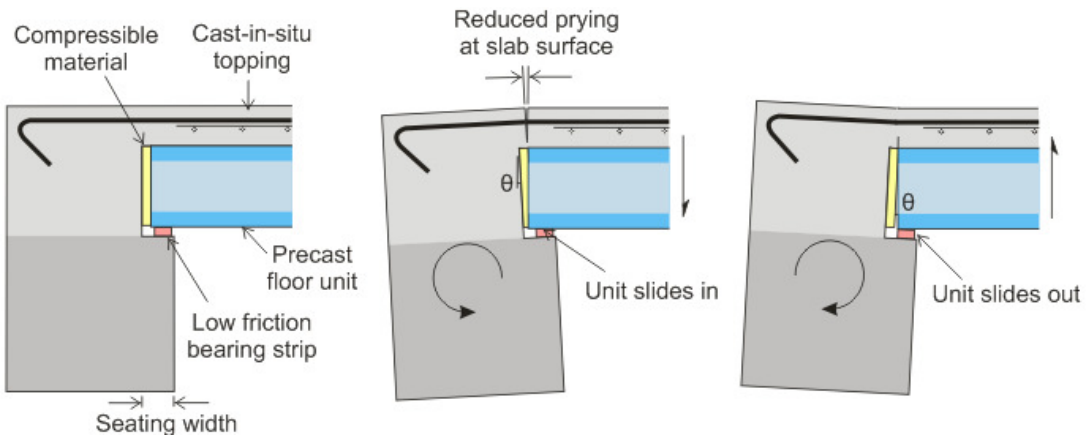

Figure 3-33: Recommended precast floor unit seating detail to reduce prying at slab surface (Matthews et al., 2003)

Figure 3-34 illustrates the minimum seating width required by NZS3101:2006 for conventional monolithic beams of 75 mm plus construction tolerances. Allowing for 17 mm tolerance, this gives a required seating width of 92 mm. In some cases, this value underestimates the actual required seating width.

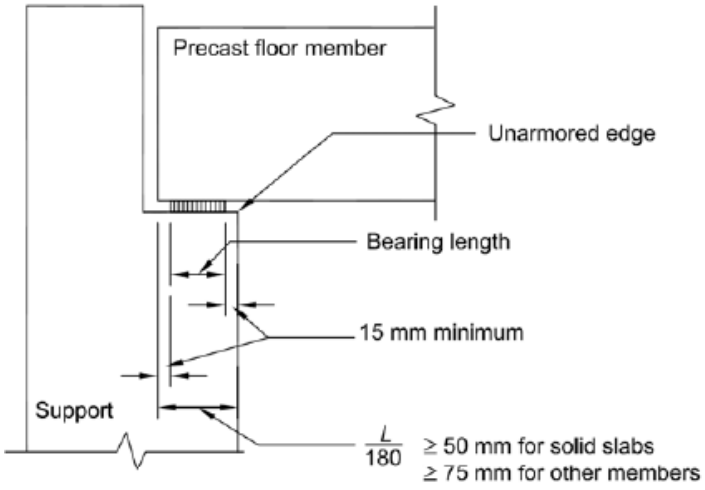

Figure 3-34: Current NZS3101:2006 seating width requirements

Recently, the Department of Housing and Building released a draft publication (2009) with a more detailed seating width estimation, which highlighted shortcomings in the current NZS3101 provisions for conventional RC beams. The methodology is summarised below.

The contributions to seating width that must be allowed for are:

1) Residual seating after an extreme earthquake event of 20 mm (for hollow-core, flat slab and rib precast units)

2) Reduction in seating width due to spalling of the support or unit of 20 mm

3) Allowances for floor creep and shrinkage at each end of 0.5 mm/m of floor span

4) Total construction tolerance of 17 mm as per CAE precast guidelines (1991)

5) Beam elongation at the mid-depth of the beam – an upper-bound value estimated from experimental testing to be:

$$\delta_l = \theta_b h_b < 0.04 h_b \qquad \text{...(3-26)}$$

Where θ_b is the expected beam rotation and h_b is the beam depth.

6) Geometric displacement of the floor relative to the support of:

$$\delta_g = \theta_b \left(\frac{h_b}{2} - t_{slab} \right) \qquad \text{...(3-27)}$$

Where t_{slab} is the total depth of the floor slab.

For a 300 mm thick, 10 m long slab and 1000 mm deep beam with expected beam rotations of 3.5%, the method estimates a required seating width of 104 mm, which is higher than that currently required by NZS3101:2006.

Fortunately, because slotted-beams exhibit negligible beam elongation, seating width requirements for floors spanning parallel to slotted-beams can be reduced. The same methodology above can be used, with the omission of Step 5, and by modifying the geometric contribution in Step 6 to account for rotation about the concrete top-hinge instead of the beam centreline.

Figure 3-35a illustrates the geometric elongation which occurs during gap-opening rotations of the slotted-beam running parallel to the span of the floor units. This movement causes the floor unit to slide off the support a distance δ_{geo}, which can be calculated as:

$$\delta_{geo} = \theta_b \left(t_{slab} - c \right) \qquad ...(3\text{-}28)$$

The seating width requirement for this contribution can be conservatively estimated from the above expression by taking the neutral axis depth, c, to be zero. Note that the geometric movement of the slab will be less than the elongation observed at the beam centreline, δ_{el}^{+}, and is only dependent on the depth of the slab, t_{slab}.

Conversely, Figure 3-35b illustrates the geometric contraction that occurs during gap-closing rotations. This movement causes the floor unit to slide into the support, squashing the compressible backer a distance t_{backer}. This displacement can be calculated using the same expression used to calculate the geometric elongation in Equation 3-28. The thickness of the compressible backer and seating width required for this movement can then be conservatively estimated by adopting the depth of the top longitudinal reinforcement, d', as the neutral axis depth, c, as in Equation 3-29.

$$t_{bac\,\mathrm{ker}} = \theta_b \left(t_{slab} - d' \right) \qquad ...(3\text{-}29)$$

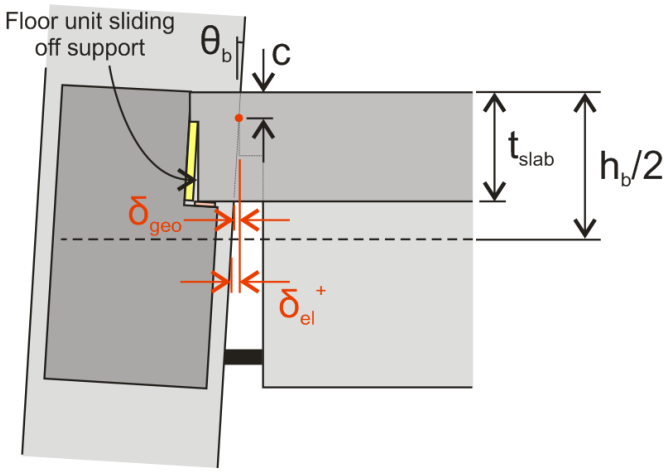

(a) Geometric elongation during gap-opening rotations

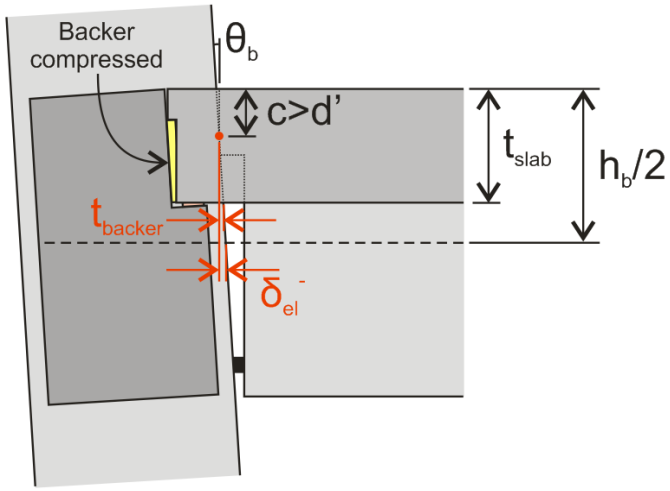

(b) Geometric contraction during gap-closing rotations

Figure 3-35: Seating width requirements for movement of slab relative to support

So using the Department of Housing and Building method modified for slotted-beams, for a 300 mm thick, 10 m long slab and 1000 mm deep slotted-beam with expected beam rotations of 3.5%, the seating width required can be estimated to be 81 mm (See calculation below). This is significantly less than that required for conventional monolithic beams using the Department of Housing and Building methodology and NZS3101:2006. Note that this seating width includes the compressible backer thickness of 8.4 mm, so the actual seated length of the floor unit is 73 mm.

Residual seating =	20 mm
Spalling of unit/ledge =	20 mm
Shrinkage/creep = 0.5 mm/m × 10 m floor span =	5 mm
Construction tolerance =	17 mm
Geometric movement off support = 0.035 rad × 300 mm =	10.5 mm
Compressible backer thickness = 0.035 rad × (300-60) mm =	8.4 mm
Required seating width for slotted-beam =	**81 mm**

Tie reinforcement is required to ensure the corbel does not crack and spall off. To allow this tie reinforcement to be placed, additional longitudinal bars (trimmers) are required as shown in Figure 3-36. For slotted-beams, these bars should be curtailed before passing through the slot, to prevent them from affecting the moment capacity and behaviour of the slotted-beam.

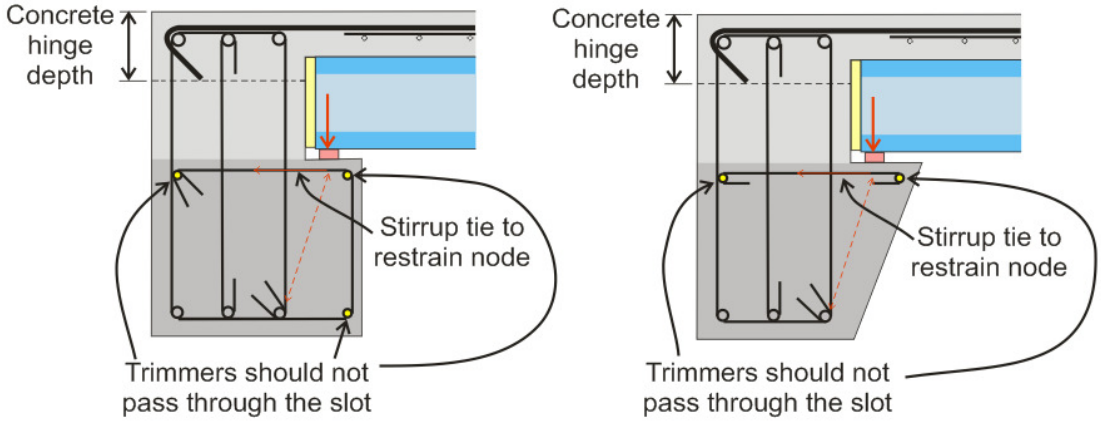

Figure 3-36: Recommended details for seating reinforcement

3.9 Design Example

Table 3-4 provides a design example for a slotted reinforced concrete beam connection. To illustrate the difference in design compared to a monolithic beam, a conventional design in accordance with NZS3101:2006 is also given side-by-side. The design is for the highlighted beam connection in the portion of a generic frame illustrated in Figure 3-37 below. Also shown are the earthquake actions as determined from the seismic design. The beam dimensions are 700 mm by 400 mm with an effective beam depth of 630 mm, and the column dimensions are 950 mm by 600 mm. The concrete strength is 40 MPa. For simplicity, only seismic actions have been considered and gravity actions have been ignored in this particular example.

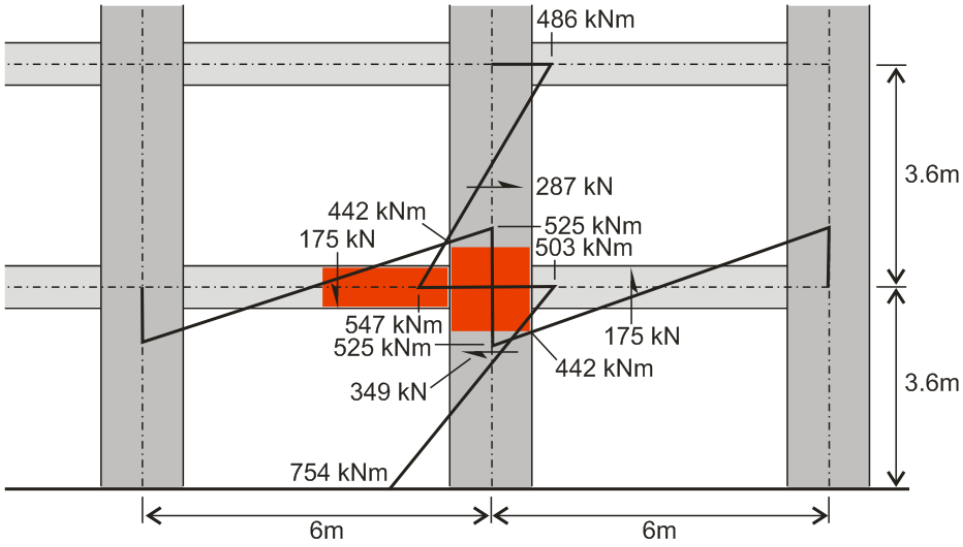

Figure 3-37: Seismic design actions from Direct Displacement-based Design

Table 3-4: Design example comparing a slotted-beam design versus a conventional reinforced concrete beam design according to NZS3101:2006
(Note: CL X.X references refer to clauses in NZS3101:2006 and § X.X references refer to relevant sections in this thesis)

RC beam according to NZS3101:2006	Slotted-beam
Design for flexure (CL 7.4):	***Design for flexure (§ 3.1.1):***
For bottom reinforcement try 3-D32 & 1-D28, A_s=3028 mm^2	For bottom reinforcement try 3-D32 & 1-D28, A_s=3028 mm^2
$\phi M_n = \phi A_s f_y (d - a/2) \geq M^*$ $= 0.85 \times 3028 \times 300(630 - 67/2)$ $= 461\text{kNm}$ $\geq M^* = 442\,\text{kNm} \quad \rightarrow \text{ok}$	$\phi M_n^+ = \phi A_s f_y (d - a/2) \geq M^*$ $= 0.85 \times 3028 \times 300(630 - 67/2)$ $= 461\text{kNm}$ $\geq M^* = 442\,\text{kNm} \quad \rightarrow \text{ok}$
The negative moment demand is the same as the positive moment demand, so adopt the same quantity of top reinforcement.	The negative moment capacity for a slotted-beam is not the same as the positive moment capacity and should be checked separately.

	$\phi M_n^- = \phi A_s f_y (d - d') \geq M^*$ $= 0.85 \times 3028 \times 300(630 - 70)$ $= 432\text{kNm}$ $< M^* = 442\,\text{kNm}$, but within 5% so ok Top reinforcement should be sized to limit cracking and elongation through the top-hinge. The limit $A_s' f_y' / A_s f_y > 2.0$ is suggested as a reasonable guide (§ 3.1.2). Trying the maximum practical solution of 4-HD32, $\frac{A_s' f_y'}{A_s f_y} = \frac{3217 \times 500}{3028 \times 300} = 1.8 \quad \rightarrow \text{ok}$
Reinforcement ratio checks (CL 9.4.3.3-4): $\rho_{\max} = \frac{f_c'+10}{6 f_y} \leq 0.025$ $= \frac{40+10}{6 \times 300} = 0.028 > 0.025$ $= 0.025$ $\rho_{\min} = \frac{\sqrt{f_c'}}{4 f_y} = \frac{\sqrt{40}}{4 \times 300} = 0.0053$	*Reinforcement ratio checks (§ 3.1.1):* The maximum reinforcement ratio from NZS3101:2006 still applies to slotted-beams: $\rho_{\max} = \frac{f_c'+10}{6 f_y} \leq 0.025$ $= \frac{40+10}{6 \times 300} = 0.028 > 0.025$ $= 0.025$ The minimum reinforcement ratio however is different and specified based upon low cycle fatigue concerns. A value between 0.006 and 0.008 is currently suggested: $\rho_{\min} = 0.007$ $\rho = \frac{A_s}{bd} = \frac{3028}{400 \times 630} = 0.012$ $> \rho_{\min}\ \&\ < \rho_{\max} \quad \rightarrow \text{ok}$

$$\rho = \rho' = \frac{A_s}{bd} = \frac{3028}{400 \times 630} = 0.012$$
$$> \rho_{\min} \;\&\; < \rho_{\max} \quad \rightarrow \text{ok}$$

Anchorage of longitudinal reinforcement in interior columns (CL 9.4.3.5.2):

For both top and bottom reinforcement:

$$\frac{d_b}{h_c} \le 3.3 \alpha_f \alpha_d \frac{\sqrt{f_c'}}{\alpha_o f_y}$$
$$\frac{d_b}{h_c} = \frac{32}{950} = \frac{1}{30}$$
$$\le 3.3 \times 1 \times 1 \times \frac{\sqrt{40}}{1.25 \times 300} = \frac{1}{18} \quad \rightarrow \text{ok}$$

Because flexural behaviour is governed by yielding of bottom reinforcement, these checks do not apply to top reinforcement.

Anchorage of longitudinal reinforcement in interior columns (§ 3.6):

For bottom reinforcement:

Adopting the expression from Equation 3-17,

$$\frac{d_b}{h_c'} \le 2.66 \alpha_f \alpha_d \frac{\sqrt{f'_c}}{\alpha_o f_y}$$
$$\frac{d_b}{h_c'} = \frac{32}{750} = \frac{1}{23.4}$$
$$\le 2.66 \times 1 \times 1 \times \frac{\sqrt{40}}{1.3 \times 300} = \frac{1}{23.2} \quad \rightarrow \text{ok}$$

$$h_c' = \min(0.8 h_c, h_c - 2c_o - 2s_j)$$
$$= \min(0.8 \times 950, 950 - 2 \times 60 - 2 \times 40)$$
$$= 750\,\text{mm}$$

Because testing revealed greater strain hardening in slotted-beams, a higher material overstrength term of α_o=1.3 has been assumed (§ 3.6).

For top reinforcement:

For top bars, CL 9.4.3.5.2 can be used. In addition, because no strain hardening is expected, α_o can be taken as 1.1 instead of 1.4 (for Grade 500 reinforcement):

$$\frac{d_b}{h_c} \le 3.3\alpha_f \alpha_d \frac{\sqrt{f_c'}}{\alpha_o f_y}$$

$$\frac{d_b}{h_c} = \frac{32}{950} = \frac{1}{30} \le 3.3\times 1\times 1\times \frac{\sqrt{40}}{1.1\times 500} = \frac{1}{26}$$

Section design unique to Slotted-beams:

Concrete top-hinge depth, d_c:

This is usually taken less than 0.25*d* to limit prying at the floor level, but greater than 0.2*d* to allow sufficient room for diagonal reinforcement (§ 6.2.6).

$$\therefore d_c = 0.25d = 0.25\times 630 \approx 160\,\text{mm}$$

Slot width, L_{slot}:

This should be wide enough to accommodate maximum expected rotations without contact of the beam soffit and the column face. Assuming a maximum rotation of 0.04 rad,

$$L_{slot} = \theta(h_b - d') = 0.04(700 - 70) \approx 25\,\text{mm}$$

Unbonded length, (L_{ub}):

The unbonded length should be as long as possible to improve low cycle fatigue resistance, but should terminate before the bottom bend of diagonal shear hangers (§ 3.2 and § 3.5). This will generally be between 0.9(*d-d'*) and (*d-d'*) for a 45° hanger.

$$\therefore L_{ub} = 0.9(d - d') = 0.9(630 - 70) \approx 500\,\text{mm}$$

Anti-buckling and confinement:	***Anti-buckling and confinement (§ 3.4):***
PPHZ region requiring special detailing:	*Two regions (L_{2hb} and L_{ub}) requiring special detailing:*
Potential plastic hinge zone from CL 9.4.2a: $L_{PPHZ} = 2h_b = 1400\,\text{mm}$	Because of the top-hinge mechanism, a slotted-beam does not form a plastic hinge zone in the conventional sense. However, due to yield penetration of bottom longitudinal reinforcement into the beam beyond the unbonded length, special detailing is still required within $2h_b$ of the column face similar to CL 9.4.2a in NZS3101:2006. $\therefore L_{2hb} = 2h_b = 1400\,\text{mm}$ In addition, due to a greater likelihood of buckling along the unbonded length, special detailing beyond the current code is also required in this region. $\therefore L_{ub} = 500\,\text{mm}$ as calculated earlier
Spacing within PPHZ (CL 9.4.5d):	*Spacing within L_{2hb}:* In this region, adopt CL 9.4.5d from NZS3101:2006 as described in § 3.4:
$s \le \min(d/4, 6d_b) = \min(630/4, 6\times 28)$ $= 150\,\text{mm}$	$s \le \min(d/4, 6d_b) = \min(630/4, 6\times 28)$ $= 150\,\text{mm}$ *Spacing within L_{ub}:* Along the unbonded length, the stirrup spacing should be reduced further from code provisions. A spacing of $4d_b$ in conjunction with steel debonding tubes was found to

	prevent buckling during testing. $\therefore s \le 4d_b = 112$ mm, take $s = 100$ mm
Spacing outside PPHZ (CL 9.3.9.4.12): $s \le \min(0.5d, 600\,\text{mm}) = \min(0.5\times 630, 600) = 300\,\text{mm}$	*Spacing outside L_{2hb} (CL 9.3.9.4.12):* $s \le \min(0.5d, 600\,\text{mm}) = \min(0.5\times 630, 600) = 300\,\text{mm}$ Outside the unbonded length, the beam is essentially the same as a conventional beam. Thus existing code provisions can be used.
Area of tie for anti-buckling (CL 9.4.5b): The current code provision requires that the capacity of the tension tie should be able to resist 1/16th of the yield force of the group of bars it restrains at $6d_b$ centres: $A_{te} = \frac{\Sigma A_b f_y}{96 f_{yt}} \frac{s}{d_b} = \frac{804\times 300\times 150}{96\times 300\times 32} = 39\,\text{mm}^2$	*Area of tie for anti-buckling:* Outside the unbonded length, CL 9.4.5b from NZS3101:2006 can be used: $A_{te} = \frac{\Sigma A_b f_y}{96 f_{yt}} \frac{s}{d_b} = \frac{804\times 300\times 150}{96\times 300\times 32} = 39\,\text{mm}^2$ Because buckling is more likely within the unbonded length, the tie area may need to be increased in this region. Until further research is conducted, it is suggested that ties be designed to resist 1/16th of the yield force of the group of bars it retrains at $4d_b$ centres, instead of $6d_b$ centres: $A_{te} = \frac{\Sigma A_b f_y}{16 f_{yt}} \frac{s}{4d_b} = \frac{804\times 300\times 100}{16\times 300\times 112} = 45\,\text{mm}^2$
All bars must be restrained with its own separate tie (CL 9.4.5).	All bars should be restrained with its own separate tie (CL 9.4.5).

Adopt 4-legs R10 stirrups,

$A_{te} = 78.5\,\text{mm}^2 \geq 39\,\text{mm}^2 \quad \rightarrow \text{ok}$

Overstrength Actions:

Overstrength beam moment at column face:

$$M_o = \frac{\lambda_o}{\phi}(\phi M_n) = \frac{1.25}{0.85} \times 461 = 678 \text{ kNm}$$

Flexural overstrength factor:

$$\phi_o = \frac{\Sigma M_o}{\Sigma M_E} = \frac{678 + 678}{442 + 442} = 1.53$$

Overstrength beam shear:

$$V_{Eo}{}^* = \frac{M_o{}^+ + M_o{}^-}{L_n} = \frac{678 + 678}{5.05} = 269\,\text{kN}$$

Adopt 4-legs R10 stirrups,

$A_{te} = 78.5\,\text{mm}^2 \geq 45\,\text{mm}^2 \quad \rightarrow \text{ok}$

Overstrength Actions:

Overstrength beam moments at column face:

$$M_o{}^+ = \frac{\lambda_o}{\phi}(\phi M_n{}^+) = \frac{1.3}{0.85} \times 461 = 705\,\text{kNm}$$

$$M_o{}^- = \frac{\lambda_o}{\phi}(\phi M_n{}^-) = \frac{1.4}{0.85} \times 432 = 712\,\text{kNm}$$

Note: Experimental tests revealed higher overstrength factors on the order of 1.3 and 1.4 for positive and negative moments respectively (See Table 4-6 and Figure 5-37b) and hence these values have been adopted in this example.

Flexural overstrength factor:

$$\phi_o = \frac{\Sigma M_o}{\Sigma M_E} = \frac{705 + 712}{442 + 442} = 1.60$$

Overstrength beam shear:

$$V_{Eo}{}^* = \frac{M_o{}^+ + M_o{}^-}{L_n} = \frac{705 + 712}{5.05} = 281\,\text{kN}$$

Note: Because shear in a monolithic beam is resisted via diagonal compression fields in the web, CL 9.3.9.3.1 allows the beam shear force demand to be taken as that a distance *d* out from the column face. This is not the case for slotted beams because shear is carried into the joint via diagonal shear reinforcement. Therefore the shear force demand for a

slotted-beam should be taken as that at the column face (§ 3.2).

Design for Shear:

Maximum nominal shear stress (CL 7.5.2):

$$v_{\max} = \min(0.2 f_c', 8\,\text{MPa}) = 8\,\text{MPa}$$

$$v_n = \frac{V^*}{\phi b_w d} = \frac{269000}{1 \times 400 \times 630} = 1.1\,\text{MPa}$$
$$< v_{\max} \quad \rightarrow \text{ok}$$

Design for shear in PPHZ:

The code assumes no concrete contribution in the PPHZ (CL 9.4.4.1.3a).

$$\therefore V_s \geq \frac{V^*}{\phi} - V_c = \frac{269}{1} - 0 = 269\,\text{kN}$$

Shear reinforcement is conventionally provided in the form of vertical stirrups according to CL 9.3.9.4.2:

$$A_v \geq \frac{V_s}{f_{yt}} \frac{s}{d} = \frac{269000}{300} \times \frac{150}{630} = 213\,\text{mm}^2$$

Minimum shear reinforcement (CL 9.4.4.1.6):

Design for Shear:

Maximum nominal shear stress (CL 7.5.2):

$$v_{\max} = \min(0.2 f_c', 8\,\text{MPa}) = 8\,\text{MPa}$$

$$v_n = \frac{V^*}{\phi b_w d} = \frac{281000}{1 \times 400 \times 630} = 1.1\,\text{MPa}$$
$$< v_{\max} \quad \rightarrow \text{ok}$$

This check guards against diagonal compression field failure via concrete crushing. This check should still be carried out because outside of the unbonded length the shear mechanism is the same as a monolithic beam.

Design for shear through slotted section:

Due to the small section, it is reasonable and conservative to assume no concrete shear contribution in the top-hinge.

$$\therefore V_s \geq \frac{V^*}{\phi} - V_c = \frac{281}{1} - 0 = 281\,\text{kN}$$

Shear reinforcement through the top-hinge should be provided via diagonal hangers according to CL 9.3.9.4.4 (§ 3.2):

$$V_s = A_v f_{yt} \sin\alpha = 281\,\text{kN}$$
$$\leq 0.25\sqrt{f_c'} b_w d = 398\,\text{kN}$$

$$A_{v,\min} = \frac{\sqrt{f_c'}}{12}\frac{b_w s}{f_{yt}} = \frac{\sqrt{40}}{12}\frac{400\times150}{300}$$
$$= 105\,\text{mm}^2$$

Check 4-legs R10 at 150 mm,

$A_v = 4\times78.5 = 314\,\text{mm}^2 > 213\,\text{mm}^2 \rightarrow$ ok

Design for shear outside PPHZ (CL 9.3.9.3.4):

$$v_b = (0.07+10\rho)\sqrt{f_c'}$$
$$= (0.07+10\times0.012)\sqrt{40}$$
$$= 1.2\,\text{MPa}$$

$$V_c = v_c A_{cv} = k_d k_a v_b b_w d$$
$$= 1\times0.9\times1.2\times400\times630 = 272\,\text{kN}$$
$$\geq V^* \rightarrow \text{ok}$$

Therefore, simply provide minimum shear reinforcement (CL 9.3.9.4.15),

$$\therefore A_v \geq \frac{V_s}{f_{yt}\sin\alpha} = \frac{281000}{500\times\sin45^o}$$
$$\geq 795\,\text{mm}^2$$

Try 2-HD25 inclined at 45°,

$A_v = 2\times491 = 982\,\text{mm}^2 > 795\,\text{mm}^2 \rightarrow$ ok

The development length of the hanger beyond the lower bend can be calculated according to CL 8.6.3.2:

$$L_d = \frac{(0.5\alpha_a f_{yh})}{\sqrt{f'_c}} d_{bh}$$
$$= \frac{(0.5\times1\times500)}{\sqrt{40}}\times25$$
$$= 988\,\text{mm}$$

Design for shear outside slotted section (CL 9.3.9.3.4):

Because there is little damage to concrete outside the slotted section, NZS3101:2006 provisions can be used.

$$v_b = (0.07+10\rho)\sqrt{f_c'}$$
$$= (0.07+10\times0.012)\sqrt{40}$$
$$= 1.2\,\text{MPa}$$

$$V_c = v_c A_{cv} = k_d k_a v_b b_w d$$
$$= 1\times0.9\times1.2\times400\times630 = 272\,\text{kN}$$
$$< V^* = 281\,\text{kN, but within 5\%}$$

Therefore, simply provide minimum shear reinforcement (CL 9.3.9.4.15),

$$A_{v,\min} = \frac{\sqrt{f_c'}}{16}\frac{b_w s}{f_{yt}} = \frac{\sqrt{40}}{16}\frac{400\times300}{300}$$
$$= 158\,\text{mm}^2$$

Check 4-legs R10 at 300 mm,

$A_v = 4\times78.5 = 314\,\text{mm}^2 > 158\,\text{mm}^2 \rightarrow \text{ok}$

Column Design Actions:

Column design actions are computed from beam overstrength actions plus some amplification for dynamic effects.

Note: the formulations below differ from NZS3101 because different dynamic amplification factors from Priestley et al. (2007) were used in accordance with the direct displacement-based design which was used to determine design actions.

$$V_{col}^{\ *} = \phi_o V_E + 0.1\mu V_{E,base}$$
$$= 1.53\times287 + 0.1\times2.39\times287$$
$$= 508\,\text{kN}$$

$$\omega_{f,c} = 1.15 + 0.13(\mu/\phi_o - 1)$$
$$= 1.15 + 0.13(2.39/1.53 - 1)$$
$$= 1.22$$

$$M_{col}^{\ *} = \phi_o \omega_{f,c} M_E - 0.3 h_b V_{col}^{\ *}$$
$$= 1.53\times1.22\times547 - 0.3\times0.7\times508$$
$$= 914\,\text{kNm}$$

$$A_{v,\min} = \frac{\sqrt{f_c'}}{16}\frac{b_w s}{f_{yt}} = \frac{\sqrt{40}}{16}\frac{400\times300}{300}$$
$$= 158\,\text{mm}^2$$

Check 4-legs R10 at 300 mm,

$A_v = 4\times78.5 = 314\,\text{mm}^2 > 158\,\text{mm}^2 \rightarrow \text{ok}$

Column Design Actions:

Column design actions are computed from beam overstrength actions plus some amplification for dynamic effects.

Note: the formulations below differ from NZS3101 because different dynamic amplification factors from Priestley et al. (2007) were used in accordance with the direct displacement-based design which was used to determine design actions.

$$V_{col}^{\ *} = \phi_o V_E + 0.1\mu V_{E,base}$$
$$= 1.60\times287 + 0.1\times2.39\times287$$
$$= 528\,\text{kN}$$

$$\omega_{f,c} = 1.15 + 0.13(\mu/\phi_o - 1)$$
$$= 1.15 + 0.13(2.39/1.60 - 1)$$
$$= 1.21$$

$$M_{col}^{\ *} = \phi_o \omega_{f,c} M_E - 0.3 h_b V_{col}^{\ *}$$
$$= 1.60\times1.21\times547 - 0.3\times0.7\times528$$
$$= 948\,\text{kNm}$$

Once column design actions have been determined, the process for designing columns simply follows NZS3101:2006.

Interior beam-column Joint Design:

Joint shear demand (Eq. C15.4):

$$V_{jho}^{*} = \lambda_o f_y (A_{s1} + A_{s2}) - V_{col}$$
$$= 1.25 \times 300 \times (3028 + 3028) - 508000$$
$$= 1763\,\text{kN}$$

Horizontal joint reinforcement (CL 15.4.4.1a):

$$\frac{6V_{ojh}^{*}}{f'_c b_j h_c} = \frac{6 \times 1763000}{40 \times 600 \times 950} = 0.46 \le 0.85$$
$$\text{use} = 0.85$$
$$\alpha_i = 1.4\alpha_n = 1.4$$
$$A_{jh} = \frac{6V_{ojh}^{*}}{f'_c b_j h_c}\left(\frac{\alpha_i f_y A_s^{*}}{f_{yh}}\right) \ge 0.4\frac{V_{ojh}^{*}}{f_{yh}}$$
$$= 0.85 \times \frac{1.4 \times 300 \times 3028}{500} \ge 0.4\frac{1763000}{500}$$
$$= 2162\,\text{mm}^2 \ge 1410\,\text{mm}^2$$

Try 5 sets of 4-legs XR12,

$$A_{jh} = 5 \times 4 \times 113 = 2262\,\text{mm}^2$$
$$> 2162\,\text{mm}^2 \rightarrow \text{ok}$$

Interior beam-column Joint Design:

Joint shear demand (§ 3.7.1):

$$V_{jho}^{*} = 2\lambda_o A_s f_y - V_{col}$$
$$= 2 \times 1.3 \times 3028 \times 300 - 528000$$
$$= 1834\,\text{kN}$$

Again λ_o=1.3 has been assumed to account for higher overstrength in slotted-beams.

Horizontal joint reinforcement:

For the truss mechanism, NZS3101:2006 provisions can be used:

$$\frac{6V_{ojh}^{*}}{f'_c b_j h_c} = \frac{6 \times 1834000}{40 \times 600 \times 950} = 0.48 \le 0.85$$
$$\text{use} = 0.85$$
$$\alpha_i = 1.4\alpha_n = 1.4$$
$$A_{jh} = \frac{6V_{ojh}^{*}}{f'_c b_j h_c}\left(\frac{\alpha_i f_y A_s^{*}}{f_{yh}}\right) \ge 0.4\frac{V_{ojh}^{*}}{f_{yh}}$$
$$= 0.85 \times \frac{1.4 \times 300 \times 3028}{500} \ge 0.4\frac{1834000}{500}$$
$$= 2162\,\text{mm}^2 \ge 1467\,\text{mm}^2$$

Try 5 sets of 4-legs XR12,

$$A_{jh} = 5 \times 4 \times 113 = 2262\,\text{mm}^2$$
$$> 2162\,\text{mm}^2 \rightarrow \text{ok}$$

Note: Additional reinforcement is then required to sustain the excess strut force at the bottom of the joint from the concrete strut mechanism. Analytical studies showed that this was between 25-40% of the reinforcement required for the truss

	mechanism when beneficial effects of axial load are ignored. Therefore conservatively adopting 40%: $\Delta A_{jh} = 0.40 A_{jh} = 865\,\text{mm}^2$ Try 2 sets of 4-legs XR12, $\Delta A_{jh} = 2 \times 4 \times 113 = 905\,\text{mm}^2$ $> 865\,\text{mm}^2 \rightarrow \text{ok}$ This additional reinforcement should be placed in the bottom half of the joint.
Assuming two dummy stirrup sets immediately adjacent to inner beam bars, 5+2=7 sets can be vertically spaced at 80 mm. Checking the maximum stirrup spacing according to CL 15.4.4.4: $s = 80\,\text{mm} < s_{\max} = \min(6d_b, b/4, 200\,\text{mm})$ $= 150\,\text{mm} \rightarrow \text{ok}$	For the top half of the joint, adopt the same vertical spacing as the monolithic joint of 80 mm. The maximum stirrup spacing according to CL 15.4.4.4 is therefore verified. For the bottom half of the joint, another two stirrup sets are required. For ΔA_{jh}, the dummy stirrup immediately adjacent to the bottom beam bars can be included, so now only one extra set is needed. To fit this in, reduce the spacing in the bottom half of the joint to 60 mm.
The detailing for the monolithic interior joint is shown in Figure 3-38a. *Vertical joint reinforcement (CL 15.4.5.1):* $\alpha_v = \frac{0.7}{1 + \frac{N_o^*}{f_c' A_g}} = \frac{0.7}{1+0}$ $= 0.7$	The detailing of the slotted-beam interior joint is shown in Figure 3-38b. *Vertical joint reinforcement (CL 15.4.5.1):* $\alpha_v = \frac{0.7}{1 + \frac{N_o^*}{f_c' A_g}} = \frac{0.7}{1+0}$ $= 0.7$

$A_{jv} = \alpha_v A_{jh} \frac{f_{yh}}{f_{yv}} \frac{h_b}{h_c}$ $= 0.7 \times 2162 \times \frac{500}{300} \times \frac{700}{950}$ $= 1859\,\text{mm}^2$ Check column intermediate bars of 8-D25, $A_v = 8 \times 491 = 3927\,\text{mm}^2$ $> 1859\,\text{mm}^2 \rightarrow$ ok	$A_{jv} = \alpha_v A_{jh} \frac{f_{yh}}{f_{yv}} \frac{h_b}{h_c}$ $= 0.7 \times 2162 \times \frac{500}{300} \times \frac{700}{950}$ $= 1859\,\text{mm}^2$ Check column intermediate bars of 8-D25, $A_v = 8 \times 491 = 3927\,\text{mm}^2$ $> 1859\,\text{mm}^2 \rightarrow$ ok

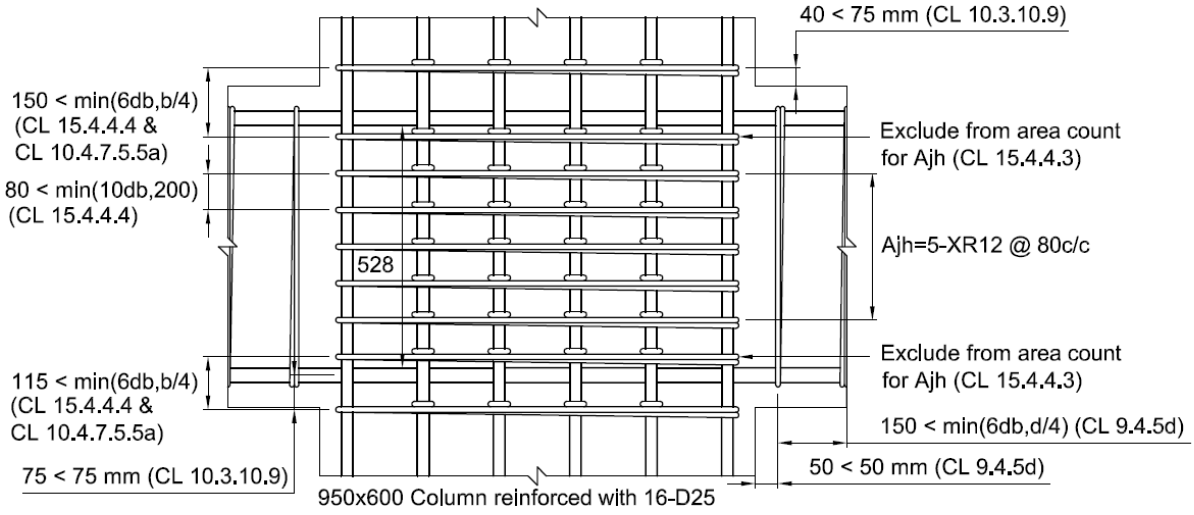

(a) Monolithic beam according to NZS3101:2006

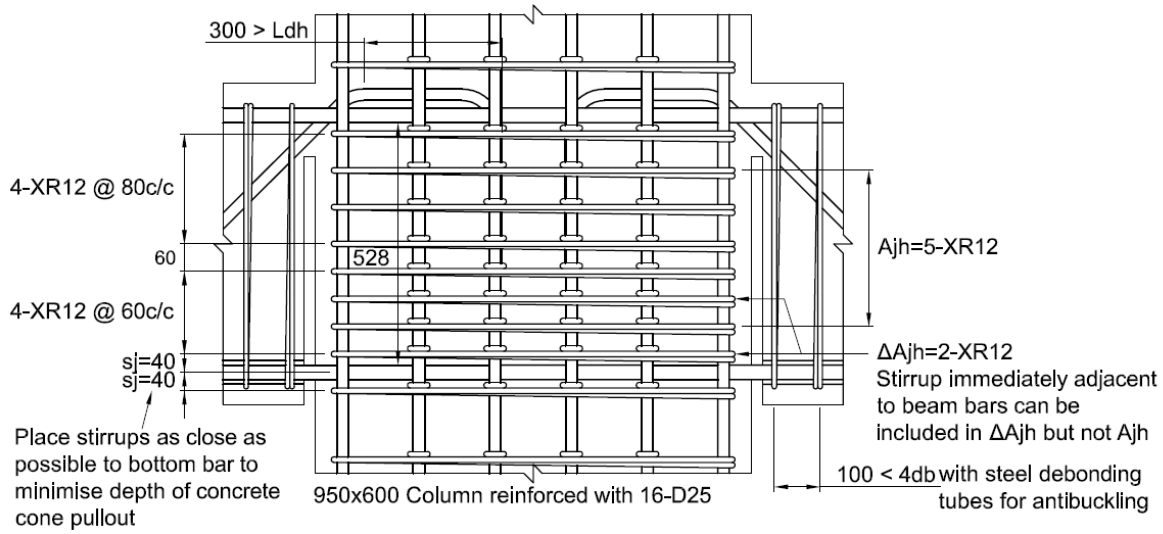

(b) Slotted-beam

Figure 3-38: Detailing of monolithic and slotted interior beam-column joints

CHAPTER 4 EXPERIMENTAL INVESTIGATION OF 2D BEAM-COLUMN JOINT SUBASSEMBLIES

Three in-plane beam-column joint subassemblies were tested under quasi-static cyclic loading. The first two specimens, RCB1 and SB1, were exterior beam-column joints. Specimen RCB1 was a conventional monolithic section, whilst specimen SB1 adopted a slotted-beam connection. The third specimen, SB2, was an interior beam-column joint with slotted-beam connections on both sides. Specimen RCB1 was designed according to NZS3101:2006, and acted as a benchmark for comparison with the slotted beam specimens. All three subassemblies had identical geometry, were 2/3 scale and designed for moderate seismicity.

The purpose of testing these specimens was to:

- Compare the response and behaviour of a slotted-beam to a conventional monolithic connection
- Verify the reduction in damage and beam elongation in slotted-beams compared to conventional monolithic beams
- Observe the shear transfer mechanism across the slotted section through the use of diagonal steel hangers
- Observe the effect of different reinforcement details for a slotted beam. Namely, altering the grade of steel for top longitudinal bars and diagonal shear hangers, and altering the hanger location.
- Assess whether current NZS3101 provisions for anti-buckling and d_b/h_c ratios for bond are applicable to slotted-beams
- Verify moment-rotation backbone curve predictions

These specimens were the first of two sets of tests performed as part of the overall experimental investigation. Quasi-static testing was later extended to an in-plane interior joint subassembly with a floor slab. For details of this test refer to CHAPTER 5.

4.1 Test Specimens

4.1.1 Exterior Monolithic Beam Specimen RCB1

Figure 4-1 shows structural drawings for the exterior monolithic beam specimen RCB1. The column had a scaled interstorey height of 2 m and the beam had a cantilever span length of 1.5 m. The beam had equal top and bottom longitudinal reinforcement of 4-D12 Grade 300 bars (lower characteristic yield strength of 300 MPa) and concrete had a specified 28 day compressive strength of 30 MPa.

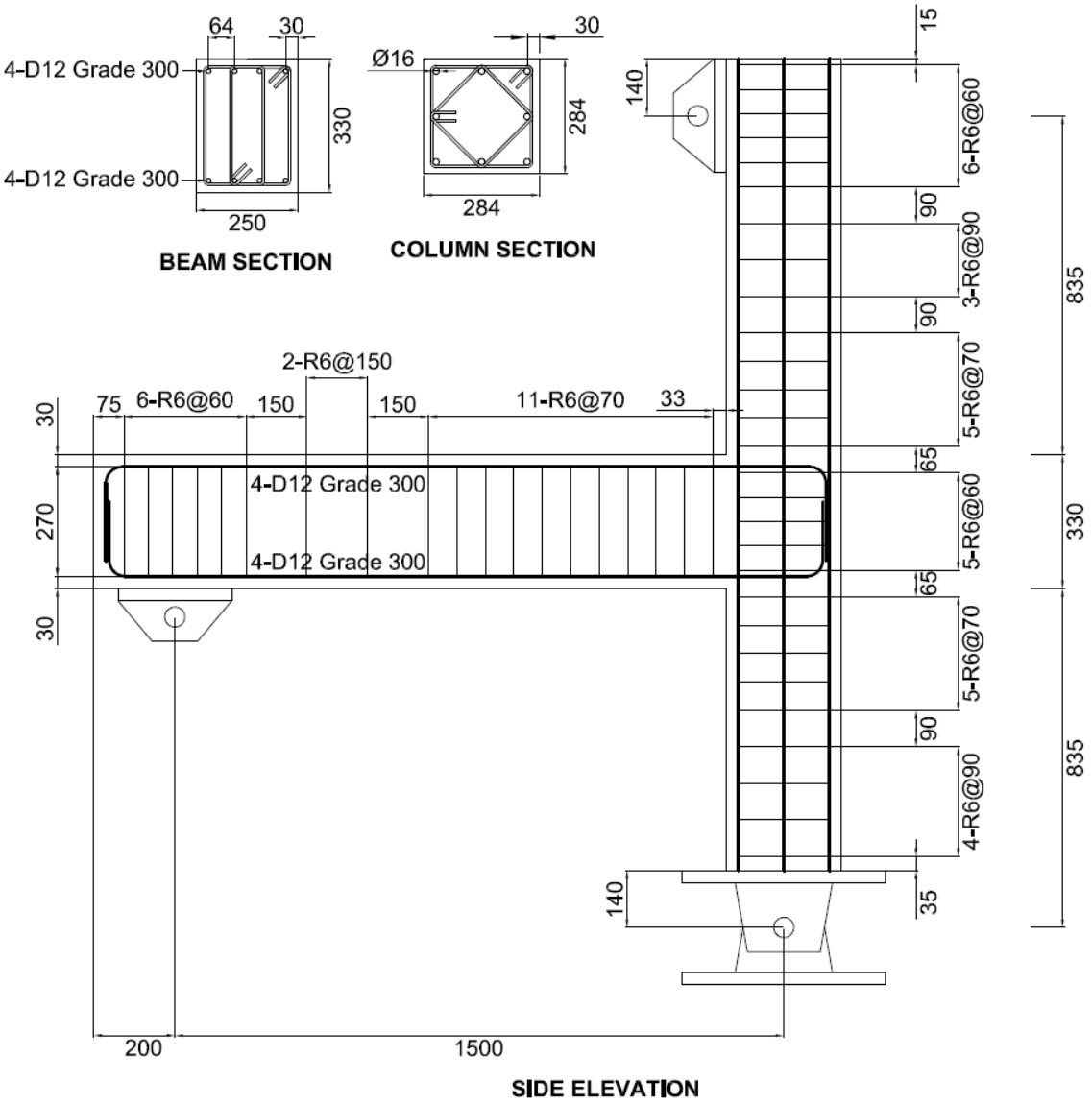

Note: All steel is Grade 300. Concrete f'c is 30 MPa.

Figure 4-1: Exterior monolithic beam specimen RCB1

4.1.2 Exterior Slotted Beam Specimen SB1

Figure 4-2 shows structural drawings of the exterior slotted beam specimen SB1, which had identical geometry to benchmark specimen RCB1. The slot adjacent to the column face was 15 mm wide, and was sized to accommodate 4.5% drifts without contact between the beam soffit and column face. To transfer shear from the beam into the joint, two 12 mm diameter deformed bars inclined at 45° were placed between the main longitudinal reinforcement. To improve low cycle fatigue resistance, bottom reinforcement was unbonded along a 230 mm length adjacent to the slot using plastic tubes. Due to greater shear forces expected in the joint, more joint steel was required compared to RCB1. Concrete had a specified 28 day compressive strength of 30 MPa.

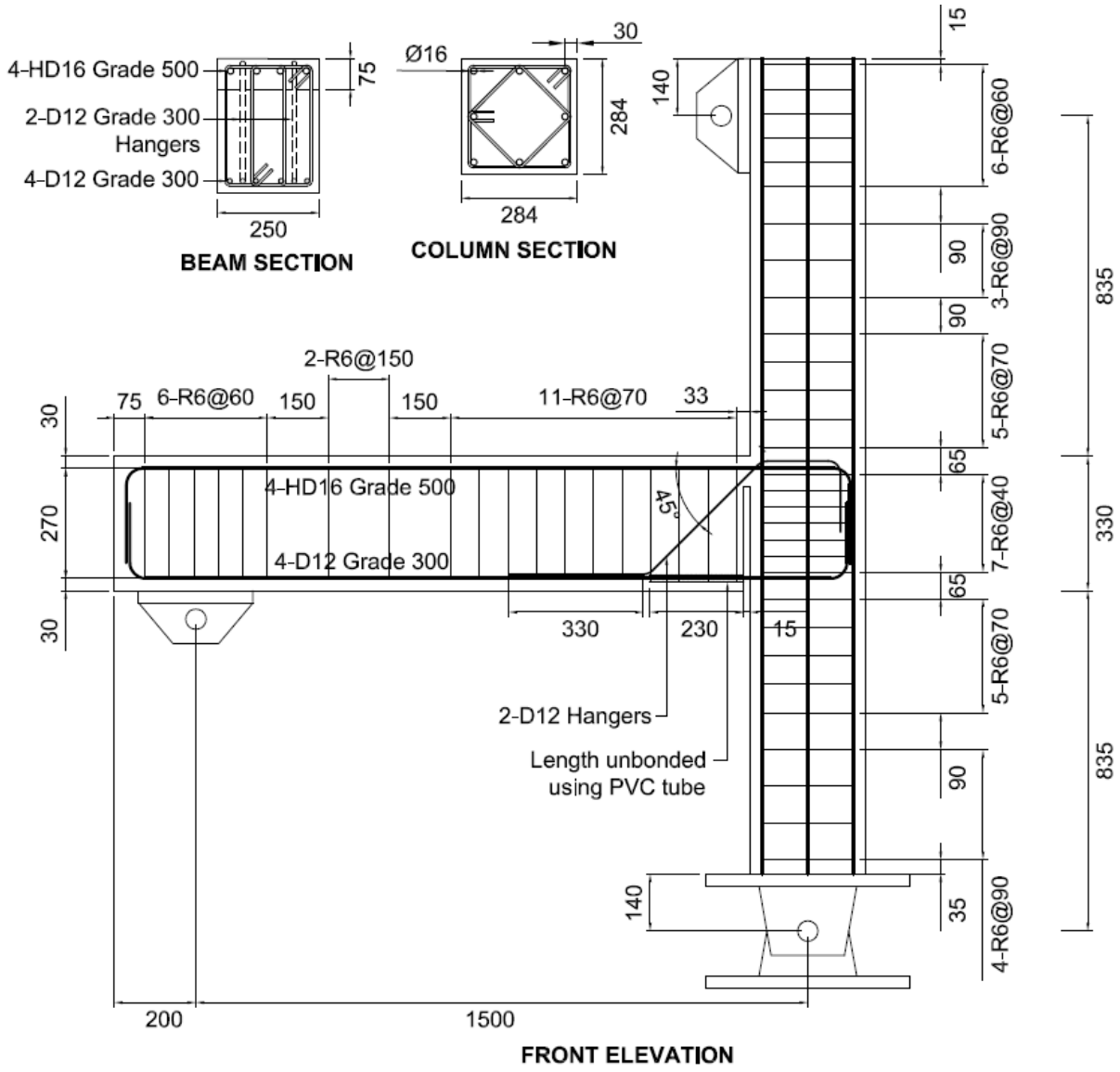

Note: All steel is Grade 300, except for the top beam reinforcement, which is Grade 500. Concrete f'c is 30 MPa.

Figure 4-2: Exterior slotted beam specimen SB1

An important detailing feature is that the upper bend of the diagonal hangers was located well-within the column, away from the slotted hinge as shown in Figure 4-3. This was to ensure compression struts forming at the bend during gap closing moments are captured within the column and do not pass through the slot. This was an additional connection detail to the specimens tested by Ohkubo (1999) to reduce shear deformations occurring through the slotted section.

Figure 4-3: Hanger bend located within column

Top longitudinal reinforcement used larger 16 mm diameter deformed bars and Grade 500 steel (lower characteristic yield strength of 500 MPa) to ensure yielding did not occur. Preliminary hand calculations showed potential yielding if Grade 300 steel was used. This is due to additional forces coming from compression at the bottom of the concrete top-hinge during gap closing moments as shown back in Figure 3-1b.

4.1.3 Interior Slotted Beam Specimen SB2

Figure 4-4 shows structural drawings for interior slotted beam specimen SB2. Specimen SB2 was constructed after the exterior joint specimens were tested. The purpose of this specimen was to verify provisions for bond between concrete and steel through an interior joint, test alternative reinforcement details, and to mitigate inelastic bar buckling that was observed in the test of specimen SB1. Like previously tested specimens, concrete had a specified 28 day compressive strength of 30 MPa.

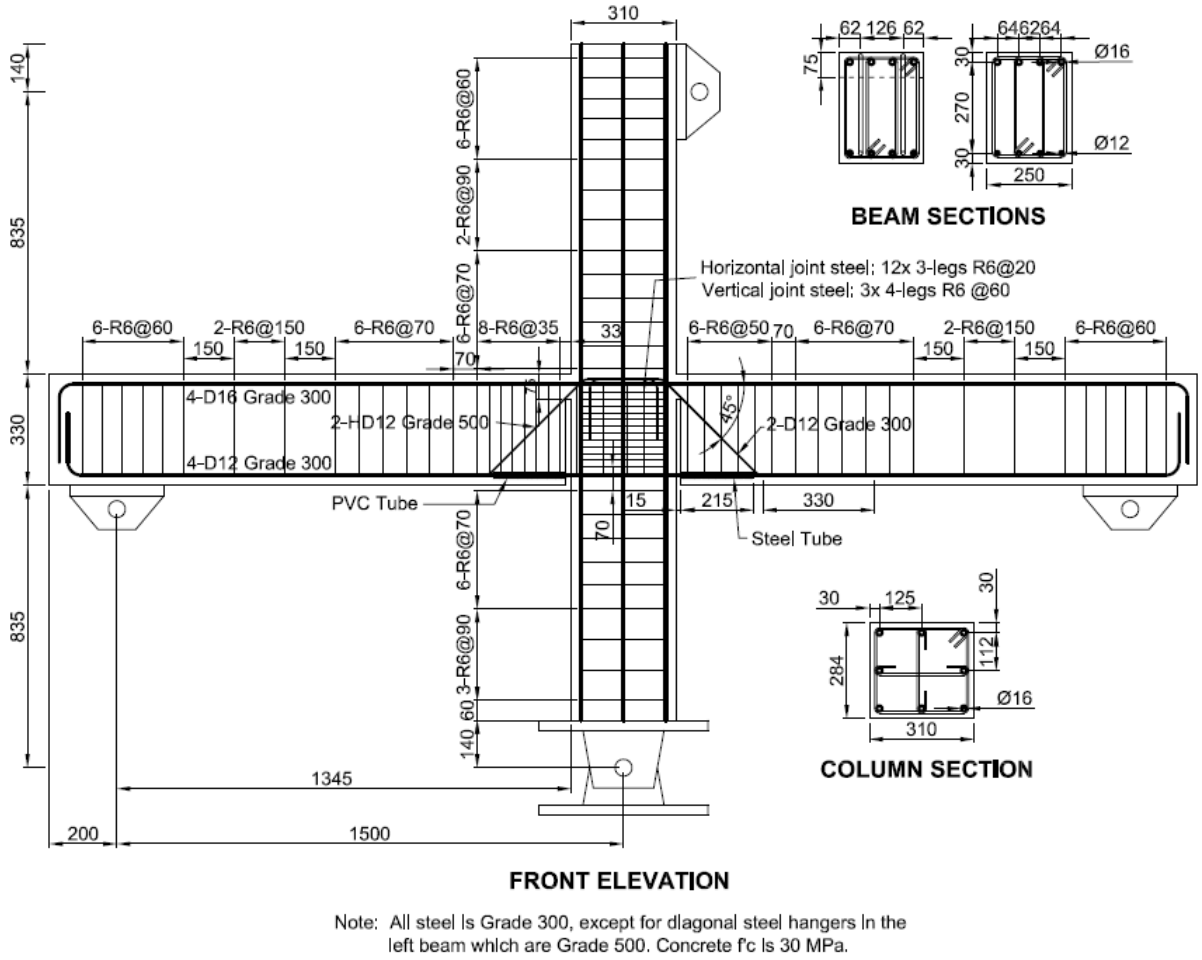

Figure 4-4: Interior slotted beam specimen SB2

SB2 had identical geometry and main bar layout to specimen SB1, except for a wider 310 mm column to attempt to provide adequate bond to bottom longitudinal bars passing through the joint. Provisions given in Paulay and Priestley (1992) were modified to account for overstrength compression and tension yield forces induced in bottom bars on both sides of the joint. Unfortunately testing later showed these modifications to be inadequate and bond-slip failure occurred. The modified provision and its shortcomings are described and discussed in Section 4.3.12.

To delay inelastic bar buckling, stirrup spacing along the unbonded length in the left-hand-side (LHS) beam was reduced to 35 mm. In addition, an extra stirrup was placed in the cover concrete of the column on the other side of the slot. In the right-hand-side (RHS) beam, the stirrup spacing was reduced to 50 mm, with steel tubes (wall thickness of 1.6 mm) to debond bottom reinforcement and provide additional buckling restraint.

In the test of specimen SB1, Grade 500 top longitudinal reinforcement was found to be sufficient to prevent yielding of this reinforcement. To observe the effect of allowing top

reinforcement to yield, Grade 300 bars were used in specimen SB2. Permitting yielding in the top reinforcement allows the grade and/or quantity of top steel to be reduced. This is at the expense of greater deformations, beam elongation and hence cracking. Preliminary calculations estimated twice the top steel deformation when Grade 300 bars were used instead of Grade 500 bars.

In the test of specimen SB1, diagonal steel hangers yielded from flexural deformations but with no observable detriment to the response. For the left-hand-side beam in specimen SB2, hangers were changed to Grade 500 steel to observe if non-yielding hangers altered the response. In addition, diagonal hangers were shifted lower, closer to the expected neutral axis to reduce hanger strains.

4.1.4 Material Properties

For all three specimens, concrete used had a specified 28 day compressive strength of 30 MPa and maximum aggregate size of 13 mm. During casting, 100 mm diameter by 200 mm high concrete cylinders were prepared and cured in a fog room. These were tested later after 7 days, 28 days and on the day the specimens were tested. Testing was carried out using an Avery Universal Testing Machine. Concrete compressive strengths obtained are shown in Table 4-1 and Table 4-2.

Table 4-1: Unconfined concrete compressive strengths for exterior joint specimens RCB1 and SB1

	Compressive strength (MPa)				
Test	**Cylinder #1**	**Cylinder #2**	**Cylinder #3**	**Average**	**Std dev**
7 day	20.8	22.2	19.1	20.7	1.54
28 day	26.6	26.4	25.5	26.2	0.59
RCB1 test day (73 days)	31.5	32.5	33.0	32.3	0.76
SB1 test day (91 days)	31.9	37.5	34.4	34.6	2.81

Table 4-2: Unconfined concrete compressive strengths for interior joint specimen SB2

	Compressive strength (MPa)				
Test	**Cylinder #1**	**Cylinder #2**	**Cylinder #3**	**Average**	**Std dev**
7 day	17.6	17.5	18.0	17.7	0.26
28 day	23.0	26.0	25.0	24.7	1.53
SB2 test day (63 days)	31.6	29.2	28.4	29.8	1.66

Similarly reinforcing steel samples were tested in axial tension via Avery Universal Testing Machine. Three samples for each type of bar used were tested. Average stress-strain

properties obtained are summarised in Table 4-3 and Table 4-4. The strain hardening coefficient, p, refers to the exponential coefficient from the steel constitutive relationship given in Equation 6-7.

Table 4-3: Reinforcing steel properties for exterior joint specimens RCB1 and SB1

Property	Bar size and grade			
	D12 Grade300	D16 Grade300	HD16 Grade500	R6 Grade300
Young's modulus, E_s (MPa)	194000	183000	184000	200000
Yield strength, f_y (MPa)	329	316	542	418
Ultimate strength, f_u (MPa)	462	458	686	494
Yield strain, ε_y	0.0017	0.0017	0.0029	0.0021
Onset of strain hardening, ε_{sh}	0.008	0.021	0.014	0.006
Strain at ultimate stress, ε_u	0.188	0.209	0.150	0.102
Strain hardening coefficient, p	5	5	5	5

Table 4-4: Reinforcing steel properties for interior joint specimen SB2

Property	Bar size and grade			
	D12 Grade300	HD12 Grade500	D16 Grade300	R6 Grade300
Young's modulus, E_s (MPa)	185000	198000	202000	196273
Yield strength, f_y (MPa)	327	554	326	423
Ultimate strength, f_u (MPa)	451	671	477	506
Yield strain, ε_y	0.0018	0.0028	0.0016	0.0022
Onset of strain hardening, ε_{sh}	0.028	0.015	0.021	0.017
Strain at ultimate stress, ε_u	0.202	0.167	0.203	0.126
Strain hardening coefficient, p	4	5	5	5

4.1.5 Specimen Construction

All joint subassemblies were constructed at the University of Canterbury. Steel was ordered cut to length and bent from the factory. The steel cages were assembled as shown in Figure 4-5a & b and Figure 4-6a & b. The beams and bottom half of the columns were caged separately, before being combined and caging the remainder of the column.

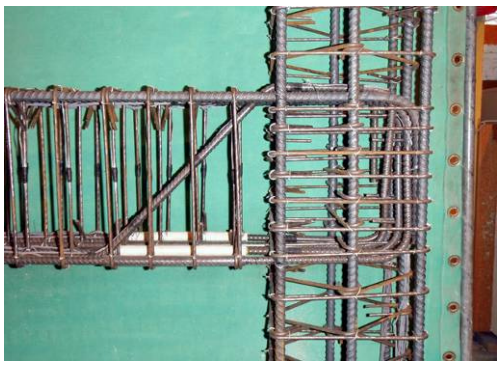

(a) SB1 connection details

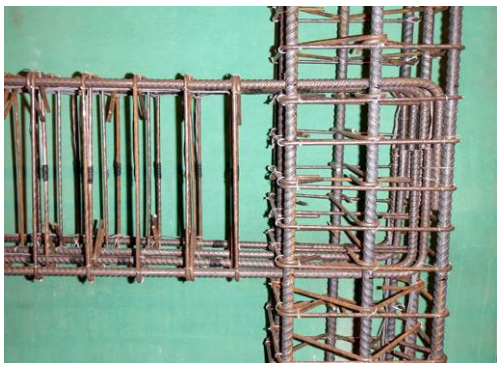

(b) RCB1 connection details

(c) Unbonded length in SB1

(d) Formwork use to create SB1 slot

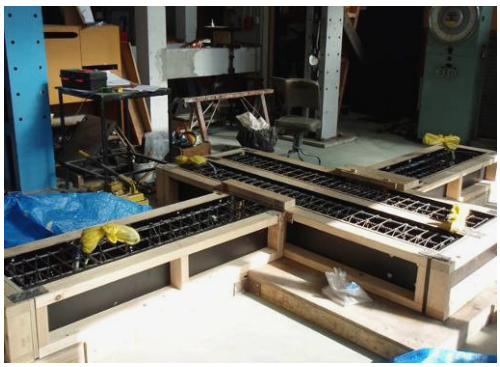

(e) RCB1 and SB1 in formwork

(f) Casting and concrete vibration

(g) Specimen SB1 in test rig

(h) RCB1 potentiometer setup

Figure 4-5: Construction of 2D exterior joint subassemblies RCB1 and SB1

(a) SB2 reinforcement cage

(b) SB2 connection details

(c) Unbonded length using Plastic tubes

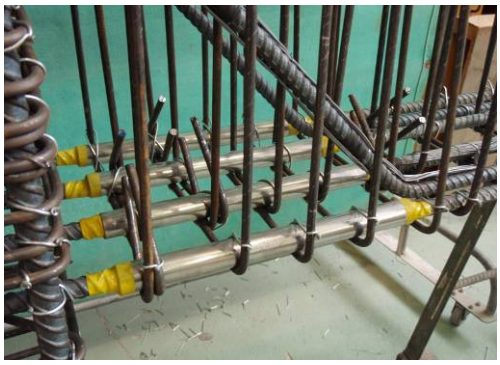

(d) Unbonded length using Steel tubes

(e) SB2 in formwork

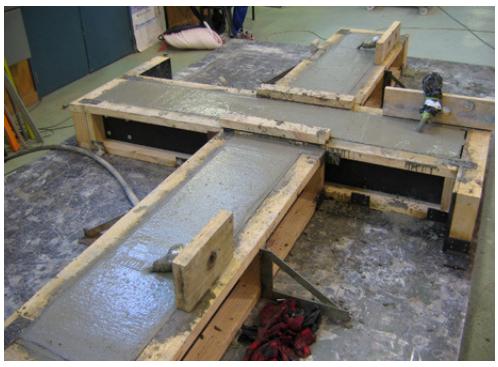

(f) Cast specimen

(g) Specimen SB2 in test rig

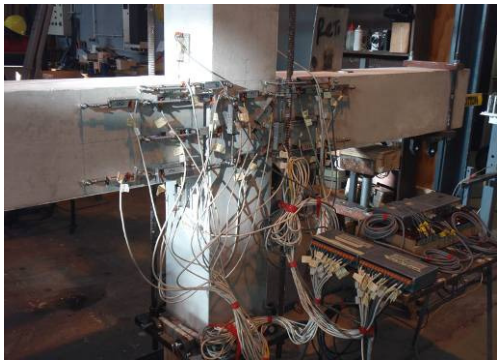

(h) SB2 potentiometer setup

Figure 4-6: Construction of 2D interior joint subassembly SB2

During caging, 120 Ohm electrical strain gauges were attached to longitudinal and transverse steel. This consisted of cleaning the steel surface of dirt and rust, attaching the instrument with cyanoacrylate adhesive, and protecting the strain gauge with Shinkoh SN/4 waterproofing glue and rubber mastic tape. For instrumented locations and purpose see Section 4.2.3.

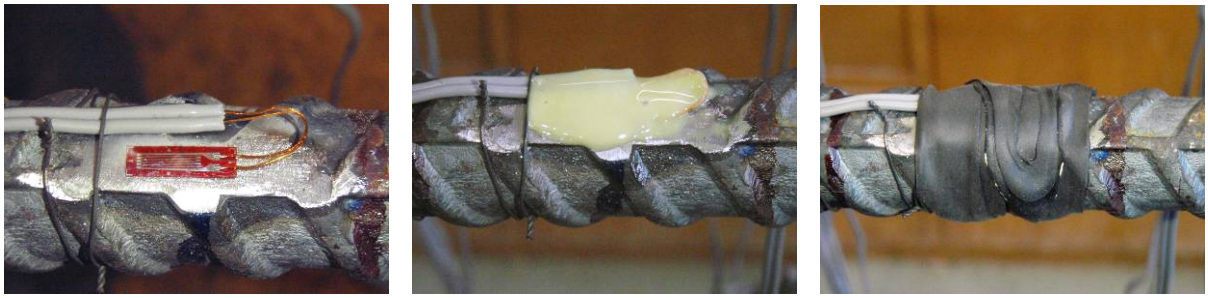

(a) Attached strain gauge **(b) Water proofing** **(c) Wrapped in rubber tape**

Figure 4-7: Installation of strain gauges

Bottom reinforcement adjacent to the slot was unbonded by encasing the bars in plastic PVC/irrigation pipe or steel tubes as shown in Figure 4-5c and Figure 4-6c & d. Larger tubes were used on some bars to allow for the attachment of strain gauges along the unbonded length. To ensure a tight fit to prevent buckling, the clearance between the steel tubes and bars was filled with grout.

Formwork for casting of concrete was constructed from plywood and No. 1 Framing timber used as stiffeners as in Figure 4-5e and Figure 4-6e. A polystyrene sheet with thin steel plates on either side was used to create the formwork for the slot as shown by Figure 4-5d. This was to allow for easy removal after casting by dissolving the polystyrene with acetone.

The concrete ready mix was provided from a local commercial plant. A 28 day design compressive strength of 30 MPa and maximum aggregate size of 13 mm was specified. To allow the placement of concrete around steel-congested joints, a 120 mm slump was ordered. For ease of casting, specimens were cast on their side. Electrical vibrators were used to distribute the fresh concrete around the mould and remove air voids (Figure 4-5f and Figure 4-6f). The surface was given a smooth finish, and cured for 7 days.

Once the concrete had set, the specimens were mounted in the test rig as shown in Figure 4-5g and Figure 4-6g. Linear potentiometers were then mounted on the rear face of the specimen using aluminium brackets screwed onto 6 mm threaded rods embedded in the concrete. Load cells were zeroed while connections were loose to ensure a true zero load.

4.2 Experimental Set-up

4.2.1 Test Rig

Exterior and interior joint specimens were tested in a joint subassembly test rig at the University of Canterbury. A schematic of the test rig is shown in Figure 4-8.

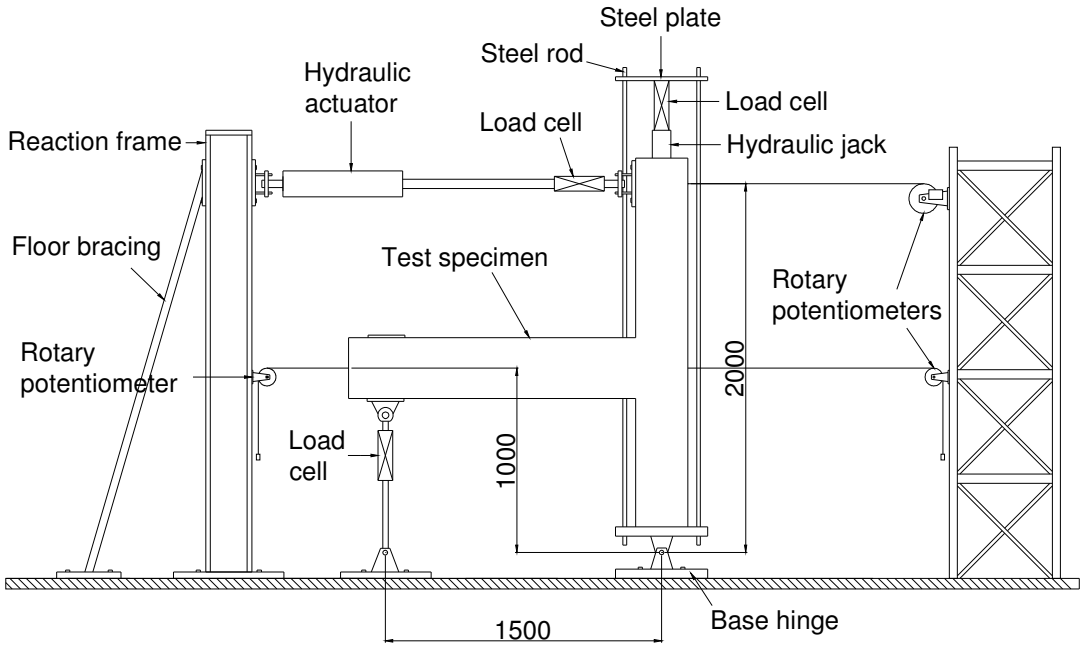

(a) Set-up for exterior joint specimens

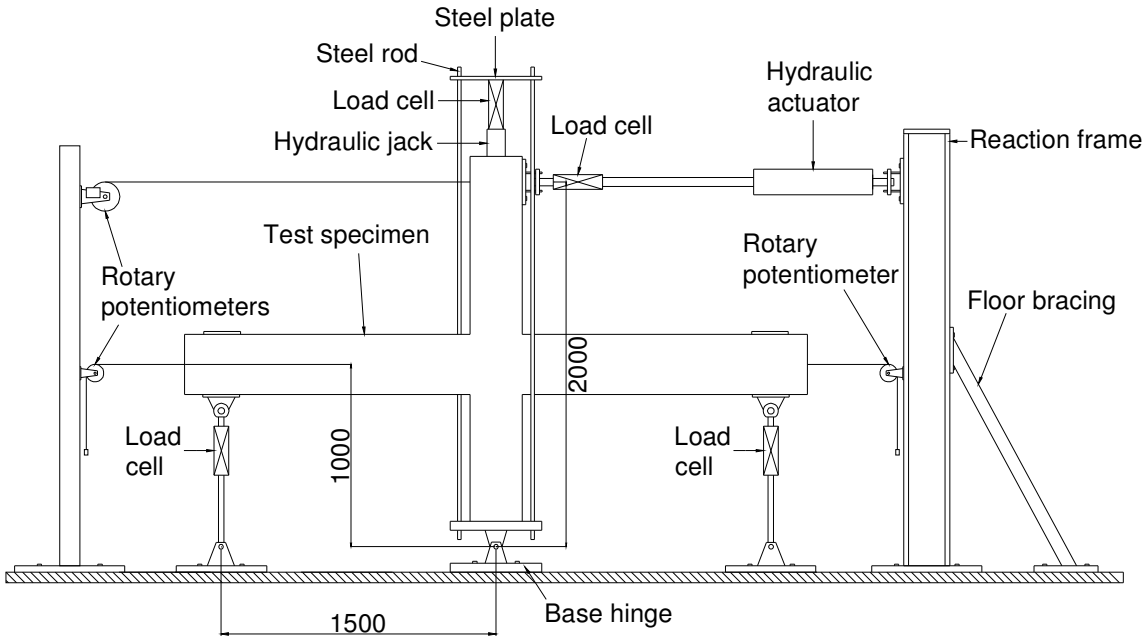

(b) Set-up for interior joint specimen

Figure 4-8: Joint subassembly test rig

The drift sequence was applied via a hydraulic actuator acting laterally at the top of the column. A rotary potentiometer at the top of the column provided measurement of lateral displacements. A 400 kN capacity load cell measured column axial load, and three 150 kN capacity load cells measured column lateral load and beam end reactions.

During testing, a constant compressive axial load of 100 kN was applied to the column via a hydraulic jack. Although column axial loads in reality vary during earthquake loading, past researchers have shown well-designed joint response to be independent of column axial stress (Bakir, 2003). Given this and that shear failure was not expected to occur in the column or joint panel zone, this simplifying assumption was considered reasonable.

4.2.2 Loading Protocol

Beam-column joint subassemblies were subject to cyclic quasi-static loading to simulate seismic actions. A displacement controlled loading system was used which applied increasing lateral force at the top of the column until a specified lateral drift was reached. The drift sequence in Figure 4-9 was adopted in accordance with American Concrete Institute (ACI) acceptance criteria for moment frames (ACI Committee 374, 2005). Test specimens were subject to 3 cycles at drift levels of 0.1%, 0.2%, 0.5%, 0.75%, 1.0%, 1.5%, 2.0%, 2.5%, 3.5% and 4.5%. A smaller cycle, one third of the previous drift, followed each large drift set to close gaps between aggregates in the concrete.

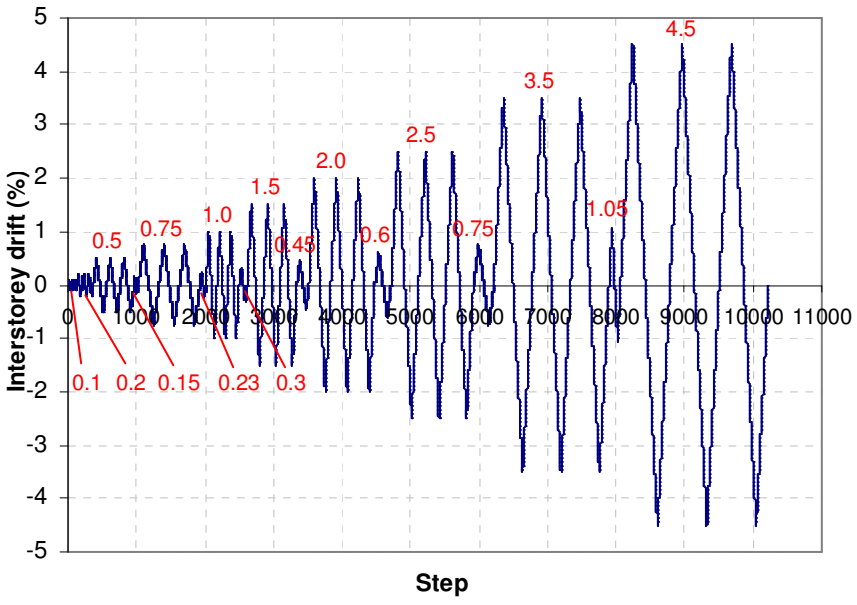

Figure 4-9: Quasi-static loading protocol

The loading direction sign convention adopted in this thesis is shown in Figure 4-10. Positive loading and positive displacement was taken as the direction that created a positive bending moment in the left-hand-side beam – that is, tension on the underside.

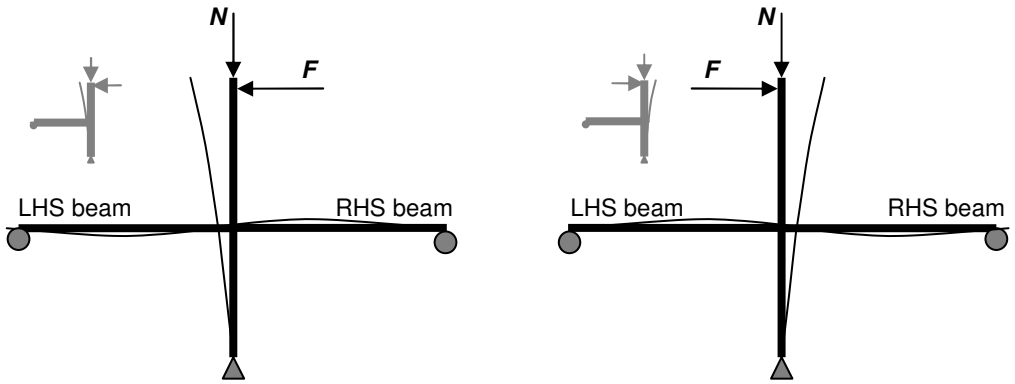

(a) Positive loading **(b) Negative loading**

Figure 4-10: Loading direction sign convention

4.2.3 Instrumentation

Strain Gauges

Local strains in reinforcing bars were measured using electrical resistance wire strain gauges (Tokyo Sokki FLA-5-11-3L and FLA-3-11-3L). 5 mm long strain gauges were used on deformed bars and 3mm long strain gauges were used on the stirrups. Both had a gauge resistance of 120 Ohms. Figure 4-11 shows the locations of the strain gauges in each specimen.

For the exterior joint specimens, one strain gauge was used at each location, which was attached to the outside surface of the bar. Two gauges across the beam cross-section were used at each location marked in the figure to provide some redundancy against strain gauge failure during casting and testing.

For the interior joint specimen, two strain gauges were used at each location with one on either side of the bar. This was so flexural stresses in the bars could be corrected for later, and to provide some redundancy against strain gauge failure.

For both exterior and interior joint specimens, strain gauges along longitudinal reinforcement were used to measure strains across the slotted section and also the strain penetration on either side.

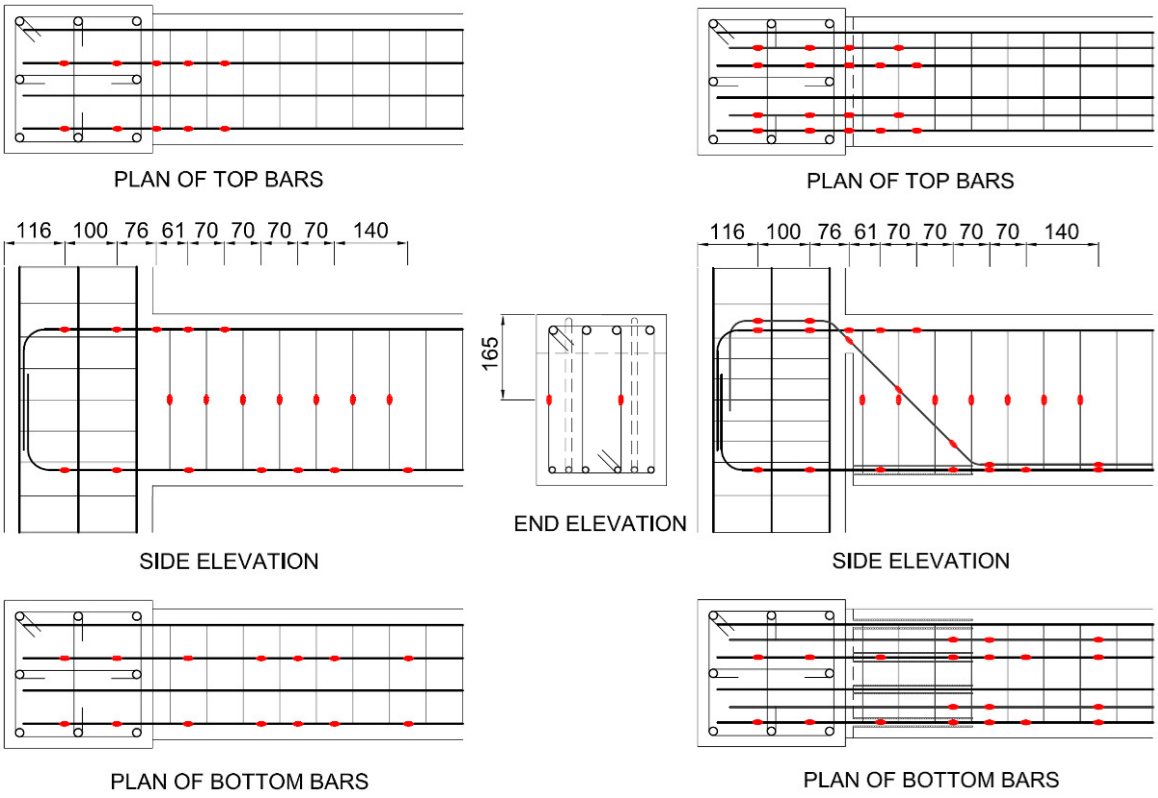

(a) Benchmark exterior joint specimen RCB1 **(b) Slotted exterior joint specimen SB1**

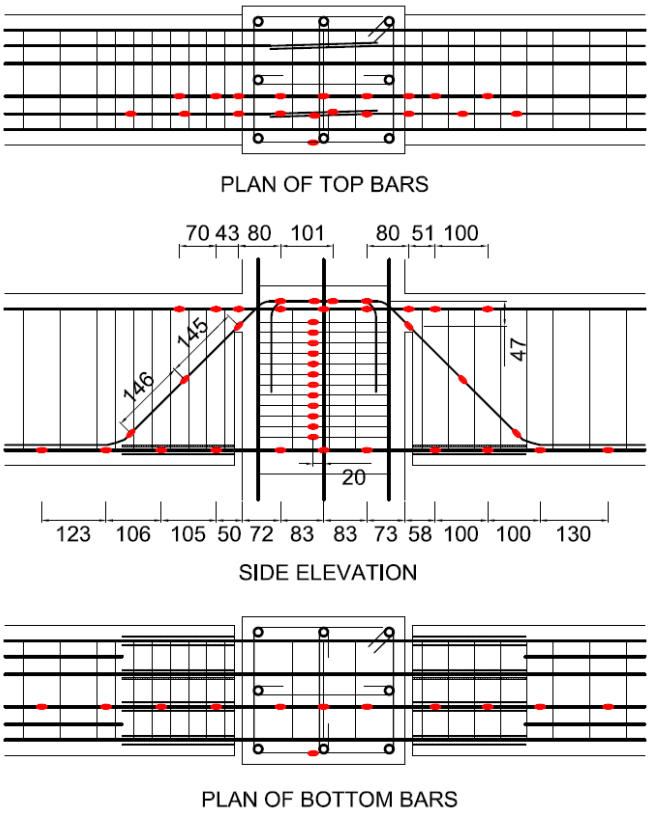

(c) Slotted interior joint specimen SB2

Figure 4-11: Location of strain gauges

For the exterior joint specimens, the diagonal hangers and seven lines of stirrups were strain gauged to observe the transfer of shear stresses from the stirrups to the hanger. During closing moments, bottom longitudinal reinforcement will be compression due to flexure, but due to shear, the diagonal hanger should remain in tension. Strain gauges on the lower anchorage length of the hanger and adjacent bottom reinforcement were placed to observe the strain differences between these shear and flexural reinforcements.

For the interior joint specimen, beam stirrups were not instrumented due to data available from the previous test of SB1. However, horizontal joint stirrups were strain gauged to observe the distribution of stresses in the joint shear reinforcement.

Linear Potentiometers

Linear potentiometers provided measurement of beam and joint deformations. The linear potentiometer set-up for each specimen is shown in Figure 4-12.

Three pairs of potentiometers across the beam column interface were used to estimate fixed end rotations. An additional pair was used in slotted specimens SB1 and SB2, located 10 mm below the top fibre of the beam. This provided more information for fixed end rotation calculations and was also used to estimate the neutral axis depth within the concrete top-hinge.

Cross diagonal potentiometers within the joint panel zone were used to calculate joint shear deformation. This was repeated in the beam plastic hinge zone for specimens RCB1 and SB1 to allow a comparison of shear deformations.

Potentiometers fixed to the column above and below the beam measured vertical deformations across the slot. The lower potentiometer for slotted specimens was located further from the column face to accommodate opening and closing of the slot.

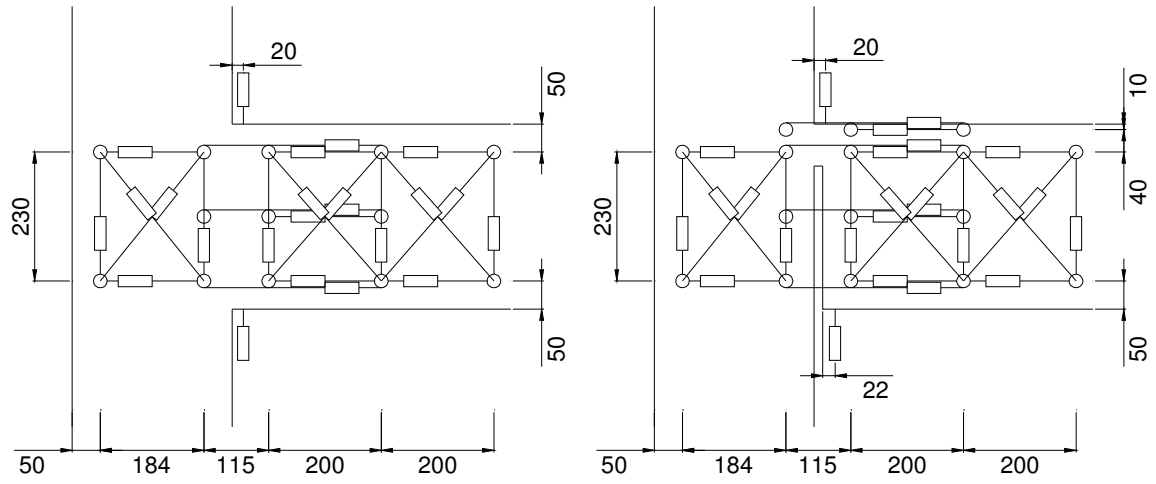

(a) Benchmark exterior joint specimen RCB1 **(b) Slotted exterior joint specimen SB1**

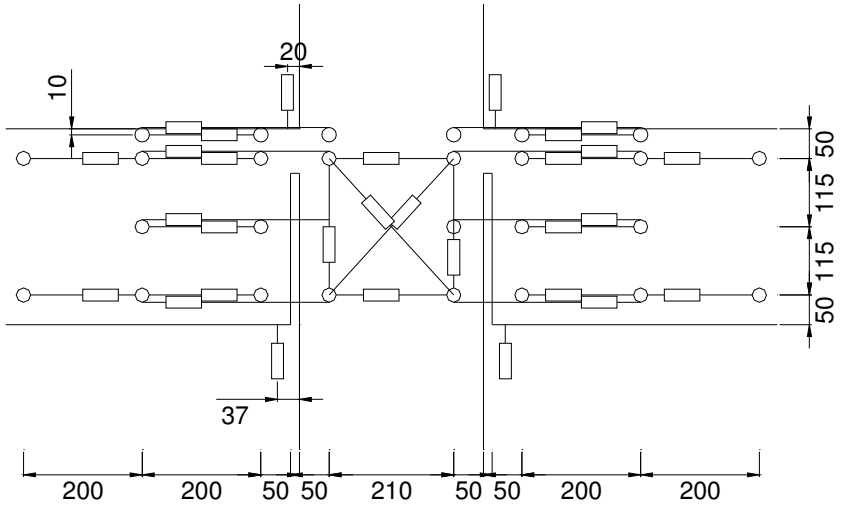

(c) Slotted interior joint specimen SB2

Figure 4-12: Location of linear potentiometers

Rotary Potentiometers

Three rotary potentiometers were used to measure the lateral displacement at the top of the column, at the joint and at the beam free ends. These were located as shown in Figure 4-8. The potentiometers attached to the joint and beam free ends were used to measure beam elongation. These measurements included both material and geometric elongation contributions.

Load Cells

Load measurements were provided via load cells. 150 kN load cells were used to measure the applied horizontal load and reaction force at the beam ends, and a 400 kN load cell was used

to measure the vertical axial load in the column (See Figure 4-8). Load cells were calibrated in compression by Avery Universal Testing Machine. The obtained calibration factors were then assumed to be effective for the particular load cell in tension.

4.3 Test Results

This section summarises the results from the testing of specimens RCB1, SB1 and SB2. Results for all three specimens are looked at simultaneously to allow a comparison of their response.

4.3.1 General Behaviour and Force-drift Response

Figure 4-13 shows the lateral force versus drift response for the exterior monolithic benchmark specimen RCB1. First cracking occurred in the beam near the beam-column interface at a drift of 0.15%, and was followed by yielding of longitudinal reinforcement at 0.5% drift, at an applied lateral force of 23.3 kN. The figure shows a stable, typical reinforced concrete hysteresis up to 3.5% drift. The slight pinching of the hysteresis can be explained by vertical shear sliding along the main flexural crack which was clearly visibly at 2.0% drift. At 3.5% drift, significant cover concrete spalling occurred exposing beam reinforcement on both top and bottom surfaces of the beam adjacent to the column face. Further spalling and strength degradation continued in drift cycles to 4.5%, where upon out-of-plane twisting of the beam caused the test to be stopped after the second 4.5% drift cycle.

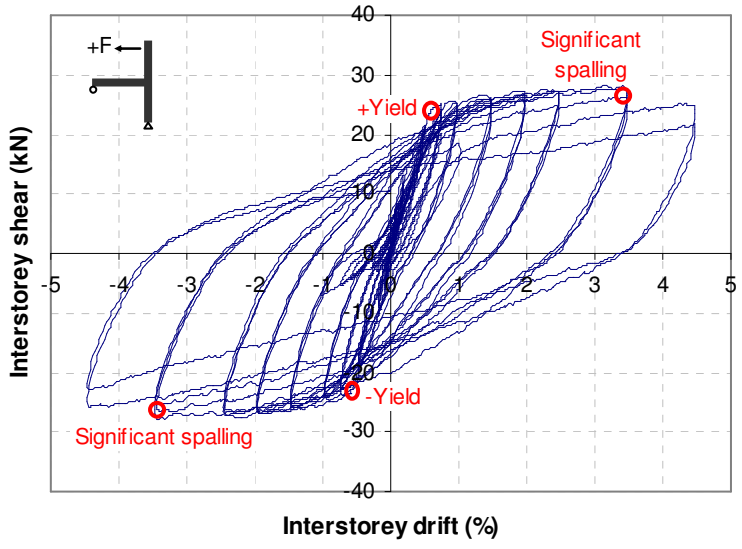

Figure 4-13: Lateral force versus drift response for monolithic beam specimen RCB1

Figure 4-14 shows the lateral force versus drift response for the exterior slotted-beam specimen SB1. First cracking was observed at a higher drift than RCB1 at 0.24%. First cracking occurred in the beam adjacent to the top-hinge and at the beam soffit just outside the unbonded length of bottom longitudinal reinforcement. The positive yield point was the same as RCB1 at 0.5% drift and a lateral force of 23.3 kN. Negative yield however occurred at a greater drift of -0.65% but a smaller lateral force of -21.4 kN. Minor spalling was observed at 2.5% drift, and beam cracking around the slot was significantly less than the cracking within the plastic hinge zone of the benchmark specimen. Unlike RCB1, the slotted specimen showed a much 'fatter' steel-like hysteresis and greater post-yield hardening up to the first gap-closing drift at -3.5%. Table 4-5 and Table 4-6 summarises overstrength factors observed at peak drift levels during the test of specimens RCB1 and SB1 respectively. The post-yield response of specimen SB1 was approximately 10% greater than that of specimen RCB1. This greater post-yield hardening is the result of additional cyclic strain hardening in the bottom reinforcement as it yields extensively in both tension and compression.

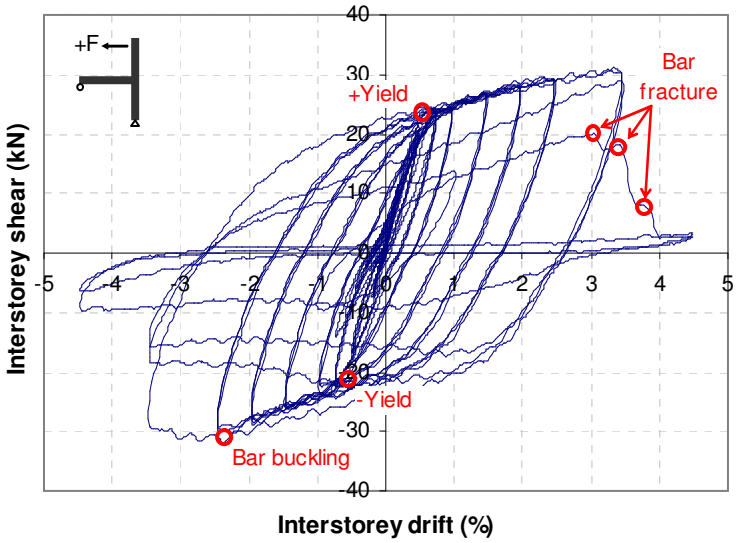

Figure 4-14: Lateral force versus drift response for slotted-beam specimen SB1

Table 4-5: Observed overstrength factors from test of specimen RCB1

Interstorey drift (%)	1.0	1.5	2.0	2.5	3.5
φ_o^+ gap opening drifts	1.16	1.20	1.23	1.24	1.26
φ_o^- gap closing drifts	1.13	1.19	1.23	1.23	1.23

Note: $\varphi_o = M/M_n$, $M_n^+ = M_n^- = A_s f_y(d-a/2) = 39.2$ kNm

Table 4-6: Observed overstrength factors from test of specimen SB1

Interstorey drift (%)	1.0	1.5	2.0	2.5	3.5
φ_o^+ gap opening drifts	1.13	1.22	1.29	1.33	1.36
φ_o^- gap closing drifts	1.12	1.27	1.34	1.47	1.40

Note: $\varphi_o = M/M_n$, $M_n^+ = A_s f_y(d-a/2) = 39.2$ kNm, $M_n^- = A_s f_y(d-d') = 36.6$ kNm

Continuing the description of specimen SB1's response, during the first gap-closing cycle to -3.5% drift, bottom longitudinal reinforcement buckled, resulting in a slight drop in strength and major cracking of the beam soffit. In subsequent bottom steel compression cycles, strength degraded to 50% of the peak value and major spalling of the beam soffit was observed as shown in Figure 4-15a. On the first bottom steel tension cycle to 4.5%, all four bottom bars fractured in succession resulting in a rapid loss in strength as highlighted in Figure 4-14 and Figure 4-15b. This was attributed to prior buckling inducing high tensile strains at the extreme fibres of the bars, which subsequently fractured when the whole bar was subject to tension. The third cycle at 4.5% drift was not carried out because the specimen exhibited negligible strength.

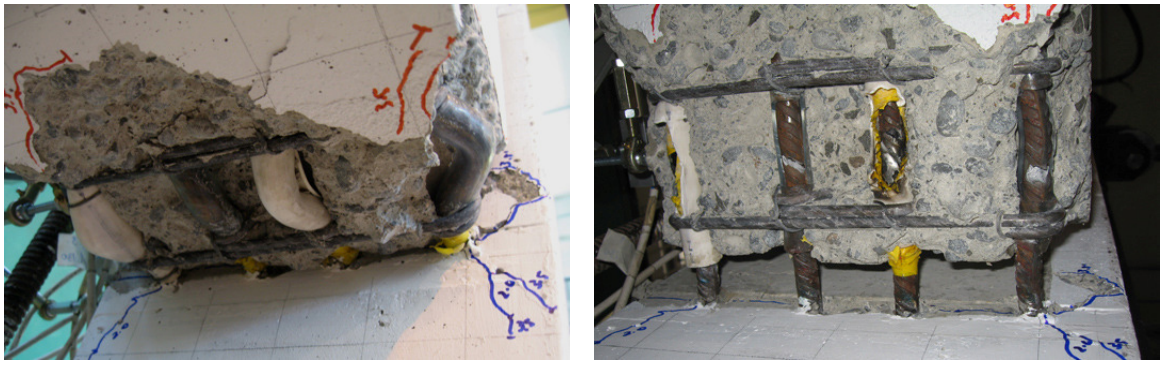

(a) Buckling at -3.5% drift **(b) Fracture at 4.5% drift**

Figure 4-15: Bottom bar buckling and fracture in specimen SB1

Figure 4-16 shows the lateral force-drift response for the interior slotted-beam specimen SB2. Figure 4-16a shows the total subassembly interstorey shear, whilst Figure 4-16b and Figure 4-16c show the interstorey shear force contributions from the left-hand-side (LHS) and right-hand-side (RHS) beams respectively. For specimen SB2, first cracking in both beams occurred at a higher drift than SB1 between 0.3% and 0.5% drift. Similarly, yielding occurred at a higher drift of 0.70-0.75% for gap-opening rotations at a lateral force of 22.7-22.9 kN. For gap-closing rotations, the yield point was similar to SB1 and occurred at 0.64-0.66% drift and a lateral force of 19.1-19.7 kN.

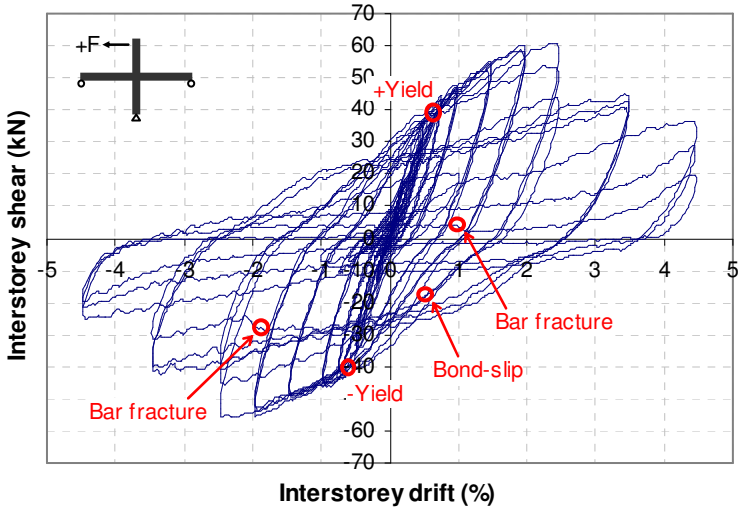

(a) Total subassembly response

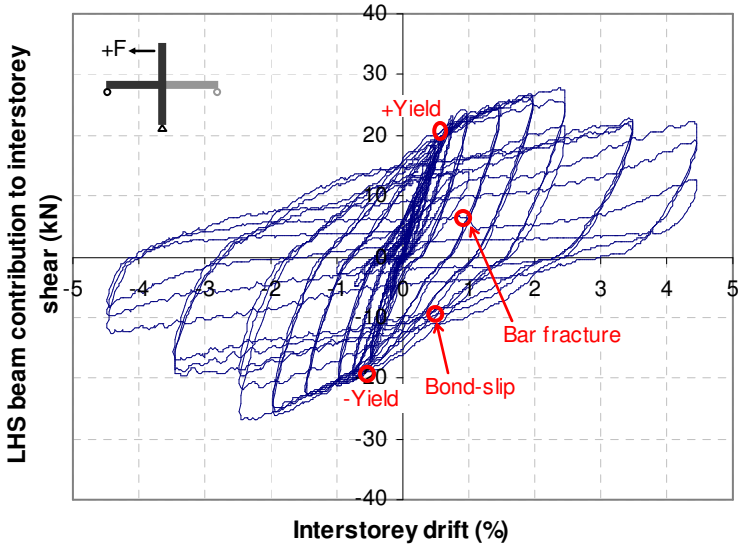

(b) LHS beam contribution to subassembly response

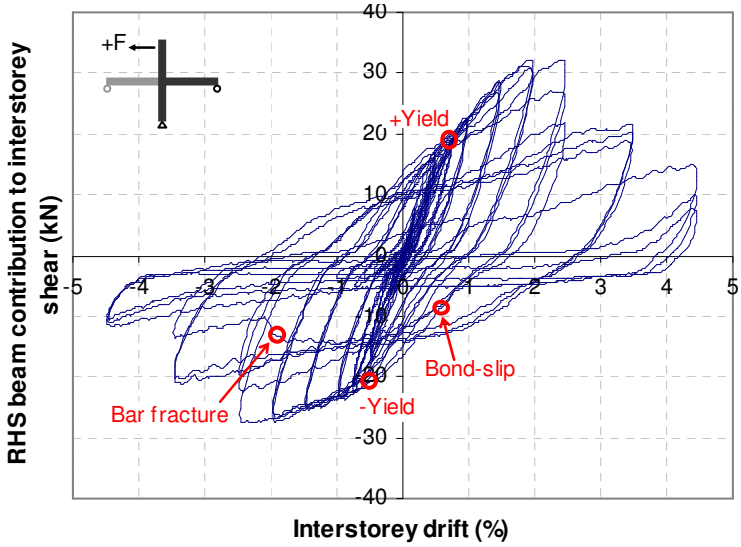

(c) RHS beam contribution to subassembly response

Figure 4-16: Lateral force versus drift response for slotted-beam specimen SB2

Like SB1, SB2 showed significantly less cracking than the monolithic benchmark. However, all three charts in Figure 4-16 show a slightly pinched reinforced concrete hysteresis like RCB1. This is attributed to greater strain penetration into the interior column and limited slip of bottom longitudinal reinforcement within the interior joint region. SB2 showed the same increased post-yield hardening like SB1. However, at gap-closing drifts between 1.5 and 2.5%, the RHS beam shows an unusually steep post-yield stiffness, with a peak shear force contribution greater than 30 kN reached at 2.0% drift. This may be partially caused by grout in the de-bonding steel tubes acting in compression.

During the second 2.5% drift cycle, Figure 4-16 shows approximately 25% strength degradation. This is due to bond-slip failure of the bottom longitudinal reinforcement through the interior joint. In subsequent cycles at higher drifts, the hysteresis is severely pinched and strength continues to degrade as the bars are pulled back and forth through the joint, deteriorating the bond further. The column depth provided was clearly not sufficient. This is discussed more in-depth in Section 4.3.12.

During the third 3.5% drift cycle, a bar in the RHS beam fractured in tension. The same bar later fractured in the LHS beam during the third 4.5% drift cycle. This is shown in Figure 4-17. Unfortunately because of the strength degradation resulting from bond-slip, the test of SB2 was unable to reveal whether the additional stirrups and steel tubes would be sufficient to prevent buckling of the bottom longitudinal reinforcement at 3.5% drift. The bars in the LHS beam did buckle between the stirrups adjacent to the slot at 4.5% drift whereas no buckling was observed in the RHS beam. The LHS beam had stirrups spaced at 35 mm but with plastic debonding tubes, whereas the RHS beam had a stirrup spacing of 50 mm and steel debonding tubes.

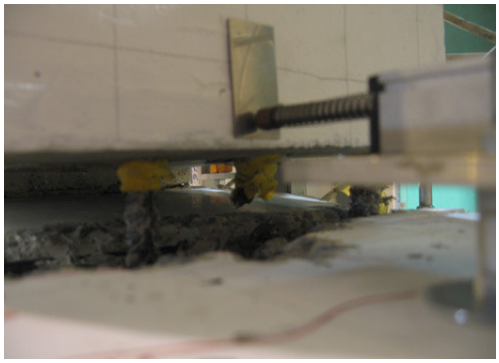

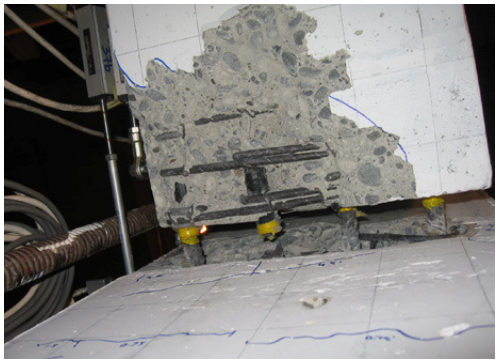

(a) Fracture in RHS at 3.5% drift (b) Buckling and fracture in LHS at 4.5% drift

Figure 4-17: Bottom bar buckling and fracture in specimen SB2

4.3.2 Crack Development and Observed Damage

Table 4-7 summarises crack widths for specimens RCB1, SB1 and SB2 at each peak drift level. Reported on are widths of the main flexural crack within the plastic hinge zone of RCB1 or concrete top-hinges of SB1 and SB2, crack widths in the joint due to strain penetration of longitudinal beam bars into the joint region, and joint crack widths due to joint shear. The locations of these cracks are illustrated in Figure 4-18. Note that no joint shear cracking was observed for specimen RCB1. Beam and column cracks where longitudinal reinforcement remained elastic were insignificant and remained between hairline (HL) and 0.15 mm in width for all three specimens. First cracking in the beam was observed earlier in the monolithic benchmark specimen RCB1 at 0.15% drift, whereas cracks did not appear in the slotted-beam specimens until drifts of 0.25-0.5%. This is because the slot acted as an artificial crack which could accommodate further displacements before first cracking was observed.

Table 4-7: Hinge zone, strain penetration and joint shear crack widths at peak drifts

Drift Level	Measured crack widths (mm)							
	Hinge zone cracks			Strain penetration cracks			Joint shear cracks	
	RCB1	SB1	SB2	RCB1	SB1	SB2	SB1	SB2
0.1%								
0.2%	HL-0.1							
0.5%	0.1-0.15	HL-0.1	0.1-0.15	0.1	0.15	0.1		
0.75%	0.35-0.5	0.25	0.2-0.3	0.15	0.15	0.15-0.25		0.1-0.2
1.0%	0.7-1.3	0.45	0.35-0.45	0.15	0.25	0.15-0.3	HL	0.15-0.25
1.5%	1.6-2.2	0.5-0.75	0.6-0.7	0.2	0.25	0.2-0.35	HL	0.15-0.25
2.0%	2.6-4	0.8-1.3	0.85-1	0.2	0.3	0.25-0.4	HL	0.15-0.35
2.5%	4-6	1-1.6	1.3-1.7	0.2	0.3	0.25-0.75	HL-0.1	0.15-0.45
3.5%	4-7	1.2-2.5	1.4-1.8	0.25	0.4	0.15-0.4	HL-0.15	0.15-0.25
4.5%	Spalling	1-3	~3	0.15	0.15	0.1-0.25	HL	0.1-0.15

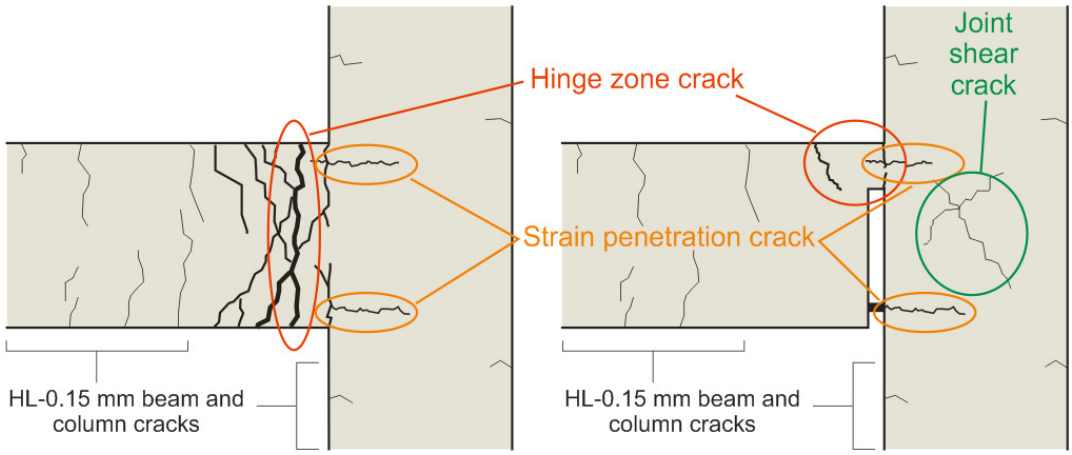

(a) Monolithic beam specimen **(b) Slotted-beam specimen**

Figure 4-18: Illustration of crack locations referred to in Table 4-7

Figure 4-19 and Figure 4-20 show photos illustrating the development of cracks in the three specimens. It is clear that the conventional beam exhibited significantly more cracking than both the slotted-beam specimens. Table 4-7 shows that crack widths within the plastic hinge zone were 2-3 times greater than those in the slotted beams. The main crack for specimen RCB1 was a vertical crack which formed 33 mm from the column face. It was characterised by multiple cracks extending into the plastic hinge zone as it formed. In contrast, the main crack for both SB1 and SB2 was a single crack which formed at the beam-column interface in the top-hinge.

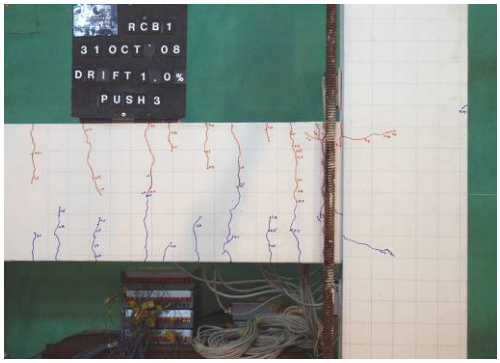

(c) RCB1 -1.0% drift

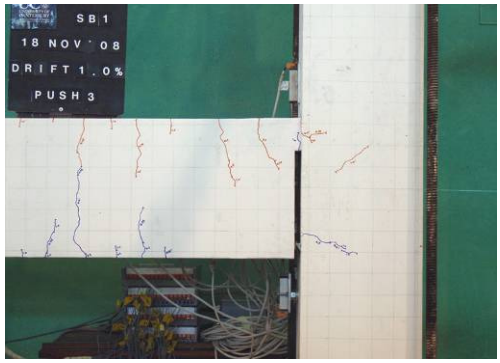

(d) SB1 -1.0% drift

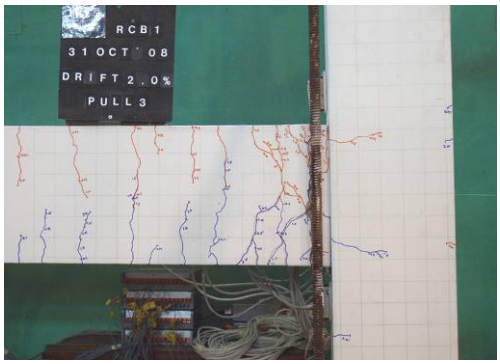

(e) RCB1 2.0% drift

(f) SB1 2.0% drift

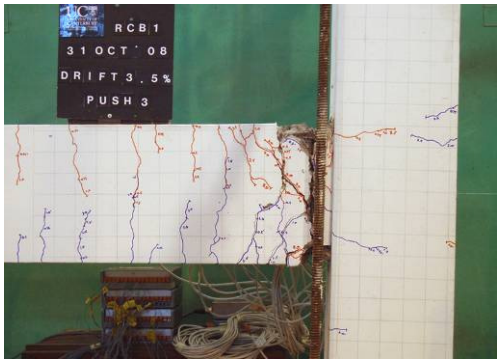

(g) RCB1 -3.5% drift

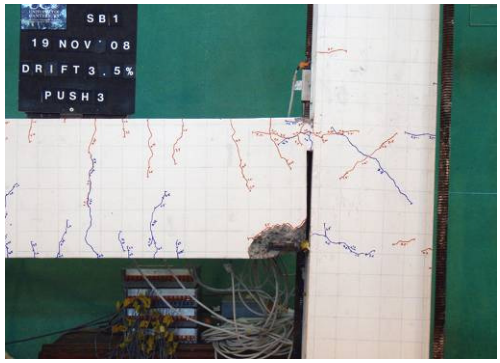

(h) SB1 -3.5% drift

Figure 4-19: Comparison of crack development in specimens RCB1 and SB1

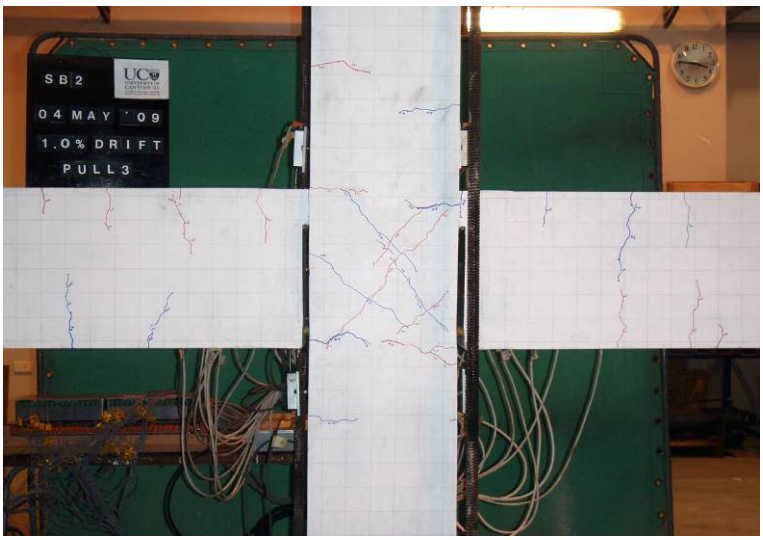

(a) SB2 -1.0% drift

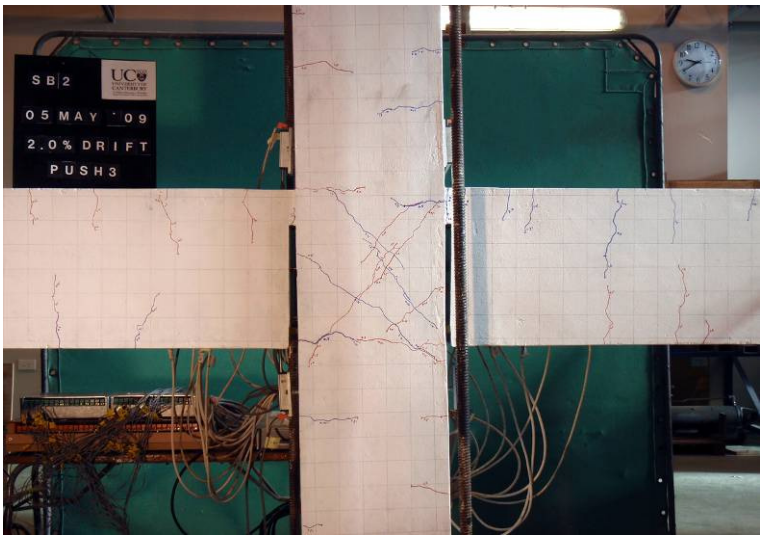

(b) SB2 2.0% drift

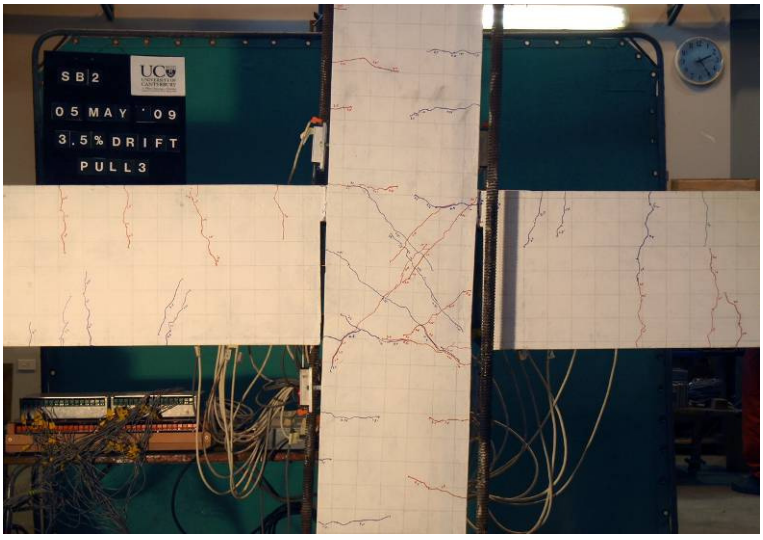

(c) SB2 -3.5% drift

Figure 4-20: Crack development in specimen SB2

At drifts of 1.5%, light spalling along the main flexural crack was observed in specimen RCB1. This worsened exposing transverse reinforcement at 2.5% drift, and continued on to major spalling of cover concrete resulting in a loss of strength at 3.5% drift. Both top and bottom longitudinal reinforced became exposed. For slotted specimen SB1, light spalling at the top of the beam was not observed until 2.5% drift. For both slotted specimens, major spalling only occurred at the beam soffit when bottom reinforcement buckled at 3.5% and 4.5% drift for specimens SB1 and SB2 (LHS beam) respectively.

Only the slotted specimens showed joint shear cracking, however in both cases, there was sufficient joint reinforcement that the joint remained elastic and the cracks closed when the specimen was unloaded. The extent of joint cracking in specimen SB1, which was not observed in RCB1, suggests greater joint shear forces in a slotted-beam than a conventional beam, as expected. This may be attributed to greater post-yield hardening observed in slotted-beams as discussed in Section 4.3.1. Being an interior joint, shear cracking was more extensive in specimen SB2 than in specimen SB1 as expected.

In specimen SB2, Grade 300 steel was used for top longitudinal reinforcement instead of Grade 500 steel which was used in specimen SB1. This was to observe the effect of allowing top reinforcement to yield. Table 4-7 shows no noticeable increase in cracking in SB2 compared to SB1 when limited yielding is allowed in the top longitudinal reinforcement.

Figure 4-21a is a photo of strain penetration cracking in specimen SB1. These horizontal cracks extending into the joint were the result of yield penetration of longitudinal bars into the joint, which were observed in all three test specimens. Table 4-7 shows these cracks were wider in the slotted-beam specimens compared to the monolithic benchmark. This is due to more extensive tension-compression yielding of the bottom reinforcement in slotted-beams. When bond-slip failure occurred in interior specimen SB2 at 2.5% drift, this crack widened to 0.75 mm and extended across the entire width of the column.

Figure 4-21b is a photo of the concrete cone pullout failure which occurred in the RHS beam of specimen SB2. When bond-slip failure occurred, earlier strain penetration cracks combined to form a conical wedge which spalled out as the bars slipped through the joint. A partially formed cone was observed in exterior specimen SB1, but due to adequate anchorage from 90° end-hooks, it did not fully form and spall out.

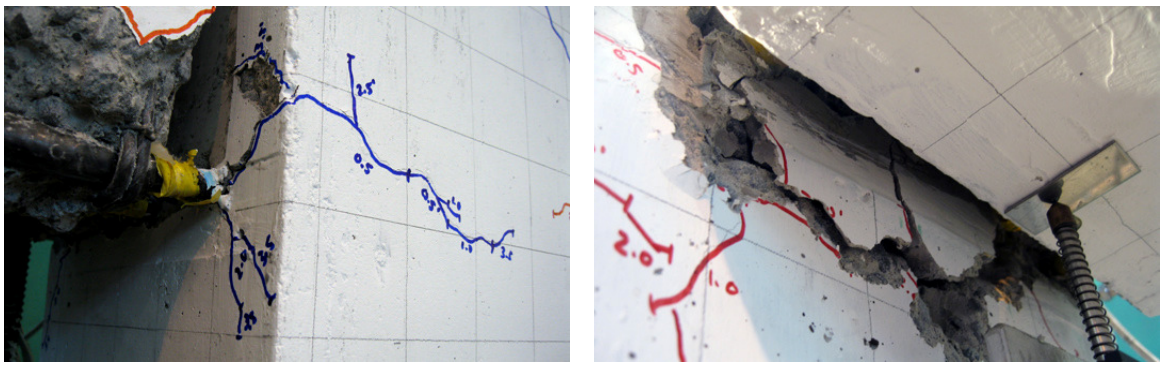

(a) Strain penetration cracking in SB1 (b) Concrete cone pullout in RHS beam of SB2

Figure 4-21: Strain penetration cracking and concrete cone pullout in slotted beams

Prior to bottom reinforcement buckling and bond-slip failure, the slotted-beam specimens exhibited significantly less cracking and spalling than the conventional benchmark specimen. Figure 4-22 highlights the difference in damage sustained between conventional and slotted-beams. These tests showed that slotted-beams present a system requiring minimal repair after moderate earthquakes with drift demands less than 2.5%.

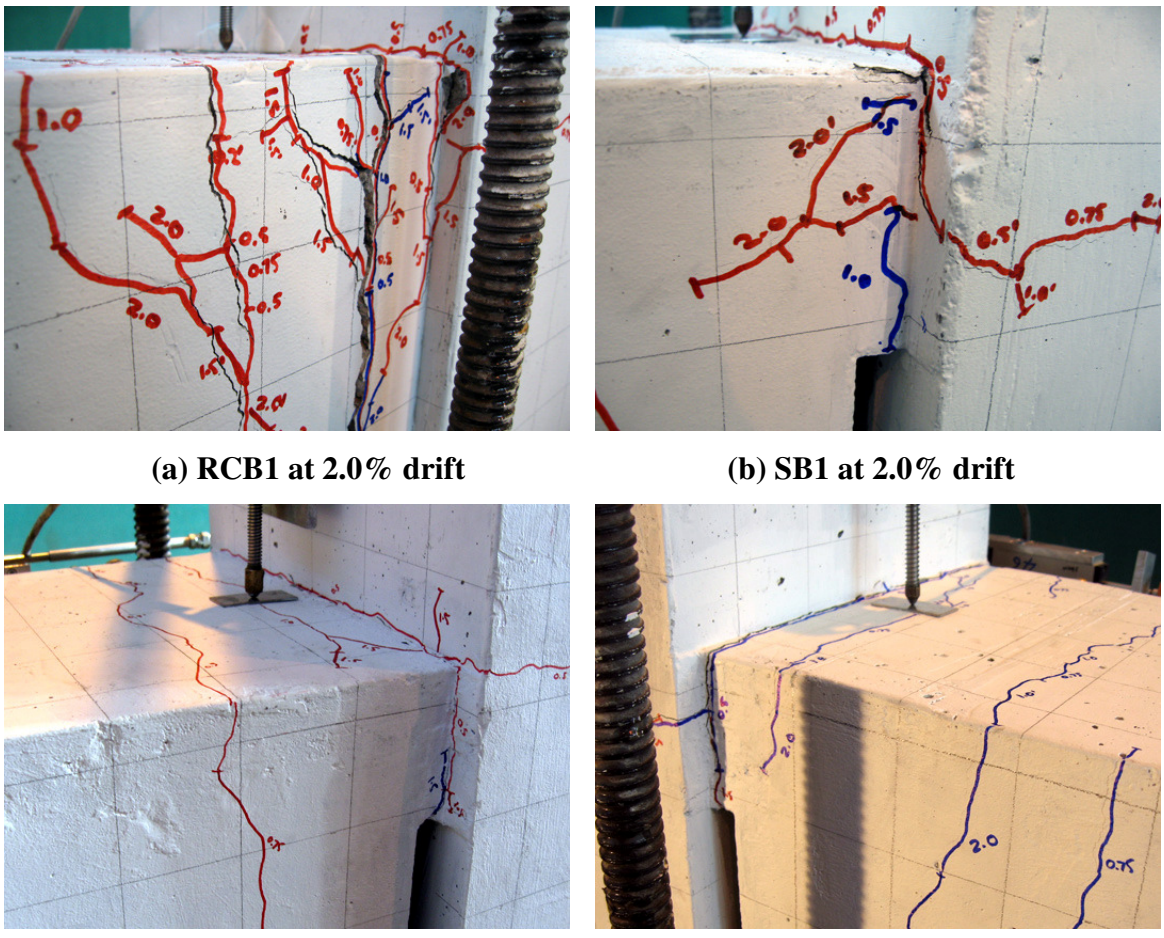

(a) RCB1 at 2.0% drift **(b) SB1 at 2.0% drift**

(c) SB2 LHS beam at 2.0% drift **(d) SB2 RHS beam at 2.5% drift**

Figure 4-22: Comparison of damage observed in the three specimens

4.3.3 Elastic Stiffness and Peak-to-peak Stiffness

Theory suggests that the elastic stiffness of slotted-beams should be slightly less than an equivalent monolithic beam due to the unbonded length of bottom longitudinal reinforcement. Figure 4-23 shows the force-drift response for each beam specimen for drift cycles up to 1.0% and proves this to generally be the case. Figure 4-23c and d show both beams in specimen SB2 to have a lower cracked stiffness than RCB1 (shown in Figure 4-23a), and Figure 4-23b shows specimen SB1 had a reduced stiffness for negative drifts. For positive drifts, SB1 does exhibit an identical stiffness to RCB1, but due to low steel strains at this stage, it is possible strains had not yet propagated far enough into the beam for the de-bonding to become apparent. From these tests, it can be concluded that slotted-beams have a lower elastic stiffness than conventional beams, but the difference can be considered small and inconsequential.

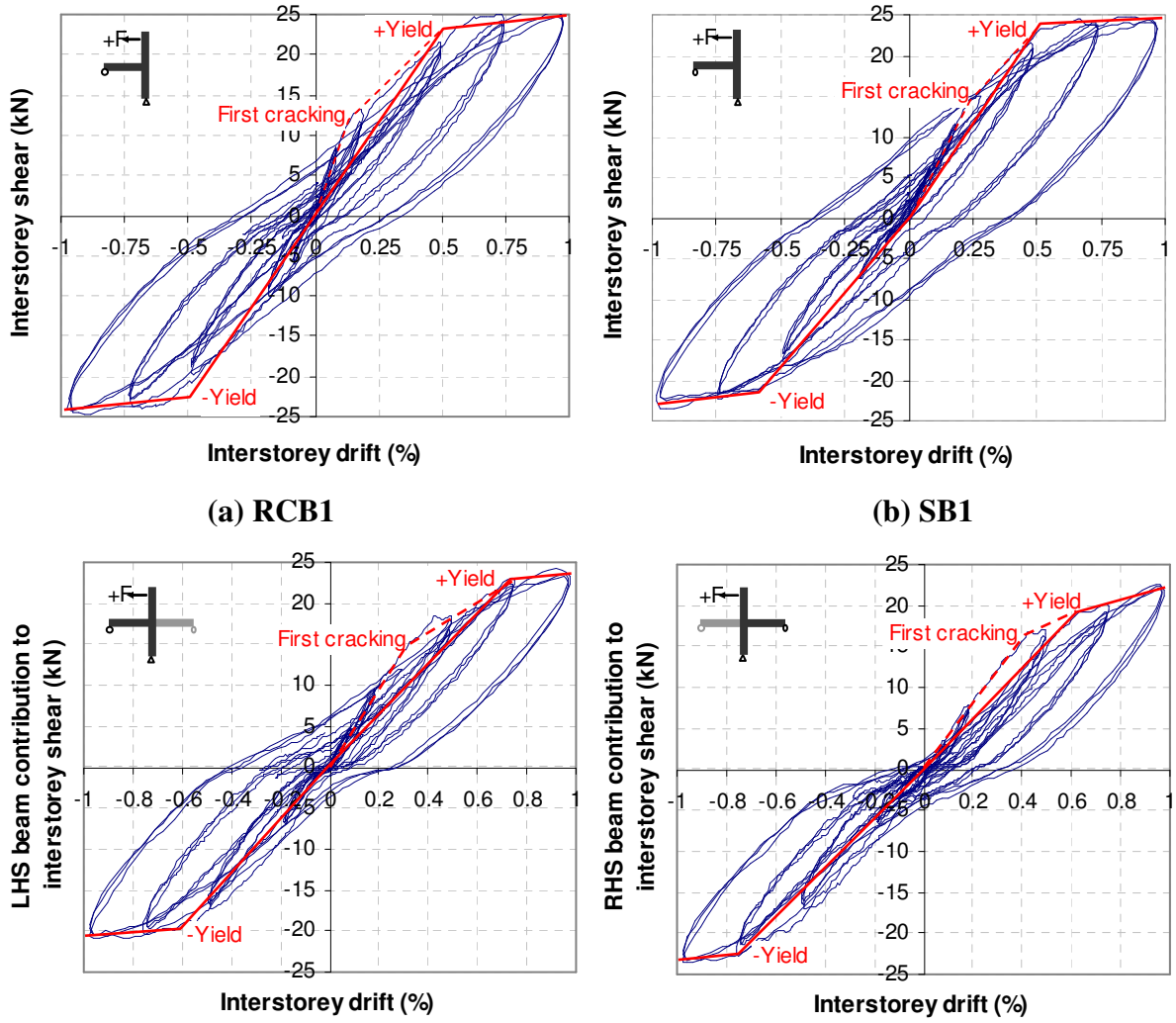

(a) RCB1 **(b) SB1**

(c) SB2 LHS beam **(d) SB2 RHS beam**

Figure 4-23: Force-drift responses up to 1.0% drift cycle

Provided the response of the bottom longitudinal reinforcement is stable, stiffness and strength-wise, the response of a slotted-beam should be comparable to that of a monolithic beam. Figure 4-24 plots the peak-to-peak secant stiffness with drift for each test and shows this to be the case. The peak-to-peak secant stiffness was defined in Section A.2 and is often used to measure strength and stiffness degradation. The figure shows the peak-to-peak stiffness response for all three specimens to be very similar up to a drift of 2.5%. At 2.5% drift, the peak-to-peak stiffness of specimen SB2 decreases due to bond-slip failure, and after 3.5% drift, the peak-to-peak stiffness of specimen SB1 decreases due to bar buckling and subsequent fracture.

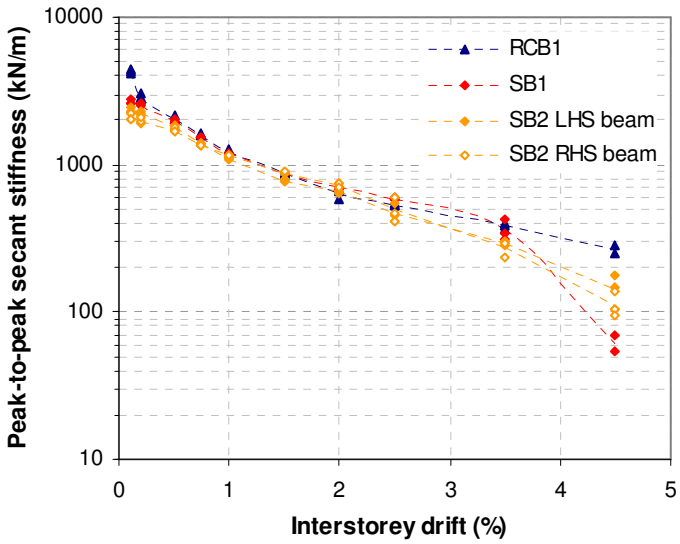

Figure 4-24: Peak-to-peak secant stiffness

4.3.4 Energy Dissipated per Cycle

Figure 4-25 plots the hysteretic energy dissipated per cycle as equivalent viscous damping for each of the three specimens tested. For the elastic cycles at drifts less than 0.5%, the average equivalent viscous damping for all specimens is about 3-5% as is commonly assumed for elastic damping. Because of greater concrete cracking in the monolithic specimen RCB1, it shows a greater amount of damping during elastic cycles compared to the slotted-beam specimens. By 0.75% drift, all specimens had yielded resulting in a significant increase in energy dissipation.

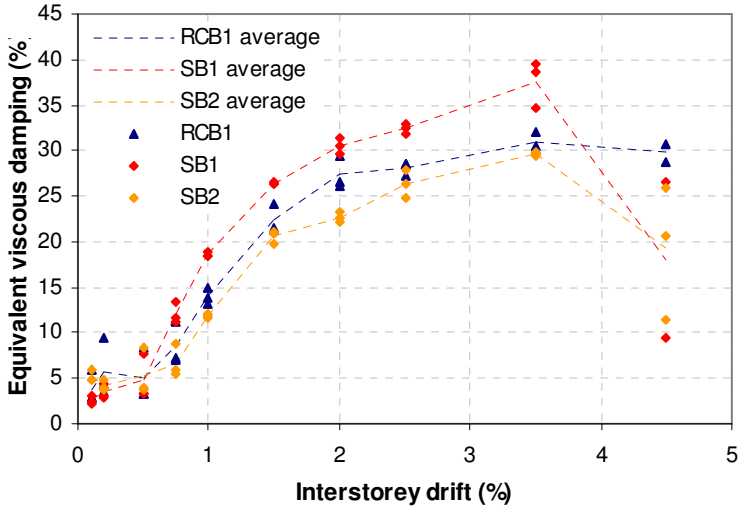

Figure 4-25: Hysteretic energy dissipated per drift cycle

For drifts between 0.75% and 3.5%, specimen SB1 produced 5-10% more damping than its monolithic beam equivalent RCB1. This is due to the fatter hysteretic response produced from cyclic yielding of bottom longitudinal reinforcement in tension and compression. However, this dropped rapidly at 4.5% drift after significant strength degradation due to bar fracture. In contrast, the energy dissipated by the interior slotted-beam specimen SB2 was slightly less than the monolithic benchmark. This can be attributed to a more pinched hysteretic response from bond-slip through the interior joint. Thus it can be concluded that the energy dissipated by a slotted-beam is comparable to, if not greater, than that of a monolithic beam provided sufficient anchorage is provided to bottom longitudinal beam reinforcement.

4.3.5 Beam Elongation

Figure 4-26 shows the measured elongation at the beam centreline across each plastic hinge zone or slotted section for the three specimens tested. This elongation was measured using linear potentiometers crossing the plastic hinge zone of RCB1 or slotted section of SB1 and SB2. Figure 4-26a compares the beam elongation from monolithic specimen RCB1 and slotted specimen SB1. The reduction in beam elongation for a slotted-beam is clearly evident. During 3.5% drift cycles, RCB1 exhibited a maximum residual beam elongation of 15.7 mm when passing through 0% drift, whereas SB1 exhibited 1.2 mm maximum elongation when passing through 0% drift.

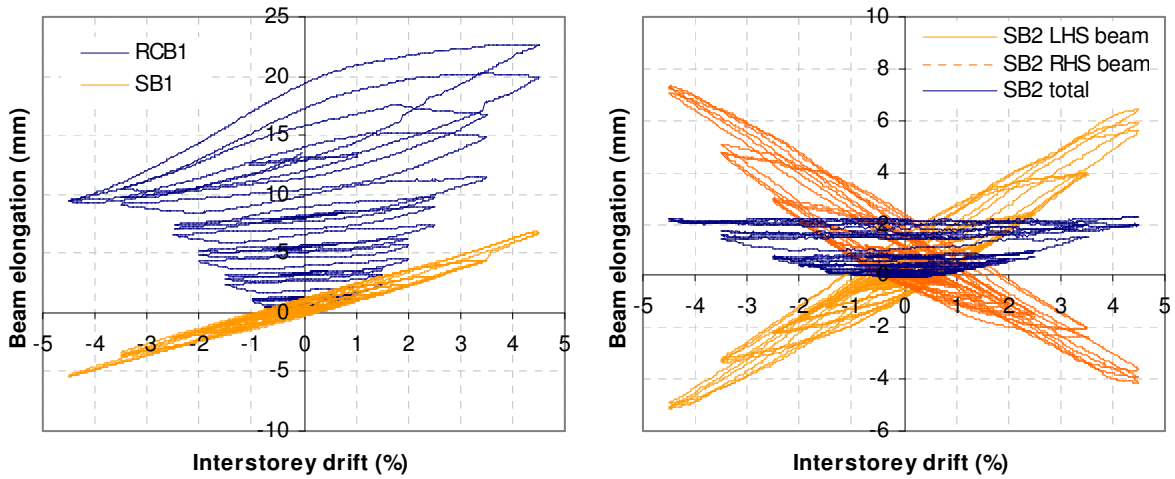

(a) Exterior specimens RCB1 & SB1 **(b) Interior specimen SB2**

Figure 4-26: Measured beam elongation

Figure 4-26b shows the beam elongation measured in the LHS and RHS beams of specimen SB2, and the total subassembly elongation from both beams. For positive drifts, the LHS beam elongates via opening of the slot, while the RHS beam contracts via closing of the slot. This is vice versa for negative drifts. So when the whole subassembly is considered, elongation/contractions from both beams cancel such that the total beam elongation remains less than 2.3 mm.

Unlike specimen SB1, specimen SB2 did not use Grade 500 top reinforcement such that yielding of top reinforcement was permitted. The purpose of this was to observe the effect on cracking and beam elongation when top reinforcement was allowed to yield. Figure 4-27 compares the elongation across the slotted section for the three slotted-beams tested. It is shown that the beam elongation in the LHS beam of SB2 was only slightly greater than that observed in SB1. During 3.5% drift cycles, the LHS beam had a maximum residual elongation of 1.5 mm when passing through 0% drift, compared to 1.2 mm in SB1.

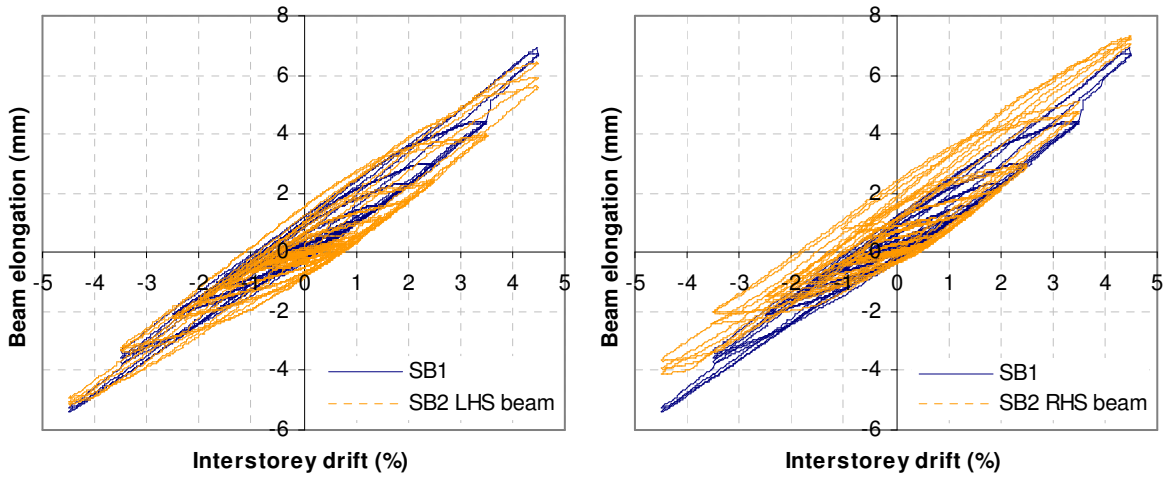

(a) SB1 versus SB2 LHS beam **(b) SB1 versus SB2 RHS beam**

Figure 4-27: Comparison of beam elongation observed in slotted-beam specimens

In contrast, the RHS beam had a greater residual elongation of 2.4 mm, which was twice that of specimen SB1 as expected, but much greater than the LHS beam. The most likely explanation for this is because the LHS beam used Grade 500 steel for the diagonal hangers whereas the RHS beam used Grade 300 steel. Hanger steel in the LHS beam remained elastic and would have helped limit flexural deformations and hence beam elongation. In both cases, the effect is minor when compared to conventional monolithic beams, and allowing limited yielding of top reinforcement has little effect on beam elongation.

4.3.6 Vertical Sliding across Slotted-section

Figure 4-28 shows the vertical sliding measured across the slotted-section of specimens SB1 and SB2. The vertical movement was estimated as described in Section A.5. It is shown that for all three beams the vertical movement across the slot was minimal – less than 1 mm for gap-opening drifts and less than 0.5 mm for gap-closing drifts. It can thus be concluded that diagonal shear reinforcement provides an adequate shear transfer mechanism capable of restraining vertical sliding of the beam at the column face.

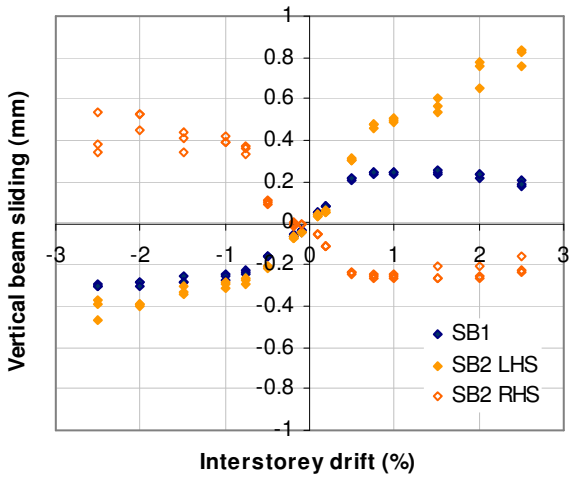

Figure 4-28: Vertical sliding across slotted-section

After yield at 0.75% drift, the vertical movement plateaus slightly with as the beam shear force also plateaus. Vertical displacements did continue to increase more significantly in specimen SB2 compared to specimen SB1. The likely reason for this is because specimen SB2 used Grade 300 top longitudinal reinforcement, whereas specimen SB1 used Grade 500 reinforcement. As a result, yielding of this reinforcement occurred in specimen SB2 but not in SB1. Yielding implies greater crack widths, which would reduce concrete friction/interlock, resulting in the greater vertical movement illustrated above.

4.3.7 Decomposition of Interstorey Drift

Figure 4-29 shows the decomposition of interstorey drift for the three specimens tested for positive and negative drifts. For each specimen, the total interstorey drift is broken down into its separate contributions from beam fixed-end rotation, elastic beam and column flexure, and elastic joint shear. Beam and column shear contributions have been regarded as negligible and are omitted. Fixed-end rotation for the monolithic specimen RCB1 has been taken as the total angle of rotation across the plastic hinge length. It is shown that the response of specimen SB1 for positive drifts is fairly similar to specimen RCB1. This is because the gap-opening mechanics of a slotted-beam is quite similar to that of a monolithic beam. The negative drift response of specimen SB1 is, however, noticeably different and unusual. Because of greater top longitudinal beam reinforcement, a higher elastic flexural stiffness would be expected, such that a greater proportion of beam deformation would be accommodated via fixed-end rotation. However linear potentiometer data for SB1 revealed the opposite and negative fixed-rotations across the slot were less than positive fixed-end rotations. This was not the case for interior specimen SB2, where larger rotations were

measured for gap-closing drifts. This suggests possibly erroneous potentiometer measurements for SB1, which can be attributed to incorrect calibration factors or poor potentiometer alignment.

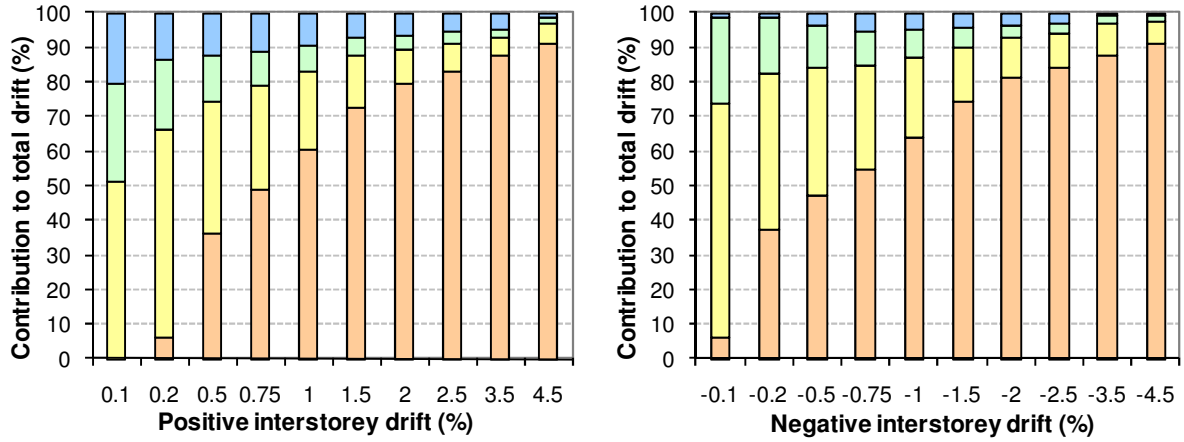

(a) Monolithic beam specimen RCB1

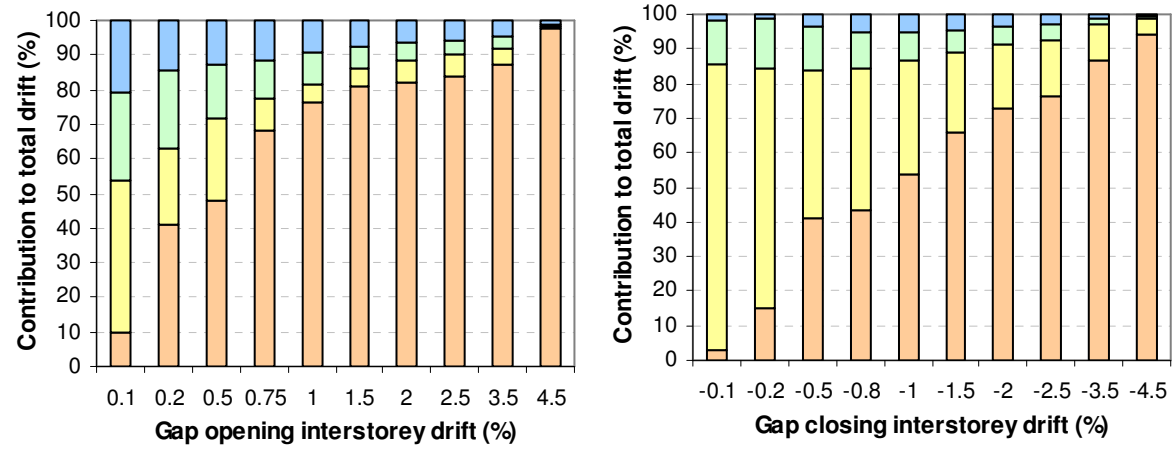

(b) Slotted-beam specimen SB1

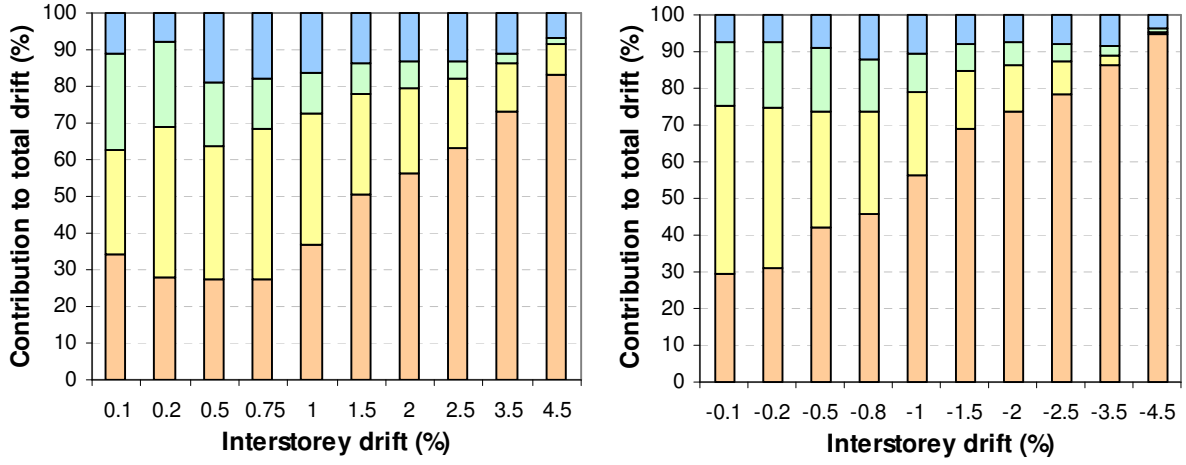

(c) Slotted-beam specimen SB2

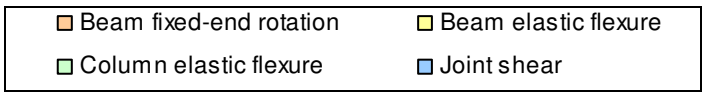

Figure 4-29: Decomposition of interstorey drift

Figure 4-29c shows the decomposition of interstorey drift for specimen SB2. Because the behaviour from both beams in SB2 is considered, the response for positive and negative drifts is similar. Also noticeable is a slightly greater proportion of deformation from column flexure and joint shear compared to the exterior joints. This is because of twice as much force demand from two beams framing into the same joint.

4.3.8 Bottom Longitudinal Reinforcement Strain Profile

Figure 4-30 shows the bottom reinforcement strain profile for slotted specimens SB1 and SB2. Apparent in all four charts is the extensive yielding in tension during gap opening rotations, and yielding in compression during gap closing rotations. Note that omitted data points are due to strain gauge failure from either over-extension or bar slip.

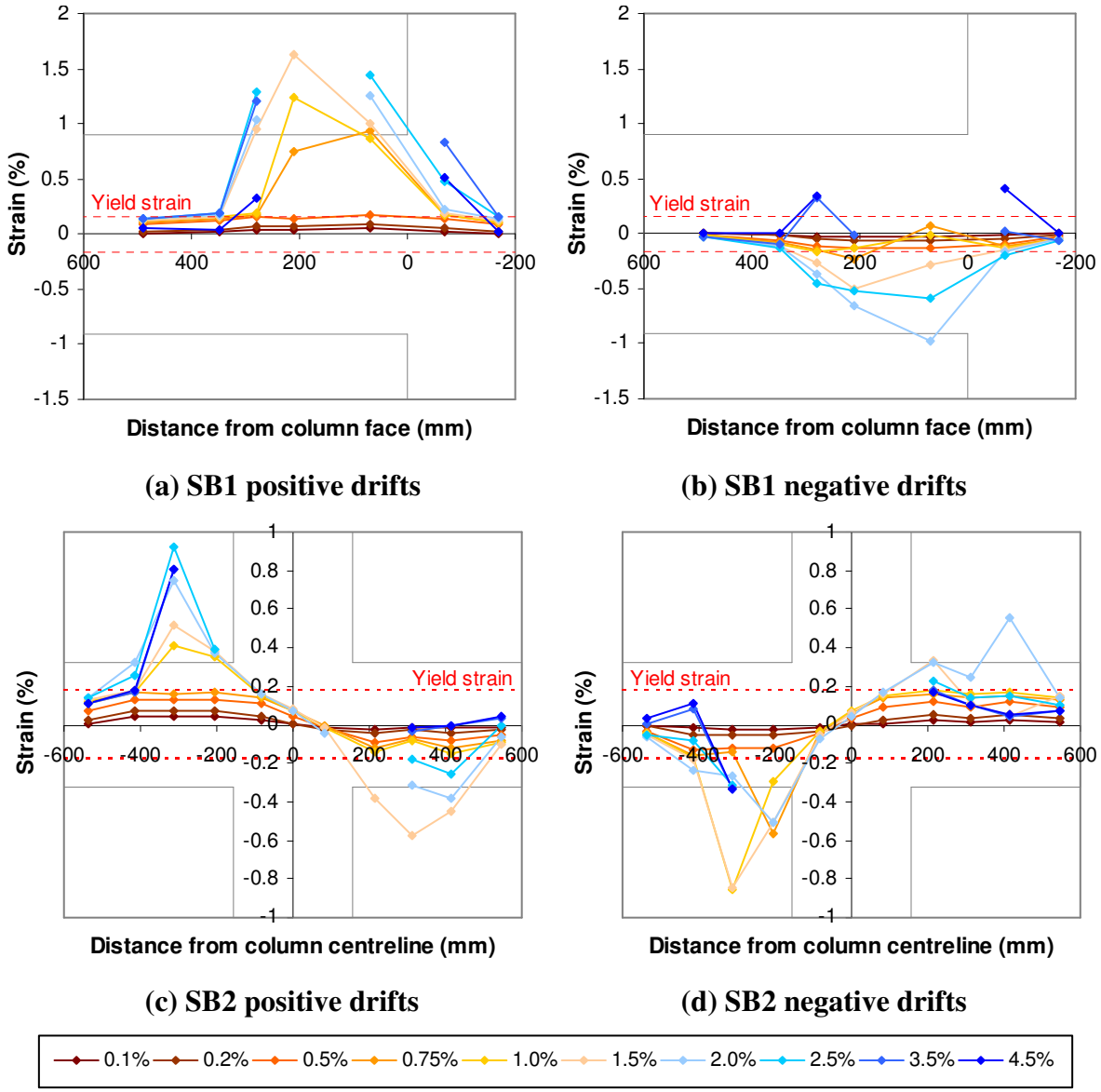

(a) SB1 positive drifts

(b) SB1 negative drifts

(c) SB2 positive drifts

(d) SB2 negative drifts

Figure 4-30: Strain profile in bottom reinforcement at peak drifts

Figure 4-30c and d highlight the extensive strain penetration into the interior joint region, which eventually resulted in bond-slip failure. At drifts of 0.5%, tensile strains had already penetrated beyond the column centreline indicating limited slip had occurred. By 1.5% drift, tensile strains had progressed across three-quarters the column depth, after which strain gauges within the joint failed – most likely damaged due to bar slip.

Paulay and Priestley (1992) and Priestley et al. (2007) have suggested the empirical expression $L_{sp}=0.022f_y d_b$ to estimate the yield penetration length in conventional reinforced concrete beams. Numerically integrating the strain profiles above at drifts of 1.5%, 2.0%, 2.5% and 3.5% gave average yield penetration lengths of $0.011f_y d_b$, $0.02f_y d_b$ and $0.039f_y d_b$ for specimens SB1, SB2 LHS beam and SB2 RHS beam respectively. The reduced strain penetration length for SB1 is most likely the result of the 90° end hook in the joint providing fixed anchorage. Similarly, the greater strain penetration in specimen SB2 might be the result of poor anchorage in the joint. Given the scatter in values, $L_{sp}=0.022f_y d_b$ appears to be a reasonable value to adopt until further test data is available.

4.3.9 Top Longitudinal Reinforcement Strain Profile

Figure 4-31 shows the top longitudinal reinforcement strain profile for slotted specimens SB1 and SB2. It can be seen that strains approximately double when Grade 300 reinforcement is used in specimen SB2 compared to the Grade 500 reinforcement in SB1. Despite this, strains remained below 0.8% and hence the controlled beam elongation and cracking response observed during testing. Oddly, specimen SB2 exhibited tensile strains during gap-opening rotations when compression would be expected. This is most likely the result of larger residual tensile strains, from previous gap-closing cycles, allowing compressive stresses to occur at positive strains. Note that omitted data points in the RHS beam of specimen SB2 is due to strain gauge failure prior to testing.

Strain gauge data can be used to determine appropriate strain lengths for top longitudinal reinforcement. The strain length combines the total length of strain penetration into the joint with the strain penetration into the beam. It is the reinforcement length which, when multiplied by the peak strain in the slotted-section, produces the same axial deformation obtained from integrating the actual strain profile along the bar's length. Palermo (2004) suggests a strain length of $2L_{sp}$ for yielding reinforcement in dry-jointed ductile precast rocking connections. L_{sp} is the strain penetration length taken as $0.022f_y d_b$, which is measured either side of the rocking interface to give $2L_{sp}$ as the strain length. For reinforcement that

remains elastic, Palermo (2004) suggests a reduced strain length of $4/3L_{sp}$. Adopting said strain lengths of $2L_{sp}$ and $4/3L_{sp}$ in a similar fashion to slotted-beams, whilst keeping L_{sp} variable, integration of the strain profiles below estimate L_{sp} to be $0.02f_y d_b$ and $0.023f_y d_b$ for specimens SB1 and SB2 respectively. Therefore $2L_{sp}$ is an appropriate expression for the strain length of yielding top longitudinal reinforcement in slotted-beams, where L_{sp} is taken as $0.022f_y d_b$. Similarly, when top longitudinal reinforcement is elastic, $4/3L_{sp}$ is an appropriate expression for estimating the strain length.

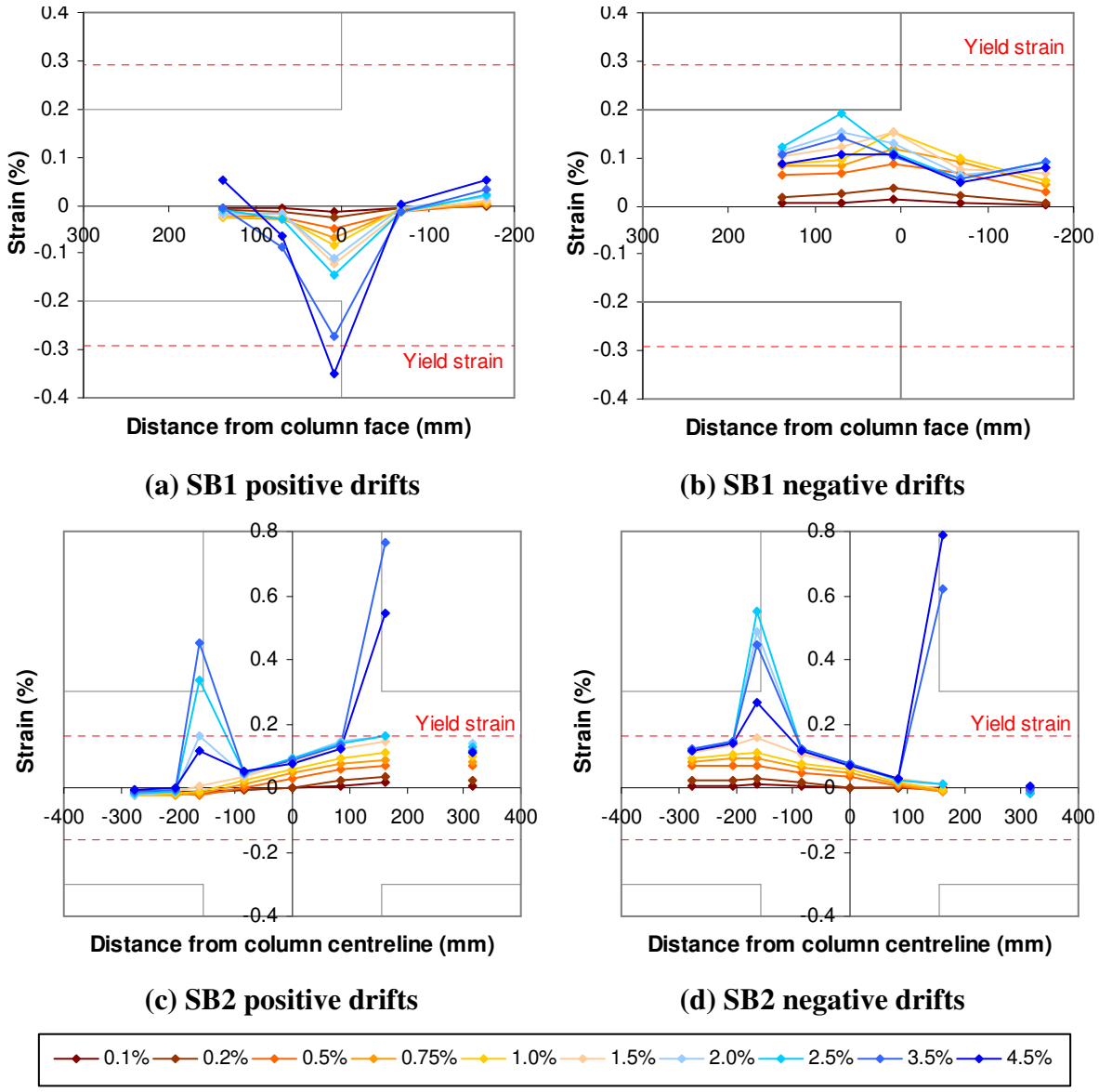

Figure 4-31: Strain profile in top reinforcement at peak drifts

4.3.10 Hanger Reinforcement Strain Profile

Figure 4-32 shows the diagonal shear reinforcement strain profile at peaks drifts for slotted specimens SB1 and SB2. Unfortunately, because hanger reinforcement in specimen SB1 was

only instrumented on one side of the bar, the strains in charts a and b are not accurate near the column face due to bending strains in the reinforcement.

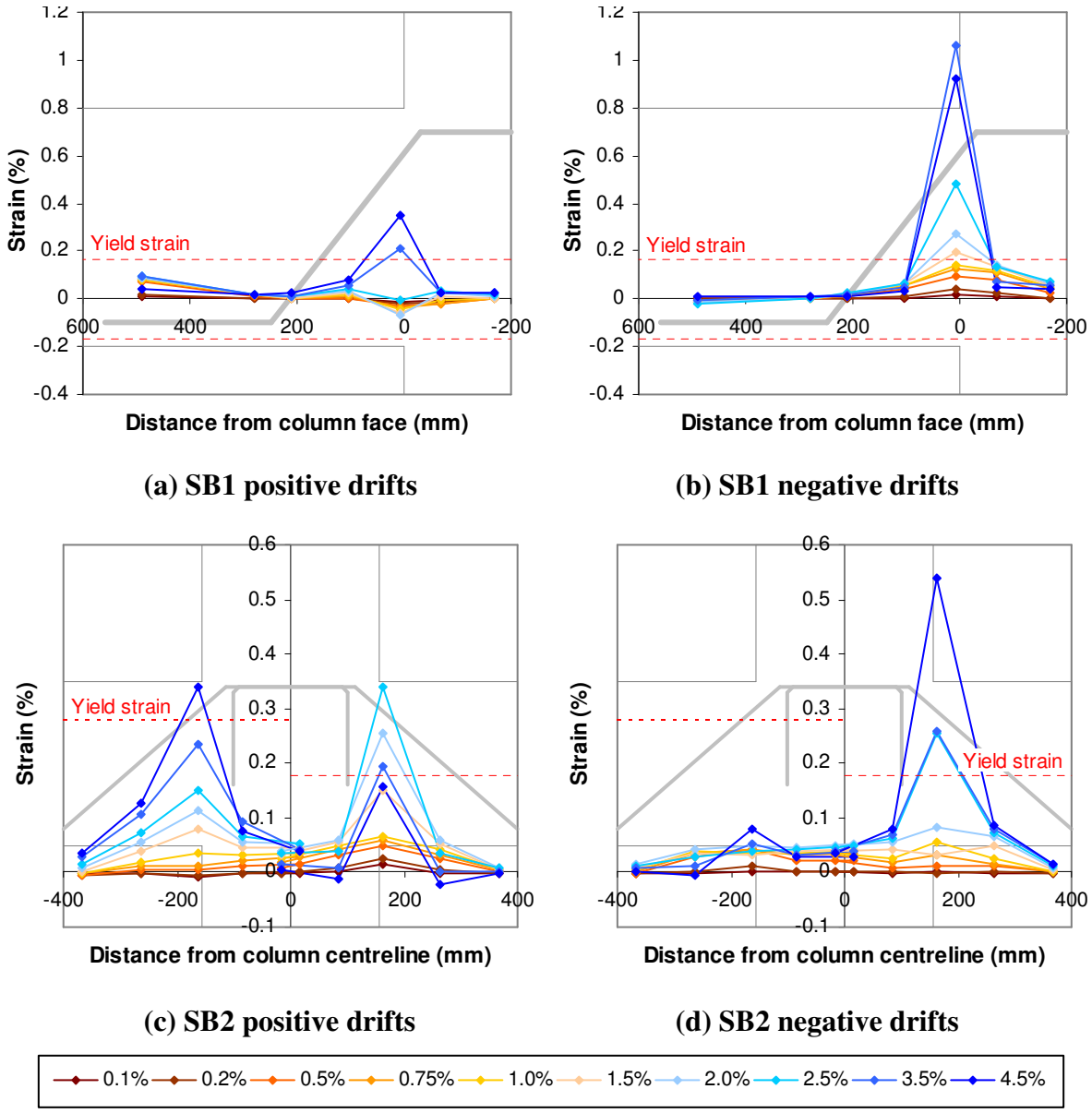

(a) SB1 positive drifts **(b) SB1 negative drifts**

(c) SB2 positive drifts **(d) SB2 negative drifts**

Figure 4-32: Strain profile in diagonal hanger at peak drifts

Apparent in all four charts is a peak strain through the slotted section adjacent to the column face. Although the purpose of the hanger is to carry shear, this peak strain is primarily caused by flexural deformations opening a crack at the beam-column interface rather than shear deformations. Evidence of flexural deformations governing strains within the hanger are positive strains for both gap-opening and gap-closing rotations. If shear was governing the strains within the hanger, strains would be negative during gap-opening rotations and positive during gap-closing rotations. Furthermore, positive and negative strains at the same location, on opposite faces of the bar, in specimen SB2 indicate bending of the hangers at this

interface crack. Because of this complex shear-flexure interaction, the respective proportions of strain from shear and flexure are difficult to quantify. Whilst hangers yield in both specimens, because this is caused by flexure, no significant shear sliding occurs.

Figure 4-32a and b show that hanger strains in specimen SB1 were greater during gap closing (negative) drifts than they were for gap opening (positive) drifts. However, Figure 4-32c and d show the opposite for specimen SB2. This is because the hangers in specimen SB1 were located at a depth of 42 mm below the top fibre of the beam at the column face, whereas the hangers in specimen SB2 were located at a depth of 55 mm. During gap opening drifts, the neutral axis depth lingered around 30 mm, and during gap closing drifts, it increased to around 60 mm. So during gap opening drifts, the hanger in SB1 was closer to the neutral axis, hence the smaller strains; and during gap closing drifts, the hanger was further from the neutral axis, hence the larger strains. The vice versa can be said for specimen SB2. This is further evidence of flexure governing strains in the diagonal reinforcement rather than shear, and also highlights the importance of locating the shear hanger as close as possible to the neutral axis to minimise yielding.

In specimen SB1, the bottom anchorage length of the hanger was instrumented. Figure 4-32a and b show that this length of the hanger behaved in flexure, that is, it acted in tension during an upwards beam shear and in compression during a downwards beam shear. Either side of the bottom bend, strains were minimal indicating the bend provided sufficient anchorage and that such a long anchorage length was not needed.

Assuming a strain penetration length in diagonal reinforcement of $L_{sp}=0.022f_y d_b$ either side of the concrete top-hinge, integration of the hanger strain profiles for specimen SB2 revealed a strain length of $1.96L_{sp}$ and $2.25L_{sp}$ for the LHS and RHS beams respectively. The strain length is the reinforcement length which, when multiplied by the peak strain in the slotted-section, produces the same axial deformation obtained from integrating the actual strain profile along the bar's length. Thus for the given test, $2L_{sp}$ appears to be a reasonable assumption for the strain length of diagonal shear reinforcement. This value is adopted when determining the axial stiffness of hangers in Sections 3.8.3 and 7.1.2.

4.3.11 Shear Transfer Mechanism

In conventional reinforced concrete beams, shear is carried partially by the concrete and by stirrup reinforcement. However, in a plastic hinge zone, concrete deteriorates significantly

such that stirrups must carry the shear into the column. This is illustrated well in Figure 4-33a and b which shows the stirrup strain profile for specimen RCB1. Stirrup strains begin to increase 250 mm from the column face, illustrating the transfer of shear stresses from the concrete to the steel.

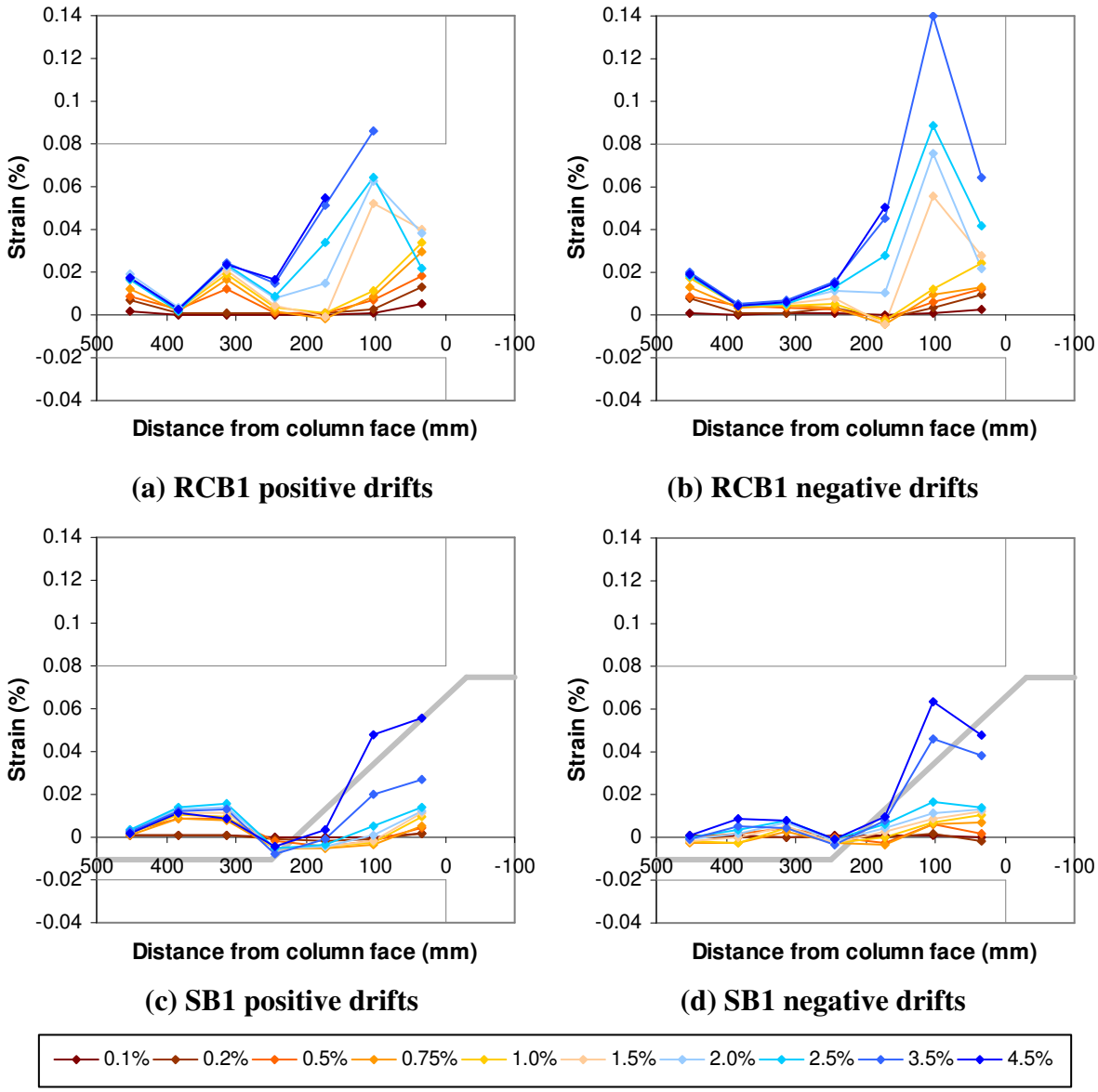

(a) RCB1 positive drifts **(b) RCB1 negative drifts**

(c) SB1 positive drifts **(d) SB1 negative drifts**

Figure 4-33: Stirrup strain profile at peak drifts

Slotted-beams are different. Because of the reduced concrete section in a slotted-beam, diagonal shear reinforcement is used to transfer shear from the beam into the column. Figure 4-33c and d shows the stirrup strain profile for slotted specimen SB1. The sudden decrease in stirrup strains at the lower bend of the diagonal shear reinforcement is due to the transfer of shear carried by the stirrups to the diagonal deformed bars. Stirrup strains do increase again

closer to the column face at higher drifts, but this is probably the result of buckling restraint of bottom longitudinal reinforcement and not shear-transfer.

Although zero concrete shear contribution is assumed through the concrete top-hinge of a slotted-beam for design, Figure 4-34 shows evidence of the concrete top-hinge carrying some shear. The figure plots the total beam shear force and the vertical force component in the hangers at peak drifts for specimen SB2. Hanger forces were calculated from recorded strains in the slotted section. For both beams, the vertical force in hanger reinforcement is not always consistent with the beam shear force. As discussed in Section 4.3.10, this is because hanger strains are more strongly influenced by flexure rather than shear. However during gap closing drifts, hanger reinforcement is in tension from both flexure and shear such that some consistency should be seen. For negative (gap closing) drifts of the LHS beam and smaller positive (gap closing) drifts of the RHS beam, the vertical shear carried by the diagonal hanger is less than the total beam shear; which suggests that some shear must be carried by the concrete top-hinge. Unfortunately, this shear contribution is difficult to quantify, and cannot be relied upon to be always present.

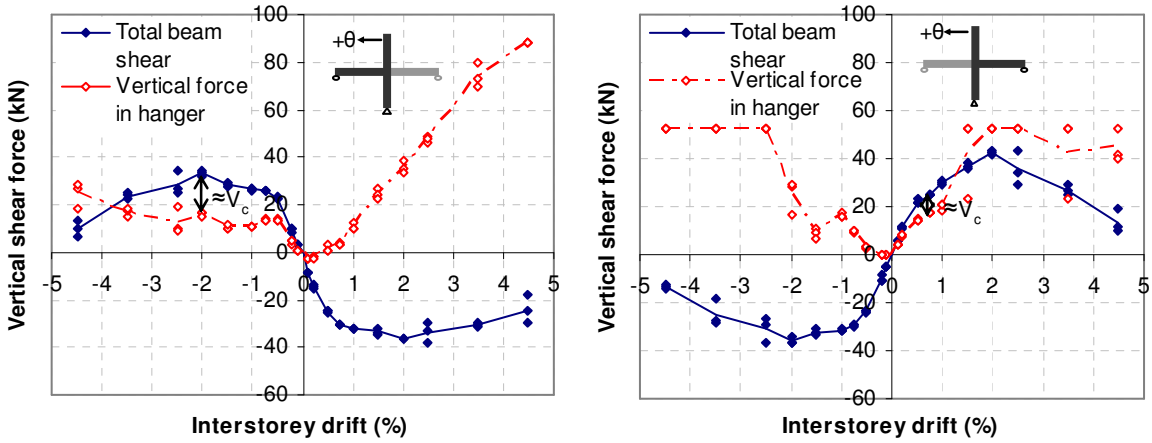

(a) LHS beam **(b) RHS beam**

Figure 4-34: Evidence of concrete shear contribution in specimen SB2

4.3.12 SB2 Bond-slip Failure Analysis

Testing of SB2 revealed that the provided column depth of 310 mm did not provide enough bond to prevent slip of bottom longitudinal reinforcement through the joint. At 2.5% drift, bond-slip of bottom reinforcement occurred. This section describes the assumptions used to determine the column depth and explains why these provisions were insufficient.

The design equation used to determine the column depth for specimen SB2 was modified from theory given in Paulay and Priestley (1992). Assuming unity for all modification factors, the basic equation given in Paulay and Priestley can be expressed as:

$$\frac{d_b}{h_c'} \leq \frac{4u_a}{\xi_m \lambda_o f_y} \qquad ...(4\text{-}1)$$

Where d_b is the longitudinal bar diameter, h_c' is the effective column depth providing bond, u_a is the average bond stress/strength, ξ_m is a factor accounting for the extent of yielding in the longitudinal reinforcement and λ_o is the overstrength factor.

h_c' is normally assumed to be $0.8h_c$, and this assumption was adopted for the design of specimen SB2. λ_o is normally taken as 1.25 for Grade 300 reinforcement, and this too was adopted in the design. Paulay and Priestley recommend ξ_m=1.55 for conventional reinforced concrete beams, but for slotted-beams where yield push and pull occurs of either side of the joint ξ_m =2.0 is more appropriate. From the bond stress distribution shown in Figure 4-35, u_a can be approximately taken to be $0.67u_{max}$. Given that Eligehausen et al. (1983) observed peak bond stresses of $u_{max}=2.5\sqrt{f'_c}$, this gives $u_a=1.675\sqrt{f'_c}$.

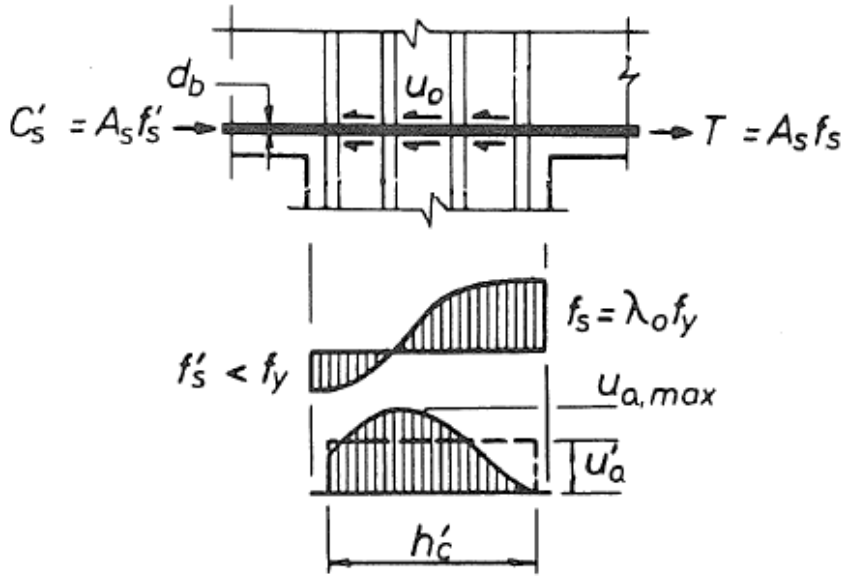

Figure 4-35: Bond stress distribution in conventional reinforced concrete beams (Paulay & Priestley, 1992)

Combining all of the above and given that D12 reinforcement was used, the required column depth is then:

$$h_c = 310\text{ mm} \geq \frac{\xi_m \lambda_o f_y}{4u_a} \times \frac{d_b}{0.8} = \frac{2 \times 1.25 \times 300}{4 \times 1.675\sqrt{30}} \times \frac{12}{0.8} = 307\text{ mm}$$

Later forensic studies of the failure revealed that certain assumptions made above were not appropriate. Firstly, it has been shown that slotted-beams exhibit greater post-yield hardening due to the cyclic yielding of the bottom reinforcement, so the adopted value for λ_o of 1.25 was un-conservative. At 2.5% drift when bond-slip occurred, the overstrength factor for bottom longitudinal reinforcement already exceeded 1.3.

Secondly, the assumption of h_c'=0.8h_c is somewhat arbitrary, and concrete cone pullout failure as illustrated in Figure 4-36 meant that the effective column depth was actually reduced to below 0.7h_c. It is interesting to note that the concrete cone angle was approximately 45° and intersected with the stirrups immediately adjacent to longitudinal bar on the RHS column face. An extra stirrup was included in the cover concrete of the LHS column face, and this helped to reduce the depth of cone pullout. In future, it is recommended that horizontal stirrups be placed immediately adjacent to the longitudinal beam bar to provide confinement against this concrete cone pullout. This behaviour is not so pronounced in conventional beams, due to some confinement being provided by adjacent beam concrete. But it becomes apparent in slotted-beams due to the presence of the slot and extensive tension-compression yielding.

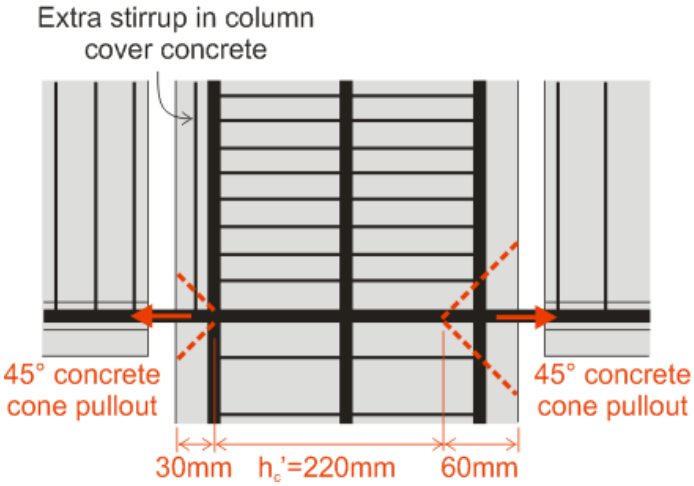

Figure 4-36: Concrete cone pullout failure in specimen SB2

Lastly, the assumption that u_a=0.67u_{max}=1.675√f'$_c$ may not apply to slotted beams as the bond stress distribution changes slightly altering the u_a/u_{max} ratio. Section 3.6 discusses this more in-depth. Just prior to bond-slip failure, average bond stress values on the order of 1.48√f'$_c$ were achieved as shown in Figure 4-37.

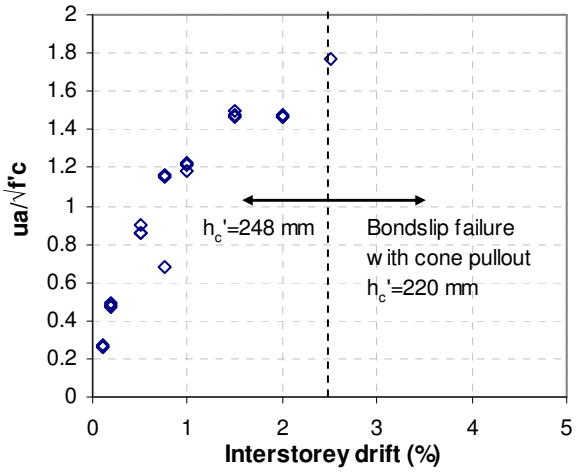

Figure 4-37: Average bond stress at peak drifts

Adopting the observed values for λ_o and h_c' at 2.5% drift and u_a=1.48√f'$_c$, it can be shown that the provided column depth was insufficient and hence the observed bond-slip failure.

$$h_c = 310\,\text{mm} \le \frac{\xi_m \lambda_o f_y}{4u_a} \times \frac{d_b}{0.7} = \frac{2 \times 1.3 \times 300}{4 \times 1.48\sqrt{30}} \times \frac{12}{0.7} = 412\,\text{mm}$$

4.3.13 SB2 Transverse Joint Reinforcement Strain Distribution

Figure 4-38 shows the horizontal joint reinforcement strain distribution at peak drifts for specimen SB2. It is shown that yielding does not occur and enough reinforcement was provided. It is also shown that strains increase towards the bottom of the joint, suggesting increasing joint shear carried by lower stirrups. This distribution is the result of the joint shear behaviour described in Section 3.7.2. Traditionally, the contribution to the concrete strut mechanism comes from concrete compression forces and reinforcement forces transferred via bond. However, because there is no concrete compression at the bottom of a slotted-beam, the excess strut force from the top of the joint must be resisted by joint stirrups at the bottom of the joint.

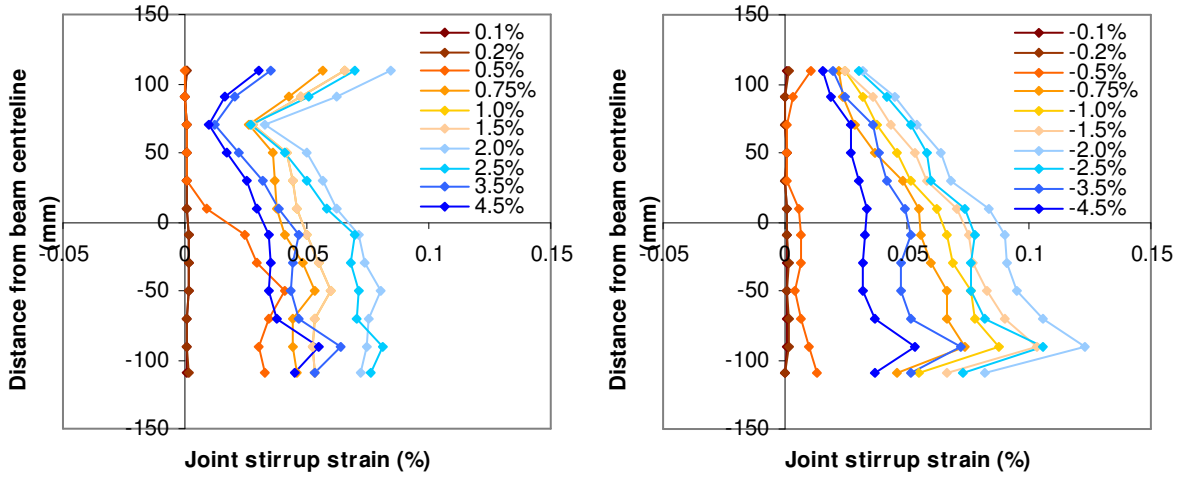

(a) Positive drifts **(b) Negative drifts**

Figure 4-38: SB2 horizontal joint reinforcement strain distribution at peak drifts

Table 4-8 summarises the proportion of total joint shear carried by horizontal stirrups, V_{sh}/V_{jh}, for specimen SB2 as calculated from strain gauge data at drifts of ±1.0%, ±1.5%, ±2.0% and ±2.5%. Also tabulated are values calculated for a theoretical, equivalent monolithic beam specimen RCB2, subject to the same joint shear demand – these values were calculated according to Equation 3-21, using actual column neutral axis depth data from moment-curvature analysis. It is shown that the total joint shear carried by stirrups for slotted specimen SB2 was between 40-60% of the total shear demand, which was higher than 43% expected for an equivalent monolithic beam. This 30-40% increase is the excess strut force from the top of the joint which must be resisted by stirrups at the bottom of the joint.

Table 4-8: Proportion of horizontal joint shear carried by joint stirrups

		SB2	RCB2	Excess strut force
V_{jh} (kN)	ξ_b	V_{sh}/V_{jh}	V_{sh}/V_{jh}	$\Delta V_{sh}/V_{sh,RCB2}$
252	2.05	0.40	0.42	-0.06
265	2.05	0.43	0.41	0.06
278	2.00	0.47	0.41	0.15
298	1.95	0.49	0.43	0.15
-252	1.90	0.45	0.42	0.08
-265	1.88	0.49	0.41	0.20
-278	1.77	0.56	0.41	0.36
-298	1.73	0.57	0.43	0.34

Table 4-8 summarises values for the factor ξ_b, which were back calculated using Equation 3-22. ξ_b is a factor which, when multiplied by the average bond force along the total column depth, gives the average bond force along the column neutral axis depth which contributes to the strut mechanism. For conventional monolithic beams, 1.25 is adopted by NZS3101:2006. However because the bond stress mechanism is slightly different for a

slotted-beam, it is expected that this factor will increase slightly (See Sections 3.6 and 3.7.2). Indeed this was the case for specimen SB2, which had values ranging between 1.73 and 2.05 as shown in Table 4-8.

4.3.14 Comparison and Discussion of Damage Limit States

Damage limit states are often used to help define performance levels for various structural elements in a building. ASCE Standard 41-06 (2007) defines three performance levels – Immediate Occupancy (IO), Life Safety (LS) and Collapse Prevention (CP); and specifies damage limits for each of these categories. This section compares the occurrence of various damage limit states in the tested slotted-beam and monolithic beam specimens, and discusses these limits in relation to the three aforementioned performance levels. Figure 4-39 plots theoretical moment-rotation backbone curves for both specimens RCB1 and SB1, and annotates damage states observed during testing. Also annotated for the monolithic specimen are beam rotation limits for each performance level as currently specified in ASCE/SEI 41-06 (2007). Theoretical backbone curves have been used for clarity, and because they agree well with experimental results until strength degradation occurred at rotations greater than 0.03 radians.

Immediate Occupancy (IO) is defined as the post-earthquake damage state where the structure remains safe to occupy. The building retains its pre-earthquake strength and stiffness, and although minor structural repairs may be appropriate, these are not required prior to re-occupancy. For conventional concrete frames at this performance level, ASCE/SEI 41-06 specifies a maximum transient drift limit of 1.0% and negligible permanent drifts. For beams elements, a maximum plastic rotation of 0.010 radians is specified. Floor cracks should be limited to distributed-hairline cracking with some larger cracks not exceeding 3.2 mm (1/8”) in width. The limit state C3.2 in Figure 4-39 corresponds to the occurrence of 2.1 mm (=2/3-scale×3.2 mm) flexural cracks in the tested beam specimen. Given that floor crack widths will be very similar to beam crack widths immediately adjacent to the beam, for specimen RCB1 it can be seen that this floor crack width limit corresponds well with the IO beam rotation limit. However for the slotted-beam specimen, the C3.2 limit state does not occur until a much larger rotation of 0.033 radians. Because slotted-beams were developed as a non-tearing floor solution, floor crack width limits will no longer govern the performance level of the structure. The slotted-connection itself was able to sustain large rotations up to 0.02 radians with only minor damage and no strength loss. The only

significant damage that occurred was the yielding of bottom longitudinal reinforcement. Immediate occupancy for slotted-beam frames will therefore only be governed by 1% maximum transient drift limits and negligible residual drift limits. These drift limits ensure damage to internal partitions is minimal and the functionality of the structure is not compromised by permanent deformations.

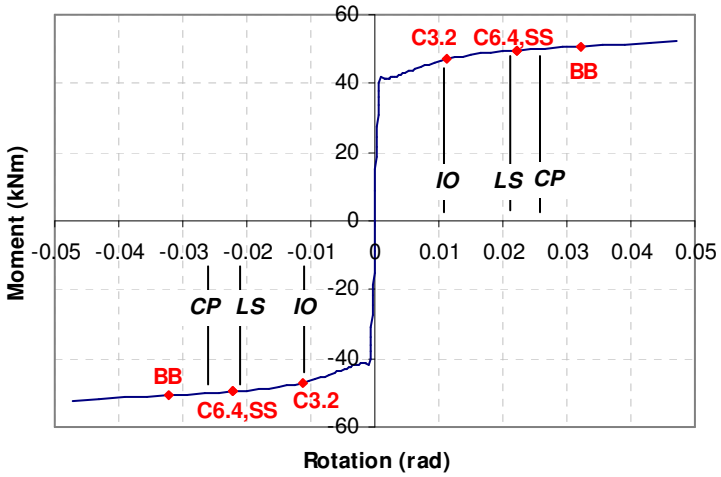

(a) Monolithic beam specimen RCB1

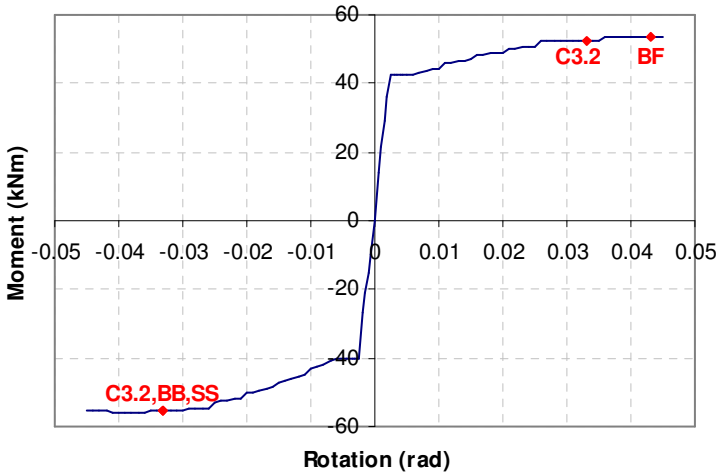

(b) Slotted-beam specimen SB1

Damage limit-state abbreviations:
C3.2 = 3.2 mm flexural crack width (2.1 mm @ 2/3-scale)
C6.4 = 6.4 mm flexural crack width (4.2 mm @ 2/3-scale)
SS = Severe spalling
BB = Bar buckling
BF = Bar fracture

Figure 4-39: Comparison of observed limit states in specimens RCB1 and SB1

Life Safety (LS) is defined as the post-earthquake damage state where the structure has damaged components, but still has some residual strength and stiffness in all stories which

provides a safe margin against partial or total collapse. It should be possible to repair the structure, which should be carried out prior to re-occupancy; however this may not be practical for economic reasons. For this performance level, a maximum transient drift limit of 2% and a residual drift limit of 1% are specified. For conventional RC beam elements, a maximum plastic rotation of 0.02 radians is given. Damage to floors should be limited to a maximum crack width of 6.4 mm (1/4"), and local crushing and spalling. The limit states C6.4 and SS in Figure 4-39 respectively correspond to the occurrence of 4.3 mm (=2/3-scale×6.4 mm) flexural crack widths and severe spalling in the tested beam specimen. Figure 4-39a shows these damage states occurred close to the LS rotation limit for monolithic specimen RCB1. However for specimen SB1, C6.4 and SS damage states did not occur until a higher rotation greater than 0.03 radians. So again floor damage will not govern the performance level of structures with slotted-beams. Spalling in the slotted-beam specimen was the result of bar buckling (BB), which results in severe strength and stiffness degradation; and thus the BB limit state exceeds the LS performance level. Even so, this still occurred at a rotation far in excess of LS rotation limits for conventional beams, such that the LS performance level for slotted-beams is likely to be governed by transient and residual drift limits. Given that slotted frames exhibit far less damage and smaller residual drifts (See numerical analyses in Section 7.3), beam plastic rotation limits and transient drift limits for the Life Safety performance level could be increased when slotted-beams are used instead of conventional RC beams. From the performance of tested specimens, increasing the plastic rotation limit from 0.02 radians to 0.025 radians when slotted-beams are used appears reasonable. Similarly, increasing the transient drift limit from 2.0% to 2.5% when slotted-beams are used also seems appropriate.

Collapse Prevention (CP) is defined as the post-earthquake damage state where the structure has little residual strength and stiffness and is near collapse. The structure will have large permanent drifts, but gravity bearing elements should still function. For conventional concrete frames, ASCE/SEI 41-06 specifies a maximum transient and permanent drift limit of 4%, and a maximum plastic rotation of 0.025 radians in beams. Floor damage at CP is described as extensive crushing with observable offsets across cracks. For monolithic specimen RCB1, the CP rotation limit of 0.025 radians appears quite low given that 4% drifts are allowed. Strength degradation from bar buckling (BB) did not occur until 0.033 radians of rotation, and damage observed in the specimen at this rotation is more consistent with the CP floor damage description than at 0.025 radians. The author is not fully aware of the

rationale behind this beam rotation limit adopted, but believes this could be increased. For the slotted-beam specimen SB1, bar buckling (BB) and bar fracture (BF) limit states provide a good indication of the CP performance level. This is because both result in severe strength and stiffness loss, but the gravity shear carrying capacity of the top-hinge system is still maintained via diagonal hangers. Even though bottom bars will become ineffective, contact between the beam soffit and column face will provide some protection against total collapse at large transient or residual drifts. Damage to the floor slab will still be minimal, such that floor damage still does not provide much indication of the structure's performance level. To guard against P-delta instability, the 4% drift limit for Collapse Prevention should be maintained for slotted-beams. However to allow this drift and bar buckling limit states to be reached, the beam plastic rotation limit could most likely be increased to around 0.03-0.035 radians.

CHAPTER 5 EXPERIMENTAL INVESTIGATION OF 2D INTERIOR JOINT SUBASSEMBLY WITH FLOOR SLAB

After testing the three beam-column subassemblies RCB1, SB1 and SB2 (See CHAPTER 4), an in-plane interior beam-column specimen SB3 was tested with a floor slab under a similar quasi-static protocol. Specimen SB3 was taken from a five-storey prototype building designed using a displacement-based design method (Priestley, Calvi and Kowalsky, 2007) and assuming Wellington design spectra from NZS1170.5:2004.

Unlike the previous beam-column subassemblies which were 2/3-scale, specimen SB3 was half-scale, but designed for a higher seismicity. A precast floor slab with cast-in-situ topping was included on one side of the beam. This slab had an imposed static gravity load equivalent to the load combination $G+\psi_c Q$ from NZS1170.1:2004.

The purpose of testing this specimen was to:

- Observe the effect of beam torsion resulting from eccentric floor gravity loads
- Verify proposed theory for designing interior joints connecting slotted-beams
- Verify revised provisions for bond to reinforcement passing through an interior joint
- Observe floor slab effects and damage
- Verify reduced stirrup spacing and/or steel tubes as a method to prevent/delay buckling of bottom longitudinal reinforcement

5.1 Test Specimen

5.1.1 Five-storey Prototype Frame Building

Specimen SB3 was taken from the first floor of the five-storey prototype frame building shown in Figure 5-1. To include floor gravity loads, the external seismic frame supporting one-way spanning floor units was considered. A relatively small bay length of 6 m was adopted to match the available span between points of contra-flexure in the scaled test-rig of 3 m. Seismic weights of 1930 kN were assumed for levels one to four for each external frame, while a weight of 1600 kN was assumed at the roof level. The frame was designed

according the direct displacement-based design method given in Priestley et al. (2007) and designed for Wellington seismicity using NZS1170.5 design spectra. For a design drift of 2.0% and equivalent viscous damping of 20.5%, this yielded an inelastic base shear demand of 813 kN per seismic frame.

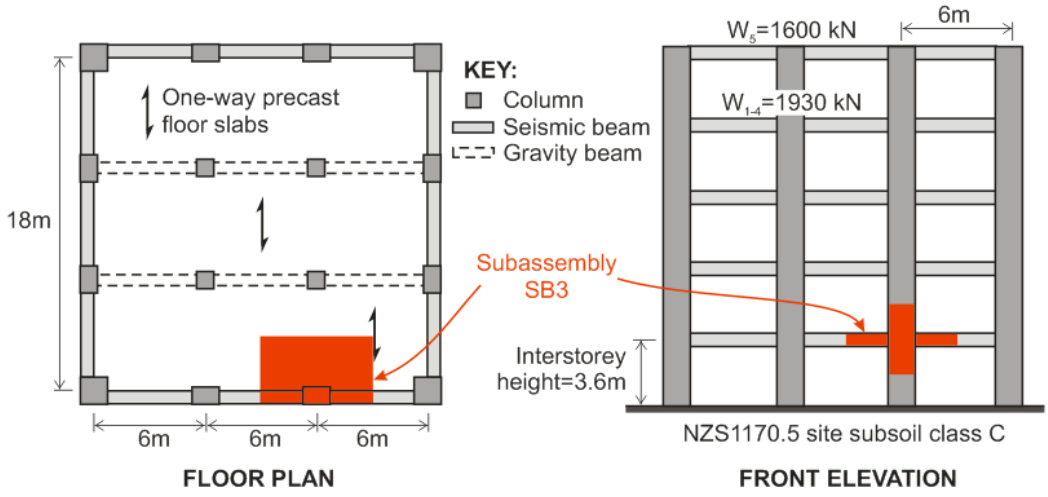

Figure 5-1: Five-storey prototype frame building

5.1.2 Interior Slotted Beam Specimen SB3 with Floor Slab

Specimen SB3 was a half-scale, interior beam-column subassembly, with a precast floor spanning off one side of the beam. The scaled specimen had a column interstorey height of 2 m, beam cantilever spans of 1.225 m and a floor clear span of 1.4 m. Figure 5-2 shows structural drawings of the beam-column subassembly. Bottom longitudinal reinforcement in the beam comprised two 16 mm diameter Grade 300 deformed bars (D16) and one 12 mm diameter Grade 300 deformed bar (D12). These Grade 300 bars had a lower characteristic yield strength of 300 MPa. To limit elongation in the concrete top-hinge, top longitudinal reinforcement compromised three 16 mm diameter Grade 500 (lower characteristic yield strength of 500 MPa) deformed bars (HD16). This reinforcement combination gave an $A_s'f_y'/A_sf_y$ ratio of 1.95.

To prevent/delay buckling of bottom longitudinal reinforcement, stirrup spacing along the unbonded length of bottom reinforcement was reduced to 35 mm in the left-hand-side (LHS) beam and 50 mm in the right-hand-side (RHS) beam. In addition, steel tubes with 2 mm wall thickness were used to debond the bottom bars in the RHS beam. To fill in the clearance between the steel tube and reinforcing bar, bars were wrapped with insulation tap, as oppose to filling with grout like in specimen SB2. The LHS beam of SB3 simply used plastic tubes to debond bottom longitudinal reinforcement. These anti-buckling details were adopted in the

previous interior joint specimen SB2, however premature bond-slip failure meant these new provisions could not be properly tested.

Learning from the bond-slip failure which occurred in specimen SB2, an overly large column depth of 600 mm was adopted to ensure sufficient bond to bottom longitudinal reinforcement passing through the joint. In addition, a higher 28 day concrete compressive strength of 40 MPa was specified.

To provide sufficient combined shear-torsion resistance through the concrete top-hinge, three diagonal shear hangers were used instead of two. In Section 3.8.3, it was shown that combined earthquake beam shear and eccentric floor gravity loads can overstress the internal hanger in tension. For this reason, two of the three hangers were located on the floor slab side of the beam. Figure 5-6 shows photos of the constructed "three-hanger" detail.

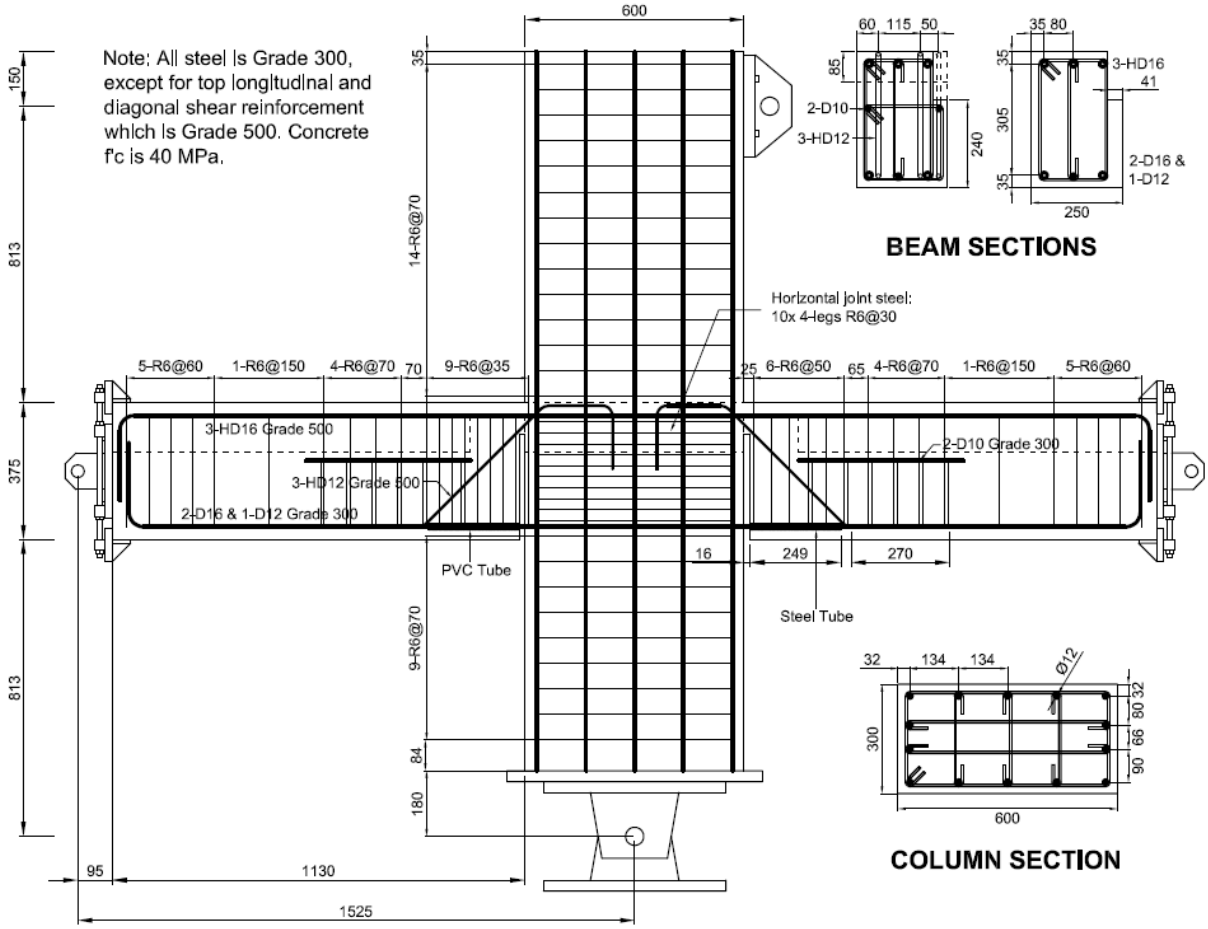

Figure 5-2: Specimen SB3 with floor slab – Front elevation of beam

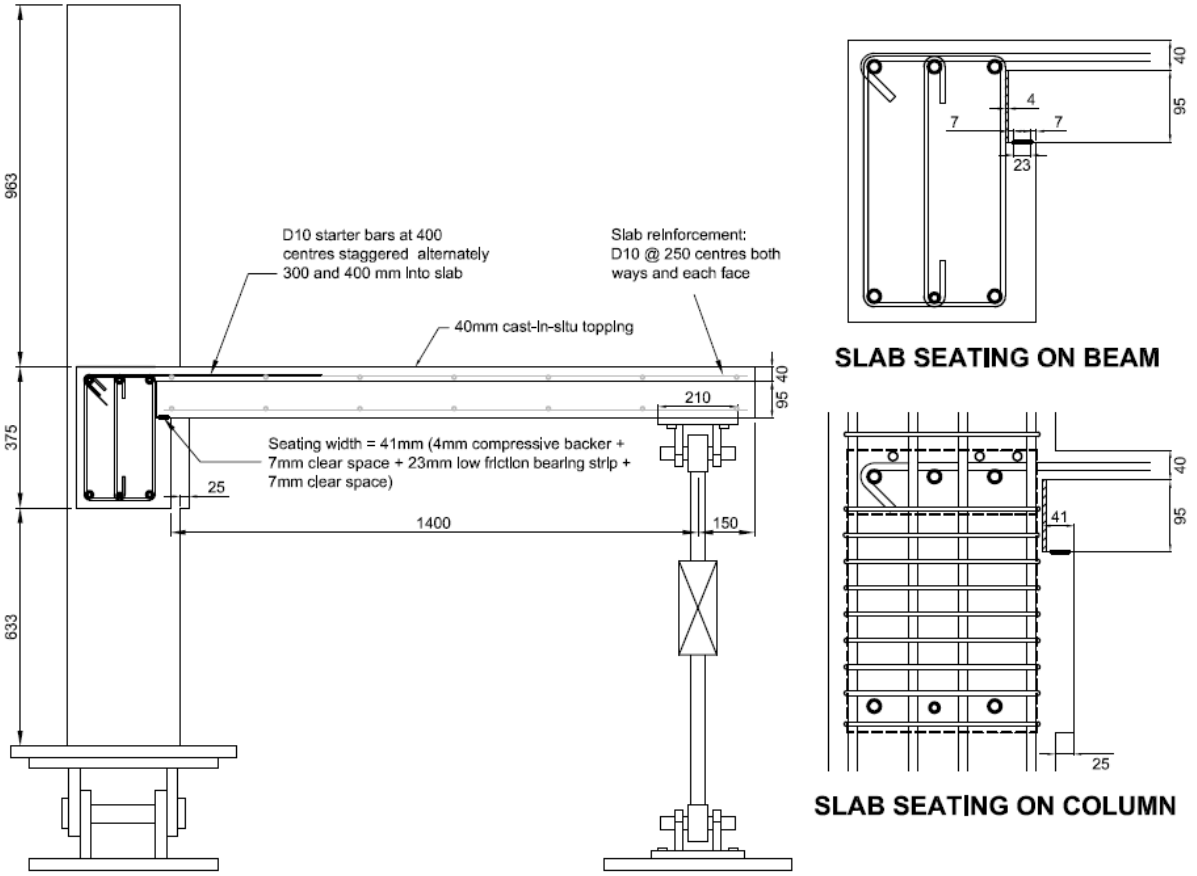

Figure 5-3: Specimen SB3 with floor slab – End elevation

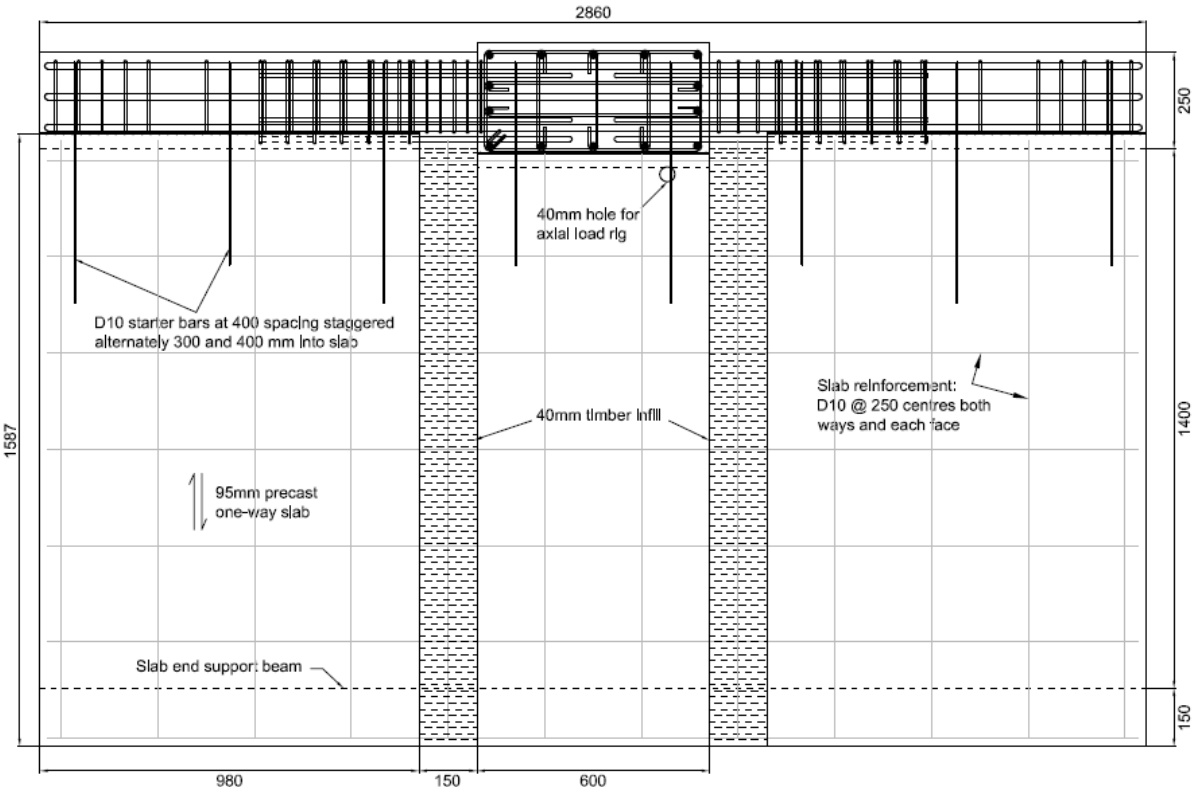

Figure 5-4: Specimen SB3 with floor slab – Plan

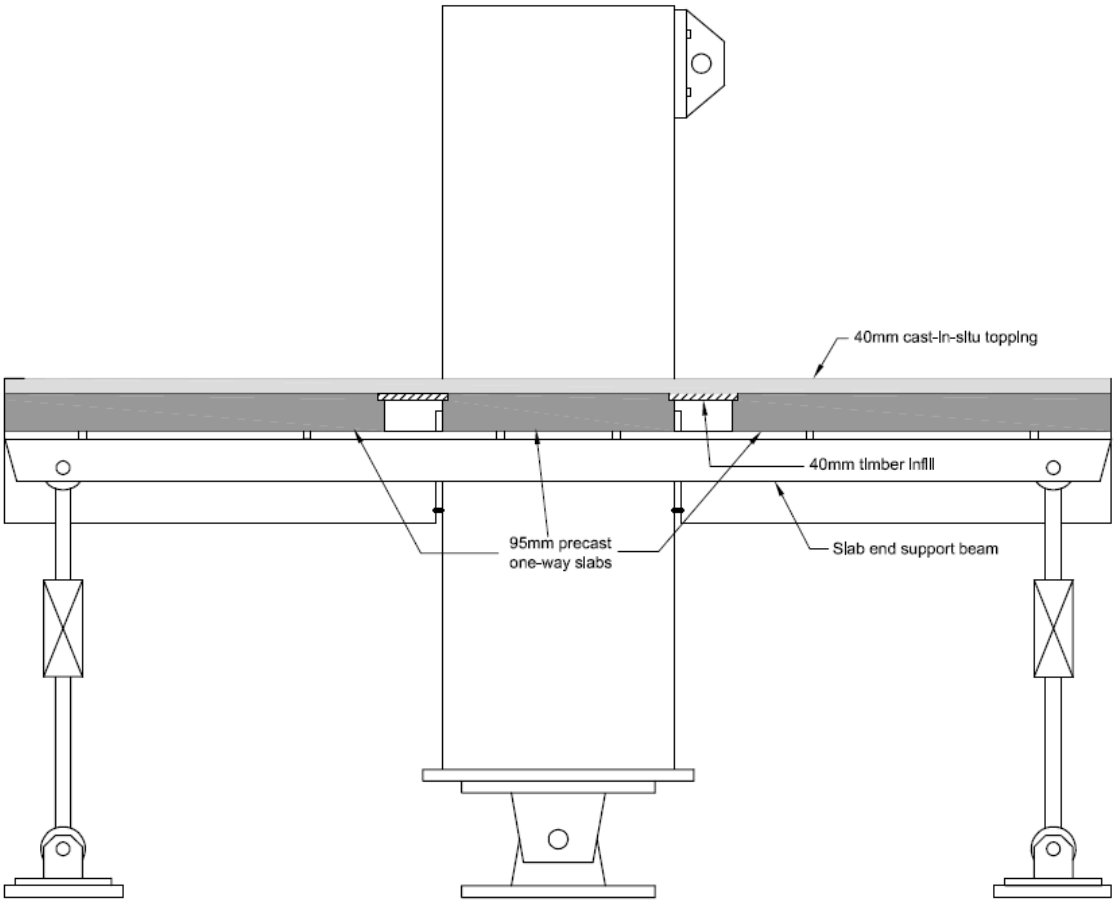

Figure 5-5: Specimen SB3 with floor slab – End elevation of floor slab

Figure 5-3 to Figure 5-5 show structural drawings of the precast floor units seated on the beam-column subassembly with 40 mm thick cast-in-situ topping. Two floor units seated directly onto the beams, while a third was seated on a 25 mm concrete ledge that was cast as part of the column. Because of the large column depth, a floor unit had to be seated onto the column. Timber infills closed the 150 mm gap between adjacent precast floor units and served a dual purpose. Firstly, it allowed the floor adjacent to the concrete top-hinge to be cast thinner than the top-hinge to reduce prying effects. Secondly, it allowed the innermost diagonal hanger to be located within the beam corbel concrete, to maximise the hanger lever-arm resisting beam torsion.

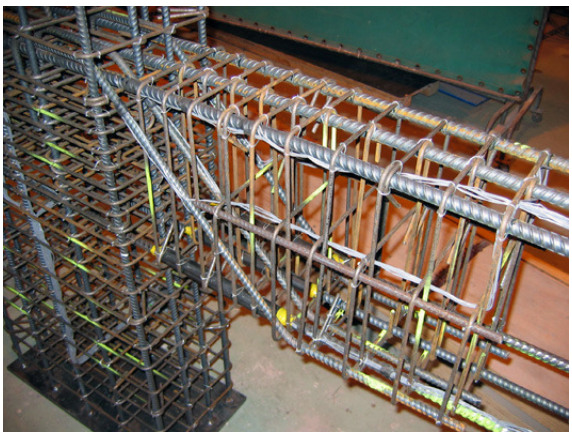

(a) Reinforcement cage

(b) Casting of bottom half of beam

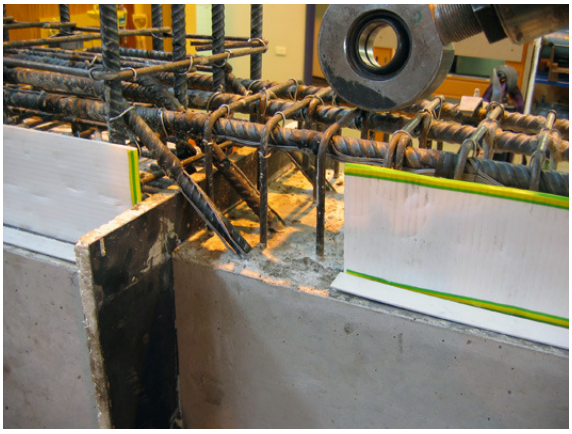

(c) Slab seating width

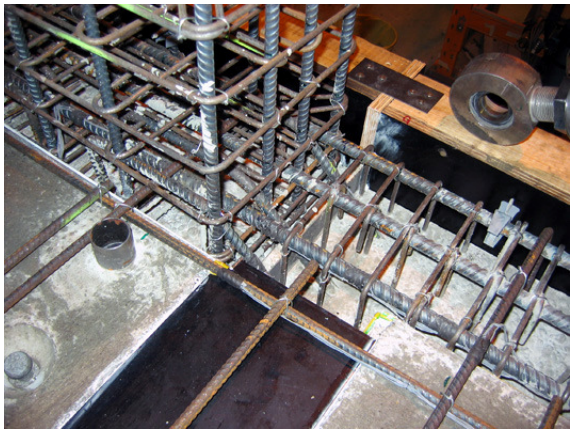

(d) Slab seated on beam

Figure 5-6: Photos of constructed detail using three diagonal hangers

Figure 5-3 shows slab seating details in the beams and column. The seating width of 41 mm was calculated using modified recommendations from the Department of Housing and Building (2009) which were described in Section 3.8.4. To accommodate rotations of the floor relative to the beam, slabs were seated on low friction McDowell bearing strips, with a 5 mm thick Corflute sheet used as a compressible backer. Precast floor units and topping were designed in accordance with the current design standard NZS3101:2006.

5.1.3 Material Properties

Concrete used had a higher specified 28 day compressive strength of 40 MPa to improve bond to longitudinal reinforcement through the interior joint. To fit aggregate through the congested half-scale specimen, the smallest, readily available, maximum aggregate size of 13 mm was specified. The specimen was poured in three stages. For each pour, 100 mm diameter by 200 mm high concrete cylinders were prepared and tested after 7 days, 28 days and/or on the day the specimen was tested. Testing was carried out using an Avery Universal

Testing Machine. Concrete compressive strengths obtained from each pour are summarised in Table 5-1.

Table 5-1: Unconfined concrete compressive strengths for specimen SB3

		Compressive strength (MPa)				
Pour #	**Test**	**Cylinder #1**	**Cylinder #2**	**Cylinder #3**	**Average**	**Std dev**
#1 – Precast slabs, bottom half of beam-column	7 day	29.8	32.6	25.5	29.3	3.58
	28 day	34.4	41.6	33.0	36.3	4.61
	SB3 test (40 day)	34.8	41.4	36.0	37.4	3.52
#2 – Top half of beam and floor topping	7 day	37.5	34	39.3	36.9	2.70
	SB3 test (25 day)	46.5	50.2	54.1	50.3	3.80
#3 – Column above floor slab	7 day	34.4	34.4	33.2	34.0	0.69
	SB3 test (21 day)	41.3	40.2	39.5	40.3	0.91

Likewise, reinforcing steel samples were tested in axial tension via Avery Universal Testing Machine. Three samples for each type of bar used were tested. Average stress-strain properties obtained are summarised in Table 5-2. The strain hardening coefficient, p, refers to the exponential coefficient from the steel constitutive relationship given in Equation 6-7.

Table 5-2: Reinforcing steel properties for specimen SB3

	Bar size and grade					
Property	**D10 Grade300**	**D12 Grade300**	**HD12 Grade500**	**D16 Grade300**	**HD16 Grade500**	**R6 Grade300**
E_s (MPa)	198000	185000	185000	166000	179000	205000
f_y (MPa)	386	324	538	343	529	412
f_u (MPa)	501	448	666	470	659	505
ε_y	0.0019	0.0018	0.0029	0.0021	0.0030	0.0020
ε_{sh}	0.016	0.025	0.015	0.002	0.020	0.003
ε_u	0.171	0.211	0.152	0.175	0.148	0.115
p	5	4	4	6	5	5

5.1.4 Specimen Construction

To accommodate the use of precast floor units and simulate precast-emulation construction methods used in industry, specimen SB3 was constructed in three stages.

In Stage #1, the specimen was caged and strain gauged in the same fashion as the previous test specimens, which is well-described in Section 4.1.5. The beam and the bottom half of the column was caged separately, before being combined as shown in Figure 5-7a.

(a) Combining beam-column cages

(b) Completed reinforcement cage

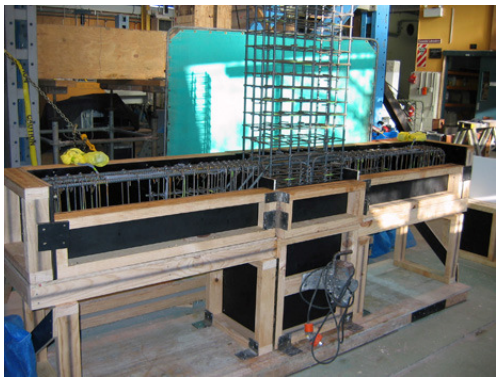

(c) Joint subassembly in formwork

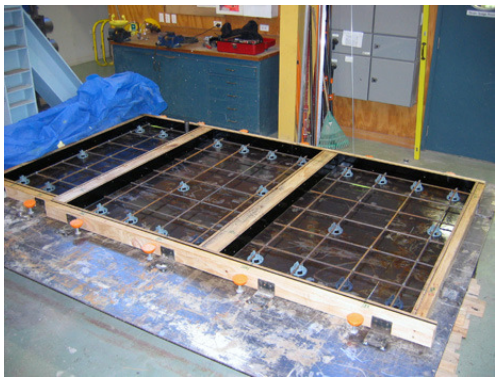

(d) Precast floor unit formwork

(e) Casting of joint subassembly

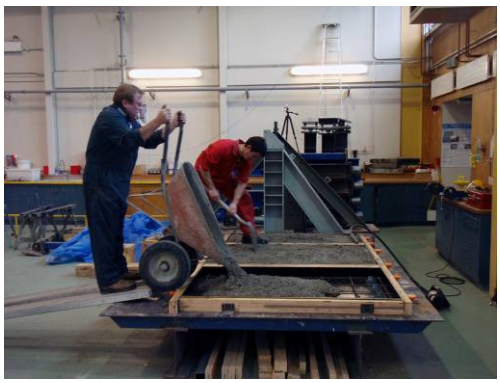

(f) Casting of precast floor units

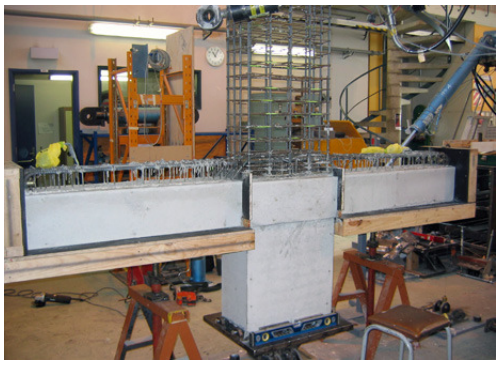

(g) Half-precast beam-column

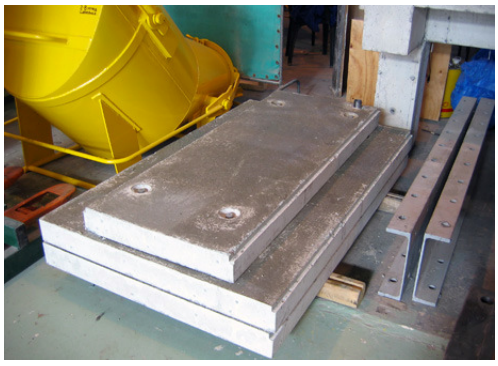

(h) Precast floor units

Figure 5-7: Construction stage #1 – Construction of precast elements

The beam-column subassembly was then cast up-standing, but only up to where the floor units were to be seated as shown in Figure 5-7g. The precast floor units were cast separately at the same time. Formwork was constructed from plywood and No. 1 Framing timber. Like previous specimens, a polystyrene sheet with thin steel plates on either side was used to create the formwork for the slot. Concrete ready mix was provided from a local commercial plant and had a specified 28 day compressive strength of 40 MPa. To allow the placement of concrete around steel-congested joints, a 120 mm slump was ordered with a maximum aggregate size of 13 mm.

Stage #2 construction commenced 7 days after the first pour. The beam-column subassembly was lifted into the test rig, and the precast floor units were lifted and seated on the beam. Formwork and reinforcement for the floor topping were setup and then casted as shown in Figure 5-8c and d.

(a) Bearing strip & compressible backer

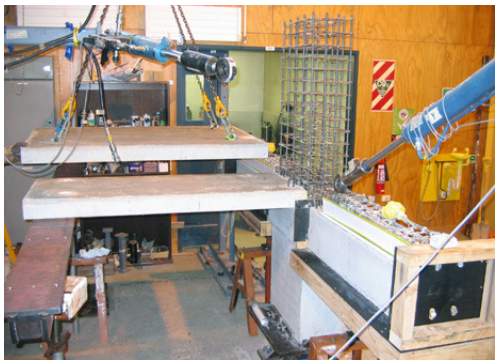

(b) Seating of precast floor units

(c) Topping reinforcement & formwork

(d) Casting of floor topping

Figure 5-8: Construction stage #2 – Seating of precast floor units on beam and casting of floor topping

The final stage of construction simply required casting of the remainder of the column. This was cast in-situ as shown in Figure 5-9a. Once the concrete had set, the specimen was painted, and linear potentiometers were setup on the rear face of the specimen. Lateral and

axial rams were connected to the top of the column, and beam and slab end pins were connected. Load cells were zeroed while connections were loose to ensure a true zero load.

(a) Casting of column

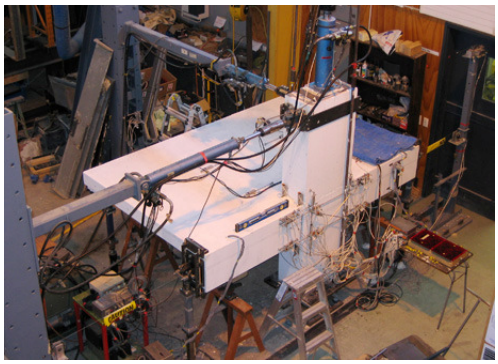

(b) Completed specimen

Figure 5-9: Construction stage #3 – Casting of top column

5.1.5 Scaling of Test Specimen

SB3 was a half-scale specimen taken from a full-scale prototype five-storey frame building. Because gravity loads were being applied to the subassembly during the test, additional attention was given to scaling to ensure similitude requirements were satisfied.

Table 5-3: Summary of scale factors for reinforced concrete models

Quantity	Dimension	True model	Practical model
Material-related properties:			
Stress	FL^{-2}	S_σ	1
Strain	-	1	1
Elastic modulus	FL^{-2}	S_σ	1
Poisson's ratio	-	1	1
Specific weight	FL^{-3}	S_σ/S_l	$1/S_l$
Geometry:			
Linear dimension/displacement	L	S_l	S_l
Angular displacement	-	1	1
Area of reinforcement	L^2	S_l^2	S_l^2
Loading:			
Concentrated load	F	$S_\sigma S_l^2$	S_l^2
Line load	FL^{-1}	$S_\sigma S_l$	S_l
Pressure	FL^{-2}	S_σ	1
Moment	FL	$S_\sigma S_l^3$	S_l^3

Harris and Sabnis (1999) provide guidelines for the scaling of reinforced concrete models. Table 5-3 summarises scale factors for a true model, where S_σ and S_l are stress and length scale factors respectively. A true model requires that material properties such as strength and

stiffness be scaled proportionally according to S_σ. However given the inherent non-linearity of concrete and unavailability of a feasible scaled reinforcing material, such models are not practical. Thus it is more common to adopt S_σ as unity to produce a more practical model as given in the last column of Table 5-3. The geometry and applied gravity loads for specimen SB3 were scaled according to this criteria given S_l=0.5.

5.2 Experimental Set-up

5.2.1 Test Rig

Specimen SB3 was tested in the same test-rig as the previous specimen SB2, which is described in detail in Section 4.2.1. Slight additions were then made to accommodate the floor slab, which are shown below in Figure 5-10. The free-end of the floor slab was seated on a custom welded double-tee steel beam, which in turn was supported on two pin-ended struts. Ball joints were used to allow the slab-end to rotate, and 150 kN load cells were included in the supports to measure the gravity load carried by these slab pins. Like previous specimens, a constant axial load (150 kN in this case) was applied to the column during testing.

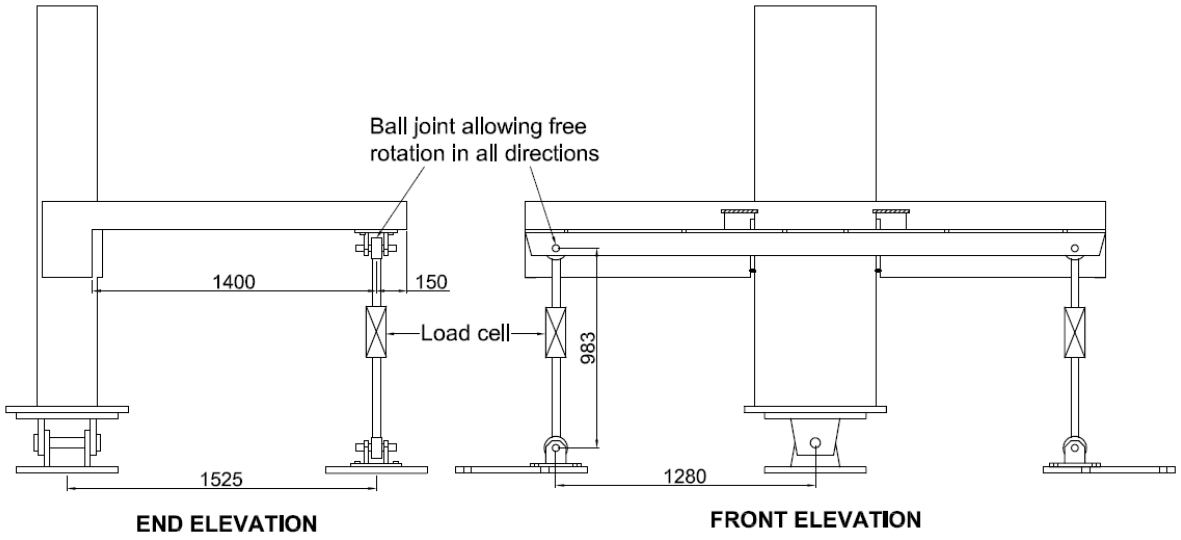

Figure 5-10: Slab supports added to the test rig setup

5.2.2 Loading Protocol

Specimen SB3 was subjected to a displacement controlled, cyclic quasi-static test to simulate earthquake actions. The same drift protocol applied to previous test specimens was adopted, except that for this test, the drift protocol was specified in terms of beam drift, θ_{bc}, instead of

interstorey drift, θ_c, as defined in Figure 5-11. The reason for this redefinition was because the large column depth significantly reduced beam cantilever lengths, such that the imposed beam rotation was much greater than the applied interstorey drift. Without this redefinition, applied beam rotations became excessively severe.

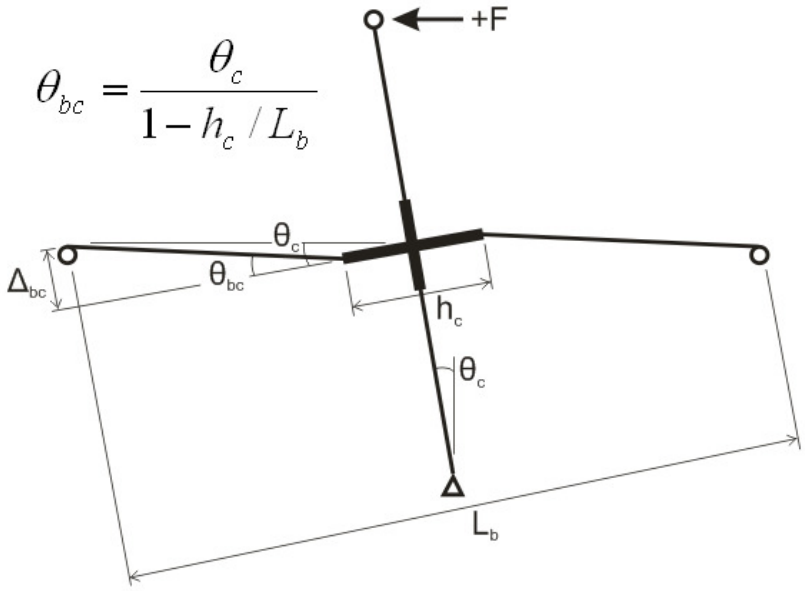

Figure 5-11: Loading protocol sign convention and definition of drifts

The beam drift protocol is shown in Figure 5-12 and was adopted in accordance with American Concrete Institute (ACI) acceptance criteria for moment frames (ACI Committee 374, 2005). It consisted of 3 cycles at beam drift levels of 0.1%, 0.2%, 0.5%, 0.75%, 1.0%, 1.5%, 2.0%, 2.5%, 3.5% and 4.5%. A smaller cycle one third of the previous drift followed each set of three cycles. Given a column depth of 600 mm and a beam span length of 3000 mm, to achieve this beam drift sequence, the interstorey drift applied had to be 80% of the desired beam drift.

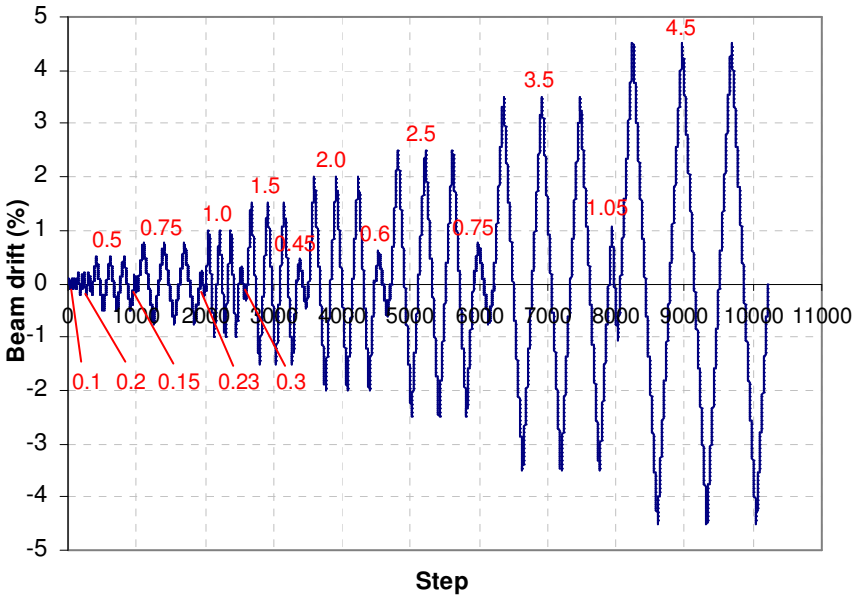

Figure 5-12: Quasi-static loading protocol

To compare the severity of applied rotations to each slotted-beam connection tested, Figure 5-13 plots the measured beam fixed-end rotation against the applied drift protocol. It is shown that beams from specimens SB1 and SB2 had similar fixed-end rotations. However fixed-end rotations for specimen SB3 were slightly less severe, especially during gap opening drifts and at higher drift levels.

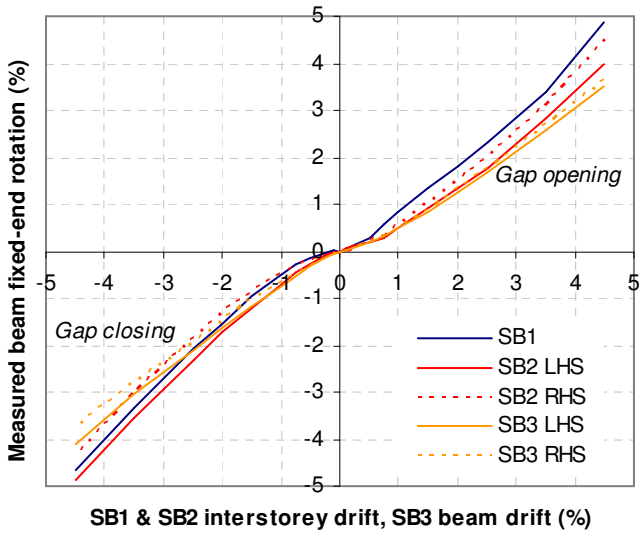

Figure 5-13: Comparison of measured beam fixed-end rotations during testing for slotted specimens SB1, SB2 and SB3

5.2.3 Floor Gravity Load

One of the objectives for testing this specimen with a floor slab was to observe the effect of beam torsion resulting from eccentric floor gravity loads as described in Section 3.8.3. To simulate the gravity load combination $G+\psi_c Q$ from NZS1170.1:2004, the floor of the test specimen was loaded with 3.1 tonnes of steel weights and lead ingots as shown in Figure 5-14a and b. Steel masses weighed 0.341 kN each and lead ingots weighed 0.239 kN each.

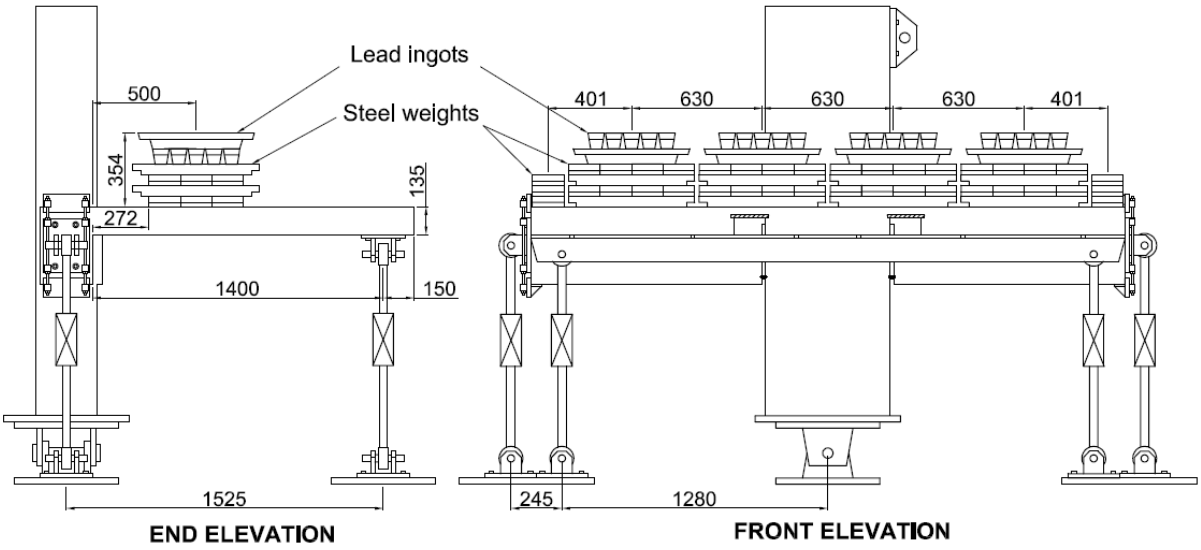

(a) Location and setup of steel and lead weights

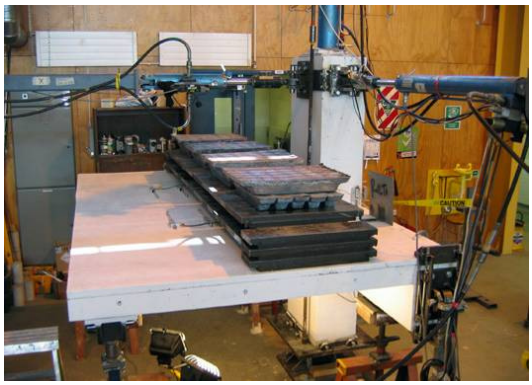

(b) Weights setup on specimen

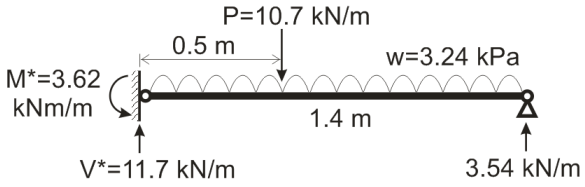

(c) Imposed gravity and reactions

Figure 5-14: Imposed floor gravity load using steel weights and lead ingots

The quantity of mass and their location was chosen to best approximate the gravity shear and slab end-moment applied to the beam, in the five-storey prototype frame of V^* = 12.5 kN/m and M_n = 2.07 kNm/m respectively. Figure 5-14c shows the resulting theoretical reactions from the imposed gravity load on the test specimen. Note that the end moment demand of M^* = 3.62 kNm/m was set greater than M_n = 2.07 kNm/m in attempt to yield starter bars and

create the worst-case torsional demands. Unfortunately, due to twisting of the beam, yielding of starter bars did not occur. This is discussed further in the results section.

5.2.4 Instrumentation

Strain Gauges

Local strains in reinforcing bars were measured using electrical resistance wire strain gauges (Tokyo Sokki FLA-5-11-3L and FLA-3-11-3L). Strain gauges were located along beam longitudinal reinforcement, diagonal hangers, joint stirrups, floor topping reinforcement and on starter bars as shown in Figure 5-15.

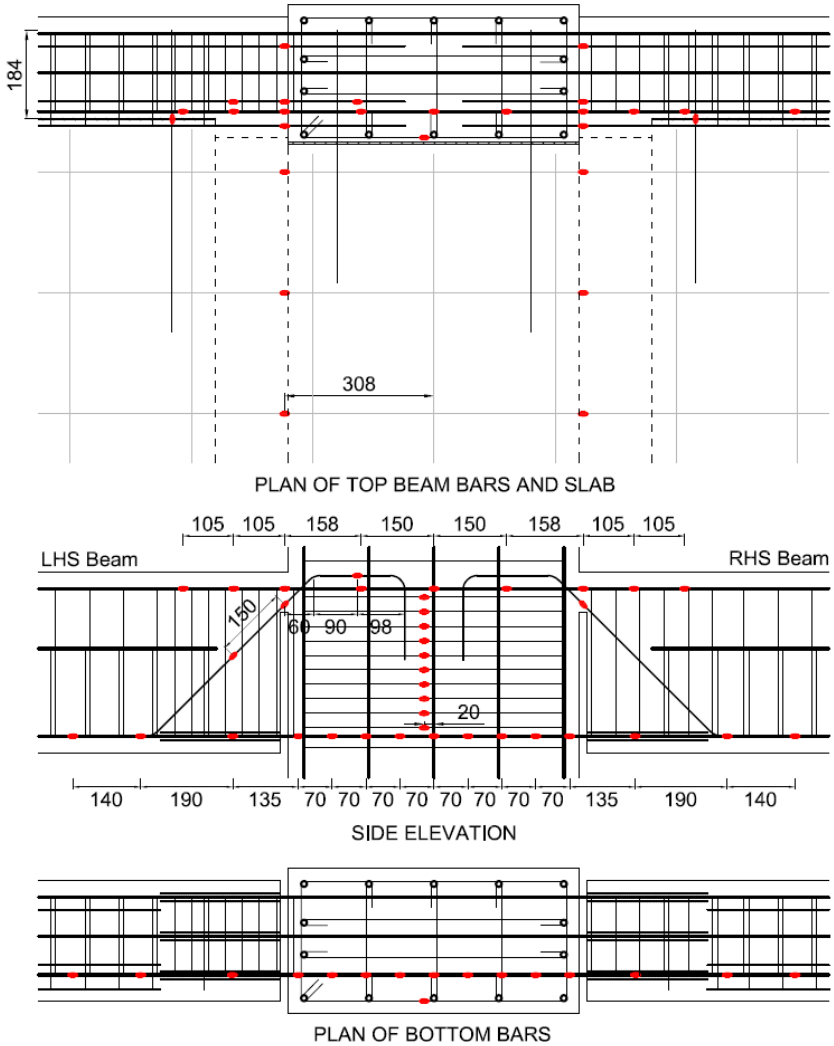

Note: All strain gauges are 5mm gauges, except for gauges on stirrups which are 3mm.

Figure 5-15: Location of strain gauges in specimen SB3

To measure strains in the critical slotted section and the strain penetration either side, one top and one bottom longitudinal bar was instrumented in both beams adjacent to the column and

within the joint. Reinforcement that would be subject to flexural bending, that is those within the slotted section and along the unbonded length, were instrumented on both sides to allow measured strains to be averaged. The bottom bar passing through the interior joint, was heavily instrumented with gauges spaced every 70 mm. The purpose of this was to allow the bond stress distribution to be determined via differentiating the internal stress distribution along the bar. Joint stirrups were instrumented to allow the horizontal joint shear carried by the truss mechanism, V_{sh}, to be calculated. To measure the extent of slab reinforcement activation, three bars in the floor topping closest to the beam which ran parallel with the beam were strain gauged.

Linear Potentiometers

Linear potentiometers provided measurement of column, beam, joint and slab deformations. The linear potentiometer set-up for specimen SB3 is shown in Figure 5-16 below.

Three pairs of potentiometers crossing the beam-column interface were used to estimate fixed end rotations and the neutral axis depth within the concrete top-hinge. Cross diagonal potentiometers within the joint panel zone were used to calculate joint shear deformations. Vertical potentiometers on the column provided measurements to determine the column neutral axis depth. To measure the extent of slab activation, six potentiometers crossing the timber infill were included on top of the slab. Lastly, to measure beam torsional deformations, spring potentiometers were placed above and below each beam, and to the side of the LHS beam.

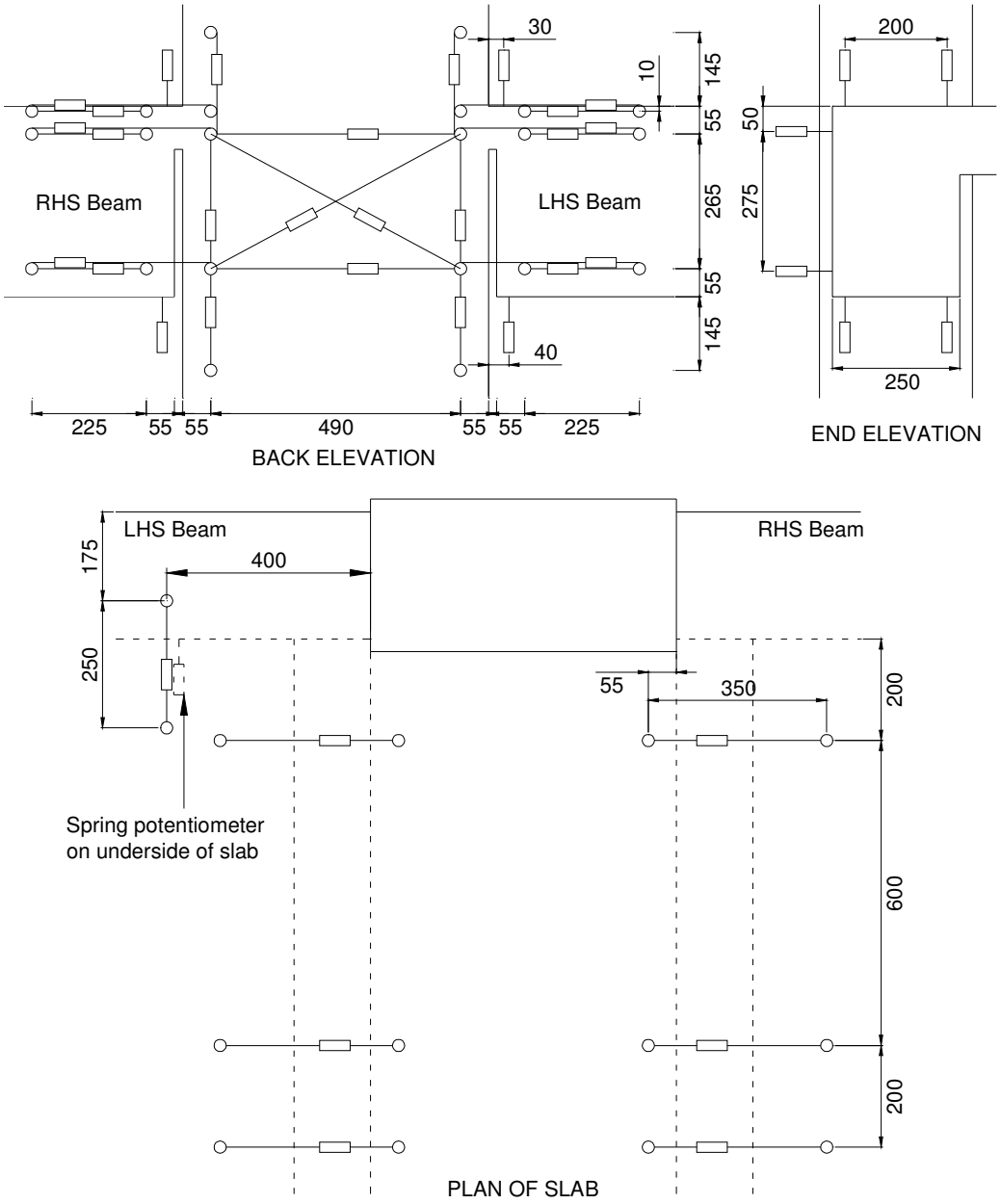

Figure 5-16: Linear potentiometer setup for specimen SB3

Rotary Potentiometers

Three rotary potentiometers were used to measure lateral displacements at the top of the column and at the beam free ends. These were located as shown in Figure 4-8b. The potentiometers attached to the beam free ends were used to measure both geometric and material beam elongation contributions.

Load Cells

Load measurements were provided via load cells. 150 kN load cells were used to measure the applied horizontal load and beam and slab end-reactions. A 440 kN load cell was used to

measure the vertical axial load in the column (See Figure 4-8b). Load cells were calibrated in compression by Avery Universal Testing Machine. The obtained calibration factors were then assumed to be effective for the particular load cell in tension.

5.3 Test Results

5.3.1 General Behaviour and Force-drift Response

Figure 5-17 shows the total interstorey shear versus beam drift response for specimen SB3. First cracking in the beam was observed at 0.5% beam drift, and was followed by yielding of bottom longitudinal reinforcement at approximately 0.69% beam drift, at a lateral force of 68 kN. The specimen exhibited a stable, steel-like hysteretic response up to 4.5% beam drift. The column depth of 600 mm and concrete strength of 40 MPa provided sufficient anchorage to bottom reinforcement passing through the joint, such that no significant bond-slip was observed.

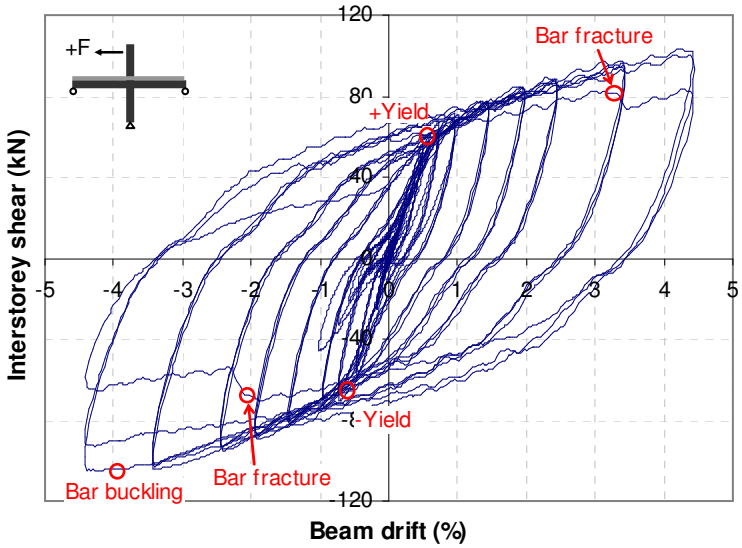

Figure 5-17: Total interstorey shear force versus beam drift response for specimen SB3

On the first cycle to -4.5% beam drift, buckling of bottom longitudinal bars in the LHS beam occurred. This resulted in spalling of the beam soffit, and strength degradation in subsequent gap-closing cycles. No buckling resulting in strength degradation or spalling was observed in the RHS beam. The RHS beam employed a stirrup spacing of 50 mm ($\approx 4d_b$) and steel tubes along the unbonded length to successfully prevent buckling of bottom longitudinal reinforcement. The LHS beam, however, adopted a smaller stirrup spacing of 35 mm, including an extra stirrup in cover concrete of the column, with plastic tubes to provide

debonding. As a similar observation was made with specimen SB2, it can be concluded that the use of steel tubes with a larger stirrup spacing is more effective at preventing buckling than a smaller stirrup spacing with plastic tubes.

On the last cycle to 4.5% beam drift, fracture of a single bottom longitudinal bar in each beam occurred during their respective gap-opening cycles. The remaining bottom bars fractured when an extra fourth cycle to 4.5% beam drift was applied. Note this extra cycle has not been plotted in the figure above. Also note that 4.5% beam drift corresponds to 3.6% interstorey drift.

Specimen SB3 exhibited significantly more post-yield hardening than previously tested slotted-beam specimens. Table 5-4 summarises positive and negative overstrength factors for beam drifts above 1.0%. These ratios are 3 to 13% higher than those given in Table 4-6 for specimen SB1. The most likely cause of this is the floor slab contributing to the flexural strength of each connection. Two slabs contributions were observed: Firstly, an effective slab width contribution due to beam deformations extending into the slab from shear lag; and secondly, a contribution from torsion of the central floor unit seated on the column. The flexural contribution from floor units is discussed further in Section 5.3.6.

Table 5-4: Observed overstrength factors from test of specimen SB3

Beam drift (%)	1.0	1.5	2.0	2.5	3.5	4.5
φ_o^+ gap opening drifts	1.17	1.29	1.41	1.46	1.60	1.65
φ_o^- gap closing drifts	1.16	1.24	1.41	1.47	1.62	1.70

Note: $\varphi_o = M/M_n$, $M_n^+ = A_s f_y(d-a/2) = 51.1$ kNm, $M_n^- = A_s f_y(d-d') = 47.1$ kNm

5.3.2 Crack Development and Observed Damage

Like previous slotted-beam specimens tested herein, specimen SB3 exhibited very little damage and cracking compared to what would be expected with a conventional monolithic beam-column connection. Table 5-5 summarises maximum crack widths observed at peak drift levels. Reported on are cracks within the concrete top-hinge area, floor cracks adjacent to the top-hinge, torsional cracks on the underside of the central precast floor unit, cracks in the joint due to longitudinal reinforcement strain penetration, beam cracks where reinforcement remains elastic, and beam-column (BC) joint crack widths due to joint shear. Figure 5-18 illustrates the locations of these cracks. It shows that crack widths within the concrete top-hinge remain small, within 2 mm for drifts up to 2.5%. Strain penetration cracks

also remain small within 0.3 mm. This is consistent with what was observed previously in specimens SB1 and SB2 (See Section 4.3.2).

Table 5-5: Maximum crack widths at peak drifts for specimen SB3

Beam drift	Max crack widths (mm)					
	Concrete top-hinge	Slab adjacent to top-hinge	Slab torsion	Strain penetration	Elastic beam	Joint shear
0.1%						
0.2%						
0.5%	HL-0.1	HL				
0.75%	0.15-0.35	0.15-0.35		0.1-0.15	HL-0.1	
1.0%	0.45-0.55	0.15-0.4	0.2-0.3	0.15	HL-0.1	
1.5%	0.75-0.9	0.35-0.65	0.35-0.45	0.2	HL-0.15	
2.0%	1-1.2	0.55-0.7	0.35-0.45	0.2-0.25	HL-0.15	
2.5%	1.2-1.4	0.8-1	0.3-0.45	0.2-0.25	HL-0.15	
3.5%	1.4-3	0.75-0.9	0.35-0.55	0.25-0.3	HL-0.15	0.1
4.5%	2-4	0.9-1.3	0.6-0.8	0.15-0.3	0.1-0.15	0.15

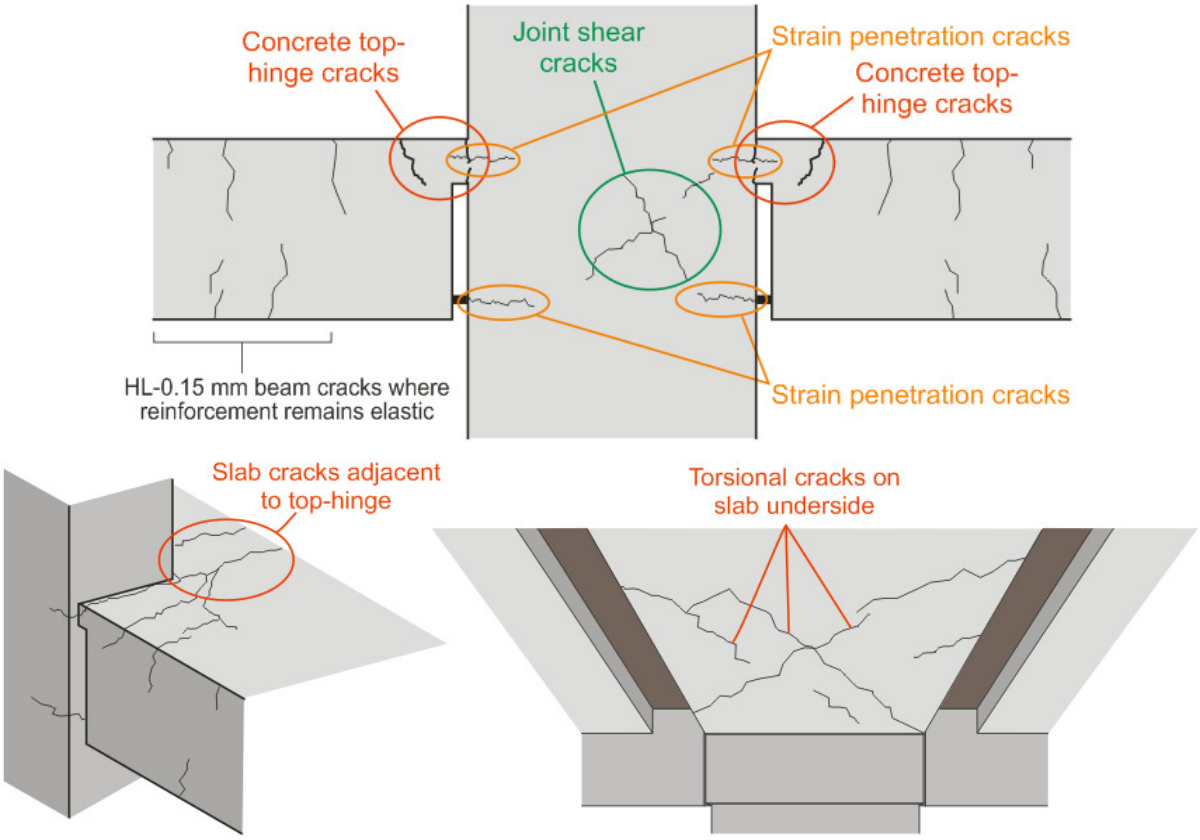

Figure 5-18: Illustration of crack locations referred to in Table 5-5

Figure 5-19 illustrates the development of cracks on the face of the beam-column subassembly. All flexural cracks along the beam and column lengths where reinforcement remained elastic were less that 0.15 mm and closed on unloading. No cracking was observed in the joint until 3.5% drift. Significant flexural cracking was concentrated into one or two cracks passing through the concrete top-hinge as shown in Figure 5-20. This same figure also highlights the relatively low concrete damage sustained by the slotted connection.

Main flexural cracks in the concrete top-hinge extended out into the slab after joining to form a single crack, as seen in Figure 5-20a, c and e, which ran the entire length of the slab as shown in Figure 5-21b. This crack did not exceed 0.15 mm in width at the end of the slab. Cross-diagonal cracking was observed on top, but more significantly underneath the central floor unit which was seated on the column as shown in Figure 5-21b and c. This was the result of torsion of the slab about its longitudinal axis as the column rotated, while the free-end of the slab was restrained in a horizontal position by the supporting steel beam. The most likely reason for the significant crack widths on the underside of the precast unit is most likely due to a combination of torsion and imposed gravity loads creating tension on the underside.

No spalling of concrete was observed until 2.5% beam drift. Spalling first occurred in the form of concrete cone pullout at the column face within the gapped section as shown in Figure 5-22a. This was caused by strain penetration of bottom longitudinal bars into the joint as they were pulled in tension during gap opening rotations. Spalling was of cover concrete and not core concrete confined by transverse joint reinforcement. Therefore the spalling did not detrimentally affect the anchorage of the bottom bars. Significant spalling of the LHS beam soffit occurred at 4.5% beam drift as a result of buckling of bottom longitudinal reinforcement as seen in Figure 5-22b. No buckling was observed in the RHS beam such that its soffit remained undamaged throughout the test.

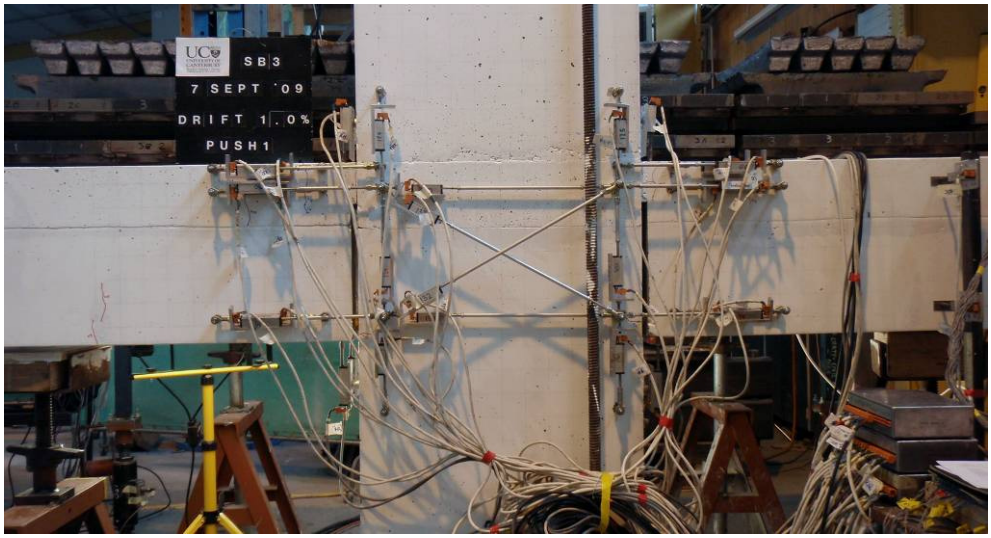

(a) Beam drift +1.0%

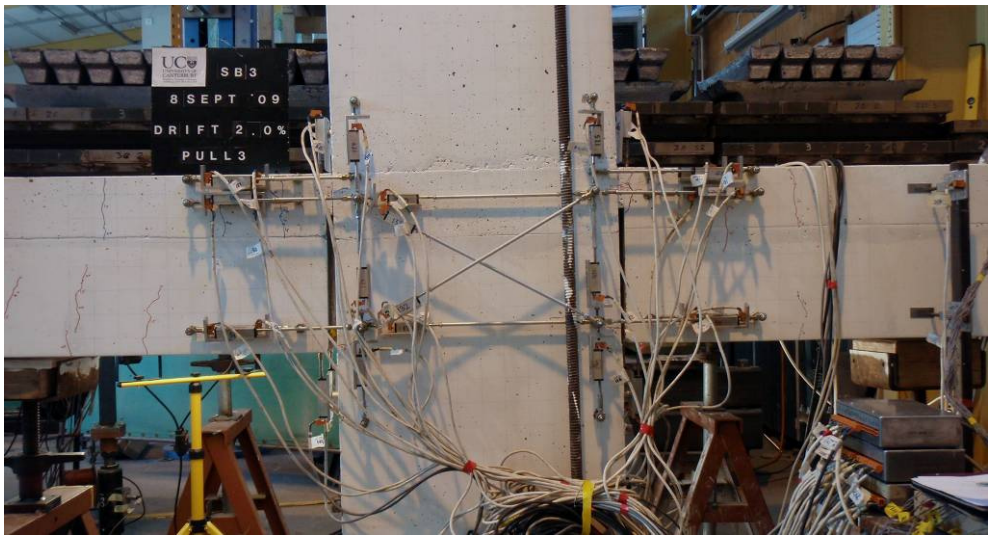

(b) Beam drift -2.0%

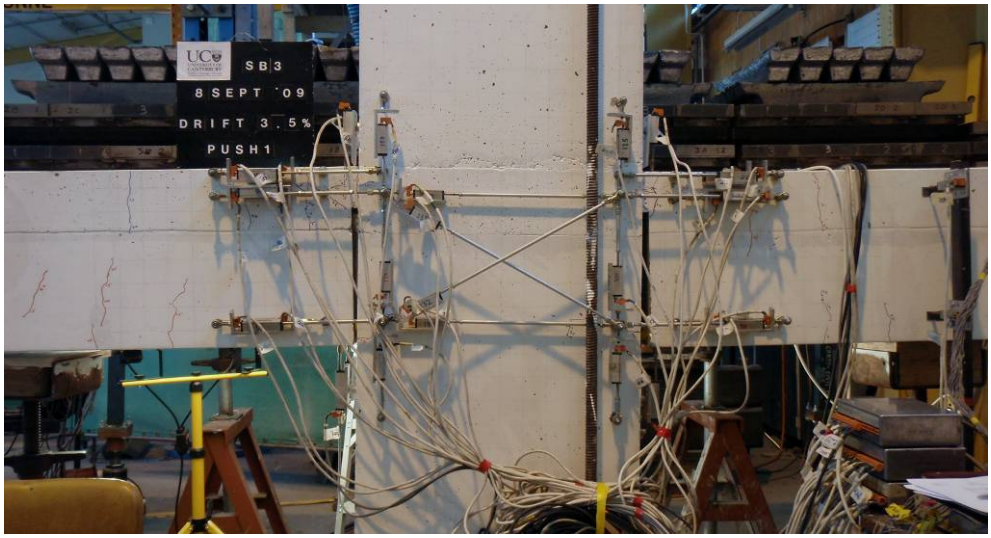

(c) Beam drift +3.5%

Figure 5-19: Beam-column crack development

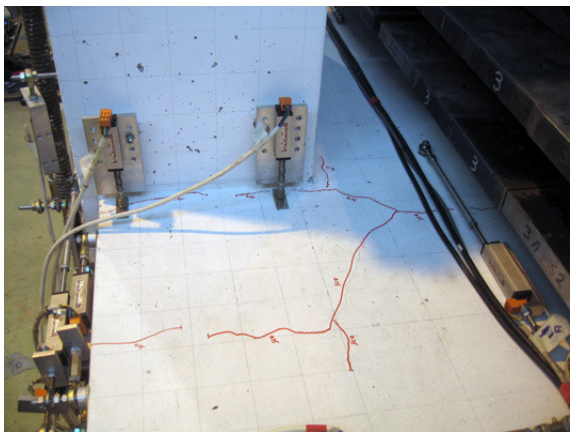

(a) LHS beam at 1.0% drift

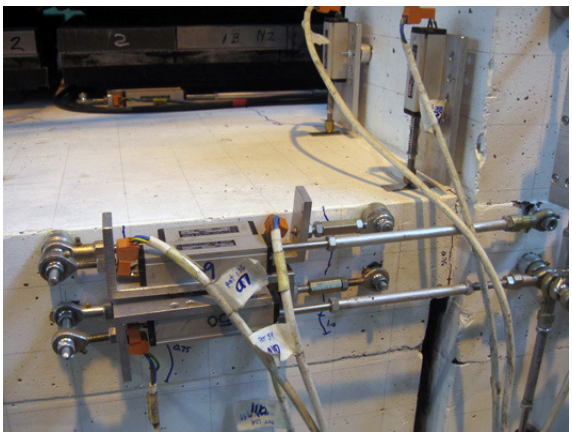

(b) RHS beam at 1.0% drift

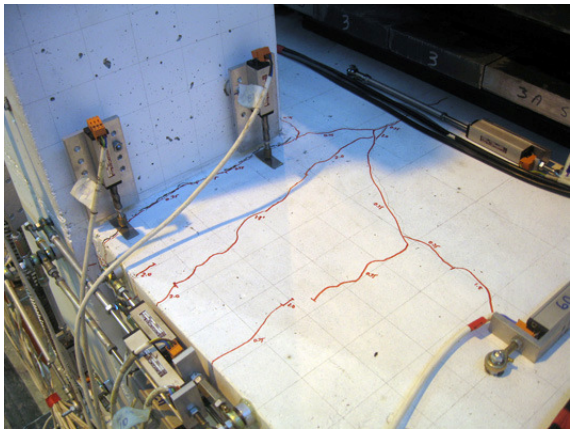

(c) LHS beam at 2.0% drift

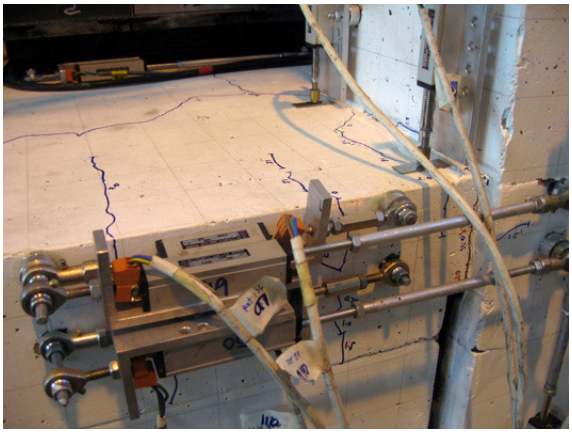

(d) RHS beam at 2.0% drift

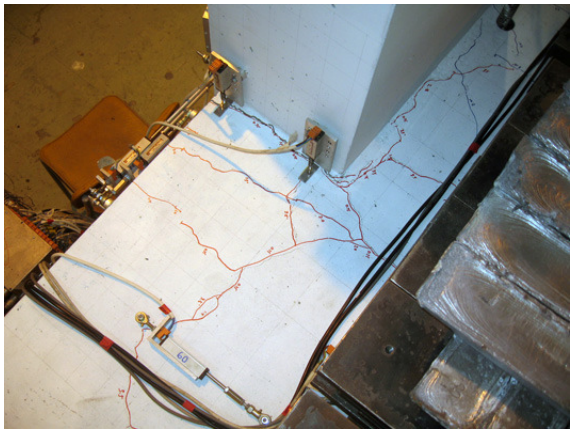

(e) LHS beam at 3.5% drift

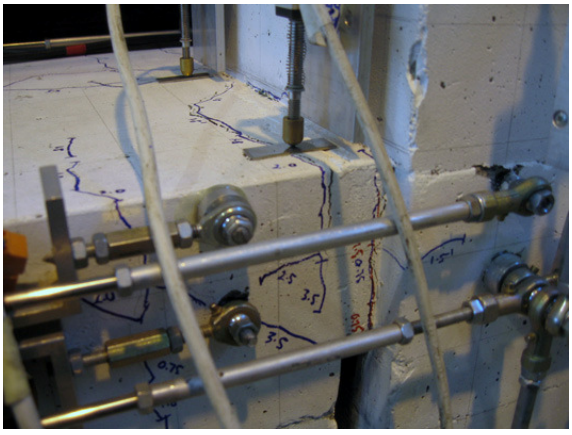

(f) RHS beam at 3.5% drift

Figure 5-20: Concrete top-hinge crack development

(a) Floor crack pattern adjacent to beam

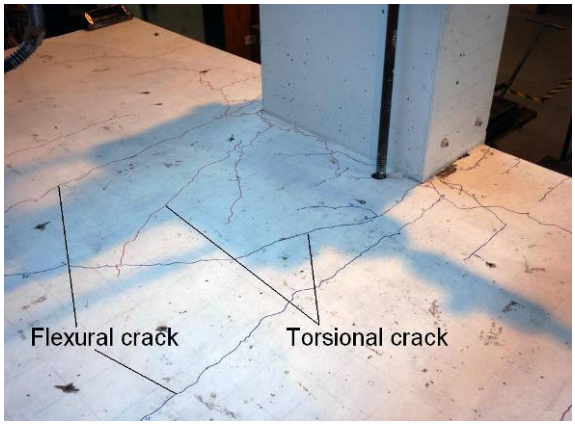

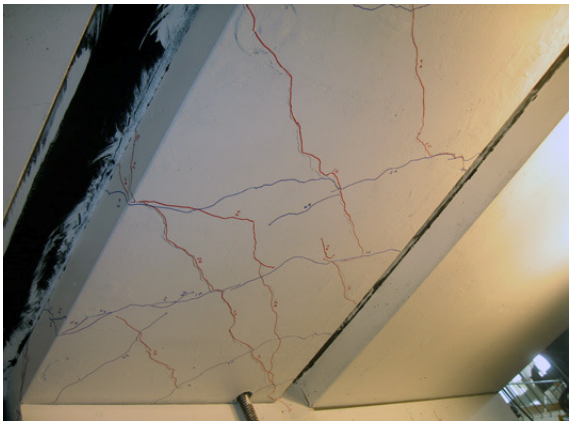

(b) Floor crack pattern **(c) Torsional cracks under central floor unit**

Figure 5-21: Floor slab crack patterns at the end of testing

(a) Concrete cone pullout in LHS column face **(b) Spalling of LHS beam soffit**

Figure 5-22: Spalling damage

5.3.3 Energy Dissipated per Cycle

Figure 5-23 plots the hysteretic energy dissipated per cycle as equivalent viscous damping for specimen SB3 alongside previously tested specimen SB1 for comparison. It is shown that both specimens showed similar amounts of energy dissipation. In Section 4.3.4, it was shown that specimen SB1 showed greater energy dissipation than an equivalent monolithic connection. Therefore, it can be concluded that slotted-beams exhibit a greater level of hysteretic damping than conventional beams. This increase in damping can be attributed to the extensive tension-compression plastic straining which occurs in the bottom longitudinal reinforcement.

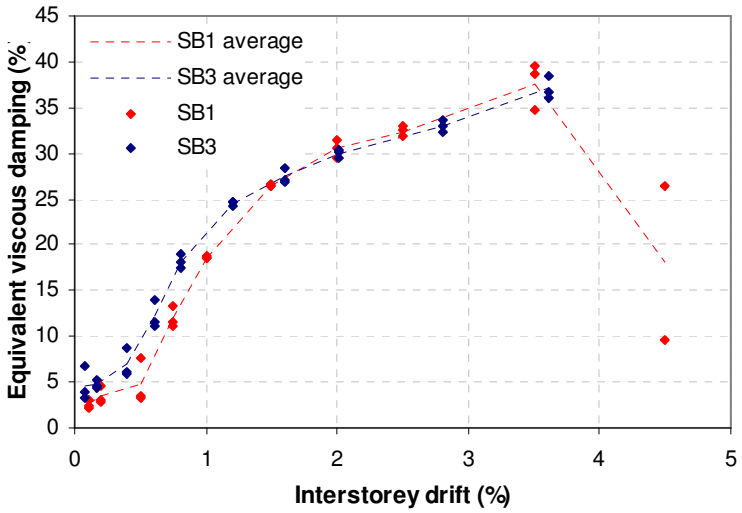

Figure 5-23: Hysteretic energy dissipated per drift cycle

5.3.4 Beam Elongation

Figure 5-24 plots the measured elongation at the beam centrelines for the LHS and RHS connections in specimen SB3, and the combined elongation of the two connections together. This elongation was measured using linear potentiometers crossing the slotted section. Like previously tested slotted-beams, specimen SB3 exhibited negligible beam elongation. Because yielding of top reinforcement did not occur with this specimen, there was less elongation than interior joint specimen SB2, even though SB3 had a larger concrete top-hinge depth. Specimen SB2's total subassembly elongation exceeded 2 mm, whilst total elongation for SB3 remained less than this. Extra restraint would also have been provided by the 3-HD12 diagonal hangers.

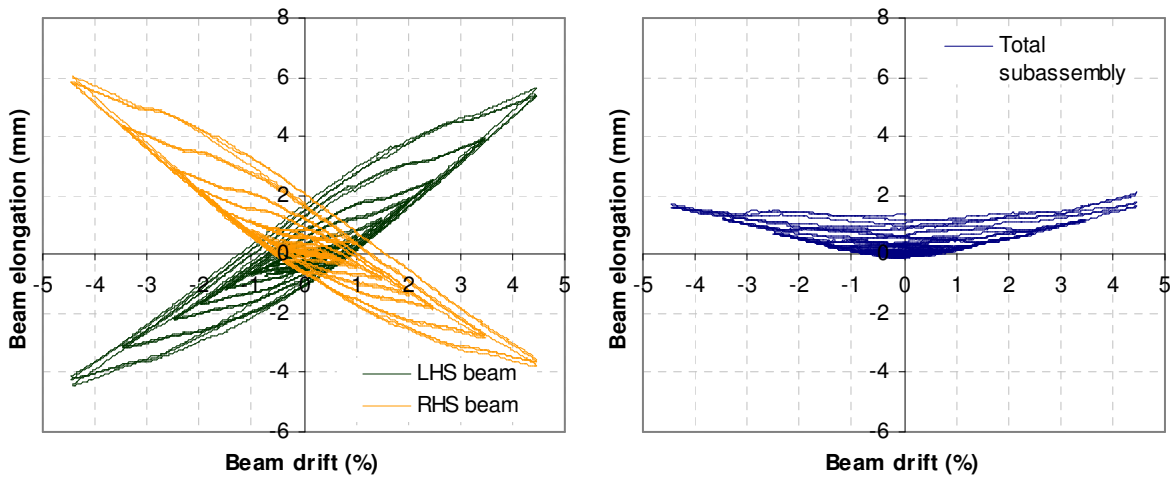

(a) Beam elongation **(b) Subassembly elongation**

Figure 5-24: Measured beam elongation

5.3.5 Reinforcement Strain Profiles

Figure 5-25 shows the strain profile in the bottom longitudinal reinforcement at peak drift levels. As expected significant yielding occurs along the unbonded length and a yield penetration length either side. Integration of this strain profile yielded a strain penetration length into the beam-column joint of $0.019 f_y d_b$ for the LHS beam and $0.020 f_y d_b$ for the RHS beam. Small strains within the central 450 mm of the joint indicate sufficient anchorage of the bars along this length.

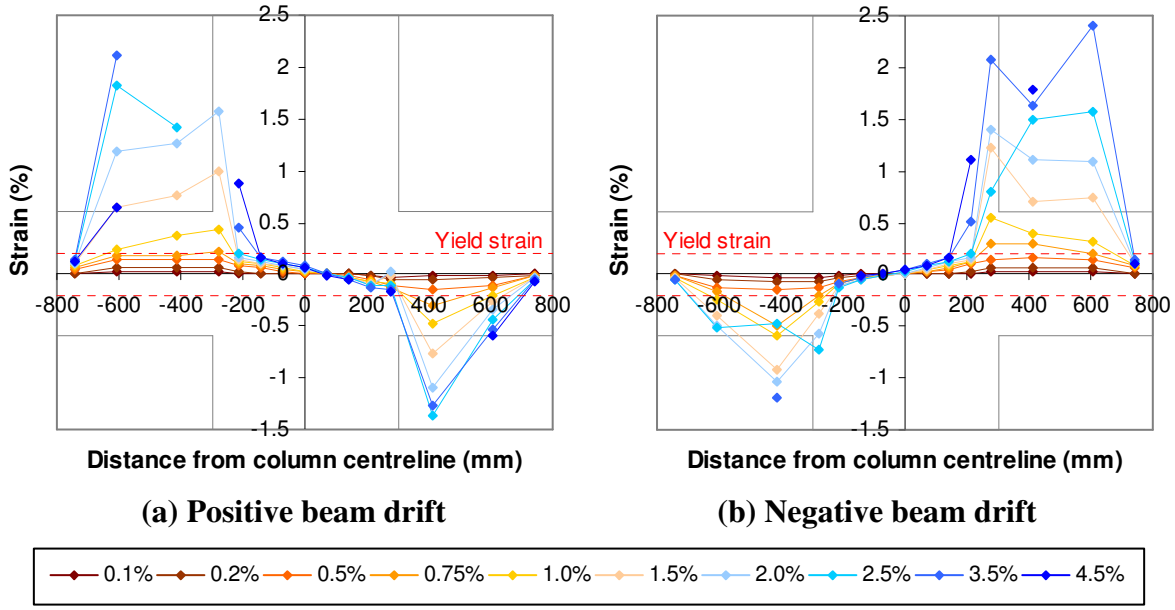

(a) Positive beam drift **(b) Negative beam drift**

Figure 5-25: Bottom longitudinal reinforcement strain profile at peak drifts

Due to multiple strain gauge failure prior to testing, the strain profile for top longitudinal reinforcement has not been plotted. However, available strain gauge data did reveal that this reinforcement remained elastic up to 3.5% beam drift.

Figure 5-26 shows the strain profile along the central diagonal hanger in the LHS beam. It is shown that the peak strain occurs through the slotted-section of the beam. For both positive and negative rotations, strains are positive due to flexural deformations within the concrete top-hinge governing strains rather than by shear. The hangers were consistently on the tensile side of the neutral axis at peak beam drifts.

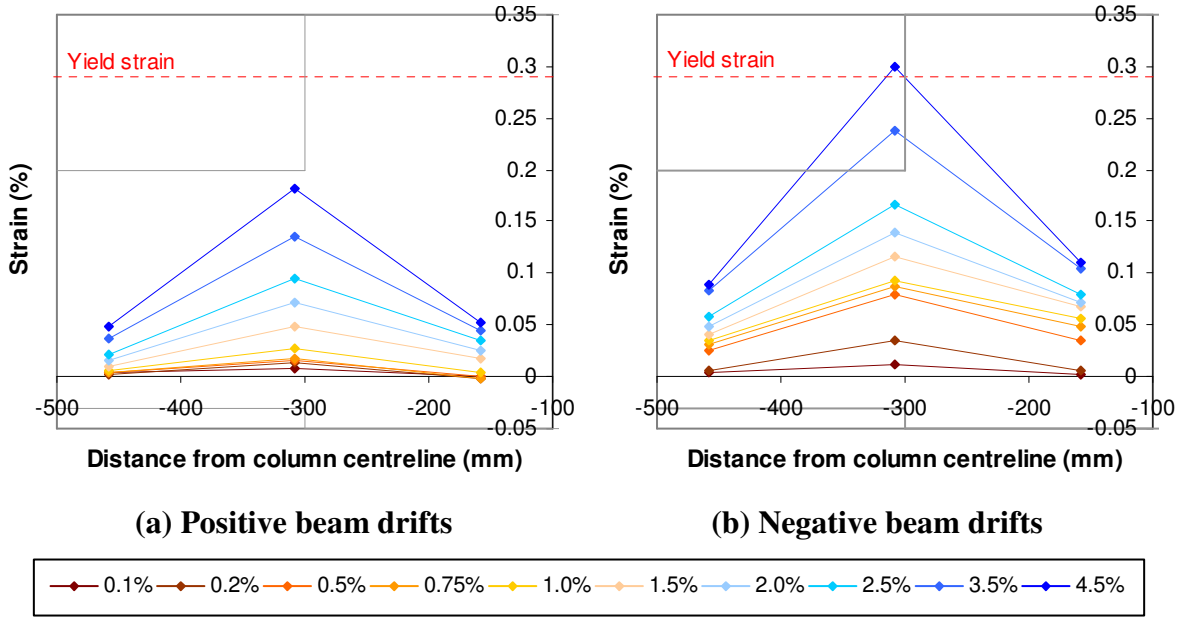

(a) Positive beam drifts **(b) Negative beam drifts**

Figure 5-26: Strain profile along central diagonal hanger in LHS beam at peak drifts

The strain length is the reinforcement length which, when multiplied by the peak strain in the slotted-section, produces the same axial deformation obtained from integrating the actual strain profile along the bar's length. Integrating the strain profile assuming $L_{sp} = 0.022 f_y d_b$ yielded a total strain length of approximately $4/3 L_{sp}$. This is less than $2L_{sp}$ which was calculated for previously tested specimen SB2.

5.3.6 Slab Flexural Contributions

One of the benefits of a slotted-beam's top-hinge connection over a monolithic connection is that deformations are concentrated at the bottom of the beam, away from the level of the floor slab. As a result, contributions to the flexural strength of the beam from floor slab reinforcement and concrete are reduced, limiting beam overstrength actions that need to be resisted by adjacent columns.

To illustrate the extent of the slab initiated in flexure, Figure 5-27 plots deformations on the top surface of the slab and reinforcement strains in the floor slab adjacent to the concrete top-hinge. During gap-opening rotations (Figures a and d), slab deformations at the surface are compressive. Vice versa, during gap-closing rotations (Figures b and c), deformations are tensile. It is shown that beam deformations extending into the slab reduce significantly within 500 mm of the beam edge. Integrating the deformed profile for compression, an effective slab width of 436 mm is calculated. Here the effective slab width has been taken as the slab width which, when multiplied by the deformation at the top surface of the beam, gives the same result as integrating the actual slab surface deformations along the width of the slab.

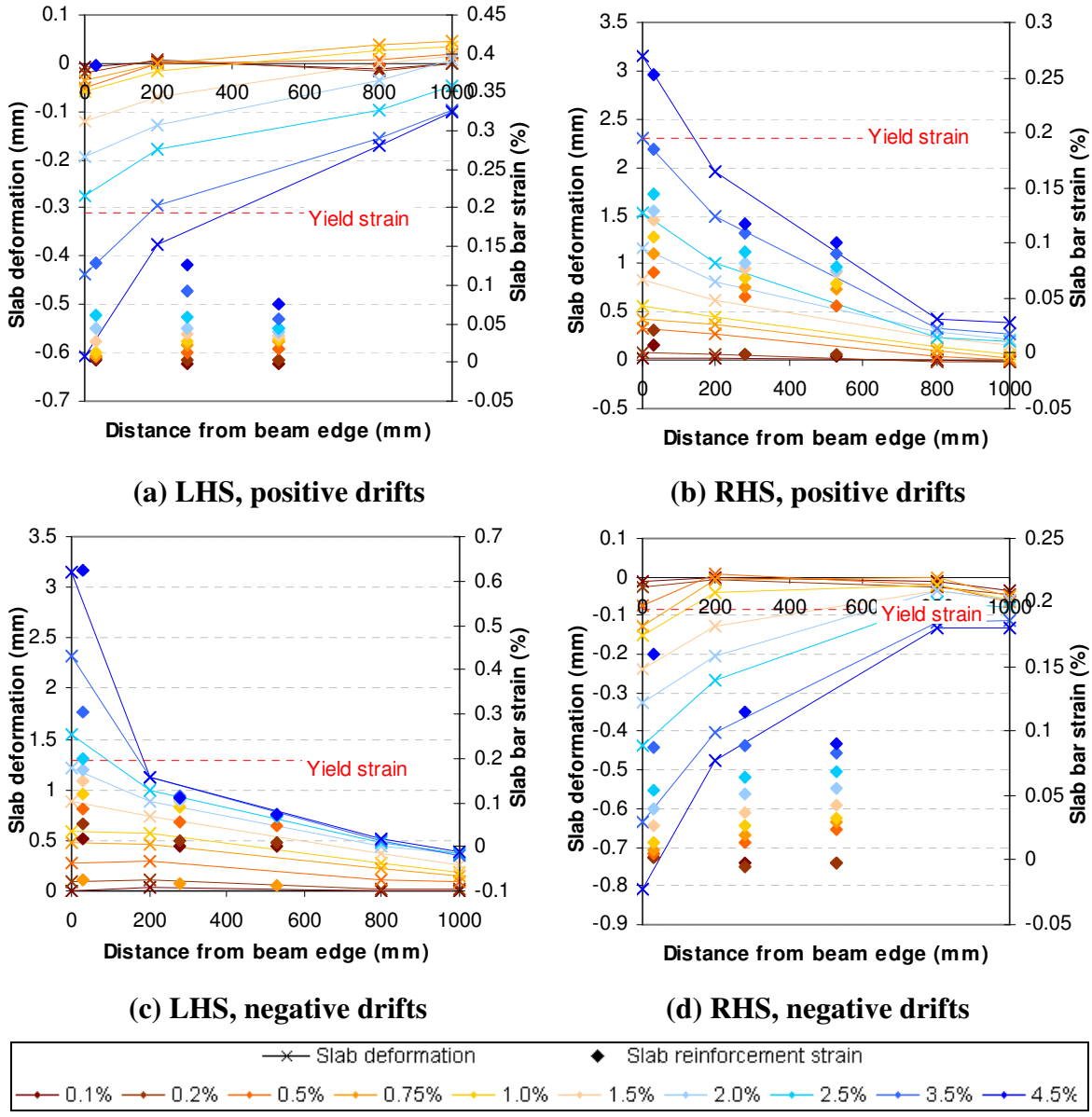

Figure 5-27: Flexural deformations on the top surface of the floor slab and slab reinforcement strains adjacent to the concrete top-hinge at peak drifts

For both gap-opening and closing rotations, slab reinforcement strains are always tensile. The author is not fully aware of the cause of this, but this could be the result of the neutral axis depth, or activation of slab reinforcement in tension due to torsion of the central floor unit. Integrating the strain profile for gap opening rotations, an effective slab width of 315 mm is calculated. Here the effective slab width is the width of slab that includes sufficient slab reinforcement which, when assumed to have the same strain as top longitudinal beam reinforcement, produces the same total force as in the actual slab reinforcement.

Figure 5-28 plots the experimental force-drift response against theoretically calculated contributions from the slotted-connection and effective slab widths calculated above. Theoretical curves were derived using the moment-rotation procedure given in CHAPTER 6. It is shown there is a significant shortfall between the observed response and what is predicted from theory. Therefore there may be contributions to the connection strength other than the connection itself and an effective slab width.

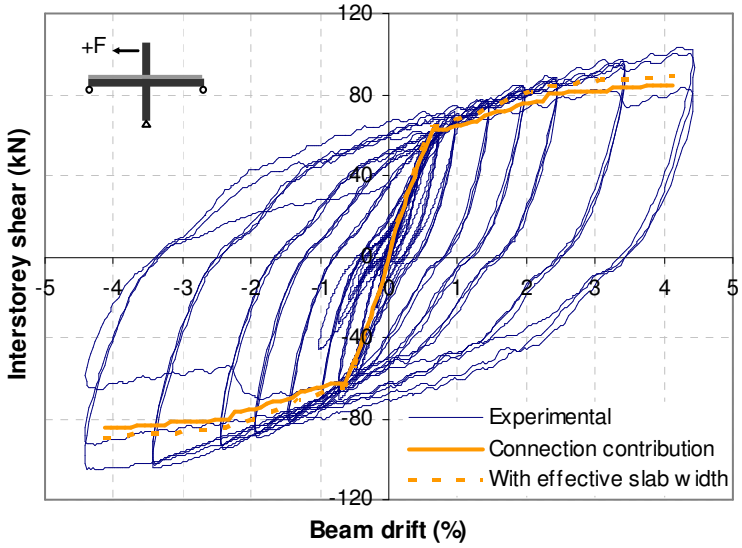

Figure 5-28: Comparison of experimental force-drift response with theoretical contributions from slotted-connection and floor slab

One other contribution that can be identified is from torsion of the central precast floor unit as illustrated in Figure 5-29. Being seated on the column, the central floor unit rotates with the column as drift is applied. However, the free end of the floor unit is restrained to the level supporting beam it is seated on. This induces a resisting torque and explains the cross-diagonal cracking observed in the central floor unit. It is likely that torsion of precast floor units (or transverse beams) framing into columns will be less significant in real buildings. This is because both ends of the floor unit or transverse beam will be connected to columns

which can both rotate as drift is applied. So the boundary conditions at the free end of the floor slab in the test of specimen SB3 did not properly replicate the real world case. Three-dimensional biaxial testing is required to confirm the significance of torsion in transverse elements framing into columns.

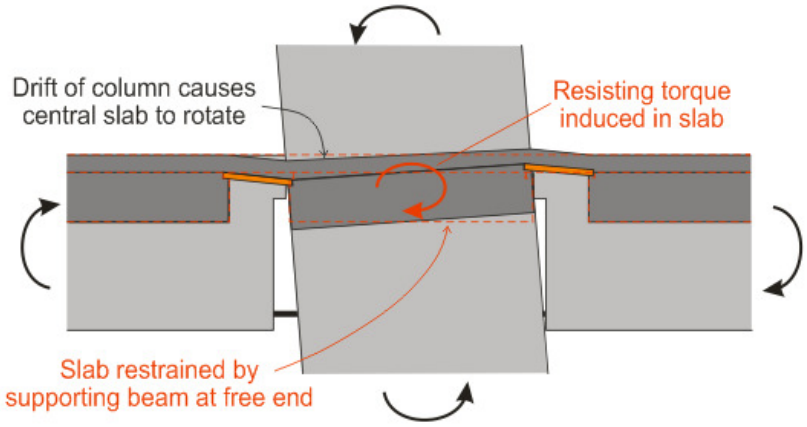

Figure 5-29: Illustration of torsion induced in central precast floor unit

5.3.7 Beam Torsion from Eccentric Floor Gravity Loads

One of the objectives for testing specimen SB3 was to observe beam torsion resulting from eccentric floor gravity loads. It was intended to create worst-case torsional demands on the beam of a downwards shear and moment as shown in Figure 5-30a. However because the flexural stiffness of the slab was much higher than the torsional stiffness of the beam, the beam twisted downwards and the slab rotated upwards relative to the slab as shown in Figure 5-30b. So during testing, the gravity shear was present, but not the floor end-moment. Biaxial testing is recommended to properly test worst-case torsional demands on a slotted-beam.

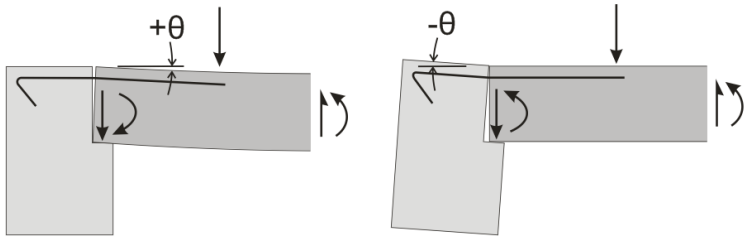

(a) Intended effect **(b) Actual behaviour**

Figure 5-30: Rotation of slab relative to beam

Figure 5-31 plots the beam twist measured from various potentiometer pairs (pots) setup around each beam. The LHS beam showed positive rotations of up to 0.011 radians in response to the eccentric gravity shear. These rotations were greater during gap-closing drifts

than during gap-opening drifts. This was the result of a shift in the gravity shear imposed by the steel/lead weights as the specimen moved laterally.

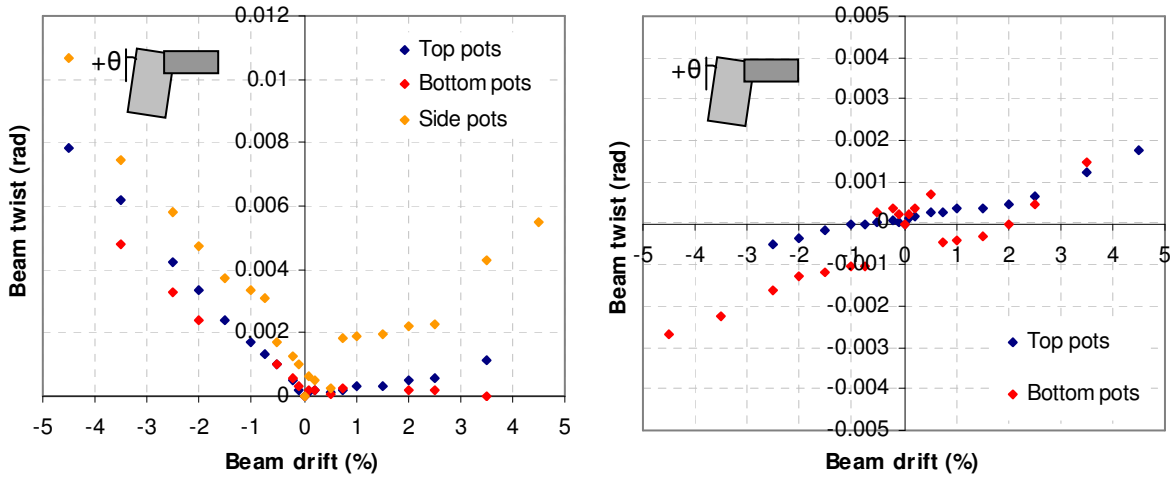

(a) LHS beam **(b) RHS beam**

Figure 5-31: Measured beam rotation at peak drifts

The RHS beam (Figure 5-31b) showed positive rotations for gap-closing drifts, and negative rotations for gap-opening drifts. During construction, it was observed that the RHS floor unit did not sit flat on the beam, but showed a gap on the column side. It is likely this caused gravity shears to pass through the beam end-support rather than through the column. Hence the RHS slotted-connection may have been subject to a smaller eccentric gravity shear than the LHS connection, which possibly explains why beam twist was less in the RHS beam.

Figure 5-32 plots hanger strains through the top-hinge section at peak drifts for both beams. Charts a and d show gap-opening behaviour, while charts b and c show gap-closing behaviour. In all cases, strains were tensile as deformations were governed by flexure in the concrete top-hinge. Comparing the relative distribution of the strains, the necessity of two inner hangers to support the floor slab is apparent. Despite there being two hangers on the inner side of the beam, strains in these hangers were significantly higher than that in the outer hanger for gap-closing rotations.

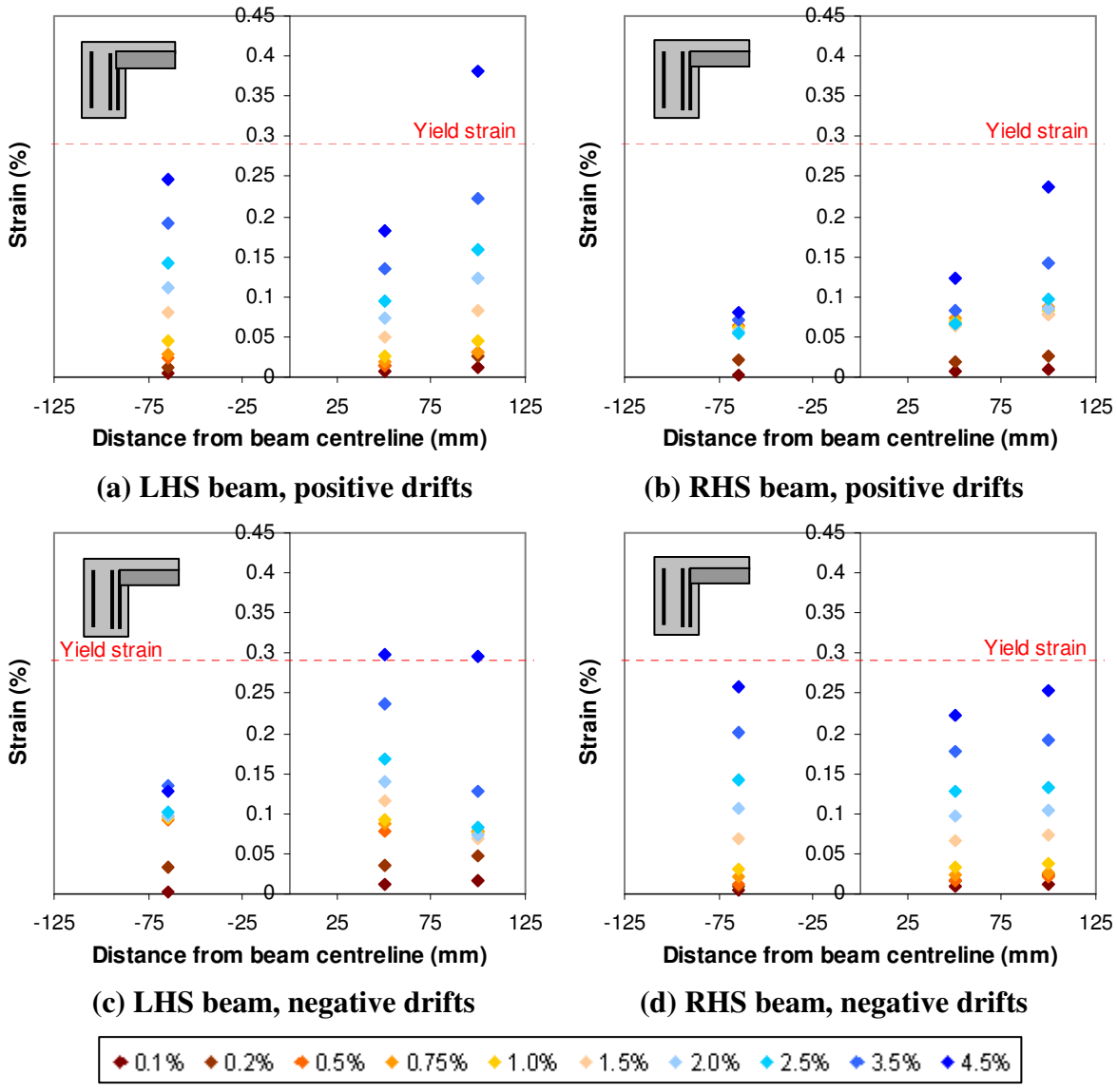

(a) LHS beam, positive drifts **(b) RHS beam, positive drifts**

(c) LHS beam, negative drifts **(d) RHS beam, negative drifts**

Figure 5-32: Hanger strains through top-hinge section

The strains shown above are composed of three contributions illustrated in Figure 5-33 – a vertical seismic shear component, an eccentric gravity shear which wants to twist the beam and large tensile strains from flexural deformations in the concrete top-hinge. Gap-closing rotations create the worst case tension in the two inner hangers from shear actions. This is why strains in the inner hangers can become significantly higher than strains in the outer hanger as shown in Figure 5-32b and c, despite there being two hangers. This torsional effect was discussed more in-depth in Section 3.8.3.

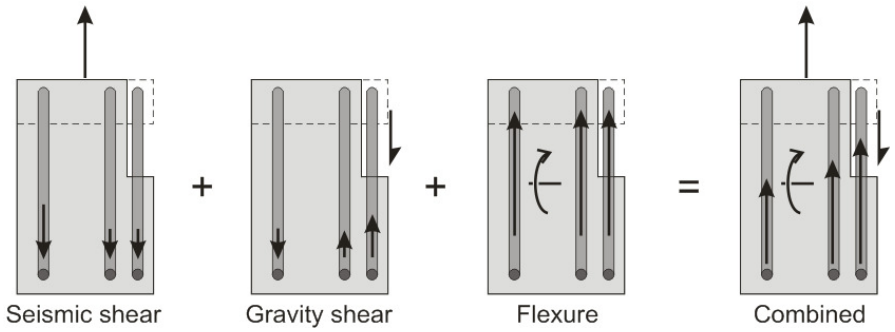

(a) Gap-opening rotation

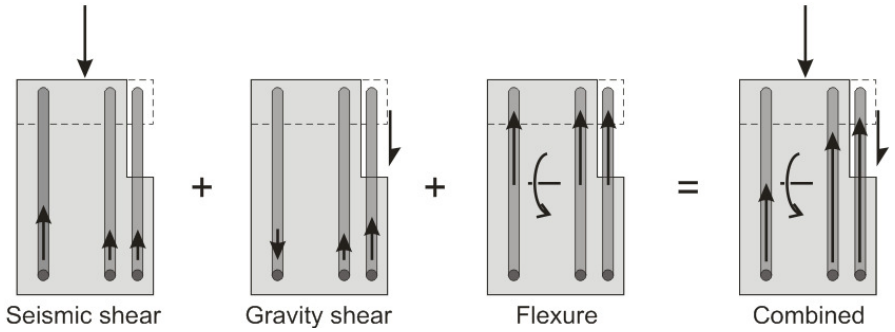

(b) Gap-closing rotation

Figure 5-33: Breakdown of strains in diagonal shear hangers

5.3.8 Bond Stress Profile along Bottom Longitudinal Reinforcement

Figure 5-34 plots the internal axial stress distribution along the bottom longitudinal reinforcement passing through the interior joint as obtained from strain gauge data. Note that missing data points are due to strain gauge failure from over-extension. From horizontal equilibrium, any change in stress must be due to the transfer of stresses to the concrete via bond. Therefore differentiating this profile must give the bond stress distribution as shown in Figure 5-35. To assist with the following explanations, Figure 5-36 provides a simplified illustration of these bond stresses.

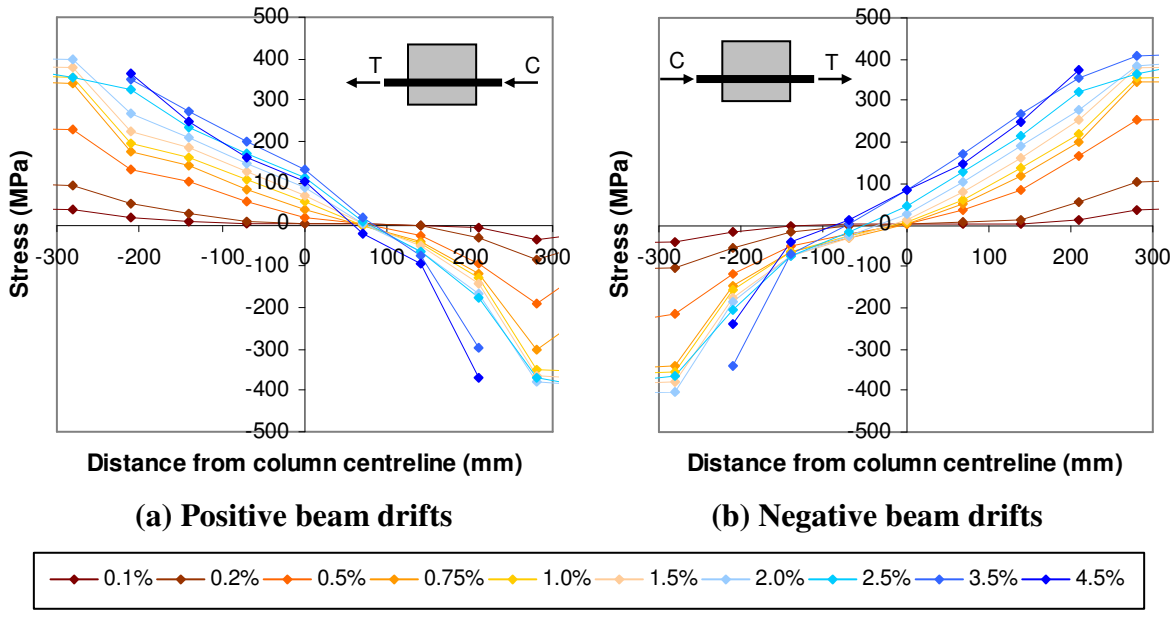

(a) Positive beam drifts (b) Negative beam drifts

Figure 5-34: Stress distribution along bottom longitudinal reinforcement passing through the interior joint at peak drifts

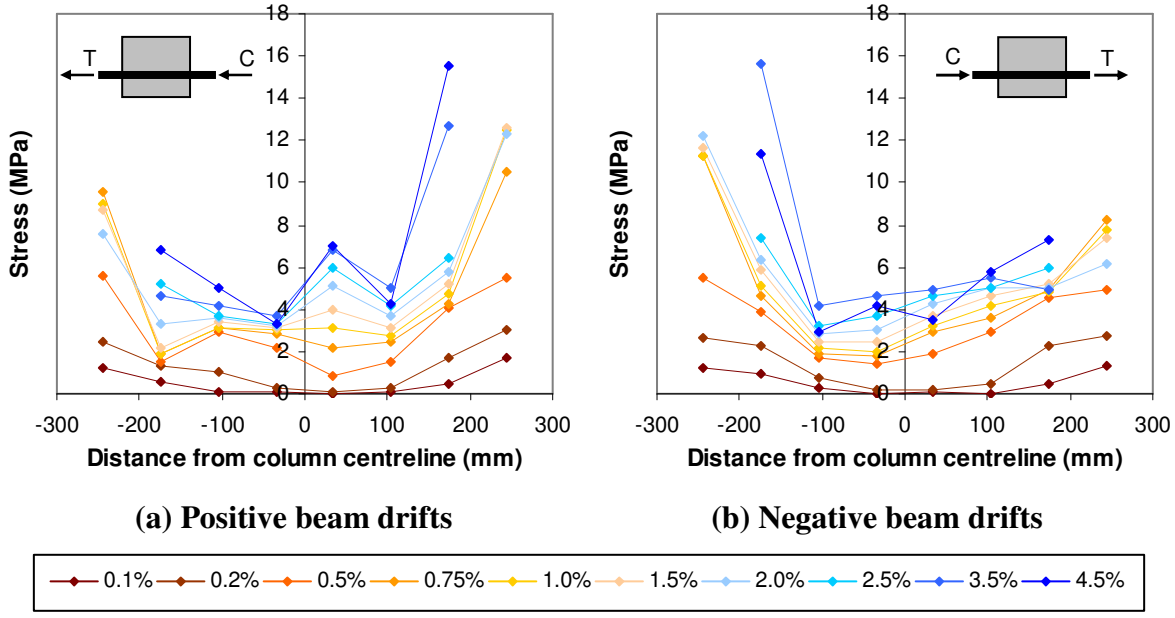

(a) Positive beam drifts (b) Negative beam drifts

Figure 5-35: Bond stress distribution along bottom longitudinal reinforcement passing through the interior joint at peak drifts

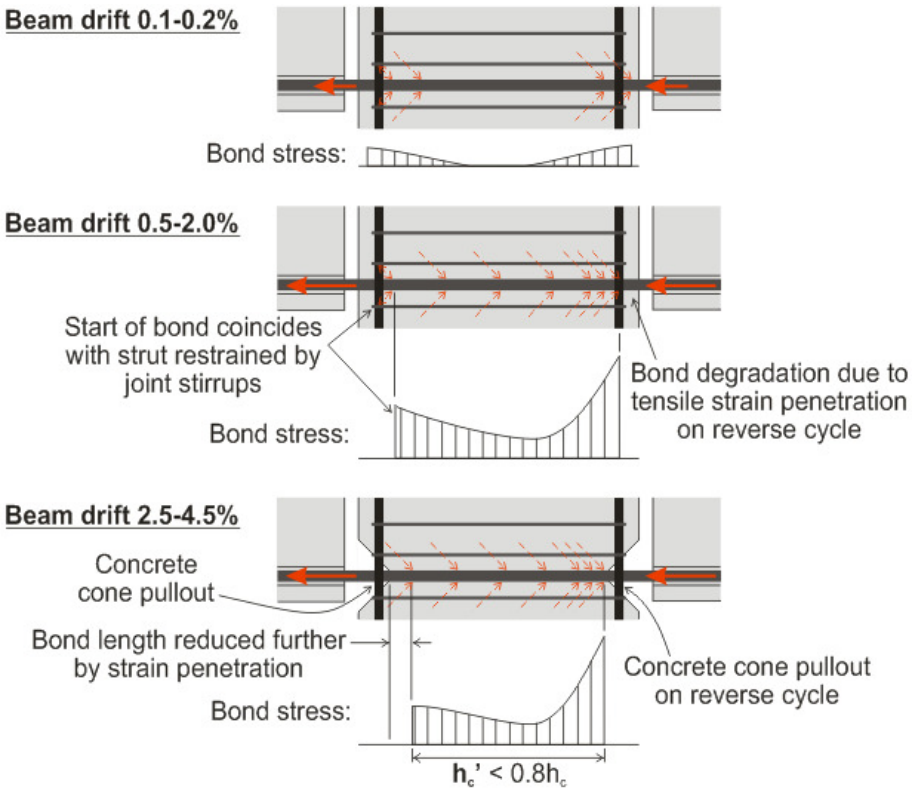

Figure 5-36: Simplified illustration of bond-stress distribution in specimen SB3

During small elastic cycles at beam drifts of 0.1 to 0.2%, bond stress existed primarily at the edges of the joint. This is because steel strains were small and had not yet propagated into the joint. Before yielding of bottom longitudinal reinforcement occurred, strains propagated further and mobilised bond at the centre of the joint at 0.5% drift.

After steel yielded at 0.75% beam drift, the bond stress distribution resembled a shape similar to that given in the second diagram of Figure 5-36. Bond stresses were higher on the side of the joint where reinforcement was in compression, but rapidly decreased within the first third of the column depth. After this, the bond stress remained relatively constant, before increasing towards the tension side of the reinforcement. Bond stresses are likely higher on the compression side because of additional confinement from the column's flexural compression zone, and also because partially degraded concrete can still provide bond by means of granular interlock when the bar is in compression.

Figure 5-34 shows there was no stress transfer in the cover concrete on the side of the joint where the bar was in compression. This is probably due to the degradation of bond from tensile strain penetration during reverse cycles. Similarly, there was no stress transfer, on the side where reinforcement was in tension, in the cover concrete plus some additional depth. This is probably because struts providing stress transfer must be restrained either by joint

stirrups or concrete in tension. The latter can only exist if there has been no prior degradation of the concrete from yield penetration.

At 2.5% beam drift, concrete cone pullout at the column face occurred due to cumulative damage to the cover concrete from reverse-cyclic strain penetration. This led to a further reduction in the column depth providing bond as shown in the third diagram of Figure 5-36. This occurs after multiple cycles of reverse loading, and is the critical limit state which must be considered when ensuring sufficient anchorage to longitudinal reinforcement.

Note that it is well accepted that the bond stress distribution is not uniquely defined and that it changes with bar diameter, the level of bar straining, the number of reverse cycles, and the length providing anchorage (Paulay and Priestley, 1992). Therefore the bond stress distribution shown above is not definitive and may change with other factors.

5.3.9 Anchorage of Bottom Longitudinal Reinforcement in Joint

In light of the bond-slip failure which occurred in previously tested specimen SB2, a large column depth of 600 mm and high concrete strength of 40 MPa was specified for specimen SB3. These provisions provided sufficient anchorage to bottom longitudinal reinforcement and a stable cyclic response was achieved. This section briefly revisits the assumptions made during the initial design and compares them with actual experimental data in hopes of seeking a more efficient design.

Specimen SB3 was designed according to theory given in Section 3.6, conservatively assuming a maximum average bond stress of $1.2\sqrt{f'_c}$, a steel material overstrength factor of 1.5, and an effective column depth providing bond of the lesser of $0.8h_c$ or h_c minus 45° concrete cone pullouts which intersect column stirrups on both sides. The former value of $0.8h_c$ governed the effective column depth. Applying Equation 3-16 then gave:

$$h_c > \frac{\xi_m \lambda_o f_y}{4u_a} \times \frac{d_b}{0.8} = \frac{2 \times 1.5 \times 300}{4 \times 1.2\sqrt{40}} \times \frac{16}{0.8} = 593 \text{ mm}$$

Figure 5-37 plots experimentally observed values for the average bond stress and material overstrength factor at each peak drift. The bottom longitudinal reinforcement stress for producing these plots was obtained from experimental strain gauge data. For the bond stress values reached, no bond failure occurred. However, it can be seen that the average bond stress did not reach the assumed value of $1.2\sqrt{f'_c}$. This is because the assumed material

overstrength factor of 1.5 overestimated the experimentally observed value, which did not exceed 1.4 as shown in Figure 5-37b.

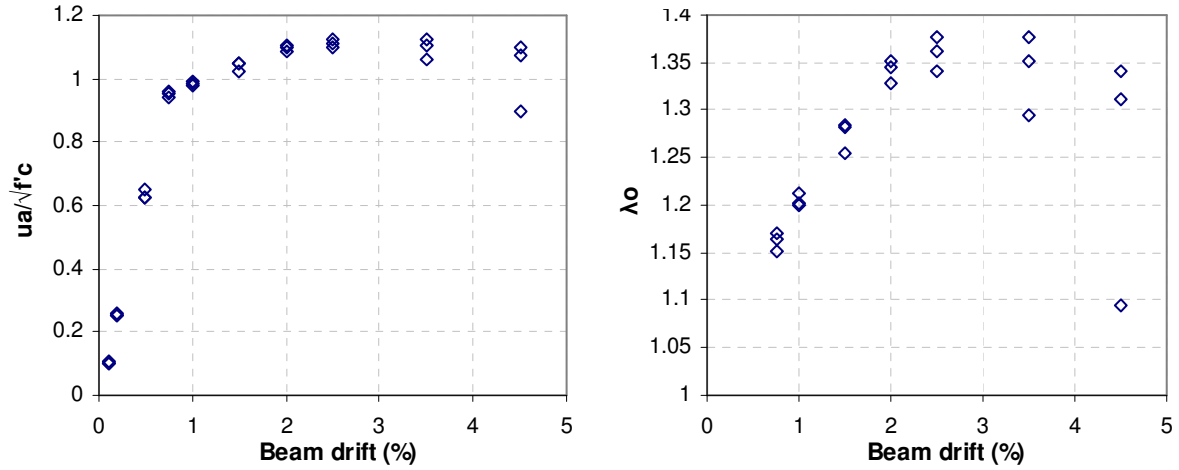

(a) Average bond stress **(b) Material overstrength factor**

Figure 5-37: Experimentally observed values

Assuming a higher maximum average bond stress of $1.4\sqrt{f'_c}$ and adopting λ_o=1.4 from Figure 5-37b, it may have been possible to provide a column depth of 500 mm as given by:

$$h_c > \frac{\xi_m \lambda_o f_y}{4u_a} \times \frac{d_b}{0.8} = \frac{2 \times 1.4 \times 300}{4 \times 1.4\sqrt{40}} \times \frac{16}{0.8} = 474 \text{ mm}$$

Note this equation is very dependent on the maximum average bond stress assumed, and significant testing is required to ascertain a safe value for design. Past tests on slotted beams have obtained average bond stresses of between $1.0\sqrt{f'_c}$ and $1.3\sqrt{f'_c}$ without bond-slip failure occurring (Ohkubo et al., 2004; Leslie, 2010). Just prior to bond failure occurring in specimen SB2, an average bond stress of $1.48\sqrt{f'_c}$ was reached. From the bond stress distributions given in Figure 5-35, a maximum u_a/u_{max} ratio of 0.51 was reached at 2.5% beam drift, when cone pullout occurred. Assuming a peak bond stress of $u_{max}=2.5\sqrt{f'_c}$ (Eligehausen et al., 1983), this gives a maximum average bond stress of $u_a=1.275\sqrt{f'_c}$. Thus test results suggest a reduction in the maximum average bond stress from $u_a=1.675\sqrt{f'_c}$ which is assumed for conventional beams. However, insufficient test data is available to actually say what this value should be for a slotted-beam.

5.3.10 Joint Shear Response

Figure 5-38 plots the joint stirrup strain profile at peak drifts. It shows that joint reinforcement remained elastic throughout the entire test. Note that the joint stirrup yield

strain of 0.20% is outside the scale of both charts. The figure also shows that horizontal joint reinforcement was not mobilised until beam drifts of 3.5%. Due to the large column depth and high strength concrete, the concrete tensile strength was capable of carrying the entire horizontal joint shear for most of the test. From a peak estimated joint shear force of 330 kN and applied axial load of 150 kN, a principle joint tensile stress of 2.3 MPa can be calculated. Given the high concrete strength of 40 MPa, it is therefore not surprising that joint reinforcement was not mobilised. One of the purposes of testing this specimen was to evaluate the respective proportions of horizontal joint shear carried by the concrete strut mechanism and truss mechanism. Unfortunately transverse joint steel was never properly mobilised and this could not be carried out.

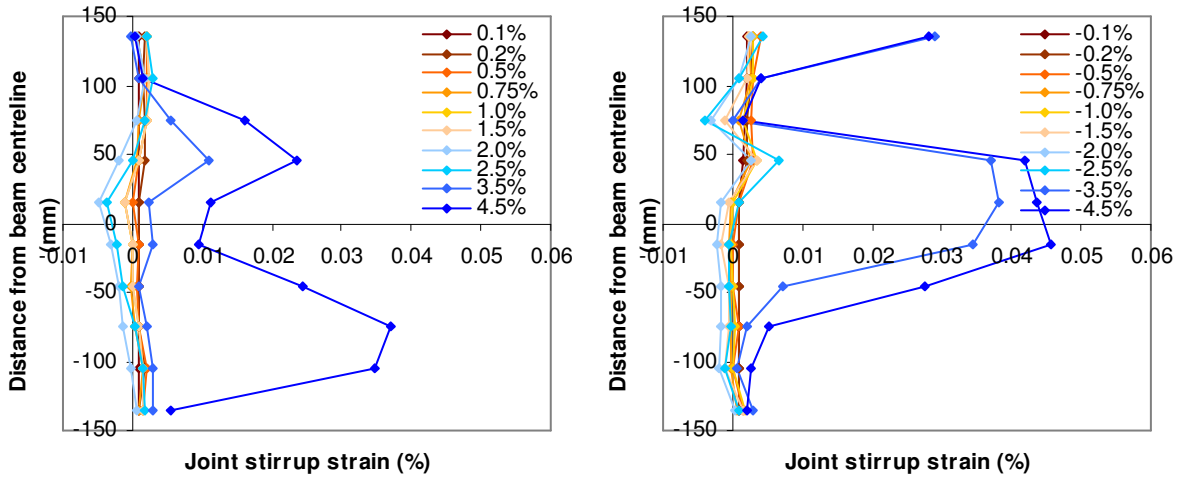

(a) Positive beam drifts **(b) Negative beam drifts**

Figure 5-38: Joint stirrup strain profile at peak drifts

CHAPTER 6 MOMENT-ROTATION ANALYSIS

An analytical procedure was developed to theoretically predict the backbone moment-rotation response of a slotted-beam connection. The method draws on concepts proposed by Pampanin, Priestley and Sritharan (2000) for the analysis of dry-jointed ductile precast rocking connections. Due to the presence of the slot and unbonded length, common assumptions of Bernoulli plane sections are no longer valid. Thus the procedure adopts a moment-rotation formulation as oppose to the common moment-curvature formulation for conventional reinforced concrete sections. The procedure is approximate, but simple enough that it can be implemented via a spreadsheet. It was used to perform a sensitivity study on beam design parameters (See Section 6.2) and was verified against experimental results (See Section 6.3).

6.1 Outline of Procedure

Firstly, a neutral axis depth is assumed and a fixed-end rotation imposed on the connection. From deformation compatibility, which is illustrated in Figure 6-1, axial deformations in the concrete, longitudinal reinforcement and diagonal hanger reinforcement can be obtained. From these deformations, strains can be computed, followed by stresses, and finally forces in the concrete and steel components. Sections 6.1.1 to 6.1.3 describe the constitutive models used to obtain concrete and steel forces from deformations.

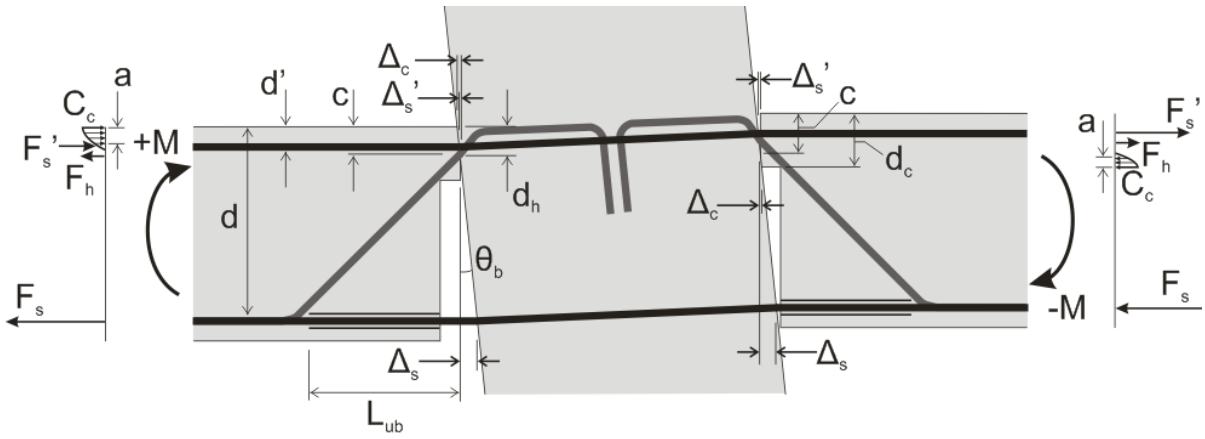

Figure 6-1: Gap opening and closing mechanism

Horizontal equilibrium (Equation 6-1) is then applied to iterate for the actual neutral axis depth and forces. The moment capacity can then be calculated by taking moments about the neutral axis as given by Equation 6-2.

Horizontal equilibrium: $F_s + F_s' + F_h - C_c = 0$ ...(6-1)

$$\begin{aligned} &\text{Gap opening}: M_n = F_s(d-c) + F_s'(d'-c) + F_h(d_h - c) + C_c(a/2 - c) \\ &\text{Gap closing}: M_n = F_s(d-c) + F_s'(d'-c) + F_h(d_h - c) + C_c(d_c - a/2 - c) \end{aligned} \quad \text{...(6-2)}$$

M_n = Nominal moment capacity

F_s = Force in bottom longitudinal reinforcement

F'_s = Force in top longitudinal reinforcement

F_h = Horizontal force component in diagonal hanger reinforcement

C_c = Force in concrete acting in compression

d = Depth from top surface of beam to bottom longitudinal reinforcement

d' = Depth from top surface of beam to top longitudinal reinforcement

d_h = Depth from top surface of beam to diagonal hanger reinforcement at the beam-column interface

d_c = Concrete top-hinge depth

c = Neutral axis depth (measured from the top surface of the beam)

a = Whitney equivalent rectangular concrete stress block depth

Note that the moment-rotation method adopts an actual non-linear concrete stress profile, and not Whitney equivalent rectangular concrete stress blocks. The Whitney rectangular concrete stress block depth *a*, is simply used in Figure 6-1 and Equation 6-2 to indicate the centroid of the concrete compression stress field. This centroid occurs at *a*/2 below the top of the concrete top-hinge during positive rotations, and at *a*/2 above the bottom of the concrete top-hinge during negative rotations.

The sign convention and vector sense adopted for this thesis is gap-opening moments and rotations as positive; and gap-closing moments and rotations as negative. In terms of component deformations, elongation is taken as positive and contraction as negative. Similarly, tensile forces are positive and compressive forces are negative.

6.1.1 Computation of Longitudinal Reinforcement Forces

From Figure 6-1, the axial deformation in longitudinal reinforcement can be calculated from:

$$\Delta_s = \theta_b (d - c) \text{ and } \Delta_s' = \theta_b (d' - c) \quad \text{...(6-3)}$$

An apostrophe (‘) denotes top reinforcement, while no apostrophe denotes bottom reinforcement.

Bottom reinforcement strain can be computed from axial deformation by dividing by a strain length which accounts for the unbonded length, L_{ub}, with strain penetration, L_{sp}, on each side. The strain length is the length which, when multiplied by the peak strain in the slotted-section, produces the same axial deformation obtained from integrating the actual strain profile along the bar’s length. Pampanin et al. (2000) derived the following expression to estimate the steel strain from a computed axial deformation:

$$\varepsilon_s = \frac{\Delta_s + 2/3 L_{sp} \alpha \varepsilon_y}{L_{ub} + 2L_{sp}} \quad \text{...(6-4)}$$

It should be noted that the strain length is never constant but increases with the magnitude of applied strain and the number of cycles. However, usually a constant strain length is assumed and found to still give reasonable results. The α-factor accounts for greater strain penetration at higher levels of strain. For strains above yield but before strain hardening, α is equal to 1.0. For strains after the onset of strain hardening, α is taken as greater than 1.0. The response is normally very insensitive to this α-factor, and often α=1 can simply be adopted.

Top reinforcement strain can be computed in a similar fashion. However, if top reinforcement remains elastic, strain penetration is less extensive. Palermo (2004) modified the expression above for elastic behaviour to give:

$$\varepsilon_s' = \frac{\Delta_s'}{4/3 L_{sp}'} \quad \text{...(6-5)}$$

If top reinforcement then yields, Equation 6-4 can be applied by taking the unbonded length L_{ub} as zero. In both Equations 6-4 and 6-5, L_{sp} is the yield penetration length. This length is dependent on the bar diameter, stress in the bar, concrete confinement and the condition of the bond to reinforcement. Many empirical expressions for this length have been suggested

by researchers (Corley, 1966; Mattock, 1967; Panagiotakos and Fardis, 2001) in the context of plastic hinge lengths in conventional reinforced concrete beams. However in this case, the following empirical expression from Paulay and Priestley (1992) will be adopted:

$$L_{sp} = 0.022 f_y d_b \qquad ...(6\text{-}6)$$

Integration of strain gauge data from tests carried out on slotted-beams, in CHAPTER 4 and CHAPTER 5, revealed yield penetration lengths of 0.011, 0.019, 0.02, 0.023 and 0.039 times $f_y d_b$. Therefore the expression above appears to be appropriate for slotted-beams. Note that yield penetration lengths are shorter for deformed bars in compression compared to when they are in tension. This is because concrete can provide additional stiffness via bond transfer in compression. For simplicity, the same yield penetration length is assumed for both tension and compression. This assumption has little effect on the results.

From computed strains, the stress and thus force in longitudinal reinforcement can be found. The constitutive stress-strain model proposed by Mander, Priestley and Park (1984) modified by Rodriguez, Botero and Villa (1999) was adopted for this study and is given below.

$$\begin{aligned}
&\varepsilon_s \le \varepsilon_y : && f_s = E_s \varepsilon_s \\
&\varepsilon_y < \varepsilon_s \le \varepsilon_{sh} : && f_s = f_y \\
&\varepsilon_{sh} < \varepsilon_s \le \varepsilon_u : && f_s = f_u + (f_y - f_u)\left(\frac{\varepsilon_u - \varepsilon_s}{\varepsilon_u - \varepsilon_{sh}}\right)^p \\
&\text{where :} && p = \frac{\log\left(\frac{f_u - f_{sh1}}{f_u - f_y}\right)}{\log\left(\frac{\varepsilon_u - \varepsilon_{sh1}}{\varepsilon_u - \varepsilon_{sh}}\right)}
\end{aligned} \qquad ...(6\text{-}7)$$

(ε_s, f_s) is the steel strain and stress, (ε_y, f_y) corresponds to the yield point, (ε_{sh}, f_y) defines the onset of strain hardening, (ε_u, f_u) defines the ultimate strength, and (ε_{sh1}, f_{sh1}) is an intermediate point on the strain hardening curve.

This stress-strain relationship was assumed for both tension and compression envelopes, which is a valid assumption until buckling occurs. Steel stress-strain models including the effects of buckling have been proposed by authors such as Dhakal and Maekawa (2002) and Bae, Mieses and Bayrak (2005). But due to their complexity, these were not included in this simplified backbone moment-rotation analysis.

Another factor that much be considered in the constitutive stress-strain model, is that due to effects of cyclic loading. Due to Bauschinger effect and strain hardening, the stress in cyclically loaded steel for a given strain can be higher than that given by the monotonic stress-strain response. Thompson and Park (1978) showed that the monotonic steel stress-strain curve could approximate the backbone curve for the cyclic response, provided the origin of the monotonic curve was shifted horizontally by the amount equivalent to the residual plastic strain after unloading. This is illustrated in Figure 6-2, and accounts for cyclic loading effects producing a pseudo-cyclic backbone curve. This correction can be incorporated into the steel constitutive model by replacing ε_s in Equation 6-7 with ε_{shift} given in Equation 6-8. Note this requires the rotation sequence to be known, such that the peak strain reached before reversal, $\varepsilon_{s,old}$, is also known.

$$\varepsilon_{shift} = \varepsilon_s - \varepsilon_{sp}$$
$$\text{Where :} \quad \varepsilon_{sp} = \varepsilon_{s,old} - \varepsilon_y > 0 \qquad \text{...(6-8)}$$

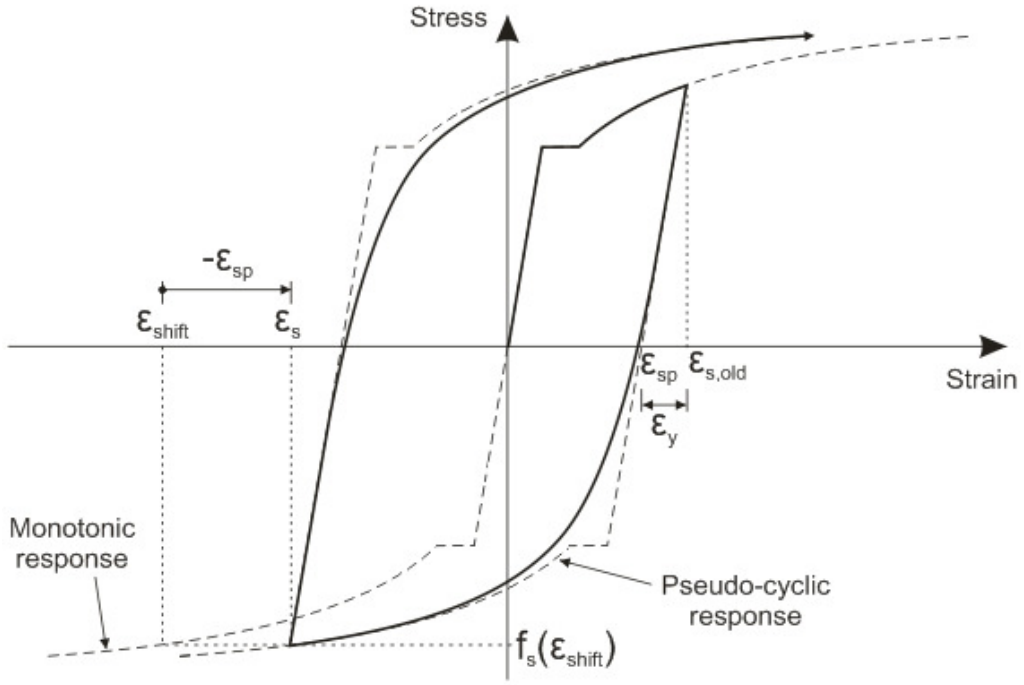

Figure 6-2: Pseudo-cyclic steel stress-strain using shifted monotonic stress-strain curve

6.1.2 Computation of Concrete Top-hinge Force

Concrete strains for conventional monolithic sections are usually calculated based on curvatures as oppose to rotations. As a result, evaluating concrete strains using a moment-rotation formulation is less clear. Two methods adopted in this study are given below.

The first method involves computing the concrete deformation at the extreme compression fibre. From Figure 6-1, this is:

$$\begin{aligned} &\text{Gap opening}: \Delta_c = \theta_b \times c \\ &\text{Gap closing}: \ \Delta_c = \theta_b (d_c - c) \end{aligned} \qquad \text{...(6-9)}$$

The corresponding concrete strain can then be computed by dividing by a strain length over which the deformation occurs. What this length should be is unclear and difficult to determine. Current literature is limited and intuitively this length would change with the extent of deformation and damage. For simplicity and assuming strain compatibility between the top longitudinal reinforcement and surrounding concrete, a strain length similar to the adjacent top reinforcement when in compression seems reasonable. From experimental strain gauge data from tests carried out, this length appears to be between $2/3L_{sp}$' and $4/3L_{sp}$'. Thus the expression below is suggested.

$$\varepsilon_c = \frac{\Delta_c}{L_{pc}'} \qquad \text{...(6-10)}$$

$$\text{Where } L_{pc}' \text{ is between } 2/3L_{sp}' \text{ and } 4/3L_{sp}'$$

The second method for estimating concrete strain is the "monolithic beam analogy" proposed by Pampanin et al. (2000) for dry-jointed ductile precast rocking connections. This analogy avoids the problem of assuming a strain length, and instead adopts the concrete curvature in a monolithic section subject to the same beam displacement at the point of contra-flexure. From this displacement compatibility condition, the concrete strain can be computed from:

$$\varepsilon_c = \left[\frac{\theta_b L_{cant}}{\left(L_{cant} - \frac{L_p}{2} \right) L_p} + \phi_y \right] \times c \qquad \text{...(6-11)}$$

L_{cant} is the cantilever length of the beam from the column face to the assumed point of contra-flexure, c is the neutral axis depth, and φ_y and L_p are the yield curvature and plastic hinge length for a monolithic RC beam respectively. The plastic hinge length can be taken as $L_p = 0.08L_{cant} + L_{sp} \geq 2L_{sp}$ (Paulay and Priestley, 1992), where L_{sp} is given by Equation 6-6.

The monolithic beam analogy assumption is appropriate for a slotted beam during gap-opening rotations, as the slotted section is equivalent to a monolithic section with only the

addition of an unbonded length. However, it is less clear how applicable this assumption is during gap-closing rotations. It can also be argued that the assumed strain length for the first method is equally as uncertain. Regardless of this, a parametric analysis carried out showed the force-drift response to be relatively insensitive to both methods, and both assumptions were found to give good comparison with experimental results. This is because the neutral axis remains within the concrete top-hinge, such that forces within the top-hinge have a small lever arm and thus have little effect on the moment achieved.

From the concrete strain, and assuming a linear strain distribution, the concrete compressive force can then be computed from a concrete stress-strain relationship. The Mander model (Mander, Priestley and Park, 1988) was adopted for this study and is given in Equation 6-12 and shown in Figure 6-3 below.

$$
\begin{aligned}
f_c &= \frac{f'_{cc}\, xr}{r-1+x^r} \\
x &= \frac{\varepsilon_c}{\varepsilon_{cc}} \\
\varepsilon_{cc} &= \varepsilon_{co}\left[1+5\left(\frac{f'_{cc}}{f'_{co}}-1\right)\right] \\
r &= \frac{E_c}{E_c - E_{\sec}} \\
E_c &= 5000\sqrt{f'_{co}} \\
E_{\sec} &= \frac{f'_{cc}}{\varepsilon_{cc}}
\end{aligned}
\qquad \text{...(6-12)}
$$

f'_{co} is the peak unconfined compressive strength, f'_{cc} is the peak confined compressive strength, and ε_{co} is the concrete strain at the peak unconfined stress. ε_{co} is often taken between 0.0015 and 0.002 (Mander et al., 1988; Paulay and Priestley, 1992).

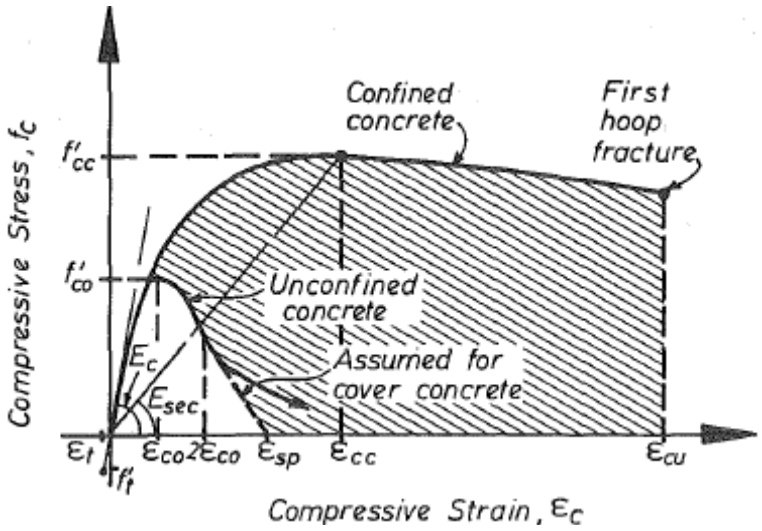

Figure 6-3: Mander constitutive concrete stress-strain model for confined and unconfined concrete (Mander et al., 1988)

Although the concrete top-hinge is not confined by any transverse steel, some lateral confinement will exist from the adjacent column and beam concrete. It is difficult to quantify how much confinement is actually present, and indeed this will change for gap-opening and gap-closing rotations. From parametric studies carried out, assuming f'_{cc}/f'_{co} between 1 and 1.1 appears to give good agreement with experimental observations. Furthermore, above this value, the response is not very sensitive to additional levels of confinement. This is because the concrete strain range never increases far enough for the post-peak ductility from confinement to become apparent. If some confinement is assumed, the ultimate concrete strain ε_{cu} can be estimated from (King, 1986):

$$\varepsilon_{cu} = \varepsilon_{sp} + 0.04\left(\frac{f'_{cc}}{f'_{co}} - 1\right) \qquad ...(6\text{-}13)$$

Where ε_{sp} is the unconfined spalling strain, which can be taken between 0.006 and 0.0064.

If zero confinement is assumed, that is concrete is unconfined, after the concrete strain exceeds $2\varepsilon_{co}$, the concrete stress-strain curve is assumed to degrade linearly until zero stress is reached at the unconfined spalling strain ε_{sp} (See Figure 6-3). In equation form, this can be expressed as:

$$\varepsilon_c > 2\varepsilon_{co}: \quad f_c = \left(\frac{f'_{co}(2\varepsilon_{co}/\varepsilon_{cc})r}{r-1+(2\varepsilon_{co}/\varepsilon_{cc})^r}\right)\left(1-\frac{\varepsilon_c - 2\varepsilon_{co}}{\varepsilon_{sp} - 2\varepsilon_{co}}\right) \qquad ...(6\text{-}14)$$

6.1.3 Computation of Diagonal Hanger Reinforcement Force

Although diagonal hangers are only included to carry shear, because they possess a horizontal force component, they do influence the flexural behaviour of the connection. In fact, experimental strain gauge data showed strains in diagonal reinforcement to be governed more by flexural deformations than shear (See Section 4.3.10). The same experiments showed that diagonal hangers also helped to restrain elongation through the top-hinge and subsequently yielding of top longitudinal reinforcement. It would therefore be useful to be able to estimate the effect of diagonal hangers on the flexural response – firstly, to limit elongation in the top-hinge; and secondly, to locate hangers as close as possible to the neutral axis to limit flexural strains within diagonal shear reinforcement.

Obtaining actual strains and forces in the diagonal hanger is quite complex due to flexural and shear interactions which are inseparable. Horizontal deformations from flexure are likely to deform diagonal bars in an s-bend as shown in Figure 6-4. At the same time vertical shear will seek to bend the bar further for gap-opening rotations and straighten the bar for gap-closing rotations. The hanger bar does not remain straight, and has flexural strains as well as axial strains. It is also no longer at its original inclination through the main flexural crack. Local crushing of concrete around the bar may also influence the way the bar bends.

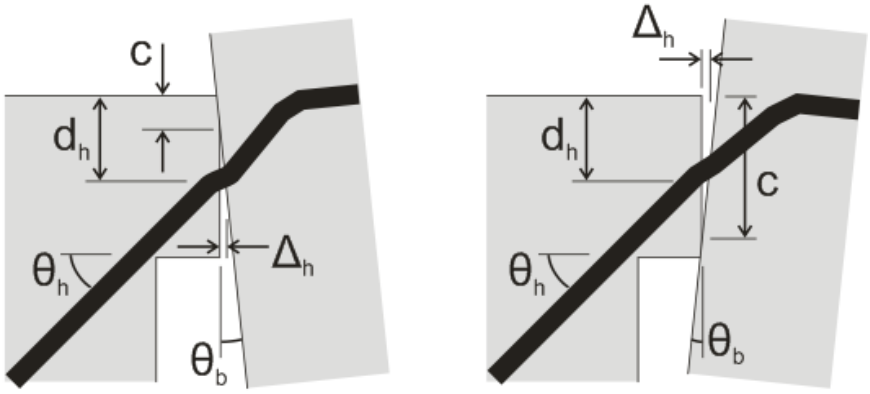

(a) Gap opening rotation **(b) Gap closing rotation**

Figure 6-4: Flexural deformations in hanger

So for simplicity, the analytical procedure that follows ignores vertical shear and evaluates the force in the hanger based solely upon flexural deformations. Also because the deformed inclination of the hanger is not known, its original inclination shall be assumed and assumed to remain unchanged.

Experimental tests showed flexural deformations in the concrete top-hinge to be accommodated predominantly by a crack at the beam-column interface as shown in Figure 6-4. Thus the deformation in the diagonal hanger can be approximated as:

$$\Delta_h = \theta_b (d_h - c) \qquad ...(6\text{-}15)$$

Similar to the longitudinal reinforcement, the strain in the hanger can be computed by dividing by a strain length. Strain gauge data from tests carried out showed values between $4/3L_{sp}$ and $2L_{sp}$ to be appropriate, where L_{sp} is given by Equation 6-6. Therefore:

$$\varepsilon_h = \frac{\Delta_h}{L_{p,h}} \qquad ...(6\text{-}16)$$

Where : $L_{p,h}$ is between $4/3L_{sp}$ and $2L_{sp}$

From the computed strain, the axial stress can be found using the steel constitutive relationship given in Equation 6-7. From the stress, the horizontal force component in the diagonal hanger estimated from Equation 6-17 and entered into the horizontal force equilibrium equation to evaluate the neutral axis depth and moment capacity.

$$F_h = A_h f_{s,h} \cos\theta_h \qquad ...(6\text{-}17)$$

Although this method of analysis does not properly represent the behaviour of the hanger, due to the small lever arm, the inclusion or exclusion of the hanger force yields negligible difference in the force-drift response. Including hanger forces only comes in useful for estimating where the hanger should be located to minimise flexural strains.

6.2 Parametric and Sensitivity Analyses

This section summarises the results of parametric analyses carried out using the proposed moment-rotation procedure. Initially a sensitivity study was carried out on parameters whose values had to be assumed by the moment-rotation procedure. Namely, the bottom reinforcement strain penetration length, top reinforcement strain length, the method adopted to estimate concrete strains and the level of concrete confinement. Later, a parametric study was carried out to assess the effect of altering the concrete top-hinge depth, top-to-bottom steel ratio, slab contributions and the effect of the diagonal shear reinforcement on flexure.

Parametric analyses were carried out using two benchmark slotted-beam sections as shown in Figure 6-5. The first beam section was identical to tested specimen SB1, whilst the second beam was a 700 mm deep full-scale prototype section, with bottom reinforcement of three 32 mm diameter and one 28 mm diameter Grade 300 deformed bars. Concrete strengths were 30 MPa and 40 MPa for sections SB1 and the full-scale prototype respectively, and unbonded lengths of 245 mm and 500 mm were assumed for sections SB1 and the full-scale prototype respectively. The main difference between the two sections was that specimen SB1 had a top-to-bottom steel ratio, $A_s'f_y'/A_sf_y$, ratio of 3.0 and a bottom reinforcement ratio, ρ, of 0.006; whereas the full-scale prototype had $A_s'f_y'/A_sf_y$=1.8 and ρ=0.012. Therefore a greater amount of yielding of top reinforcement was to be expected in the full-scale prototype. Unless otherwise stated, beam design parameters in Figure 6-5 and assumptions given in Table 6-1 were adopted for parametric analyses.

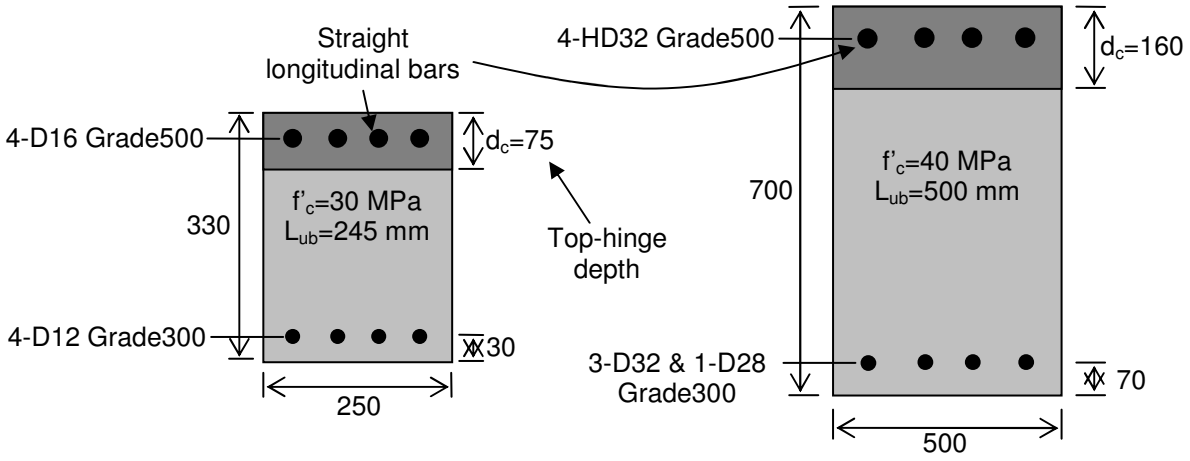

(a) Tested specimen SB1 **(b) Full-scale prototype**

Figure 6-5: Benchmark slotted-beam sections used for parametric analysis (diagonal hanger bars not shown)

Table 6-1: Benchmark parameters assumed for parametric analysis

Parameter	Benchmark
Strain penetration length, L_{sp}	$0.022f_yd_b$
Top reinforcement strain length, L_p'	$4/3L_{sp}'$
Method to estimate, ε_c	Monolithic beam analogy
Concrete confinement, f'_{co}/f'_c	1
Loading type	Monotonic
Hanger forces included	No (if yes, d_h=0.72d_c)

Results plots for both benchmark specimens are provided, but were normalised to allow easier comparison. Moments were normalised by dividing by the positive yield moment of the benchmark section, M_{y+}. Similarly, the neutral axis depth and top longitudinal

reinforcement strains were normalised by dividing by the effective beam depth, d, and the top reinforcement yield strain, ε_y', respectively.

6.2.1 Sensitivity to Bottom Reinforcement Strain Penetration Length

The expression for the yield penetration length of $0.022 f_y d_b$ that Paulay and Priestley (1992) suggested was empirically derived from extensive experimental data. Due to scatter, the actual yield penetration length will vary from this value, and indeed this was observed in the slotted-beam tests carried out. Figure 6-6 shows plots of normalised moment against rotation for both benchmark specimens for different strain penetration lengths assumed for the bottom longitudinal reinforcement.

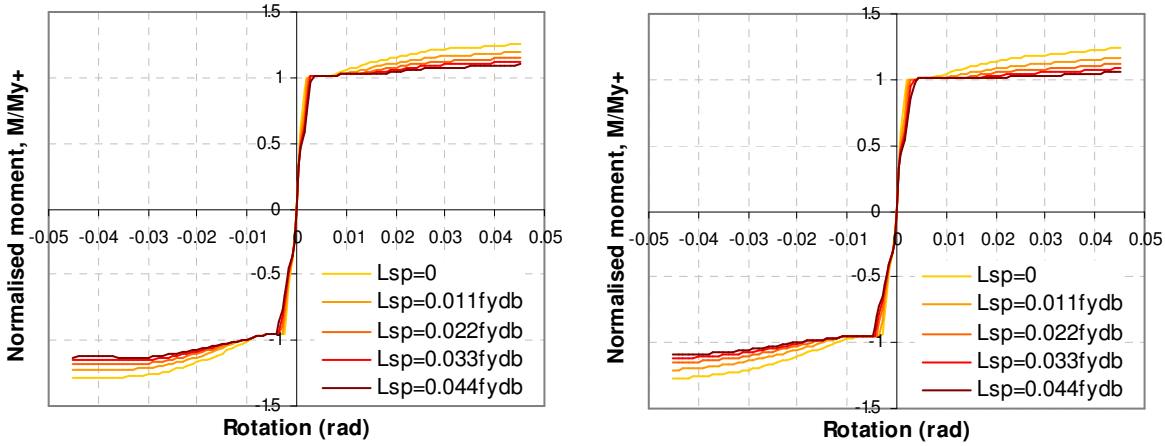

(a) Section SB1 **(b) Full-scale prototype section**

Figure 6-6: Sensitivity analysis - Bottom reinforcement strain penetration length

The response is very intuitive, the shorter the strain penetration length, the greater the bottom reinforcement strain and hence moment capacity for a given drift. Decreasing the strain penetration length increases the elastic stiffness, and rate of post-yield hardening. Because the moment capacity of a slotted-beam is governed by the bottom reinforcement, it is sensitive to the assumed strain penetration length for this reinforcement.

6.2.2 Sensitivity to Top Reinforcement Strain Length

As outlined in Section 6.1.1, a strain length, L_p', of $4/3L_{sp}$' can be adopted for non-yielding top longitudinal reinforcement and a length of $2L_{sp}$' for yielding top reinforcement. Figure 6-7 shows the effect of altering this value on the moment-rotation response, the neutral axis depth and top reinforcement strains.

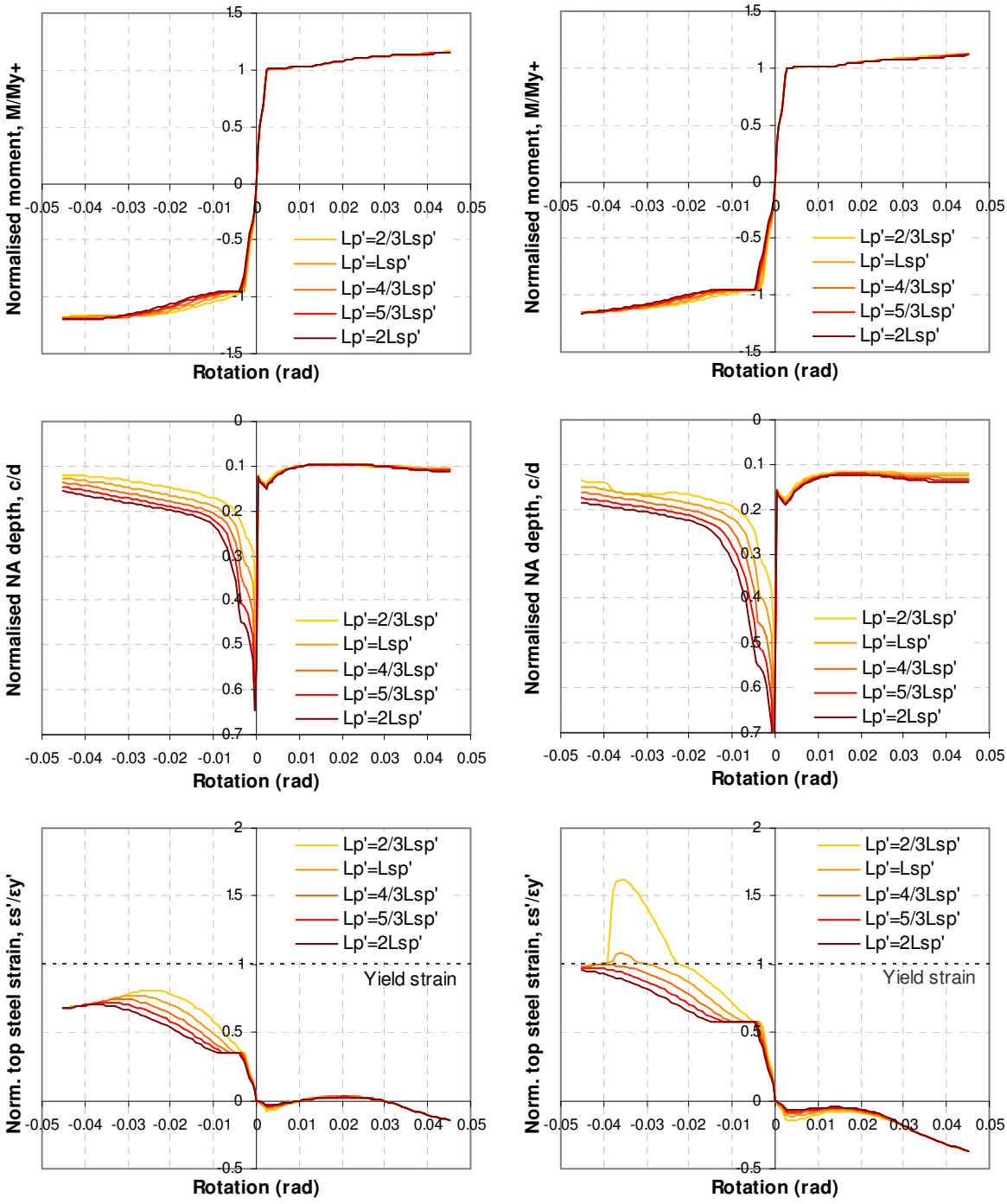

(a) Section SB1 **(b) Full-scale prototype section**

Figure 6-7: Sensitivity study – Top reinforcement strain length

Figure 6-7 shows that the strain length has negligible effect on the positive (gap-opening) response for both beams. This is because the neutral axis depth remains close to the depth of the top reinforcement which is at $0.1d$ and $0.11d$ for section SB1 and the full-scale prototype respectively. During positive rotations, compression within the section is governed primarily by the surrounding concrete as for a monolithic section. For this reason, the monolithic beam

analogy assumed to estimate concrete strains is very applicable. However, this is not so for negative (gap-closing) rotations.

For negative (gap-closing) rotations, the top reinforcement strain length has a greater influence on the response because top reinforcement is the only component providing tension in the horizontal direction. A shorter assumed strain length increases top reinforcement forces, therefore reducing the neutral axis depth to maintain horizontal equilibrium. This in turn increases the lever arm of concrete in compression about the top reinforcement, which slightly increases the moment capacity as seen for both sections.

In addition, Figure 6-7b illustrates the effects of top reinforcement yielding in the full-scale prototype when L_p' is less than L_{sp}'. Note that top reinforcement will only yield in tension during negative (gap-closing) rotations. It can be seen that top reinforcement yielding has little effect on the moment-rotation response. It does however lower the neutral axis depth, which will in turn increase permanent deformations and cracking at the top surface of the beam. These effects are not desirable. However, it will be shown later that these can be limited by reducing the concrete top-hinge depth and ensuring sufficient top reinforcement is provided. The sudden reduction in the neutral axis depth and top reinforcement strain at a rotation of 0.037 radians in Figure 6-7b represents crushing failure of the concrete, and is the consequence of assuming an unconfined concrete constitutive relationship.

6.2.3 Sensitivity to Concrete Strain Length & Monolithic Beam Analogy

In Section 6.1.2, two methods for estimating the concrete strain were proposed. The first method estimated the concrete strain by dividing the computed deformation by a concrete strain length, L_{pc}', assumed reasonably to be between $2/3L_{sp}'$ and $4/3L_{sp}'$. The second method estimated concrete strain via a monolithic beam analogy. Figure 6-8 shows the moment-rotation response for the two benchmark sections for a range of assumed concrete strain lengths and also for when the monolithic beam analogy was adopted.

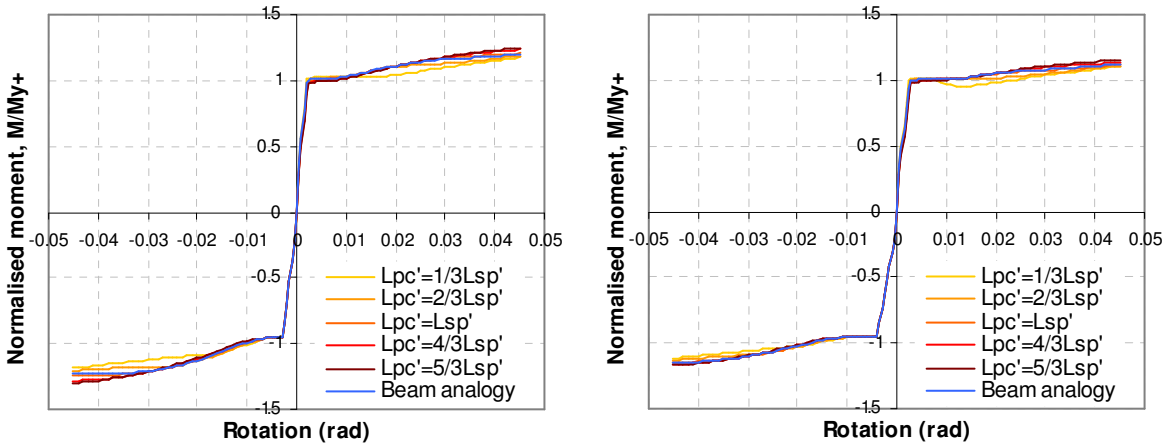

(a) Section SB1 **(b) Full-scale prototype section**

Figure 6-8: Sensitivity study – Concrete strain length and monolithic beam analogy

The figure shows that the elastic and early post-yield response is very insensitive to the assumed concrete strain length. This is because the neutral axis remains within the concrete top-hinge, such that concrete forces have a small lever arm. Effects of the parameter only come into play at higher drifts where concrete crushing can occur. For low strain lengths, concrete strains are higher so early degradation in the response is observed from concrete crushing. Interestingly, the response adopting the monolithic beam analogy lies within the response lines assuming strain penetration lengths of $2/3L_{sp}$' and $4/3L_{sp}$'. In Section 6.3, it is shown that both methods give good agreement with experimental results, and for the purposes of predicting the moment-rotation response, both methods are verified.

6.2.4 Sensitivity to Level of Concrete Confinement

Although the concrete top-hinge is not confined by any transverse steel, because of its very small length-to-depth ratio, some confinement will be provided by the adjacent column and beam concrete. Figure 6-9 shows the effect of assuming different levels of confinement in the concrete top-hinge for both beam sections. f'_c is the peak unconfined concrete compressive strength and f'_{cc} is the peak confined concrete compressive strength. The ratio f'_{cc}/f'_c then represents the level of concrete confinement.

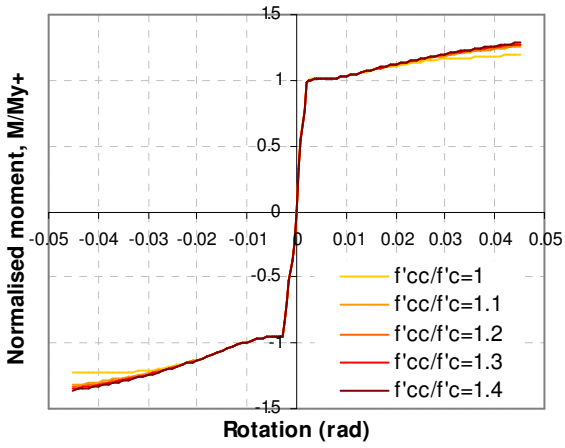

(a) M-θ response of Section SB1

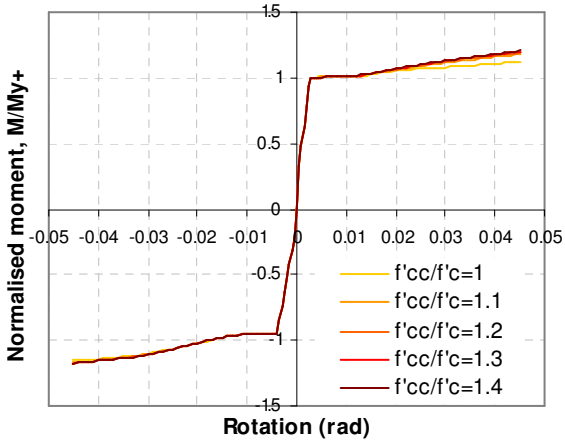

(b) M-θ response of full-scale prototype

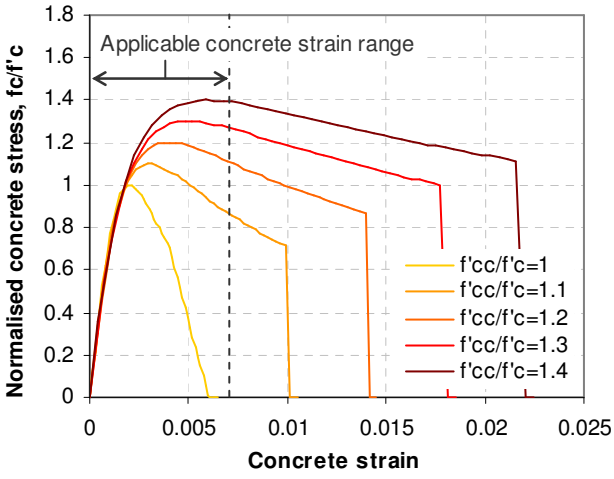

(c) Concrete constitutive stress-strain relationship

Figure 6-9: Sensitivity study – Level of concrete confinement

Both Figures a and b show a small increase in moment capacity at higher rotations when a low level of confinement of f'_{cc}/f'_c=1.1 is assumed, but no significant change is observed with additional levels of confinement. This is because the applicable concrete strain range is less than 0.007. Within this range, there is little difference between the concrete stress-strain curves with f'_{cc}/f'_c values greater than 1.1; a significant difference is apparent when compared to the curve with zero confinement as shown in Figure 6-9c. Due to uncertainty in determining the actual level of confinement, it is recommended that zero confinement be conservatively assumed. Due to the relative insensitivity to the level of confinement chosen, this assumption still gives good correlation with experimental results.

6.2.5 Parametric Study of Unbonded Length

To improve the low cycle fatigue resistance of the slotted-beam, a length of the bottom longitudinal reinforcement is unbonded. Figure 6-10 shows the normalised moment-rotation response for the two benchmark sections, for different unbonded lengths, L_{ub}, expressed as a proportion of the distance between the top and bottom longitudinal reinforcement, (*d-d'*). By increasing the unbonded length, bottom reinforcement strains are reduced and hence the slight reduction in moment capacity, initial stiffness and strain hardening. Maximum realistic unbonded lengths that can be achieve will range between 0.9(*d-d'*) and *d-d'* for a 45° diagonal hanger given geometry restrictions. Within this range, the moment-rotation response of the slotted-connection is relatively insensitive to the unbonded length. Analytically, altering the unbonded length has the same effect as altering the assumed strain penetration length (See Section 6.2.1).

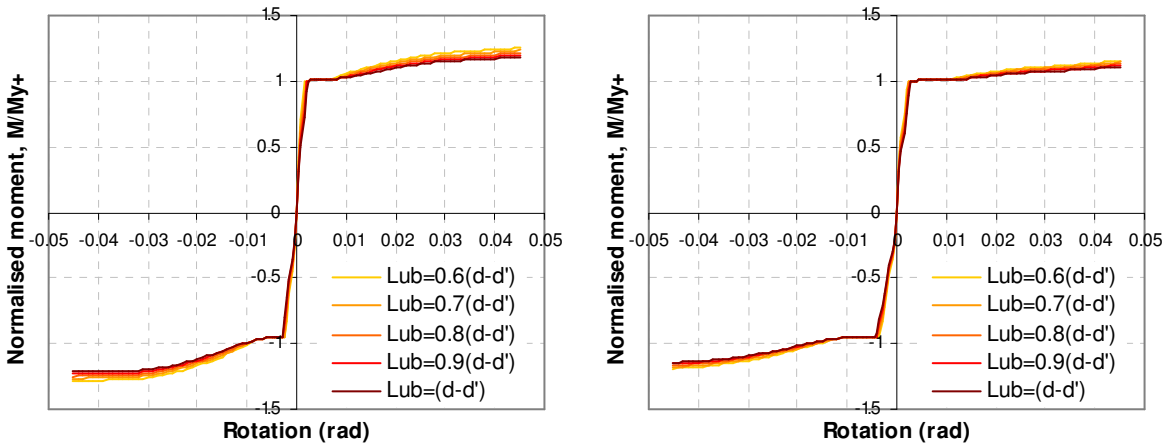

(a) M-θ response of Section SB1 **(b) M-θ response of full-scale prototype**

Figure 6-10: Parametric study – Unbonded length

6.2.6 Parametric Study of Concrete Top-hinge Depth

Figure 6-11 shows the results of a parametric study assessing the effect of altering the concrete top-hinge depth. Confinement levels corresponding to that within equivalent monolithic sections of f'_{cc}/f'_{c}=1.3 and 1.37 have been assumed for slotted sections SB1 and the full-scale prototype respectively. This is because as the top-hinge depth is increased, confinement from the adjacent beam and column will increase, which will tend toward that for a monolithic section. Because it has been shown that the response is relatively insensitive to high levels of confinement, for simplicity, confinement levels corresponding to the full monolithic section have been assumed.

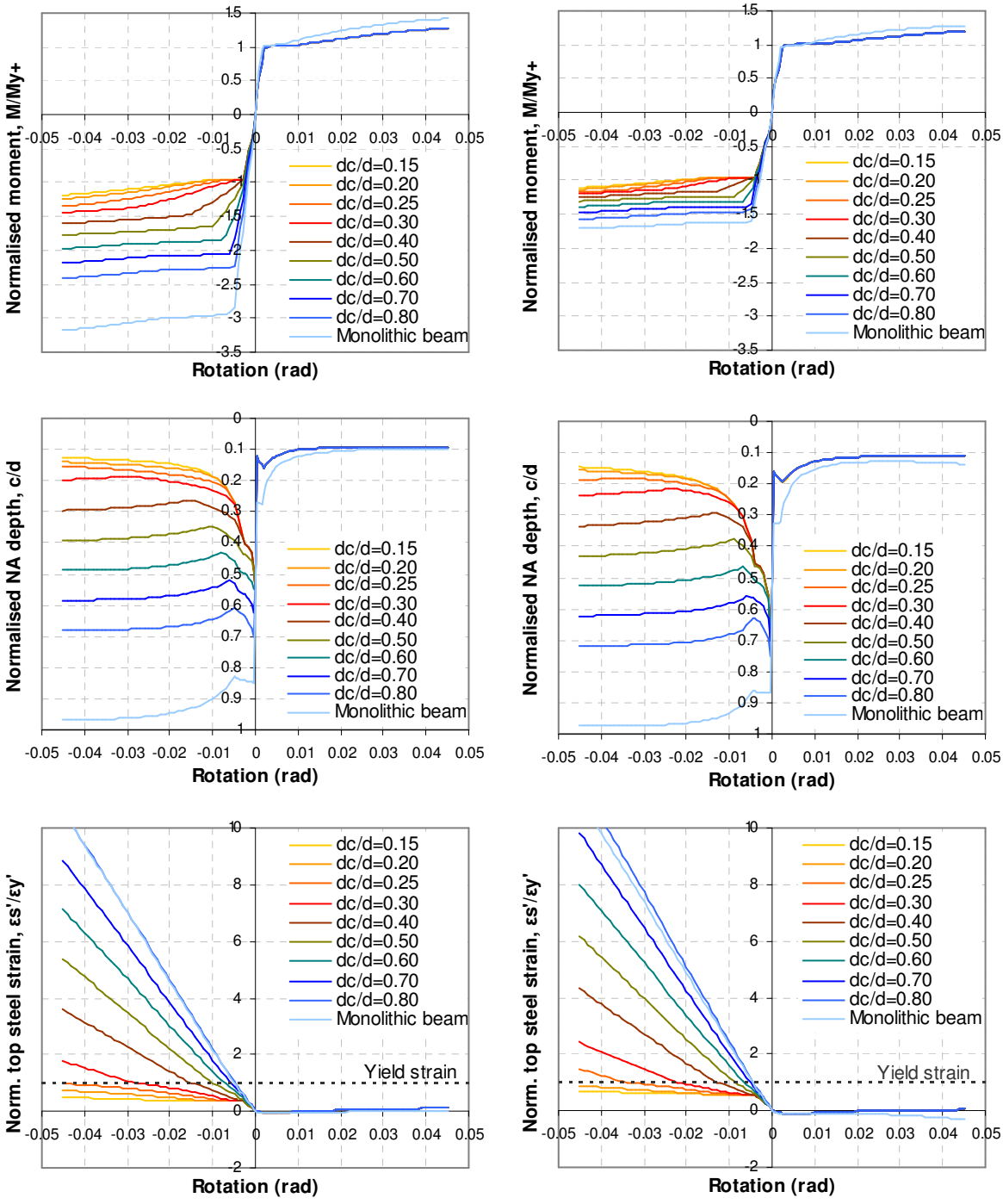

(a) Section SB1 (f'_{cc}/f'_c=1.3) **(b) Full-scale prototype section (f'_{cc}/f'_c=1.37)**

Figure 6-11: Parametric study – Concrete top-hinge depth

Figure 6-11 shows that as the top-hinge depth, d_c, is increased (and the slot depth is reduced), the moment-rotation and neutral axis response approaches that of an equivalently reinforced monolithic section. This is simply because the slotted-beam is becoming more like a monolithic section with the addition of an unbonded length. The negative moment capacity increases as the hinge depth is increased because top longitudinal reinforcement has a larger area and yield force compared to that of the bottom longitudinal reinforcement. So as the slot

is reduced, the response becomes governed by tensile yielding of top reinforcement rather than compression yielding of the bottom reinforcement. Because it has been assumed that concrete has zero tensile strength, it is understandable that increasing the concrete hinge depth has no effect on the positive (gap-opening) response of the section.

It is shown that increasing the top-hinge depth, d_c, increases top reinforcement tensile strains during negative (gap-closing) rotations; and when yielding occurs, strains continue to increase but at a faster rate. This is because as the hinge depth increases, the neutral axis drops, creating a prying effect which increases deformations at the top of the beam. Therefore, yielding of top reinforcement can be controlled by limiting the depth of the concrete top-hinge. For section SB1, top reinforcement yielding occurs when the hinge depth exceeds 0.25d; and for the full-scale prototype, yielding occurs when the hinge depth exceeds 0.20d. 0.20d and 0.25d represent the smallest concrete top-hinge depths that can be realistically achieved due to the concrete cover required to house the top reinforcement and diagonal shear hangers. Thus another method to limit top reinforcement yielding is required. This can be done by altering the ratio between top and bottom longitudinal reinforcement, which is studied next.

6.2.7 Parametric Study of Top-to-bottom Reinforcement Ratio

To limit yielding of top longitudinal reinforcement and concrete top-hinge deformations, top longitudinal reinforcement is designed to be larger than bottom longitudinal reinforcement. The top-to-bottom reinforcement ratio is herein defined as $A_s'f_y'/A_sf_y$.

Figure 6-12 shows the moment-rotation response and top longitudinal reinforcement strains for both benchmark specimens for different values of $A_s'f_y'/A_sf_y$. From all four graphs, it is shown that increasing the quantity of top reinforcement has negligible effect on the positive (gap-opening) response of the section. This is because compression of the concrete top-hinge and tensile yielding of the bottom longitudinal reinforcement govern the behaviour similar to a monolithic section.

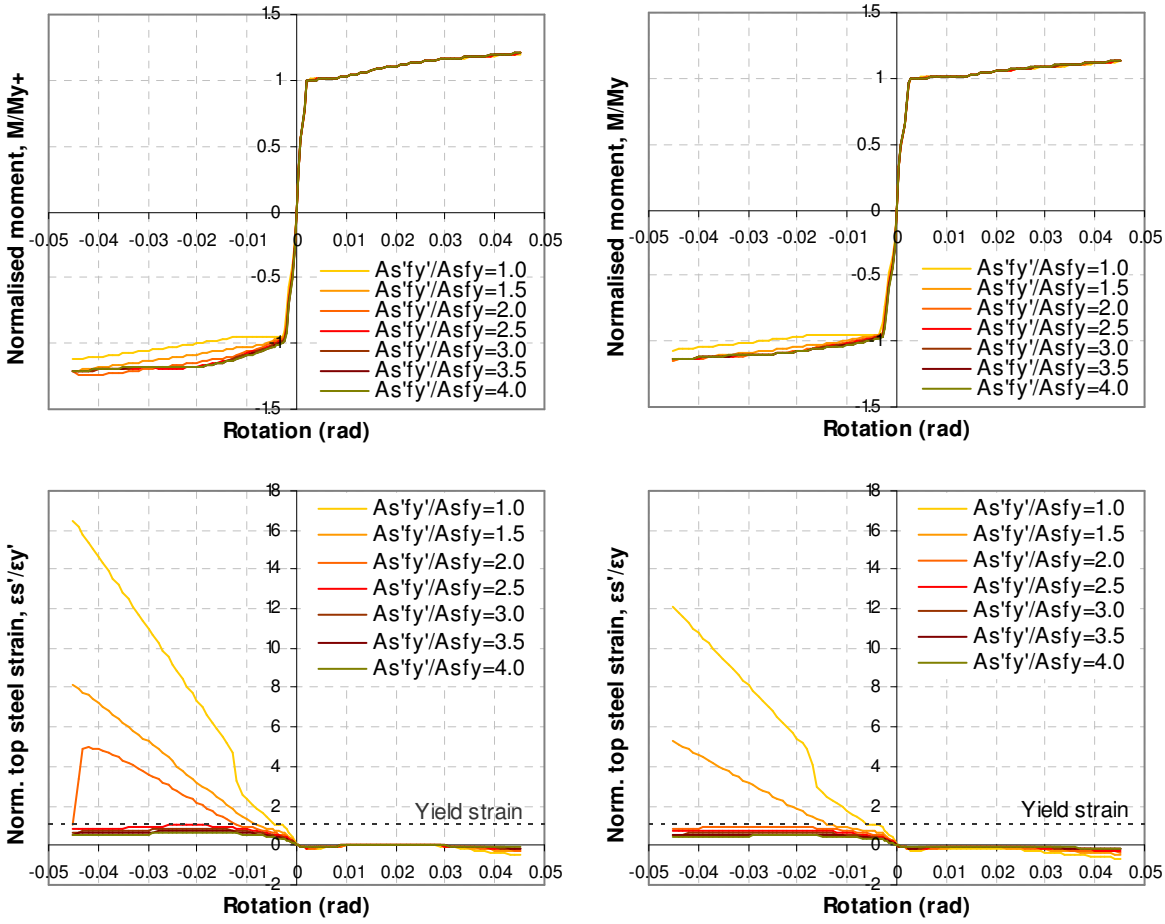

(a) Section SB1 **(b) Full-scale prototype section**

Figure 6-12: Parametric study – Top-to-bottom steel ratio

For negative (gap-closing) rotations, as $A_s'f_y'/A_sf_y$ is increased, the post-yield moment response increases. This is because increasing $A_s'f_y'/A_sf_y$ increases the tension component in the section. Because bottom reinforcement has yielded in compression, this increase in tension must be resisted by an increase in compression at the bottom of the concrete top-hinge. Although near the neutral axis, this increase in force is enough to increase the moment capacity slightly as shown. If there is too much top reinforcement, subsequent strength degradation occurs due to concrete crushing as observed for section SB1 beyond -0.025 radians when $A_s'f_y'/A_sf_y$ is greater than 3.0.

The top-to-bottom reinforcement ratio should be sufficient to limit yielding of top longitudinal reinforcement and deformations through the top-hinge. For top-to-bottom reinforcement ratios greater than 2.5, top reinforcement remains elastic for both sections. For $A_s'f_y'/A_sf_y$=2.0, strains remain elastic for the full-scale prototype and within six times the yield strain for section SB1. Therefore a ratio between 2.0 and 2.5 can be regarded as an

acceptable guide for design. The largest values of $A_s'f_y'/A_sf_y$ that can be realistically achieved are in the range of 1.5 to 2.5. This is best achieved by using Grade 300 steel for bottom reinforcement and Grade 500 steel for top reinforcement.

6.2.8 Effect of Cyclic Strain Hardening

Because the bottom longitudinal reinforcement in a slotted-beam is subject to extensive yielding in compression as well as in tension, slotted-connections will tend to exhibit significantly more post-yield hardening from cyclic straining. This is because the stress in cyclically loaded steel for a given strain can be higher than that given by the monotonic stress-strain response (Discussed in Section 6.1.1). Figure 6-13 compares the monotonic backbone curve to a pseudo-cyclic backbone curve for both benchmark specimens. For the pseudo-cyclic response, each section was subject to a sequence of three cycles of rotation at ±0.001, ±0.002, ±0.005, ±0.0075, ±0.01, ±0.015, ±0.02, ±0.025, ±0.035, and ±0.045 radians.

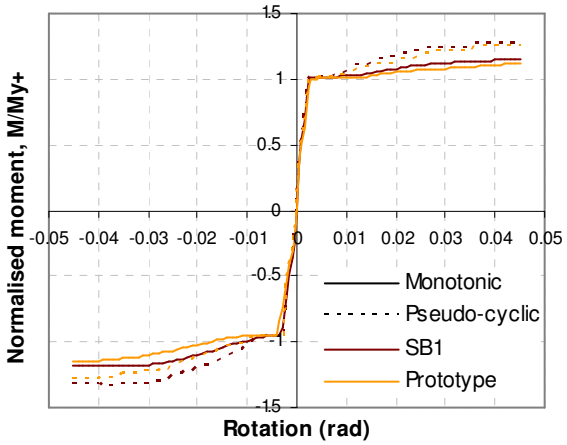

Figure 6-13: Monotonic versus pseudo-cyclic response

It is shown that there is significantly more post-yield hardening in the pseudo-cyclic response compared to the monotonic curve. Of course the extent of this additional hardening is very much dependent on the load history applied. For this particular cyclic drift sequence, there is a 10-15% increase in the post-yield moment capacity. Cyclic loading does not affect the elastic response of the connection, and this increase in strain hardening only occurs if there are both positive and negative strain excursions in bottom longitudinal reinforcement.

6.2.9 Effect of Diagonal Hanger Reinforcement on Flexural Response

Section 6.1.3 describes an approximate method for considering the flexural actions induced within diagonal shear reinforcement. Figure 6-14 shows the moment-rotation response of

both benchmark sections when different sized shear hangers are included and when flexural forces from the hanger are ignored. Both plots show that the inclusion of hanger flexural forces has little effect on the response of the connection. This is because the hanger is located within the concrete top-hinge, near the neutral axis, such that it has little influence on moment capacity. Thus for the purposes of predicting the moment-rotation response of a slotted-beam, flexural actions in the shear hanger can be ignored. Although this was not apparent from the moment-rotation procedure, experimental results did apparently show that hanger reinforcement did help to limit top longitudinal reinforcement strains and elongation through the top-hinge.

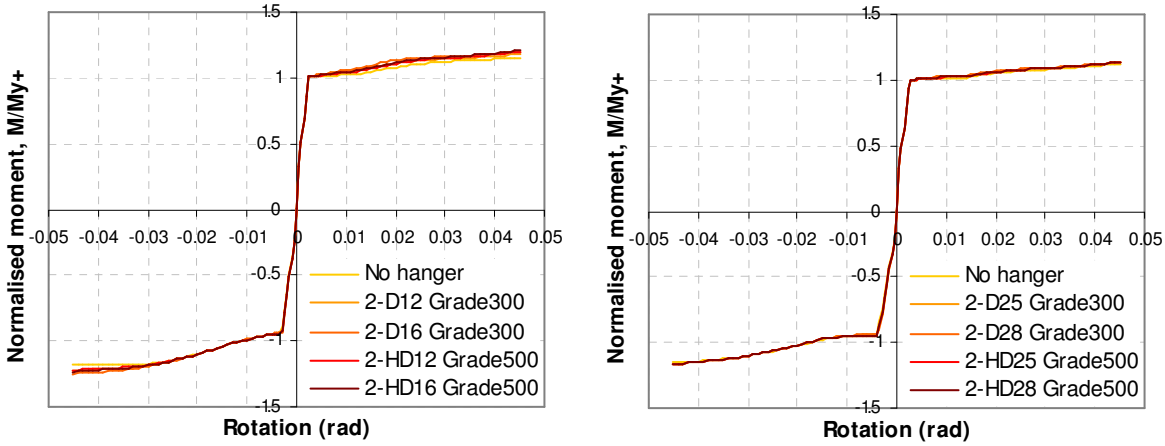

(a) Section SB1 **(b) Full-scale prototype section**

Figure 6-14: Parametric study – Effect of diagonal shear hanger on flexural response

6.2.10 Effect of Diagonal Hanger Reinforcement depth on Strains

Figure 6-15 plots the hanger strains for both benchmark sections when the hanger is located at different depths between 0.4 and 0.8 times the concrete top-hinge depth, d_c, measured from the top surface of the concrete hinge. Here SB1 has been given 2-D12 hangers and the full-scale prototype 2-D32 hangers. It can be seen that the depth of the hanger does influence flexural strains within the hanger, and if yielding is to be minimised, it is important to locate the hangers as close as possible to the neutral axis. To minimise strains for both positive and negative rotations, Figure 6-15 shows a hanger depth between $0.5d_c$ and $0.6d_c$ to be the most optimum. However, it must be remembered that this moment-rotation procedure ignores shear actions. For positive rotations, an upwards shear will induce negative axial strains in the hanger; while for negative rotations, a downwards shear will induce positive axial strains.

This suggests that a depth greater than $0.6d_c$ from the top surface of the concrete top-hinge may be more appropriate.

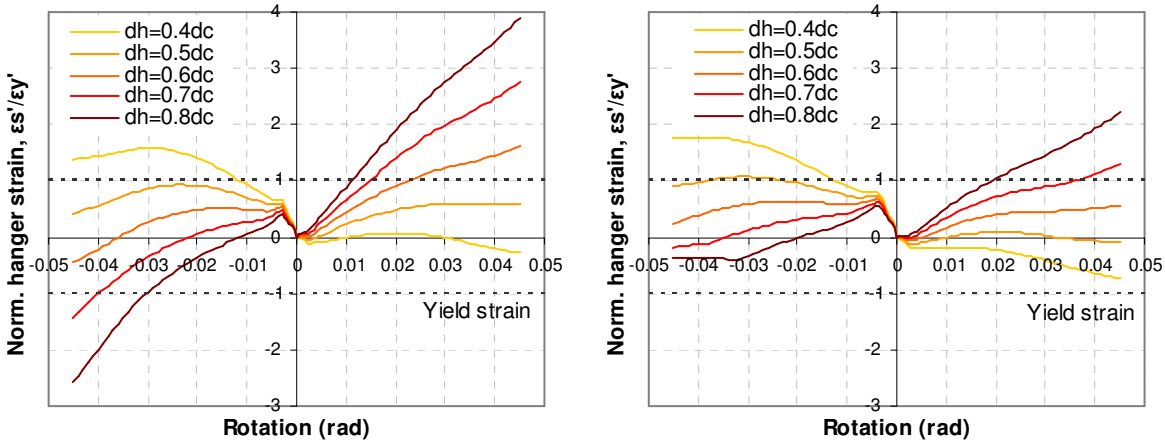

(a) Section SB1 **(b) Full-scale prototype section**

Figure 6-15: Parametric study – Effect of hanger depth on hanger strains

From Figure 6-11, when the concrete top-hinge depth, d_c, is between $0.2d$ and $0.25d$, the neutral axis depth, c (measured from the top of the beam), remains predominantly around $0.1d$ for gap-opening rotations and $0.2d$ for gap-closing rotations. d is the depth to bottom longitudinal reinforcement measured from the top of the beam. This equates to an average neutral axis depth between $0.6d_c$ and $0.75d_c$ when expressed as a proportion of the top-hinge depth, d_c. Therefore to minimise strains within diagonal hanger reinforcement, theoretically hangers should be located at approximately these depths.

Tested specimens SB1, SB2 and SB3 had hanger depths, d_h, of $0.56d_c$, $0.73d_c$ and $0.71d_c$ respectively. The hanger in specimen SB1 was found to have large tensile strains during gap-closing rotations suggesting the hanger was located too high. The hangers in specimens SB2 and SB3 showed a much more even distribution of hanger strains between gap-opening and gap-closing. Therefore hanger depths between $0.7d_c$ and $0.75d_c$ appear to be the most optimum from theory and experimental testing.

6.2.11 Effect of Effective Slab Width Contributions

If there is a floor slab built integrally into the slotted-beam, then slab concrete and reinforcement may influence the response of the connection. Figure 6-16 illustrates the effect of including increasing slab widths to the strength of the slotted section. The effective slab width, b_f, has been expressed as a multiple of the beam effective depth, d, and is measured

from the side of the beam to the edge of the effective flange. For both sections, a slab depth equal to the depth of the top-hinge was assumed. A common slab mesh arrangement was assumed, namely 8 mm diameter Grade 500 deformed bars (HD8) at 200 mm centres for the 2/3-scale section SB1 and 12 mm diameter Grade 500 deformed bars (HD12) at 300 mm centres for the full-scale prototype.

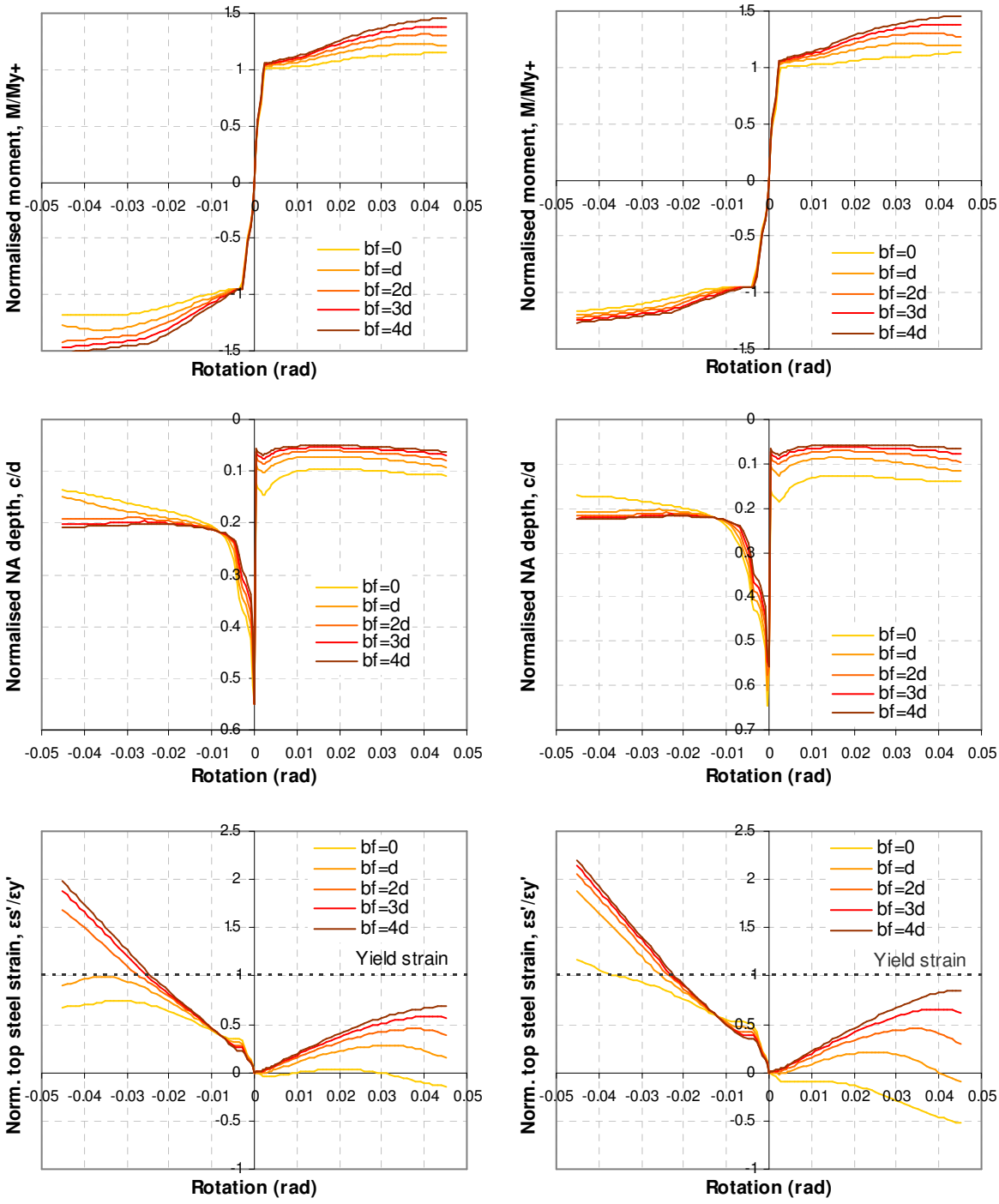

(a) Section SB1 **(b) Full-scale prototype section**

Figure 6-16: Parametric study – Effect of including slab flexural contributions

The moment-rotation plots in Figure 6-16 show the inclusion of an effective slab width only has a minor effect on the positive yield moment. A 2% increase is observed when an effective flange width of d is assumed; and a maximum increase of 5% is observed when the effective width is increased to $4d$. The effective slab width has no effect on the negative yield moment. Because the strength of the connection is governed by yielding of bottom longitudinal reinforcement, it is reasonable to omit effective slab width contributions from the calculation of the nominal moment capacity, M_n.

A greater effect is observed in the post-yield strain hardening response. At a positive rotation of 0.0035 radians, a 9% increase in the moment is observed when $b_f = d$, and a 23% increase is observed when $b_f = 4d$.

The inclusion of an integrated slab also has an influence on the deformations within the concrete top-hinge. As the slab width considered is increased, there is an increase in the concrete compressive force, such that neutral axis must shift to maintain horizontal equilibrium. As shown by the normalised neutral axis plots in Figure 6-16, during positive (gap-opening) rotations the neutral axis shifts upwards, and for negative (gap-closing) rotations it shifts downwards. This induces a prying effect, which increases deformations in the top-hinge and damage to the floor slab.

The effect of the floor slab is very much dependent on the effective width that must be considered. Recorded floor deformations in specimen SB3 revealed an effective slab width on the order of 1 to 1.5 times the effective beam depth should be expected. However because the effective flange activated is also dependent on the torsional stiffness of any transverse beam or slab framing into the column, determination of this width is not that simple and has been regarded as outside the scope of this research project.

6.3 Comparison of Moment-rotation Procedure with Experimental Results

This section compares the proposed moment-rotation procedure described in Section 6.1 with the observed response from experimental tests. Lateral force verse drift backbone curves were derived using the procedure, assuming elastic beam and column deformations from equations given in Section A.6.

6.3.1 Lateral Force versus Drift

Figure 6-17 compares theoretical lateral force versus drift backbone curves with the observed cyclic response for specimen SB1. The dashed line is the theoretical curve adopting a monotonic steel stress-strain relationship. Whilst the elastic portion of the monotonic response showed good agreement, it can be seen that neglecting the cyclic response of bottom longitudinal reinforcement greatly underestimates the post-yield hardening. The experimental post-yield response is the result of greater strain hardening in bottom reinforcement as it undergoes extensive plastic straining in tension as well as in compression.

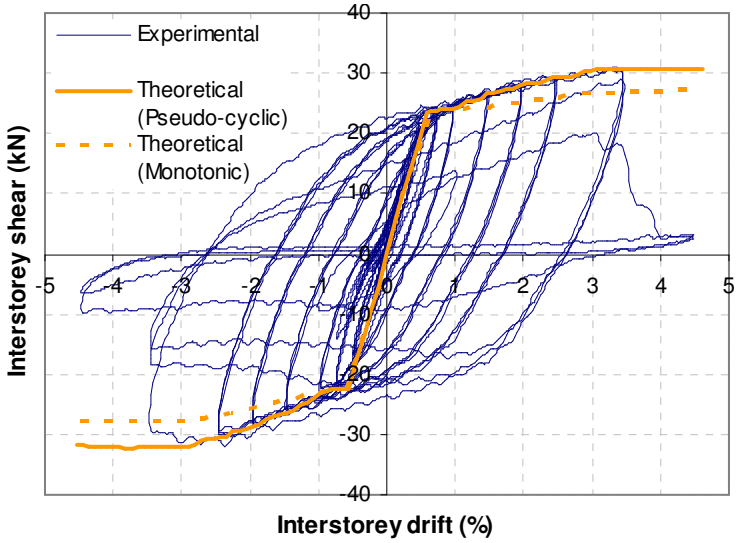

(a) Overall response

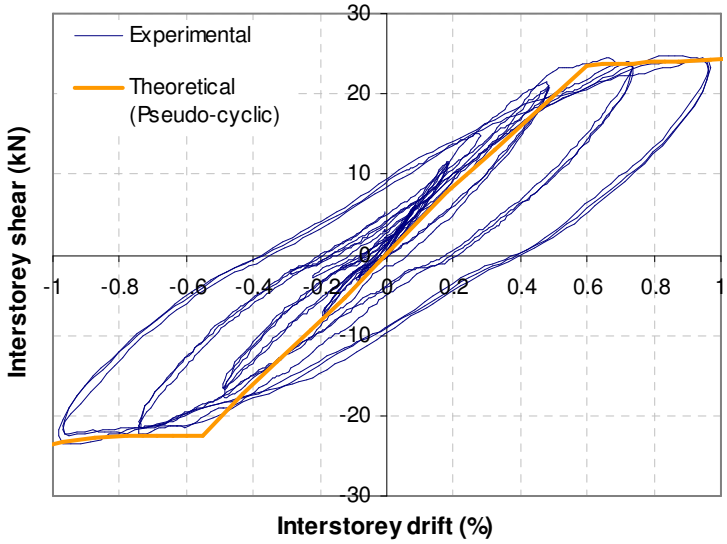

(b) Close up of elastic cycles

Figure 6-17: Comparison of theoretical backbone predictions with experimental results of specimen SB1

The solid yellow line is the theoretical curve utilising the pseudo-cyclic steel stress-strain relationship described in Section 6.1.1. Experimental strain gauge data revealed a reduced strain penetration length in the bottom longitudinal reinforcement of L_{sp}=0.011$f_y d_b$, instead of 0.022$f_y d_b$, and was modified accordingly in the theoretical prediction. It is shown in Figure 6-17a that the moment-rotation procedure provides a very accurate prediction of the cyclic backbone response, until buckling occurred in the test specimen at 3.5% drift. Figure 6-17b provides a close up of the smaller elastic cycles, and shows satisfactory predictions of the elastic stiffness and yield force at 24 kN and -23 kN respectively.

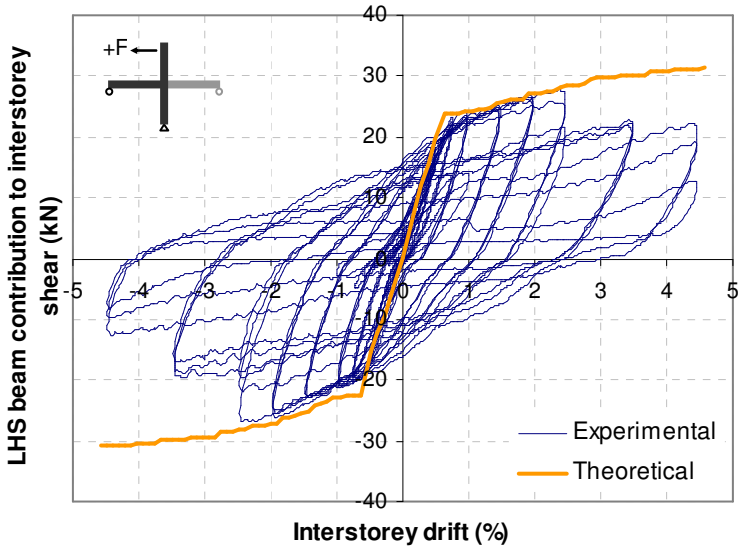

(a) Left-hand-side beam

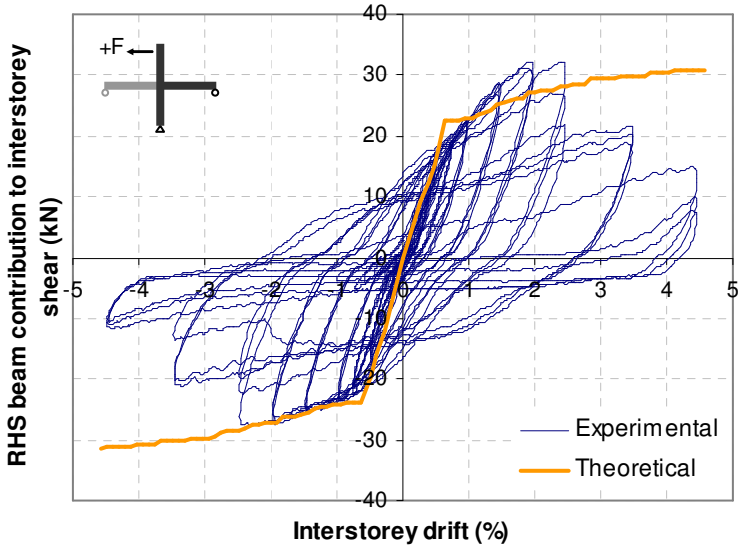

(b) Right-hand-side beam

Figure 6-18: Comparison of theoretical backbone predictions with experimental results of Specimen SB2

Figure 6-18 compares theoretical backbone predictions with the cyclic response of both beams in specimen SB2. The match between experimental and theoretical lines is not as close as with specimen SB1, although a reasonable correlation still exists up until 2.5% drift when bond-slip failure occurred. The moment-rotation procedure gives a good prediction of the elastic stiffness; however it overestimates the gap-closing yield force in both beams. Figure 6-18b shows an unusual increase in post-yield strength after 1.0% positive drift. The author is not fully aware of the cause of this, but this could be the result of grout in the steel de-bonding tube acting in compression, thus localising compressive strains in the length of bar crossing the slot. The discrepancy between theory and experimental results could be from a number of reasons; namely, variations in steel and concrete properties, bond-slip altering the behaviour of the specimen, incorrect assumptions made in estimating elastic beam and column deformations, and the omission shear-flexure interaction in the concrete top-hinge in the moment-rotation procedure.

6.3.2 Neutral Axis Depth

Figure 6-19 compares the neutral axis depth calculated using the moment-rotation procedure to that observed during the tests of specimen SB1 and SB2. Here, the neutral axis depth is measured from the top of the concrete-hinge. For both specimens, the theoretical procedure gives a reasonable prediction of the actual neutral axis for gap-opening rotations – that is, positive drifts for specimen SB1 and the LHS beam of SB2, and negative drifts for the RHS beam of SB2. This is most likely because the monolithic beam analogy used to estimate the concrete strain is most applicable for gap-opening rotations. In addition, the assumption of zero concrete confinement is consistent with the little confinement that would be provided to top-fibre cover concrete.

For gap-closing rotations, there is less correlation between actual data and theory. This is probably because the monolithic beam analogy and assumptions of zero confinement are less applicable for gap-closing behaviour. Concrete in compression on the underside of the top-hinge does not behave like that in a monolithic beam, and additional confinement would be expected from the adjacent column face and beam concrete. Furthermore, during gap-closing rotations, shear is carried across the slot by the diagonal reinforcement. This would create a highly disturbed region of stresses in the top-hinge, including shear-flexure interaction which is not considered in this simple moment-rotation analysis. Note that the large discrepancy at drifts below 1.0% is most likely due to the omission of the concrete tensile strength in the

simplified theoretical procedure, and inaccuracies in the experimental results which arises due to the relatively small magnitude of deformations taking place at low drifts.

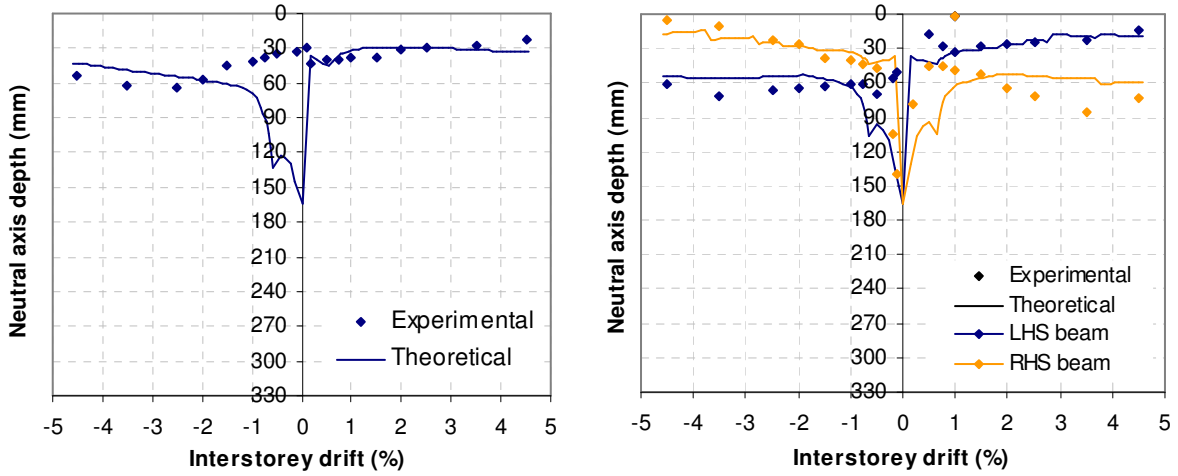

(a) Specimen SB1 **(b) Specimen SB2**

Figure 6-19: Comparison of theoretical and experimental neutral axis depths

Despite the difference between the predicted and experimentally observed neutral axis depths, it was shown earlier that the theory still gave a good prediction of the lateral force versus drift response. This is because the moment capacity of a slotted section is governed by the force in bottom longitudinal reinforcement, and is relatively insensitive to the exact location of the neutral axis depth. Horizontal equilibrium in the section, however, is very sensitive to the location of the neutral axis depth. Therefore, the actual neutral axis depth cannot be accurately predicted unless forces in the section can be accurately calculated. This is limited to the accuracy of strain predictions and constitutive stress-strain relationships assumed.

6.3.3 Concrete and Steel Deformations

Figure 6-20 compares theoretical and experimentally measured concrete and steel deformations for Specimens SB1 and SB2. Here the concrete deformation is the compressive deformation at the top of the top-hinge during gap-opening and at the bottom of the top-hinge during gap-closing. Experimental component deformations were measured by linear potentiometers crossing the width of the slot. For all beams there is fairly good correlation between theoretical and experimental deformations. All predicted deformations are within 2 mm of observed values. The slight difference which does exist is most likely the result of the inaccurately predicted neutral axis depth which was discussed in the previous section.

However, given that the procedure is a simple analytical tool which can be implemented with a spreadsheet, the experimental tests provide good validation of the proposed procedure.

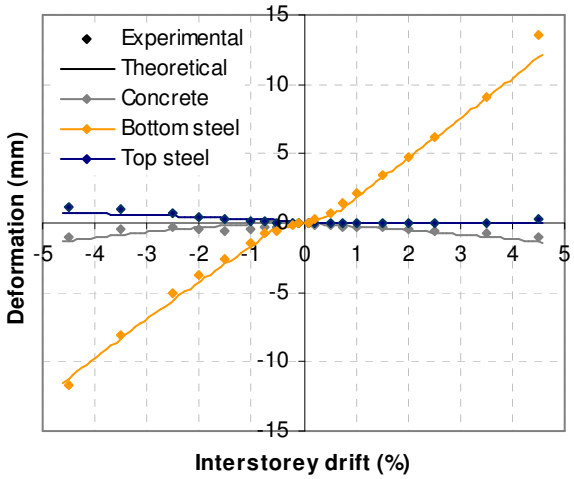

(a) Specimen SB1

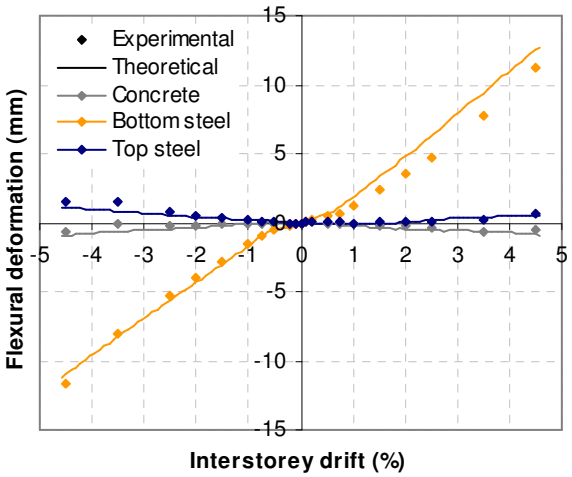

(b) Specimen SB2, LHS beam

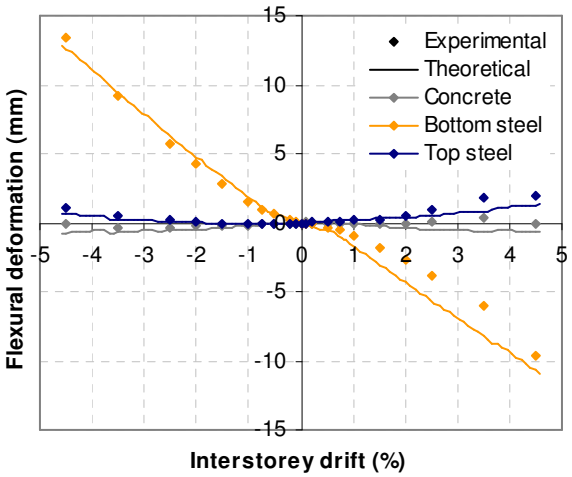

(c) Specimen SB2, RHS beam

Figure 6-20: Comparison of theoretical and experimental material component axial deformations

CHAPTER 7 NUMERICAL MODELLING AND INVESTIGATION OF FRAME RESPONSE

This chapter outlines numerical investigations carried out on slotted-beam connections. Two models were developed to represent the response of the slotted-connection. The first was a multi-spring model which modelled individual material deformations via a series of axial springs, and the second was a simplified lumped plasticity model which simply replicated the global response of the connection. The multi-spring model was based upon the plastic hinge element for conventional reinforced concrete beams that was developed by Peng (2009).

The two slotted-connection models were verified with experimental test results, and later, the multi-spring model was used in the analysis of a five-storey, three-bay frame. To allow a comparison of the frame response using slotted-connections with that using traditional monolithic connections a second reinforced concrete frame was setup using Peng's plastic hinge element. This element was used to include effects of beam elongation, as oppose to traditional frame elements with Takeda hysteresis loops which do not account for beam elongation.

Numerical analyses were carried out using Ruaumoko2D, a programme developed at the University of Canterbury by Carr (2005). For simplicity, two-dimensional analyses were carried out rather than three-dimensional studies.

7.1 Numerical Models of Frame Connections

7.1.1 Multi-spring Plastic Hinge Element for RC Beams (Peng, 2009)

Figure 7-1 shows a schematic of the multi-spring plastic hinge element developed by Peng (2009). The element was developed to model the effects beam elongation in traditional reinforced concrete beams. It consists of ten axial concrete springs and two longitudinal steel springs to represent the flexural response of the plastic hinge, and two diagonal concrete springs to represent the shear-strut behaviour in the web. To model cyclic material behaviour, it adopts the cracked concrete hysteresis given in Maekawa, Pimanmas and Okamura (2003) for the concrete springs, and the steel hysteresis rule from Dhakal and Maekawa (2002) without buckling for the steel springs.

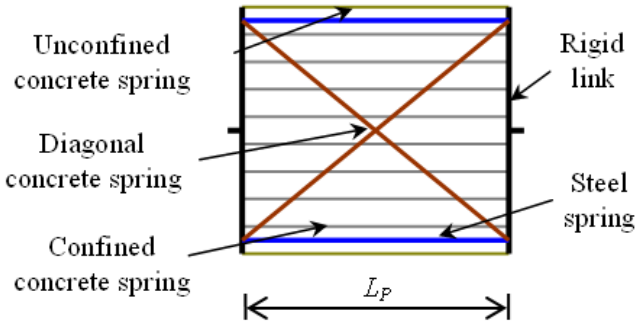

Figure 7-1: Schematic of multi-spring plastic hinge element (Peng, 2009)

Two parameters which govern the response of the element are the plastic hinge length, L_p, and the effective length of the steel springs, L_{yield}. Peng suggests that L_p be taken as the length required to include sufficient stirrups to resist the shear force at flexural yield. It can be calculated according to Equation 7-1, where V_{yc} is the beam shear at flexural yield, A_v is the area of transverse steel at a spacing s, and f_{vy} is the stirrup yield strength. L_{yield} should be taken as the length over which the reinforcement yields, which Peng proposes can be calculated as in Equation 7-2. L_{cant} is the cantilevered span of the beam, L_{sp} is the length of strain penetration, M_{max} is the maximum beam moment expected, M_y is the beam yield moment, and *d-d'* is the distance between top and bottom longitudinal reinforcement. For conventional reinforced concrete beams, a M_{max}/M_y ratio on the order of 1.2 can be expected and was assumed. For this project, the strain penetration length, L_{sp}, was taken as $0.022 f_y d_b$ (Paulay and Priestley, 1992).

$$L_p = \frac{V_{yc} s}{A_v f_{vy}} \qquad \text{...(7-1)}$$

$$L_{yield} = \frac{M_{\max} - M_y}{M_{\max}} L_{cant} + \frac{d - d'}{2} + L_{sp} \qquad \text{...(7-2)}$$

The compressive strength of the diagonal struts should be taken as $0.34 f'_c$ and their effective width, D, taken as in Equation 7-3, where θ_{strut} is the inclination of the diagonal struts from horizontal. Other default values for hysteretic parameters are given in Peng (2009), and were adopted for this project.

$$D = L_p \sin \theta_{strut} \qquad \text{...(7-3)}$$

7.1.2 Multi-spring Model for Slotted-beams

Figure 7-2 shows a schematic of the multi-spring model that was developed for slotted-beam connections. Like the previously described plastic hinge element developed by Peng (2009), axial springs were used to represent the concrete and longitudinal reinforcement. Nodes were located based on the geometry of the slotted-beam as shown superimposed upon the physical slotted-connection. Longitudinal reinforcement springs were given a Dodd-Restrepo cyclic steel hysteresis (1995) to allow Baushinger effect and effects of cyclic strain hardening to be modelled. To accurately model cyclic unloading and reloading branches, the Dodd-Restrepo model parameter *OmegaF*, which accounts for Baushinger effect, was taken between 0.9 and 1.0.

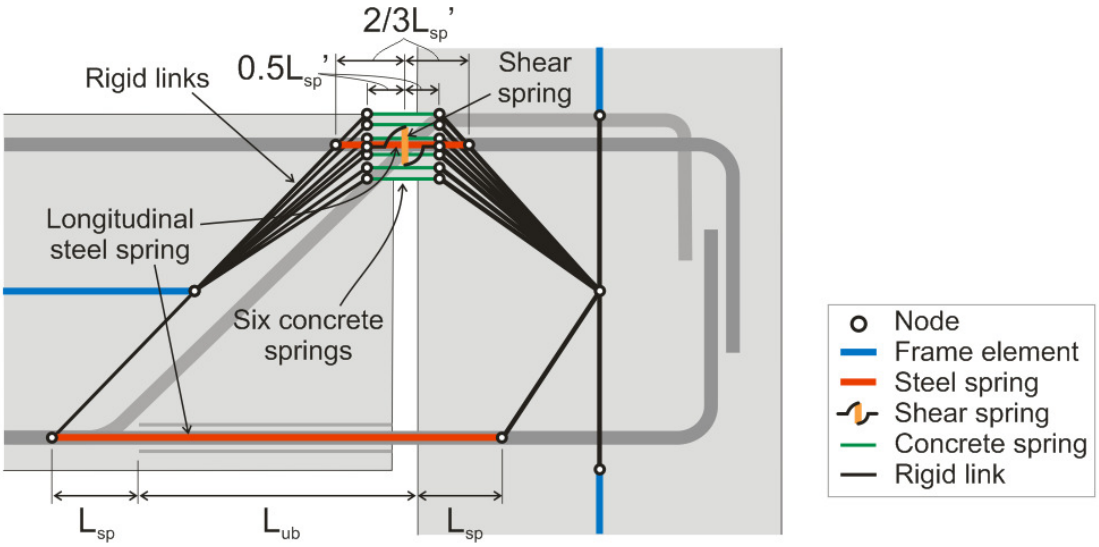

Figure 7-2: Multi-spring model for slotted reinforced concrete beam connections

The concrete top-hinge was represented using six springs distributed on the basis of Lobatto integration as carried out by Spieth, Carr, Pampanin, Murahidy and Mander (2004). This was to model the reality of greater local stiffness at the centre of the section and decreasing stiffness towards the edges. Table 7-1 shows the weighting and position from the centre of the top-hinge for each spring. To determine the position of a spring, multiply the tabulated value by half the height of the concrete top-hinge. Similarly, to get the individual spring stiffness or strength, multiply the tabulated weighting by half the total concrete top-hinge stiffness or strength respectively. Lobatto integration was used as oppose to Gauss Quadrature to allow springs to be placed at the edges of the concrete section. Spieth et al. found a minimum of six springs was required to give similar results to that given by Gauss

Quadrature. To model the cyclic concrete behaviour, the cracked concrete hysteresis given in Maekawa, Pimanmas and Okamura (2003) was adopted.

Table 7-1: Concrete spring position and weighting from Lobatto integration (Spieth et al., 2004)

Spring number, i	Position, ± y_i	Weighting, w_i
1, 6	± 1.0	0.06666667
2, 5	± 0.76505532	0.37847496
3, 4	± 0.28523152	0.55485838

For simplicity, the shear response of the slotted-section was represented by a single vertical shear spring, which had a stiffness equal to the vertical component of the diagonal reinforcement stiffness. It was assumed the concrete did not carry any shear, which is reasonable given that the concrete section is small. The diagonal inclination of hanger reinforcement was also ignored, because it would have little influence on the flexural response being located close to the neutral axis (See Section 6.2.9). These simplifying assumptions avoided the problem of determining appropriate node locations for diagonal springs, which are not clearly defined from the connection geometry.

To verify the above simplifying assumptions for shear, an alternative model shown in Figure 7-3 was investigated. This model had diagonal springs to represent shear in the concrete top-hinge and diagonal steel hangers. The use of diagonal struts to represent concrete shear comes from a similar strut-and-tie analogy used in the plastic hinge element developed by Peng (2009). It was found that the inclusion of these diagonal springs had little effect on the results.

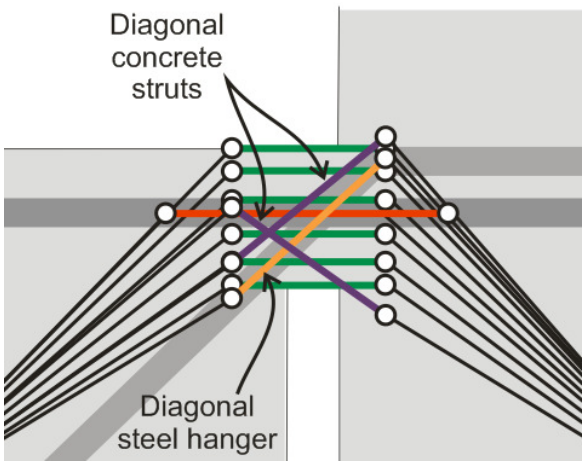

Figure 7-3: Alternative model with diagonal springs in the top-hinge for shear

Axial spring stiffness was calculated using AE/L – the cross-sectional area multiplied by the elastic modulus and divided by a length. The length, L, adopted for each component is summarised in Table 7-2. These values were based on strain lengths verified by strain gauge data from the experimental tests carried out. L_{ub} is the unbonded length of bottom longitudinal reinforcement, and L_{sp} is the strain penetration length which can be taken as $0.022 f_y d_b$ (Paulay and Priestley, 1992). f_y and d_b and the yield force (in MPa) and diameter (in mm) of the reinforcement considered respectively. The apostrophe (‘) with L_{sp} is used to indicate that f_y and d_b for top longitudinal reinforcement should be used when calculating L_{sp}’. Similarly, the subscript h with L_{sp} indicates that f_y and d_b for diagonal shear reinforcement should be used when calculating L_{sph}.

Table 7-2: Lengths, *L*, used to calculate spring stiffness, *AE/L*

Spring component	Length, *L*
Concrete top-hinge	L_{sp}’
Top longitudinal reinforcement	$4/3L_{sp}$’
Bottom longitudinal reinforcement	$L_{ub}+2L_{sp}$
Diagonal shear reinforcement	$2L_{sph}$

Due to numerous springs framing into single nodes, numerical simulations with multi-spring elements require very small time steps and/or displacement steps. As a result they tend to be computationally demanding and relatively time-consuming. For this particular multi-spring model in Ruaumoko2D, there was occasional instability with the Dodd-Restrepo hysteresis rule. It was not discovered why this occurred, but the instability could usually be resolved by increasing the stiffness of the vertical shear spring, using large displacement theory, or increasing the time-step and enabling Newton-Raphson iterations.

Despite the additional effort in setting up these multi-spring models, the advantage is that they can model the beam elongation response and provide information on steel and concrete deformations. In addition, because information on constitutive relationships for individual material components is readily available, little hysteresis calibration is required.

7.1.3 Simplified Lumped Plasticity Model for Slotted-beams

To provide a simpler alternative to the multi-spring model, Figure 7-4 illustrates a lumped plasticity model which represents the slotted-connection with a single, nonlinear rotational spring. Because the flexural response of a slotted beam is governed by tension-compression yielding of bottom longitudinal reinforcement, the cyclic behaviour of the connection can be

modelled by giving the rotational spring a steel hysteresis rule. This model ignores beam elongation, but because slotted-beams exhibit negligible beam elongation, this may be of little consequence. This model does not require small time-steps like the multi-spring model, and so is ideal for analyses of frames where only the global response of the connection is required.

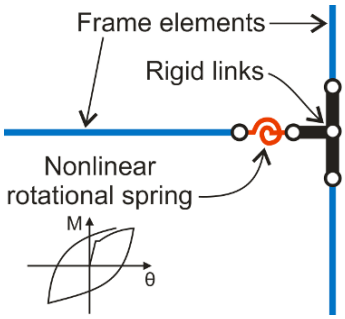

Figure 7-4: Lumped plasticity model for slotted-connections

Dodd-Restrepo (1995) and Bounded Ramberg-Osgood (1943) steel hysteresis rules were adopted in this project. Backbone parameters for the Dodd-Restrepo rule were determined from monotonic moment-rotation backbone curves, which were derived using the analytical procedure in CHAPTER 6. It was found that values for the Baushinger effect parameter, *OmegaF*, between 0.8 and 1.0 gave reasonable correlation with experimental results. To give reasonable correlation with experimental data, the Ramberg-Osgood hysteresis rule had to be calibrated with results via trial-and-error.

7.2 Verification of Models with Experimental Results

To allow frame connection models to be verified against experimental results, models of tested specimens RCB1 and SB1 were setup. Because of bond-slip failure in specimen SB2 and the addition of floor units in SB3, these specimens did not provide ideal data for comparison. Figure 7-5 shows schematics of the models set up. Beams were modelled using elastic Giberson beam elements, and columns were modelled using concrete beam-column elements. The same displacement protocol applied to test specimens, which was described in Section 4.2.2, was applied to the models. A maximum lateral displacement step of 0.01 mm at the top of the column was adopted in multi-spring analyses. Further reductions beyond this yielded no appreciable change in results.

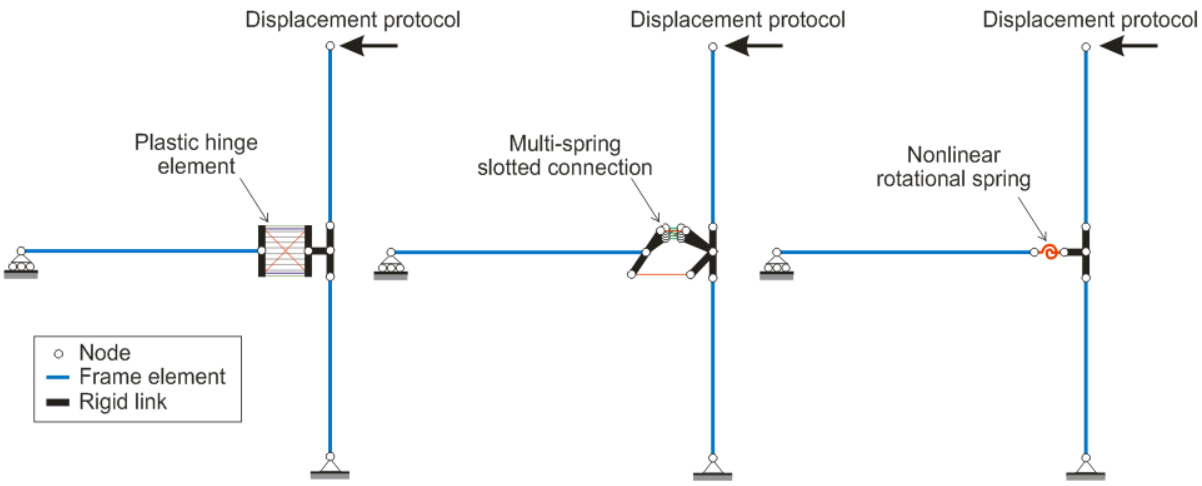

(a) Model of RCB1 **(b) Multi-spring model of SB1** **(c) Lumped plasticity model of SB1**

Figure 7-5: Joint subassembly models

To briefly illustrate the results from Peng's plastic hinge element, Figure 7-6 compares the response of the analytical model with the experimental response of specimen RCB1. It shows that the element is capable of accurately modelling the global force-drift response of the subassembly, as well as the beam elongation response. The spike in the force-drift response near yield is a result of the sudden change in stiffness at yield. This unresolved anomaly was also encountered by Peng.

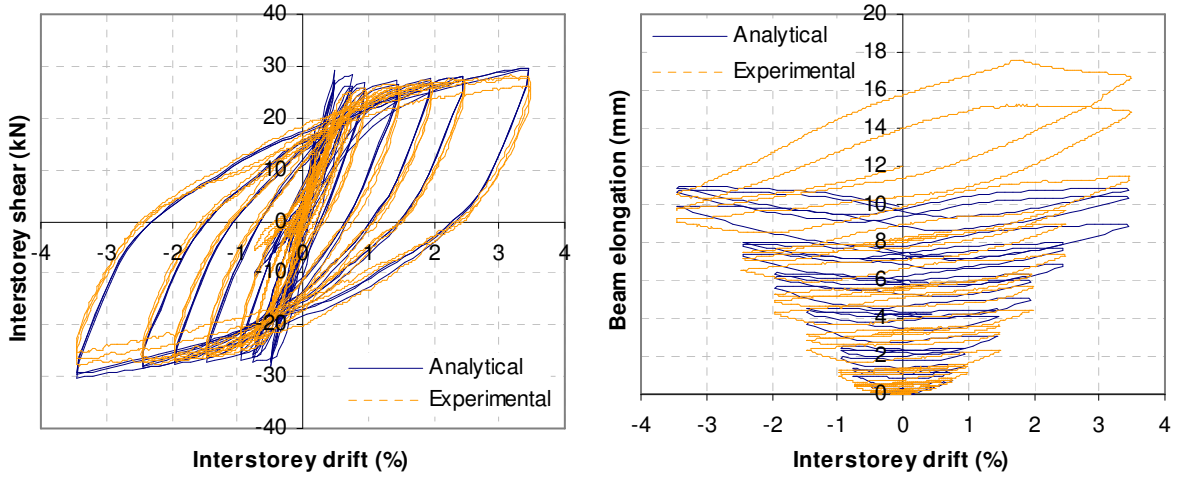

(a) Global response **(b) Beam elongation**

Figure 7-6: Comparison of analytical and experimental results for specimen RCB1

Figure 7-7 compares results from the multi-spring model for slotted-connections with the experimental results from specimen SB1. Figure 7-7a shows the model gives reasonably good agreement with the experimentally observed force-drift response. The peak response

envelope is well predicted and the Dodd-Restrepo hysteresis is able to model the additional post-yield hardening due to cyclic loading. However, in terms of the unloading-reloading response, the model gives slightly fatter loops and is unable to reproduce the slight pinching observed in the test response. This pinching is more prominent during gap-closing (decreasing) rotations, which is most likely the result of minor buckling of bottom longitudinal reinforcement within tubes providing the unbonded length. For this particular model, the parameter *OmegaF* was taken as 1.0.

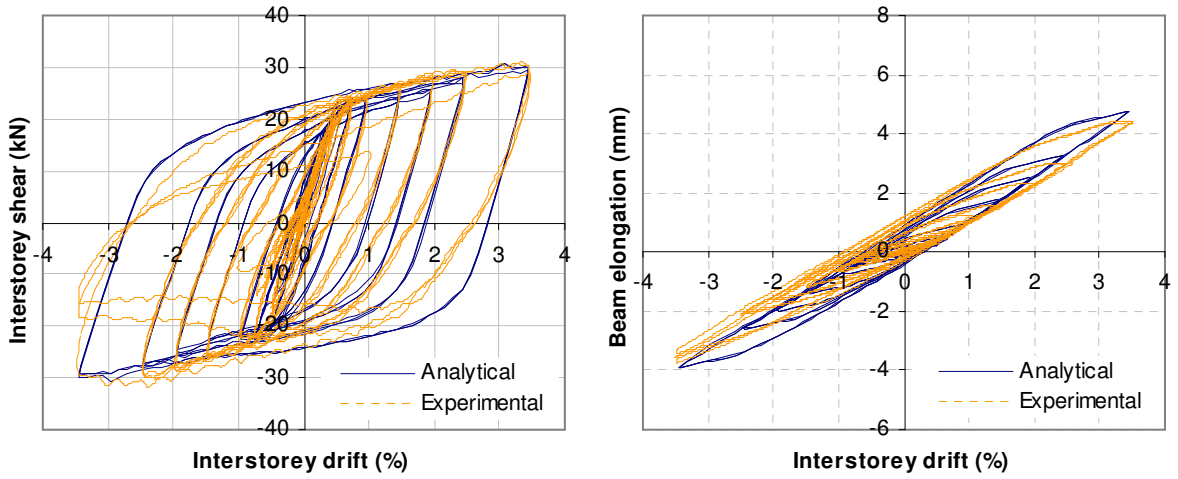

(a) Global response **(b) Beam elongation**

Figure 7-7: Comparison of multi-spring model and experimental results for specimen SB1

Slight strength degradation can be seen for the multi-spring model on successive cycles at the same drift. This is inherent to the Dodd-Restrepo hysteresis rule which reduces the peak tensile strength as a function of the peak compressive strain. Note that the sudden strength degradation shown in the experimental results at 3.5% drift is due to buckling of bottom longitudinal reinforcement, which the model is unable to account for.

Figure 7-7b compares the analytical and experimental beam elongation response. Beam elongation was measured at the beam centreline, across the slotted section. It shows the multi-spring model is capable of reproducing the actual beam elongation in specimen SB1 with reasonable accuracy.

Although not reported on in this thesis, multi-spring models for specimens SB2 and SB3 were investigated. These models did not show the same correlation with the experimental beam elongation response seen here with specimen SB1. They over-predicted the elongation or contraction at peak drifts by approximately 1 mm, and the beam elongation versus drift

hysteretic loops were not as fat as that observed experimentally. This may be partly due to bond-slip failure and the inclusion of floor units in specimens SB2 and SB3 respectively, which were not included in the numerical models.

Figure 7-8 compares the global response from the lumped plasticity model with experimental results. It shows the Dodd-Restrepo hysteresis, in Figure 7-8a, is not quite capable of attaining the same peak post-yield envelope. This is because the simple model cannot account for the slight increases in strength from the movement of the neutral axis within the top-hinge. It can represent the unloading/reloading response well. For the figure shown, the parameter *OmegaF* was taken as 0.8. Figure 7-8b shows that the Bounded Ramberg-Osgood hysteresis is capable of representing the hysteretic response of the slotted-beam extremely well. Peak shears and the slightly pinched steel unloading and reloading branches correspond well with experimental results. The drawback is that this hysteresis is not path-dependent and requires direct calibration with cyclic experimental data. On closer inspection the yield point is also not accurately predicted.

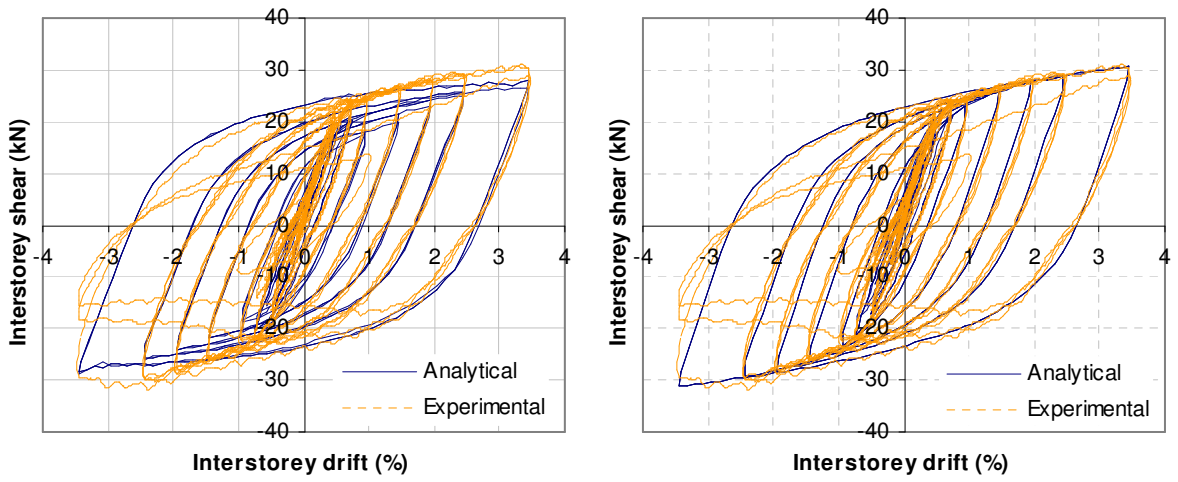

(a) Dodd-Restrepo Hysteresis **(b) Bounded Ramberg-Osgood Hysteresis**

Figure 7-8: Comparison of lump plasticity model and experimental results for specimen SB1

7.3 Numerical Investigation of Frame Response

The multi-spring model presented in Section 7.1.2 was implemented into a five-storey prototype frame to investigate the frame response using slotted-beam connections when subject to earthquake excitation. To allow a comparison with a conventional RC frame, a second frame was also setup using Peng's plastic hinge element (2009) for monolithic beams.

A pushover analysis was first carried out to verify the direct displacement-based design of the frames, and was followed by non-linear time history analyses with eight earthquake records.

7.3.1 Five-Storey Frame Models

The five-storey frame analysed came from the prototype building in Figure 7-9 below. The seismic frame running parallel with one-way spanning floor units was considered. It had three bays, each 6 m in width, and an interstorey height of 3.6 m. Beam and column dimensions are summarised in Table 7-3. While the column depth of 500 mm was chosen for a conventional reinforced concrete frame, this theoretically would not provide sufficient anchorage to beam bottom longitudinal reinforcement passing through interior columns in the slotted-beam frame. A column depth on the order of 600-700 mm would be required to anchor 25 mm diameter Grade 300 deformed bars (D25). However, when such a large column depth was used, the structure was unable to reach its design drift of 2.0%. Because the non-linear hysteretic response of the frame was of interest, it was important that the design drift was reached. Thus the smaller column depth of 500 mm was adopted, and it was suggested that the bond issue was resolved via other means such as smaller diameter bars, mechanical anchorages and/or high strength concrete.

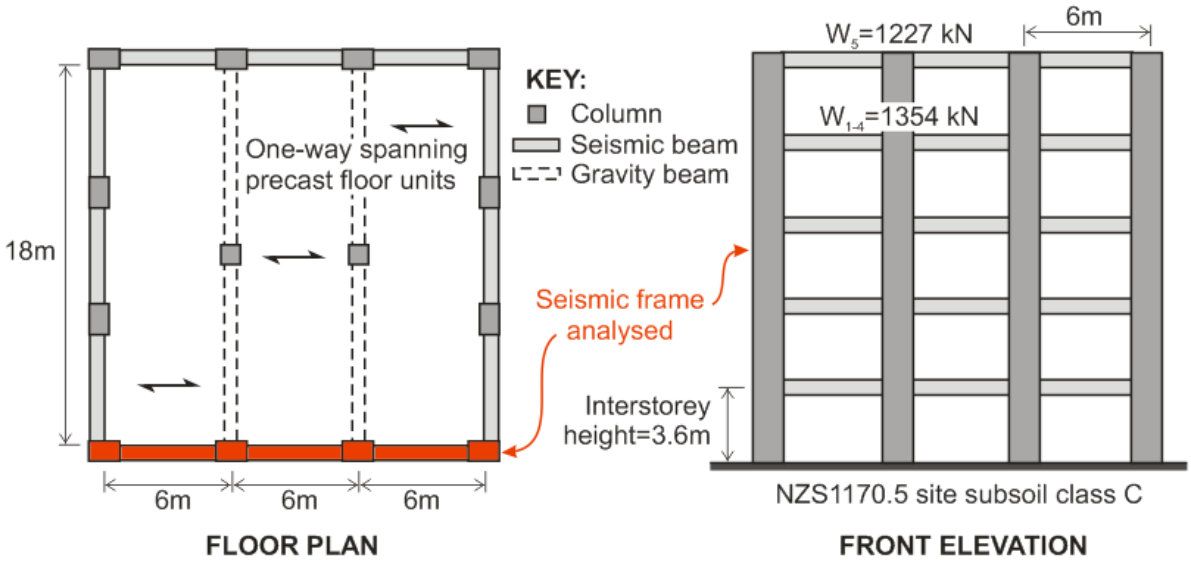

Figure 7-9: Five-storey prototype frame building

Table 7-3: Beam and column dimensions in prototype building

Element	Dimension (mm×mm)
Beam in external seismic frame	500×300
Beam in internal gravity frame	500×300
Column in external seismic frame	500×400
Column in internal gravity frame	400×400

To calculate static gravity loads, a combined floor load ($G+\psi_c Q$) of 7.5 kPa and 6.9 kPa was assumed for levels one to four and the roof level respectively. P-delta effects from gravity loads acting on the external seismic frame were considered. However, P-delta effects from gravity loads on the internal gravity frame were ignored. Seismic weights of 1354 kN were assumed for levels one to four for each seismic frame, and a weight of 1227 kN was assumed at the roof level for each seismic frame.

The frame was designed according to the direct displacement-based design method given in Priestley et al. (2007), and was designed for Wellington seismicity using NZS1170.5 design spectra. Table 7-4 summarises parameters assumed for the design spectra and displacement-based design. For a design drift of 2.0%, an inelastic base shear demand of 547 kN per seismic frame was calculated. P-delta effects were omitted from the determination of seismic design actions, as it was found that it resulted in less than a 5% increase in base shear.

Table 7-4: Parameters assumed for design spectra and displacement-based design

NZS1170.5 Design Spectra	
Location	Wellington
Soil class	C (Shallow soil)
Importance level	2
Annual exceedance probability	1/500
Hazard factor, Z	0.4
Return period factor, R_u	1.0
Near-fault factor, $N(T,D)$	1.0
Direct Displacement-based Design	
Design drift, θ_{design}	2.0%
Design displacement, Δ_d	214 mm
Equivalent viscous damping, ξ_{eq}	21.6%
Effective height, H_e	12.7 m
Effective mass, m_e	580.9 tonnes
Effective period, T_e	3.00 s
Effective stiffness, K_e	2555 kN/m
Base shear, V_{base}	547 kN

Base shear was distributed to frame members based on equilibrium considerations and the equivalent static analysis force distribution from NZS1170.5:2004. Both slotted-beam and monolithic frames were designed for the same column-face beam moments. Frame member design was first carried out in accordance with NZS3101:2006 using a strength reduction

factor, φ, of 0.85 and lower characteristic material strengths. A pushover analysis (See Section 7.3.2) showed that this led to an over-designed frame, and so the frame was redesigned adopting φ as 1.0 and using average material strengths. Refer to APPENDIX C for design details of each frame.

Figure 7-10 shows a graphical representation of the slotted and monolithic frame models in Ruaumoko2D. Ground floor columns were modelled as inelastic concrete beam-column elements with Takeda hysteresis loops. Because all other columns should remain elastic according to capacity design principles, these were modelled as elastic frame elements. Any yielding would only be transient, so this simplification should not greatly affect the frame response. Beams were modelled using elastic Giberson beam elements and beam connections were modelled as described in Section 7.1. For all frame elements, effective moments of inertia for cracked sections were adopted in accordance with NZS3101:2006.

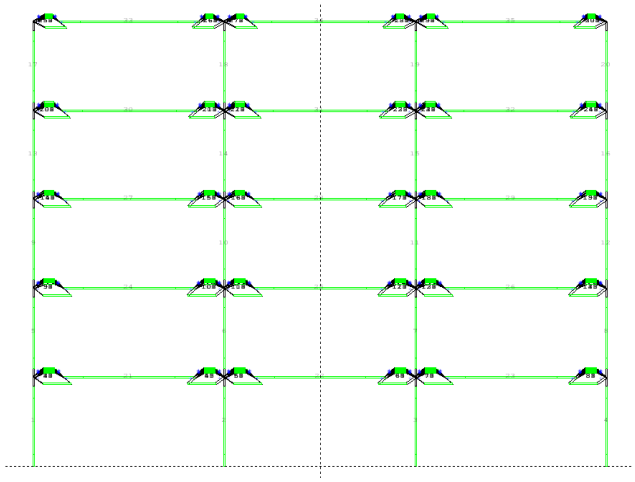

(a) Slotted frame

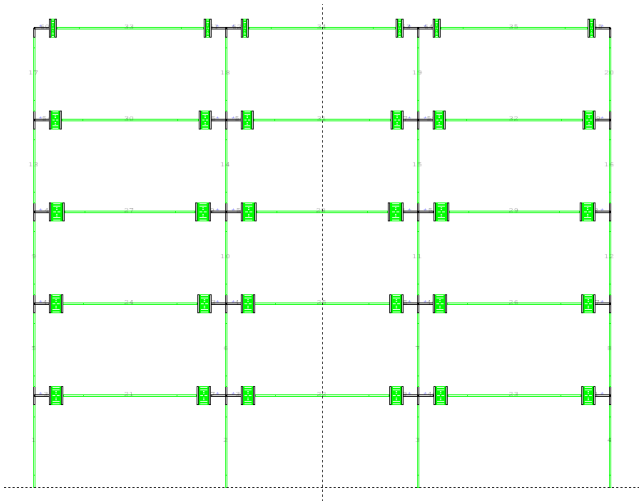

(b) Monolithic frame

Figure 7-10: Ruaumoko frame models

For time history analyses with the slotted-beam frame, time-steps ranging between 0.0001 s and 0.0008 s were used with Newton-Raphson iterations enabled. For some earthquake records, instability occurred when the time-step was too small, so occasionally a larger time-step was used with the maximum number of Newton-Raphson iterations increased to ensure convergence. Analyses that included P-delta effects were performed using large-displacement theory because the frame model was found to be less stable with small-displacement theory.

For analyses with the monolithic frame, a time-step of 0.000025 s was used for all analyses. A smaller time-step was used because Peng (2009) found the plastic hinge element to be less stable when Newton-Raphson iterations were enabled. For analyses including P-delta effects, small displacement theory with a P-delta stiffness correction was used. This was because the plastic hinge element was less stable when run using large displacement theory.

7.3.2 Pushover Analysis

To verify the displacement-based design of the frames, a pushover analysis was carried out on each frame. A force-controlled pushover was used because perfectly plastic yield plateaus meant an adaptive pushover would terminate early when the stiffness reduced to zero. An equivalent static force distribution from NZS1170.5:2004 was adopted and considered appropriate because it was the force distribution assumed when designing frame members. Because this was simply a verification of the displacement-based design, P-delta effects were ignored for pushover analyses. This was appropriate because P-delta effects were small enough to be ignored during the displacement-based design itself.

Figure 7-11a shows the pushover response for both slotted and monolithic frames as originally designed according to NZS3101:2006 using lower characteristic material strengths and a strength reduction factor, φ, of 0.85. Also plotted is the NZS1170.5:2004 elastic design spectra in acceleration-displacement (AD) format. Spectral accelerations have been converted to base shears by multiplying by the effective mass of the frame, m_e. It is shown that both frames are over-designed and achieve base shears 45-60% higher than the code spectra at the design displacement of 214 mm. Given a strength reduction factor, φ, of 0.85, average material strengths which are 10% higher than lower characteristic strengths, and strain hardening estimated at 20%, a strength increase of 55% (1.1×1.20/0.85=1.55) is not unusual.

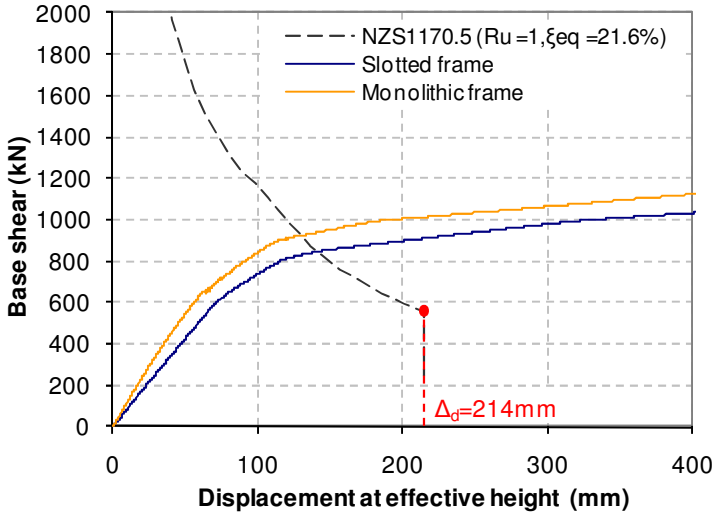

(a) Frames designed using φ=0.85 and lower characteristic material strengths

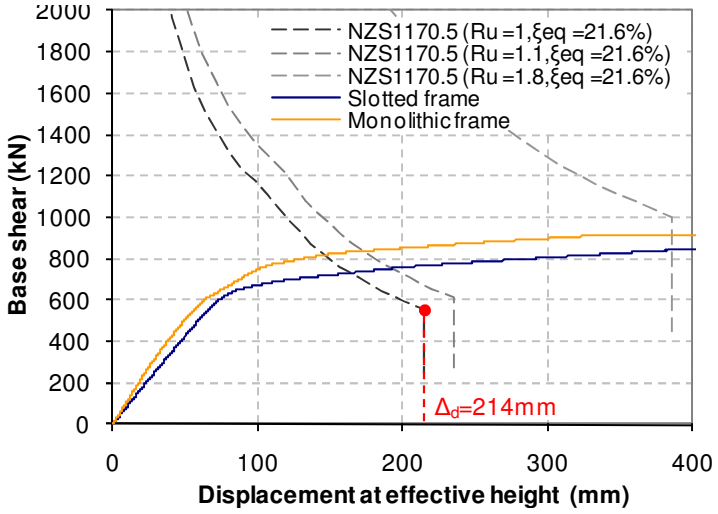

(b) Frames redesigned using φ=1.0 and average material strengths

Figure 7-11: Frame pushover response

To provide closer agreement with the displacement-based design, both frames were redesigned assuming φ equal to 1.0 and using average material strengths. Because this is not a conservative design and a target displacement response is desired, adopting average material strengths and a strength reduction factor of 1.0 is appropriate. Figure 7-11b plots the pushover response for the redesigned frames and compares them to the design spectra. The redesigned frames show a better agreement with the design spectra. Both frames still achieve higher base shears than the code spectra at the design displacement, but this is simply due to strain hardening and the fact that designed connection strengths are usually slightly higher than the demand. To ensure the design drift of 2.0% was reached, the design earthquake spectrum was increased by increasing the return period factor, R_u, from 1.0 to 1.1. This corresponds to an increase in design earthquake (DE) from a 1/500 year event to a 1/667 year

event. Although according to the pushover response, this is not sufficient to attain the design displacement, time history analyses showed that peak drifts of 2.0% were reached. A possible reason for the discrepancy between the displacement-based design and time history analyses is a slight overestimation in the assumed level of damping. Also plotted in Figure 7-11b is the code spectra for a maximum credible earthquake (MCE), that is, a 1/2500 year event (R_u=1.8) as according to NZS1170.5:2004. For this event, the maximum displacement at the effective height is 386 mm, which corresponds to a maximum interstorey drift of 3.6%.

Comparing the pushover response of both frames in Figure 7-11b, it can be seen that the slotted frame has a lower elastic stiffness than the conventional monolithic frame. This is due to the slot and unbonded length in slotted-beam connections. The unbonded length reduces the rate of strain (and hence stress) accumulation in bottom longitudinal reinforcement, and the slot reduces the stiffness of the connection during gap-closing rotations.

The slotted frame also exhibits a lower yield base shear than the monolithic frame. This is because the gap-closing yield moment for a slotted-beam is smaller than the gap-opening yield moment. For an equally-reinforced monolithic connection, the absolute magnitudes of positive and negative yield moments are equal and the same as the gap-opening yield moment in a slotted-connection. So during the pushover, half the slotted-connections are yielding at a smaller moment than in the monolithic frame. Although this resulted in a slight increase in the design displacement during the pushover analysis, earthquake time history analyses later showed that displacements actually decrease due to greater damping in slotted-connections.

7.3.3 Earthquake Records Used and Scaling

Non-linear earthquake time history analyses were carried on both slotted and monolithic frames using the eight earthquake records summarised in Table 7-5. Each record was scaled according to NZS1170.5:2004 for a 1/667 year design earthquake (DE) and a 1/2500 year maximum credible earthquake (MCE). The fundamental translationary elastic period for the monolithic frame model was 1.68 s. Because slotted-beam connections are more flexible, the slotted-beam frame had a longer fundamental period of 1.94 s. To allow the same excitation to be applied to both frames, all records were scaled to the average fundamental period of 1.81 s. Figure 7-12 shows the acceleration spectra for the earthquake records as scaled to design level and maximum credible earthquake code spectra.

Table 7-5: Earthquake records used and scale factors

Earthquake event	Year	Station	Moment Mag.	Duration (s)	Scale factor DE	Scale factor MCE
Imperial Valley1	1940	El Centro	7	64	1.33	2.17
Imperial Valley2	1979	UNAM/UCSD 6617 Cucapah	6.53	40	1.49	2.43
Imperial Valley3	1979	UNAM/UCSD 6621 Chihuahua	6.53	40	1.57	2.57
Superstition hills	1987	USGS 5210 Wildlife Liquif. Array	6.54	44	0.90	1.47
Landers	1992	CDMG 22074 Yermo Fire Station	7.28	44	1.79	2.93
Turkey1	1999	ERD Bolu	7.14	56	0.89	1.45
Turkey2	1999	Duzce	7.2	26	0.63	1.02
Hokkaido	2003	HKD085	8.3	78	0.82	1.33

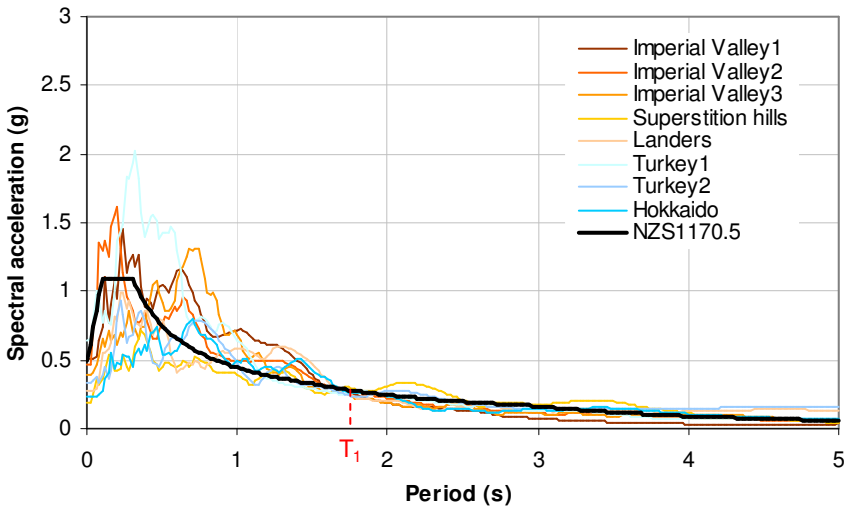

(a) Design earthquake (DE)

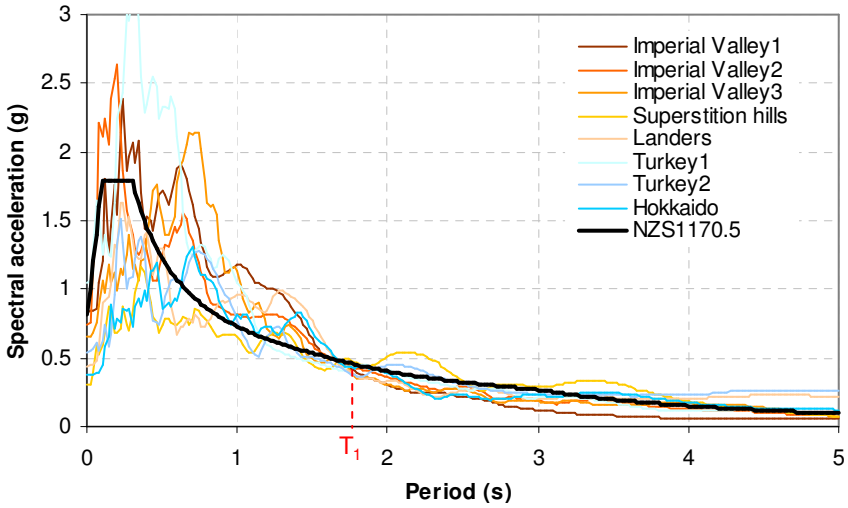

(b) Maximum credible earthquake (MCE)

Figure 7-12: Scaled earthquake acceleration spectra

7.3.4 Earthquake Time History Analysis Results

This section presents and discusses the results from the earthquake time history analyses. Figure 7-13 plots peak response envelopes averaged across the eight earthquake records used. Plotted on each chart is the response for both slotted and monolithic frames, for 1/667 year design earthquakes (DE) and 1/2500 year maximum credible earthquakes (MCE). Unless stated otherwise, all analyses included P-delta effects.

From the initial displacement-based design, maximum drifts of 2.0% and 3.6% were expected for design level and maximum credible earthquakes respectively for both frames. Figure 7-13a plots the peak transient interstorey drift envelopes. Although both frames only show peak drifts of approximately 1.6% and 2.4% for DE and MCE events respectively, it should be remembered that this is the peak drift envelope averaged across eight earthquake records. An absolute maximum drift envelope across all eight records (not shown) showed drifts of 1.8-2.2% across all five stories for a design earthquake, and showed drifts of 3-5% for a maximum credible earthquake. Thus earthquake time history analyses returned maximum drifts consistent with the initial design.

Figure 7-13a shows that peak drifts for the slotted and monolithic frames were fairly similar. Interstorey drifts were measured up the second column to minimise effects of floor elongation on measured drifts. Maximum drifts for both frames occurred in second and third floors, and maximum credible earthquake drifts were 50-100% larger than design earthquake drifts for both frames. Drifts for the slotted frame on average were only slightly less than those in the monolithic frame. Of particular interest is the difference in distribution of the peak drift envelopes – the monolithic frame showed larger drifts towards the bottom of the frame, whereas the slotted frame showed larger drifts at the top of the frame. A possible explanation for this is the stiffness degradation that occurs in conventional monolithic connections. Beams on lower levels are likely to yield first due to higher storey shear demands. After any reasonable yield excursion, the stiffness in a conventional beam plastic hinge quickly degrades such that drifts are concentrated in these lower storeys as oppose to being distributed to the upper levels. Another possible cause of early stiffness degradation in lower floor connections is beam elongation. Beam elongation will occur in the first floor, but because elongation cannot occur at the ground level, this will induce additional drifts and rotations in first floor beams. Because slotted-beams do not exhibit any stiffness degradation, this drift concentration in bottom levels does not occur.

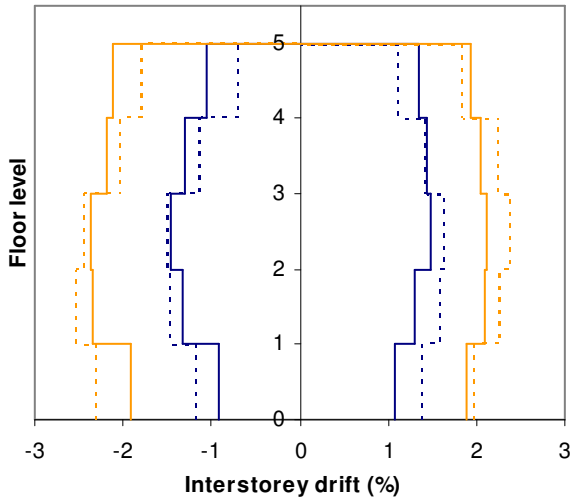

(a) Interstorey drifts

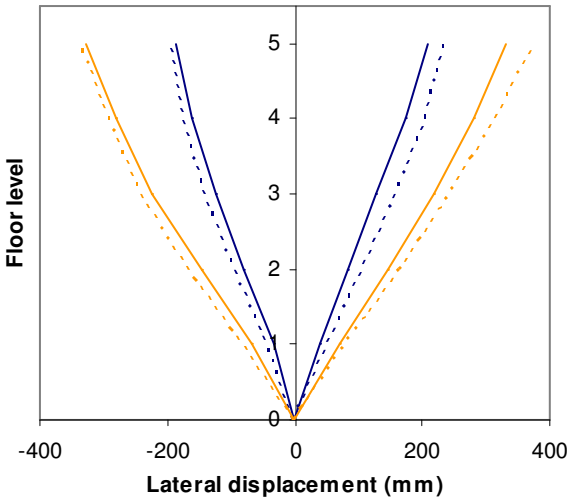

(b) Floor displacements

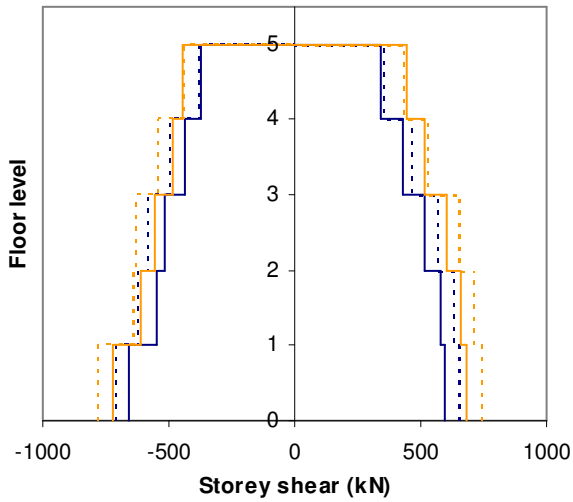

(c) Storey shears

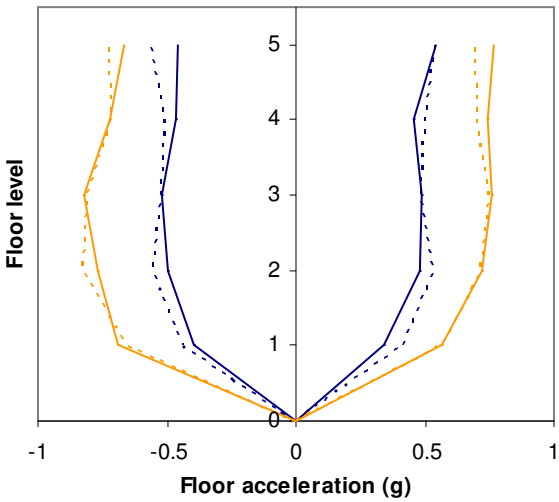

(d) Floor accelerations

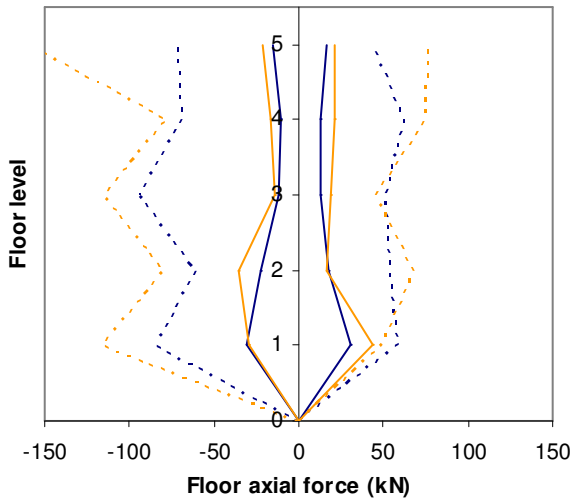

(e) Centre-bay beam axial force

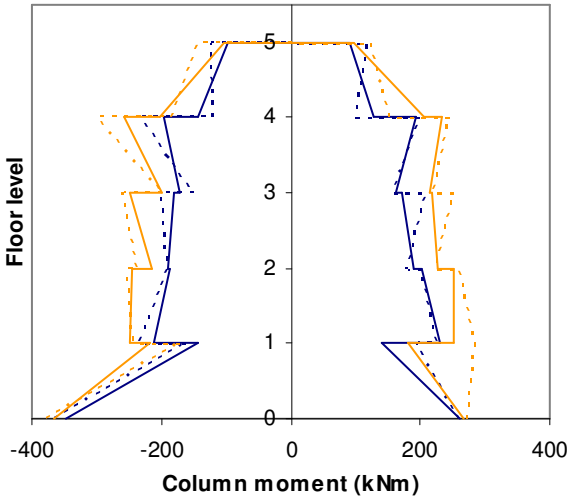

(f) RHS exterior column moments

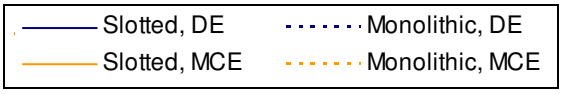

Figure 7-13: Average peak response envelopes from earthquake time history analyses

Figure 7-13b shows the peak floor displacement envelope averaged across the eight earthquake records for each frame. It shows floor displacements in the slotted frame were slightly less than those in the monolithic frame for both design level and maximum credible earthquakes. Drifts and displacements in the slotted frame are most likely less than those in the monolithic frame due to the larger damping in slotted-connections and the absence of stiffness degradation which occurs in conventional connections. The hysteretic response of the two connections is discussed further, later in this section.

Figure 7-13c plots the peak storey shear envelope averaged across the eight earthquake records for each frame. It shows storey shears in the slotted frame are slightly less than in the monolithic frame for both design level and maximum credible earthquakes. This is simply because the gap-closing moment capacity of a slotted connection is slightly less than its gap-opening moment capacity, whereas the absolute magnitudes of positive and negative yield moments in a monolithic beam are identical. Because storey shears are limited by yielding of beam connections, the maximum credible earthquake results in a slight increase in storey shears from additional strain hardening.

Figure 7-13d plots the peak floor acceleration envelopes, for each frame, averaged across the eight earthquake records. It can be seen that there is little difference in floor accelerations between slotted and monolithic frames. For the design earthquake, accelerations were slightly lower in the slotted frame. This could be attributed to either greater damping in slotted-beams or slotted-beams having a lower initial flexural stiffness compared to conventional beams. This difference was less apparent for the maximum credible earthquake events.

Figure 7-13e plots the peak axial force envelope in centre-bay beams for each frame. Again the peak envelope has been averaged across the eight earthquake records. It shows that significantly larger tensile and compressive axial forces are induced in the monolithic frame beams compared to the slotted frame beams. These beam axial forces are the result of beam elongation in each floor. To help describe how beam elongation induces these axial forces, Figure 7-14 illustrates the floor elongation and beam axial forces in both frames during the Duzce 1999 design level earthquake record at t=7.0 s. t=7.0 s is just after a large spike in horizontal acceleration, during which the bulk of beam elongation occurred. For the monolithic frame, in Figure 7-14b, the first floor had elongated 15.4 mm. Because column bases are fixed, ground floor columns will act to restrain this elongation via column shear,

which induces 52.2 kN compression in the first floor beam. The second floor had elongated a greater amount, equal to 18.3 mm. However second floor beams were not in compression but in tension. This is because first floor elongation is pushing exterior columns outwards at such a wide angle, that at the height of the second floor, second floor beams act to pull the columns back in. This induces the 11.2 kN tension in the second floor beam. Similar to the first floor, the third floor is in compression due to columns restraining a floor elongation of 15.2 mm. The same corollary from the first three floors applies to the remaining floors, but with smaller induced axial forces, because the difference in floor elongation between these floors is not as significant. Because slotted-beams exhibit negligible beam elongation, floor elongation in the slotted frame was minimal (less than 1 mm in Figure 7-14a) and hence the smaller axial forces induced in beams. Note that the pattern of tension and compression in floors up the height of either frame is not uniquely defined, but changes with the earthquake record and during the earthquake itself. The only requirement is that horizontal force equilibrium must be satisfied.

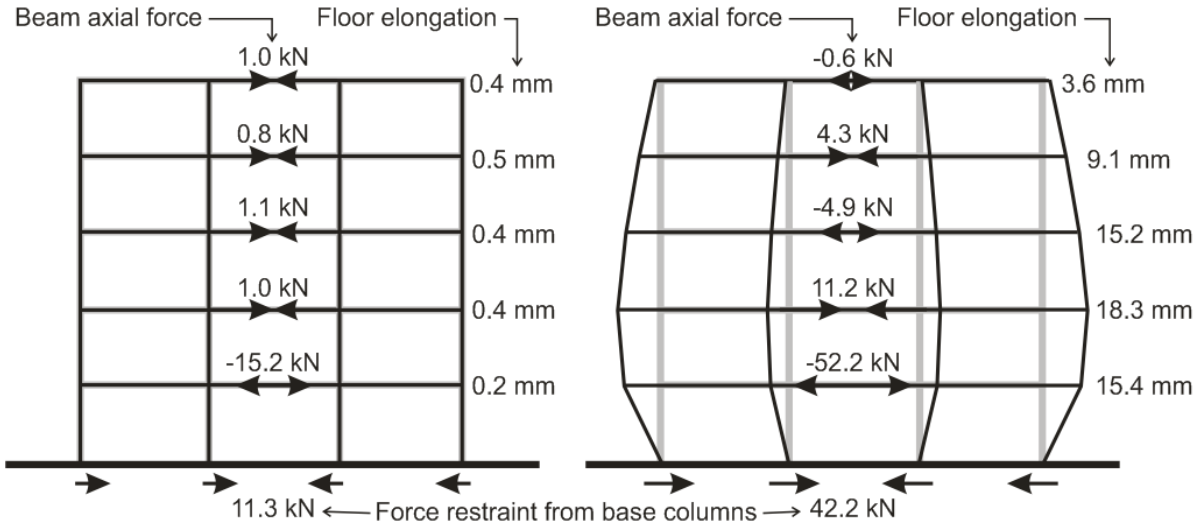

(a) Slotted frame **(b) Monolithic frame**

Figure 7-14: Floor elongation and central-bay beam axial forces during Duzce 1999 design level earthquake record at t=7.0 s

Induced beam axial forces from beam elongation are of interest because they can alter beam moment capacities. In conventional RC beams, compressive axial forces will increase the moment capacity, whereas tensile axial forces will decrease the moment capacity. This is not quite so for slotted-beams. For gap-opening rotations, because the strength is governed by tensile yielding of bottom longitudinal reinforcement, compressive axial forces will increase the moment capacity and tensile axial forces will decrease the moment capacity – just like

with a conventional beam. However, for gap-closing moments, because the strength is governed by compression yielding of bottom longitudinal reinforcement, compressive axial forces will now decrease the moment capacity and tensile axial forces will now increase the moment capacity. So for a conventional beam, a compressive axial load will result in a strength increase at both ends of the beam. However for a slotted-beam, it will result in a strength increase at one end of the beam and a strength decrease at the other. So given this and the fact that beam axial forces were significantly less in the slotted frame, issues of increased overstrength beam moments induced by floor axial forces will be minimal in a slotted beam frame when compared to a conventional frame.

To compare column moment demands generated from overstrength beam actions, Figure 7-13f plots the peak moment envelope in the right-hand-side exterior column for both slotted and monolithic frames. This is the peak envelope up the height of the frame averaged across the eight earthquake records. It shows that column moment demands in both frames are very similar, with the column moments in the monolithic frame on average being slightly higher than those in the slotted frame. This could partially be due to axial force effects in the beams as discussed in the previous paragraph, but may also be due to the gap-closing moment capacity of slotted-beams being less than the moment capacity of monolithic beams (See Section 3.1.1). Given these two contributions, it would be expected that column moment demands would be significantly higher in the monolithic frame than in the slotted frame compared to the difference seen in Figure 7-13f. However, it must be remembered that greater post-yield hardening was observed in slotted-beams during experimental testing from cyclic strain hardening effects. For the slotted frame analysed, this means greater beam moments, and therefore greater column moments demands.

One of the main reasons for using multi-spring connection models in frame analyses was to observe effects of beam elongation. Figure 7-15 compares peak floor elongation envelopes averaged across the eight earthquakes for each frame. This floor elongation is the total elongation from the six plastic hinges or top-hinges in each floor, measured at the beam centreline. As expected, floor elongation in the slotted frame was negligible, on the order of 1 mm and 3 mm for design and maximum credible earthquakes respectively. This was reasonably consistent across the eight earthquake records.

Floor elongation in the monolithic frame was significantly greater, with a maximum elongation of 18 mm for a design level earthquake and 41 mm for a maximum credible

earthquake. It should be noted that these are average values and that there was reasonable scatter in the results for the monolithic frame. Floor elongation values had a maximum standard deviation of 11 mm and 13 mm for design and maximum credible earthquakes respectively. This means that 95-percentile values, which are often considered in engineering, are 36 mm for a design earthquake and 62 mm for a maximum credible earthquake for the monolithic frame. Assuming floor elongation is distributed evenly across the six beam-column connections, this translates to a 6 mm and 10 mm floor crack for design and maximum credible earthquakes respectively from beam elongation alone. Obviously this elongation could be distributed across multiple smaller cracks, but this still gives an indication of reasonable floor damage when compared to the slotted frame which exhibits negligible beam elongation.

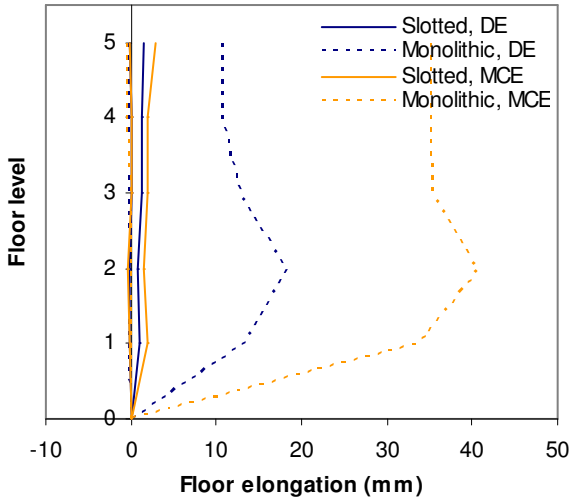

Figure 7-15: Average peak floor elongation envelopes from earthquake time history analyses

It should be remembered that the analyses carried out were only two-dimensional and did not consider the effects of floor units spanning parallel with the frame. Previous studies carried out by Peng (2009) and Lau et al. (2007) showed that floor units help to restrain beam elongation by inducing axial compression in elongating beams. The floor elongation values quoted above will therefore be upper bound values. However, additional axial compression in beams also suggests increases in beam plastic hinge strength, in addition to floor slab contributions which must be considered. Thus overstrength column moment demands in a monolithic frame will be significantly higher than what is suggested in Figure 7-13f. Because slotted-beams exhibit negligible beam elongation, induced axial compression from floor units will be minimal, floor slab contributions to flexural overstrengths will be minimal, and thus

columns will not be subject to the same overstrength demands as in a conventional monolithic frame. This was confirmed in the experimental test of a frame subassembly using slotted-beams with floor units by Leslie (2010).

Figure 7-16 shows the hysteretic response of a level 2 beam connection from both frames when subject to the Landers 1992 earthquake record. This moment-rotation response is typical of that seen with the other earthquake records. In both DE and MCE plots, the fatter hysteretic response of the slotted-connection and stiffness degradation in the monolithic connection is apparent. Monolithic connections seemed to be characterised by one or two large rotation excursions, followed by smaller cycles at a degraded stiffness. The large excursion would be when the majority of beam elongation occurred, and hence the degraded stiffness after the excursion. The smaller cycles which followed showed little hysteretic energy dissipation. Conversely, slotted-beam connections showed a greater number of larger cycles and hence a greater amount of hysteretic energy dissipation. Although the model could not represent stiffness degradation from bar buckling, buckling was unlikely as rotations remained less than 0.03 radians for all earthquake records, except a maximum credible event with the Superstition Hills 1987 record.

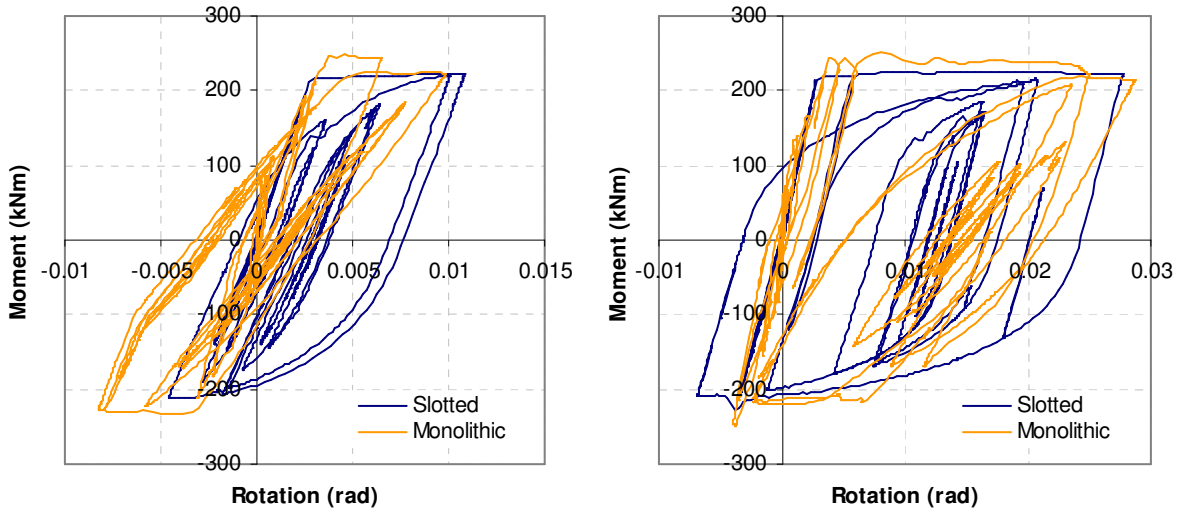

(a) Design earthquake **(b) Maximum credible earthquake**

Figure 7-16: Hysteretic response of level 2, centre bay, right-hand-side connection during analysis with the Landers 1992 earthquake record

To provide an indication of building performance, Figure 7-17a and b re-plots average peak drift envelopes for both frames against performance level drift limits specified in American Standard ASCE/SEI 41-06. This standard defines three major performance levels – Immediate Occupancy (IO), Life Safety (LS) and Collapse Prevention (not shown in figure).

The definition of each performance level and a discussion on appropriate damage limit states for slotted-beams for each performance level was given in Section 4.3.14.

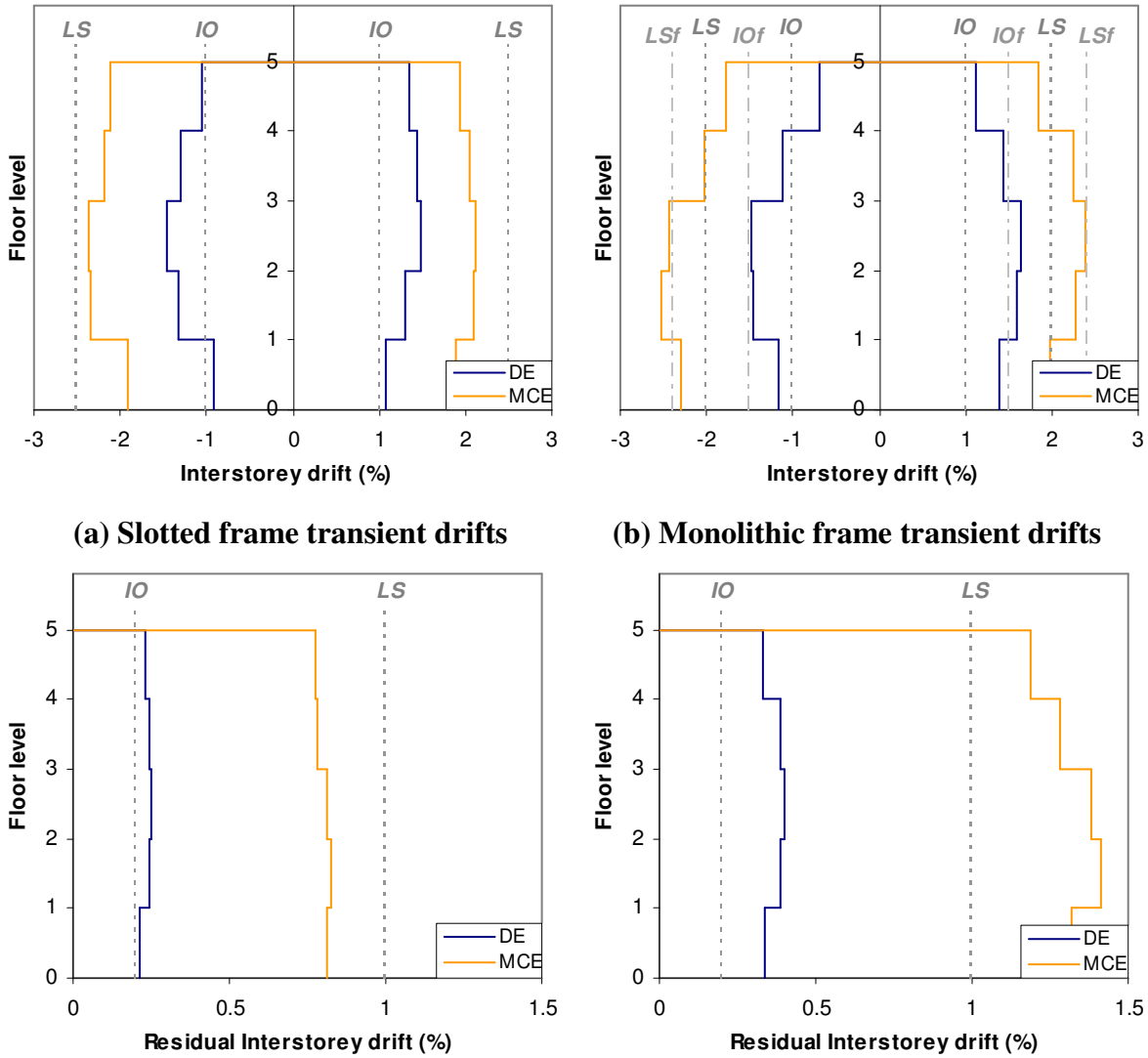

(a) Slotted frame transient drifts **(b) Monolithic frame transient drifts**

(c) Slotted frame residual drifts **(d) Monolithic frame residual drifts**

Performance level abbreviations:
IO = Immediate occupancy (based on drift limits)
LS = Life safety (based on drift limits)
IOf = Immediate occupancy (based on floor damage)
LSf = Life safety (based on floor damage)

Figure 7-17: Comparison of average peak drift envelopes from earthquake time history analyses with ASCE/SEI 41-06 performance levels

Figure 7-17a and b shows that for a design level earthquake, the average building response for both frame types exceeds Immediate Occupancy performance levels but is well within Life Safety limits. Immediate Occupancy requires that the structure is safe for re-occupancy post-event without urgent repair. As was discussed in Section 4.3.14, because slotted-beams

exhibit minimal floor and connection damage for rotations up to 0.02 radians, Immediate Occupancy is not governed by structural damage, but rather 1% transient drifts to ensure minor damage to internal building partitions. So although, both frames exceed transient IO drift limits, the structural damage sustained by the slotted frame will be far less than the damage in the conventional frame. To help illustrate this, performance level limits for floor diaphragms are also shown in Figure 7-17 as IOf for Immediate Occupancy and LSf for Life Safety. IOf and LSf require that floor cracks remain less than 3.2 mm (1/8") and 6.4 mm (1/4") respectively. Appropriate drift limits corresponding to IOf and LSf floor damage states were extrapolated from experimental tests carried out. Figure 7-17b shows that the floor damage in the monolithic frame exceeds IOf and LSf limits for design and maximum credible earthquakes respectively. However for the slotted frame, these floor damage limits are outside the drift scale of Figure 7-17a.

For a maximum credible earthquake, Figure 7-17b shows that the average response of the monolithic frame exceeds Life Safety drift limits, whereas Figure 7-17a shows that the slotted frame remains within Life Safety drift limits. Life Safety allows moderate structural damage to occur provided there remains a safe margin against collapse. It also suggests the structure is capable of being repaired prior to re-occupation; although in some cases this may be uneconomical. Because slotted-beams sustain minor damage up to 0.025 radians, in Section 4.3.14, it was suggested that the Life Safe drift limit for slotted-beams be increased to 2.5% from 2.0%, which is used for conventional beams. Under a maximum credible earthquake, although collapse did not occur, it would not be possible to repair the monolithic frame as it exceeds Life Safety limits. However for the slotted frame, provided accumulated plastic strains in bottom longitudinal reinforcement are not excessive, repair would be a very practical option given that floor damage is minimal.

It should be emphasised that drifts plotted in Figure 7-17a and b are peak values averaged across the eight earthquake records. They therefore do not represent the maximum possible response. Performance level wise, the maximum response of the monolithic frame appears to be worse than the maximum response of the slotted frame. In seven of the eight design earthquake records, at least one floor in the monolithic frame exceeded the 2.0% design drift and thus the Life Safety drift criteria. For the slotted frame, only in two of the eight DE records did at least one floor exceed 2.0% drift, and in no case did drifts exceed the LS limit of 2.5%. For the Superstition Hills 1987 maximum credible earthquake record, the monolithic frame reached a peak transient drift of 4.7% in the first and second floors,

whereas the slotted frame reached a peak drift of 3.9% in the same floors. ASCE/SEI 41-06 specifies a 4% drift limit for the Collapse Prevention performance level. Based on this criterion, collapse of the monolithic frame was quite possible, whereas the slotted frame would only be considered on the verge of collapse.

Figure 7-17c and d plots average residual drifts for both frames. For both earthquake levels, the monolithic frame exhibited higher residual drifts than the slotted frame. For a design earthquake, the maximum average residual drift was 0.39% for the monolithic frame and 0.22% for the slotted frame. For a maximum credible earthquake, they were 1.37% and 0.79% for the monolithic and slotted frames respectively. Because conventional beams exhibit stiffness degradation, smaller permanent deformations would have been expected in the monolithic frame. Degraded unloading stiffness's promote the reduction of permanent deformations during smaller cycles at the end of an earthquake record – called 'building shakedown'. However, for the two frames analysed this was not the case. A possible explanation for this is less damping in the monolithic frame. This would mean larger peak drifts, which were observed, and hence larger permanent deformations that the structure was unable to recover from. A second possibility is a greater post-yield stiffness in the slotted frame from cyclic strain hardening of bottom longitudinal reinforcement. A greater post-yield stiffness helps to guard against the accumulation of drifts in a particular direction, whereas negative post-yield stiffness's promote the accumulation of permanent drifts. Hysteretic moment-rotation plots showed that slotted-beam connections had on average a slightly greater post-yield stiffness than monolithic connections. In some plots, monolithic connections were seen to have a negative post-yield stiffness as a result of P-delta effects.

To provide an indication of building performance in terms of permanent deformations, also plotted in Figure 7-17c and d are permanent drift limits specified in ASCE/SEI 41-06. ASCE/SEI 41-06 specifies "negligible" permanent drifts for Immediate Occupancy performance levels. For the figure, a value of 0.2% has been assumed in accordance with the recommended serviceability limit for columns in NZS1170.0:2002. For a design earthquake, Figure 7-17c shows that the average response of the slotted frame has only just exceeded Immediate Occupancy limits. It is therefore quite possible that in some cases a slotted frame structure will be able to be safely reoccupied after a design earthquake. Note it is normally expected that a structure would have exceeded Immediate Occupancy limits but remained Life Safe under a design earthquake. This is the case for the monolithic frame which convincingly exceeded IO residual drift limits. Similarly for a maximum credible earthquake,

the slotted frame remains within Life Safety permanent drift limits, whereas the monolithic frame exceeds them. So not only does a slotted frame exhibit less damage than a conventional RC frame, for this particular frame, permanent deformations are also significantly less.

To briefly illustrate the influence of P-delta effects on the frame response, Figure 7-18 plots peak interstorey drift envelopes averaged across the eight design level earthquakes, comparing analyses with and without P-delta effects, for each frame. It is shown that P-delta had little effect on peak transient drifts. This is consistent with the direct displacement-based design, which resulted in less than a 5% increase in design base shear when P-delta effects were considered. Figure 7-18b shows that P-delta effects caused a reasonable increase in permanent drifts. This is because P-delta effectively reduces the post-elastic stiffness of the structure, which promotes the accumulation of drifts in one direction. From Figure 7-18b it is not apparent whether slotted frames are more greatly influenced by P-delta than conventional frames, and both frames appear to be equally affected.

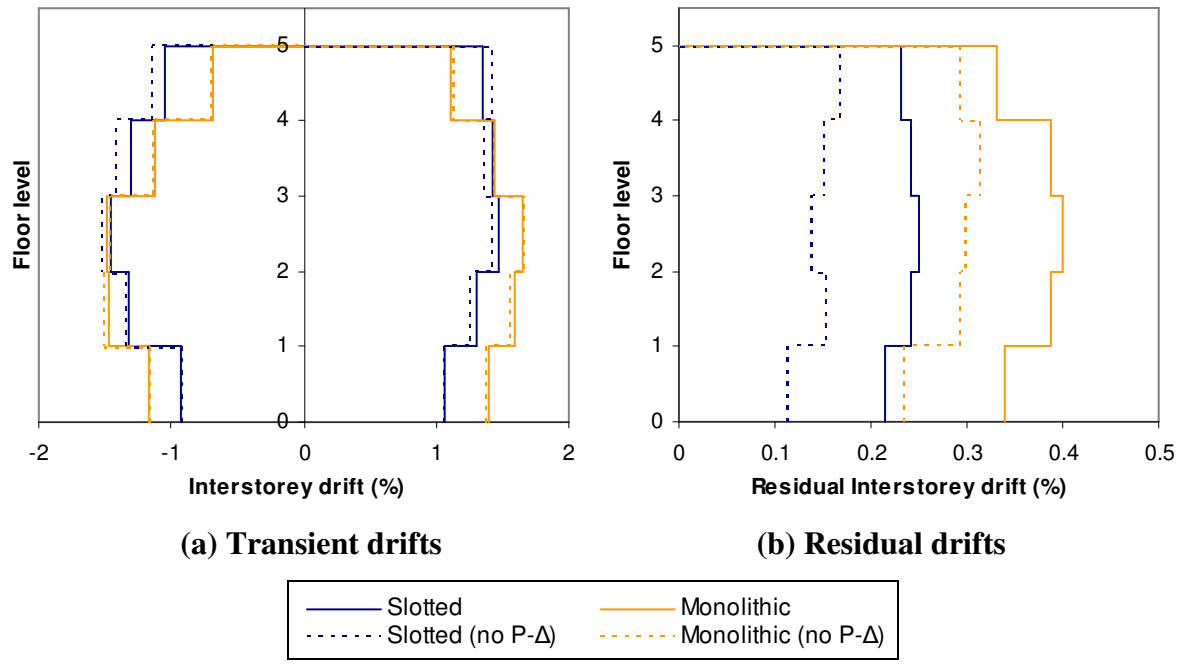

(a) Transient drifts **(b) Residual drifts**

Figure 7-18: Influence of P-delta effects on interstorey drifts

In brief conclusion, earthquake time history analyses showed the average peak response of slotted and monolithic frames to be quite similar. The slotted frame did show slightly smaller drifts and displacements due to greater hysteretic damping. Although peak drifts were similar, a frame with slotted-beams would show significantly less damage than a conventional frame for the same drifts. Beam elongation was on average 10 to 20 times

greater in the monolithic frame and thus more floor damage would be expected. Due to greater damping and a greater post-yield stiffness, the slotted-beam frame also exhibited much smaller residual drifts. The effect of axial loads induced in beams was also discussed, and it was explained that beam overstrength moments are likely to be much higher in a monolithic frame than in a slotted frame. This is due to axial beam compression and floor slab contributions increasing the strength of plastic hinges in a monolithic frame. Slotted-beams are not influenced in the same way by axial beam compression, and because of negligible beam elongation, floor slab contributions will also be minimal. This has positive implications when it comes to designing adjacent columns which must resist these overstrength beam actions.

CHAPTER 8 CONCLUSIONS

8.1 Summary

The research presented in this thesis sought to develop a simple non-tearing floor frame connection that could be used as a substitute for conventional reinforced concrete design. The slotted reinforced concrete beam was investigated as a likely solution. It consists of a conventional reinforced concrete beam, modified with a narrow vertical slot at the column face, running approximately three quarters of the beam depth. The inclusion of the slot allows seismic rotations to occur about the remaining concrete "top-hinge", such that deformations are accommodated via opening and closing of the gap. This minimises beam elongation, which is seen in conventional reinforced concrete beams, and concentrates deformations away from the floor slab level such that damage to adjacent floors is minimised.

The reconfiguration of the beam-column connection to produce a slotted reinforced concrete beam raised several design issues which needed to be addressed in this project. These were the shear transfer across the top-hinge, buckling of bottom longitudinal reinforcement, greater low cycle fatigue demands, the anchorage of bottom reinforcement in interior joints, interior joint design, detailing with floor units and slab effects such as beam torsion resulting from gravity loads. These issues were conceptually investigated in-turn in CHAPTER 3, and where possible, design and detailing recommendations were made.

The experimental program consisted of quasi-static cyclic tests on in-plane beam-column joint subassemblies. The first stage, described in CHAPTER 4, involved the testing of 2/3-scale exterior and interior joint subassemblies using slotted-beams, and a conventional exterior joint which acted as a benchmark. This was to compare the response of slotted-beams with conventional RC beams and to verify some of the design recommendations made in CHAPTER 3. Testing was then extended to a ½-scale interior joint with one-way spanning floor-units with gravity load. This was reported on in CHAPTER 5. The purpose of this test was to investigate joint and bond behaviour and beam torsion resulting from eccentric floor gravity loads.

In CHAPTER 6, a simple analytical procedure was developed to predict the moment-rotation response of slotted-beams. The procedure was used to perform sensitivity studies on various

beam parameters and used to determine appropriate limits for the concrete top-hinge depth, the location of diagonal reinforcement, and the top-to-bottom reinforcement ratio. The procedure was verified against results from experimental tests.

Lastly, CHAPTER 7 reports on the numerical investigation carried out on slotted reinforced concrete beams. A multi-spring model was developed to represent the flexural response of slotted-beams and was verified against experimental test results. This was implemented into a two-dimensional five-storey frame, which was investigated using non-linear time history analysis with eight earthquake records. To compare the slotted-beam frame response with the response of a conventional frame, analyses were also performed on a second frame using the reinforced concrete (RC) plastic hinge element developed by Peng (2009).

8.2 Conclusions

This section summarises the main conclusions which can be drawn from the research presented in this thesis. This is followed by a summary of the advantages and disadvantages of slotted-beams in relation to conventional reinforced concrete (RC) beams at the end of this section.

From the conceptual investigation of design issues identified for slotted reinforced concrete beams, the following conclusions can be drawn:

- To limit elongation and cracking through the concrete top-hinge, larger top longitudinal reinforcement than bottom longitudinal reinforcement in the beam is required. From parametric studies, a top-to-bottom reinforcement ratio, $A_s'f_y'/A_sf_y$, on the order of 2.0 is recommended.

- Because bottom longitudinal reinforcement in slotted-beams yield extensively in compression, these bars are more at risk to buckling. This buckling can be successfully restrained by decreasing the stirrup spacing and providing the unbonded length with steel tubes to provide lateral support for the reinforcement.

- Because the plastic strain accumulation in bottom longitudinal reinforcement is 2-3 times greater than in conventional RC beams, slotted-beams are more at risk to low cycle fatigue failure. It was theoretically shown that slotted-connections could satisfy American Concrete Institute (2005) acceptance criteria for new connections provided

the unbonded length was maximised ($L_{ub} \approx 0.9(d\text{-}d')$) and a minimum bottom reinforcement ratio limit between 0.006-0.008 was specified.

- In slotted-beams, because of tension-compression yielding of bottom longitudinal reinforcement on both sides of interior columns, bond conditions are more severe in interior beam-column joints which connect slotted-beams. Theory and information from testing suggest that column depths 50% larger than required by NZS3101:2006 bond provisions are needed to provide sufficient anchorage to bottom beam longitudinal reinforcement. This can be mitigated to some extent by using smaller diameter bars and higher strength concrete through the joint zone.

- Because of no flexural concrete compression at the bottom of slotted-beams connected to beam-column joints, additional horizontal joint stirrups are required to support the diagonal concrete strut mechanism in the joint. Theory and testing suggests joint reinforcement should be increased by 25-40% of that required by NZS3101:2006. This additional reinforcement should be located in the bottom half of the joint.

- Because of the reduced concrete section in slotted-connections, beam torsion from gravity loads on floor slabs seated on one side of a slotted-beam is a concern. It was theoretically shown that this could be mitigated by using a detail with three diagonal hangers to provide combined shear and torsional resistance.

- Because slotted reinforced concrete beams exhibit $1/8^{th}$ to $1/10^{th}$ of the beam elongation expected in conventional RC beams, floor seating widths for slotted-beams can be reduced. A method for estimating required seating widths was given in Section 3.8.4.

From the experimental investigations performed on in-plane beam-column joint subassemblies, the following conclusions can be drawn:

- Slotted reinforced concrete beams exhibit significantly less damage and cracking than conventional RC beams for the same drift. This reduction in damage is observed in the beam itself as well as in adjacent floor units. Part of this reduction in damage is because slotted-beams exhibit negligible beam elongation compared to conventional beams.

- The diagonal hanger detail tested successfully transfers beam shear across the slotted section with negligible vertical shear sliding. To minimise flexural strains in diagonal hangers, hangers should be located at a depth between 0.7 and 0.75 times the depth of the concrete top-hinge, d_c, where the hanger crosses the beam-column interface.

- Due to cyclic plastic straining of bottom longitudinal reinforcement in tension and compression, slotted-beams exhibit greater post-yield strain hardening than conventional RC beams. This additional strain hardening is dependent on the strain history applied.

- Provided a stable hysteretic response is achieved (that is, there is no bond-slip or bar buckling), slotted-beams exhibit 5-10% more hysteretic energy dissipation than conventional RC beams.

- Because of extensive compression yielding, bottom longitudinal reinforcement in slotted-beams is likely to buckle when current NZS3101:2006 anti-buckling provisions are used. For specimen SB3, it was found that reducing the maximum stirrup spacing to $4d_b$ along the unbonded length of bottom longitudinal reinforcement, and using steel tubes for the unbonded length was sufficient to prevent buckling. Specimen SB3 was the in-plane interior beam-column joint subassembly with slotted-beams and a precast concrete slab on one side of the subassembly.

- Existing NZS3101:2006 bond provisions for beam reinforcement passing through interior joints are insufficient to prevent bond-slip of bottom longitudinal reinforcement in slotted-beams.

- Because flexural deformations are concentrated away from the floor slab level, slab contributions to beam flexural overstrengths are significantly less in slotted-beams compared to conventional RC beams. A 60% increase over nominal strengths was observed during the test of specimen SB3, compared to increases of up to 100% observed by other researchers for conventional beams (Peng, 2009; Lau et al., 2007).

From the numerical investigations performed on slotted reinforced concrete beams, the following conclusions can be drawn:

- The hysteretic flexural response of a slotted-beam connection can be accurately represented by a multi-spring model which was developed.

- The average response of a frame using slotted-beam connections is reasonably similar to a conventional RC frame. Slight differences are mentioned below.

- Peak floor accelerations and storey shears are slightly less in slotted-beam frames compared to conventional RC frames. This is because slotted-beam frames exhibit a slightly lower initial stiffness and a lower yield base shear.

- Peak interstorey drifts and lateral displacements are slightly less in slotted-beam frames compared to conventional RC frames. This is because slotted-connections exhibit greater hysteretic energy dissipation and a stable hysteretic response with no strength or stiffness degradation.

- The most significant difference discovered was that slotted-beam frames exhibit smaller residual drifts than conventional frames. For the five-storey frame considered, a 40% reduction was observed. The author attributes this to greater hysteretic energy dissipation and a greater post-yield stiffness in slotted-beam connections.

To allow an easier evaluation of the differences between slotted-beams and conventional RC beams, below is a summary of the main advantages and disadvantages of slotted-beams in relation to conventional RC beams.

Main advantages:

- **Low damaging:** Compared to conventional RC beams, slotted-beams exhibit significantly less cracking and damage in the connection and floor slab for the same drift level.

- **Negligible beam elongation:** This means significant reductions in damage to adjacent floor diaphragms and reduced slab contributions to beam flexural overstrengths. This also allows seating widths for floor units to be reduced.

- **Smaller column moment demands:** Because slab contributions to beam overstrength moments are significantly less compared to conventional RC beams, column moment demands are smaller in frames with slotted-beams.

- **Lower residual drifts:** Due to greater damping and a greater post-yield stiffness, frames with slotted-beams exhibit smaller residual drifts.

- **Can be constructed using the same methods as conventional RC beams:** Because slotted-beams are so similar conventional RC beams, they can be constructed using the same precast-emulation methods commonly used in New Zealand. This makes slotted-beams a practical substitute for conventional reinforced concrete beams.

Main disadvantages:

- **Larger column depths required:** Because bond conditions are more severe in slotted-beams, larger column depths are required to provide sufficient bond to bottom beam longitudinal reinforcement.

- **Low cycle fatigue:** Because the plastic strain accumulation in bottom longitudinal reinforcement is 2-3 times greater than in a conventional RC beam, slotted-beams are more at risk to low cycle fatigue failure.

- **Larger top longitudinal reinforcement required:** To limit elongation and cracking through the concrete top-hinge, larger top longitudinal reinforcement is required.

- **More beam-column joint steel required:** Because of no concrete compression at the bottom a slotted-beam connected to a beam-column joint, additional horizontal joint stirrups are required to support the diagonal concrete strut mechanism in the joint.

So although a few changes are required to resolve design issues associated with slotted reinforced concrete beams, given the numerous benefits in terms of low damage and negligible beam elongation, the concept is certainly a viable substitute for conventional reinforced concrete construction. There are a few areas requiring further research, which are discussed in the following section.

8.3 Recommended Future Research

During this research project, several areas requiring further investigation were highlighted. These are described in the paragraphs below.

Because the bottom longitudinal reinforcement in slotted-beams yields extensively in compression, they are more susceptible to buckling. Experimental testing showed current NZS3101:2006 anti-buckling provisions to be insufficient, but also showed that buckling could be prevented by reducing the stirrup spacing to $4d_b$ and using steel tubes to provide the

unbonded length. Further experimental testing should be carried out to further verify the $4d_b$ stirrup spacing provision, and to determine steel tube wall thickness and stirrup tie diameter requirements. It is recommended that some of this testing is carried out at full-scale.

Past research has identified that the low cycle fatigue resistance of mild steel is strain rate dependent. Peak strain rates on the order of 5×10^{-2} – 8×10^{-2} strain/s can be expected in the bottom longitudinal reinforcement of a slotted-beam during a seismic event. At these strain rates, the fracture toughness of mild steel has been shown to decrease (Srinivas and Kamat, 2001). Conceptual low cycle fatigue investigations carried out in this project ignored strain rate effects, and in addition, quasi-static testing performed did not simulate actual strain rates which would be expected during an earthquake. Therefore further research is recommended to determine whether realistic dynamic strain rates will severely compromise the low cycle fatigue resistance of slotted-beams. For New Zealand applications, testing should be carried out using New Zealand mild steel.

Bond-slip of bottom longitudinal reinforcement passing through interior columns has been identified as an issue with slotted-beams. Tentative modifications to existing design equations in NZS3101:2006 have been suggested. However, due to limited test data available, a specific value for the average bond strength could not be given. Further experimental testing should be carried out to obtain a distribution of values to allow an optimum but safe value to be chosen. It is recommended that testing be carried out in the form of full joint subassemblies, as oppose to mock subassemblies of a single bar passing through a block of concrete. This is because the bond stress is influenced by joint shear and column flexural stresses. As an alternative solution, anchorage of bottom longitudinal reinforcement with mechanical anchors could also be investigated, instead of relying on bond from ribbed deformed bars.

Section 3.8.2 briefly discussed effective flange contributions, from adjacent floor slabs, to the flexural strength of slotted-beams. It was theorised that effective flange contributions would be significantly less for a slotted-beam compared to a conventional RC beam. This is because negligible beam elongation would limit the extent of slab activation and strength enhancements from beam axial compression. This was confirmed in the test of specimen SB3 and tests by Leslie (2010). However, further research should be carried out to develop appropriate effective flange width recommendations for calculating the overstrength moment

of slotted-beams. This is necessary to accurately predict design actions in columns, which are to remain elastic according to the Capacity Design Philosophy adopted in NZS3101:2006.

The test of specimen SB3, reported on in CHAPTER 5, was an attempt to verify the torsional resistance of slotted-beams when subject to combined eccentric floor gravity and seismic loads. Although the specimen behaved satisfactorily, the test was unable to replicate the worst case torsional demands on the slotted-beam. Worst case torsional demands will occur under biaxial seismic loading where the transverse component causes the floor unit to rotate downwards relative to the beam it is seated on. Therefore to check this case, it is recommended that a three-dimensional biaxial test is carried out with floor units and imposed gravity loads.

Due to the composite nature of reinforced concrete, the anisotropy of concrete, and the transfer of stresses between steel and concrete via bond, the behaviour of stresses within a slotted-beam and within a beam-column joint connecting slotted-beams is very complex. Because of the concrete top-hinge and diagonal shear reinforcement, common assumptions in conventional RC beams of Bernoulli plane sections no longer apply. Therefore, the author believes it would be useful if three-dimensional finite element modelling of slotted-beams was carried out. This would allow an investigation into the distribution of stresses within beam-column joints and within the disturbed zone of the concrete top-hinge. This would provide useful information for developing recommendations for the design of joint reinforcement and proper anchorage of diagonal hanger reinforcement.

Finally, as an extension to the simple slotted reinforced concrete beam concept, it is suggested that a solution using replaceable external steel dissipaters, as oppose to cast-in deformed bars, be investigated. Although the current concept has the advantage of being a simple direct substitute for conventional construction, at the end of a severe earthquake, it is expected that the damage accumulation in bottom reinforcement will be too extensive that they will have to be replaced if the structure is to be used again. This would be a very costly repair. A solution using external dissipaters would provide a much cheaper repair option. In addition, the coupling system used to connect the external dissipaters to the column could be designed such that issues of bond-anchorage and additional joint reinforcement no longer exist. As with the current concept, every attempt should be made to ensure the new concept is cheap and easy to construct.

CHAPTER 9 REFERENCES

ACI Committee 374. (2005). *Acceptance criteria for moment frames based on structural testing and commentary*. ACI Technical Document 374.1-05.

ACI Committee 408 (1992). *State-of-the-art report on bond under cyclic loads*. ACI Report 408.2R-92.

ACI-ASCE Committee 326 (1962). Shear and Diagonal Tension. *Proceedings of ACI, Vol.59*; No.1, P.1-30; No.2, P.277-334; No.3, P.1148-1157.

Amaris, A., Pampanin, S., Bull, D. K., & Carr, A. J. (2007). Development of a Non-tearing Floor Solution for Jointed Precast Frame Systems. *Proceedings of the 2007 New Zealand Society for Earthquake Engineering (NZSEE) Conference, Paper 14*, Palmerston North, New Zealand, March 30 - April 1.

Amaris, A., Pampanin, S., Bull, D. K., & Carr, A. J. (2008). Experimental Investigation on a Hybrid Jointed Precast Frame with Non-tearing Floor Connections. *Proceedings of the 2008 New Zealand Society for Earthquake Engineering, Paper 26*, Wairakei, New Zealand, April 11-13.

Amaris, A., Pampanin, S., Bull, D. K., & Carr, A. J. (2008). Experimental Performance of Hybrid Frames Systems with Non-tearing Floor Connections. *Proceedings of the 14th World Conference on Earthquake Engineering (WCEE)*, Beijing, China, October 12-17.

American Society of Civil Engineers (2007). *Seismic Rehabilitation of Existing Buildings*. ASCE Standard ASCE/SEI 41-06, American Society of Civil Engineers, Reston, Virginia.

Arnold, D. M. (2004). *Development and experimental testing of a seismic damage avoidance designed beam to column connection utilising draped unbonded post-tensioning*. Masters Dissertation, Department of Civil Engineering, University of Canterbury, Christchurch, New Zealand.

Bae, S., Mieses, A. M., & Bayrak, O. (2005). Inelastic buckling of reinforcing bars. *Journal of Structural Engineering, 131*(2), 314-321.

Bakir, P. G. (2003). Seismic resistance and mechanical behaviour of exterior beam-column joints with crossed inclined bars. *Structural Engineering and Mechanics, 16*(4), 493-517.

Bentz, E. C. (2000). *Sectional Analysis of Reinforced Concrete Members*. PhD Thesis, Department of Civil Engineering, University of Toronto.

Bentz, E. C., Vecchio, F. J., & Collins, M. P. (2006). Simplified modified compression field theory for calculating shear strength of reinforced concrete elements. *ACI Structural Journal, 103*(4), 614-624.

Brown, J., & Kunnath, S. K. (2004). Low-cycle fatigue failure of reinforcing steel bars. *ACI Materials Journal, 101*(6), 457-466.

Bull, D. K. (2003). Understanding the Complexities of Designing Diaphragms in Buildings for Earthquakes. *Symposium to Celebrate the Lifetime Contributions of Tom Paulay and Bob Park*, Christchurch.

Carr, A. J. (2005) *Ruaumoko Manual Volume 2: User Manual for the 2-Dimensional Version Ruaumoko2D*. Department of Civil Engineering, University of Canterbury, Christchurch.

CAE (1991). *Guidelines for the use of structural precast concrete in buildings*. Report of a study group of the NZ Concrete Society and the NZ National Society for Earthquake Engineering. Centre for Advanced Engineering, Christchurch.

Cheok, G. S., & Lew, H. S. (1990). *Performance of 1/3-scale model precast concrete beam-column connections subjected to cyclic inelastic loads*. Gaithersburg, MD: National Institute of Standards and Technology.

Cheok, G. S., & Lew, H. S. (1991). Performance of precast concrete beam-to-column connections subject to cyclic loading. *PCI Journal, 36*(3), 56-67.

Cheok, G. S., & Lew, H. S. (1993). Model precast concrete beam-to-column connections subject to cyclic loading. *PCI Journal, 38*(4), 80-92.

Cheok, G. S., & Stone, W. C. (1991). *Performance of 1/3-scale model precast concrete beam-column connections subjected to cyclic inelastic loads - report no. 2*. Gaithersburg, MD: National Institute of Standards and Technology.

Cheok, G. S., & Stone, W. C. (1993). *Performance of 1/3-scale model precast concrete beam-column connections subjected to cyclic inelastic loads - report no. 3*. Gaithersburg, MD: National Institute of Standards and Technology.

Cheok, G., Stone, W., Stanton, J., & Seagren, D. (1994). Beam-to-column connections for precast concrete moment-resisting frames, *Proc. 4th JTCC-PRESSS*. Tsukuba.

Cheung, P. C., Park, R., & Paulay, T. (1991). *Seismic Design of Reinforced Concrete Beam Column Joints with Floor Slab Support*. Research Report 91-4, Department of Civil Engineering, University of Canterbury, Christchurch.

Chopra, A. K. (2001). *Dynamics of structures: Theory and application to earthquake engineering* (2 ed.): Prentice Hall, Upper Saddle River, New Jersey.

Coffin, J. L. F. (1954). Study of effects of cyclic thermal stresses on ductile metal. *American Society of Mechanical Engineers - Transactions, 76*(6), 931-949.

Collins, M. P., & Mitchell, D. (1980). Shear and Torsion Design of Prestressed and Non-prestressed Concrete Beams. *PCI Journal, 25*(5), 32-101.

Corley, G. W. (1966) Rotation capacity of reinforced concrete beams. *ASCE Journal Structural Division, 92*(10), 121-146.

Davies, M. N. (2004). *Seismic damage avoidance design of beam-column joints using unbonded post-tensioning: Theory, experiments and design example*. Masters dissertation, Department of Civil Engineering, University of Canterbury, Christchurch, New Zealand.

Department of Building and Housing (2009) *Seismic Performance of Hollow Core Floor Systems: Guidelines for Design Assessment and Retrofit*. Preliminary draft publication prepared by SESOC, NZSEE, NZCS, and supported by the Department of Housing and Building, New Zealand.

Dhakal, R. P. (2000). *Enhanced fiber model in highly inelastic range and seismic performance assessment of reinforced concrete*. Doctoral Dissertation. Department of Civil Engineering, University of Tokyo, Japan.

Dhakal, R. P., & Maekawa, K. (2002). *Modeling for postyield buckling of reinforcement. Journal of Structural Engineering, 128*(9), 1139-1147.

Dhakal, R. P., & Maekawa, K. (2002). Path-dependent cyclic stress-strain relationship of reinforcing bar including buckling. *Engineering Structures, 24*(11), 1383-1396.

Dodd, L. L., & Restrepo-Posada, J. I. (1995). Model for Predicting Cyclic Behaviour of Reinforcing Steel. *Journal of Structural Engineering, ASCE, 121*(3), 433-445.

Eligehausen, R., Popov, E. P., & Bertero, V. V. (1983). *Local bond stress-slip relationships of deformed bar under generalized excitation*. Report UCB/EERC-83/23, Earthquake Engineering Research Centre, University of California, Berkeley.

Fédération internationale du béton (2000). *Bond of reinforcement in concrete: State of the art report*. CEB-FIB Bulletin 10, International Federation for Structural Concrete, Lausanne, Switzerland.

Fenwick, R. C., & Davidson, B. J. (1995) Elongation in ductile seismic-resistant reinforced concrete frames. *ACI SP-157, Recent Developments in Lateral Force Transfer in Buildings*, 143-170.

Fenwick, R. C., & Megget, L. M. (1993). Elongation and load deflection characteristics of reinforced concrete members containing plastic hinges. *Bulletin of the New Zealand National Society for Earthquake Engineering, 26*(1), 28-41.

Hall, J. F. (1995). Northridge earthquake of January 17, 1994 reconnaissance report. *Earthquake Spectra, 11*(S2), 1-514.

Harris, H. G. and Sabnis, G. M. (1999). *Structural Modeling and Experimental Techniques*. CRC Press, Boca Raton, London, New York and Washington D.C.

Housner, G. W. (1963). Behaviour of inverted pendulum structures during earthquakes. *Bulletin of the Seismological Society of America, 53*(2), 403-417.

Huang, Z., Engstrom, B., & Magnusson, J. (1996). *Experimental investigation of the Bond and Anchorage Behaviour of Deformed Bar in High Strength Concrete*. Chalmers University of Technology, Division of Concrete Structures, Report 95:4, Goteborg.

Kim, J. H., & Mander, J. B. (1999). *Truss Modeling of Reinforced Concrete Shear-Flexure Behaviour*. MCEER Technical Report, MCEER-99-0005, University at Buffalo, State University of New York.

King, D. J. (1986). *Computer programs for concrete column design*. Masters Thesis, University of Canterbury, Christchurch.

Koh, S. K., & Stephens, R. I. (1991). Mean stress effects on low cycle fatigue for a high strength steel. *Fatigue and Fracture of Engineering Materials and Structures, 14*(4), 413-428.

Krawinkler, H. (1983). Recommendations for experimental studies on the seismic behaviour of steel components and materials. *John A. Blume Centre Report No. 61*, Department of Civil Engineering, Stanford University.

Lau, D. B. N., Fenwick, R. C., & Davidson, B. J. (2007). *Influence of Precast Prestressed Flooring on the Seismic Performance of Reinforced Concrete Perimeter Frame Buildings*. School of Engineering Report No. 653, Department of Civil and Environmental Engineering, University of Auckland, Auckland, New Zealand.

Leslie, B. (2010). *The Development and Validation of a Non-tearing Floor Precast Concrete Structural System for Seismic Regions*. Masters Thesis, University of Canterbury, Christchurch, New Zealand.

Li, L. (2006). *Further experiments on the seismic performance of structural concrete beam-column joints designed in accordance with the principles of damage avoidance*. Masters dissertation, Department of Civil Engineering, University of Canterbury, Christchurch, New Zealand.

Lindsay, R. (2004). *Experiments on the seismic performance of hollow-core floor systems in precast concrete buildings*. Masters Dissertation, Department of Civil Engineering, University of Canterbury, Christchurch, New Zealand.

Maekawa, K., Pimanmas, A., & Okamura, H. (2003). *Nonlinear mechanics of reinforced concrete*. Spon Press, Taylor Francis Group, London and New York.

Mander, J. B., Priestley, M. J. N., & Park, R. (1984). *Seismic design of bridge piers.* Research Report No. 84-2, Department of Civil Engineering, University of Canterbury, Christchurch, New Zealand.

Mander, J. B., Priestley, M. J. N., & Park, R. (1988). Theoretical stress-strain model for confined concrete. *Journal of Structural Engineering, 114*(8), 1804-1826.

Mander, J. B., Priestley, M. J. N., & Park, R. (1988). Observed stress-strain behaviour of confined concrete. *Journal of Structural Engineering, 114*(8), 1827-1849.

Mander, J. B., Panthaki, F. D., & Kasalanati, A. (1994). *Low-cycle fatigue behaviour of reinforcing steel. Journal of Materials in Civil Engineering, 6*(4), 453-468.

Manson, S. S. (1953). Behaviour of materials under conditions of thermal stress. *National Advisory Committee for Aeronautics - Technical Notes, 105*.

Matthews, J. G. (2004). *Hollow-core floor slab performance following a severe earthquake*. PhD Thesis, Department of Civil Engineering, University of Canterbury, Christchurch.

Matthews, J. G., Bull, D. K., & Mander, J. B. (2003). Preliminary results from the testing of a precast hollow-core floor slab building. *Proceedings of the 2003 Pacific Conference on Earthquake Engineering*, Christchurch, New Zealand.

Mattock, A. H. (1967) Discussion of rotational capacity of reinforced concrete beams by W. D. G. Corley. *ASCE Journal Structural Division, 93*(2), 519-522.

Megget, L. M. & Fenwick, R. C. (1989). Seismic behaviour of a reinforced concrete portal frame sustaining gravity loads. *Bulletin of NZ National Society for Earthquake Engineering, 22*(1), 39-49.

Muir, C. (2009) *Comparison of strain hardening behaviour of non-tearing and traditional reinforced concrete beams*. Undergraduate Research Project Report, Department of Civil Engineering, University of Canterbury, Christchurch.

Miner, M. A. (1945). Cumulative damage in fatigue. *American Society of Mechanical Engineers - Journal of Applied Mechanics, 12*(3), 159-164.

Nakaki, S. D., Stanton, J. F., & Sritharan, S. (1999). An overview of the PRESSS five-storey precast test building. *PCI Journal, 44*(2), 26-39.

Ohkubo, M., & Hamamoto, T. (2004). Developing reinforced concrete slotted beam structures to reduce earthquake damage and to enhance seismic structural performance, *Proc. 13th World Conference on Earthquake Engineering*. Vancouver.

Ohkubo, M., Matsuoka, T., Yoshioka, T., & Anderson, D. L. (1999). Shear transfer mechanism of reinforced concrete beams with a slot at the beam-end. *Proc. Of Japan Concrete Institute, 21*(3), 301-306.

Palermo, A. (2004). *The use of controlled rocking in the seismic design of bridges*. PhD Dissertation. Technical University of Milan, Italy.

Palmieri, L., & French, C. (1996). *Evaluation of Ductile Connections for Precast Frame Systems - Volume 1*. PhD Dissertation, University of Minnesota.

Palmieri, L., & French, C. (1996). Performance of ductile connections in precast concrete frames, *Proc. 11th World Conference on Earthquake Engineering*. Acapulco.

Palmieri, L., Saqan, E., French, C., & Kreger, M. (1996). Ductile connections for precast concrete frame systems. *ACI, 162*, 313-356.

Pampanin, S. (2005). Emerging Solutions for High Seismic Performance of Precast/Prestressed Concrete Buildings. *Journal of Advanced Concrete Technology, 3*(2), 207-223.

Pampanin, S., Amaris, A., Akguzel, U. and Palermo, A. (2006) Experimental Investigations on High-Performance Jointed Ductile Connections for Precast Frames. *Proceedings of the First European Conference on Earthquake Engineering and Seismology (ECEES)*, Geneva, Switzerland, September 3-8.

Pampanin, S., Pagani, C., & Zambelli, S. (2004). Cable-stayed and suspended post-tensioned solution for precast concrete frames: The Brooklyn system. *Proc. of NZ Concrete Industry Conference, Queenstown*.

Pampanin, S., Priestley, M. J. N., & Sritharan, S. (2000). *PRESSS Phase 3: The five-storey precast test building vol. 3-4 - Frame direction response*. Report No. SSRP-2000/08. Department of Structural Engineering, University of California, San Diego.

Panagiotakos, T. B., & Fardis, M. N. (2001) Deformations of reinforced concrete members at yielding and ultimate. *ACI Structural Journal, 98*(2), 135-148.

Paulay, T., & Priestley, M. J. N. (1992). *Seismic design of reinforced concrete and masonry buildings*. New York: Wiley.

Park, R. (1986). Seismic design considerations for precast concrete construction in seismic zones. *Seminar on precast concrete construction, Japan Society for the Promotion of Science – United States National Science Foundation*, Tokyo, Vol. 1, p. 1-38.

Park, R. (2002). Seismic design and construction of precast concrete buildings in New Zealand. *PCI Journal, 47*(5), 60-75.

Park, R., & Paulay, T. (1975). *Reinforced Concrete Structures*. New York: John Wiley & Sons Inc.

Park, R., & Ruitong, D. (1988). A comparison of the behaviour of reinforced concrete beam-column joints designed for ductility and limited ductility. *Bulletin of the New Zealand National Society for Earthquake Engineering, 21*(4), 255-278.

Peng, B. H., Fenwick, R. C., Dhakal, R. P. & Bull, D. K. (2008). Experimental study on the seismic performance of RC moment resisting frames with precast-prestressed floor units. *Proceedings of the New Zealand Society of Earthquake Engineering Annual Conference*, Taupo, New Zealand.

Peng, B. H. H., Dhakal, R. P., Fenwick, R. C., & Carr, A. J. (2009). Modelling of RC moment resisting frames with precast-prestressed flooring system. *Proceedings of the 2009 New Zealand Society for Earthquake Engineering, Christchurch*, New Zealand, April 3-5.

Peng, B. H. H. (2009). *Seismic performance assessment of reinforced concrete buildings with precast concrete floor systems*. PhD Thesis, Department of Civil and Natural Resources Engineering, University of Canterbury, Christchurch, New Zealand.

Priestley, M. J. N. (1991). Overview of PRESSS research program. *PCI Journal, 36*(4), 50-57.

Priestley, M. J. N., Calvi, G. M., & Kowalsky, M. J. (2007). *Displacement-based seismic design of structures*. Pavia, Italy: IUSS Press.

Priestley, M. J. N., & MacRae, G. A. (1996). Seismic tests of precast beam-to-column joint subassemblages with unbonded tendons. *PCI Journal, 41*(1), 64-80.

Priestley, M. J. N., Sritharan, S., Conley, J. R., & Pampanin, S. (1999). Preliminary results and conclusions from the PRESSS five-storey precast concrete test building. *PCI Journal, 44*(6), 42-67.

Priestley, M. J. N., & Tao, J. R. T. (1993). Seismic response of precast prestressed concrete frames with partially debonded tendons. *PCI Journal, 38*(1), 58-69.

Ramberg, W., & Osgood, W. R. (1943). *Description of stress-strain curves by three parameters*. Technical Note No. 902, National Advisory Committee for Aeronautics, Washington DC

Restrepo, J., Park, R. & Buchanan, A. (1990). *Seismic load tests on mid-span connections between precast concrete beams*. NZ Concrete Society, Technical Report TR10, 55-71.

Rodriguez, M. E., Botero, J. C., & Villa, J. (1999). Cyclic stress-strain behaviour of reinforcing steel including effect of buckling. *Journal of Structural Engineering, 125*(6), 605-612.

SEAOC Vision 2000 Committee. (1995). *Performance-based seismic engineering*. Structural Engineers Association of California, Sacramento, California.

Spieth, H. A., Carr, A. J., Pampanin, S., Murahidy, A. G., & Mander, J. B. (2004). *Modelling of Precast Prestressed Concrete Frame Structures with Rocking Beam-Column Connections*. Research report 2004-01, University of Canterbury, Christchurch.

Srinivas, M., & Kamat, S. V. (2001). Effect of strain rate on fracture toughness of mild steel. *Materials Science and Technology, 17*(5), 529-535.

Standards Association of New Zealand (2006). *Concrete Structures Standard.* New Zealand Standard NZS3101, Wellington, New Zealand.

Standard Association of New Zealand (2002-04). *Structural Design Actions*. New Zealand Standard NZS1170, Wellington, New Zealand.

Stone, W. C., Cheok, G. S., & Stanton, J. F. (1995). Performance of hybrid moment-resisting precast beam-column concrete connections subjected to cyclic loading. *ACI Structural Journal (American Concrete Institute), 92*(2), 229.

Thompson, K. J., & Park, R. (1978). Stress-strain model for Grade 275 reinforcing steel with cyclic loading. *Bulletin of the New Zealand National Society for Earthquake Engineering, 111*(2), 101-109.

Vandewalle, L. (1992). Theoretical prediction of the ultimate bond strength between a reinforcement bar and concrete. *Comité euro-international du béton, Internacional conference: bond in concrete: from research to practice*, Riga, Latvia, October 15-17.

Wyllie, L. A., & Filson, J. R. (1989). Armenia Earthquake Reconnaissance Report. *Earthquake Spectra, EERI Pub. 89-101*(Special supplement).

Zerke, H. E. & Durrani, A. J. (1989). Seismic response of connections in two bay reinforced concrete frame subassemblies. *ASCE Journal of Structural Engineers, 11*(4), 2829-2844.

Zerke, H. E. & Durrani, A. J. (1990). Seismic response of connections in two bay reinforced concrete frame subassemblies with a floor. *ACI Structural Journal, 87*(4), 406-415.

Zhu, S., & Jirsa, J. O. (1983). *Study of bond deterioration in reinforced concrete beam-column joints.* PMFSEL Report No. 83-1, Department of Civil Engineering, University of Texas at Austin.

APPENDIX A PROCESSING OF EXPERIMENTAL RESULTS

A.1 Crack Observation

To allow clear observation and recording of cracks, the specimens were painted white and a 50 mm by 50 mm grid drawn on each face. At the peak drifts of the first and third loading cycles, cracks were marked in blue and red for positive and negative loading respectively. Crack widths were recorded and photos taken of the specimen.

A.2 Peak-to-peak Stiffness Degradation

Peak-to-peak secant stiffness is a measure often used to observe the degradation of strength and stiffness with drift. It is defined below:

$$k_p = \frac{F_{+ve} - F_{-ve}}{\Delta_{+ve} - \Delta_{-ve}} \qquad \text{...(A- 1)}$$

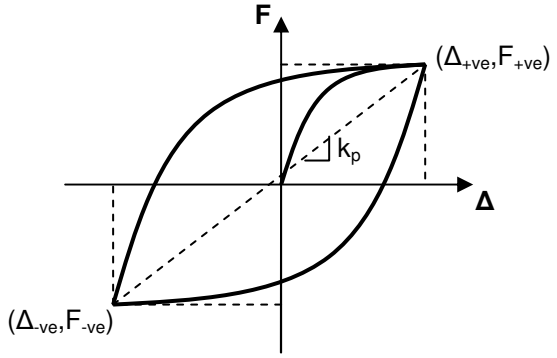

Figure A- 1: Peak-to-peak secant stiffness

A.3 Energy Dissipated per Cycle

The hysteretic energy dissipated each drift cycle during testing, E_D, can be computed by numerically integrating the area within the force-displacement response. This is expressed mathematically in Equation A-2.

$$E_D = \sum_{cycle} (\Delta_{i+1} - \Delta_i) \frac{(F_i + F_{i+1})}{2} \qquad \text{...(A- 2)}$$

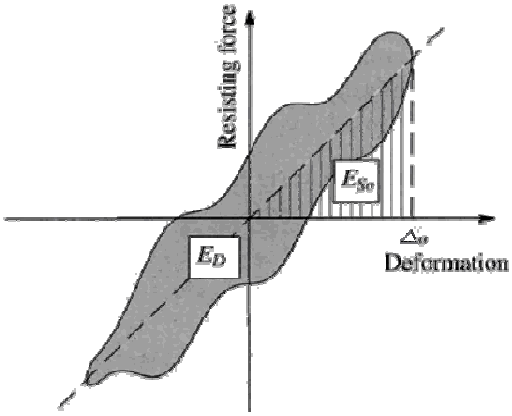

Figure A- 2: Hysteretic energy dissipated in a cycle of harmonic vibration determined from experiment (Chopra, 2001)

Due to the complexity of hysteretic damping models, it is common to express the energy dissipated as equivalent viscous damping. This is done by equating the hysteretic energy dissipated to the energy dissipated by an elastic system with the same amplitude. The following expression for equivalent viscous damping, ξ_{eq}, is given in Chopra (2001):

$$\xi_{eq} = \frac{1}{4\pi}\frac{E_D}{E_{So}} \qquad \text{...(A- 3)}$$

$$\text{where : } E_{So} = k\Delta_o^{\,2}/2$$

E_{So} is the strain energy, Δ_o is the peak displacement of the cycle and k is the secant stiffness determined from the experiment.

A.4 Measured Beam Elongation

The beam elongation measured at the beam centreline was calculated using the horizontal linear potentiometers crossing the beam-column interface or slot as given below:

$$\delta_{el} = \frac{\delta_{bottom} - \delta_{top}}{2} \qquad \text{...(A- 4)}$$

δ_{top} and δ_{bottom} are the deformations in the top and bottom potentiometers respectively, taking the average of which gives the measured beam elongation. Potentiometer extension and beam elongation was taken as positive. Theoretically beam elongation can be calculated from the difference in displacements measured by rotary potentiometers attached to the beam ends and joint, however later processing of these measurements revealed unusual results.

A.5 Estimation of Vertical Sliding across Slotted-section

Vertical sliding of the beam across the slotted-section was measured using spring potentiometers placed on the underside of the beam. To remove the component of vertical movement resulting from beam end-rotation, the following formula was used:

$$\Delta_{bv} = \delta_{pot,v} - x_{pot}\theta_b \qquad \text{...(A- 5)}$$

Where Δ_{bv} is the vertical movement across the slotted-section, $\delta_{pot,v}$ is the measured displacement in the spring potentiometer, x_{pot} is the horizontal distance of the potentiometer from the column face and θ_b is the measured beam end-rotation as given by Equation A-9. Spring potentiometers were placed on the top face of the beam, however due to lifting of the concrete from Poisson's ratio effect and spalling, data from these instruments were not usable.

A.6 Decomposition of Lateral Displacement

The lateral displacement of the specimen measured at the top of the column can be decomposed into the various deformation contributions from column flexure, beam flexure, beam fixed-end rotation and joint shear as shown in Figure A- 3 and Equation A-6. This section describes the method used to estimate each of these sources of deformation. Note that due to sufficient shear reinforcement being provided, column and beam shear deformations have been assumed sufficiently small to be neglected.

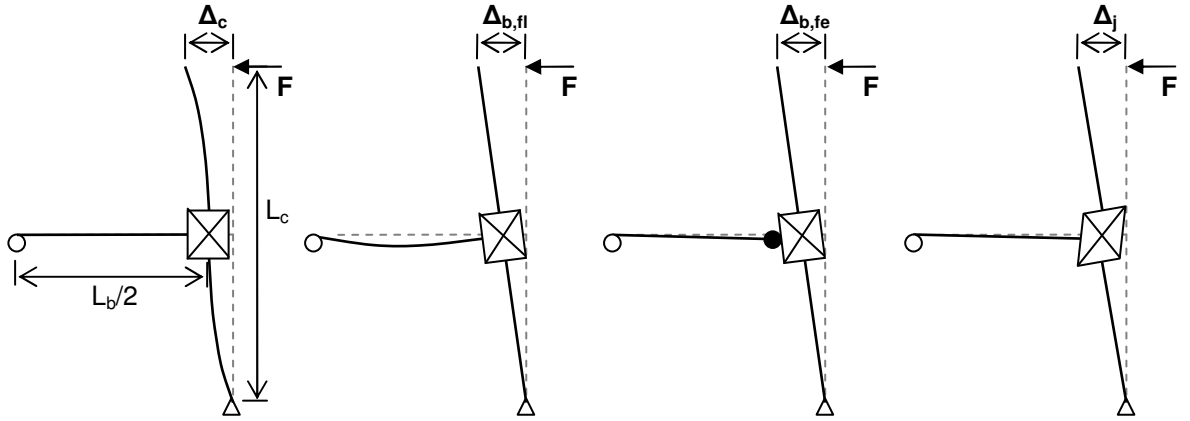

(a) Column Flexure (b) Beam flexure (c) Beam fixed-end rotation (d) Joint shear

Figure A- 3: Decomposition of lateral displacement

$$\Delta_{total} = \Delta_c + \Delta_{b,fl} + \Delta_{b,fe} + \Delta_j \quad \text{...(A- 6)}$$

Column Flexure

Moment-area theorem can be used to derive the following expression for the deformation due to elastic column flexure:

$$\Delta_c = \frac{F(L_c - h_b)^3}{12E_cI_c} \quad \text{...(A- 7)}$$

F is the lateral force applied at the top of the column, L_c and L_b are column and beam lengths as shown in Figure A- 3 and h_b is the beam depth. E_c is the elastic modulus of the concrete which was taken as E_c=3320$\sqrt{f'_c}$+6900 from NZS3101:2006. I_c is the effective column moment of inertia, as calculated from Response-2000 – a reinforced concrete moment-curvature analysis program (Bentz, 2000).

Beam Flexure

Similarly, moment-area theorem can be used to derive the following expression for the deformation due to elastic beam flexure:

$$\text{Exterior joint}: \Delta_{b,fl} = F\left(\frac{L_c}{L_b}\right)^2 \frac{(L_b - h_c)^3}{6E_cI_b}$$
$$\text{Interior joint}: \Delta_{b,fl} = F\left(\frac{L_c}{L_b}\right)^2 \frac{(L_b - h_c)^3}{12E_cI_b} \quad \text{...(A- 8)}$$

h_c is the column depth and I_b is the effective beam moment of inertia. Note that due to greater top longitudinal reinforcement in slotted-beam specimens, the beam sections were stiffer for negative (gap-closing) drifts. For specimens SB1 and SB2, I_b was taken as $0.33I_g$ for positive drifts and $0.47I_g$ for negative drifts as calculated from Response-2000 (Bentz, 2000).

Beam Fixed-end Rotation

The beam fixed-end rotation was estimated using the horizontal linear potentiometers crossing the beam-column interface or slot as given below:

$$\theta_b = \frac{\delta_{bottom} - \delta_{top}}{h_p} \quad \text{...(A- 9)}$$

δ_{top} and δ_{bottom} are the deformations in the top and bottom potentiometers respectively and h_p is the vertical distance between them. From geometry, the resulting lateral displacement at the top of the column is then:

$$\Delta_{b,fe} = \frac{L_c}{L_b}\theta_b (L_b - h_c) \qquad \text{...(A- 10)}$$

Joint Shear

Joint shear deformation was estimated using five of the six potentiometers placed on the joint as given in Figure A- 4 and Equation A-11.

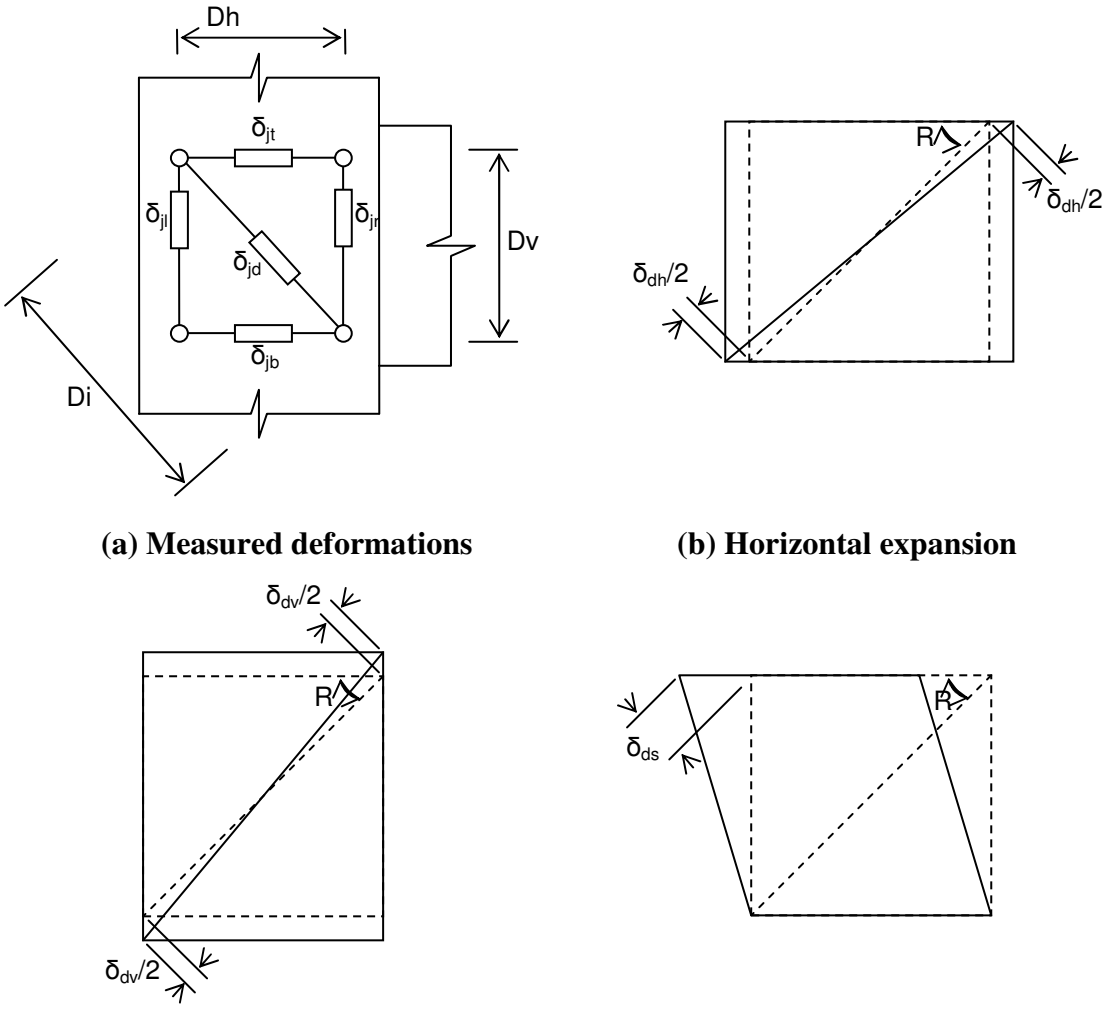

(a) Measured deformations **(b) Horizontal expansion**

(c) Vertical expansion **(d) Shear deformation**

Figure A- 4: Estimation of joint shear deformation

$$\text{Joint shear distortion}: \gamma_j = \frac{\Delta_s}{Dv}$$

$$\begin{aligned} \text{where}: \quad \Delta_s &= \frac{|\delta_{ds}|}{\cos R} \\ \delta_{ds} &= \delta_{jd} - \delta_{dh} - \delta_{dv} \\ \delta_{dh} &= \frac{\delta_{jt} + \delta_{jb}}{2} \cos R \\ \delta_{dv} &= \frac{\delta_{jl} + \delta_{jr}}{2} \sin R \end{aligned} \qquad \text{...(A- 11)}$$

As depicted in Figure A- 5, the resulting lateral displacement at the top of the column due to joint deformation can then be computed as:

$$\begin{aligned} \Delta_j &= \gamma_1 (L_b - h_c) \frac{L_c}{L_b} + \gamma_2 (L_c - h_b) - \gamma_2 h_c \frac{L_c}{L_b} - \gamma_1 h_b \\ &= \gamma_j \left(L_c - h_c \frac{L_c}{L_b} \right) - \gamma_j h_b \end{aligned} \qquad \text{...(A- 12)}$$

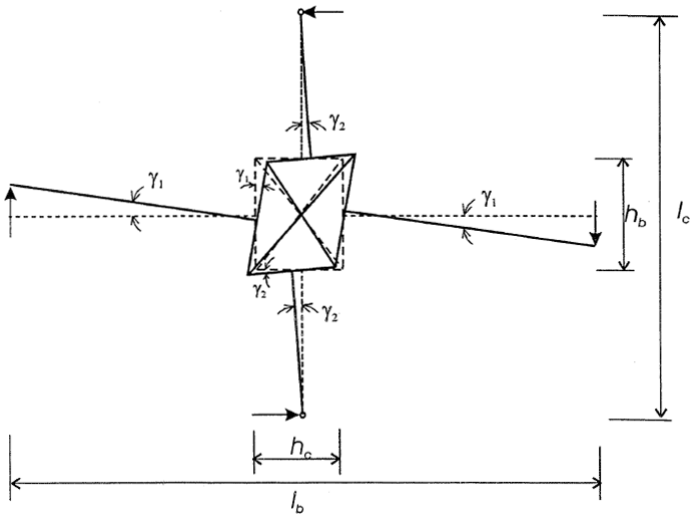

Figure A- 5: Lateral displacement due to joint shear deformation

To allow experimental results to be compared to theoretical predictions, elastic joint deformation also needed to be estimated from existing theory. From equilibrium, horizontal joint shear force, V_{jh}, can be written as:

$$\text{Exterior joint : } V_{jh} = \frac{M_b}{jd}\left(1 - \frac{L_b}{L_c}\frac{jd}{(L_b - h_c)}\right)$$
$$\text{Interior joint : } V_{jh} = \frac{M_b}{jd}\left(1 - \frac{L_b}{L_c}\frac{jd}{(L_b - h_c)}\right) \qquad \text{...(A- 13)}$$

Where M_b is the beam moment at the column face and jd is the moment lever arm which was approximated at $0.9d$. A full derivation of this equation from equilibrium is given in Matthews (2004).

Using a variable angle truss model for reinforced concrete beam-columns, Kim and Mander (1999) derived the following simplified solution for the cracked elastic shear stiffness:

$$K_j = \frac{\rho_v n \cot^2 \alpha}{1 + 4\rho_v n\left(\frac{b_w}{b_{ws}}\right)(1 + 0.39\cot^2 \alpha)^2} E_c A_j \qquad \text{...(A- 14)}$$

Where :

$\rho_v = \text{beam - column joint steel ratio } = \dfrac{A_{sh}}{b_w s}$

$n = \dfrac{E_s}{E_c}$

$\alpha = \text{aspect ratio of the joint}$

$A_j = \text{Horizontal cross sectional area of the joint}$

$\dfrac{b_w}{b_{ws}} = \dfrac{V_s + V_c + V_p}{V_s}$

$V_s = A_{sh} f_{yh} jd / s$

$V_c = 0.2\sqrt{f'_c}\, b_w d$

$V_p = \text{axial compression force on joint}$

Knowing V_{jh} and K_j, the theoretical joint shear deformation can then be computed (Matthews, 2004):

$$\gamma_j = \frac{V_{jh}}{K_j} \qquad \text{...(A- 15)}$$

A.7 Neutral Axis Depth Estimation

Three horizontal linear potentiometers crossing the slot in specimens SB1 and SB2 were used to measure flexural deformations and interpolate the neutral axis depth using the following formula:

$$c = \frac{\delta_1 d_2 - \delta_2 d_1}{\delta_1 - \delta_2} \qquad \text{...(A- 16)}$$

δ_1 and δ_2 are the measured deformations in the potentiometers immediately above and below the neutral axis respectively, and d_1 and d_2 are the distances to the respective potentiometers from the top fibre of the beam.

A.8 Component Deformation Estimation

Three horizontal linear potentiometers crossing the slot in specimens SB1 and SB2 were used to interpolate the deformations in the longitudinal reinforcement and at the extreme concrete compression fibre using the following formula:

$$\Delta_{component} = \delta_1 + \frac{(\delta_2 - \delta_1)}{(d_2 - d_1)}(d_{component} - d_1) \qquad \text{...(A- 17)}$$

δ_1 and δ_2 are the measured deformations in the potentiometers nearest the steel/concrete component considered, d_1 and d_2 are the distances to the respective potentiometers from the top fibre of the beam, and $d_{component}$ is the distance to the steel/concrete component considered from the top of the beam.

APPENDIX B EXPERIMENTAL TESTING PHOTOGRAPHIC LOG

This appendix provides additional photographs illustrating the development of cracks and damage in the tested specimens.

B.1 Specimen RCB1

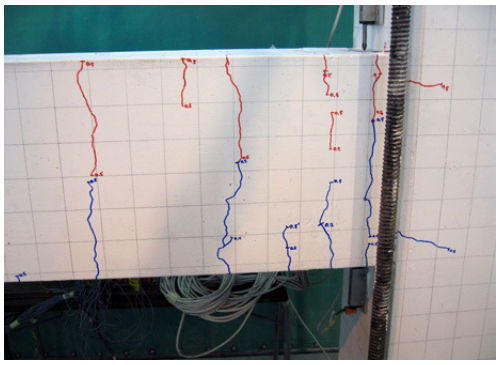

(a) Drift = 0.5%

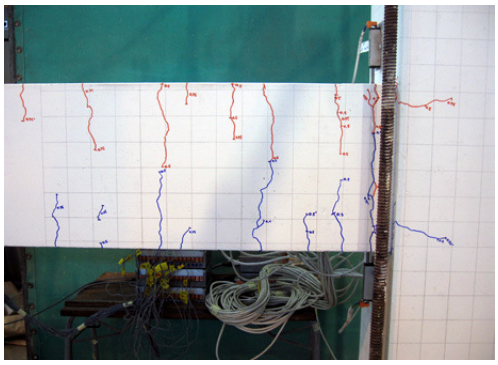

(b) Drift = 0.75%

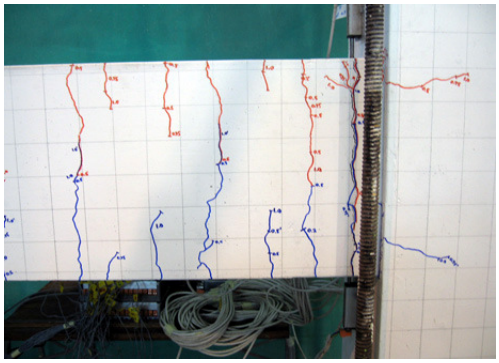

(c) Drift = 1.0%

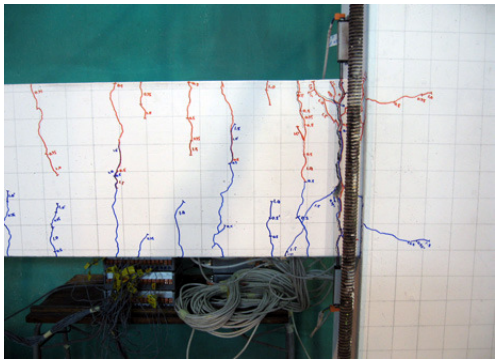

(d) Drift = 1.5%

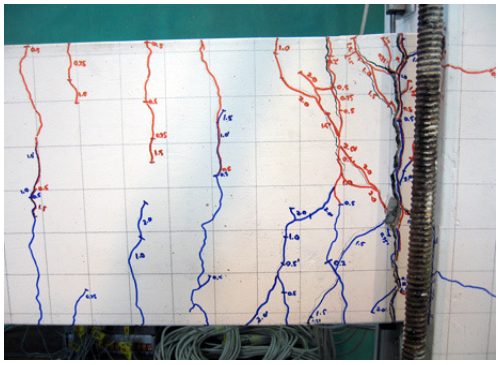

(e) Drift = 2.0%

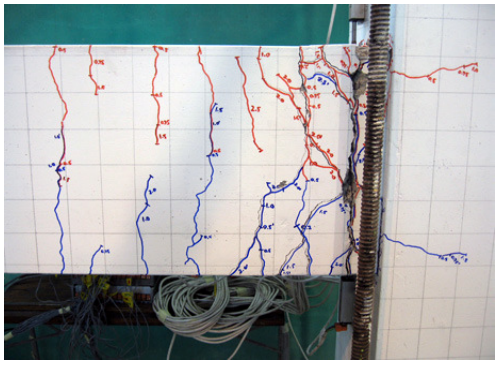

(f) Drift = 2.5%

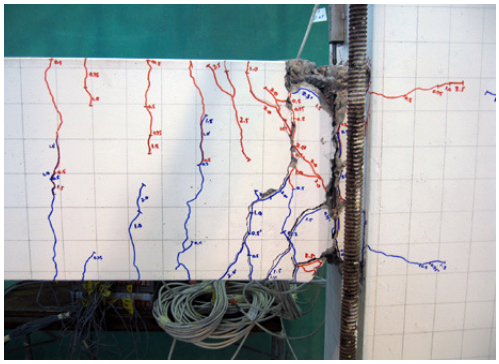

(g) Drift = 3.5%

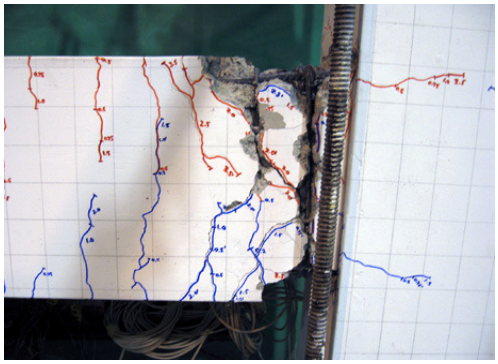

(h) Drift = 4.5%

Figure B- 1: Crack development in monolithic specimen RCB1

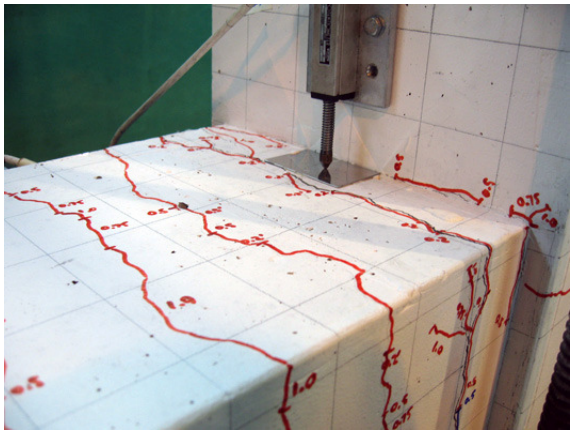

(a) Top of beam at 1.0% drift (SLS)

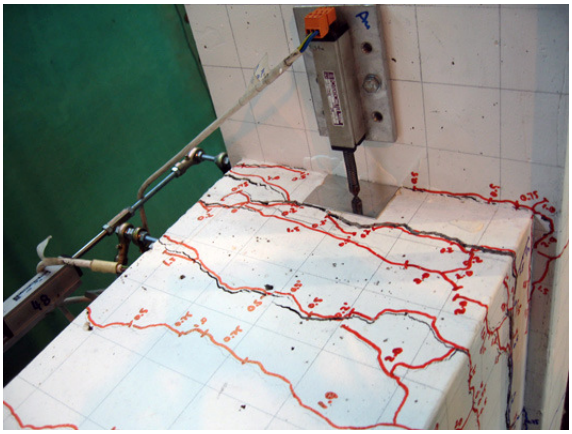

(b) Top of beam at 2.0% drift (Design ULS)

(c) Spalling at 2.5% drift

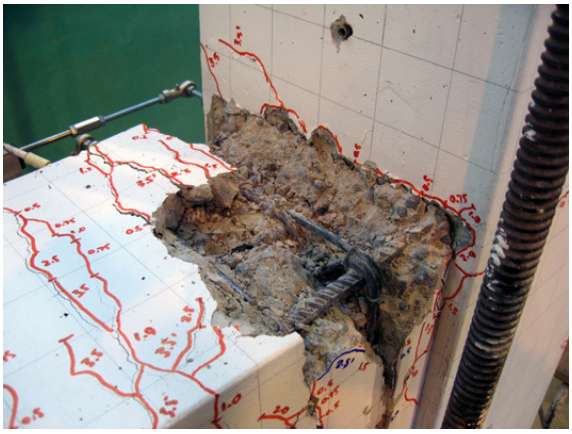

(d) Severe spalling at 3.5% drift

Figure B- 2: Damage highlights in monolithic specimen RCB1

B.2 Specimen SB1

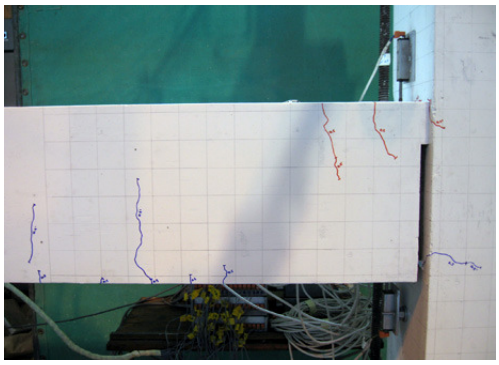

(a) Drift = 0.5%

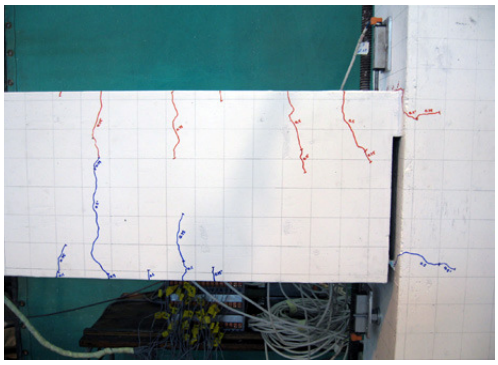

(b) Drift = 0.75%

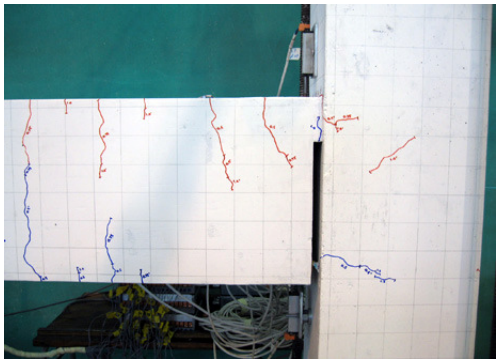

(c) Drift = 1.0%

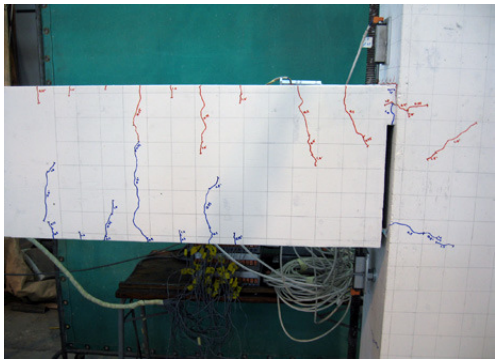

(d) Drift = 1.5%

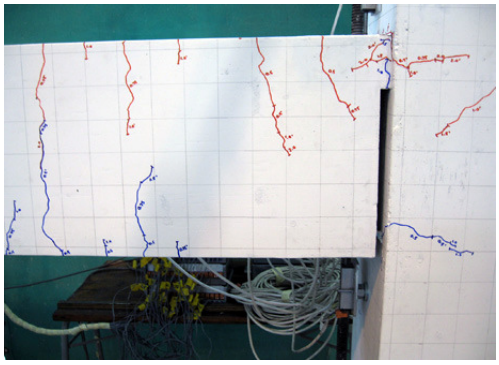

(e) Drift = 2.0%

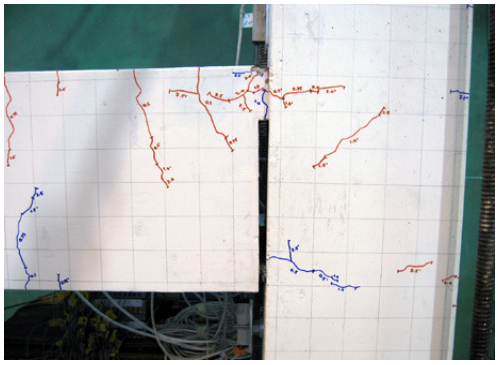

(f) Drift = 2.5%

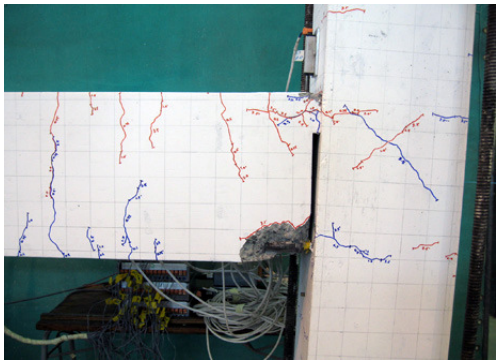

(g) Drift = 3.5%

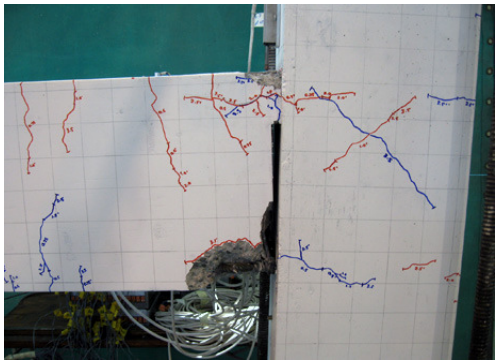

(h) Drift = 4.5%

Figure B- 3: Crack development in slotted specimen SB1

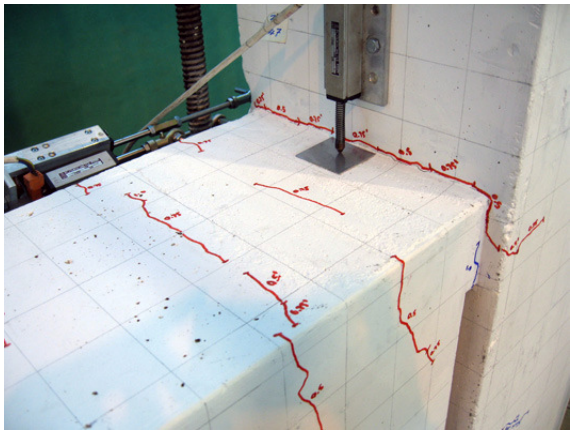

(a) Top of beam at 1.0% drift (SLS)

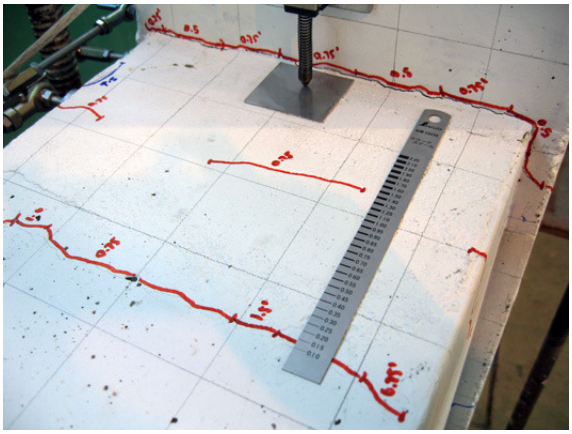

(b) Top of beam at 2.0% drift (Design ULS)

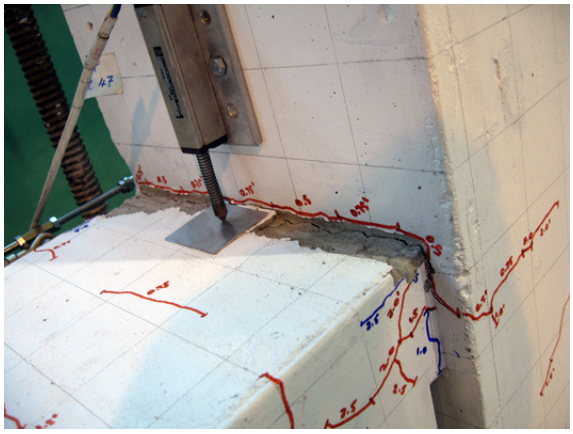

(c) Top of beam at 2.5% drift

(d) Bar buckling at 3.5% drift

Figure B- 4: Damage highlights in slotted specimen SB1

B.3 Specimen SB2

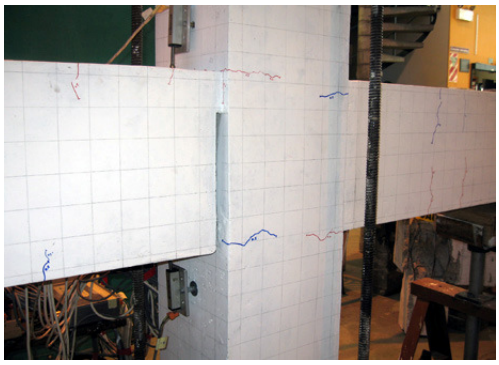

(a) Drift = 0.5%

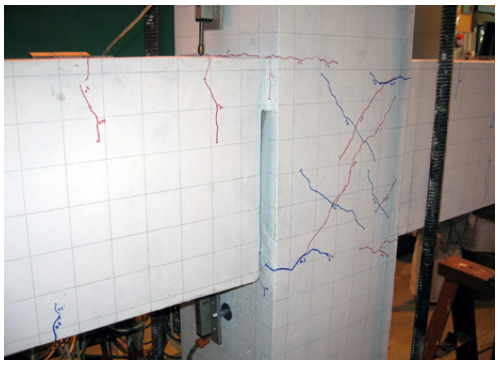

(b) Drift = 0.75%

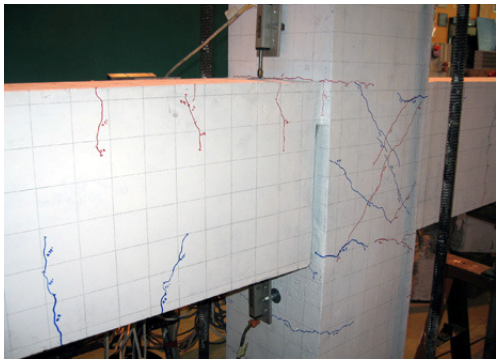

(c) Drift = 1.0%

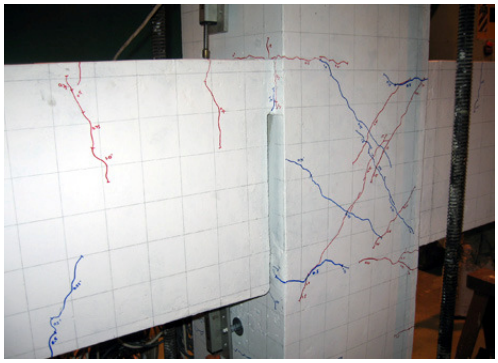

(d) Drift = 1.5%

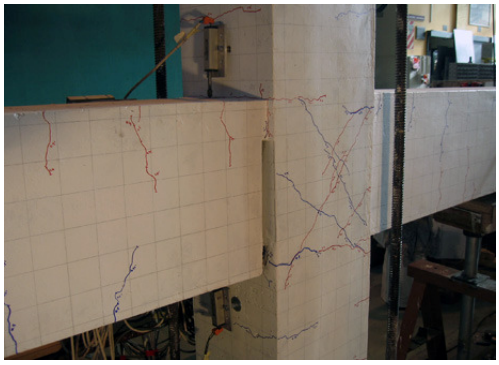

(e) Drift = 2.0%

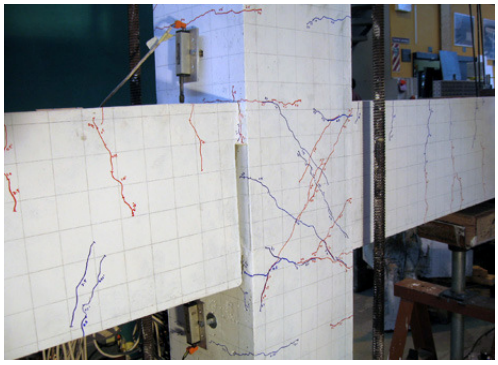

(f) Drift = 2.5%

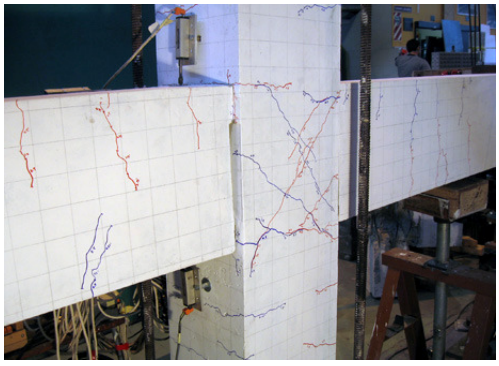

(g) Drift = 3.5%

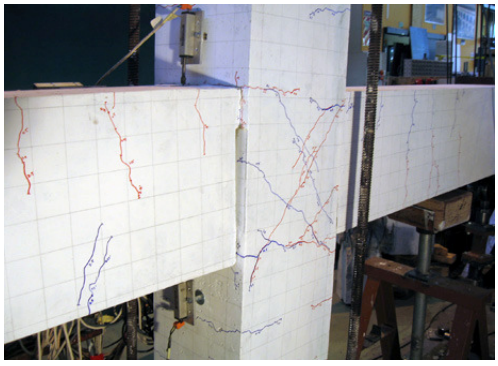

(h) Drift = 4.5%

Figure B- 5: Crack development in slotted specimen SB2

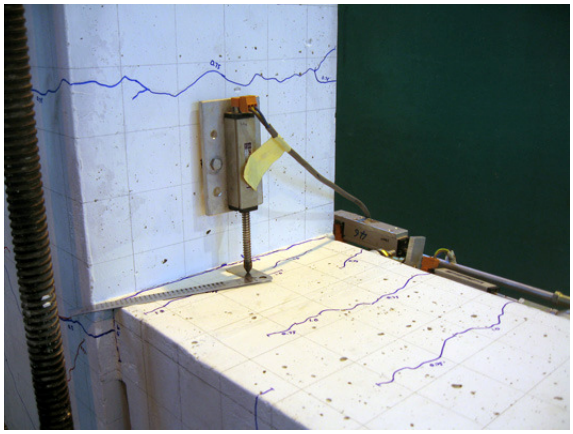

(a) RHS beam at 1.0% drift (SLS)

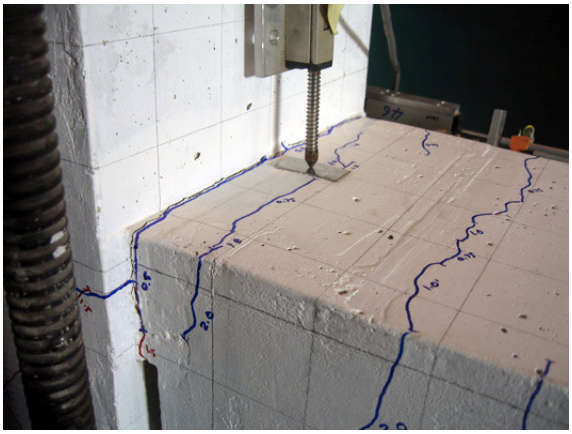

(b) RHS beam at 2.0% drift (Design ULS)

(c) Bond-slip/cone pullout at 2.5% drift

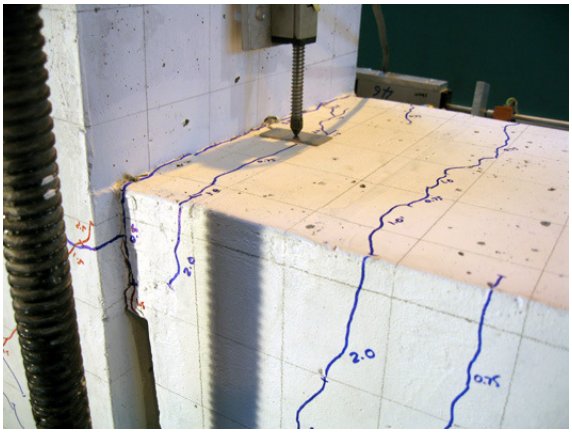

(d) RHS beam at 3.5% drift

Figure B- 6: Damage highlights in slotted specimen SB2

B.4 Specimen SB3

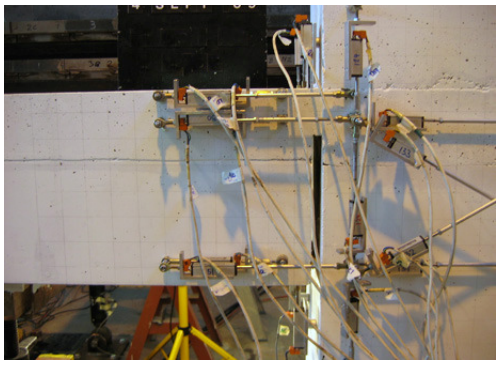

(a) Drift = 0.5%

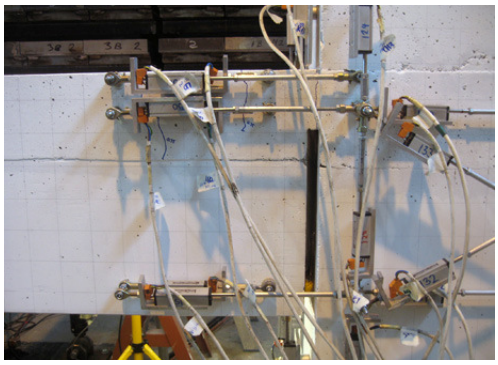

(b) Drift = 0.75%

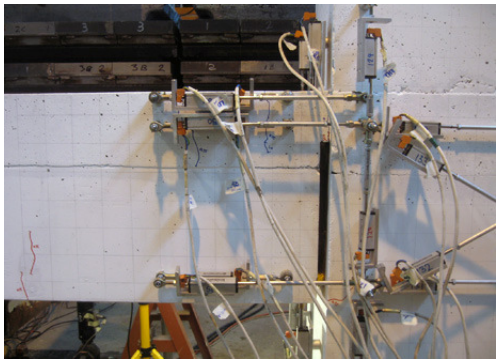

(c) Drift = 1.0%

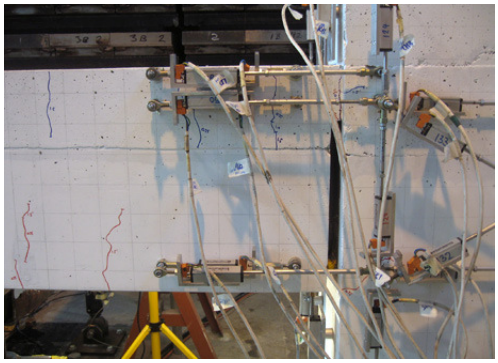

(d) Drift = 1.5%

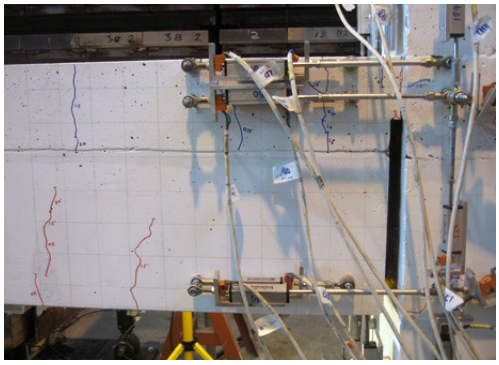

(e) Drift = 2.0%

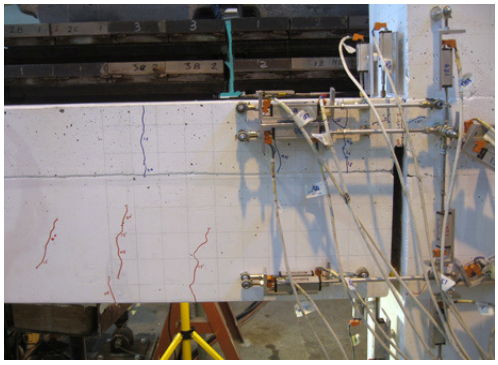

(f) Drift = 2.5%

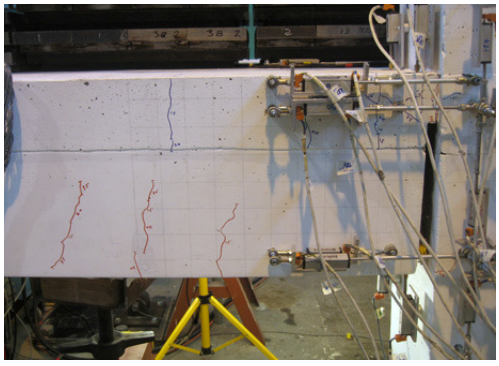

(g) Drift = 3.5%

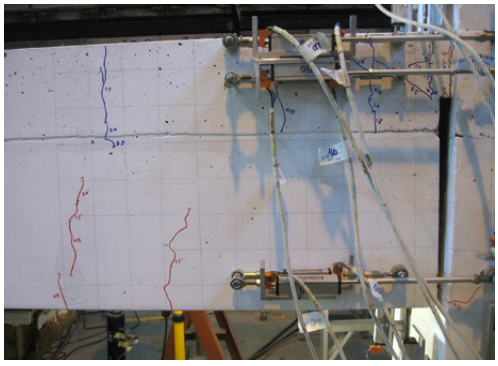

(h) Drift = 4.5%

Figure B- 7: Crack development on back face of slotted specimen SB3 RHS beam

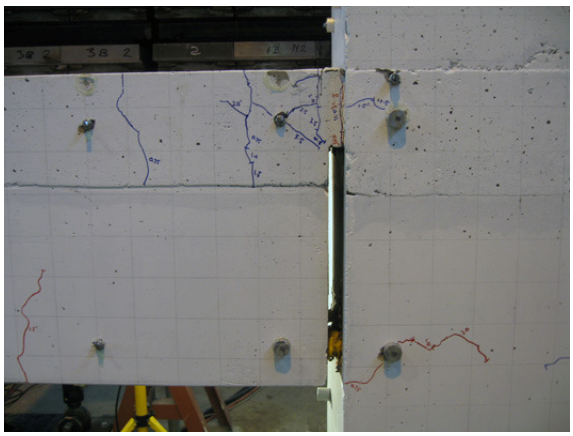

(a) Back face of RHS beam

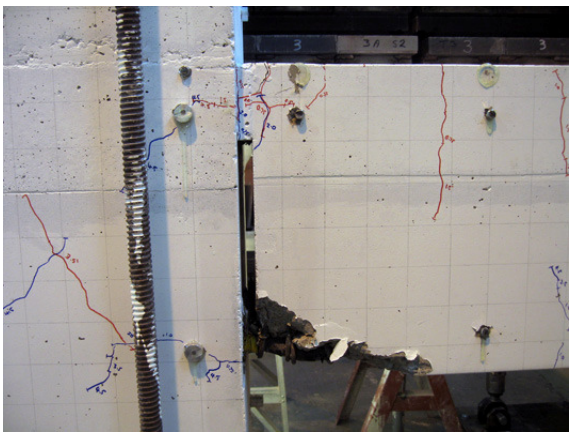

(b) Back face of LHS beam

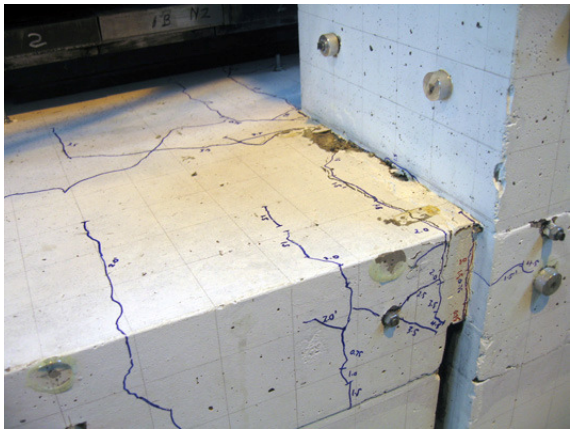

(d) Top of RHS beam

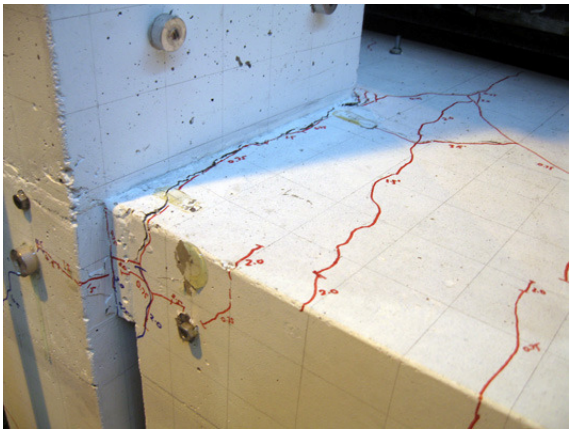

(e) Top of LHS beam

(f) Top of floor slab

Figure B- 8: Damage in slotted specimen SB3 after testing

APPENDIX C DATAFILES FOR RUAUMOKO2D MODELS

C.1 Subassembly Model of Specimen SB1

```
SPECIMEN SB1 MULTI-SPRING MODEL
* Units: kN, m, Seconds

! IPANL IFMT    IPLAS   IPCONM  ICTYPE  IPVERT  INLGEO  IPNF    IZERO   ORTHO   IMODE
  8     0       1       0       2       1       1       0       0       0       0
! NNP   NMEM    NTYPE   M       MODE1   MODE2   GRAV    C1      C2      DT      TIME    FACTOR
  30    14      10      3       1       2       9.81    5       5       0.002   1025    1
! KP    KPA     KPLOT   JOUT    DSTORT  DFACT   XMAX    YMAX    NLEVEL  NUP     IRESID  KDUMP
  0     250     250     0       1       1       0.5     0.5     2       2       0       0
! MAXIT MAXCIT  FTEST   WAVEX   WAVEY   THETA   DXMAX   DYMAX   D       OMEGA   F
  10    10      0.0001  0       0       0       0.5     0.5

NODES
! N     X       Y       Nx      Ny      Nr      Kup-x   Kup-y   Kup-r   IOUT
  1     1.5     0       1       1       0       0       0       0       0       ! Column base
  2     1.5     0.835   1       1       1       0       0       0       0
  3     1.5     1       0       0       0       0       0       0       0       ! Joint centre
  4     1.5     1.165   1       1       1       0       0       0       0
  5     1.5     2       0       0       0       -1      0       0       0       ! Column top
  6     1.343   1       0       0       0       0       0       0       0       ! Beam slot end
  7     0       1       0       1       0       0       0       0       0       ! Beam free end
  8     1.402   0.865   1       1       1       0       0       0       0       ! Bottom steel
  9     1.069   0.865   1       1       1       0       0       0       0
  10    1.485   1.135   1       1       1       0       0       0       0       ! Top steel
  11    1.231   1.135   1       1       1       0       0       0       0
  12    1.358   1.128   1       1       1       0       0       0       0       ! Shear spring
  13    1.343   1.128   1       1       1       0       0       0       0
  14    1.453   1.165   1       1       1       0       0       0       0       ! Concrete hinge 1
  15    1.263   1.165   1       1       1       0       0       0       0
  16    1.453   1.156   1       1       1       0       0       0       0       ! Concrete hinge 2
  17    1.263   1.156   1       1       1       0       0       0       0
  18    1.453   1.138   1       1       1       0       0       0       0       ! Concrete hinge 3
  19    1.263   1.138   1       1       1       0       0       0       0
  20    1.453   1.117   1       1       1       0       0       0       0       ! Concrete hinge 4
  21    1.263   1.117   1       1       1       0       0       0       0
  22    1.453   1.099   1       1       1       0       0       0       0       ! Concrete hinge 5
  23    1.263   1.099   1       1       1       0       0       0       0
  24    1.453   1.090   1       1       1       0       0       0       0       ! Concrete hinge 6
  25    1.263   1.090   1       1       1       0       0       0       0
  26    1.388   1.183   1       1       1       0       0       0       0       ! Diagonal strut 1
  27    1.265   1.046   1       1       1       0       0       0       0
  28    1.388   1.063   1       1       1       0       0       0       0       ! Diagonal strut 2
  29    1.325   1.135   1       1       1       0       0       0       0
  30    1.495   0       1       1       1       0       0       0       0       ! Dummy node

DRIFT ANGLE
  1     5

ELEMENTS
! N     MT      I       J       i       j       IOUT
  1     1       1       3       0       2       0       ! Bottom column
  2     1       3       5       4       0       0       ! Top column
  3     2       6       7       0       0       0       ! Beam
  4     3       3       6       8       9       0       ! Bottom steel
  5     4       3       6       10      11      0       ! Top steel
  6     5       3       6       12      13      0       ! Shear spring
  7     6       3       6       14      15      0       ! Concrete hinge spring 1
  8     7       3       6       16      17      0       ! Concrete hinge spring 2
  9     8       3       6       18      19      0       ! Concrete hinge spring 3
  10    8       3       6       20      21      0       ! Concrete hinge spring 4
  11    7       3       6       22      23      0       ! Concrete hinge spring 5
  12    6       3       6       24      25      0       ! Concrete hinge spring 6
  13    9       1       30      0       0       0       ! Diagonal strut 1
  14    10      1       30      0       0       0       ! Diagonal strut 2

PROPS
! N     MTYPE   LABEL
  1     FRAME   'Column'
! ITYPE IPIN    ICOND   IHYST   ILOS    IDAMG   ICOL    IGA     IDUCT
  2     0       0       4       0       0       3       0       0
! E     G       A       AS      I       WGT     END1    END2    FJ1     FJ2
  25E6  10.4E6  0.0807  0.0721  2.54E-4 2.02    0.000   0.000   0.000   0.000
! RA    RF      H1      H2
  0.01  0.01    0.211   0.211
```

```
! PYC   PB      MB      M1B     M2B     M0      PYT     IEND
  -2871 -2000   67.5    103.3   109.3   62.2    678     0
! ALFA  BETA    NF      KKK
  0.25  0.45    1       2

! N     MTYPE   LABEL
  2     FRAME   'Beam'
! ITYPE IPIN    ICOND   IHYST   ILOS    IDAMG   ICOL    IGA     IDUCT
  1     0       0       0       0       0       0       0       0
! E     G       A       AS      I       WGT     END1    END2    FJ1     FJ2
  25E6  10.4E6  0.0825  0.0750  3.13E-4 2.06    0.000   0.000   0.000   0.000

! N     MTYPE   LABEL
  3     SPRING  'Bottom steel'
! ITYPE IHYST   ILOS    IDAMG   KX      KY      GJ      WGT     RF      RT      PSX     PSY     PSZ
        THETA   ITRUSS  IOP     SL
  1     39      0       0       264500  0       0       0.035   0       0       0       0       0
        0       0       0       0
! FX+   FX-     FY+     FY-     MZ+     MZ-
  149.3 -149.3  0       0       0       0
! ESH   ESU     FSU     OMEGAF
 0.0033 0.0625  209.2   1.0

! N     MTYPE   LABEL
  4     SPRING  'Top steel'
! ITYPE IHYST   ILOS    IDAMG   KX      KY      GJ      WGT     RF      RT      PSX     PSY     PSZ
        THETA   ITRUSS  IOP     SL
  1     39      0       0       582300  0       0       0.062   0       0       0       0       0
        0       0       0       0
! FX+   FX-     FY+     FY-     MZ+     MZ-
  435.9 -435.9  0       0       0       0
! ESH   ESU     FSU     OMEGAF
 0.0035 0.0381  551.6   1.0

! N     MTYPE   LABEL
  5     SPRING  'Shear spring'
! ITYPE IHYST   ILOS    IDAMG   KX      KY      GJ      WGT     RF      RT      PSX     PSY     PSZ
        THETA   ITRUSS  IOP     SL
  1     39      0       0       0       178472  0       0.017   0       0       0       0       0
        0       0       0       0
! FX+   FX-     FY+     FY-     MZ+     MZ-
  52.8  -52.8   0       0       0       0
! ESH   ESU     FSU     OMEGAF
 0.0017 0.0328  104.6   1.0

! N     MTYPE   LABEL
  6     SPRING  'Concrete hinge 1 6'
! ITYPE IHYST   ILOS    IDAMG   KX      KY      GJ      WGT     RF      RT      PSX     PSY     PSZ
        THETA   ITRUSS  IOP     SL
  1     54      0       0       85079   0       0       0.075   0       0       0       0       0
        0       0       0       0
! FX+   FX-     FY+     FY-     MZ+     MZ-
  2.2   -21.6   0       0       0       0
! TLIMT CLIMIT  BETA    Fbo     L       TFACTOR CFACTOR eTT
 0.0025 0.005   1.0     0.2     1.0     1.0     1.0

! N     MTYPE   LABEL
  7     SPRING  'Concrete hinge 2 5'
! ITYPE IHYST   ILOS    IDAMG   KX      KY      GJ      WGT     RF      RT      PSX     PSY     PSZ
        THETA   ITRUSS  IOP     SL
  1     54      0       0       483001  0       0       0075    0       0       0       0       0
        0       0       0       0
! FX+   FX-     FY+     FY-     MZ+     MZ-
  12.4  -122.8  0       0       0       0
! TLIMT CLIMIT  BETA    Fbo     L       TFACTOR CFACTOR eTT
 0.0025 0.005   1.0     0.2     1.0     1.0     1.0

! N     MTYPE   LABEL
  8     SPRING  'Concrete hinge 3 4'
! ITYPE IHYST   ILOS    IDAMG   KX      KY      GJ      WGT     RF      RT      PSX     PSY     PSZ
        THETA   ITRUSS  IOP     SL
  1     54      0       0       708098  0       0       0075    0       0       0       0       0
        0       0       0       0
! FX+   FX-     FY+     FY-     MZ+     MZ-
  18.2  -180.0  0       0       0       0
! TLIMT CLIMIT  BETA    Fbo     L       TFACTOR CFACTOR eTT
 0.0025 0.005   1.0     0.2     1.0     1.0     1.0

! N     MTYPE   LABEL
  9     SPRING  'Diagonal strut 1'
! ITYPE IHYST   ILOS    IDAMG   KX      KY      GJ      WGT     RF      RT      PSX     PSY     PSZ
        THETA   ITRUSS  IOP     SL
  1     54      0       0       323299  0       0       0       0       0       0       0       0
        0       0       0       0
! FX+   FX-     FY+     FY-     MZ+     MZ-
  8.3   -82.2   0       0       0       0
! TLIMT CLIMIT  BETA    Fbo     L       TFACTOR CFACTOR eTT
 0.0025 0.005   1.0     0.2     1.0     1.0     1.0
```

```
! N     MTYPE   LABEL
  10    SPRING  'Diagonal strut 2'
! ITYPE IHYST   ILOS    IDAMG   KX      KY      GJ      WGT     RF      RT      PSX     PSY     PSZ
        THETA   ITRUSS  IOP     SL
  1     54      0       0       190576  0       0       0       0       0       0       0       0
        0       0       0       0
! FX+   FX-     FY+     FY-     MZ+     MZ-
  4.9   -48.4   0       0       0       0
! TLIMT CLIMIT  BETA    Fbo     L       TFACTOR CFACTOR eTT
 0.0025 0.005   1.0     0.2     1.0     1.0     1.0

WEIGHTS 0
! N     WX      WY      WM
  1
  30

LOADS
! N     FX      FY      FM
  1     0       0       0
  2     0       0       0
  3     0       0       0
  4     0       0       0
  5     0       -100    0
  6     0       0       0
  7     0       0       0
  8     0       0       0
  9     0       0       0
  10    0       0       0
  11    0       0       0
  12    0       0       0
  13    0       0       0
  14    0       0       0
  15    0       0       0
  16    0       0       0
  17    0       0       0
  18    0       0       0
  19    0       0       0
  20    0       0       0
  21    0       0       0
  22    0       0       0
  23    0       0       0
  24    0       0       0
  25    0       0       0
  26    0       0       0
  27    0       0       0
  28    0       0       0
  29    0       0       0
  30    0       0       0

EQUAKE drift_all.txt
! IBERG ISTART  DELTAT  ASCALE  END     VEL     DIS     TSCALE
  3     1       0.001   -1      -1      0       0       1
```

C.2 Slotted-beam Frame Model

C.2.1 Frame Details

Table C- 1: Frame details

Parameter	Value
Number of bays	3
Number of storeys	5
Bay width	6 m
Interstorey height	3.6 m

Table C- 2: Member dimensions

Column Dimension	Value
Depth, h_c	500 mm
Width, b_c	400 mm
Beam Dimension	**Value**
Depth, h_b	500 mm
Width, b	300 mm
Effective depth, d	450 mm
Top-hinge depth, d_c	110 mm
Slot width, L_{slot}	20 mm
Unbonded length, L_{ub}	360 mm

Table C- 3: Member reinforcement

Beam member	Bottom reinforcement	Top reinforcement	Shear reinforcement
Level 1 beams	3-D25 & 1-D20	4-HD25	2-D20 at 45°
Level 2 beams	2-D25 & 2-D20	4-HD25	2-D20 at 45°
Level 3 beams	4-D20	2-HD25 & 2-HD20	2-D20 at 45°
Level 4 beams	2-D20 & 2-D16	4-HD20	2-D16 at 45°
Level 5 beams	2-D16 & 2-D12	4-HD16	2-D12 at 45°
Column member	**Longitudinal reinforcement**		
Base column	10-D20 distributed evenly around perimeter		

Table C- 4: Steel properties assumed

Material property	Grade300 steel	Grade500 steel
Elastic modulus, E	200 GPa	200 GPa
Yield strength, f_y	325 MPa	540 MPa
Ultimate strength, f_u	457 MPa	670 MPa
Yield strain, ε_y	0.001625	0.0027
Strain hardening strain, ε_{sh}	0.025	0.016
Ultimate strain, ε_u	0.2	0.15
Strain hardening factor, p	4	5

C.2.2 Ruaumoko2D Datafile

```
FIVE-STOREY FRAME USING SLOTTED-BEAMS
* Units: kN, m, Seconds

! IPANL IFMT    IPLAS   IPCONM  ICTYPE  IPVERT  INLGEO  IPNF    IZERO   ORTHO   IMODE
2       0       1       0       2       0       1       0       0       1       0
! NNP   NMEM    NTYPE   M       MODE1   MODE2   GRAV    C1      C2      DT      TIME    FACTOR
594     305     35      25      1       25      9.81    5       5       0.0001  26      1
! KP    KPA     KPLOT   JOUT    DSTORT  DFACT   XMAX    YMAX    NLEVEL  NUP     IRESID  KDUMP
0       65      65      0       1       5       0.8     0.8     6       2       1       0
! MAXIT MAXCIT  FTEST   WAVEX   WAVEY   THETA   DXMAX   DYMAX   D       OMEGA   F
20      20      0.0001  0       0       0       1       1

NODES
! N     X       Y       Nx      Ny      Nr      Kup-x   Kup-y   Kup-r   IOUT
1       0       0       1       1       1       0       0       0       0       ! Ground level
2       6       0       1       1       1       0       0       0       0
3       12      0       1       1       1       0       0       0       0
4       18      0       1       1       1       0       0       0       0
5       0       3.6     0       0       0       0       0       0       0       ! Level 1
6       6       3.6     0       0       0       0       0       0       0
7       12      3.6     0       0       0       0       0       0       0
8       18      3.6     0       0       0       0       0       0       0
9       0       7.2     0       0       0       0       0       0       0       ! Level 2
10      6       7.2     0       0       0       0       0       0       0
11      12      7.2     0       0       0       0       0       0       0
12      18      7.2     0       0       0       0       0       0       0
13      0       10.8    0       0       0       0       0       0       0       ! Level 3
14      6       10.8    0       0       0       0       0       0       0
15      12      10.8    0       0       0       0       0       0       0
16      18      10.8    0       0       0       0       0       0       0
17      0       14.4    0       0       0       0       0       0       0       ! Level 4
18      6       14.4    0       0       0       0       0       0       0
19      12      14.4    0       0       0       0       0       0       0
20      18      14.4    0       0       0       0       0       0       0
21      0       18      0       0       0       0       0       0       0       ! Level 5
22      6       18      0       0       0       0       0       0       0
23      12      18      0       0       0       0       0       0       0
24      18      18      0       0       0       0       0       0       0
25      0.615   3.6     0       0       0       0       0       0       0       ! Level 1 beams
26      5.385   3.6     0       0       0       0       0       0       0
27      6.615   3.6     0       0       0       0       0       0       0
28      11.385  3.6     0       0       0       0       0       0       0
29      12.615  3.6     0       0       0       0       0       0       0
30      17.385  3.6     0       0       0       0       0       0       0
31      0.609   7.2     0       0       0       0       0       0       0       ! Level 2 beams
32      5.391   7.2     0       0       0       0       0       0       0
33      6.609   7.2     0       0       0       0       0       0       0
34      11.391  7.2     0       0       0       0       0       0       0
35      12.609  7.2     0       0       0       0       0       0       0
36      17.391  7.2     0       0       0       0       0       0       0
37      0.591   10.8    0       0       0       0       0       0       0       ! Level 3 beams
38      5.409   10.8    0       0       0       0       0       0       0
39      6.591   10.8    0       0       0       0       0       0       0
40      11.409  10.8    0       0       0       0       0       0       0
41      12.591  10.8    0       0       0       0       0       0       0
42      17.409  10.8    0       0       0       0       0       0       0
43      0.574   14.4    0       0       0       0       0       0       0       ! Level 4 beams
44      5.426   14.4    0       0       0       0       0       0       0
45      6.574   14.4    0       0       0       0       0       0       0
46      11.426  14.4    0       0       0       0       0       0       0
47      12.574  14.4    0       0       0       0       0       0       0
48      17.426  14.4    0       0       0       0       0       0       0
49      0.543   18      0       0       0       0       0       0       0       ! Level 5 beams
50      5.457   18      0       0       0       0       0       0       0
51      6.543   18      0       0       0       0       0       0       0
52      11.457  18      0       0       0       0       0       0       0
53      12.543  18      0       0       0       0       0       0       0
54      17.457  18      0       0       0       0       0       0       0
55      0.078   3.400   1       1       1       0       0       0       0       ! LEVEL1
CONNECTION1, Bottom steel
56      0.782   3.400   1       1       1       0       0       0       0
57      0.052   3.800   1       1       1       0       0       0       0       ! Top steel
58      0.448   3.800   1       1       1       0       0       0       0
59      0.250   3.795   1       1       1       0       0       0       0       ! Shear spring
60      0.270   3.795   1       1       1       0       0       0       0
61      0.102   3.850   1       1       1       0       0       0       0       ! Concrete strut 1
62      0.399   3.850   1       1       1       0       0       0       0
63      0.102   3.837   1       1       1       0       0       0       0       ! Concrete strut 2
64      0.399   3.837   1       1       1       0       0       0       0
65      0.102   3.811   1       1       1       0       0       0       0       ! Concrete strut 3
66      0.399   3.811   1       1       1       0       0       0       0
67      0.102   3.779   1       1       1       0       0       0       0       ! Concrete strut 4
```

```
68      0.399   3.779   1       1       1       0       0       0       0
69      0.102   3.753   1       1       1       0       0       0       0       ! Concrete strut 5
70      0.399   3.753   1       1       1       0       0       0       0
71      0.102   3.740   1       1       1       0       0       0       0       ! Concrete strut 6
72      0.399   3.740   1       1       1       0       0       0       0
73      5.218   3.400   1       1       1       0       0       0       0       ! LEVEL1
CONNECTION2, Bottom steel
74      5.922   3.400   1       1       1       0       0       0       0
75      5.552   3.800   1       1       1       0       0       0       0       ! Top steel
76      5.948   3.800   1       1       1       0       0       0       0
77      5.730   3.795   1       1       1       0       0       0       0       ! Shear spring
78      5.750   3.795   1       1       1       0       0       0       0
79      5.602   3.850   1       1       1       0       0       0       0       ! Concrete strut 1
80      5.899   3.850   1       1       1       0       0       0       0
81      5.602   3.837   1       1       1       0       0       0       0       ! Concrete strut 2
82      5.899   3.837   1       1       1       0       0       0       0
83      5.602   3.811   1       1       1       0       0       0       0       ! Concrete strut 3
84      5.899   3.811   1       1       1       0       0       0       0
85      5.602   3.779   1       1       1       0       0       0       0       ! Concrete strut 4
86      5.899   3.779   1       1       1       0       0       0       0
87      5.602   3.753   1       1       1       0       0       0       0       ! Concrete strut 5
88      5.899   3.753   1       1       1       0       0       0       0
89      5.602   3.740   1       1       1       0       0       0       0       ! Concrete strut 6
90      5.899   3.740   1       1       1       0       0       0       0
91      6.078   3.400   1       1       1       0       0       0       0       ! LEVEL1
CONNECTION3, Bottom steel
92      6.782   3.400   1       1       1       0       0       0       0
93      6.052   3.800   1       1       1       0       0       0       0       ! Top steel
94      6.448   3.800   1       1       1       0       0       0       0
95      6.250   3.795   1       1       1       0       0       0       0       ! Shear spring
96      6.270   3.795   1       1       1       0       0       0       0
97      6.102   3.850   1       1       1       0       0       0       0       ! Concrete strut 1
98      6.399   3.850   1       1       1       0       0       0       0
99      6.102   3.837   1       1       1       0       0       0       0       ! Concrete strut 2
100     6.399   3.837   1       1       1       0       0       0       0
101     6.102   3.811   1       1       1       0       0       0       0       ! Concrete strut 3
102     6.399   3.811   1       1       1       0       0       0       0
103     6.102   3.779   1       1       1       0       0       0       0       ! Concrete strut 4
104     6.399   3.779   1       1       1       0       0       0       0
105     6.102   3.753   1       1       1       0       0       0       0       ! Concrete strut 5
106     6.399   3.753   1       1       1       0       0       0       0
107     6.102   3.740   1       1       1       0       0       0       0       ! Concrete strut 6
108     6.399   3.740   1       1       1       0       0       0       0
109     11.218  3.400   1       1       1       0       0       0       0       ! LEVEL1
CONNECTION4, Bottom steel
110     11.922  3.400   1       1       1       0       0       0       0
111     11.552  3.800   1       1       1       0       0       0       0       ! Top steel
112     11.948  3.800   1       1       1       0       0       0       0
113     11.730  3.795   1       1       1       0       0       0       0       ! Shear spring
114     11.750  3.795   1       1       1       0       0       0       0
115     11.602  3.850   1       1       1       0       0       0       0       ! Concrete strut 1
116     11.899  3.850   1       1       1       0       0       0       0
117     11.602  3.837   1       1       1       0       0       0       0       ! Concrete strut 2
118     11.899  3.837   1       1       1       0       0       0       0
119     11.602  3.811   1       1       1       0       0       0       0       ! Concrete strut 3
120     11.899  3.811   1       1       1       0       0       0       0
121     11.602  3.779   1       1       1       0       0       0       0       ! Concrete strut 4
122     11.899  3.779   1       1       1       0       0       0       0
123     11.602  3.753   1       1       1       0       0       0       0       ! Concrete strut 5
124     11.899  3.753   1       1       1       0       0       0       0
125     11.602  3.740   1       1       1       0       0       0       0       ! Concrete strut 6
126     11.899  3.740   1       1       1       0       0       0       0
127     12.078  3.400   1       1       1       0       0       0       0       ! LEVEL1
CONNECTION5, Bottom steel
128     12.782  3.400   1       1       1       0       0       0       0
129     12.052  3.800   1       1       1       0       0       0       0       ! Top steel
130     12.448  3.800   1       1       1       0       0       0       0
131     12.250  3.795   1       1       1       0       0       0       0       ! Shear spring
132     12.270  3.795   1       1       1       0       0       0       0
133     12.102  3.850   1       1       1       0       0       0       0       ! Concrete strut 1
134     12.399  3.850   1       1       1       0       0       0       0
135     12.102  3.837   1       1       1       0       0       0       0       ! Concrete strut 2
136     12.399  3.837   1       1       1       0       0       0       0
137     12.102  3.811   1       1       1       0       0       0       0       ! Concrete strut 3
138     12.399  3.811   1       1       1       0       0       0       0
139     12.102  3.779   1       1       1       0       0       0       0       ! Concrete strut 4
140     12.399  3.779   1       1       1       0       0       0       0
141     12.102  3.753   1       1       1       0       0       0       0       ! Concrete strut 5
142     12.399  3.753   1       1       1       0       0       0       0
143     12.102  3.740   1       1       1       0       0       0       0       ! Concrete strut 6
144     12.399  3.740   1       1       1       0       0       0       0
145     17.218  3.400   1       1       1       0       0       0       0       ! LEVEL1
CONNECTION6, Bottom steel
146     17.922  3.400   1       1       1       0       0       0       0
147     17.552  3.800   1       1       1       0       0       0       0       ! Top steel
148     17.948  3.800   1       1       1       0       0       0       0
149     17.730  3.795   1       1       1       0       0       0       0       ! Shear spring
150     17.750  3.795   1       1       1       0       0       0       0
```

```
151     17.602  3.850   1       1       1       0       0       0       0       ! Concrete strut 1
152     17.899  3.850   1       1       1       0       0       0       0
153     17.602  3.837   1       1       1       0       0       0       0       ! Concrete strut 2
154     17.899  3.837   1       1       1       0       0       0       0
155     17.602  3.811   1       1       1       0       0       0       0       ! Concrete strut 3
156     17.899  3.811   1       1       1       0       0       0       0
157     17.602  3.779   1       1       1       0       0       0       0       ! Concrete strut 4
158     17.899  3.779   1       1       1       0       0       0       0
159     17.602  3.753   1       1       1       0       0       0       0       ! Concrete strut 5
160     17.899  3.753   1       1       1       0       0       0       0
161     17.602  3.740   1       1       1       0       0       0       0       ! Concrete strut 6
162     17.899  3.740   1       1       1       0       0       0       0
163     0.089   7       1       1       1       0       0       0       0       ! LEVEL2
CONNECTION1, Bottom steel
164     0.771   7       1       1       1       0       0       0       0
165     0.052   7.4     1       1       1       0       0       0       0       ! Top steel
166     0.448   7.4     1       1       1       0       0       0       0
167     0.250   7.395   1       1       1       0       0       0       0       ! Shear spring
168     0.270   7.395   1       1       1       0       0       0       0
169     0.102   7.450   1       1       1       0       0       0       0       ! Concrete strut 1
170     0.399   7.450   1       1       1       0       0       0       0
171     0.102   7.437   1       1       1       0       0       0       0       ! Concrete strut 2
172     0.399   7.437   1       1       1       0       0       0       0
173     0.102   7.411   1       1       1       0       0       0       0       ! Concrete strut 3
174     0.399   7.411   1       1       1       0       0       0       0
175     0.102   7.379   1       1       1       0       0       0       0       ! Concrete strut 4
176     0.399   7.379   1       1       1       0       0       0       0
177     0.102   7.353   1       1       1       0       0       0       0       ! Concrete strut 5
178     0.399   7.353   1       1       1       0       0       0       0
179     0.102   7.340   1       1       1       0       0       0       0       ! Concrete strut 6
180     0.399   7.340   1       1       1       0       0       0       0
181     5.229   7       1       1       1       0       0       0       0       ! LEVEL2
CONNECTION2, Bottom steel
182     5.911   7       1       1       1       0       0       0       0
183     5.552   7.4     1       1       1       0       0       0       0       ! Top steel
184     5.948   7.4     1       1       1       0       0       0       0
185     5.730   7.395   1       1       1       0       0       0       0       ! Shear spring
186     5.750   7.395   1       1       1       0       0       0       0
187     5.602   7.450   1       1       1       0       0       0       0       ! Concrete strut 1
188     5.899   7.450   1       1       1       0       0       0       0
189     5.602   7.437   1       1       1       0       0       0       0       ! Concrete strut 2
190     5.899   7.437   1       1       1       0       0       0       0
191     5.602   7.411   1       1       1       0       0       0       0       ! Concrete strut 3
192     5.899   7.411   1       1       1       0       0       0       0
193     5.602   7.379   1       1       1       0       0       0       0       ! Concrete strut 4
194     5.899   7.379   1       1       1       0       0       0       0
195     5.602   7.353   1       1       1       0       0       0       0       ! Concrete strut 5
196     5.899   7.353   1       1       1       0       0       0       0
197     5.602   7.340   1       1       1       0       0       0       0       ! Concrete strut 6
198     5.899   7.340   1       1       1       0       0       0       0
199     6.089   7       1       1       1       0       0       0       0       ! LEVEL2
CONNECTION3, Bottom steel
200     6.771   7       1       1       1       0       0       0       0
201     6.052   7.4     1       1       1       0       0       0       0       ! Top steel
202     6.448   7.4     1       1       1       0       0       0       0
203     6.250   7.395   1       1       1       0       0       0       0       ! Shear spring
204     6.270   7.395   1       1       1       0       0       0       0
205     6.102   7.450   1       1       1       0       0       0       0       ! Concrete strut 1
206     6.399   7.450   1       1       1       0       0       0       0
207     6.102   7.437   1       1       1       0       0       0       0       ! Concrete strut 2
208     6.399   7.437   1       1       1       0       0       0       0
209     6.102   7.411   1       1       1       0       0       0       0       ! Concrete strut 3
210     6.399   7.411   1       1       1       0       0       0       0
211     6.102   7.379   1       1       1       0       0       0       0       ! Concrete strut 4
212     6.399   7.379   1       1       1       0       0       0       0
213     6.102   7.353   1       1       1       0       0       0       0       ! Concrete strut 5
214     6.399   7.353   1       1       1       0       0       0       0
215     6.102   7.340   1       1       1       0       0       0       0       ! Concrete strut 6
216     6.399   7.340   1       1       1       0       0       0       0
217     11.229  7       1       1       1       0       0       0       0       ! LEVEL2
CONNECTION4, Bottom steel
218     11.911  7       1       1       1       0       0       0       0
219     11.552  7.4     1       1       1       0       0       0       0       ! Top steel
220     11.948  7.4     1       1       1       0       0       0       0
221     11.730  7.395   1       1       1       0       0       0       0       ! Shear spring
222     11.750  7.395   1       1       1       0       0       0       0
223     11.602  7.450   1       1       1       0       0       0       0       ! Concrete strut 1
224     11.899  7.450   1       1       1       0       0       0       0
225     11.602  7.437   1       1       1       0       0       0       0       ! Concrete strut 2
226     11.899  7.437   1       1       1       0       0       0       0
227     11.602  7.411   1       1       1       0       0       0       0       ! Concrete strut 3
228     11.899  7.411   1       1       1       0       0       0       0
229     11.602  7.379   1       1       1       0       0       0       0       ! Concrete strut 4
230     11.899  7.379   1       1       1       0       0       0       0
231     11.602  7.353   1       1       1       0       0       0       0       ! Concrete strut 5
232     11.899  7.353   1       1       1       0       0       0       0
233     11.602  7.340   1       1       1       0       0       0       0       ! Concrete strut 6
234     11.899  7.340   1       1       1       0       0       0       0
```

```
235     12.089  7       1       1       1       0       0       0       0       ! LEVEL2
CONNECTION5, Bottom steel
236     12.771  7       1       1       1       0       0       0       0
237     12.052  7.4     1       1       1       0       0       0       0       ! Top steel
238     12.448  7.4     1       1       1       0       0       0       0
239     12.250  7.395   1       1       1       0       0       0       0       ! Shear spring
240     12.270  7.395   1       1       1       0       0       0       0
241     12.102  7.450   1       1       1       0       0       0       0       ! Concrete strut 1
242     12.399  7.450   1       1       1       0       0       0       0
243     12.102  7.437   1       1       1       0       0       0       0       ! Concrete strut 2
244     12.399  7.437   1       1       1       0       0       0       0
245     12.102  7.411   1       1       1       0       0       0       0       ! Concrete strut 3
246     12.399  7.411   1       1       1       0       0       0       0
247     12.102  7.379   1       1       1       0       0       0       0       ! Concrete strut 4
248     12.399  7.379   1       1       1       0       0       0       0
249     12.102  7.353   1       1       1       0       0       0       0       ! Concrete strut 5
250     12.399  7.353   1       1       1       0       0       0       0
251     12.102  7.340   1       1       1       0       0       0       0       ! Concrete strut 6
252     12.399  7.340   1       1       1       0       0       0       0
253     17.229  7       1       1       1       0       0       0       0       ! LEVEL2
CONNECTION6, Bottom steel
254     17.911  7       1       1       1       0       0       0       0
255     17.552  7.4     1       1       1       0       0       0       0       ! Top steel
256     17.948  7.4     1       1       1       0       0       0       0
257     17.730  7.395   1       1       1       0       0       0       0       ! Shear spring
258     17.750  7.395   1       1       1       0       0       0       0
259     17.602  7.450   1       1       1       0       0       0       0       ! Concrete strut 1
260     17.899  7.450   1       1       1       0       0       0       0
261     17.602  7.437   1       1       1       0       0       0       0       ! Concrete strut 2
262     17.899  7.437   1       1       1       0       0       0       0
263     17.602  7.411   1       1       1       0       0       0       0       ! Concrete strut 3
264     17.899  7.411   1       1       1       0       0       0       0
265     17.602  7.379   1       1       1       0       0       0       0       ! Concrete strut 4
266     17.899  7.379   1       1       1       0       0       0       0
267     17.602  7.353   1       1       1       0       0       0       0       ! Concrete strut 5
268     17.899  7.353   1       1       1       0       0       0       0
269     17.602  7.340   1       1       1       0       0       0       0       ! Concrete strut 6
270     17.899  7.340   1       1       1       0       0       0       0
271     0.107   10.6    1       1       1       0       0       0       0       ! LEVEL3
CONNECTION1, Bottom steel
272     0.753   10.6    1       1       1       0       0       0       0
273     0.072   11      1       1       1       0       0       0       0       ! Top steel
274     0.428   11      1       1       1       0       0       0       0
275     0.250   10.995  1       1       1       0       0       0       0       ! Shear spring
276     0.270   10.995  1       1       1       0       0       0       0
277     0.116   11.050  1       1       1       0       0       0       0       ! Concrete strut 1
278     0.384   11.050  1       1       1       0       0       0       0
279     0.116   11.037  1       1       1       0       0       0       0       ! Concrete strut 2
280     0.384   11.037  1       1       1       0       0       0       0
281     0.116   11.011  1       1       1       0       0       0       0       ! Concrete strut 3
282     0.384   11.011  1       1       1       0       0       0       0
283     0.116   10.979  1       1       1       0       0       0       0       ! Concrete strut 4
284     0.384   10.979  1       1       1       0       0       0       0
285     0.116   10.953  1       1       1       0       0       0       0       ! Concrete strut 5
286     0.384   10.953  1       1       1       0       0       0       0
287     0.116   10.940  1       1       1       0       0       0       0       ! Concrete strut 6
288     0.384   10.940  1       1       1       0       0       0       0
289     5.247   10.6    1       1       1       0       0       0       0       ! LEVEL3
CONNECTION2, Bottom steel
290     5.893   10.6    1       1       1       0       0       0       0
291     5.572   11      1       1       1       0       0       0       0       ! Top steel
292     5.928   11      1       1       1       0       0       0       0
293     5.730   10.995  1       1       1       0       0       0       0       ! Shear spring
294     5.750   10.995  1       1       1       0       0       0       0
295     5.616   11.050  1       1       1       0       0       0       0       ! Concrete strut 1
296     5.884   11.050  1       1       1       0       0       0       0
297     5.616   11.037  1       1       1       0       0       0       0       ! Concrete strut 2
298     5.884   11.037  1       1       1       0       0       0       0
299     5.616   11.011  1       1       1       0       0       0       0       ! Concrete strut 3
300     5.884   11.011  1       1       1       0       0       0       0
301     5.616   10.979  1       1       1       0       0       0       0       ! Concrete strut 4
302     5.884   10.979  1       1       1       0       0       0       0
303     5.616   10.953  1       1       1       0       0       0       0       ! Concrete strut 5
304     5.884   10.953  1       1       1       0       0       0       0
305     5.616   10.940  1       1       1       0       0       0       0       ! Concrete strut 6
306     5.884   10.940  1       1       1       0       0       0       0
307     6.107   10.6    1       1       1       0       0       0       0       ! LEVEL3
CONNECTION3, Bottom steel
308     6.753   10.6    1       1       1       0       0       0       0
309     6.072   11      1       1       1       0       0       0       0       ! Top steel
310     6.428   11      1       1       1       0       0       0       0
311     6.250   10.995  1       1       1       0       0       0       0       ! Shear spring
312     6.270   10.995  1       1       1       0       0       0       0
313     6.116   11.050  1       1       1       0       0       0       0       ! Concrete strut 1
314     6.384   11.050  1       1       1       0       0       0       0
315     6.116   11.037  1       1       1       0       0       0       0       ! Concrete strut 2
316     6.384   11.037  1       1       1       0       0       0       0
317     6.116   11.011  1       1       1       0       0       0       0       ! Concrete strut 3
```

```
318     6.384   11.011  1       1       1       0       0       0       0
319     6.116   10.979  1       1       1       0       0       0       0       ! Concrete strut 4
320     6.384   10.979  1       1       1       0       0       0       0
321     6.116   10.953  1       1       1       0       0       0       0       ! Concrete strut 5
322     6.384   10.953  1       1       1       0       0       0       0
323     6.116   10.940  1       1       1       0       0       0       0       ! Concrete strut 6
324     6.384   10.940  1       1       1       0       0       0       0
325     11.247  10.6    1       1       1       0       0       0       0       ! LEVEL3
CONNECTION4, Bottom steel
326     11.893  10.6    1       1       1       0       0       0       0
327     11.572  11      1       1       1       0       0       0       0       ! Top steel
328     11.928  11      1       1       1       0       0       0       0
329     11.730  10.995  1       1       1       0       0       0       0       ! Shear spring
330     11.750  10.995  1       1       1       0       0       0       0
331     11.616  11.050  1       1       1       0       0       0       0       ! Concrete strut 1
332     11.884  11.050  1       1       1       0       0       0       0
333     11.616  11.037  1       1       1       0       0       0       0       ! Concrete strut 2
334     11.884  11.037  1       1       1       0       0       0       0
335     11.616  11.011  1       1       1       0       0       0       0       ! Concrete strut 3
336     11.884  11.011  1       1       1       0       0       0       0
337     11.616  10.979  1       1       1       0       0       0       0       ! Concrete strut 4
338     11.884  10.979  1       1       1       0       0       0       0
339     11.616  10.953  1       1       1       0       0       0       0       ! Concrete strut 5
340     11.884  10.953  1       1       1       0       0       0       0
341     11.616  10.940  1       1       1       0       0       0       0       ! Concrete strut 6
342     11.884  10.940  1       1       1       0       0       0       0
343     12.107  10.6    1       1       1       0       0       0       0       ! LEVEL3
CONNECTION5, Bottom steel
344     12.753  10.6    1       1       1       0       0       0       0
345     12.072  11      1       1       1       0       0       0       0       ! Top steel
346     12.428  11      1       1       1       0       0       0       0
347     12.250  10.995  1       1       1       0       0       0       0       ! Shear spring
348     12.270  10.995  1       1       1       0       0       0       0
349     12.116  11.050  1       1       1       0       0       0       0       ! Concrete strut 1
350     12.384  11.050  1       1       1       0       0       0       0
351     12.116  11.037  1       1       1       0       0       0       0       ! Concrete strut 2
352     12.384  11.037  1       1       1       0       0       0       0
353     12.116  11.011  1       1       1       0       0       0       0       ! Concrete strut 3
354     12.384  11.011  1       1       1       0       0       0       0
355     12.116  10.979  1       1       1       0       0       0       0       ! Concrete strut 4
356     12.384  10.979  1       1       1       0       0       0       0
357     12.116  10.953  1       1       1       0       0       0       0       ! Concrete strut 5
358     12.384  10.953  1       1       1       0       0       0       0
359     12.116  10.940  1       1       1       0       0       0       0       ! Concrete strut 6
360     12.384  10.940  1       1       1       0       0       0       0
361     17.247  10.6    1       1       1       0       0       0       0       ! LEVEL3
CONNECTION6, Bottom steel
362     17.893  10.6    1       1       1       0       0       0       0
363     17.572  11      1       1       1       0       0       0       0       ! Top steel
364     17.928  11      1       1       1       0       0       0       0
365     17.730  10.995  1       1       1       0       0       0       0       ! Shear spring
366     17.750  10.995  1       1       1       0       0       0       0
367     17.616  11.050  1       1       1       0       0       0       0       ! Concrete strut 1
368     17.884  11.050  1       1       1       0       0       0       0
369     17.616  11.037  1       1       1       0       0       0       0       ! Concrete strut 2
370     17.884  11.037  1       1       1       0       0       0       0
371     17.616  11.011  1       1       1       0       0       0       0       ! Concrete strut 3
372     17.884  11.011  1       1       1       0       0       0       0
373     17.616  10.979  1       1       1       0       0       0       0       ! Concrete strut 4
374     17.884  10.979  1       1       1       0       0       0       0
375     17.616  10.953  1       1       1       0       0       0       0       ! Concrete strut 5
376     17.884  10.953  1       1       1       0       0       0       0
377     17.616  10.940  1       1       1       0       0       0       0       ! Concrete strut 6
378     17.884  10.940  1       1       1       0       0       0       0
379     0.121   14.2    1       1       1       0       0       0       0       ! LEVEL4
CONNECTION1, Bottom steel
380     0.739   14.2    1       1       1       0       0       0       0
381     0.092   14.6    1       1       1       0       0       0       0       ! Top steel
382     0.408   14.6    1       1       1       0       0       0       0
383     0.250   14.595  1       1       1       0       0       0       0       ! Shear spring
384     0.270   14.595  1       1       1       0       0       0       0
385     0.131   14.650  1       1       1       0       0       0       0       ! Concrete strut 1
386     0.369   14.650  1       1       1       0       0       0       0
387     0.131   14.637  1       1       1       0       0       0       0       ! Concrete strut 2
388     0.369   14.637  1       1       1       0       0       0       0
389     0.131   14.611  1       1       1       0       0       0       0       ! Concrete strut 3
390     0.369   14.611  1       1       1       0       0       0       0
391     0.131   14.579  1       1       1       0       0       0       0       ! Concrete strut 4
392     0.369   14.579  1       1       1       0       0       0       0
393     0.131   14.553  1       1       1       0       0       0       0       ! Concrete strut 5
394     0.369   14.553  1       1       1       0       0       0       0
395     0.131   14.540  1       1       1       0       0       0       0       ! Concrete strut 6
396     0.369   14.540  1       1       1       0       0       0       0
397     5.261   14.2    1       1       1       0       0       0       0       ! LEVEL4
CONNECTION2, Bottom steel
398     5.879   14.2    1       1       1       0       0       0       0
399     5.592   14.6    1       1       1       0       0       0       0       ! Top steel
400     5.908   14.6    1       1       1       0       0       0       0
```

```
401     5.730   14.595  1       1       1       0       0       0       0       ! Shear spring
402     5.750   14.595  1       1       1       0       0       0       0
403     5.631   14.650  1       1       1       0       0       0       0       ! Concrete strut 1
404     5.869   14.650  1       1       1       0       0       0       0
405     5.631   14.637  1       1       1       0       0       0       0       ! Concrete strut 2
406     5.869   14.637  1       1       1       0       0       0       0
407     5.631   14.611  1       1       1       0       0       0       0       ! Concrete strut 3
408     5.869   14.611  1       1       1       0       0       0       0
409     5.631   14.579  1       1       1       0       0       0       0       ! Concrete strut 4
410     5.869   14.579  1       1       1       0       0       0       0
411     5.631   14.553  1       1       1       0       0       0       0       ! Concrete strut 5
412     5.869   14.553  1       1       1       0       0       0       0
413     5.631   14.540  1       1       1       0       0       0       0       ! Concrete strut 6
414     5.869   14.540  1       1       1       0       0       0       0
415     6.121   14.2    1       1       1       0       0       0       0       ! LEVEL4
CONNECTION3, Bottom steel
416     6.739   14.2    1       1       1       0       0       0       0
417     6.092   14.6    1       1       1       0       0       0       0       ! Top steel
418     6.408   14.6    1       1       1       0       0       0       0
419     6.250   14.595  1       1       1       0       0       0       0       ! Shear spring
420     6.270   14.595  1       1       1       0       0       0       0
421     6.131   14.650  1       1       1       0       0       0       0       ! Concrete strut 1
422     6.369   14.650  1       1       1       0       0       0       0
423     6.131   14.637  1       1       1       0       0       0       0       ! Concrete strut 2
424     6.369   14.637  1       1       1       0       0       0       0
425     6.131   14.611  1       1       1       0       0       0       0       ! Concrete strut 3
426     6.369   14.611  1       1       1       0       0       0       0
427     6.131   14.579  1       1       1       0       0       0       0       ! Concrete strut 4
428     6.369   14.579  1       1       1       0       0       0       0
429     6.131   14.553  1       1       1       0       0       0       0       ! Concrete strut 5
430     6.369   14.553  1       1       1       0       0       0       0
431     6.131   14.540  1       1       1       0       0       0       0       ! Concrete strut 6
432     6.369   14.540  1       1       1       0       0       0       0
433     11.261  14.2    1       1       1       0       0       0       0       ! LEVEL4
CONNECTION4, Bottom steel
434     11.879  14.2    1       1       1       0       0       0       0
435     11.592  14.6    1       1       1       0       0       0       0       ! Top steel
436     11.908  14.6    1       1       1       0       0       0       0
437     11.730  14.595  1       1       1       0       0       0       0       ! Shear spring
438     11.750  14.595  1       1       1       0       0       0       0
439     11.631  14.650  1       1       1       0       0       0       0       ! Concrete strut 1
440     11.869  14.650  1       1       1       0       0       0       0
441     11.631  14.637  1       1       1       0       0       0       0       ! Concrete strut 2
442     11.869  14.637  1       1       1       0       0       0       0
443     11.631  14.611  1       1       1       0       0       0       0       ! Concrete strut 3
444     11.869  14.611  1       1       1       0       0       0       0
445     11.631  14.579  1       1       1       0       0       0       0       ! Concrete strut 4
446     11.869  14.579  1       1       1       0       0       0       0
447     11.631  14.553  1       1       1       0       0       0       0       ! Concrete strut 5
448     11.869  14.553  1       1       1       0       0       0       0
449     11.631  14.540  1       1       1       0       0       0       0       ! Concrete strut 6
450     11.869  14.540  1       1       1       0       0       0       0
451     12.121  14.2    1       1       1       0       0       0       0       ! LEVEL4
CONNECTION5, Bottom steel
452     12.739  14.2    1       1       1       0       0       0       0
453     12.092  14.6    1       1       1       0       0       0       0       ! Top steel
454     12.408  14.6    1       1       1       0       0       0       0
455     12.250  14.595  1       1       1       0       0       0       0       ! Shear spring
456     12.270  14.595  1       1       1       0       0       0       0
457     12.131  14.650  1       1       1       0       0       0       0       ! Concrete strut 1
458     12.369  14.650  1       1       1       0       0       0       0
459     12.131  14.637  1       1       1       0       0       0       0       ! Concrete strut 2
460     12.369  14.637  1       1       1       0       0       0       0
461     12.131  14.611  1       1       1       0       0       0       0       ! Concrete strut 3
462     12.369  14.611  1       1       1       0       0       0       0
463     12.131  14.579  1       1       1       0       0       0       0       ! Concrete strut 4
464     12.369  14.579  1       1       1       0       0       0       0
465     12.131  14.553  1       1       1       0       0       0       0       ! Concrete strut 5
466     12.369  14.553  1       1       1       0       0       0       0
467     12.131  14.540  1       1       1       0       0       0       0       ! Concrete strut 6
468     12.369  14.540  1       1       1       0       0       0       0
469     17.261  14.2    1       1       1       0       0       0       0       ! LEVEL4
CONNECTION6, Bottom steel
470     17.879  14.2    1       1       1       0       0       0       0
471     17.592  14.6    1       1       1       0       0       0       0       ! Top steel
472     17.908  14.6    1       1       1       0       0       0       0
473     17.730  14.595  1       1       1       0       0       0       0       ! Shear spring
474     17.750  14.595  1       1       1       0       0       0       0
475     17.631  14.650  1       1       1       0       0       0       0       ! Concrete strut 1
476     17.869  14.650  1       1       1       0       0       0       0
477     17.631  14.637  1       1       1       0       0       0       0       ! Concrete strut 2
478     17.869  14.637  1       1       1       0       0       0       0
479     17.631  14.611  1       1       1       0       0       0       0       ! Concrete strut 3
480     17.869  14.611  1       1       1       0       0       0       0
481     17.631  14.579  1       1       1       0       0       0       0       ! Concrete strut 4
482     17.869  14.579  1       1       1       0       0       0       0
483     17.631  14.553  1       1       1       0       0       0       0       ! Concrete strut 5
484     17.869  14.553  1       1       1       0       0       0       0
```

```
485     17.631  14.540  1       1       1       0       0       0       0       ! Concrete strut 6
486     17.869  14.540  1       1       1       0       0       0       0
487     0.150   17.8    1       1       1       0       0       0       0       ! LEVEL5
CONNECTION1, Bottom steel
488     0.710   17.8    1       1       1       0       0       0       0
489     0.123   18.2    1       1       1       0       0       0       0       ! Top steel
490     0.377   18.2    1       1       1       0       0       0       0
491     0.250   18.195  1       1       1       0       0       0       0       ! Shear spring
492     0.270   18.195  1       1       1       0       0       0       0
493     0.155   18.250  1       1       1       0       0       0       0       ! Concrete strut 1
494     0.345   18.250  1       1       1       0       0       0       0
495     0.155   18.237  1       1       1       0       0       0       0       ! Concrete strut 2
496     0.345   18.237  1       1       1       0       0       0       0
497     0.155   18.211  1       1       1       0       0       0       0       ! Concrete strut 3
498     0.345   18.211  1       1       1       0       0       0       0
499     0.155   18.179  1       1       1       0       0       0       0       ! Concrete strut 4
500     0.345   18.179  1       1       1       0       0       0       0
501     0.155   18.153  1       1       1       0       0       0       0       ! Concrete strut 5
502     0.345   18.153  1       1       1       0       0       0       0
503     0.155   18.140  1       1       1       0       0       0       0       ! Concrete strut 6
504     0.345   18.140  1       1       1       0       0       0       0
505     5.290   17.8    1       1       1       0       0       0       0       ! LEVEL5
CONNECTION2, Bottom steel
506     5.850   17.8    1       1       1       0       0       0       0
507     5.623   18.2    1       1       1       0       0       0       0       ! Top steel
508     5.877   18.2    1       1       1       0       0       0       0
509     5.730   18.195  1       1       1       0       0       0       0       ! Shear spring
510     5.750   18.195  1       1       1       0       0       0       0
511     5.655   18.250  1       1       1       0       0       0       0       ! Concrete strut 1
512     5.845   18.250  1       1       1       0       0       0       0
513     5.655   18.237  1       1       1       0       0       0       0       ! Concrete strut 2
514     5.845   18.237  1       1       1       0       0       0       0
515     5.655   18.211  1       1       1       0       0       0       0       ! Concrete strut 3
516     5.845   18.211  1       1       1       0       0       0       0
517     5.655   18.179  1       1       1       0       0       0       0       ! Concrete strut 4
518     5.845   18.179  1       1       1       0       0       0       0
519     5.655   18.153  1       1       1       0       0       0       0       ! Concrete strut 5
520     5.845   18.153  1       1       1       0       0       0       0
521     5.655   18.140  1       1       1       0       0       0       0       ! Concrete strut 6
522     5.845   18.140  1       1       1       0       0       0       0
523     6.150   17.8    1       1       1       0       0       0       0       ! LEVEL5
CONNECTION3, Bottom steel
524     6.710   17.8    1       1       1       0       0       0       0
525     6.123   18.2    1       1       1       0       0       0       0       ! Top steel
526     6.377   18.2    1       1       1       0       0       0       0
527     6.250   18.195  1       1       1       0       0       0       0       ! Shear spring
528     6.270   18.195  1       1       1       0       0       0       0
529     6.155   18.250  1       1       1       0       0       0       0       ! Concrete strut 1
530     6.345   18.250  1       1       1       0       0       0       0
531     6.155   18.237  1       1       1       0       0       0       0       ! Concrete strut 2
532     6.345   18.237  1       1       1       0       0       0       0
533     6.155   18.211  1       1       1       0       0       0       0       ! Concrete strut 3
534     6.345   18.211  1       1       1       0       0       0       0
535     6.155   18.179  1       1       1       0       0       0       0       ! Concrete strut 4
536     6.345   18.179  1       1       1       0       0       0       0
537     6.155   18.153  1       1       1       0       0       0       0       ! Concrete strut 5
538     6.345   18.153  1       1       1       0       0       0       0
539     6.155   18.140  1       1       1       0       0       0       0       ! Concrete strut 6
540     6.345   18.140  1       1       1       0       0       0       0
541     11.290  17.8    1       1       1       0       0       0       0       ! LEVEL5
CONNECTION4, Bottom steel
542     11.850  17.8    1       1       1       0       0       0       0
543     11.623  18.2    1       1       1       0       0       0       0       ! Top steel
544     11.877  18.2    1       1       1       0       0       0       0
545     11.730  18.195  1       1       1       0       0       0       0       ! Shear spring
546     11.750  18.195  1       1       1       0       0       0       0
547     11.655  18.250  1       1       1       0       0       0       0       ! Concrete strut 1
548     11.845  18.250  1       1       1       0       0       0       0
549     11.655  18.237  1       1       1       0       0       0       0       ! Concrete strut 2
550     11.845  18.237  1       1       1       0       0       0       0
551     11.655  18.211  1       1       1       0       0       0       0       ! Concrete strut 3
552     11.845  18.211  1       1       1       0       0       0       0
553     11.655  18.179  1       1       1       0       0       0       0       ! Concrete strut 4
554     11.845  18.179  1       1       1       0       0       0       0
555     11.655  18.153  1       1       1       0       0       0       0       ! Concrete strut 5
556     11.845  18.153  1       1       1       0       0       0       0
557     11.655  18.140  1       1       1       0       0       0       0       ! Concrete strut 6
558     11.845  18.140  1       1       1       0       0       0       0
559     12.150  17.8    1       1       1       0       0       0       0       ! LEVEL5
CONNECTION5, Bottom steel
560     12.710  17.8    1       1       1       0       0       0       0
561     12.123  18.2    1       1       1       0       0       0       0       ! Top steel
562     12.377  18.2    1       1       1       0       0       0       0
563     12.250  18.195  1       1       1       0       0       0       0       ! Shear spring
564     12.270  18.195  1       1       1       0       0       0       0
565     12.155  18.250  1       1       1       0       0       0       0       ! Concrete strut 1
566     12.345  18.250  1       1       1       0       0       0       0
567     12.155  18.237  1       1       1       0       0       0       0       ! Concrete strut 2
```

```
568     12.345  18.237  1       1       1       0       0       0       0
569     12.155  18.211  1       1       1       0       0       0       0       ! Concrete strut 3
570     12.345  18.211  1       1       1       0       0       0       0
571     12.155  18.179  1       1       1       0       0       0       0       ! Concrete strut 4
572     12.345  18.179  1       1       1       0       0       0       0
573     12.155  18.153  1       1       1       0       0       0       0       ! Concrete strut 5
574     12.345  18.153  1       1       1       0       0       0       0
575     12.155  18.140  1       1       1       0       0       0       0       ! Concrete strut 6
576     12.345  18.140  1       1       1       0       0       0       0
577     17.290  17.8    1       1       1       0       0       0       0       ! LEVEL5
CONNECTION6, Bottom steel
578     17.850  17.8    1       1       1       0       0       0       0
579     17.623  18.2    1       1       1       0       0       0       0       ! Top steel
580     17.877  18.2    1       1       1       0       0       0       0
581     17.730  18.195  1       1       1       0       0       0       0       ! Shear spring
582     17.750  18.195  1       1       1       0       0       0       0
583     17.655  18.250  1       1       1       0       0       0       0       ! Concrete strut 1
584     17.845  18.250  1       1       1       0       0       0       0
585     17.655  18.237  1       1       1       0       0       0       0       ! Concrete strut 2
586     17.845  18.237  1       1       1       0       0       0       0
587     17.655  18.211  1       1       1       0       0       0       0       ! Concrete strut 3
588     17.845  18.211  1       1       1       0       0       0       0
589     17.655  18.179  1       1       1       0       0       0       0       ! Concrete strut 4
590     17.845  18.179  1       1       1       0       0       0       0
591     17.655  18.153  1       1       1       0       0       0       0       ! Concrete strut 5
592     17.845  18.153  1       1       1       0       0       0       0
593     17.655  18.140  1       1       1       0       0       0       0       ! Concrete strut 6
594     17.845  18.140  1       1       1       0       0       0       0

DRIFT ANGLE
1       5       9       13      17      21

ELEMENTS
! N     MT      I       J       i       j       IOUT
1       1       1       5       0       0       0       ! Level 1 columns
2       2       2       6       0       0       0
3       2       3       7       0       0       0
4       1       4       8       0       0       0
5       3       5       9       0       0       0       ! Level 2 columns
6       3       6       10      0       0       0
7       3       7       11      0       0       0
8       3       8       12      0       0       0
9       3       9       13      0       0       0       ! Level 3 columns
10      3       10      14      0       0       0
11      3       11      15      0       0       0
12      3       12      16      0       0       0
13      3       13      17      0       0       0       ! Level 4 columns
14      3       14      18      0       0       0
15      3       15      19      0       0       0
16      3       16      20      0       0       0
17      3       17      21      0       0       0       ! Level 5 columns
18      3       18      22      0       0       0
19      3       19      23      0       0       0
20      3       20      24      0       0       0
21      4       25      26      0       0       0       ! Level 1 beams
22      4       27      28      0       0       0
23      4       29      30      0       0       0
24      4       31      32      0       0       0       ! Level 2 beams
25      4       33      34      0       0       0
26      4       35      36      0       0       0
27      4       37      38      0       0       0       ! Level 3 beams
28      4       39      40      0       0       0
29      4       41      42      0       0       0
30      4       43      44      0       0       0       ! Level 4 beams
31      4       45      46      0       0       0
32      4       47      48      0       0       0
33      5       49      50      0       0       0       ! Level 5 beams
34      5       51      52      0       0       0
35      5       53      54      0       0       0
36      6       5       25      55      56      0       ! LEVEL1 CONNECTION1, Bottom steel
37      7       5       25      57      58      0       ! Top steel
38      8       5       25      59      60      0       ! Shear spring
39      9       5       25      61      62      0       ! Concrete strut 1
40      10      5       25      63      64      0       ! Concrete strut 2
41      11      5       25      65      66      0       ! Concrete strut 3
42      11      5       25      67      68      0       ! Concrete strut 4
43      10      5       25      69      70      0       ! Concrete strut 5
44      9       5       25      71      72      0       ! Concrete strut 6
45      6       26      6       73      74      0       ! LEVEL1 CONNECTION2, Bottom steel
46      7       26      6       75      76      0       ! Top steel
47      8       26      6       77      78      0       ! Shear spring
48      9       26      6       79      80      0       ! Concrete strut 1
49      10      26      6       81      82      0       ! Concrete strut 2
50      11      26      6       83      84      0       ! Concrete strut 3
51      11      26      6       85      86      0       ! Concrete strut 4
52      10      26      6       87      88      0       ! Concrete strut 5
53      9       26      6       89      90      0       ! Concrete strut 6
54      6       6       27      91      92      0       ! LEVEL1 CONNECTION3, Bottom steel
```

```
55      7       6       27      93      94      0       ! Top steel
56      8       6       27      95      96      0       ! Shear spring
57      9       6       27      97      98      0       ! Concrete strut 1
58      10      6       27      99      100     0       ! Concrete strut 2
59      11      6       27      101     102     0       ! Concrete strut 3
60      11      6       27      103     104     0       ! Concrete strut 4
61      10      6       27      105     106     0       ! Concrete strut 5
62      9       6       27      107     108     0       ! Concrete strut 6
63      6       28      7       109     110     0       ! LEVEL1 CONNECTION4, Bottom steel
64      7       28      7       111     112     0       ! Top steel
65      8       28      7       113     114     0       ! Shear spring
66      9       28      7       115     116     0       ! Concrete strut 1
67      10      28      7       117     118     0       ! Concrete strut 2
68      11      28      7       119     120     0       ! Concrete strut 3
69      11      28      7       121     122     0       ! Concrete strut 4
70      10      28      7       123     124     0       ! Concrete strut 5
71      9       28      7       125     126     0       ! Concrete strut 6
72      6       7       29      127     128     0       ! LEVEL1 CONNECTION5, Bottom steel
73      7       7       29      129     130     0       ! Top steel
74      8       7       29      131     132     0       ! Shear spring
75      9       7       29      133     134     0       ! Concrete strut 1
76      10      7       29      135     136     0       ! Concrete strut 2
77      11      7       29      137     138     0       ! Concrete strut 3
78      11      7       29      139     140     0       ! Concrete strut 4
79      10      7       29      141     142     0       ! Concrete strut 5
80      9       7       29      143     144     0       ! Concrete strut 6
81      6       30      8       145     146     0       ! LEVEL1 CONNECTION6, Bottom steel
82      7       30      8       147     148     0       ! Top steel
83      8       30      8       149     150     0       ! Shear spring
84      9       30      8       151     152     0       ! Concrete strut 1
85      10      30      8       153     154     0       ! Concrete strut 2
86      11      30      8       155     156     0       ! Concrete strut 3
87      11      30      8       157     158     0       ! Concrete strut 4
88      10      30      8       159     160     0       ! Concrete strut 5
89      9       30      8       161     162     0       ! Concrete strut 6
90      12      9       31      163     164     0       ! LEVEL2 CONNECTION1, Bottom steel
91      13      9       31      165     166     0       ! Top steel
92      14      9       31      167     168     0       ! Shear spring
93      15      9       31      169     170     0       ! Concrete strut 1
94      16      9       31      171     172     0       ! Concrete strut 2
95      17      9       31      173     174     0       ! Concrete strut 3
96      17      9       31      175     176     0       ! Concrete strut 4
97      16      9       31      177     178     0       ! Concrete strut 5
98      15      9       31      179     180     0       ! Concrete strut 6
99      12      32      10      181     182     0       ! LEVEL2 CONNECTION2, Bottom steel
100     13      32      10      183     184     0       ! Top steel
101     14      32      10      185     186     0       ! Shear spring
102     15      32      10      187     188     0       ! Concrete strut 1
103     16      32      10      189     190     0       ! Concrete strut 2
104     17      32      10      191     192     0       ! Concrete strut 3
105     17      32      10      193     194     0       ! Concrete strut 4
106     16      32      10      195     196     0       ! Concrete strut 5
107     15      32      10      197     198     0       ! Concrete strut 6
108     12      10      33      199     200     0       ! LEVEL2 CONNECTION3, Bottom steel
109     13      10      33      201     202     0       ! Top steel
110     14      10      33      203     204     0       ! Shear spring
111     15      10      33      205     206     0       ! Concrete strut 1
112     16      10      33      207     208     0       ! Concrete strut 2
113     17      10      33      209     210     0       ! Concrete strut 3
114     17      10      33      211     212     0       ! Concrete strut 4
115     16      10      33      213     214     0       ! Concrete strut 5
116     15      10      33      215     216     0       ! Concrete strut 6
117     12      34      11      217     218     0       ! LEVEL2 CONNECTION4, Bottom steel
118     13      34      11      219     220     0       ! Top steel
119     14      34      11      221     222     0       ! Shear spring
120     15      34      11      223     224     0       ! Concrete strut 1
121     16      34      11      225     226     0       ! Concrete strut 2
122     17      34      11      227     228     0       ! Concrete strut 3
123     17      34      11      229     230     0       ! Concrete strut 4
124     16      34      11      231     232     0       ! Concrete strut 5
125     15      34      11      233     234     0       ! Concrete strut 6
126     12      11      35      235     236     0       ! LEVEL2 CONNECTION5, Bottom steel
127     13      11      35      237     238     0       ! Top steel
128     14      11      35      239     240     0       ! Shear spring
129     15      11      35      241     242     0       ! Concrete strut 1
130     16      11      35      243     244     0       ! Concrete strut 2
131     17      11      35      245     246     0       ! Concrete strut 3
132     17      11      35      247     248     0       ! Concrete strut 4
133     16      11      35      249     250     0       ! Concrete strut 5
134     15      11      35      251     252     0       ! Concrete strut 6
135     12      36      12      253     254     0       ! LEVEL2 CONNECTION6, Bottom steel
136     13      36      12      255     256     0       ! Top steel
137     14      36      12      257     258     0       ! Shear spring
138     15      36      12      259     260     0       ! Concrete strut 1
139     16      36      12      261     262     0       ! Concrete strut 2
140     17      36      12      263     264     0       ! Concrete strut 3
141     17      36      12      265     266     0       ! Concrete strut 4
142     16      36      12      267     268     0       ! Concrete strut 5
```

```
143     15      36      12      269     270     0       ! Concrete strut 6
144     18      13      37      271     272     0       ! LEVEL3 CONNECTION1, Bottom steel
145     19      13      37      273     274     0       ! Top steel
146     20      13      37      275     276     0       ! Shear spring
147     21      13      37      277     278     0       ! Concrete strut 1
148     22      13      37      279     280     0       ! Concrete strut 2
149     23      13      37      281     282     0       ! Concrete strut 3
150     23      13      37      283     284     0       ! Concrete strut 4
151     22      13      37      285     286     0       ! Concrete strut 5
152     21      13      37      287     288     0       ! Concrete strut 6
153     18      38      14      289     290     0       ! LEVEL3 CONNECTION2, Bottom steel
154     19      38      14      291     292     0       ! Top steel
155     20      38      14      293     294     0       ! Shear spring
156     21      38      14      295     296     0       ! Concrete strut 1
157     22      38      14      297     298     0       ! Concrete strut 2
158     23      38      14      299     300     0       ! Concrete strut 3
159     23      38      14      301     302     0       ! Concrete strut 4
160     22      38      14      303     304     0       ! Concrete strut 5
161     21      38      14      305     306     0       ! Concrete strut 6
162     18      14      39      307     308     0       ! LEVEL3 CONNECTION3, Bottom steel
163     19      14      39      309     310     0       ! Top steel
164     20      14      39      311     312     0       ! Shear spring
165     21      14      39      313     314     0       ! Concrete strut 1
166     22      14      39      315     316     0       ! Concrete strut 2
167     23      14      39      317     318     0       ! Concrete strut 3
168     23      14      39      319     320     0       ! Concrete strut 4
169     22      14      39      321     322     0       ! Concrete strut 5
170     21      14      39      323     324     0       ! Concrete strut 6
171     18      40      15      325     326     0       ! LEVEL3 CONNECTION4, Bottom steel
172     19      40      15      327     328     0       ! Top steel
173     20      40      15      329     330     0       ! Shear spring
174     21      40      15      331     332     0       ! Concrete strut 1
175     22      40      15      333     334     0       ! Concrete strut 2
176     23      40      15      335     336     0       ! Concrete strut 3
177     23      40      15      337     338     0       ! Concrete strut 4
178     22      40      15      339     340     0       ! Concrete strut 5
179     21      40      15      341     342     0       ! Concrete strut 6
180     18      15      41      343     344     0       ! LEVEL3 CONNECTION5, Bottom steel
181     19      15      41      345     346     0       ! Top steel
182     20      15      41      347     348     0       ! Shear spring
183     21      15      41      349     350     0       ! Concrete strut 1
184     22      15      41      351     352     0       ! Concrete strut 2
185     23      15      41      353     354     0       ! Concrete strut 3
186     23      15      41      355     356     0       ! Concrete strut 4
187     22      15      41      357     358     0       ! Concrete strut 5
188     21      15      41      359     360     0       ! Concrete strut 6
189     18      42      16      361     362     0       ! LEVEL3 CONNECTION6, Bottom steel
190     19      42      16      363     364     0       ! Top steel
191     20      42      16      365     366     0       ! Shear spring
192     21      42      16      367     368     0       ! Concrete strut 1
193     22      42      16      369     370     0       ! Concrete strut 2
194     23      42      16      371     372     0       ! Concrete strut 3
195     23      42      16      373     374     0       ! Concrete strut 4
196     22      42      16      375     376     0       ! Concrete strut 5
197     21      42      16      377     378     0       ! Concrete strut 6
198     24      17      43      379     380     0       ! LEVEL4 CONNECTION1, Bottom steel
199     25      17      43      381     382     0       ! Top steel
200     26      17      43      383     384     0       ! Shear spring
201     27      17      43      385     386     0       ! Concrete strut 1
202     28      17      43      387     388     0       ! Concrete strut 2
203     29      17      43      389     390     0       ! Concrete strut 3
204     29      17      43      391     392     0       ! Concrete strut 4
205     28      17      43      393     394     0       ! Concrete strut 5
206     27      17      43      395     396     0       ! Concrete strut 6
207     24      44      18      397     398     0       ! LEVEL4 CONNECTION2, Bottom steel
208     25      44      18      399     400     0       ! Top steel
209     26      44      18      401     402     0       ! Shear spring
210     27      44      18      403     404     0       ! Concrete strut 1
211     28      44      18      405     406     0       ! Concrete strut 2
212     29      44      18      407     408     0       ! Concrete strut 3
213     29      44      18      409     410     0       ! Concrete strut 4
214     28      44      18      411     412     0       ! Concrete strut 5
215     27      44      18      413     414     0       ! Concrete strut 6
216     24      18      45      415     416     0       ! LEVEL4 CONNECTION3, Bottom steel
217     25      18      45      417     418     0       ! Top steel
218     26      18      45      419     420     0       ! Shear spring
219     27      18      45      421     422     0       ! Concrete strut 1
220     28      18      45      423     424     0       ! Concrete strut 2
221     29      18      45      425     426     0       ! Concrete strut 3
222     29      18      45      427     428     0       ! Concrete strut 4
223     28      18      45      429     430     0       ! Concrete strut 5
224     27      18      45      431     432     0       ! Concrete strut 6
225     24      46      19      433     434     0       ! LEVEL4 CONNECTION4, Bottom steel
226     25      46      19      435     436     0       ! Top steel
227     26      46      19      437     438     0       ! Shear spring
228     27      46      19      439     440     0       ! Concrete strut 1
229     28      46      19      441     442     0       ! Concrete strut 2
230     29      46      19      443     444     0       ! Concrete strut 3
```

```
231     29      46      19      445     446     0       ! Concrete strut 4
232     28      46      19      447     448     0       ! Concrete strut 5
233     27      46      19      449     450     0       ! Concrete strut 6
234     24      19      47      451     452     0       ! LEVEL4 CONNECTION5, Bottom steel
235     25      19      47      453     454     0       ! Top steel
236     26      19      47      455     456     0       ! Shear spring
237     27      19      47      457     458     0       ! Concrete strut 1
238     28      19      47      459     460     0       ! Concrete strut 2
239     29      19      47      461     462     0       ! Concrete strut 3
240     29      19      47      463     464     0       ! Concrete strut 4
241     28      19      47      465     466     0       ! Concrete strut 5
242     27      19      47      467     468     0       ! Concrete strut 6
243     24      48      20      469     470     0       ! LEVEL4 CONNECTION6, Bottom steel
244     25      48      20      471     472     0       ! Top steel
245     26      48      20      473     474     0       ! Shear spring
246     27      48      20      475     476     0       ! Concrete strut 1
247     28      48      20      477     478     0       ! Concrete strut 2
248     29      48      20      479     480     0       ! Concrete strut 3
249     29      48      20      481     482     0       ! Concrete strut 4
250     28      48      20      483     484     0       ! Concrete strut 5
251     27      48      20      485     486     0       ! Concrete strut 6
252     30      21      49      487     488     0       ! LEVEL5 CONNECTION1, Bottom steel
253     31      21      49      489     490     0       ! Top steel
254     32      21      49      491     492     0       ! Shear spring
255     33      21      49      493     494     0       ! Concrete strut 1
256     34      21      49      495     496     0       ! Concrete strut 2
257     35      21      49      497     498     0       ! Concrete strut 3
258     35      21      49      499     500     0       ! Concrete strut 4
259     34      21      49      501     502     0       ! Concrete strut 5
260     33      21      49      503     504     0       ! Concrete strut 6
261     30      50      22      505     506     0       ! LEVEL5 CONNECTION2, Bottom steel
262     31      50      22      507     508     0       ! Top steel
263     32      50      22      509     510     0       ! Shear spring
264     33      50      22      511     512     0       ! Concrete strut 1
265     34      50      22      513     514     0       ! Concrete strut 2
266     35      50      22      515     516     0       ! Concrete strut 3
267     35      50      22      517     518     0       ! Concrete strut 4
268     34      50      22      519     520     0       ! Concrete strut 5
269     33      50      22      521     522     0       ! Concrete strut 6
270     30      22      51      523     524     0       ! LEVEL5 CONNECTION3, Bottom steel
271     31      22      51      525     526     0       ! Top steel
272     32      22      51      527     528     0       ! Shear spring
273     33      22      51      529     530     0       ! Concrete strut 1
274     34      22      51      531     532     0       ! Concrete strut 2
275     35      22      51      533     534     0       ! Concrete strut 3
276     35      22      51      535     536     0       ! Concrete strut 4
277     34      22      51      537     538     0       ! Concrete strut 5
278     33      22      51      539     540     0       ! Concrete strut 6
279     30      52      23      541     542     0       ! LEVEL5 CONNECTION4, Bottom steel
280     31      52      23      543     544     0       ! Top steel
281     32      52      23      545     546     0       ! Shear spring
282     33      52      23      547     548     0       ! Concrete strut 1
283     34      52      23      549     550     0       ! Concrete strut 2
284     35      52      23      551     552     0       ! Concrete strut 3
285     35      52      23      553     554     0       ! Concrete strut 4
286     34      52      23      555     556     0       ! Concrete strut 5
287     33      52      23      557     558     0       ! Concrete strut 6
288     30      23      53      559     560     0       ! LEVEL5 CONNECTION5, Bottom steel
289     31      23      53      561     562     0       ! Top steel
290     32      23      53      563     564     0       ! Shear spring
291     33      23      53      565     566     0       ! Concrete strut 1
292     34      23      53      567     568     0       ! Concrete strut 2
293     35      23      53      569     570     0       ! Concrete strut 3
294     35      23      53      571     572     0       ! Concrete strut 4
295     34      23      53      573     574     0       ! Concrete strut 5
296     33      23      53      575     576     0       ! Concrete strut 6
297     30      54      24      577     578     0       ! LEVEL5 CONNECTION6, Bottom steel
298     31      54      24      579     580     0       ! Top steel
299     32      54      24      581     582     0       ! Shear spring
300     33      54      24      583     584     0       ! Concrete strut 1
301     34      54      24      585     586     0       ! Concrete strut 2
302     35      54      24      587     588     0       ! Concrete strut 3
303     35      54      24      589     590     0       ! Concrete strut 4
304     34      54      24      591     592     0       ! Concrete strut 5
305     33      54      24      593     594     0       ! Concrete strut 6

PROPS
! N     MTYPE   LABEL
1       FRAME   Base exterior column'
! ITYPE IPIN    ICOND   IHYST   ILOS    IDAMG   ICOL    IGA     IDUCT
2       0       0       4       0       0       3       0       0
! E     G       A       AS      I       WGT     END1    END2    FJ1     FJ2
2.79E7  1.16E7  0.2     0.2     0.00197 4.8     0       0.25    0       0
! RA    RF      H1      H2
0.01    0.01    0.3     0.3
! PYC   PB      MB      M1B     M2B     M0      PYT     IEND
-8809   -7200   178     503     529     190     942     0
! ALFA  BETA    NF      KKK
```

```
0.25    0.45    1       2

! N     MTYPE   LABEL
2       FRAME   Base interior column'
! ITYPE IPIN    ICOND   IHYST   ILOS    IDAMG   ICOL    IGA     IDUCT
2       0       0       4       0       0       3       0       0
! E     G       A       AS      I       WGT     END1    END2    FJ1     FJ2
2.79E7  1.16E7  0.2     0.2     0.00215 4.8     0       0.25    0       0
! RA    RF      H1      H2
0.005   0.005   0.3     0.3
! PYC   PB      MB      M1B     M2B     M0      PYT     IEND
-8809   -7200   178     503     530     196     942     0
! ALFA  BETA    NF      KKK
0.25    0.45    1       2

! N     MTYPE   LABEL
3       FRAME   Elastic column'
! ITYPE IPIN    ICOND   IHYST   ILOS    IDAMG   ICOL    IGA     IDUCT
2       0       0       0       0       0       3       0       0
! E     G       A       AS      I       WGT     END1    END2    FJ1     FJ2
2.79E7  1.16E7  0.2     0.2     0.00188 4.8     0.25    0.25    0       0

! N     MTYPE   LABEL
4       FRAME   Elastic beam'
! ITYPE IPIN    ICOND   IHYST   ILOS    IDAMG   ICOL    IGA     IDUCT
1       0       0       0       0       0       0       0       0
! E     G       A       AS      I       WGT     END1    END2    FJ1     FJ2
2.79E7  1.16E7  0.15    0.15    0.00125 3.6     0       0       0       0

! N     MTYPE   LABEL
5       FRAME   Elastic roof beam'
! ITYPE IPIN    ICOND   IHYST   ILOS    IDAMG   ICOL    IGA     IDUCT
1       0       0       0       0       0       0       0       0
! E     G       A       AS      I       WGT     END1    END2    FJ1     FJ2
2.79E+07        1.16E+07        0.15    0.15    0.00125 3.6     0       0       0       0

! N     MTYPE   LABEL
6       SPRING  'Level1 Bottom steel'
! ITYPE IHYST   ILOS    IDAMG   KX      KY      GJ      WGT     RF      RT      PSX     PSY     PSZ
        THETA   ITRUSS  IOP     SL
1       39      0       0       508248  0       0       0.14    0       0       0       0       0
        0       0       0       0
! FX+   FX-     FY+     FY-     MZ+     MZ-
580.8   -580.8  0       0       0       0
! ESH   ESU     FSU     OMEGAF
0.0176  0.141   817     1

! N     MTYPE   LABEL
7       SPRING  'Level1 Top steel'
! ITYPE IHYST   ILOS    IDAMG   KX      KY      GJ      WGT     RF      RT      PSX     PSY     PSZ
        THETA   ITRUSS  IOP     SL
1       39      0       0       991414  0       0       0.15    0       0       0       0       0
        0       0       0       0
! FX+   FX-     FY+     FY-     MZ+     MZ-
1060.0  -1060.0 0       0       0       0
! ESH   ESU     FSU     OMEGAF
0.0063  0.059   1315    1

! N     MTYPE   LABEL
8       SPRING  'Level1 Shear spring'
! ITYPE IHYST   ILOS    IDAMG   KX      KY      GJ      WGT     RF      RT      PSX     PSY     PSZ
        THETA   ITRUSS  IOP     SL
1       0       0       0       0       388464  0       0.08    0       0       0       0       0
        0       0       0       0

! N     MTYPE   LABEL
9       SPRING  'Level1 Concrete hinge 1 6'
! ITYPE IHYST   ILOS    IDAMG   KX      KY      GJ      WGT     RF      RT      PSX     PSY     PSZ
        THETA   ITRUSS  IOP     SL
1       54      0       0       103324  0       0       0.026   0       0       0       0       0
        0       0       0       0
! FX+   FX-     FY+     FY-     MZ+     MZ-4    -44     0       0       0       0
! TLIMT CLIMIT  BETA    Fbo     L       TFACTOR CFACTOR eTT
0.0025  0.005   1       0.2     1       1       1

! N     MTYPE   LABEL
10      SPRING  'Level1 Concrete hinge 2 5'
! ITYPE IHYST   ILOS    IDAMG   KX      KY      GJ      WGT     RF      RT      PSX     PSY     PSZ
        THETA   ITRUSS  IOP     SL
1       54      0       0       586584  0       0       0.150   0       0       0       0       0
        0       0       0       0
! FX+   FX-     FY+     FY-     MZ+     MZ-
24      -250    0       0       0       0
! TLIMT CLIMIT  BETA    Fbo     L       TFACTOR CFACTOR eTT
0.0025  0.005   1       0.2     1       1       1

! N     MTYPE   LABEL
11      SPRING  'Level1 Concrete hinge 3 4
```

```
! ITYPE IHYST   ILOS    IDAMG   KX      KY      GJ      WGT     RF      RT      PSX     PSY     PSZ
        THETA   ITRUSS  IOP     SL
1       54      0       0       859954  0       0       0.220   0       0       0       0       0
        0       0       0       0
! FX+   FX-     FY+     FY-     MZ+     MZ-
35      -366    0       0       0       0
! TLIMT CLIMIT  BETA    Fbo     L       TFACTOR CFACTOR eTT
0.0025  0.005   1       0.2     1       1       1

! N     MTYPE   LABEL
12      SPRING  'Level2 Bottom steel'
! ITYPE IHYST   ILOS    IDAMG   KX      KY      GJ      WGT     RF      RT      PSX     PSY     PSZ
        THETA   ITRUSS  IOP     SL
1       39      0       0       472314  0       0       0.13    0       0       0       0       0
        0       0       0       0
! FX+   FX-     FY+     FY-     MZ+     MZ-
523.3   -523.3  0       0       0       0
! ESH   ESU     FSU     OMEGAF
0.0170  0.136   736     1

! N     MTYPE   LABEL
13      SPRING  'Level2 Top steel'
! ITYPE IHYST   ILOS    IDAMG   KX      KY      GJ      WGT     RF      RT      PSX     PSY     PSZ
        THETA   ITRUSS  IOP     SL
1       39      0       0       991414  0       0       0.15    0       0       0       0       0
        0       0       0       0
! FX+   FX-     FY+     FY-     MZ+     MZ-
1060.0  -1060.0 0       0       0       0
! ESH   ESU     FSU     OMEGAF
0.0063  0.059   1315    1

! N     MTYPE   LABEL
14      SPRING  'Level2 Shear spring'
! ITYPE IHYST   ILOS    IDAMG   KX      KY      GJ      WGT     RF      RT      PSX     PSY     PSZ
        THETA   ITRUSS  IOP     SL
1       0       0       0       0       388464  0       0.08    0       0       0       0       0
        0       0       0       0

! N     MTYPE   LABEL
15      SPRING  'Level2 Concrete hinge 1 6'
! ITYPE IHYST   ILOS    IDAMG   KX      KY      GJ      WGT     RF      RT      PSX     PSY     PSZ
        THETA   ITRUSS  IOP     SL
1       54      0       0       103324  0       0       0.026   0       0       0       0       0
        0       0       0       0
! FX+   FX-     FY+     FY-     MZ+     MZ-
4       -44     0       0       0       0
! TLIMT CLIMIT  BETA    Fbo     L       TFACTOR CFACTOR eTT
0.0025  0.005   1       0.2     1       1       1

! N     MTYPE   LABEL
16      SPRING  'Level2 Concrete hinge 2 5'
! ITYPE IHYST   ILOS    IDAMG   KX      KY      GJ      WGT     RF      RT      PSX     PSY     PSZ
        THETA   ITRUSS  IOP     SL
1       54      0       0       586584  0       0       0.150   0       0       0       0       0
        0       0       0       0
! FX+   FX-     FY+     FY-     MZ+     MZ-
24      -250    0       0       0       0
! TLIMT CLIMIT  BETA    Fbo     L       TFACTOR CFACTOR eTT
0.0025  0.005   1       0.2     1       1       1

! N     MTYPE   LABEL
17      SPRING  'Level2 Concrete hinge 3 4
! ITYPE IHYST   ILOS    IDAMG   KX      KY      GJ      WGT     RF      RT      PSX     PSY     PSZ
        THETA   ITRUSS  IOP     SL
1       54      0       0       859954  0       0       0.220   0       0       0       0       0
        0       0       0       0
! FX+   FX-     FY+     FY-     MZ+     MZ-
35      -366    0       0       0       0
! TLIMT CLIMIT  BETA    Fbo     L       TFACTOR CFACTOR eTT
0.0025  0.005   1       0.2     1       1       1

! N     MTYPE   LABEL
18      SPRING  'Level3 Bottom steel'
! ITYPE IHYST   ILOS    IDAMG   KX      KY      GJ      WGT     RF      RT      PSX     PSY     PSZ
        THETA   ITRUSS  IOP     SL
1       39      0       0       389164  0       0       0.10    0       0       0       0       0
        0       0       0       0
! FX+   FX-     FY+     FY-     MZ+     MZ-
408.5   -408.5  0       0       0       0
! ESH   ESU     FSU     OMEGAF
0.0162  0.129   574     1

! N     MTYPE   LABEL
19      SPRING  'Level3 Top steel'
! ITYPE IHYST   ILOS    IDAMG   KX      KY      GJ      WGT     RF      RT      PSX     PSY     PSZ
        THETA   ITRUSS  IOP     SL
1       39      0       0       903479  0       0       0.13    0       0       0       0       0
        0       0       0       0
```

```
! FX+   FX-     FY+     FY-     MZ+     MZ-
869.4   -869.4  0       0       0       0
! ESH   ESU     FSU     OMEGAF
0.0057  0.053   1079    1

! N     MTYPE   LABEL
20      SPRING  'Level3 Shear spring'
! ITYPE IHYST   ILOS    IDAMG   KX      KY      GJ      WGT     RF      RT      PSX     PSY     PSZ
        THETA   ITRUSS  IOP     SL
1       0       0       0       0       388464  0       0.08    0       0       0       0       0
        0       0       0       0

! N     MTYPE   LABEL
21      SPRING  'Level3 Concrete hinge 1 6'
! ITYPE IHYST   ILOS    IDAMG   KX      KY      GJ      WGT     RF      RT      PSX     PSY     PSZ
        THETA   ITRUSS  IOP     SL
1       54      0       0       114805  0       0       0.026   0       0       0       0       0
        0       0       0       0
! FX+   FX-     FY+     FY-     MZ+     MZ-
4       -44     0       0       0       0
! TLIMT CLIMIT  BETA    Fbo     L       TFACTOR CFACTOR eTT
0.0025  0.005   1       0.2     1       1       1

! N     MTYPE   LABEL
22      SPRING  'Level3 Concrete hinge 2 5'
! ITYPE IHYST   ILOS    IDAMG   KX      KY      GJ      WGT     RF      RT      PSX     PSY     PSZ
        THETA   ITRUSS  IOP     SL
1       54      0       0       651760  0       0       0.150   0       0       0       0       0
        0       0       0       0
! FX+   FX-     FY+     FY-     MZ+     MZ-
24      -250    0       0       0       0
! TLIMT CLIMIT  BETA    Fbo     L       TFACTOR CFACTOR eTT
0.0025  0.005   1       0.2     1       1       1

! N     MTYPE   LABEL
23      SPRING  'Level3 Concrete hinge 3 4
! ITYPE IHYST   ILOS    IDAMG   KX      KY      GJ      WGT     RF      RT      PSX     PSY     PSZ
        THETA   ITRUSS  IOP     SL
1       54      0       0       955505  0       0       0.220   0       0       0       0       0
        0       0       0       0
! FX+   FX-     FY+     FY-     MZ+     MZ-
35      -366    0       0       0       0
! TLIMT CLIMIT  BETA    Fbo     L       TFACTOR CFACTOR eTT
0.0025  0.005   1       0.2     1       1       1

! N     MTYPE   LABEL
24      SPRING  'Level4 Bottom steel'
! ITYPE IHYST   ILOS    IDAMG   KX      KY      GJ      WGT     RF      RT      PSX     PSY     PSZ
        THETA   ITRUSS  IOP     SL
1       39      0       0       333657  0       0       0.08    0       0       0       0       0
        0       0       0       0
! FX+   FX-     FY+     FY-     MZ+     MZ-
334.8   -334.8  0       0       0       0
! ESH   ESU     FSU     OMEGAF
0.0154  0.123   471     1

! N     MTYPE   LABEL
25      SPRING  'Level4 Top steel'
! ITYPE IHYST   ILOS    IDAMG   KX      KY      GJ      WGT     RF      RT      PSX     PSY     PSZ
        THETA   ITRUSS  IOP     SL
1       39      0       0       793561  0       0       0.10    0       0       0       0       0
        0       0       0       0
! FX+   FX-     FY+     FY-     MZ+     MZ-
678.8   -678.8  0       0       0       0
! ESH   ESU     FSU     OMEGAF
0.0051  0.048   842     1

! N     MTYPE   LABEL
26      SPRING  'Level4 Shear spring'
! ITYPE IHYST   ILOS    IDAMG   KX      KY      GJ      WGT     RF      RT      PSX     PSY     PSZ
        THETA   ITRUSS  IOP     SL
1       0       0       0       0       388464  0       0.08    0       0       0       0       0
        0       0       0       0

! N     MTYPE   LABEL
27      SPRING  'Level4 Concrete hinge 1 6'
! ITYPE IHYST   ILOS    IDAMG   KX      KY      GJ      WGT     RF      RT      PSX     PSY     PSZ
        THETA   ITRUSS  IOP     SL
1       54      0       0       129155  0       0       0.026   0       0       0       0       0
        0       0       0       0
! FX+   FX-     FY+     FY-     MZ+     MZ-
4       -44     0       0       0       0
! TLIMT CLIMIT  BETA    Fbo     L       TFACTOR CFACTOR eTT
0.0025  0.005   1       0.2     1       1       1

! N     MTYPE   LABEL
28      SPRING  'Level4 Concrete hinge 2 5'
```

```
! ITYPE IHYST   ILOS    IDAMG   KX      KY      GJ      WGT     RF      RT      PSX     PSY     PSZ
        THETA   ITRUSS  IOP     SL
1       54      0       0       733230  0       0       0.150   0       0       0       0       0
        0       0       0       0
! FX+   FX-     FY+     FY-     MZ+     MZ-
24      -250    0       0       0       0
! TLIMT CLIMIT  BETA    Fbo     L       TFACTOR CFACTOR eTT
0.0025  0.005   1       0.2     1       1       1

! N     MTYPE   LABEL
29      SPRING  'Level4 Concrete hinge 3 4
! ITYPE IHYST   ILOS    IDAMG   KX      KY      GJ      WGT     RF      RT      PSX     PSY     PSZ
        THETA   ITRUSS  IOP     SL
1       54      0       0       1074943 0       0       0.220   0       0       0       0       0
        0       0       0       0
! FX+   FX-     FY+     FY-     MZ+     MZ-
35      -366    0       0       0       0
! TLIMT CLIMIT  BETA    Fbo     L       TFACTOR CFACTOR eTT
0.0025  0.005   1       0.2     1       1       1

! N     MTYPE   LABEL
30      SPRING  'Level5 Bottom steel'
! ITYPE IHYST   ILOS    IDAMG   KX      KY      GJ      WGT     RF      RT      PSX     PSY     PSZ
        THETA   ITRUSS  IOP     SL
1       39      0       0       224206  0       0       0.05    0       0       0       0       0
        0       0       0       0
! FX+   FX-     FY+     FY-     MZ+     MZ-
204.1   -204.1  0       0       0       0
! ESH   ESU     FSU     OMEGAF
0.0140  0.112   287     1

! N     MTYPE   LABEL
31      SPRING  'Level5 Top steel'
! ITYPE IHYST   ILOS    IDAMG   KX      KY      GJ      WGT     RF      RT      PSX     PSY     PSZ
        THETA   ITRUSS  IOP     SL
1       39      0       0       634470  0       0       0.06    0       0       0       0       0
        0       0       0       0
! FX+   FX-     FY+     FY-     MZ+     MZ-
434.2   -434.2  0       0       0       0
! ESH   ESU     FSU     OMEGAF
0.0041  0.038   539     1

! N     MTYPE   LABEL
32      SPRING  'Level5 Shear spring'
! ITYPE IHYST   ILOS    IDAMG   KX      KY      GJ      WGT     RF      RT      PSX     PSY     PSZ
        THETA   ITRUSS  IOP     SL
1       0       0       0       0       388464  0       0.08    0       0       0       0       0
        0       0       0       0

! N     MTYPE   LABEL
33      SPRING  'Level5 Concrete hinge 1 6'
! ITYPE IHYST   ILOS    IDAMG   KX      KY      GJ      WGT     RF      RT      PSX     PSY     PSZ
        THETA   ITRUSS  IOP     SL
1       54      0       0       161444  0       0       0.026   0       0       0       0       0
        0       0       0       0
! FX+   FX-     FY+     FY-     MZ+     MZ-
4       -44     0       0       0       0
! TLIMT CLIMIT  BETA    Fbo     L       TFACTOR CFACTOR eTT
0.0025  0.005   1       0.2     1       1       1

! N     MTYPE   LABEL
34      SPRING  'Level5 Concrete hinge 2 5'
! ITYPE IHYST   ILOS    IDAMG   KX      KY      GJ      WGT     RF      RT      PSX     PSY     PSZ
        THETA   ITRUSS  IOP     SL
1       54      0       0       916538  0       0       0.150   0       0       0       0       0
        0       0       0       0
! FX+   FX-     FY+     FY-     MZ+     MZ-
24      -250    0       0       0       0
! TLIMT CLIMIT  BETA    Fbo     L       TFACTOR CFACTOR eTT
0.0025  0.005   1       0.2     1       1       1

! N     MTYPE   LABEL
35      SPRING  'Level5 Concrete hinge 3 4
! ITYPE IHYST   ILOS    IDAMG   KX      KY      GJ      WGT     RF      RT      PSX     PSY     PSZ
        THETA   ITRUSS  IOP     SL
1       54      0       0       1343678 0       0       0.220   0       0       0       0       0
        0       0       0       0
! FX+   FX-     FY+     FY-     MZ+     MZ-
35      -366    0       0       0       0
! TLIMT CLIMIT  BETA    Fbo     L       TFACTOR CFACTOR eTT
0.0025  0.005   1       0.2     1       1       1

WEIGHTS 0
! N     WX      WY      WM
1       0       0       0
2       0       0       0
3       0       0       0
4       0       0       0
```

```
5       306.5   0       0
6       306.5   0       0
7       306.5   0       0
8       306.5   0       0
9       306.5   0       0
10      306.5   0       0
11      306.5   0       0
12      306.5   0       0
13      306.5   0       0
14      306.5   0       0
15      306.5   0       0
16      306.5   0       0
17      306.5   0       0
18      306.5   0       0
19      306.5   0       0
20      306.5   0       0
21      283.3   0       0
22      283.3   0       0
23      283.3   0       0
24      283.3   0       0

LOADS
! N     FX      FY      FM
1       0       0       0
2       0       0       0
3       0       0       0
4       0       0       0
5       0       -96     0
6       0       -236    0
7       0       -236    0
8       0       -96     0
9       0       -96     0
10      0       -236    0
11      0       -236    0
12      0       -96     0
13      0       -96     0
14      0       -236    0
15      0       -236    0
16      0       -96     0
17      0       -96     0
18      0       -236    0
19      0       -236    0
20      0       -96     0
21      0       -91     0
22      0       -222    0
23      0       -222    0
24      0       -91     0
594     0       0       0

EQUAKE  Duzce-H2.txt
! IBERG ISTART  DELTAT  ASCALE  END     VEL     DIS     TSCALE
3       1       0.001   1.585   -1      0       0       1
```

C.3 Monolithic beam Frame Model

C.3.1 Frame Details

Table C- 5: Frame details

Parameter	Value
Number of bays	3
Number of storeys	5
Bay width	6 m
Interstorey height	3.6 m

Table C- 6: Member dimensions

Column Dimension	Value
Depth, h_c	500 mm
Width, b_c	400 mm
Beam Dimension	**Value**
Depth, h_b	500 mm
Width, b	300 mm
Effective depth, d	450 mm

Table C- 7: Member reinforcement

Beam member	Bottom reinforcement	Top reinforcement	Shear reinforcement
Level 1 beams	3-D25 & 1-D20	3-D25 & 1-D20	4-legs R6 @ 110 mm
Level 2 beams	2-D25 & 2-D20	2-D25 & 2-D20	4-legs R6 @ 110 mm
Level 3 beams	4-D20	4-D20	4-legs R6 @ 110 mm
Level 4 beams	2-D20 & 2-D16	2-D20 & 2-D16	4-legs R5 @ 110 mm
Level 5 beams	2-D16 & 2-D12	2-D16 & 2-D12	4-legs R5 @ 90 mm
Column member	**Longitudinal reinforcement**		
Base column	10-D20 distributed evenly around perimeter		

Table C- 8: Steel properties assumed

Material property	Grade300 steel
Elastic modulus, E	200 GPa
Yield strength, f_y	325 MPa
Ultimate strength, f_u	457 MPa
Yield strain, ε_y	0.001625
Strain hardening strain, ε_{sh}	0.025
Ultimate strain, ε_u	0.2
Strain hardening factor, p	4

C.3.2 Ruaumoko2D Datafile

```
FIVE-STOREY FRAME USING PENG'S PLASTIC HINGE ELEMENT
* Units: kN, m, Seconds

! IPANL IFMT    IPLAS   IPCONM  ICTYPE  IPVERT  INLGEO  IPNF    IZERO   ORTHO   IMODE
2       0       1       0       2       0       2       0       0       1       0
! NNP   NMEM    NTYPE   M       MODE1   MODE2   GRAV    C1      C2      DT      TIME    FACTOR
84      65      10      25      1       25      9.81    5       5       0.000025        26      1
! KP    KPA     KPLOT   JOUT    DSTORT  DFACT   XMAX    YMAX    NLEVEL  NUP     IRESID  KDUMP
0       260     260     0       1       5       0.8     0.8     6       2       1       0
! MAXIT MAXCIT  FTEST   WAVEX   WAVEY   THETA   DXMAX   DYMAX   D       OMEGA   F
0       0       0.0001  0       0       0       1       1

NODES
! N     X       Y       Nx      Ny      Nr      Kup-x   Kup-y   Kup-r   IOUT
1       0       0       1       1       1       0       0       0       0       ! Ground level
2       6       0       1       1       1       0       0       0       0
3       12      0       1       1       1       0       0       0       0
4       18      0       1       1       1       0       0       0       0
5       0       3.6     0       0       0       0       0       0       0       ! Level 1
6       6       3.6     0       0       0       0       0       0       0
7       12      3.6     0       0       0       0       0       0       0
8       18      3.6     0       0       0       0       0       0       0
9       0       7.2     0       0       0       0       0       0       0       ! Level 2
10      6       7.2     0       0       0       0       0       0       0
11      12      7.2     0       0       0       0       0       0       0
12      18      7.2     0       0       0       0       0       0       0
13      0       10.8    0       0       0       0       0       0       0       ! Level 3
14      6       10.8    0       0       0       0       0       0       0
15      12      10.8    0       0       0       0       0       0       0
16      18      10.8    0       0       0       0       0       0       0
17      0       14.4    0       0       0       0       0       0       0       ! Level 4
18      6       14.4    0       0       0       0       0       0       0
19      12      14.4    0       0       0       0       0       0       0
20      18      14.4    0       0       0       0       0       0       0
21      0       18      0       0       0       0       0       0       0       ! Level 5
22      6       18      0       0       0       0       0       0       0
23      12      18      0       0       0       0       0       0       0
24      18      18      0       0       0       0       0       0       0
25      0.539   3.6     0       0       0       0       0       0       0       ! Level 1 beams
26      5.461   3.6     0       0       0       0       0       0       0
27      6.539   3.6     0       0       0       0       0       0       0
28      11.461  3.6     0       0       0       0       0       0       0
29      12.539  3.6     0       0       0       0       0       0       0
30      17.461  3.6     0       0       0       0       0       0       0
31      0.513   7.2     0       0       0       0       0       0       0       ! Level 2 beams
32      5.487   7.2     0       0       0       0       0       0       0
33      6.513   7.2     0       0       0       0       0       0       0
34      11.487  7.2     0       0       0       0       0       0       0
35      12.513  7.2     0       0       0       0       0       0       0
36      17.487  7.2     0       0       0       0       0       0       0
37      0.549   10.8    0       0       0       0       0       0       0       ! Level 3 beams
38      5.451   10.8    0       0       0       0       0       0       0
39      6.549   10.8    0       0       0       0       0       0       0
40      11.451  10.8    0       0       0       0       0       0       0
41      12.549  10.8    0       0       0       0       0       0       0
42      17.451  10.8    0       0       0       0       0       0       0
43      0.520   14.4    0       0       0       0       0       0       0       ! Level 4 beams
44      5.480   14.4    0       0       0       0       0       0       0
45      6.520   14.4    0       0       0       0       0       0       0
46      11.480  14.4    0       0       0       0       0       0       0
47      12.520  14.4    0       0       0       0       0       0       0
48      17.480  14.4    0       0       0       0       0       0       0
49      0.446   18      0       0       0       0       0       0       0       ! Level 5 beams
50      5.554   18      0       0       0       0       0       0       0
51      6.446   18      0       0       0       0       0       0       0
52      11.554  18      0       0       0       0       0       0       0
53      12.446  18      0       0       0       0       0       0       0
54      17.554  18      0       0       0       0       0       0       0
55      0.250   3.6     1       1       1       0       0       0       0       ! Level 1 column
faces
56      5.750   3.6     1       1       1       0       0       0       0
57      6.250   3.6     1       1       1       0       0       0       0
58      11.750  3.6     1       1       1       0       0       0       0
59      12.250  3.6     1       1       1       0       0       0       0
60      17.750  3.6     1       1       1       0       0       0       0
61      0.250   7.2     1       1       1       0       0       0       0       ! Level 2 column
faces
62      5.750   7.2     1       1       1       0       0       0       0
63      6.250   7.2     1       1       1       0       0       0       0
64      11.750  7.2     1       1       1       0       0       0       0
65      12.250  7.2     1       1       1       0       0       0       0
66      17.750  7.2     1       1       1       0       0       0       0
```

```
67      0.250   10.8    1       1       1       0       0       0       0       ! Level 3 column
faces
68      5.750   10.8    1       1       1       0       0       0       0
69      6.250   10.8    1       1       1       0       0       0       0
70      11.750  10.8    1       1       1       0       0       0       0
71      12.250  10.8    1       1       1       0       0       0       0
72      17.750  10.8    1       1       1       0       0       0       0
73      0.250   14.4    1       1       1       0       0       0       0       ! Level 4 column
faces
74      5.750   14.4    1       1       1       0       0       0       0
75      6.250   14.4    1       1       1       0       0       0       0
76      11.750  14.4    1       1       1       0       0       0       0
77      12.250  14.4    1       1       1       0       0       0       0
78      17.750  14.4    1       1       1       0       0       0       0
79      0.250   18      1       1       1       0       0       0       0       ! Level 5 column
faces
80      5.750   18      1       1       1       0       0       0       0
81      6.250   18      1       1       1       0       0       0       0
82      11.750  18      1       1       1       0       0       0       0
83      12.250  18      1       1       1       0       0       0       0
84      17.750  18      1       1       1       0       0       0       0

DRIFT ANGLE
1       5       9       13      17      21

ELEMENTS
! N     MT      I       J       i       j       IOUT
1       1       1       5       0       0       0       ! Level 1 columns
2       2       2       6       0       0       0
3       2       3       7       0       0       0
4       1       4       8       0       0       0
5       3       5       9       0       0       0       ! Level 2 columns
6       3       6       10      0       0       0
7       3       7       11      0       0       0
8       3       8       12      0       0       0
9       3       9       13      0       0       0       ! Level 3 columns
10      3       10      14      0       0       0
11      3       11      15      0       0       0
12      3       12      16      0       0       0
13      3       13      17      0       0       0       ! Level 4 columns
14      3       14      18      0       0       0
15      3       15      19      0       0       0
16      3       16      20      0       0       0
17      3       17      21      0       0       0       ! Level 5 columns
18      3       18      22      0       0       0
19      3       19      23      0       0       0
20      3       20      24      0       0       0
21      4       25      26      0       0       0       ! Level 1 beams
22      4       27      28      0       0       0
23      4       29      30      0       0       0
24      4       31      32      0       0       0       ! Level 2 beams
25      4       33      34      0       0       0
26      4       35      36      0       0       0
27      4       37      38      0       0       0       ! Level 3 beams
28      4       39      40      0       0       0
29      4       41      42      0       0       0
30      4       43      44      0       0       0       ! Level 4 beams
31      4       45      46      0       0       0
32      4       47      48      0       0       0
33      5       49      50      0       0       0       ! Level 5 beams
34      5       51      52      0       0       0
35      5       53      54      0       0       0
36      6       5       25      55      0       0       ! Level 1 plastic hinges
37      6       26      6       0       56      0
38      6       6       27      57      0       0
39      6       28      7       0       58      0
40      6       7       29      59      0       0
41      6       30      8       0       60      0
42      7       9       31      61      0       0       ! Level 2 plastic hinges
43      7       32      10      0       62      0
44      7       10      33      63      0       0
45      7       34      11      0       64      0
46      7       11      35      65      0       0
47      7       36      12      0       66      0
48      8       13      37      67      0       0       ! Level 3 plastic hinges
49      8       38      14      0       68      0
50      8       14      39      69      0       0
51      8       40      15      0       70      0
52      8       15      41      71      0       0
53      8       42      16      0       72      0
54      9       17      43      73      0       0       ! Level 4 plastic hinges
55      9       44      18      0       74      0
56      9       18      45      75      0       0
57      9       46      19      0       76      0
58      9       19      47      77      0       0
59      9       48      20      0       78      0
60      10      21      49      79      0       0       ! Level 5 plastic hinges
61      10      50      22      0       80      0
```

```
62      10      22      51      81      0       0
63      10      52      23      0       82      0
64      10      23      53      83      0       0
65      10      54      24      0       84      0

PROPS
! N     MTYPE   LABEL
1       FRAME   Base exterior column'
! ITYPE IPIN    ICOND   IHYST   ILOS    IDAMG   ICOL    IGA     IDUCT
2       0       0       4       0       0       3       0       0
! E     G       A       AS      I       WGT     END1    END2    FJ1     FJ2
2.79E+07        1.16E+07        0.2     0.2     0.00197 4.8     0       0.25    0       0
! RA    RF      H1      H2
0.01    0.01    0.3     0.3
! PYC   PB      MB      M1B     M2B     M0      PYT     IEND
-8809   -7200   178     503     529     190     942     0
! ALFA  BETA    NF      KKK
0.25    0.45    1       2

! N     MTYPE   LABEL
2       FRAME   Base interior column'
! ITYPE IPIN    ICOND   IHYST   ILOS    IDAMG   ICOL    IGA     IDUCT
2       0       0       4       0       0       3       0       0
! E     G       A       AS      I       WGT     END1    END2    FJ1     FJ2
2.79E+07        1.16E+07        0.2     0.2     0.00215 4.8     0       0.25    0       0
! RA    RF      H1      H2
0.005   0.005   0.3     0.3
! PYC   PB      MB      M1B     M2B     M0      PYT     IEND
-8809   -7200   178     503     530     196     942     0
! ALFA  BETA    NF      KKK
0.25    0.45    1       2

! N     MTYPE   LABEL
3       FRAME   Elastic column'
! ITYPE IPIN    ICOND   IHYST   ILOS    IDAMG   ICOL    IGA     IDUCT
2       0       0       0       0       0       3       0       0
! E     G       A       AS      I       WGT     END1    END2    FJ1     FJ2
2.79E+07        1.16E+07        0.2     0.2     0.00188 4.8     0.25    0.25    0       0

! N     MTYPE   LABEL
4       FRAME   Elastic beam'
! ITYPE IPIN    ICOND   IHYST   ILOS    IDAMG   ICOL    IGA     IDUCT
1       0       0       0       0       0       0       0       0
! E     G       A       AS      I       WGT     END1    END2    FJ1     FJ2
2.79E+07        1.16E+07        0.15    0.15    0.00125 3.6     0       0       0       0

! N     MTYPE   LABEL
5       FRAME   Elastic roof beam'
! ITYPE IPIN    ICOND   IHYST   ILOS    IDAMG   ICOL    IGA     IDUCT
1       0       0       0       0       0       0       0       0
! E     G       A       AS      I       WGT     END1    END2    FJ1     FJ2
2.79E+07        1.16E+07        0.15    0.15    0.00125 3.6     0       0       0       0

! N     MTYPE           LABEL
6       REINFORCED      'Level1 Plastic hinge'
! JPLAS B       D       C       HL      WGT     THETA   ISTEEL  CONC
1       0.300   0.500   0.050   0.289   1.04    0       0       0
! EC    FPC     FT      ECC     FPCC    FTC     ECV     FPCV    FTV     DB      FLEXV
3.20E7  -43225  3945    2.79E7  -40000  3795    1.91E7  -13600  2213    0.234   2
! ES    FSC     FST     Atop            Abtm            Slong
2.00E8  -325000 325000  0.001787        0.001787        0.830
! TLMIT CLIMIT  BETA    Fbo     L       TFACTOR CFACTOR eTT
1       0.005   1       0.2     1       1.5     1
! TLMIT CLIMIT  BETA    Fbo     L       TFACTOR CFACTOR eTT
1       0.005   1       0.2     1       1.5     1
! IHARD IBCKL   FYAV    eHARD1  FU      eU      FHARD2  eHARD2  RATIO   EBLKT
2       0       1       15      1.41    123     1.32    50
! TLMIT CLIMIT  BETA    Fbo     L       TFACTOR CFACTOR eTT
0.0025  0.005   1       0.2     1       1       1

! N     MTYPE           LABEL
7       REINFORCED      'Level2 Plastic hinge'
! JPLAS B       D       C       HL      WGT     THETA   ISTEEL  CONC
1       0.300   0.500   0.050   0.263   0.95    0       0       0
! EC    FPC     FT      ECC     FPCC    FTC     ECV     FPCV    FTV     DB      FLEXV
3.30E7  -43164  3942    2.79E7  -40000  3795    1.91E7  -13600  2213    0.220   2
! ES    FSC     FST     Atop    Abtm    Slong
2.00E8  -325000 325000  0.00161 0.00161 0.819
! TLMIT CLIMIT  BETA    Fbo     L       TFACTOR CFACTOR eTT
1       0.005   1       0.2     1       1.5     1
! TLMIT CLIMIT  BETA    Fbo     L       TFACTOR CFACTOR eTT
1       0.005   1       0.2     1       1.5     1
! IHARD IBCKL   FYAV    eHARD1  FU      eU      FHARD2  eHARD2  RATIO   EBLKT
2       0       1       15      1.41    123     1.32    50
! TLMIT CLIMIT  BETA    Fbo     L       TFACTOR CFACTOR eTT
0.0025  0.005   1       0.2     1       1       1

! N     MTYPE           LABEL
```

```
8       REINFORCED      'Level3 Plastic hinge'
! JPLAS B       D       C       HL      WGT     THETA   ISTEEL  CONC
1       0.300   0.500   0.050   0.299   1.08    0       0       0
! EC    FPC     FT      ECC     FPCC    FTC     ECV     FPCV    FTV     DB      FLEXV
3.40E7  -42121  3894    2.79E7  -40000  3795    1.91E7  -13600  2213    0.239   2
! ES    FSC     FST     Atop            Abtm            Slong
2.00E8  -325000 325000  0.001257        0.001257        0.801
! TLMIT CLIMIT  BETA    Fbo     L       TFACTOR CFACTOR eTT
1       0.005   1       0.2     1       1.5     1
! TLMIT CLIMIT  BETA    Fbo     L       TFACTOR CFACTOR eTT
1       0.005   1       0.2     1       1.5     1
! IHARD IBCKL   FYAV    eHARD1  FU      eU      FHARD2  eHARD2  RATIO   EBLKT
2       0       1       15      1.41    123     1.32    50
! TLMIT CLIMIT  BETA    Fbo     L       TFACTOR CFACTOR eTT
0.0025  0.005   1       0.2     1       1       1

! N     MTYPE           LABEL
9       REINFORCED      'Level4 Plastic hinge'
! JPLAS B       D       C       HL      WGT     THETA   ISTEEL  CONC
1       0.300   0.500   0.050   0.270   0.97    0       0       0
! EC    FPC     FT      ECC     FPCC    FTC     ECV     FPCV    FTV     DB      FLEXV
3.30E7  -42720  3922    2.79E7  -40000  3795    1.91E7  -13600  2213    0.224   2
! ES    FSC     FST     Atop    Abtm    Slong
2.00E8  -325000 325000  0.00103 0.00103 0.787
! TLMIT CLIMIT  BETA    Fbo     L       TFACTOR CFACTOR eTT
1       0.005   1       0.2     1       1.5     1
! TLMIT CLIMIT  BETA    Fbo     L       TFACTOR CFACTOR eTT
1       0.005   1       0.2     1       1.5     1
! IHARD IBCKL   FYAV    eHARD1  FU      eU      FHARD2  eHARD2  RATIO   EBLKT
2       0       1       15      1.41    123     1.32    50
! TLMIT CLIMIT  BETA    Fbo     L       TFACTOR CFACTOR eTT
0.0025  0.005   1       0.2     1       1       1

! N     MTYPE           LABEL
10      REINFORCED      'Level5 Plastic hinge'
! JPLAS B       D       C       HL      WGT     THETA   ISTEEL  CONC
1       0.300   0.500   0.050   0.196   0.71    0       0       0
! EC    FPC     FT      ECC     FPCC    FTC     ECV     FPCV    FTV     DB      FLEXV
3.20E7  -43529  3959    2.79E7  -40000  3795    1.91E7  -13600  2213    0.176   2
! ES    FSC     FST     Atop            Abtm            Slong
2.00E8  -325000 325000  0.000628        0.000628        0.758
! TLMIT CLIMIT  BETA    Fbo     L       TFACTOR CFACTOR eTT
1       0.005   1       0.2     1       1.5     1
! TLMIT CLIMIT  BETA    Fbo     L       TFACTOR CFACTOR eTT
1       0.005   1       0.2     1       1.5     1
! IHARD IBCKL   FYAV    eHARD1  FU      eU      FHARD2  eHARD2  RATIO   EBLKT
2       0       1       15      1.41    123     1.32    50
! TLMIT CLIMIT  BETA    Fbo     L       TFACTOR CFACTOR eTT
0.0025  0.005   1       0.2     1       1       1

WEIGHTS 0
! N     WX      WY      WM
1       0       0       0
2       0       0       0
3       0       0       0
4       0       0       0
5       306.5   0       0
6       306.5   0       0
7       306.5   0       0
8       306.5   0       0
9       306.5   0       0
10      306.5   0       0
11      306.5   0       0
12      306.5   0       0
13      306.5   0       0
14      306.5   0       0
15      306.5   0       0
16      306.5   0       0
17      306.5   0       0
18      306.5   0       0
19      306.5   0       0
20      306.5   0       0
21      283.3   0       0
22      283.3   0       0
23      283.3   0       0
24      283.3   0       0

LOADS
! N     FX      FY      FM
1       0       0       0
2       0       0       0
3       0       0       0
4       0       0       0
5       0       -96     0
6       0       -236    0
7       0       -236    0
8       0       -96     0
9       0       -96     0
```

```
10      0       -236    0
11      0       -236    0
12      0       -96     0
13      0       -96     0
14      0       -236    0
15      0       -236    0
16      0       -96     0
17      0       -96     0
18      0       -236    0
19      0       -236    0
20      0       -96     0
21      0       -91     0
22      0       -222    0
23      0       -222    0
24      0       -91     0
84      0       0       0

EQUAKE  Duzce-H2.txt
! IBERG ISTART  DELTAT  ASCALE  END     VEL     DIS     TSCALE
3       1       0.001   1.585   -1      0       0       1
```

APPENDIX D ADDITIONAL TIME HISTORY ANALYSIS RESULTS

This appendix provides time history plots of total base shear, lateral roof displacement and floor elongation in level 1. Plots are given for both slotted and monolithic frames, for both design and maximum credible earthquake events.

D.1 Design Earthquake

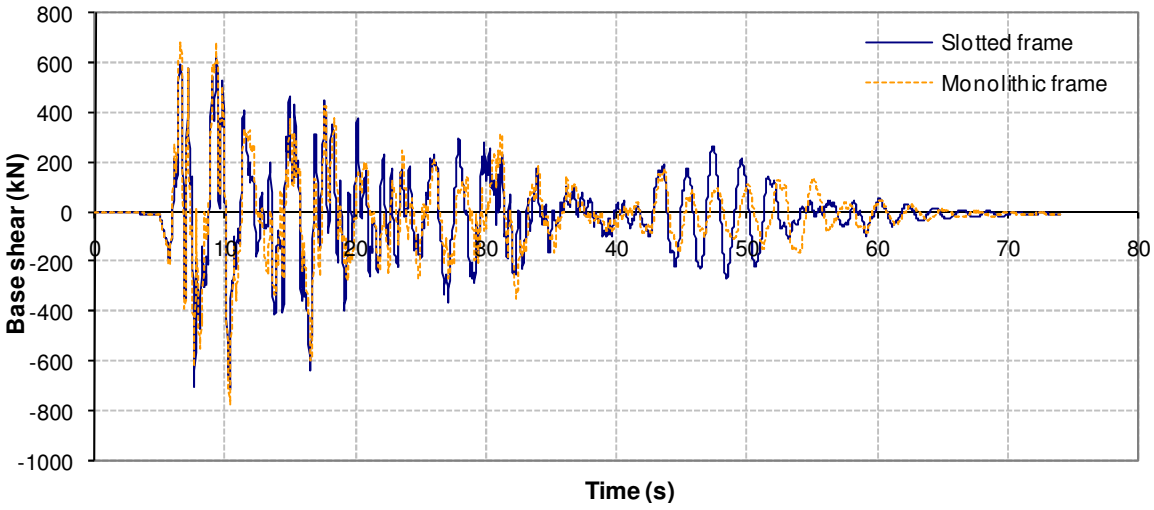

(a) Base shear response

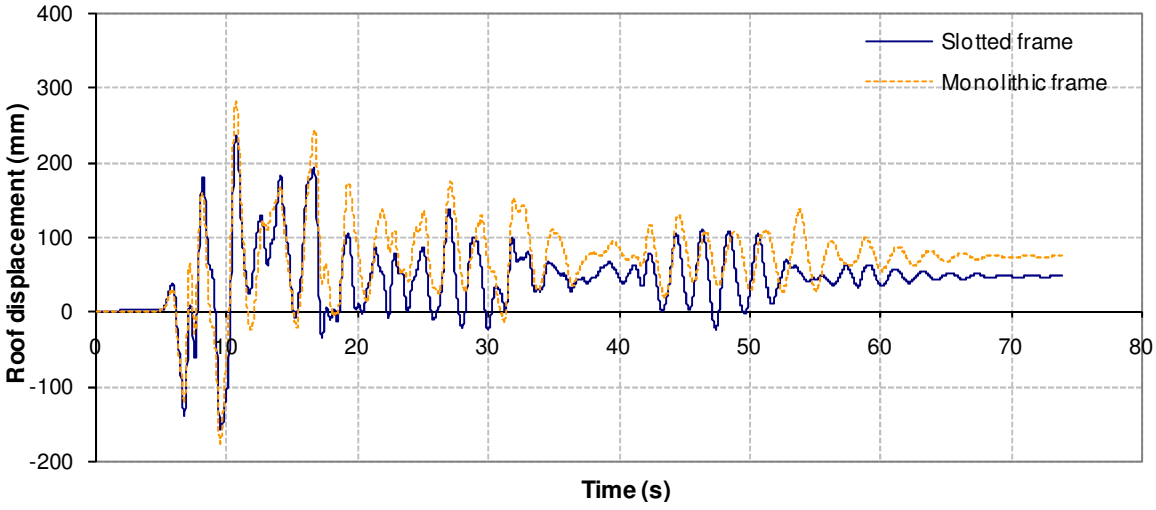

(b) Roof displacement response

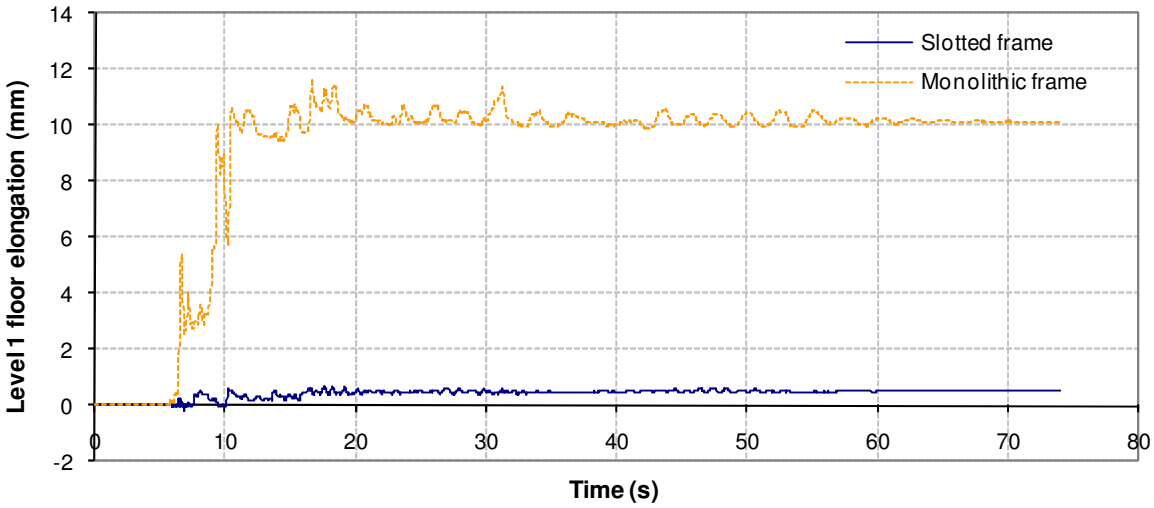

(c) Level 1 floor elongation

Figure D- 1: Imperial Valley 1 1940 earthquake record

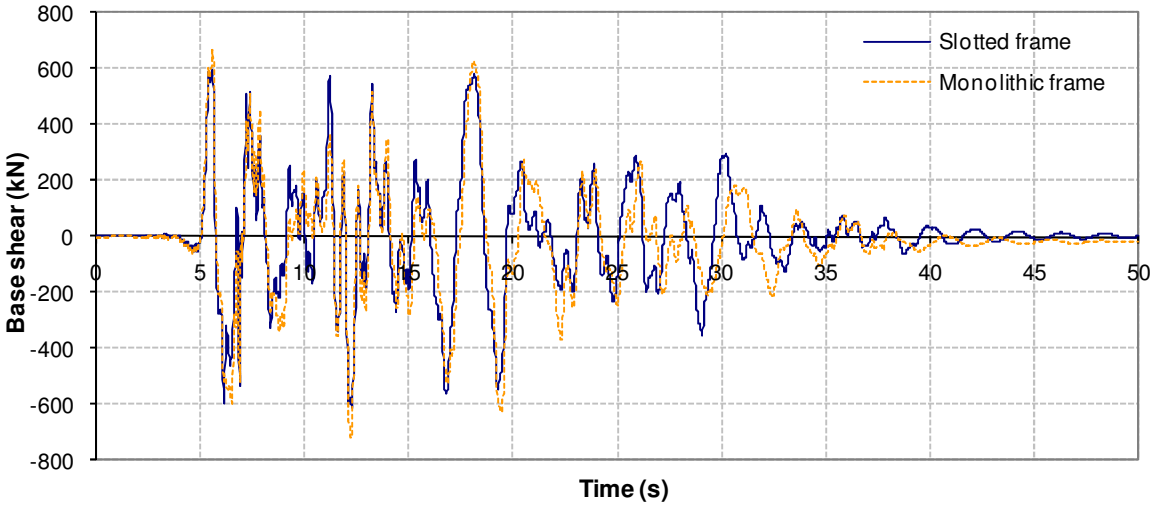

(a) Base shear response

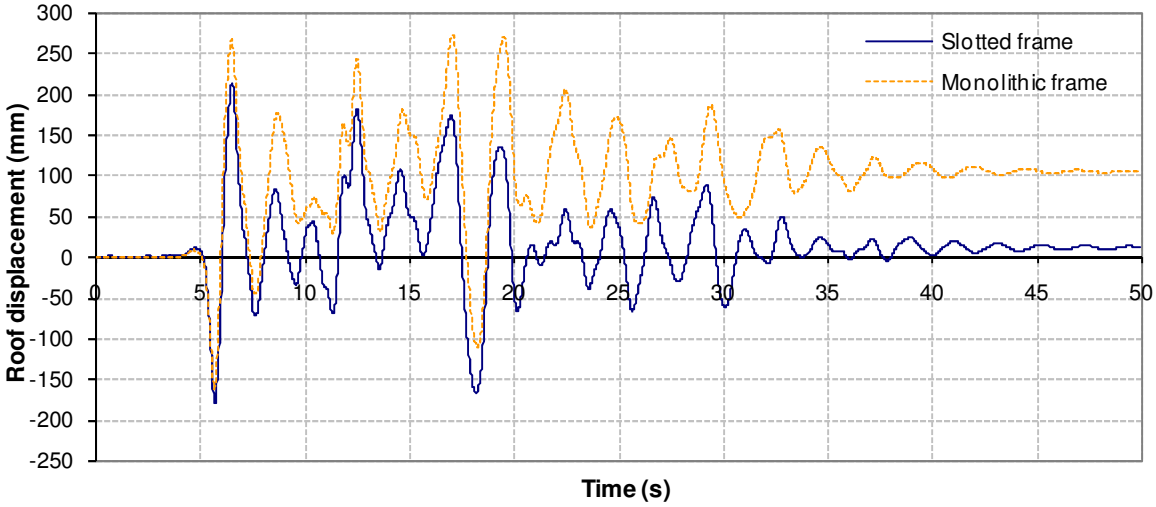

(b) Roof displacement response

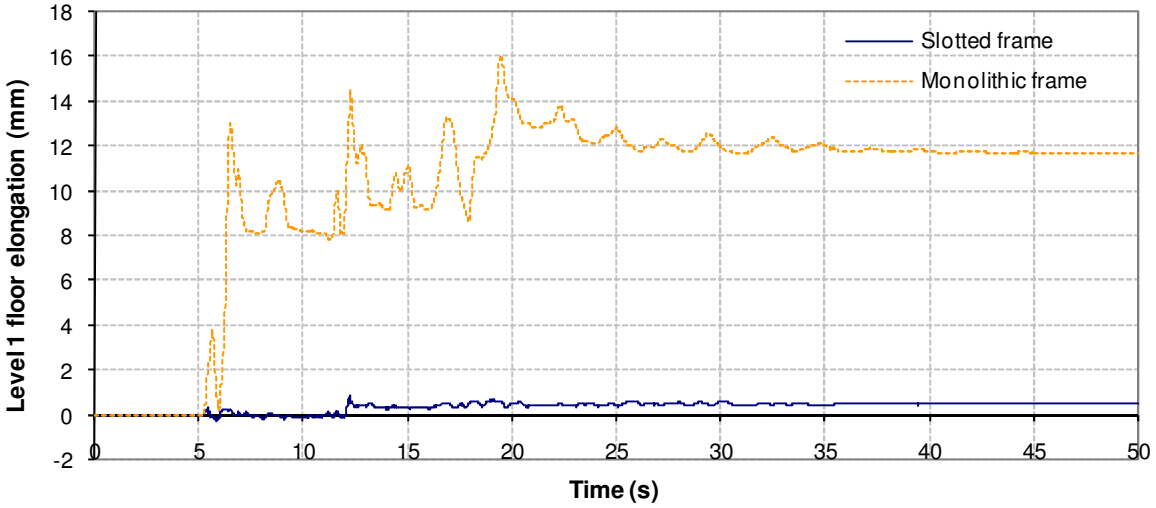

(c) Level 1 floor elongation

Figure D- 2: Imperial Valley 2 1979 earthquake record

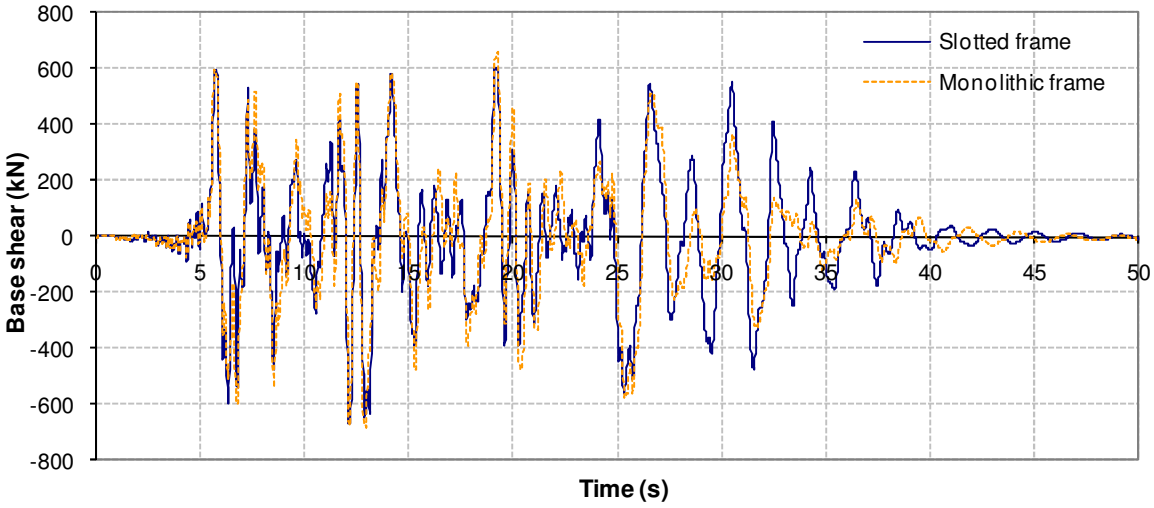

(a) Base shear response

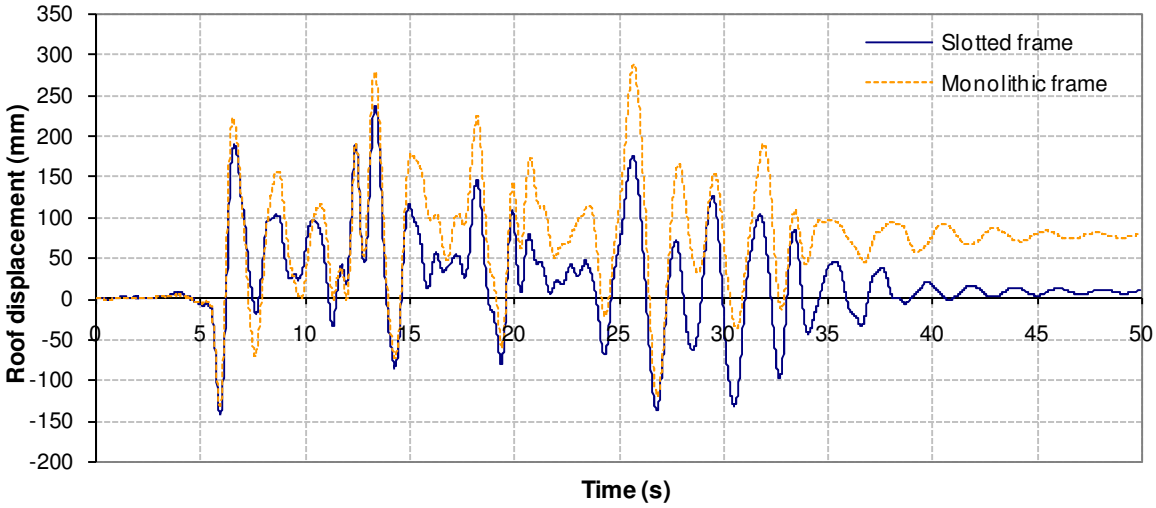

(b) Roof displacement response

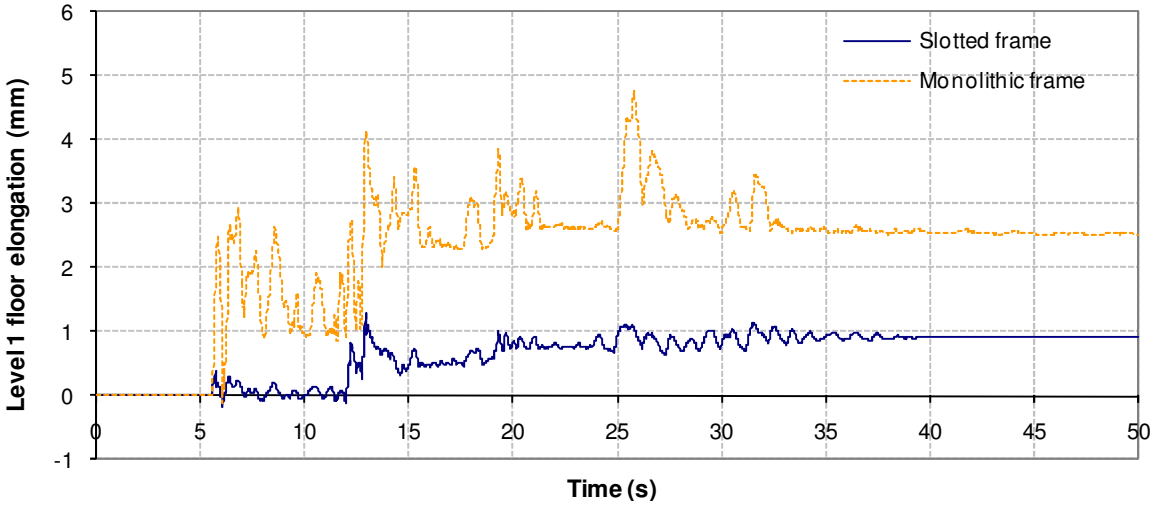

(c) Level 1 floor elongation

Figure D- 3: Imperial Valley 3 1979 earthquake record

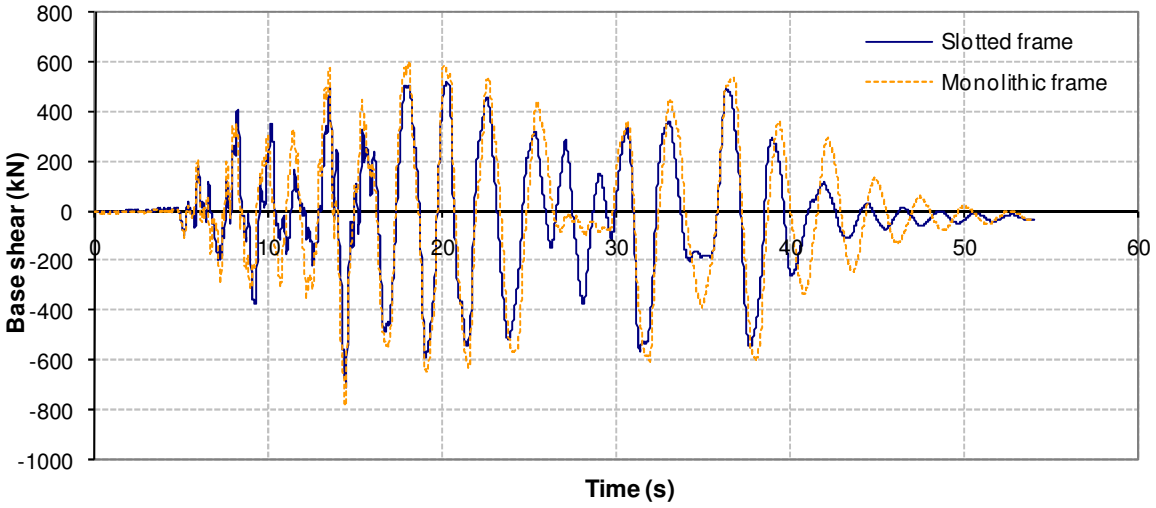

(a) Base shear response

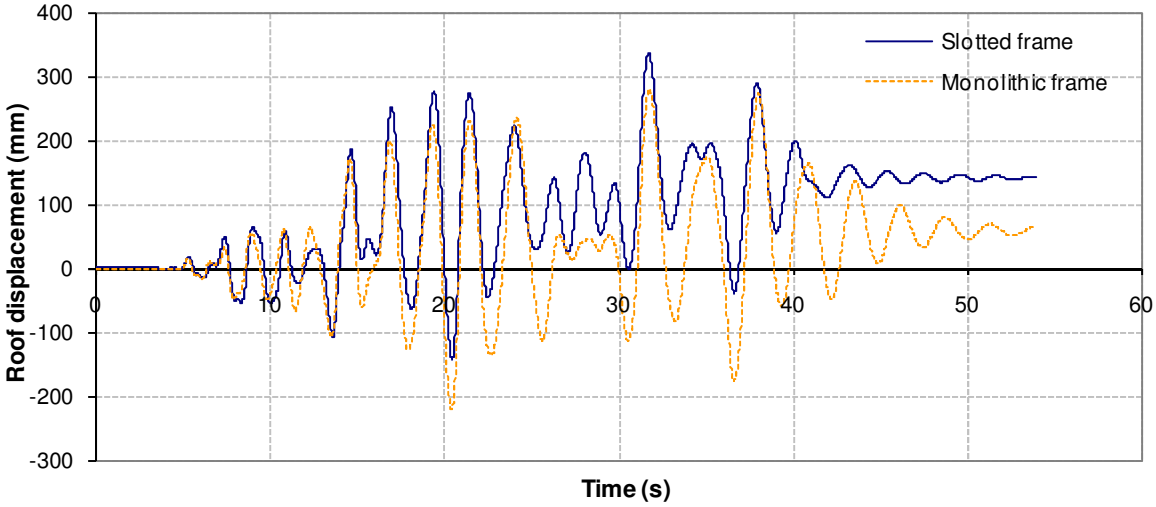

(b) Roof displacement response

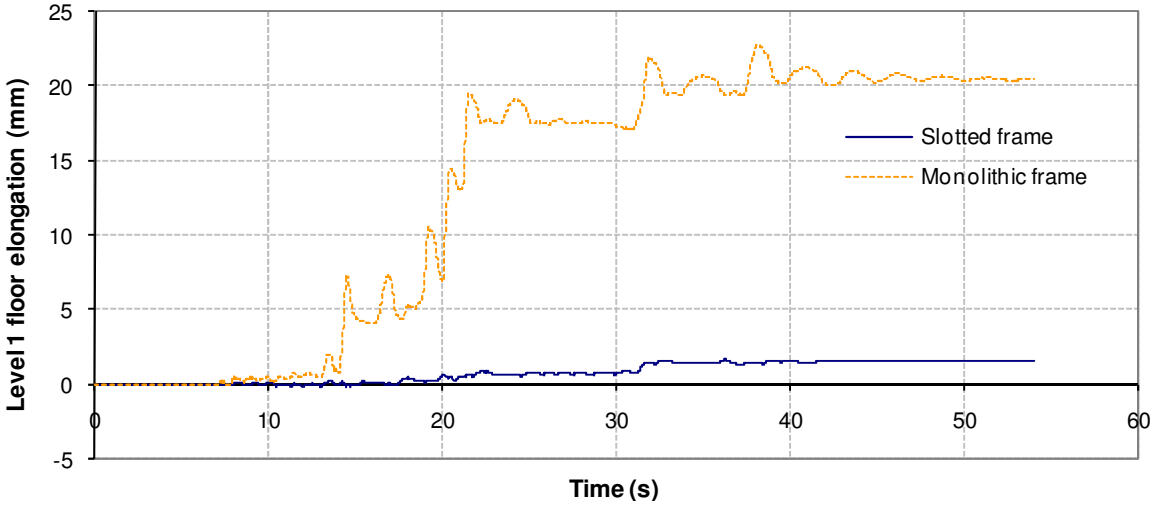

(c) Level 1 floor elongation

Figure D- 4: Superstition hills 1987 earthquake record

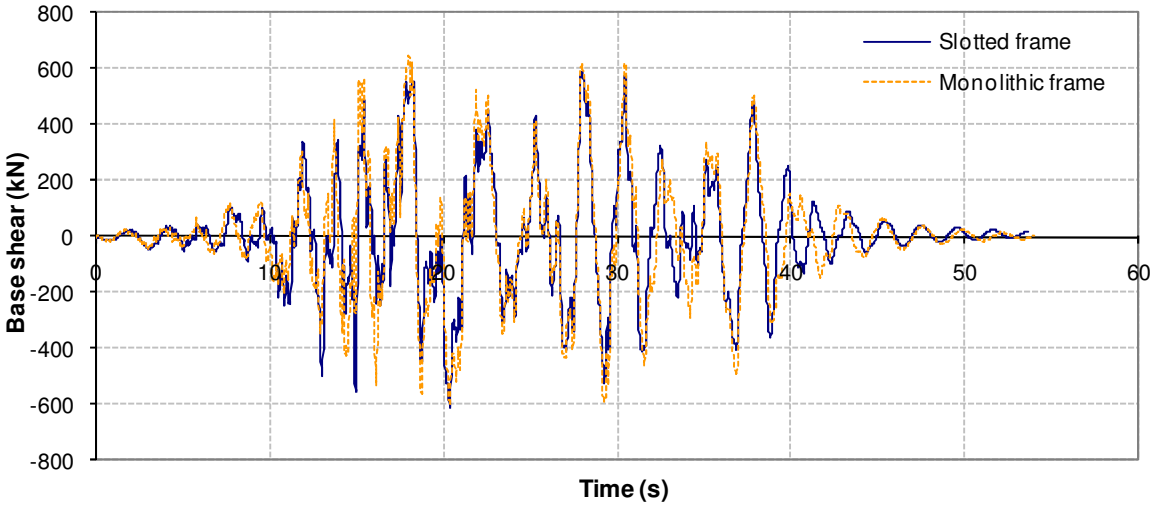

(a) Base shear response

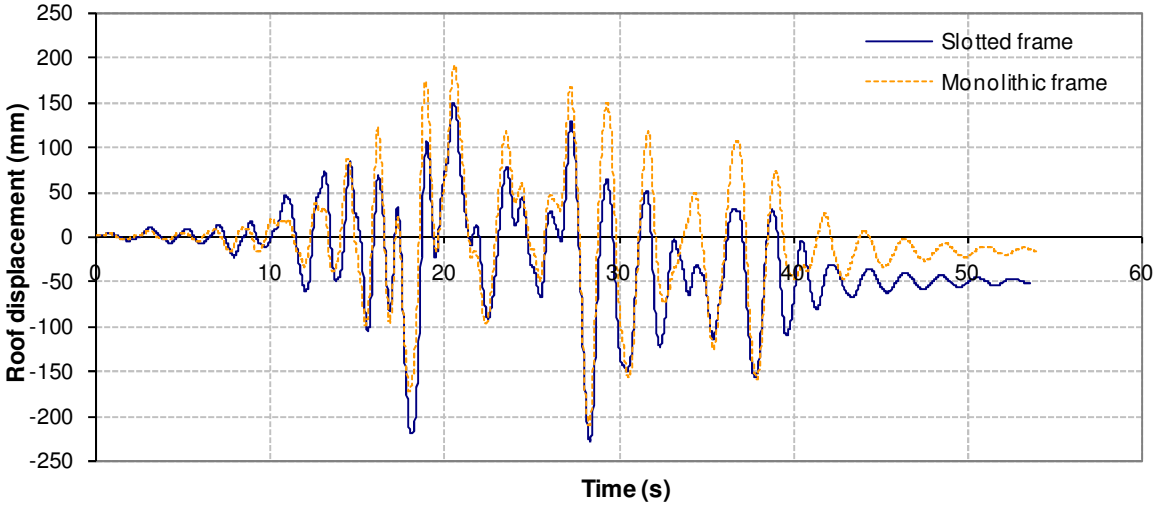

(b) Roof displacement response

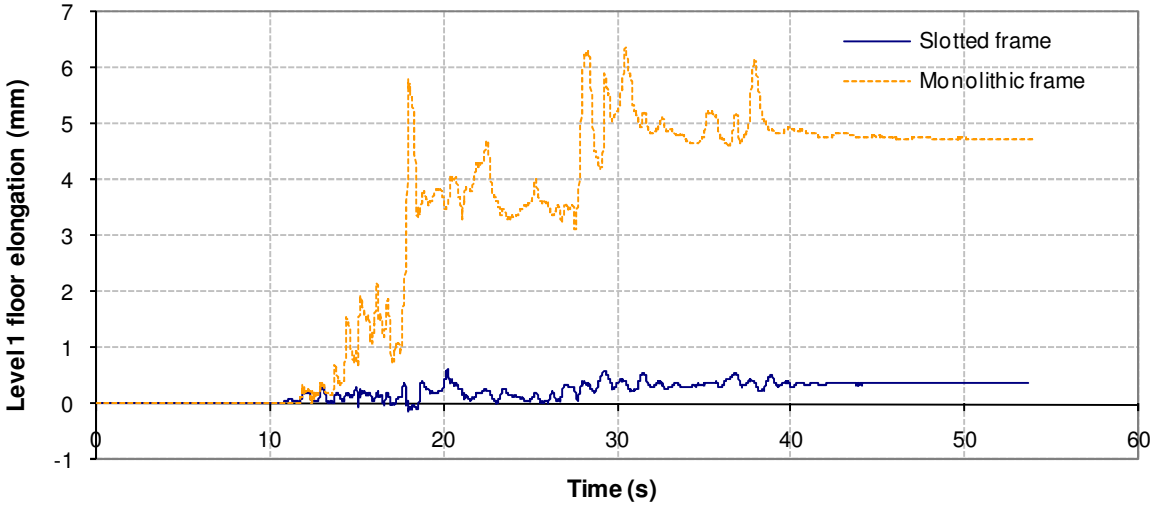

(c) Level 1 floor elongation

Figure D- 5: Landers 1992 earthquake record

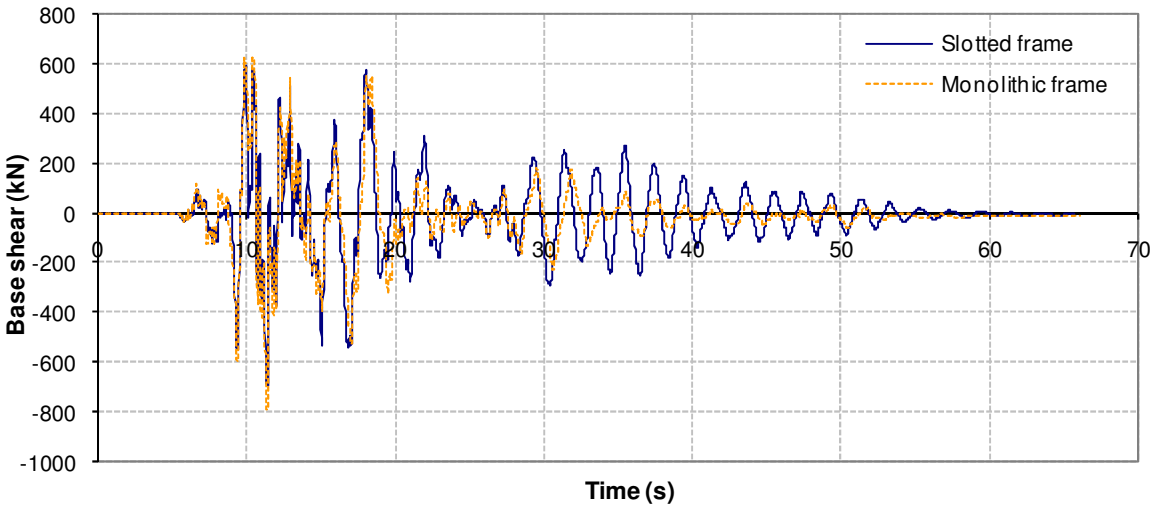

(a) Base shear response

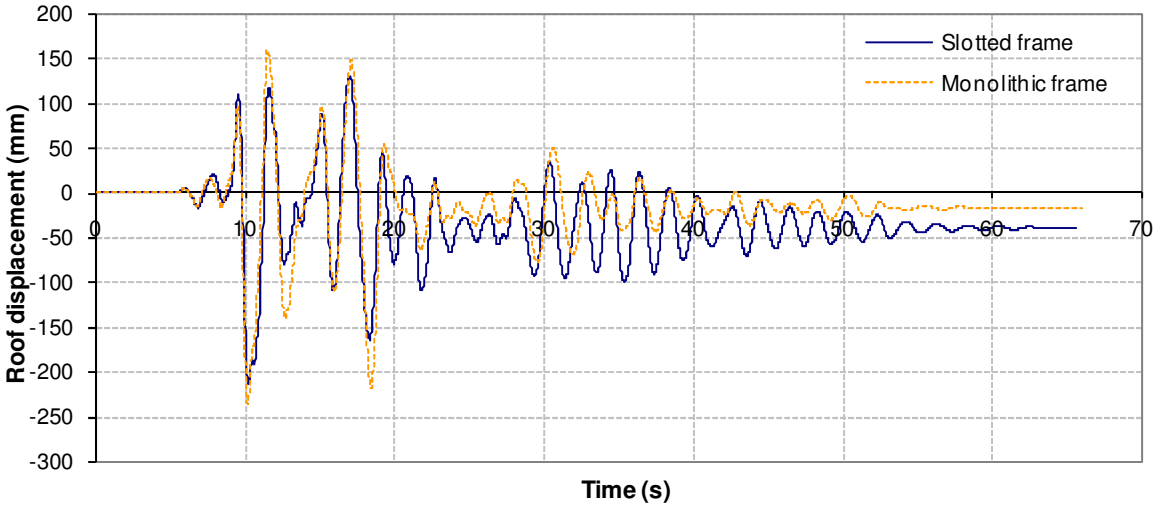

(b) Roof displacement response

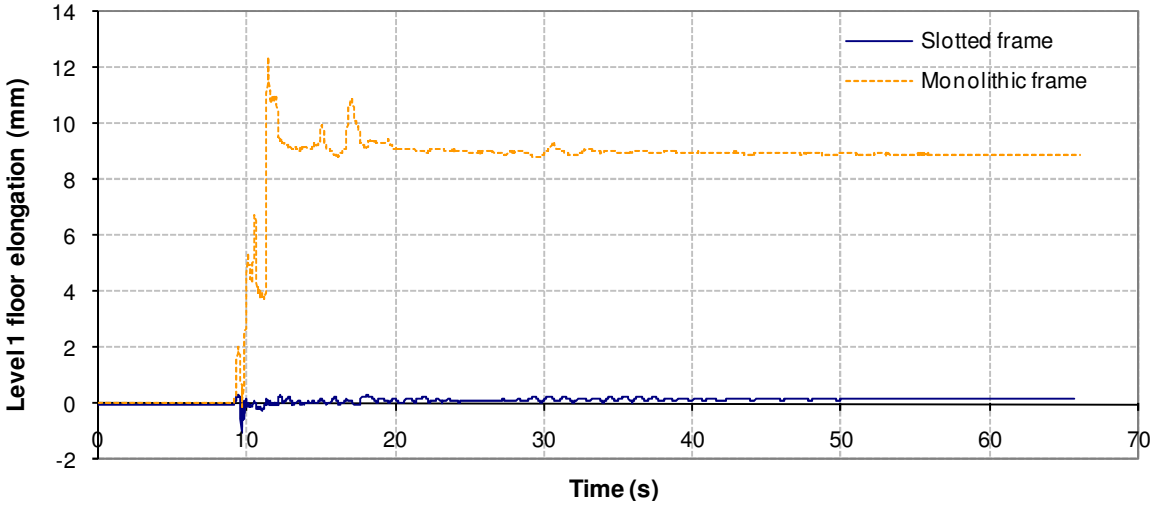

(c) Level 1 floor elongation

Figure D- 6: Turkey 1 1999 earthquake record

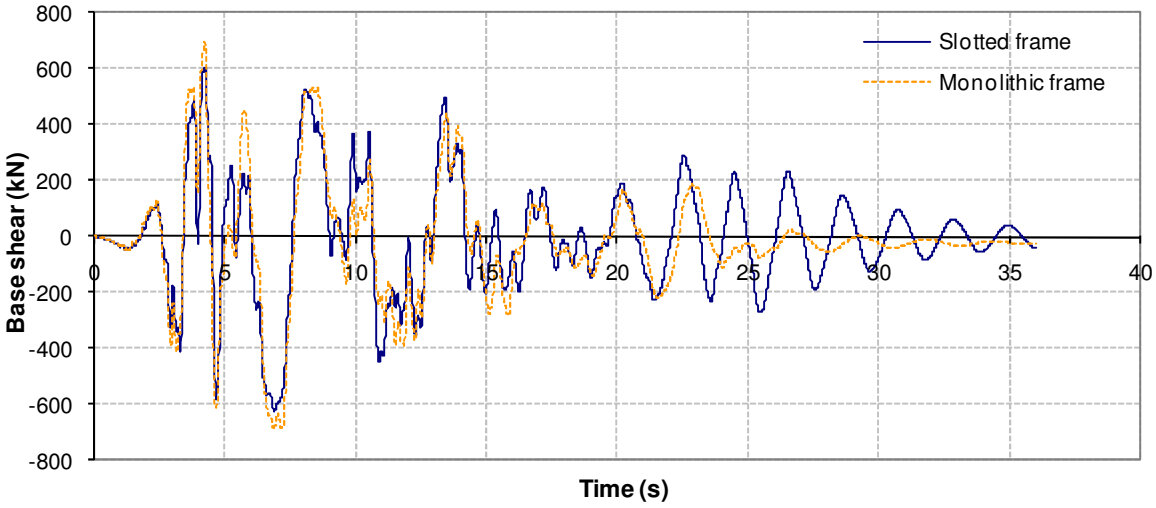

(a) Base shear response

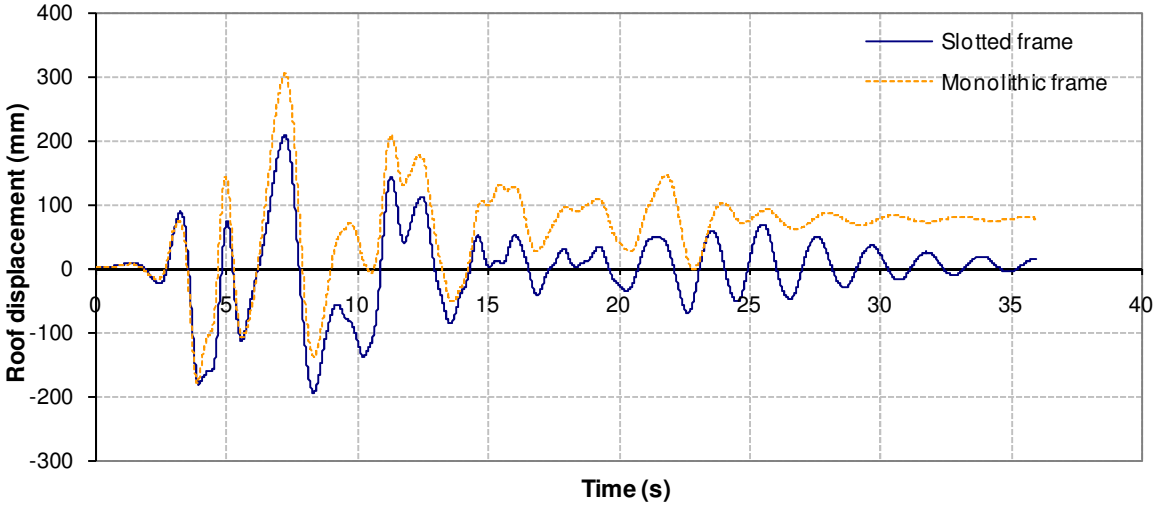

(b) Roof displacement response

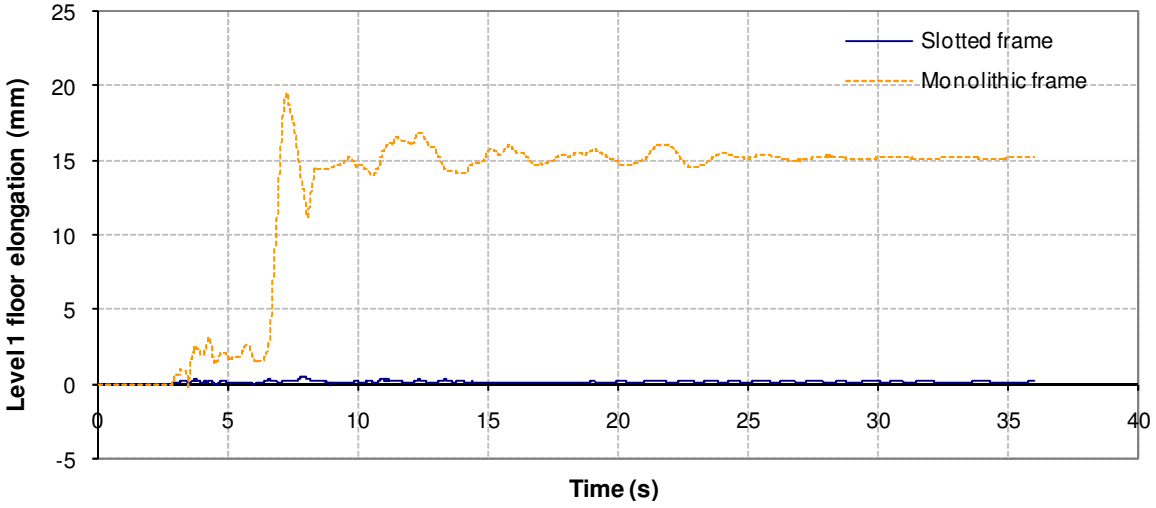

(c) Level 1 floor elongation

Figure D- 7: Turkey 2 1999 earthquake record

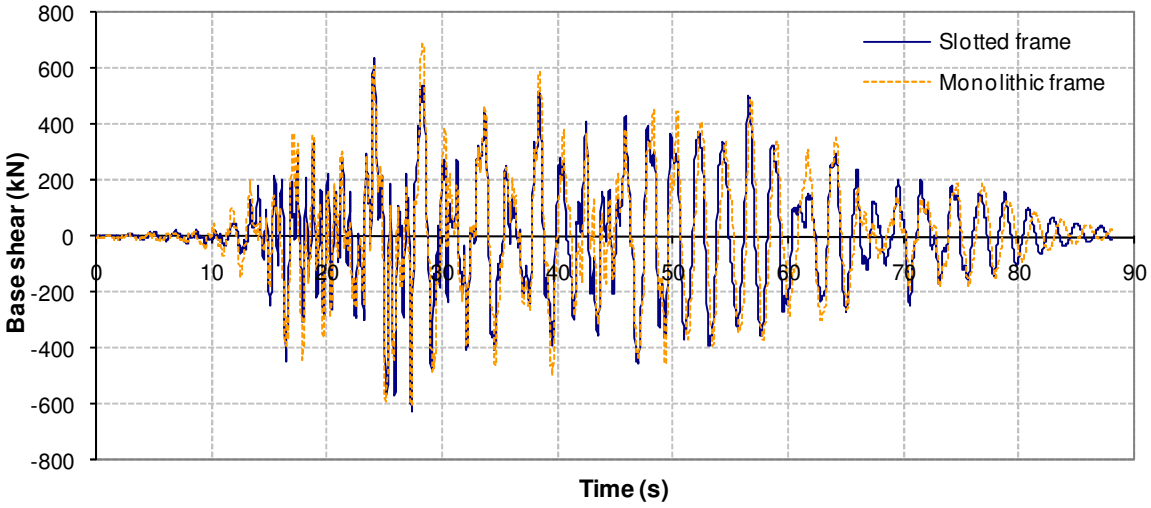

(a) Base shear response

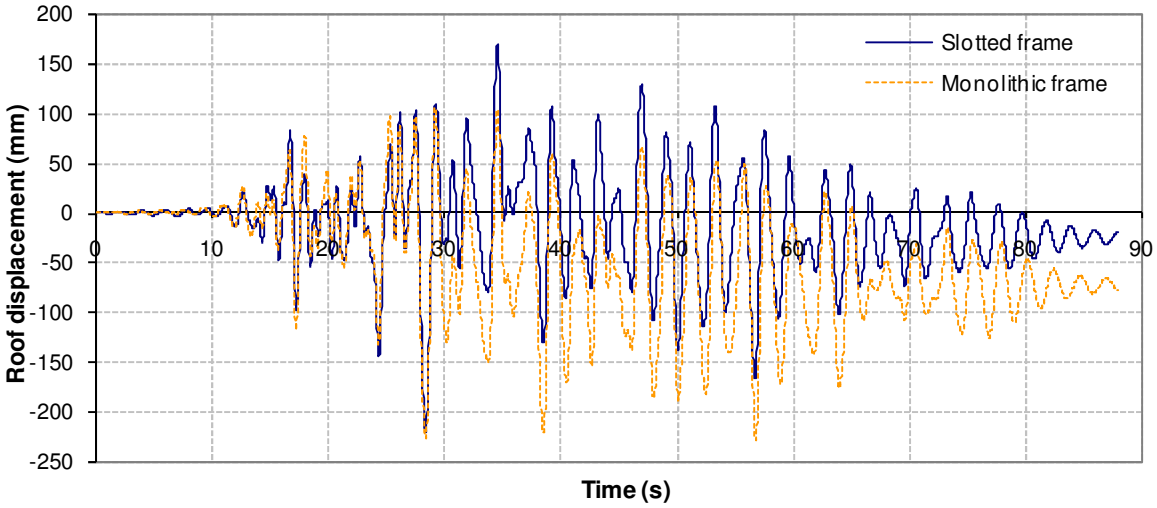

(b) Roof displacement response

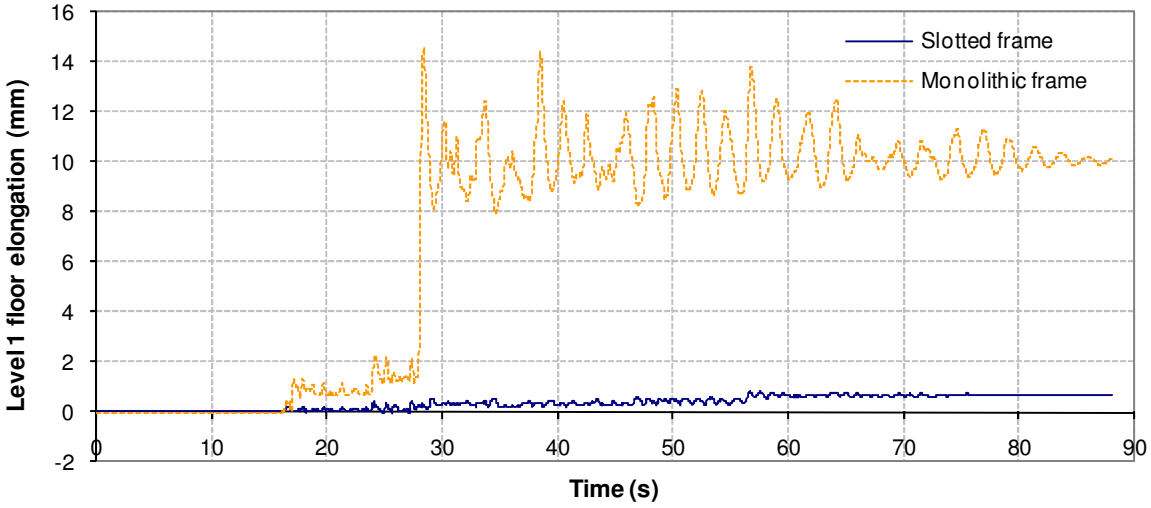

(c) Level 1 floor elongation

Figure D- 8: Hokkaido 2003 earthquake record

D.2 Maximum Credible Earthquake

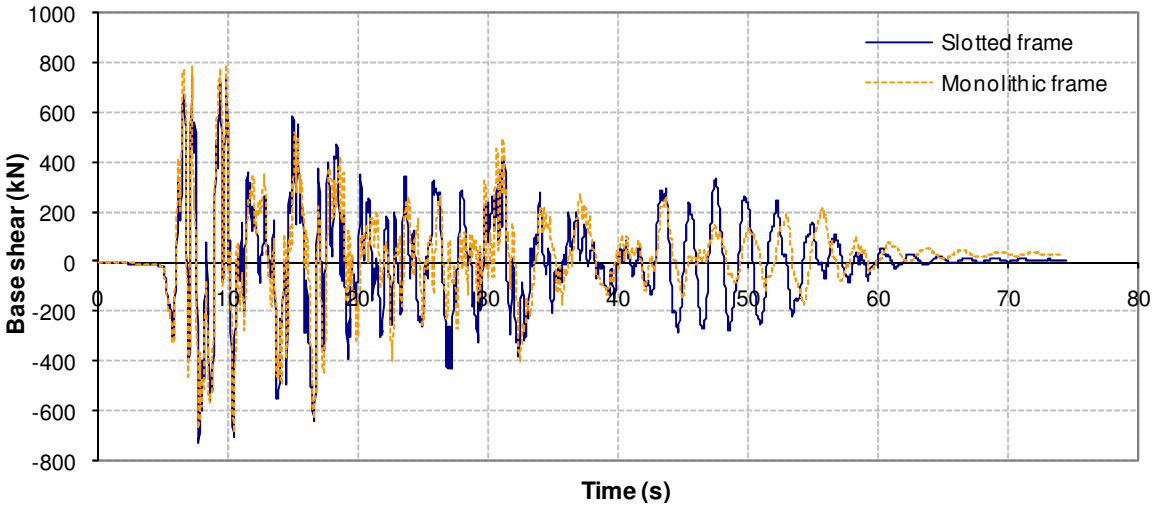

(a) Base shear response

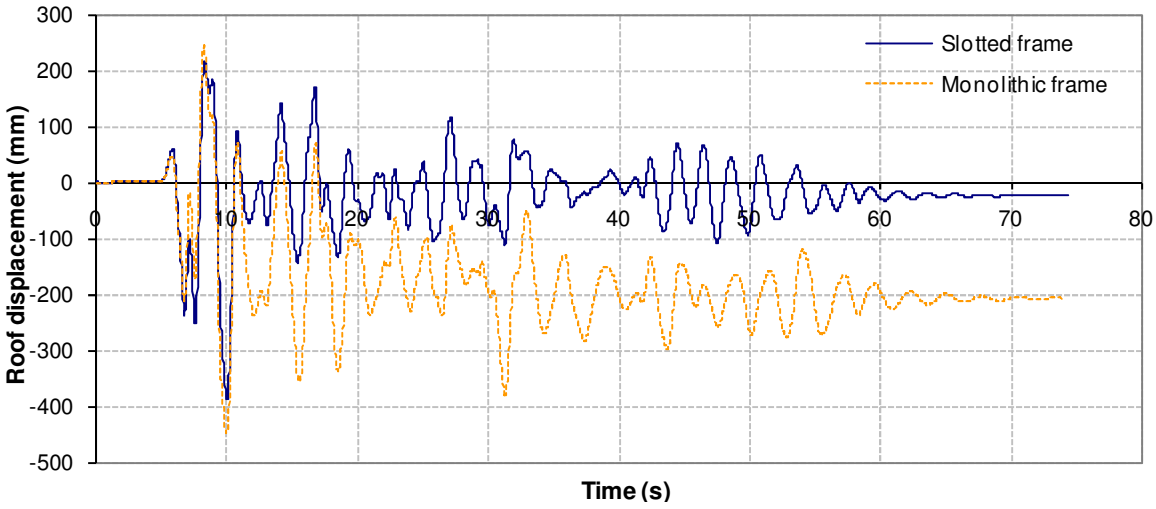

(b) Roof displacement response

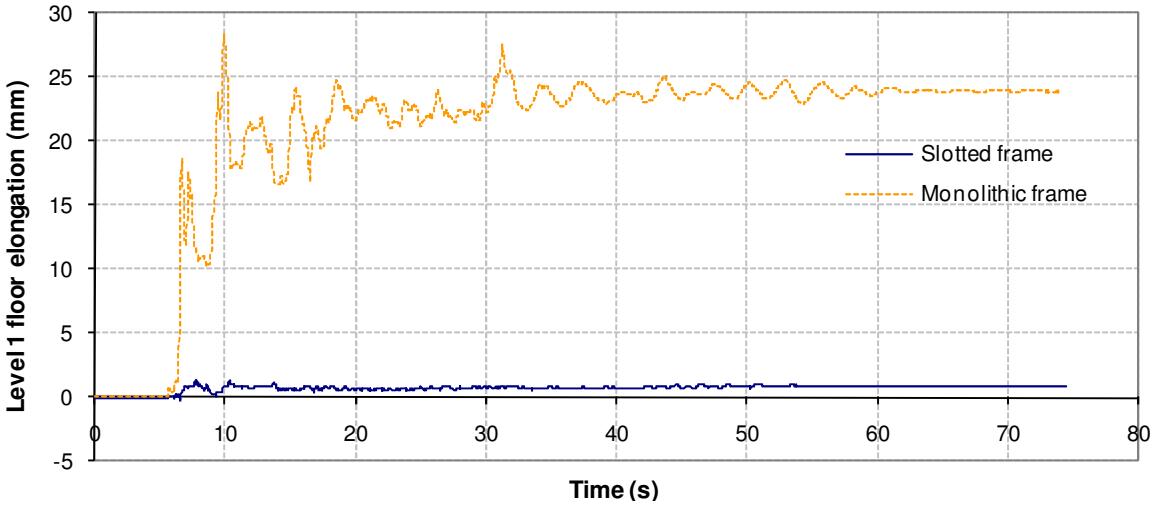

(c) Level 1 floor elongation

Figure D- 9: Imperial Valley 1 1940 earthquake record

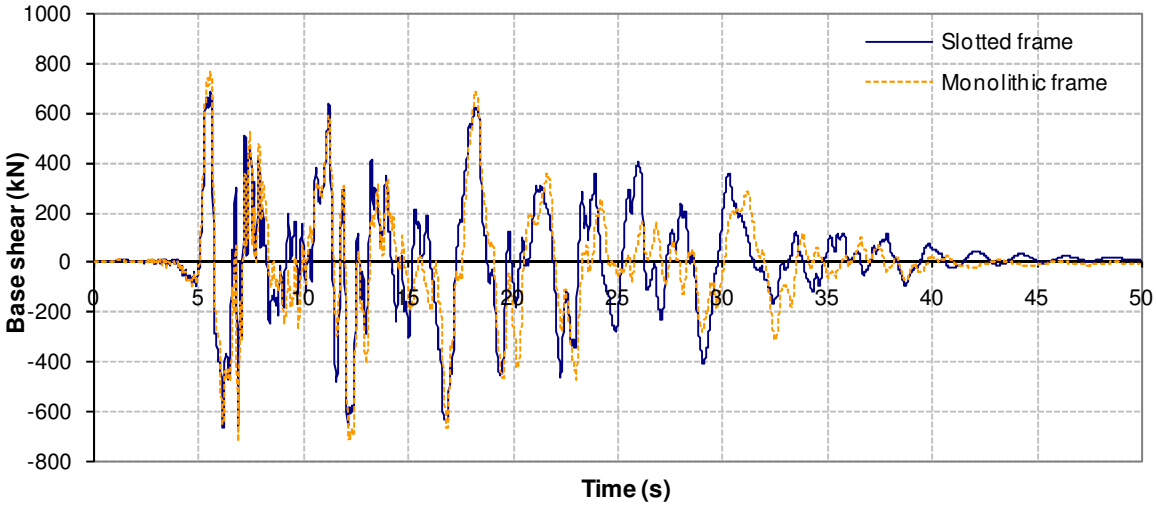

(a) Base shear response

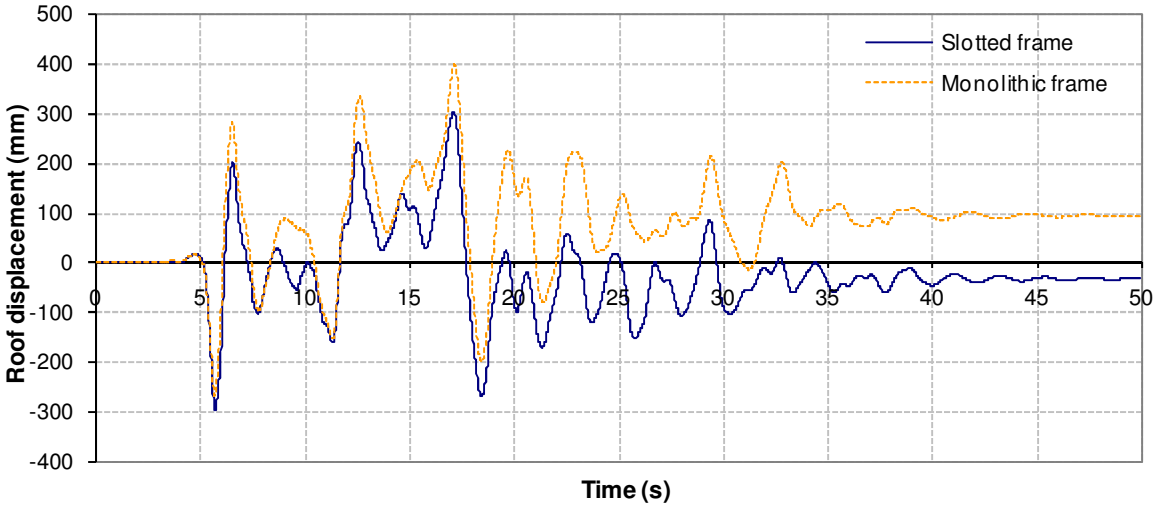

(b) Roof displacement response

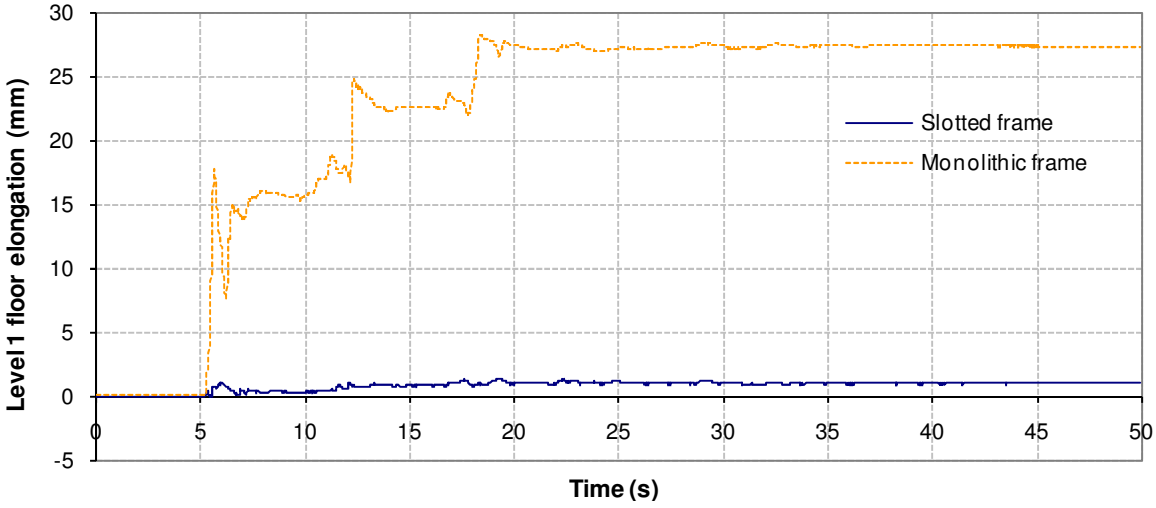

(c) Level 1 floor elongation

Figure D- 10: Imperial Valley 2 1979 earthquake record

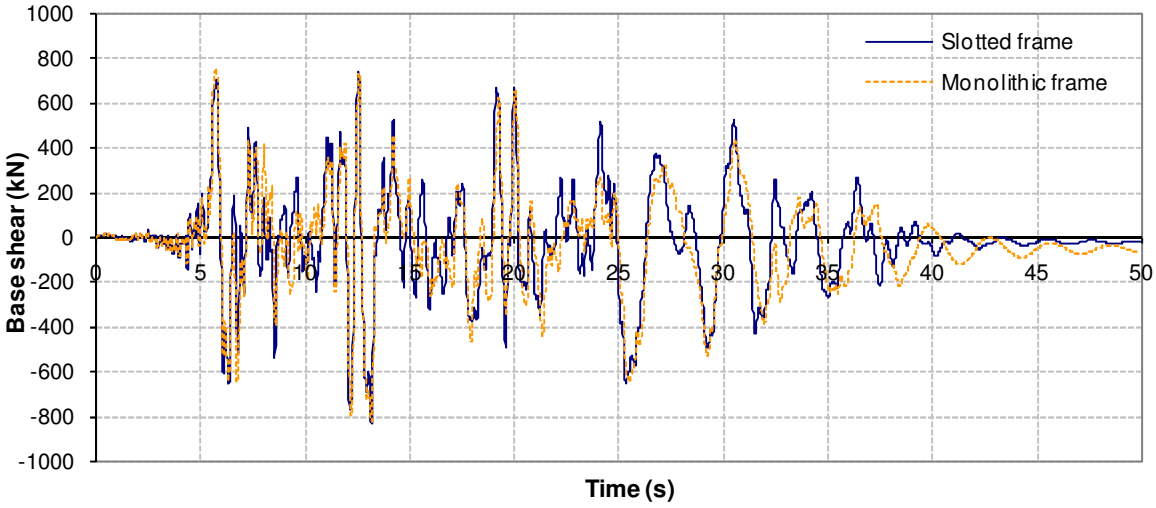

(a) Base shear response

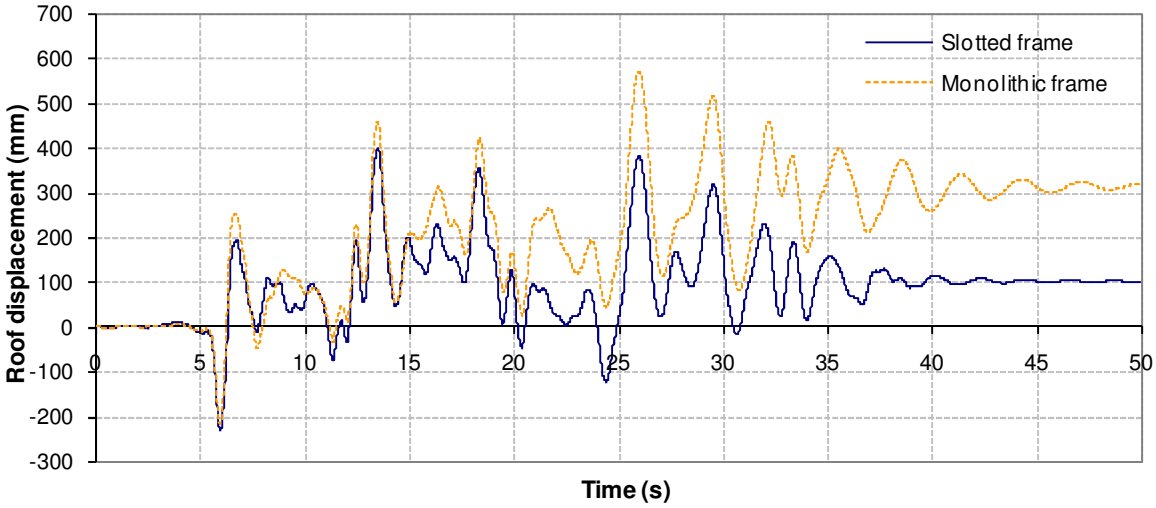

(b) Roof displacement response

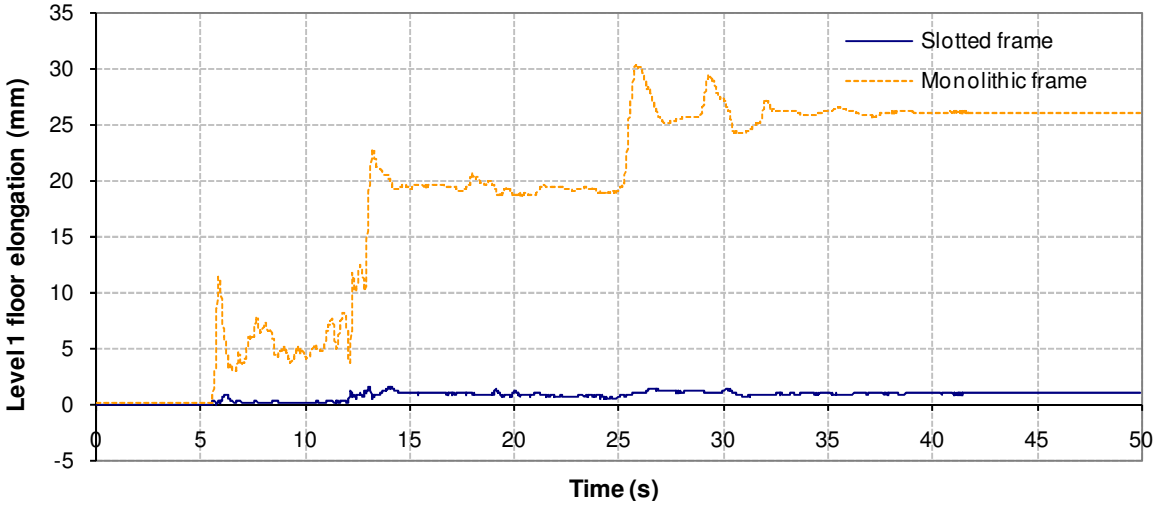

(c) Level 1 floor elongation

Figure D- 11: Imperial Valley 3 1979 earthquake record

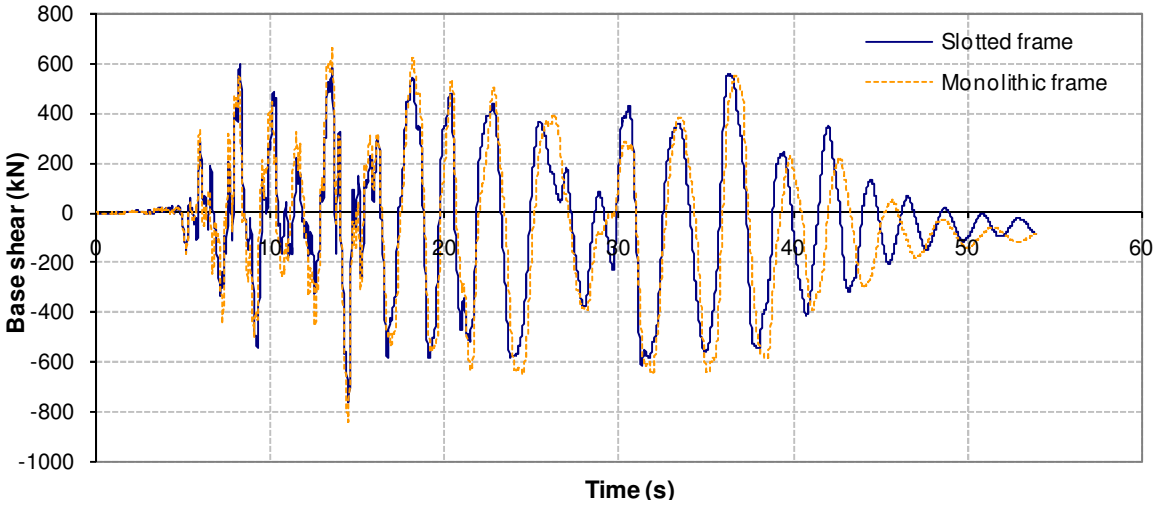

(a) Base shear response

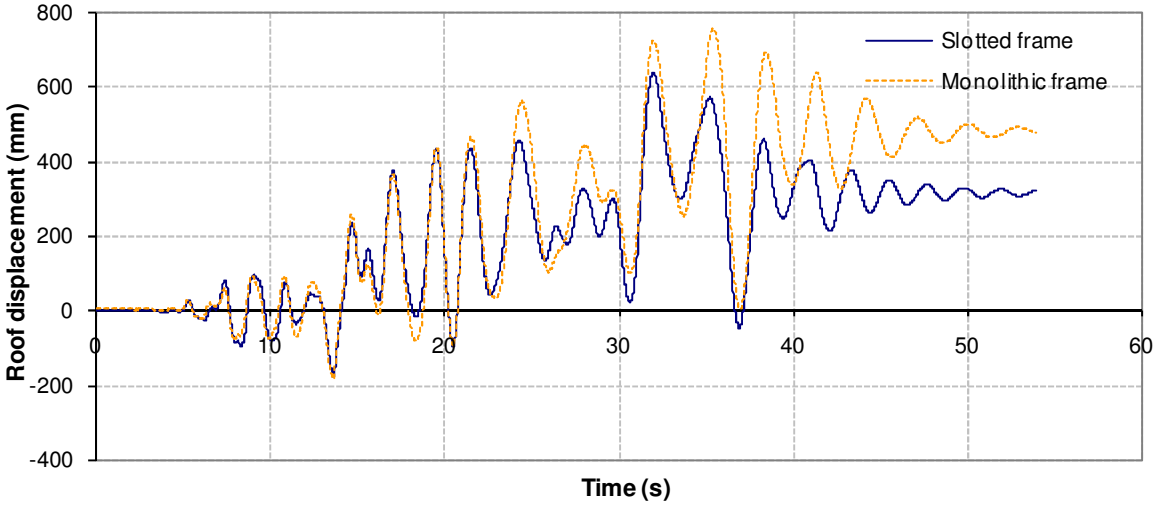

(b) Roof displacement response

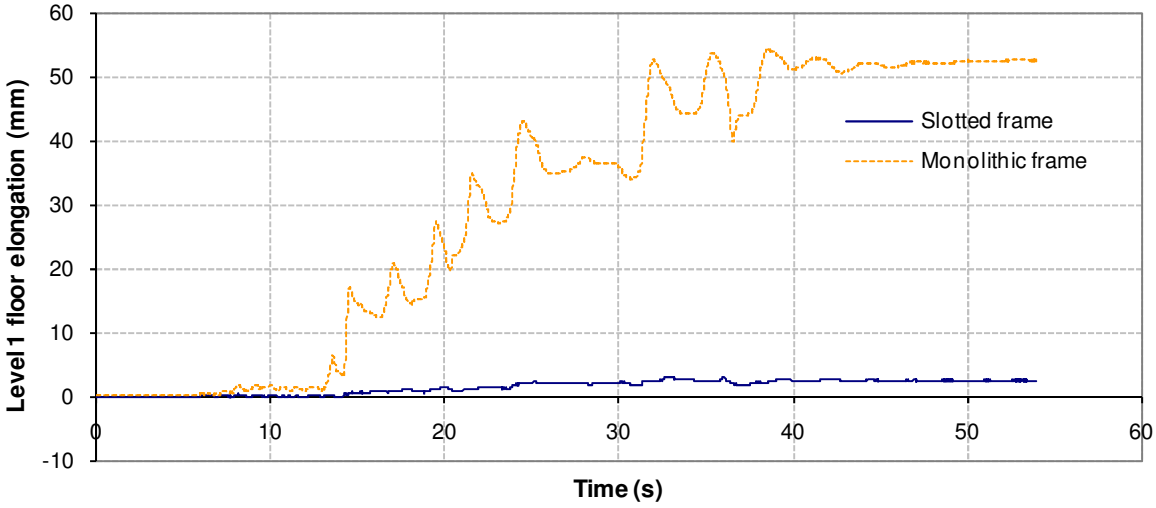

(c) Level 1 floor elongation

Figure D- 12: Superstition hills 1987 earthquake record

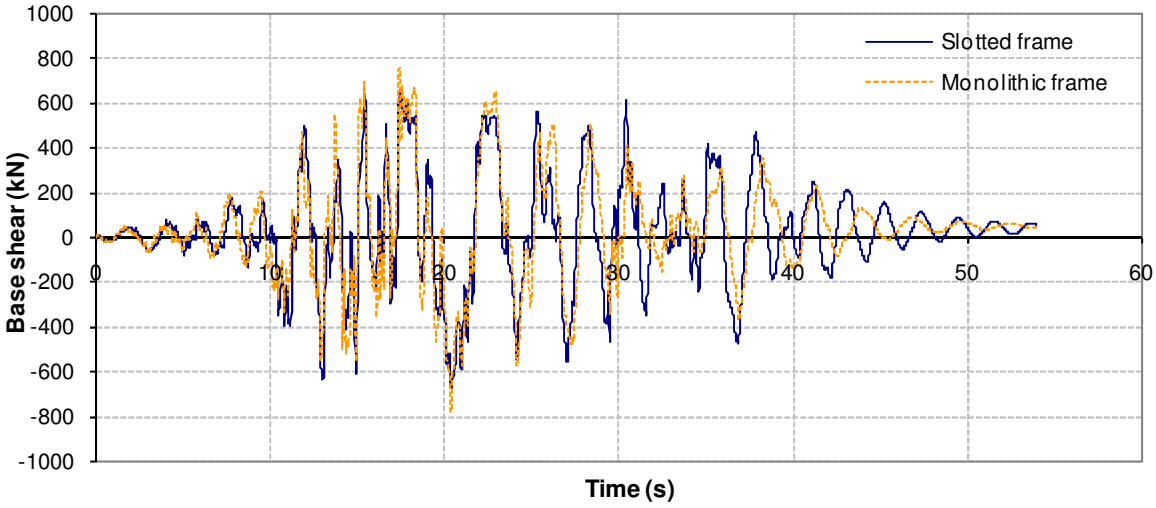

(a) Base shear response

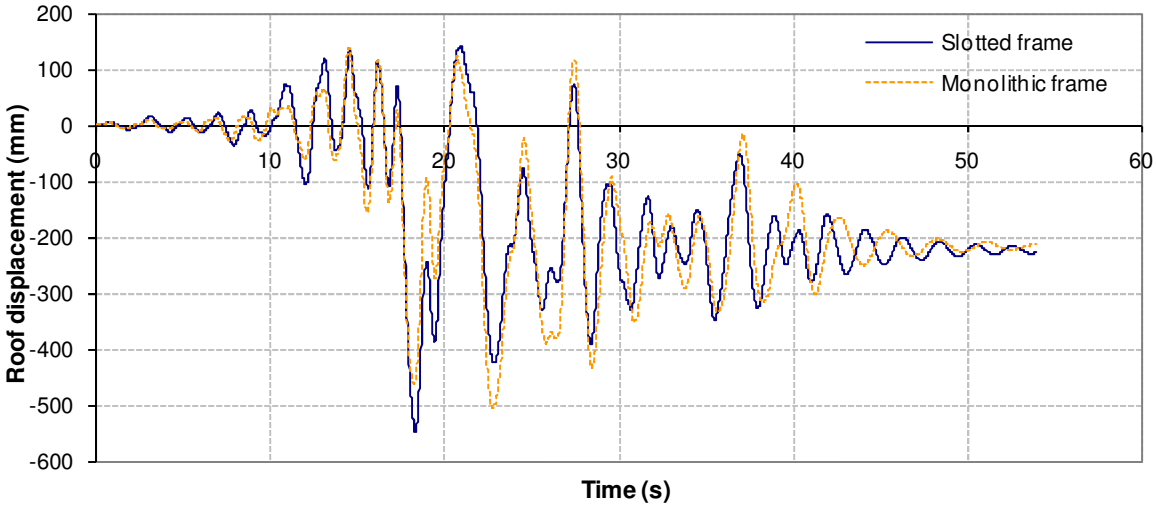

(b) Roof displacement response

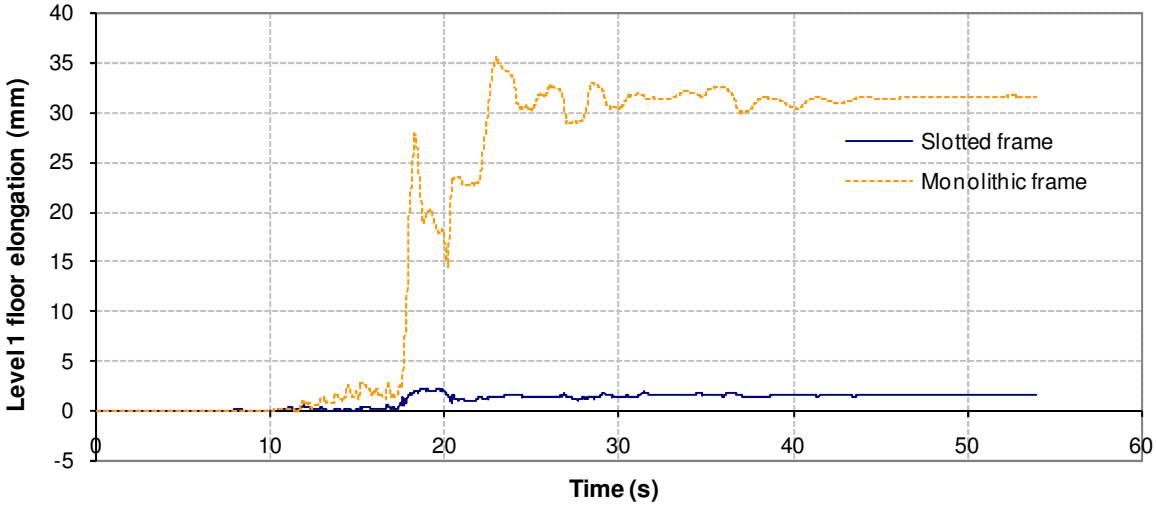

(c) Level 1 floor elongation

Figure D- 13: Landers 1992 earthquake record

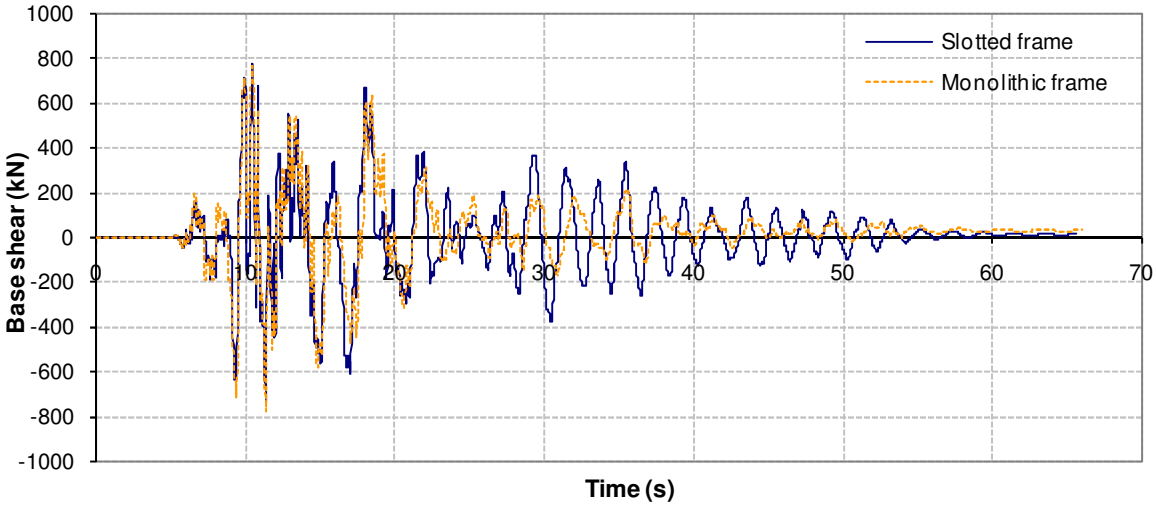

(a) Base shear response

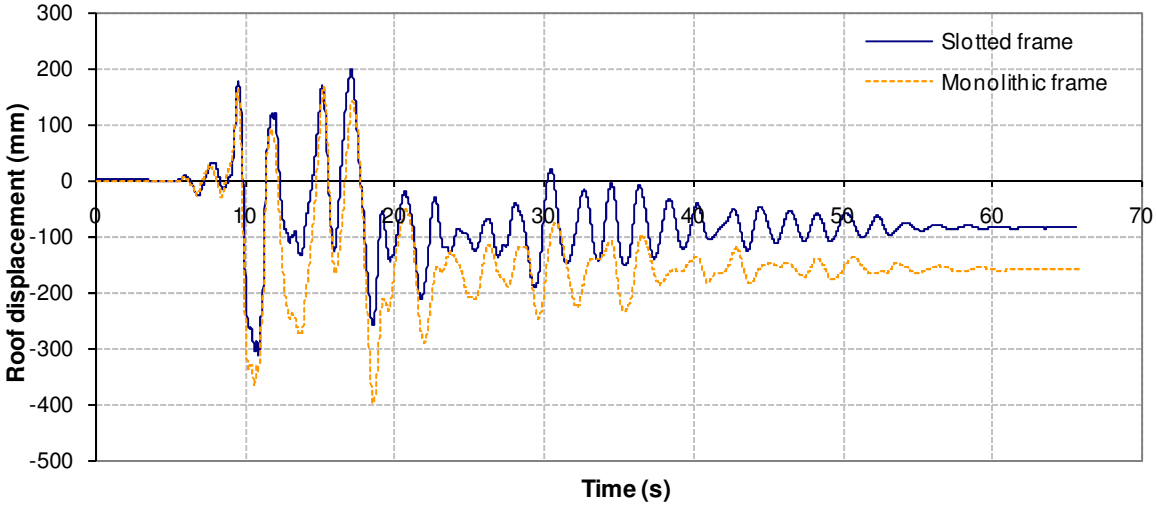

(b) Roof displacement response

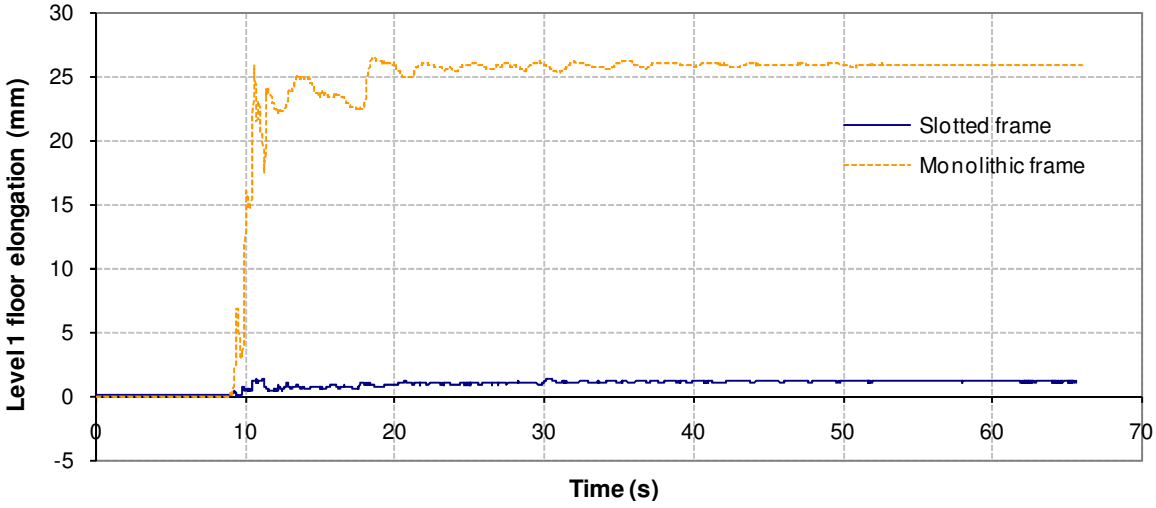

(c) Level 1 floor elongation

Figure D- 14: Turkey 1 1999 earthquake record

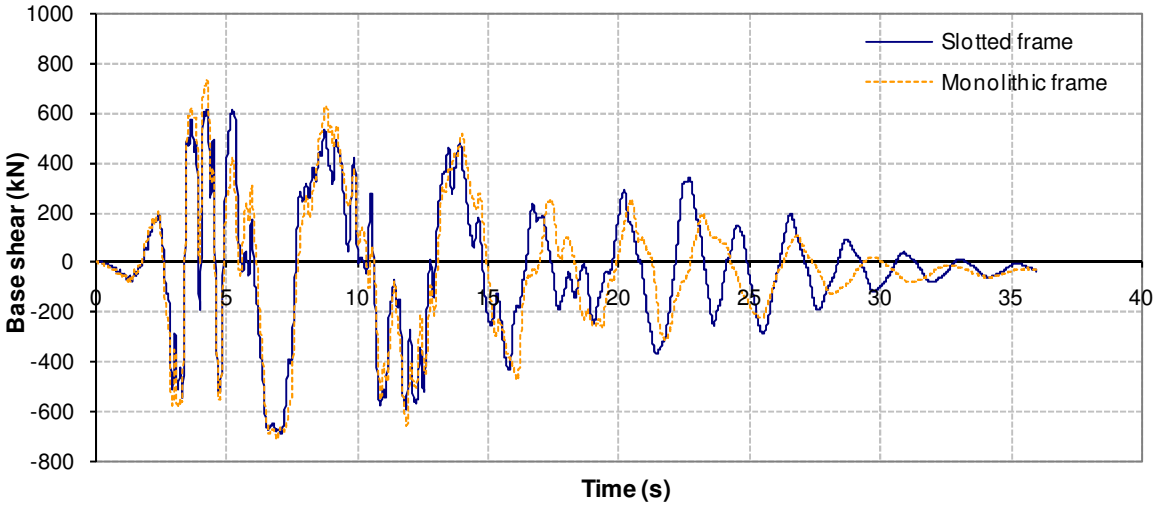

(a) Base shear response

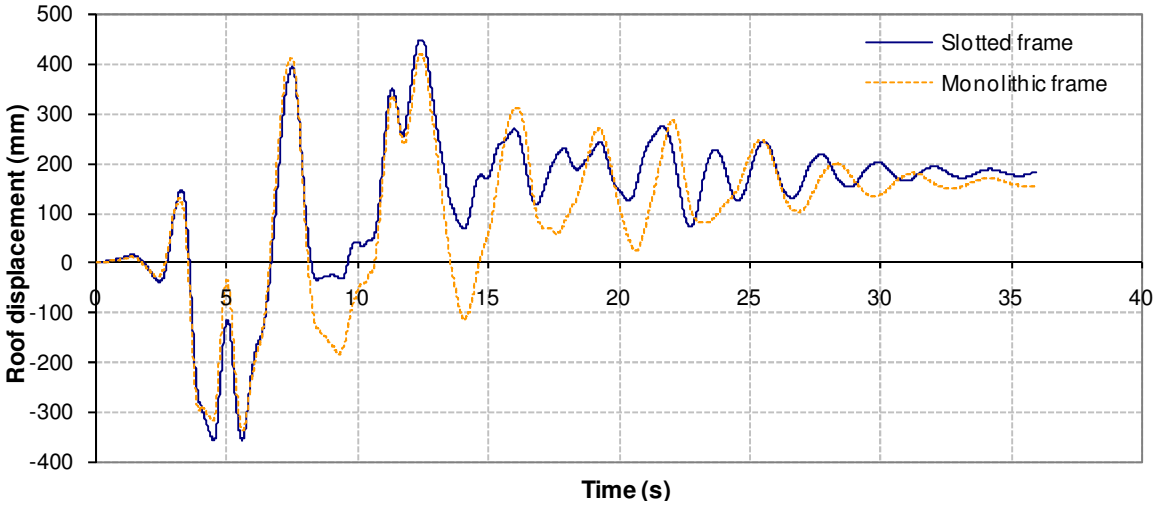

(b) Roof displacement response

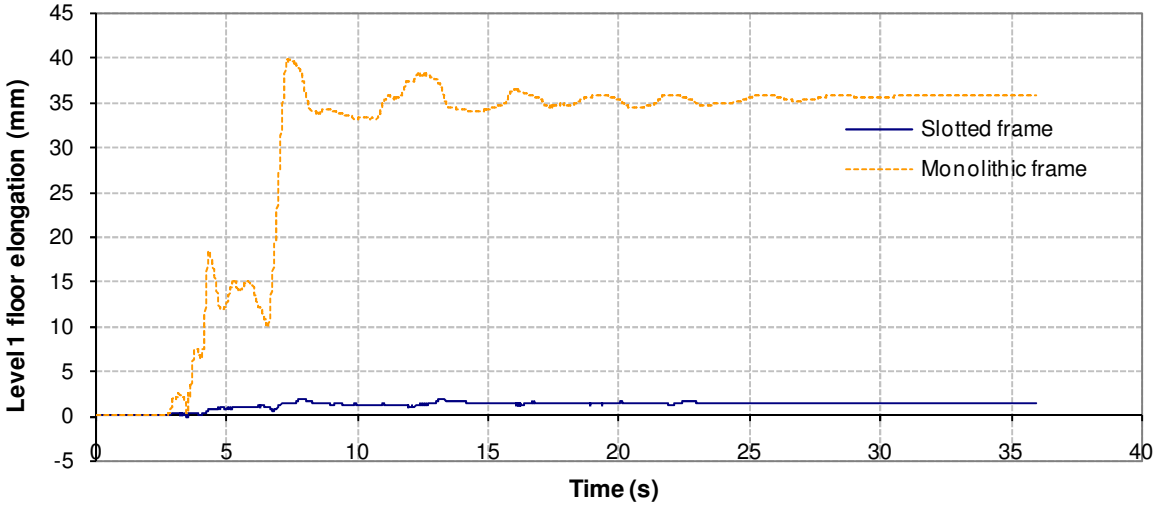

(c) Level 1 floor elongation

Figure D- 15: Turkey 2 1999 earthquake record

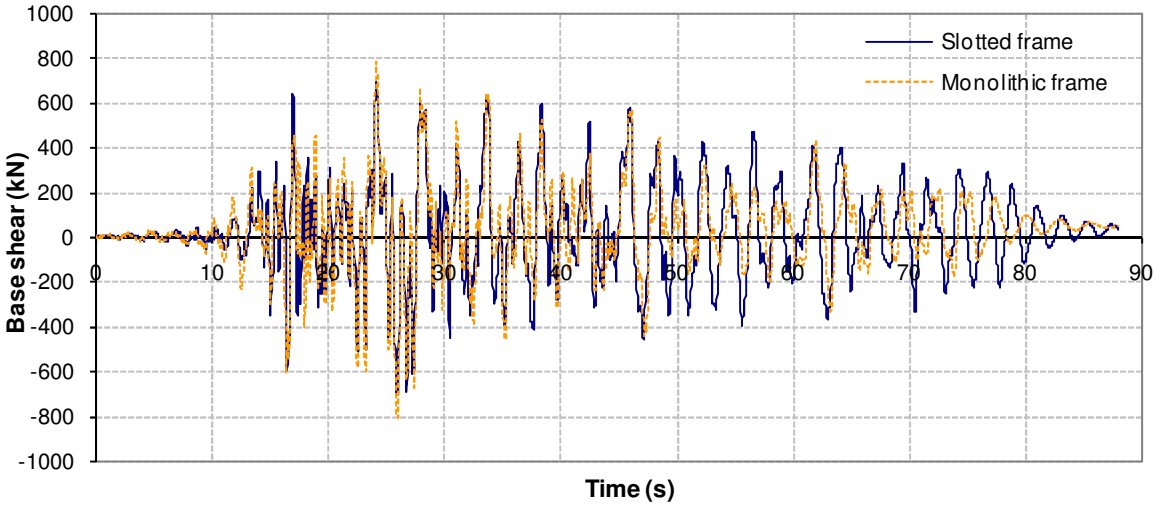

(a) Base shear response

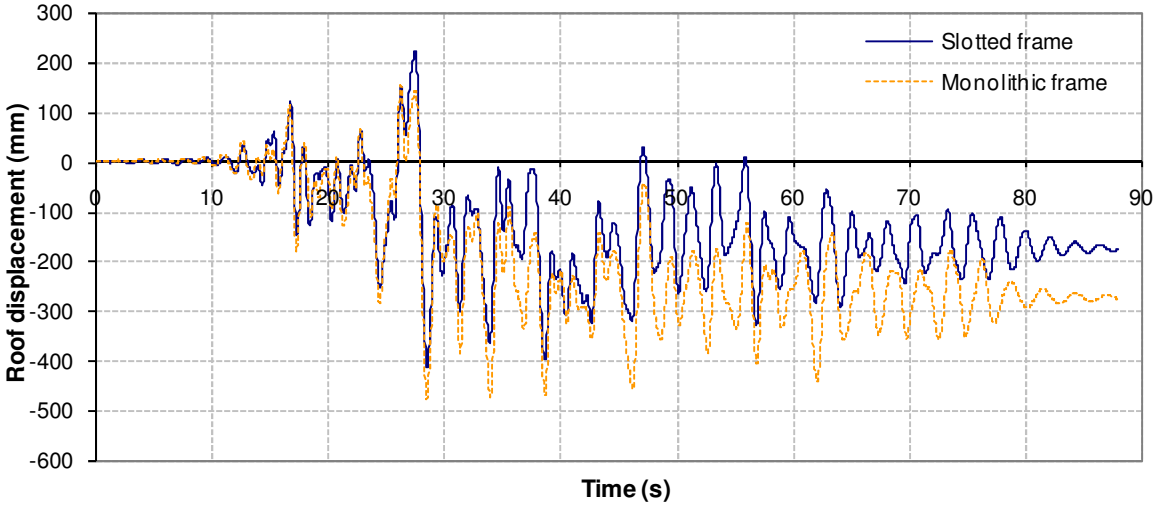

(b) Roof displacement response

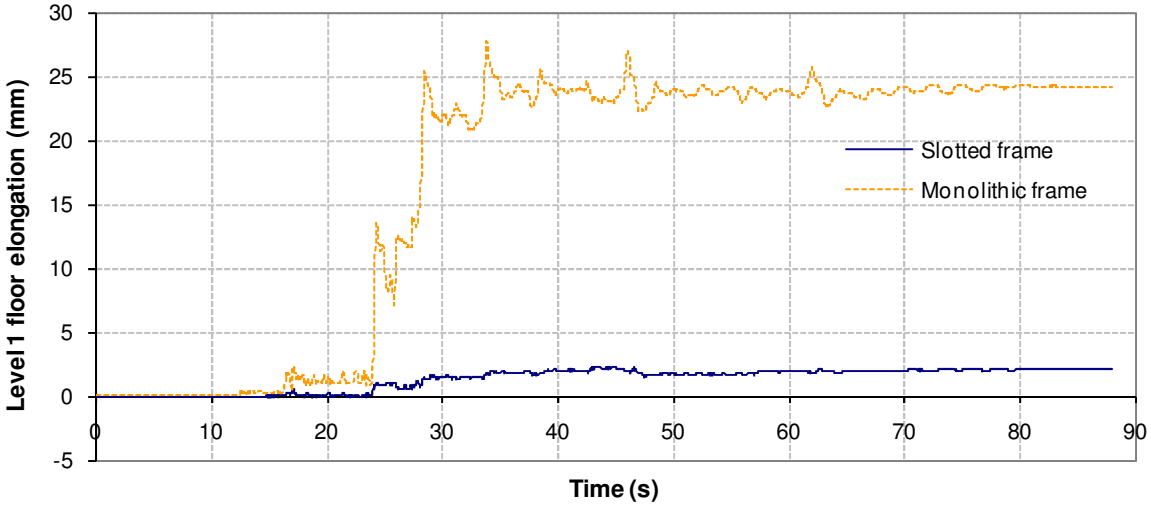

(c) Level 1 floor elongation

Figure D- 16: Hokkaido 2003 earthquake record